UNIVERSITY OF LIVERPOOL

Assessment of disease progression and monitoring response to treatment using ^{18}F-NaF PET/CT in patients with alkaptonuria

Thesis submitted in accordance with the requirements of the University of Liverpool for the degree of Doctor in Philosophy by:

Eman Habib Alawadhi

March 2021

Abstract

Alkaptonuria (AKU) is an ultra-rare, autosomal recessive metabolic disease caused by a deficiency of HGD enzyme leading to increased circulating homogentisic acid (HGA). HGA is deposited as ochronotic pigment in connective tissues, leading to multisystemic involvements including severe arthropathy and cardiovascular calcification. ^{18}F-NaF PET/CT is a sensitive imaging modality which can offer unique and accurate information concerning the radiotracer activity at the ROI using PET semiquantitative assessment methods such as standardised uptake value (SUV).

The main aims of this thesis were to investigate the utility of ^{18}F-NaF PET/CT as an imaging biomarker for detecting the early stage of bone involvement, early disc degeneration, and the early stage of microvascular calcification for AKU patients. Part of this thesis aimed to assess the progression of the disease and the response of therapy over four years for SONIA 2 patients by evaluating the changes in ^{18}F-NaF PET/CT scans.
AKU patients who were enrolled in the SONIA 2 trial and underwent ^{18}F-NaF PET/CT were included in the analysis in this thesis. HU_{mean} and SUV_{max} were measured from lumbar vertebrae, femoral head, and lumbar disc. SUV_{max}, TBR_{max}, and HU_{mean} were measured for the main cardiac arteries.

The studies presented in this thesis show four key findings:
First, high ^{18}F-NaF uptake and low HU_{mean} values were detected in the lower spine and hip lesions from ^{18}F-NaF PET/CT scan, indicating active bone turnover and low bone density in AKU patients. Bone HU_{mean} and SUV_{max} values in the spine consistently decrease with age, indicating decreased bone density, decreased osteoblastic activity, and reduced spine perfusion which may be assiocated with ochronosis and ageing.
Second, disc degeneration was strongly associated with increased SUV_{max} in PET images and high Pfirrmann scores in MR images in AKU patients. Lumbar disc SUV_{max} increased gradually with age followed by a decline in the later years, which is related to the disease progression. In the advanced disc degeneration, less binding sites would be available to bind with ^{18}F-NaF and was therefore associated with low SUV.
Third, there were no significant differences between the nitisinone-treated and non-treated patients in the adjusted mean change in ^{18}F-NaF PET/CT quantitative values for the spine. Minimal changes in the SUV_{max} and HU_{mean} over the visits have been noted in both groups, suggesting that nitisinone may not directly affect spinal tissues or the impact of nitisinone needs more time to be noticeable. In fact nitisinone might slow the progression of ochronosis by stopping further pigmentation, but it is unlikely to reverse ochronosis or treat severe damage, specifically in the lumbar spine regions.
Fourth, cardiac involvements appeared as increased ^{18}F-NaF uptake and local dense areas in ^{18}F-NaF PET/CT images, indicating cardiovascular calcification in AKU patients. Calcified vessels were detected in PET images due to the strong biological similarities between bone formation and vascular calcification as the main structural component in both events is hydroxyapatite; the ^{18}F-NaF uptake mechanism in the calcified vessels is similar to that in bone tissues.

Overall, this thesis reveals that ^{18}F-NaF PET/CT scan is a promising imaging technique to identify early musculoskeletal and cardiovascular involvements in AKU patients. This thesis proposed novel and reliable ^{18}F-NaF PET/CT semiquantitative assessment methods to assess disease progression and treatment response.

Declaration

I hereby certify that this thesis constitutes my own product. I declare that the work referred to in the thesis has not been submitted in support of an application for another degree or qualification of any other university or other institutes of learning.

Acknowledgements

I would like to thank the following people, without whom I would not have been able to complete this thesis, and without whom I would not have made it through my PhD degree!

Firstly, I would like to think my supervisor Prof James Gallagher. Jim, thank you for always supporting and guiding me through my PhD; Thank you for being positive and boosting my confidence. Your advice was vital in inspiring me to think outside the box. Without your support, this thesis would not have been possible. I would like also to thank Prof Sobhan Vinjamuri, and Prof Lakshminarayan Ranganath for giving me the opportunity to do my PhD.

Secondly, I would like to thank my lab group for their guidance, encouragement and support. I am so glad and blessed that I have you in my life. It's comforting to know that I have such caring people surrounding me. Jane Dillon, thank you for your kindness and your personal support; thank you for looking after me like a daughter. Dr Hazel Sutherland, I will forever be grateful to you for your help and your support; your continued support and help are appreciated more than you know, thank you for everything.

Dr Juliette Hughes, thank you for being an amazing friend; you are that person who always helped me; I am grateful for your support. Dr Brendan Norman, I would like to thank you for always offering me help; I really appreciate your assistance and your support. Dr Peter Wilson, you have been so kind to me, thank you. Dr Leah Taylor, I would like to thank you for your guidance at the beginning of my PhD.

Thanks also to the following people; Dr Alpesh Mistry for analysing the MR scans; Mark Baker for his guidance in the nuclear medicine department; Eftychia Psarelli and Matt Gornall for their guidance and work on the statistical analysis.

My heartfelt thanks go to my special friend, Ghada Alfateni. You and your family have been part of our family. Ghada, thank you for the wonderful times we shared together. We have shared many happy and sad times together during our PhD journey. We started together and we ended together, and we will be friends forever.

Last but not least, I would like to thank my family and friends for being with me, supporting me, and encouraging me. Mum and Dad, thank you for everything you did and still are doing for me and my kids; without your support I would not be where I am today. Thank you for always being proud of me.

Thank you to my sister Amal for always supporting me and taking care of my kids while I am writing my thesis. A very special thank you goes out to Anfal Alsebeh for motivating me; your kind words warmed my heart. Moussira Alameddine, you are a wonderful friend, I appreciate your help

My acknowledgements would not be complete without thanking my husband Yousef; I could not do it without you. My boys, Ahmad and Saqer, I know it was difficult for you to live far away from your family, but I am sure that you learned a lot in these years. I love you boys, and I hope that you now are proud of your Mum.

Abbreviations

AA	Ascending aorta
AAA	Average aortic arteries
ABP	Average blood pool
AC	Articular cartilage
ACA	Average coronary arteries
ACC	Articular calcified cartilage
AKU	Alkaptonuria
AKUSSI	Alkaptonuria severity score index
ANOVA	One-way analysis of variance
BMD	Bone mineral density
BP	Blood pool
BSA	Body surface area
BQA	Benzoquinone acetic acid
BTM	Bone turnover biomarker
CA	Circumflex artery
CAC	Coronary calcium score
CCS	Coronary calcification score
CT	Computed tomography
DA	Descending aorta
DEXA	Dual-energy x-ray absorptiometry
DICOM	Digital imaging and communications in medicine
DVU	Discovertebral unit
e+	Positron
e-	Electron

EANM	European Association of Nuclear Medicine
EBCT	Electron beam computed tomography
ECM	Extracellular matrix
FDA	Food and Drug Administration
GCCS	Global cardiac calcification score
HGA	Homogentisic acid
HGD	Homogentisate 1,2-dioxygenase
HMDP	Hydroxymethylene diphosphonate
HPPA	4-hydroxyphenylpyruvic acid
HPPD	4-hydroxyphenylpyruvate dioxygenase
HT1	Tyrosinemia type 1
HU	Hounsfield unit
IV	Intravenously
IVD	Intervertebral disc
IVC	Inferior vena cava
kBq	Kilobecquere
keV	Kiloelectronvolts
kVp	Kilovoltage peak
LAD	Left anterior descending artery
LBM	Lean body mass
LCA	Left coronary artery
LCx	Left circumflex artery
LC-MS/MS	Liquid chromatography tandem mass spectrometry
LOR	Line of response
L1	Lumbar level 1

L2	Lumbar level 2
L3	Lumbar level 3
L4	Lumbar level 4
L5	Lumbar level 5
mAs	Milliampere-seconds
MBq	Megabecquerel
mCi	Milicurie
MDP	Methylene diphosphonate
MIP	Maximum intensity projection
MRI	Magnetic resonance imaging
mSv	MilliSievert
NAC	National Alkaptonuria Centre
NaF	Sodium fluoride
NaOH	Sodium hydroxide
NCEP	National Cholesterol Education Programme
NIH	National Institute of Health
NTBC	Nitisinone
OA	Osteoarthritis
OH-	hydroxy1 group
OSEM	Ordered-subset expectation-maximization
PA	Posteroanterior
PET	Positron emission tomography
RA	Rheumatoid arthritis
RCA	Right coronary artery
ROI	Region of interest

SB	Subchondral bone
SIJ	Sacroiliac joint
SNM	Society of Nuclear Medicine
SVC	Superior vena cava
s-HGA	serum HGA
SOFIA	Subclinical ochronotic features in alkaptonuria
SONIA 1	Suitability of nitisinone in alkaptonuria 1
SONIA 2	Suitability of nitisinone in alkaptonuria 2
SPECT	Single-photon emission computed tomography
SUV	Standardised uptake value
SUV_{max}	Maximum standardised uptake value
TBR	Target to background ratio
TBR_{max}	Maximum target to background ratio
TBW	Total body weight
TOF	Time of flight
T12	Thoracic level 12
u-HGA	urine HGA
US	Ultrasound
WHO	World Health Organisation
3D	Three dimensional
^{18}F	Fluorine 18
^{18}F-NaF	18Fluorine- labelled sodium fluoride
^{18}F-FDG	18Fluorine- labelled fluorodeoxyglucose
^{18}O-H_2O	Oxygen-18 enriched water
^{99}Mo	99Mo-molybdate

^{99m}Tc	Technetium-99m
^{99m}Tc HMDP	Technetium-99m labelled hydroxymethylene diphosphonate
^{99m}Tc MDP	Technetium-99m labelled methylene diphosphonate

Table of Contents

List of the figures

Chapter 1

Chapter 2

Chapter 3

Chapter 4

Chapter 5

Chapter 6

Appendix

List of tables

Chapter 1

Chapter 2

Chapter 3

Chapter 4

Chapter 5

Chapter 6

Appendix

1 Introduction

1.1 Alkaptonuria

Alkaptonuria (AKU) is a rare multi-system genetic disorder caused by the accumulation of homogentisic acid (HGA) in connective tissues due to mutation in a specific enzyme [1]. It is now known that the cause of AKU is a deficiency of homogentisate 1,2-dioxygenase (HGD; EC 1.13.11.5), an enzyme in the pathway for metabolising ingested phenylalanine and tyrosine [1]. The deficiency of HGD in the tyrosine metabolic pathway leads to an inability to metabolise HGA to maleylacetoacetic acid (Figure 1.1). Over time, HGA accumulates and undergoes oxidation, hypothesised to result in a melanin-like polymer, which appears as a dark-brown pigment in connective tissues, termed ochronosis (Figure 1.2). HGA is excreted from the body via the urinary system. The high urinary concentration of HGA in AKU causes urine to darken upon standing or following exposure to air. HGA deposition as an ochronotic pigment in cartilage, joints, and bones leads to them to become brittle and black-brown in colour over time, which is why AKU is also known as 'black bone disease'. Pigmentation of cartilage is the direct cause of an early-onset, severe osteoarthropathy, termed ochronotic arthropathy, which is one of the central pathophysiological features of AKU.

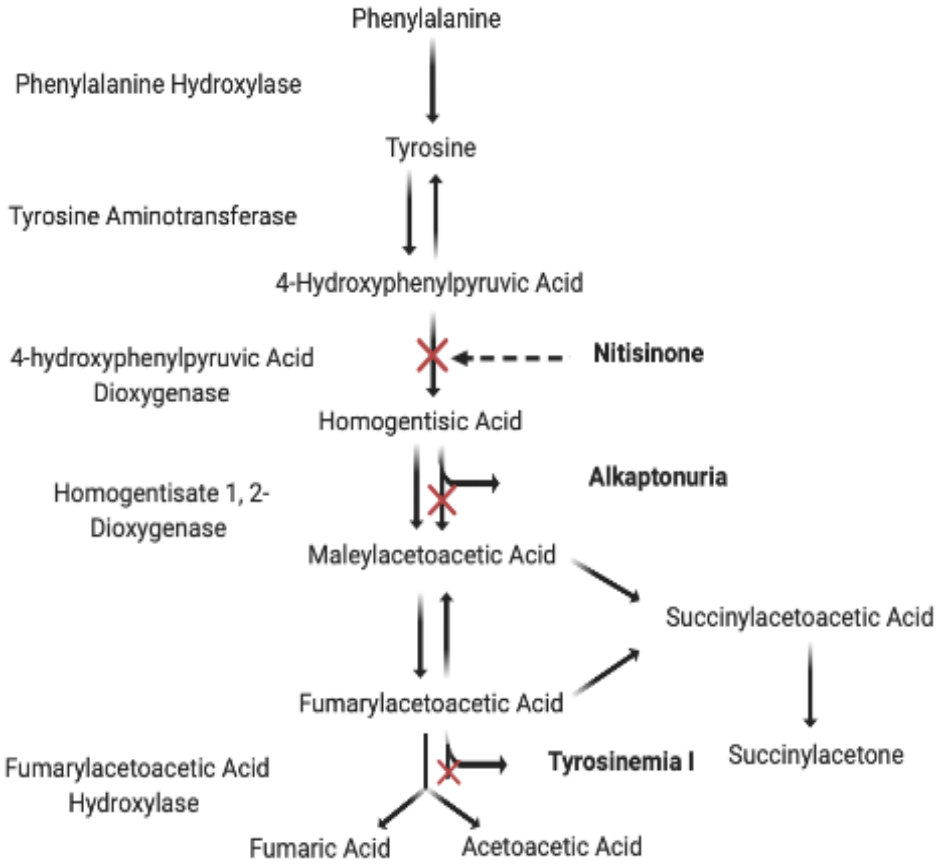

Figure 1.1. The tyrosine metabolic pathway.

The diagram illustrates the phenylalanine and tyrosine degradation pathway. The biochemical defect in alkaptonuria is the deficiency of the enzyme homogentisate 1, 2 dioxygenase (HGD). HGA is not metabolised as a consequence of HGD deficiency, and over time HGA accumulates in connective tissues as ochronotic pigment. The drug nitisinone inhibits the enzyme 4-hydroxyphenylpyruvic acid dioxygenase, blocking the production of homogentisic acid and downstream metabolites (adapted from reference [2]). In non-AKU, significant HGD enzyme expression has only been identified in the kidney and liver.

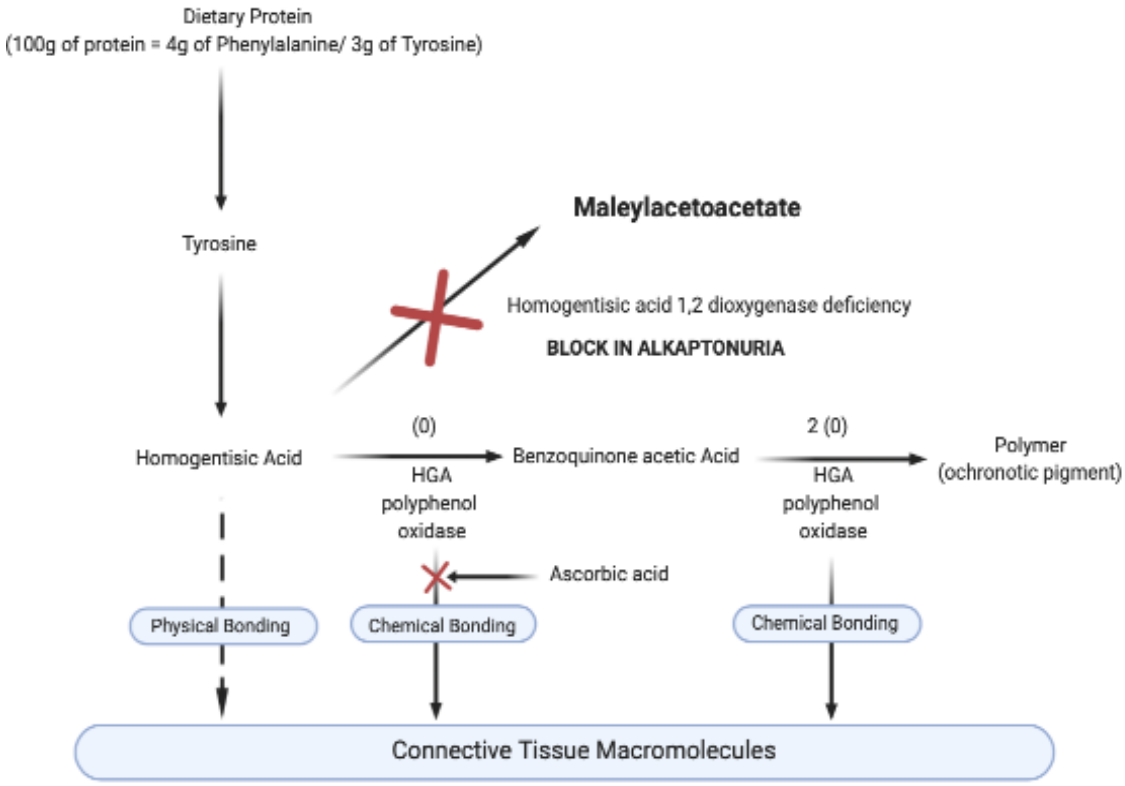

Figure 1.2. Formation of ochronotic pigment.

Dietary protein is metabolised via homogentisic acid (HGA) to maleylacetoacetate. Deficiency of the enzyme homogentisic acid 1, 2-dioxygenase in alkaptonuria leads to increased HGA. Oxidative conversion of HGA to benzoquinone acetic acid leads to the production of ochronotic pigment, which becomes bound within the connective tissue extracellular matrix (adapted from [3]).

1.1.1 History

AKU holds an iconic place in medical history, as the first disease shown to conform to Mendelian principles, with an autosomal recessive mode of inheritance [1]. The earliest case of AKU has been dated to 1500 BC, from the study of an Egyptian mummy named Harwa. Both biochemical and radiographical examination of the spine, knee, and hip of the mummy established the diagnosis [4]. It has been noted that the mummy joints were narrowed and pigmented. Clinically, the first AKU case was reported by Scribonius in 1584 in a healthy child whose urine was 'black as ink' coining the term black urine disease [5]. In 1609, Schenck reported the same clinical finding in a Carmelite monk. Subsequently, several cases were reported by Zacutus Lusitanus in 1649, by Singer in 1775, and by Marcet in 1822. In 1859, Boedecker was

the first to use the term ‘alcapton’, which described the discolouration of urine when alkali was added [1,5]. Boedecker gave the substance responsible for darkening the name ‘alkapton’, derived from Arabic alkali, and the Greek word meaning ‘to suck up oxygen greedily', which refers to the property of acid oxygen uptake in alkaline solution [5]. The term ‘ochronosis’ was first used by Virchow in 1866 to describe a case of a 67-year old male patient characterised by black pigmentation in the articular cartilage, tendons, ligaments and arteriosclerotic plaques [6]. The patient died of congestive heart failure, and the pigmented tissue which was examined microscopically, appeared as yellow/brown (ochre) in colour. Three decades later in 1891, Wolkow and Bauman identified 2,5-dihydroxyphenylacetic acid (HGA), the chemical species of the causative agent of AKU [1].

In 1902, Albrecht proposed an association between AKU and ochronotic arthropathy. A few years later, Osler diagnosed ochronosis clinically in two AKU patients. In 1908, Archibald Garrod first discribed AKU as an ‘inborn error of metabolism’, after finding that many affected individuals were the offspring of consanguineous parents. In 1909, he suggested that the deficiency of a specific enzyme that splits the aromatic ring of HGA was the cause of AKU. After more than fifty years, La Du confirmed this theory when he established that HGD, the enzyme involved in the tyrosine and phenylalanine pathway in the liver, was missing in a patient with AKU [5].

1.1.2 Epidemiology

AKU is classified as an ultra-rare disease; today, the incidence of AKU is estimated to range from one out of 250,000 to one out of 1,000,000 births worldwide [7]. However, there are specific hotspots where the incidence rate is much higher, such as in Slovakia and the Dominican Republic, where it is estimated to be one out of 19,000 [8,9]. Since 1962 [1], the cases documented amount to roughly 600 patients from 35 countries. Nowadays, more than 1000 patients have been identified with AKU worldwide [10]. According to a worldwide review on AKU, cases have been recorded in other countries, including the United States [11], Saudi Arabia [12], Turkey [13], India [6], Sudan, France [14], United Kingdom [15], Germany, Lebanon, and Jordan [16]. Jordan has been recently identified as one of the hotspots for AKU, including the diagnosis of 40 cases in one village, nine of whom were from one family [16,17].

Several possible explanations exist for the high incidence in some world regions. Living in isolated hamlets may cause genetic isolation and the founder effect, leading to increased local transmission of genetic variants, including defective alleles, from a common ancestor [9]. A possible reason for increased incidence in Arabic countries and India is a consanguineous marriage, which is more common in Arabic, Muslim and Indian cultures [5]. It is believed that there are likely many unidentified patients with AKU, particularly in countries where consanguineous marriages are more common, and in regions where healthcare challenges limit accurate diagnoses of AKU.

1.1.3 Clinical presentation

1.1.3.1 Homogentisic acid

Despite the rarity of the AKU, signs of the disease can be recognised from birth. Children with AKU are usually asymptomatic, but the main pathognomonic characteristic of the disease appears at birth and persists throughout life, which is black-brown urine (Figure 1.3.A). Darkening of urine in diapers (nappies) is often the first feature of AKU to be identified in infant patients. However, in some cases, darkening of urine may take several hours, and therefore go unnoticed by the parent or patient. In this case, an additional test may be required to confirm the AKU diagnosis, which involves adding sodium hydroxide (NaOH) to the fresh urine sample. Adding this step will lead to immediate darkening of the urine [12]. This incident can be explained by the oxidisation of a high HGA concentration in the urine by air or alkalinisation, which leads to urine discolouration. The oxidisation process converts the HGA to benzoquinone acetic acid (BQA) turning the urine black. Oxidisation of other bodily fluids, including sweat, also occurs, which can lead to noticeable discolouration of clothing in areas such as under arms.

1.1.3.2 Ochronosis

Besides the black-brown urine, the overt clinical manifestations of AKU usually do not appear until the third-fourth decades of life, due to the slow progressive nature of the disease. The non-excreted HGA by the urinary system results in increased HGA accumulation in tissues throughout the body over many years, which leads to a pathological blue-black discolouration in connective tissues; ‘ochronosis’. Ochronotic

pigment appears in the skin, as brown sclera pigmentation in the eyes and as blue-black discolouration in the pinna of the ear (Figure 1.3.C). Ear pigmentation has been reported in 70% of AKU patients, and eye pigment been noticed in 50% of AKU patients. Discolouration of other parts, including the gums, hands, and nose, has also been documented [14,18].

In the third-fourth decades of life, HGA pigment accumulates in the articular cartilage in addition to skeletal, cardiovascular, genitourinary, respiratory, ocular and cutaneous tissues. The advanced stage appears between 50 and 60 years, with rapid disease progression [19]. The symptoms worsen with age due to several reasons. One of the major reasons is decreased kidney function with age, causing a decrease in HGA urinary excretion. Another possible explanation is the cartilage degradation that occurs as part of the natural ageing process in later life, which exacerbates the existing joint damage caused by ochronosis [20].

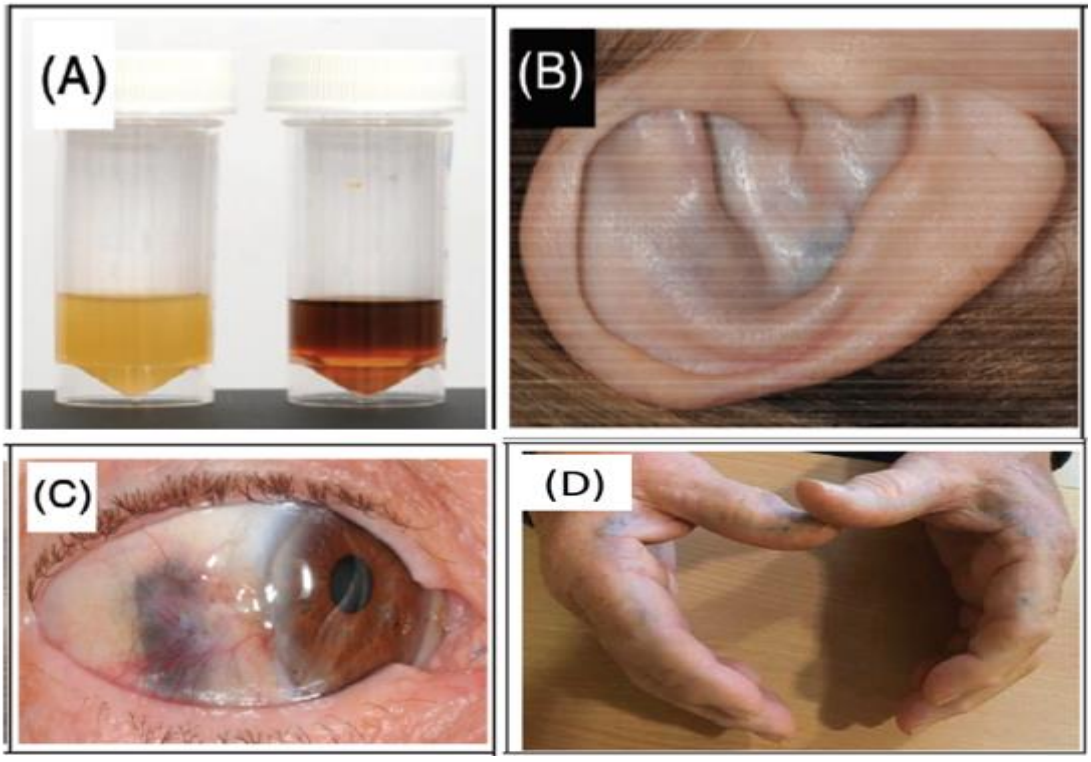

Figure 1.3. Ochronotic pigmentation features.

A. Dark urine of AKU. B. External ear cartilage pigmentation. C. Dark pigmentation of the temporal aspect of the sclera in the right eye with vessels coursing superficial to pigmentation. D. Pigment at the junction of palmar and dorsal skin of hands. Figure from [21].

1.1.3.2.1 Ochronotic arthropathy

The most severe complication of ochronosis is musculoskeletal and joint involvements, which is also known as ochronotic arthropathy (see Figure 1.4). The musculoskeletal involvement primarily affects the axial skeleton and weight-bearing joints, causing lower back and joint pain. Usually, spinal symptoms appear by the age of 30 and progress with age [19].

Ochronotic arthritis closely resembles general osteoarthritis (OA) with pain and damage to the large joints and spine. Clinically, both conditions exhibit similar abnormal morphostructural radiological changes of joints and the spine. In contrast to OA, in which osteophytic changes and lumbosacral changes are predominant, the sacroiliac joint changes are not as evident in ochronotic osteoarthropathy. The spinal degeneration changes for ochronosis include narrowing of the intervertebral discs (IVDs) with severe disc calcification, sclerosis of the endplate, osteophytosis, bony bridges, and spondylitis and disc herniation. The intervertebral vacuum phenomenon is one of the common disc degeneration findings in AKU patients. Vacuum phenomenon is a degenerative disc disorder which usually appear as gaseous collection in the IVD space and within vertebral bodies [22]. The ochronotic pigment is deposited in hyaline cartilage and both annulus fibrosis and nucleus pulposus at multiple IVD levels. The nucleus pulposus probably becomes ossified in advanced cases, which is readily recognised on spine images [23]. In 20% of ochronotic spondylosis cases, the initial presenting symptom appears as an acute rupture of the nucleus pulposus.

Although the entire spine is usually affected, lumbar spine symptoms usually occur first, followed by the thoracic then cervical regions [3]. These changes result in predominant back pain, limitation of movement, stiffness and primarily physical disabilities. In some cases, the IVD collapses and fuses at multiple spinal levels, causing possible loss of physiological curves and resulting in decreased height. In advanced cases, the IVD and synovial joints are often found to contain dark brown to black material on discectomy, most likely due to ochronotic pigment deposition in cartilage and ligaments. In a previous study examining 163 AKU patients, most patients experienced spine complications, and a smaller number of patients had knee

and hip involvement [3]. In fact, large weight-bearing joint involvement usually appears several years after the spine involvement. In ochronotic arthritis, upper extremity involvement is less commonly recognised, except in the shoulder, compared to multiple lower extremity involvement, which is more common [24]. Large peripheral joints, such as knees and hips, are most commonly affected by ochronosis. Hand, elbow and wrist involvement is rare in AKU, but numerous cases of multi-upper joint involvement have been reported, including carpal, metacarpal and distal interphalangeal joints [24].

Additionally, tendon also can be pigmented [5]. Numerous tendon-related pathologies have been reported in AKU, including radiographic findings of tendon calcification, which causes increased thickness of the tendon [14]. In the advanced stage, full-thickness tears may also be recognised in ochronotic patients who may need a casting with the ankle in the talipes equinus position or surgical repair.

It is important to highlight that the interactions with environmental factors such as gait and abnormal load-bearing can affect the extent of bone and joint involvement in AKU. Typically, joint degeneration and its associated symptoms become more progressive by 40 years of age, prompting total joint arthroplasty.

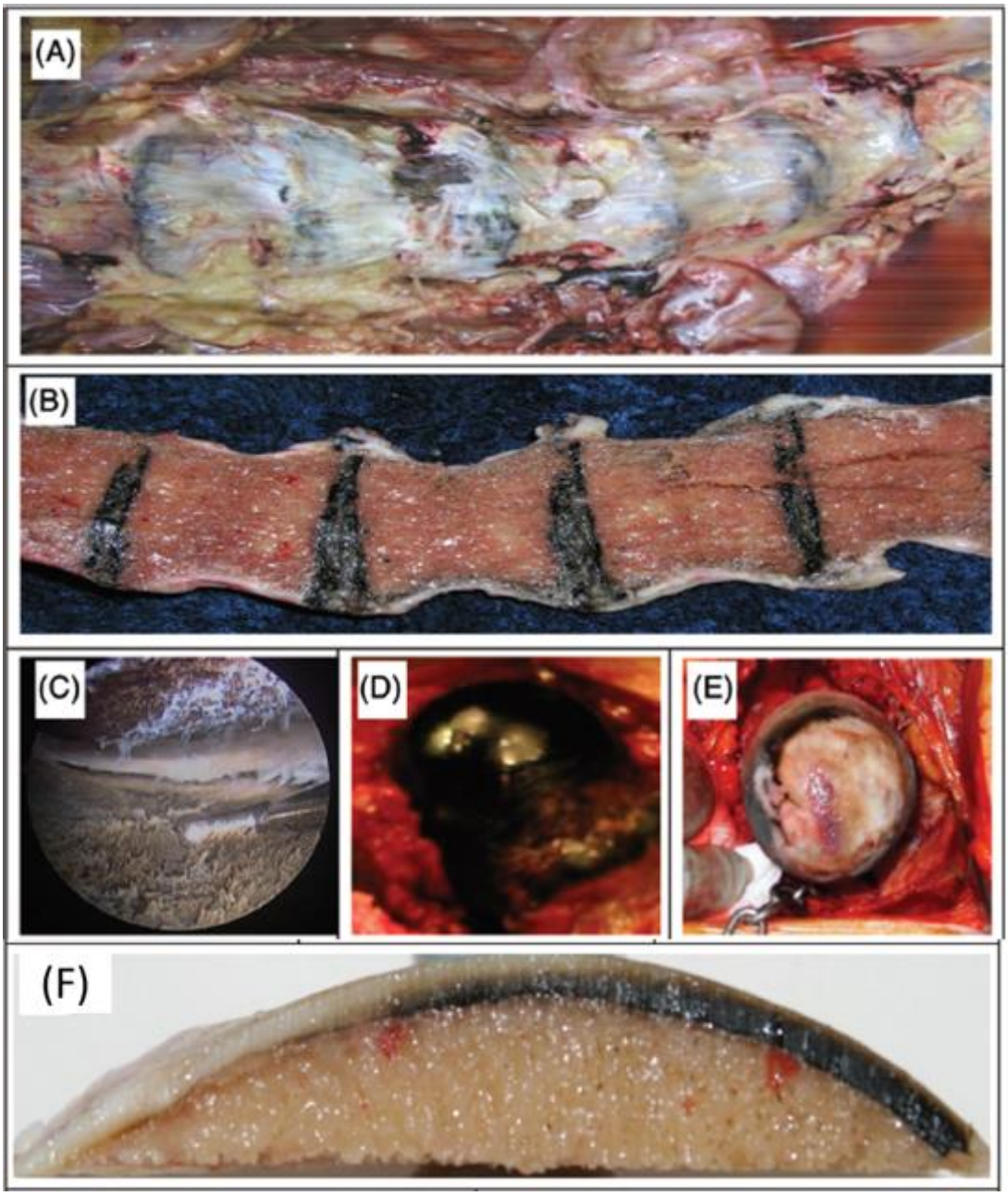

Figure 1.4. Features of ochronotic arthrophathy in human joint tissue.

A, Markedly ochronotic bulging intervertebral discs and the vertebral body is seen from within the abdominal cavity. B, spine seen from posterior or dorsal aspect showing ochronotic pigment. C, Dark pigmentation seen in arthroscopy of knee joint showing fibrillary blackened cartilage. D, appearance of pigmented head of femur showing uniform pigmentation. E, Hip joint showing rim of cartilage and marked cartilage loss with exposure of underlying bone. F, unstained cut section of femur condyle showing little pigment on left side progressing to full pigmentation on the right side. Figure from [21].

1.1.3.2.2 Cardiac ochronosis

Connective tissues of the cardiovascular system are particularly susceptible to damage by ochronosis (see Figure 1.5). Although the pathogenesis of cardiovascular ochronosis is unclear, the extensive extracellular deposits of ochronotic pigment in the cardiac tissues are present [25]. The accumulation of ochronotic pigment within cardiac connective tissues acts as a trigger for dystrophic calcification. The cardiac arteries can be affected by thickening and calcification of the arterial walls in ochronotic patients leading to aortic stenosis and mixed cardiac diseases. Although many clinical factors can be associated with calcified aortic valve disease in AKU, there is no clear statistical correlation between aortic stenosis and plasma HGA level [26,27]. This can be explained by the fact that plasma HGA level is a snapshot of the disease at the time of measuring, while the severe cardiovascular involvements are due to ochronotic pigments which deposited years ago.

Cardiovascular manifestations in AKU patients are common. There are numerous case reports of cardiac involvement in AKU, including coronary artery disease, aortic root disease, and aortic stenosis [28–32]. In very severe cases, patients may require a heart transplant [25]. AKU has been diagnosed intra-operatively during aortic valve replacement, due to presence of ochronotic pigmentation in the heart [25,33]. A partial or entire arterial wall can be covered with black patches and may be extended into the endothelium, causing valve involvement.

Fifty-eight AKU patients were evaluated to delineate the natural history of AKU by Phornphutkul *et al.* [7]. In that study, cardiac involvement appeared at the mean age of 54 years, with no clear sign of cardiac abnormality before the age of 40. Additionally, 50% of patients were found to have severe cardiovascular involvement after 59 years of age. In that study, coronary artery calcification was detected from computed tomography (CT). Interestingly, elevated serum cholesterol level was not correlated with coronary artery calcification in these patients.

In the UK National Alkaptonuria Centre (Liverpool), a systematic cardiovascular evaluation was performed to understand the cardiovascular changes for patients with AKU [34]. Pettit *et al.* [34] evaluated a series of cardiovascular investigations for 16 AKU

patients from 14 families using full electrocardiographic, echocardiographic, and coronary angiography. They found that more than 40% of AKU patientts had a significant burden of aortic valve disease by the fifth decade of life, with no explicit finding of a substantial burden of mitral valve disease or coronary artery disease. Another study by Hawaida *et al.* [27] evaluated the presence of valvular heart disease and vascular calcification for 76 AKU patients using echocardiographic screening and CT scans. In that study, a subgroup of 40 patients was enrolled in a nitisinone treatment study and underwent a non-contrast CT scan; only 17 scans were suitable for cardiac evaluation and coronary and valvular calcification evaluation. Coronary and valvular calcification was noted in CT images and scored using the Agatston cardiac scoring system at coronary, intracardiac, and aorta regions. It was found that 18% of the patients showed coronary calcification, 47% of the patients showed valvular calcification, and 65% showed aortic calcification. All patients had substantial evidence of intracardiac calcification by the age of 60. A modest relationship was also noted between the peak aortic valve velocities per patient and the number of joints replaced.

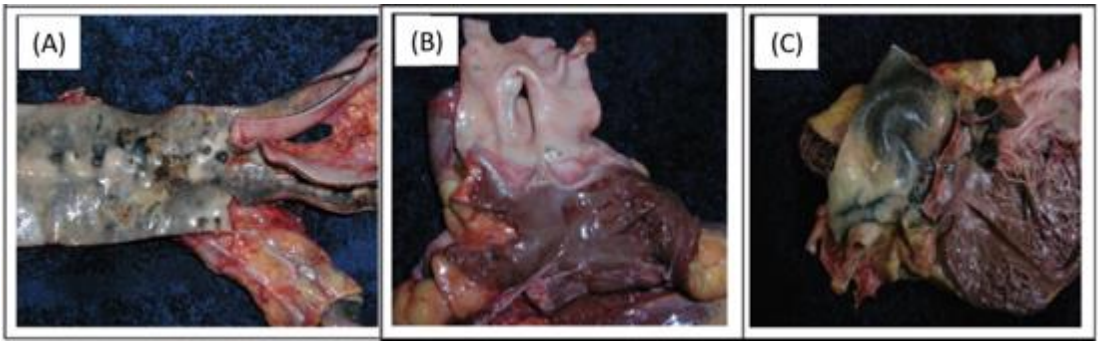

Figure 1.5. Features of cardiovascular ochronosis in human tissue.

A. Longitudinal cut section of the abdominal aorta and common iliac bifurcation, showing more pigment at bifurcation and branch point orifices. B, Low-pressure pulmonary trunk and valve showing little pigment. C, Aortic root and valve with marked pigmentation. Figure from [21].

1.1.4 Mechanism underlying AKU and connective tissue change

In AKU, excessive HGA production leads to an increase in HGA level in circulating and tissue concentrations, but the accumulation of pigment and ochronosis throughout the body is not uniform [3]. The deposition of the ochronotic pigment can be found in

all connective tissues over the body. Joint cartilage is particularly susceptible to ochronosis, which results in weakness and brittleness of the joint tissues [35]. HGA-derived pigment is most heavily deposited in large weight-bearing joints such as the hip, shoulder, elbow and knee. Within fibrocartilaginous tissues, pigmentation has been identified in the annulus fibrosis of IVDs and pubic symphysis. Pigmentation is also found within the elastic cartilage of the external ear and epiglottis. Ochronotic pigment is also deposited in non-cartilaginous tissues; it can be found in the skin, eye, brain, tendons, ligaments, perichondrium, synovial membrane and periosteum. Pigmentation has been identified in the cardiovascular system within heart valves, chordae tendineae, major coronary arteries and aortic artery.

The pathogenesis of ochronosis is still not fully understood, nor is the exact mechanism of pigment formation from HGA. Although there are still many unexplained questions about ochronosis, the initiation of pigmentation within human cartilage was elucidated. Taylor *et al*. carried out a number of investigations to investigate the initiation and progression of ochronosis in AKU [36,37]. Taylor *et al*. demonstrated that early ochronotic pigment were associated ultrastructurally with collagen periodicity [36]. Histological exanimation of an alkaptonuric hip joint capsule showed that the presence of extracellular pigmentation was associated with the collagen fibres and intracellular pigmentation within fibroblasts. Taylor *et al*. also identified that initial pigmentation appears as pericellular and intracellular pigmentation of chondrons within the calcified articular cartilage. Mechanical and biochemical damage caused by mechanical loading, chemical attack, and ageing could significantly increase the possibility of ochronosis in cartilage. It has been hypothesised that the collagen fibres may have sites where HGA can bind, and that these sites in a healthy collagen fibres are protected by proteoglycans that prevent HGA from binding. Proteoglycans can be lost due to mechanical or biochemical damage as part of age-related wear and tear, which exposes these sites to binding of HGA.

Following the initial binding of HGA, it is hypoethezsied that rapid deposition of HGA will occur as an ochronotic polymer resulting in stiffening of the collagen fibre. This process results in further mechanical damage leading to progressive ochronosis [20]. It is important to mention that collagen damage also occurs naturally in the absence of AKU because of the normal ageing.

Ochronotic pigments is extensively deposited in connective tissue, which contains type 1 collagen. HGA accumulation may alter the cross-linking structure and integrity of collagen and interactions of the macromolecules by physical binding. Chemically, HGA is oxidised to a melanin-like polymer by an enzymatic process via BQA [24]. The oxidation process leads to the formation of free radicals in connective tissue, which is also associated with tissue damage by inciting inflammation in the cartilage. Tendon can be considered a pigment deposition site as it richly contains type 1 collagen [5,38]. The ochronotic process eventually causes degradation of cartilage and joint degeneration in the axial and appendicular skeleton, which leads to premature arthritis, bone fracture, osteopenia and muscle and tendon ruptures [38].

1.1.5 Prevention and treatment options for AKU

Although AKU was described over a hundred years ago, the prevention and treatment for AKU patients was focused on symptomatic treatment and limiting the progression of ochronosis symptoms. Ascorbic acid (vitamin C), low protein diets, classic analgesic drugs, physiotherapy, joints replacement were used as a possible treatment option for AKU patients. However, these treatments were clinically ineffective and had no effect on the intrinsic cause of ochronosis. Recently, in 2020, nitisinone has been licenced for treating AKU patients [39].What follows is a description and review of past and current therapy options for AKU patients. Table 1.1 summarises all the prevention and treatment options that have been tested and reported for AKU patients.

1.1.5.1 Ascorbic acid

It has been assumed that antioxidant therapy would have a powerful effect in treating AKU patients by inhibiting the oxidation of HGA to BQA, an intermediary product in the formation of ochronotic pigment in connective tissues. From this point, it has been hypothesised that using ascorbic acid (vitamin C); a powerful antioxidant agent, as a treatment option for AKU patients, would prevent ochronosis by inhibiting the oxidative conversion of HGA to BQA (Figure 1.1 and Figure 1.2). Interestingly, based on previous studies, the most unexpected finding was that ascorbic acid has no apparent effect in treating AKU patients [18,3,40,41].

In 1940, Sealock *et al*. [40] administrated ascorbic acid (1 to 4 gram/day) to AKU patients without getting any effect on the excretion of HGA. It had been presumed that preventing the oxidation of HGA using ascorbic acid could delay the darkening of urine only. Another study was done by Wolff *et al*. [41] who investigated the effect of administrating vitamin C to AKU patients, testing the effect of vitamin C in both adult and infant. Wolff *et al*. reported that a high dose of vitamin C could possibly reduce urinary BQA and free radical formation; however, it appeared not to affect HGA excretion. Furthermore, it was suggested that vitamin C increased the levels of HGA in the urinary system, contributing to the formation of renal oxalate stones, which could be an unsuitable treatment for young infants. Additionally, several studies highlighted that antioxidant ascorbic acid therapy was not clinically useful [3,18].

1.1.5.2 Low protein diet

Another possible treatment option was lowering tyrosine in the diet, which would prevent the formation of BQA by the degradative HGA pathway. Approximately 6% of dietary protein is degraded via the HGA pathway. The idea is that reducing the dietary intake of phenylalanine and tyrosine will reduce the amount of HGA produced and therefore prevent ochronotic pigmentation. Hasas *et al*. [42] investigated the effectiveness of protein restriction in 16 AKU patients aged between 3 to 27 years old. In that study, Hasas noted that protein restriction resulted in a significant reduction of HGA urinary excretion in 12 years old and younger. The result was less evident for older age patients, suggesting that protein intake restriction may be useful for younger AKU children only. It has also been reported by Phornphutkul *et al*. [7] that no significant change in urinary HGA level been noted with protein restriction in AKU patients. Another study showed relief of joint pain in children after restricting protein intake [43]. Indeed, it is challenging to restrict a low protein diet for life, as it needs intensive specialist supervision during growth and is difficult to maintain [3].

1.1.5.3 Nitisinone

Presently, the most promising treatment for AKU patients is inhibiting 4-hydroxyphenylpyruvic acid dioxygenase (HPPD), the second enzyme in the tyrosine degeneration pathway, which is responsible for the formation of HGA. Nitisinone, 2-

(2-nitro-4-trifluoromethylbenzoyl)-cyclohexane-1,3-dione (NTBC), is a HPPD inhibitor which can block the conversion of 4-HPPA into HGA (Figure 1.1). The regulatory agencies have approved nitisinone for the treatment of hereditary tyrosinemia type 1 (HT-1). Hereditary tyrosinemia type 1 (HT-1) is another inborn tyrosine metabolism disorder which results in chronic liver and kidney disorder due to the accumulation of toxic metabolites that are downstream of HGA in the tyrosine pathway. Data from several sources have identified the reduction of HGA levels and ochronotic pigment associated with nitisinone intake.

In 1998, Anikster *et al.* [44] suggested using nitisinone to treat AKU patients as it would reduce the production of HGA. One year later, Suzuki *et al.* [45] investigated the effect of nitisinone in an AKU mouse model, and he found a reduction in urinary output of HGA. The evidence from that study suggests that nitisinone could be a possible pharmacotherapeutic agent for AKU. In 2002, two patients were treated with oral administration of nitisinone, 0.35-1.4 mg/day, twice a day, for 10 and 9 days [7]. In that study, urinary HGA excretion reduced after the course of treatment, from 6.4 g to 1.7 g per day after nine days and 2.9 to 0.13 g per day after ten days. Initial observations suggested that there may be a link between taking nitisinone and reducing ochronosis for AKU patients.

In addition to the clinical experiments, preclinical experiments of nitisinone in AKU mice were performed. Preston *et al.* [46] studied the therapeutic effect of long-term treatment with nitisinone in the AKU mouse model, examining the plasma HGA level and knee joint pigmentation. A considerable reduction in plasma HGA was reported, as well as joint ochronosis inhibition in those mice treated with nitisinone compared to non-treated mice.

Since 2005, the National Institutes of Health (NIH) has investigated the safety and efficacy of nitisinone in AKU. Suwannarat *et al.* [47] evaluated 9 AKU patients who received oral doses of nitisinone with a regular diet, starting with 0.35 mg for eight days, then followed by 1.05 mg for three months. In that study, it was noted that urinary HGA concentration reduced by 95% from 4 g/day to 0.2 g/day, and tyrosine levels increased significantly from 68 μmol/L to 760 μmol/L. Additionally, Suwannarat reported that six out of seven patients who received nitisinone for more than one week

had reported lower pain in their affected joints. A longer-term trial then followed, with a larger sample group, including treatment and non-treatment groups, between 2005 and 2009. In a 3-year randomised therapeutic trial, Introne *et al*. [48] investigated the effect of 2.1 mg/day nitisinone on 40 AKU patients including 20 patients in the treatment group and 20 patients in the non-treatment group. This study showed a sustained and marked reduction in urine HGA by 98% and plasma HGA levels by 95% throughout the study. To examine the clinical efficacy of the drug, Introne *et al*. used hip rotation examination, which did not show a statistically significant difference in the range of motion between the treated and untreated groups reporting an inconclusive outcome. These results would seem to suggest that it is possible that the joint degeneration started early in AKU patients and is irreversible even with the reduction of HGA.

The agreement of using nitisinone in AKU patients by the regulatory agency, was recently approved in 2020 [39,49]. Nitisinone has been used off-label at the National Alkaptonuria Centre (NAC) since 2012 for patients attending the Royal Liverpool University Hospital, using 2 mg/day, the same dose given in the NIH study. In 2018, NAC results were published, confirming the biochemical efficacy of nitisinone in AKU [38]. The NAC study reported that nitisinone can effectively reduce the urinary HGA level, slow morbidity progression, and may partially reverse ochronosis after taking nitisinone.

DevelopAKUre founded a series of international clinical trials to investigate the efficacy and safety of nitisinone in order to obtain marketing authorisation for the treatment of AKU, which has now been approved by the European Medicines Agency. The main three research sites are Royal Liverpool University Hospital, Liverpool, UK, the National Institute of Rheumatic Diseases, Piestany, Slovakia and Hospital Necker and Institute Necker in Paris, France. Three studies were involved; the first study was to assess the dose-response and was called ‘Suitability of Nitisinone in Alkaptonuria 1’ (SONIA 1), the second study was to determine the efficacy of nitisinone and called ‘Suitability of Nitisinone in Alkaptonuria 2 (SONIA 2), and the last study was a cross-sectional study and called ‘Sub-clinical Ochronotic Features in Alkaptonuria (SOFIA) [50].

In 2013, the Royal Liverpool University Hospital and the National Institute of Rheumatic Diseases, Piestany, started the first trial (SON1A 1). The SONIA 1 trial aimed to identify the most appropriate nitisinone dose in patients with AKU over a period of four weeks by investigating the effect of different doses in reducing urinary HGA excretion [51]. Forty patients were grouped into five groups; each group received a different daily nitisinone dose, 0 mg, 1 mg, 2 mg, 4 mg, and 8 mg. The most effective dose which reduced urinary HGA down by 98.8% and serum HGA to < 3.1 μmol/L was shown in the group treated with the highest amount of daily dosage of nitisinone 8 mg. No serious adverse events were reported in the SONIA 1 study.

In 2014, a longer-term trial called SONIA 2 started and finished in 2019. The primary objective of the SONIA 2 trial was to analyse the effectiveness of nitisinone in AKU after four years of treatment. In addition to this, the study intended to confirm whether nitisinone is safe for use by most AKU patients. All the participants engaged in SONIA 2 were recruited from all across Europe and Jordan. The SONIA 2 study was based at three different clinical sites, including Paris (France), Liverpool (UK) and Piestany (Slovakia). These sites are chosen based on the fact that there are experts in AKU and support from AKU society. In total, 138 AKU patients were identified and randomly divided into two equal groups. Out of these, 69 were treated with nitisinone reciving 10 mg/day, and the other 69 were not given nitisinone. The impact of nitisinone on the HGA level excreted into the urine and overall disease progression in the whole-body, including bone and joints, was observed over four years. Each patient attended their allocated test centre for a total of six visits. From SONIA 2 data, it would be possible to determine the effectiveness and impact of nitisinone and define whether nitisinone is safe to be used for the long term.

In 2017, the SOFIA trial started, including 30 AKU patients with a mean age of 38 years who visited the Royal Liverpool University Hospital. The objective of the SOFIA trial was to determine when microscopic and macroscopic ochronosis can be identified, and the ideal age to begin nitisinone treatment [52]. SOFIA encompassed five age groups, 4 patients in each group. A series of clinical tests and examinations were performed, including urine tests, blood tests, MRI, ear biopsy, eyes/ear photography and gait analysis. SOFIA data showed that ear pigmentation could be identified in the 20s and increased with age. From photography, eye pigmentation was first detected in

a 22 years old patient, while ear pigmentation was first detected in a 34 years old patient. Interestingly, MRI results did not show significant changes in the spine and joints before 30 years, however gait data showed abnormal results in all patients, including the young AKU patients. It was concluded from the SOFIA trial that ochronosis could begin before the age of 20 years, suggesting a paediatric study to identify when ochronosis first initiates is needed.

Ranganath *et al.* [53] tested the relationship between bone density and nitisinone therapy for 87 AKU patients who attended the NAC between 2007 and 2020 and underwent serial clinical evaluations, including DEXA and CT densitometry. In that study, patients were grouped into three groups, nitisinone-treatment group, nitisinone plus antiresorptive treatment group, and non-treatment group. The changes in regional bone density values from DEXA and CT were evaluated to detect the effect of treatment. The study focused on three body sites; the femoral neck, hip and lumbar spine. Ranganath *et al*. reported that the group of AKU patients who undertook 2 mg/day nitisinone showed a significant reduction in CT values measured at femoral neck and hip sites ($P < 0.05$ and 0.01, respectively), and slightly increase lumbar CT value ($P > 0.05$). Only patients on nitisinone plus antiresorptive had improved bone density values at all measured ROI ($P < 0.001$), and surprisingly had significantly more fractures than nitisinone-treatment group and non-treatment group. Ranganath *et al*, are suggesting the co-therapy is required to prevent bone loss in AKU patients.

1.1.5.4 Other treatment options

Although lifestyle counselling is also underused and can improve the life quality of AKU patients, the existing literature on this area have not been addressed yet [18]. Minimising joints load and avoiding hard exercises caused by active occupations, activities, or hobbies can likely have a positive impact on ochronotic arthropathy symptoms. Pain control is tackled by undertaking a variety of classic analgesic drugs such as paracetamol, non-steroidal anti-inflammatories, opioids, local anaesthetics, anticonvulsants and gabapentin; however, it is only palliative treatment and not completely effective. Physiotherapy can also help in reducing joint pain and improve mobility. At the advanced stage of ochronotic arthropathy, palliative surgery may be needed to relieve the pain and enhance life quality. Surgical procedures include joint

replacement, spine surgery and tendon repair may also needed in some cases. It has been suggested that liver transplant would successfully eradicate HGA from the body [54]. Organ replacement could improve the metabolic symptoms of AKU however it is not justified in a disease with a relatively normal lifespan. Therefore, liver or kidney transplant is not used to treat patients with AKU.

Although using nitisinone showed very successful results, it is not a perfect option as it can affect the tyrosine levels. Missing enzyme replacement would be the ideal treatment for AKU patient. Hypothetically, replacing the missing HGD enzyme with gene/enzyme therapy will prevent HGA accumulation and appearance of ochronosis in connective tissues. However, clinically, this treatment is not possible yet but may be available in the future [3].

Table 1.1. Current and future treatment options available for AKU.
Adapted from reference [3,18].

Treatment options	Summary
Ascorbic Acid (vitamin C)	Efficacy unproven increases HGA production may exacerbate the condition
Low protein diets	Efficacy in adults unproven, compliance difficult
Lifestyle counselling	Underused, lack of evidence base
Physiotherapy	Underused
Surveillance	Lack of knowledge prevents utilisation
Pain control	Widely used, palliative, incompletely effective
Palliative surgery	Effective but invasive, not universally available
Organ replacement/ Liver transplant	Unjustified in a disease with normal lifespan, lack of evidence base
Reverse pigment binding	Not yet available
Nitisinone	Not shown to alter outcomes, increases tyrosine
Enzyme replacement	Not yet available
Gene replacement	Not yet available

1.2 Skeletal system

1.2.1 Anatomy and physiology

The skeleton system consists of bone and connective tissues, which generates the body frame, and protects the vital organs [55]. Bone is characterised by its strength, rigidity, and capacity to heal and rebuild itself regularly. Bone is made up of an inorganic mineral phase of crystals bound to protein, mostly collagen [56]. The crystals contain a composite called hydroxyapatite, which consists of calcium, phosphate and hydroxyl ions. Normal bone is in a continuous state of remodelling by resorbing osteoclasts from the old and microdamaged bone to mechanically stronger and thicker new bone, which adapts to the mechanical stresses of everyday life. The bone turnover process can also be triggered or accelerated by pathological conditions like fractures, infections, bone tumors or metastases.

The skeleton is comprised of two portions: the axial and the appendicular parts. The axial skeleton composes the skull, the thoracic cage and the vertebral column, while the appendicular skeleton composes the shoulder girdle, the upper limbs, the pelvic girdle, and the lower limbs. This is an essential distinction since many disorders favour either the axial or the appendicular portions.

Anatomically, bone is composed of two components: cortical bone, also called compact bone, and trabecular bone, also called spongy or cancellous bone (see Figure 1.6). Both cortical and trabecular bone have similar matrix compositions, but with different layout and distribution. Cortical bone is restricted to the outer layer of the bone and makes up around 75% of total bone volume. Trabecular bone is restricted to the inner layer, having a much larger surface area, around 60%. Although cortical bone is a greater mass per unit volume compared to trabecular bone, the metabolic rate in trabecular regions is ten times higher than in cortical regions [55]. In total, around 5-10% of the skeleton is annually renewed.

Besides the bones, the human skeleton comprises of tendons, ligaments and cartilage that link the bones together. Articular cartilage is the highly specialised connective tissue surrounding the ends of the bones that acts as load-bearing and low frictional

coefficient which allows joint motion [57]. Articular cartilage is structurally devoid of blood circulation, lymphatics, and nerves and is strongly influenced by a harsh biomechanical and physiological environment. The most significant feature of articular cartilage is that it has little ability for healing and repairing. Usually, treatment and repair of cartilage damage are challenging for the patient and clinician; therefore, it is important to protect this structure.

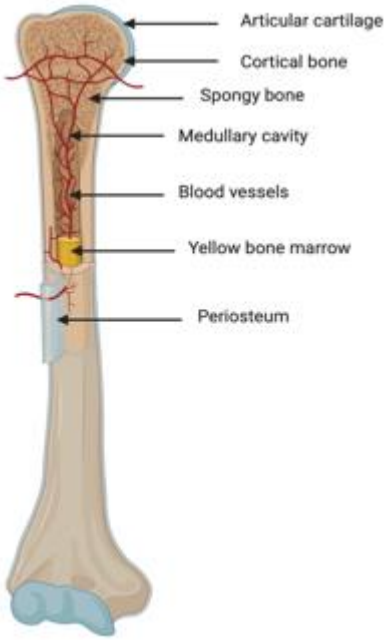

Figure 1.6. Anatomy of a bone.
The femur with its soft tissue, including articular cartilage, blood vessels, bone marrow and periosteum. Image performed by BioRender.com

1.2.1.1 Spine

The spinal column consists of bones, ligaments and intervertebral discs, functionally coordinated to allow upright movement and protect the spinal cord. The bony spinal column comprises generally of 33 vertebral bodies that are stacked from the skull to the coccyx, one on top of the other [58]. The spine consists of 33 vertebral bodies that create 5 different sections with their own distinctive features in the normal arrangement; 7 cervical vertebral bodies, 12 thoracic vertebral bodies, 5 lumbar

vertebral bodies, 5 sacral vertebral bodies which are fused together to form the sacrum and 4 vestigial vertebral bodies which are fused to form the coccyx, see Figure 1.7.

The spine consists of segments consisting of a vertebral body and IVD that adjacent surfaces of the vertebra. These discs are at risk of inflammatory and degenerative diseases. Ligaments and muscles act as a connective tissue between spinal segments, allowing for flexion, tilt, extension, and rotation.

Each IVD forms a fibrocartilaginous joint which consists normally in young and healthy IVD of three components: the annulus fibrosus, nucleus pulposus and the cartilaginous endplate [59], see Figure 1.8. Annulus fibrosus is the thick outer ring of fibrous cartilage that surrounds the nucleus pulposus. The annulus fibrosis is composed of 15–25 concentric layers that composed of type I and type II collagen. The nucleus pulposus is soft and gel-like structure within the disc functioning as a buffer between the end plates and transfers hydrostatic pressure. The cartilaginous endplate is a thin horizontal layer usually less than 1mm thick of hyaline cartilage that attaches to the border of the vertebral body.

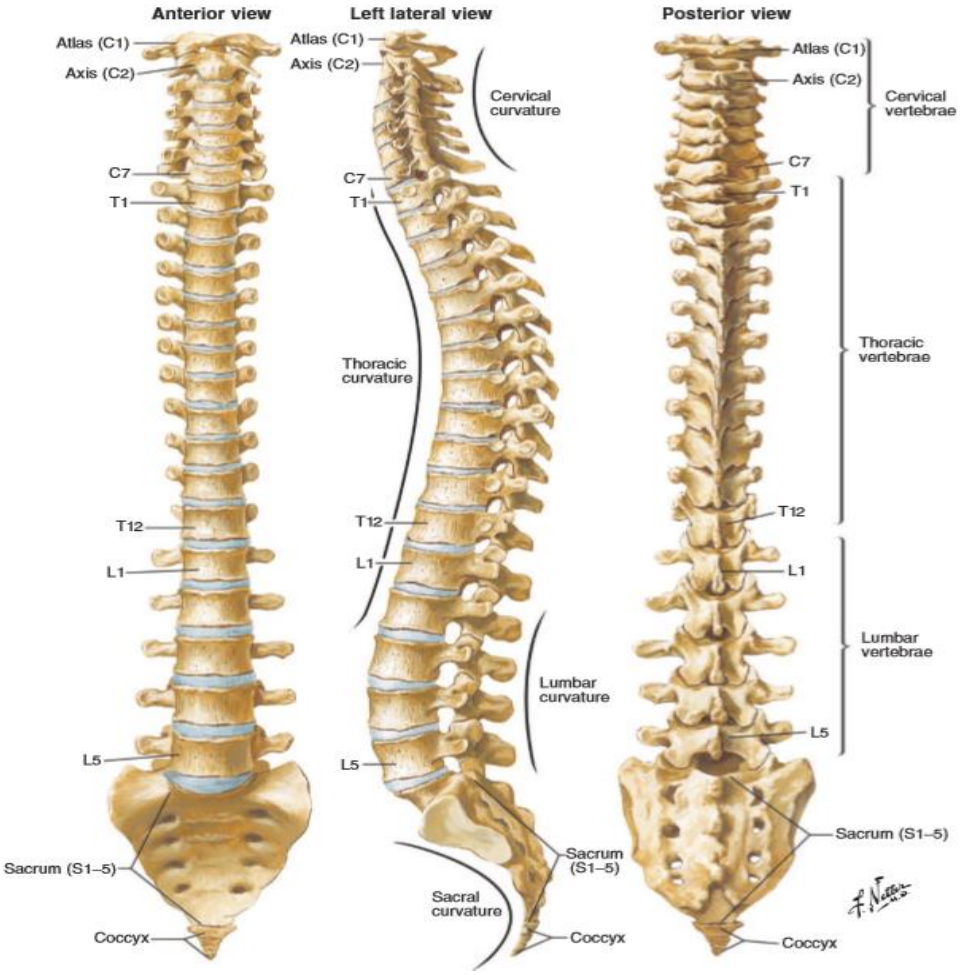

Figure 1.7. Anatomy of vertebral column (figure from [60]).

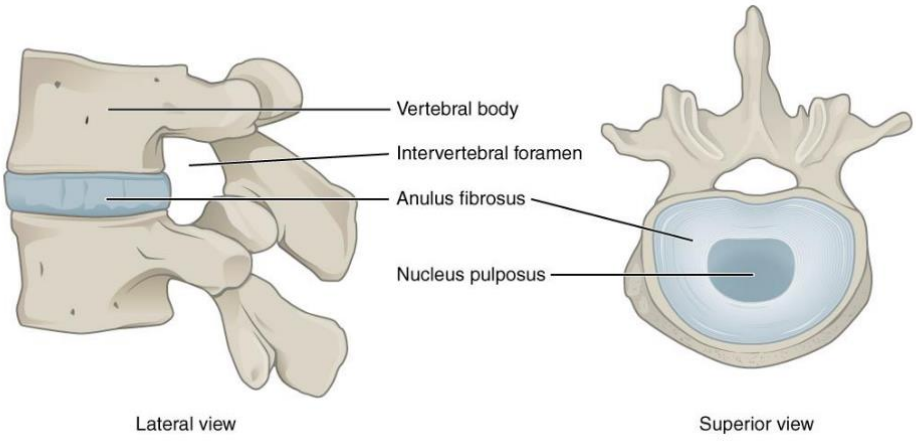

Figure 1.8. Anatomy of the intervertebral disc. Figure from [61].

1.3 Cardiovascular system

1.3.1 Anatomy and physiology

The cardiovascular system composes of principle components: the heart, blood, blood vessels, and the lymphatic system [62,63]. The heart is a cone-shaped muscular organ located wihtin the central region of the thoracic cavity, called the mediastinum. The cardiac muscle is supplied by different branches of coronary arteries. The blood vessels transfer blood throughout the body tissues via bulk flow. The main components of the vascular system are arteries, arterioles, capillaries, venules, and veins. The largest artery in the body is the aorta, divided into ascending aorta, descending aorta, and abdominal aorta. All the arteries branch from the aorta and divide into smaller vessels. The four main coronary artery branches are the left coronary artery or left main stem (LCA), left anterior descending artery (LAD), left circumflex artery (CA), and right coronary artery (RCA). There are two major veins: the inferior vena cava, which is located below the level of the heart and the superior vena cava, located above the heart.

The functional anatomy of the coronary arteries changes throughout the lifespan of humans. With ageing coronary arteries become thicker due to calcium deposition [62]. These changes typically appear in the elderly, causing detrimental cardiac damage, myocardial ischemia, and in some cases, it can cause death.

1.4 Medical imaging

Medical imaging is a process of performing a visual representation of different body parts for clinical evaluation. Structural and functional information can be established by different medical imaging techniques identifying anatomical and physiological abnormalities. Moreover, medical imaging may help address important concerns that occur during the drug development phase.

Diagnostic imaging includes multiple non-invasive imaging modalities, each with its own set of technology, equipment and protocol. Diagnostic imaging techniques include X-ray, computed tomography (CT), bone mineral density (DEXA), magnetic

resonance imaging (MRI), echocardiogram, ultrasound (US), and nuclear medicine imaging techniques such as single-photon emission computed tomography (SPECT) and positron emission tomography (PET).

Both physicians and AKU researchers are aware of the increased importance of different imaging techniques for detection, evaluation, and follow up of disease stages. With numerous ongoing research efforts involving large-scale imaging investigations, more advanced imaging would inevitably find its place in the clinical management of AKU patients. For the diagnosis of ochronosis, radiographic assessment and imaging evaluation play a critical role to identify and assess pathological changes caused by ochronosis. Therefore, imaging modalities would be a crucial part for enhancing and growing our awareness of the natural history of AKU.

1.4.1 Radiographic evaluation of ochronotic arthropathy using different imaging modalities

The radiographic features of ochronotic arthrosis should be considered carefully to avoid miss diagnosis with other arthrosis disorders such as OA. In the past, the relatively uncommon and unrecognised skeletal manifestations of ochronotic arthropathy have perhaps contributed to the scarcity of investigations performed in this disease area as it is a rare genetic disease [12,64,65]. Early diagnosis of ochronotic arthritis has a long-term impact on the patient as it allows early detection of structural bone and joint damage. The radiographic features of bone involvement in ochronotic cases were previously reported in many AKU cases [22,66–70]. Most of the AKU radiographic features were particularly similar to those which can be noted in other musculoskeletal disorders [15,71–75].

What follows is a brief description of medical imaging techniques that are mainly used to diagnose bone and bone-related disorders.

1.4.1.1 Conventional X-ray radiography

X-ray is the simplest, least expensive imaging modality, which is usually used as a reference technique in various bone and bone-related disorders. X-ray imaging has

limited sensitivity and specificity as it creates a two-dimensional (2D) anatomical image, which may fail to depict abnormalities on individual lesions where specific views including obliques are required. X-ray also has low sensitivity to assess the changes in bone loss at a follow-up imaging. It has been estimated that plain radiography cannot identify bone loss until it exceeded 25-30% of its density, which means severe damage has occured by that time [76].

While X-ray images may not show as much detail as other imaging modalities, it is usually performed at the first of nearly all musculoskeletal disorders to decide the next steps. Spinal X-ray is not recommended to be repeated frequently every year as it may not provide additional information, however, it can be used for monitoring structural damage over a long-term period [72]. The characteristic X-ray imagery associated with AKU can show significant calcification of the IVD, and joint narrowing [72].

1.4.1.2 Ultrasound (US)

Although evaluation of bone involvement and periphery of joints abnormalities in general by US is restricted, nowadays, US examination offers acceptable results in the assessment of ochronotic arthropathy [15,74]. US can permit an evaluation of bone and joint turnover for AKU patients as it can offer an image of the structural lesions and inflammatory changes during the early and late stages of ochronotic arthropathy [15]. It is important to point out that the quality of US images depends on the frequency of sound waves and the type of transducer. It deserves to be mentioned that evaluating the level of joint inflammation, abnormal bone and cartilage structure mainly depends on the experience level of the sonographers.

1.4.1.3 Dual Energy X-ray Absorptiometry (DEXA)

Clinically, bone densitometry or dual energy X-ray absorptiometry (DEXA) is a gold standard method to diagnose osteoporosis by measuring bone mineral density (BMD) from two different intensity X-ray beams [77]. The basic principle of DEXA is to calculate the absorption of the X-ray of high and low-energy transfer within the body, assuming that the body consists of two compartments: bone tissue and soft tissue. The attenuation ratio of the two X-ray beams is analysed in two anatomical sites; the first

site containing bone, the other site containing soft tissue only, then the soft tissue attenuation ratio will be subtracted away, leaving only bone attenuation ratio.

DEXA is usually measured in the anteroposterior view of the lumbar spine (L2-L4) and proximal femur. Although BMD is measured in g/cm^2, the DEXA report is more commonly referred to as T-score and Z-score. T-score is density value expressed as the standard deviation below or above the mean BMD of a healthy young reference population at the site of the same gender and the ethnicity of the patient. Z-score is the difference between the measured bone density and someone from an aged-matched cohort. Diagnoses based on bone density value measurements have been guided by a World Health Organisation (WHO) report. The WHO report recommended using a T-score equal or below -2.5 as diagnostic of osteoporosis, between -2.5 and -1 as osteopenia and equal or above -1 as normal. Table 1.2 summarises the WHO classification criteria for T-scores.

Table 1.2 WHO classification criteria for T-score from DEXA scan.

Level	T-score
Normal	> -1
Osteopenia	Between - 1 and - 2.5
Osteoporosis	< −2.5

In AKU, the ochronotic pigment in cartilage may contribute to bone mineral density loss. An imbalance between bone formation and bone resorption caused by ochronosis may increase bone fracture risk in patients with AKU. Therefore, evaluating bone density for AKU patients could be an essential diagnostic tool to assess patients at risk and who may need clinical intervention. Numerous studies found a strong inverse association between BMD measured from DEXA and joint damage, suggesting that the pathophysiological processes of osteoporosis seem to be expected for the local bone loss of individual joints [77].

Although DEXA has been successfully employed in many musculoskeletal disorders, it is not the best method fo choice for AKU patients. Yu *et al.* [78] evaluated bone density from DEXA scans in patients with a spinal degeneration condition, and he found that those patients had significant higher spinal BMD values than those without spinal

degeneration. This means that severe IVD calcification significantly over-estimates the value of lumbar bone density in DEXA scans. In ochronotic patients, extensive disc degeneration could influence the spinal DEXA measurements; therefore, the results may not reflect a true representation of bone density [79]. On the other hand, it has been reported previously that hip BMD is usually lower than spinal BMD in osteoarthritic patients, suggest that spinal BMD is not considered a significant marker for spinal osteoporosis [48,79]. Therefore, lumbar bone density measured from DEXA results in AKU patients must be interpreted with caution. A previous study reported low bone mineral density in DEXA scan at the hip region in ochronotic patients that had normal spine density [75].

1.4.1.4 Computed Tomography (CT)

Computed tomography (CT) is a medical imaging procedure using a rotating gentry with X-ray tubes performing cross-sectional images of a specific body part. CT is superior when compared with conventional osseous radiography as it offers a high-resolution tomographic analysis of osseous changes and soft tissue structure. CT images translate the X-ray attenuation of various body structures, demonstrating precisely bone details, hence making it the preferred choice to evaluate bone anatomical structures [80].

In the 1970s, bone mineral density analysis was proposed using the quantitative CT technique [81]. However, drawbacks such as high cost, the need for a large dose of ionizing radiation, comparatively long scanning duration, and the advent of DEXA contributed to the restricted use of CT in the areas of musculoskeletal research, not withstanding its initial introduction and precision. Diagnostic imaging technology has recently advanced steadily, and CT is growing considerably in both quality and quantity in clinical areas. The benefit of CT over DEXA gained interest for the second time with the development of diagnostic imaging technology.

It has been described previously in many studies when CT scans were obtained for routine clinical measurements in preoperative examinations; the images would be considered a valuable source of information and can be used to assess osteoporosis for high-risk patients [82]. This evidence suggests the possibilities of estimating bone

mineral density and evaluating the risk of fractures for AKU patients using CT images from a PET/CT scan without any additional cost or radiation exposure. The information delivered by quantitative measurements can notify the physician to initiate future investigations.

1.4.1.4.1 Semiquantitative CT assessment

With technological advances in CT systems and imaging software, CT usage was remarkably increased in bone quantitative fields, specifically for those patients who have not undergone DEXA scanning. In 2011, Hounsfield unit (HU) from the CT scan was introduced by Schreiber *et al*. [83] to predict regional spinal BMD, with several concurrent studies examining its effectiveness in predicting fracture risk.

HU is a quantitative value obtained from the linear attenuation coefficient describing radiodensity of tissues, named after Sir Godfrey Hounsfield [83]. HU are generated from the total linear X-ray absorption coefficient, which is calibrated to the water X-ray attenuation coefficient. Based on the Hounsfield scale, water is assigned a value of 0 HU, air a value of -1000 HU, bone a value of +300 to +3000 [83], soft tissue a value between +20 and +100, and fat value of around -50 HU. Metal devices have demonstrated high HU values (≥3000), which will cause marked attenuation of the radiation beam [83]. Table 1.3 shows the HU values for different body components and common joint replacement implant component. Modern imaging software allows identifying HU value for any ROI from CT scans. HU values are calculated based on the equation below:

$$\text{HU} = \frac{\mu - \mu\omega}{\mu\omega} \text{ X } 1000 \quad [83,84]$$

μ is the X-ray linear attenuation coefficient of the selected ROI

μω is linear X-ray attenuation of distilled water at room pressure and temperature

Table 1.3 Hounsfield value of body components and medical implant component measured from CT scan.

Substance	HU value
Air	-1000
Fat	Around -50 to -120
Water	0
Bone	+300 to +3000
Metal	≥ 3000
Soft tissue	Between +20 to +100

The relationship between densitometry and diagnostic CT scan semiquantitative values has been widely investigated [81,83–85]. Recently, a number of studies have shown a significant correlation between BMD and T-score measured from DEXA scan and HU values measured from the diagnostic CT scan. These studies described the role of diagnosis of osteoporosis by measuring lumbar spine bone density from diagnostic CT scans. Previous investigations have proved a linear correlation between HU values and bone density values (BMD and T-score) [81,83–86].

A considerable amount of literature has been published, estimating bone density from diagnostic CT imaging. According to the published data in this area, the average HU value that indicates a strong risk of osteoporosis was below 60. Table 1.4 summarises HU values measured from CT scans for normal, osteopenic and osteoporotic patients stratified according to WHO criteria from literature. Lee *et al*. [81] reported that patients with normal bone density at lumbar vertebra levels had a mean HU value of 120.8, osteopenic patients had a mean HU value of 78.8, and osteoporotic patients had a mean HU value of 54.7. In another study, Batawil *et al*. [85] pointed out that HU value of 100 and below demonstrated 100% sensitivity for osteoporosis in a study analysing 252 patients. Another significant study in 1867 patients showed a strong correlation of the range HU values of 110-160 at lumbar vertebrae and osteoporosis [87]. Other researchers question whether HU measurements from different body parts correlate with BMD from the DEXA scan. Pervaiz *et al*. [88] investigated the correlation between HU measurements in the proximal humerus and hip DEXA measurements. They identified a significant correlation between humerus HU values measured from CT images and hip BMD and T-score measured from DEXA scans ($P < 0.001$).

Considering all of these findings, it seems that HU measurements could provide such a promising tool to assess regional bone density. However, it is premature to say that HU values will operate as a replacement indicator for bone mineral density. As noted in Table 1.4 there is some overlap in the HU values between the classified groups. Unlike the WHO criteria for T-score from DEXA scan, the standard classification for BMD from HU quantification has not yet been established. However, such values can be used as comparison points for evaluating acceptable HU ranges which can identify patients with bone density disorders. Future studies on the current topic are therefore recommended.

Table 1.4. The mean HU values measured from diagnostic CT scan for normal, osteopenic, and osteoporotic patients from the literature.

Data display as mean value ± SD or as range values. No. of patients = number of patients.

Reference	No. of patients	Mean age	Measured ROI	HU value		
				Normal	Osteopenia	Osteoporosis
Schreiber *et al*. 2011[83]	25 adult	71.3	Lumbar spine	133.0 ± 37.6	100.8 ± 24.5	78.5 ± 32.4
Lee *et al.* 2013 [81]	128 female	66.4	Lumbar spine	120.8 ± 41.8	78.8 ± 23.0	54.7 ± 25.2
Batawil and Sabiq *et al*. 2016 [85]	114 female	58 ± 10	Lumbar spine	197.8 ± 49.7	159.1 ± 46.7	118.6 ± 52.6
Bruce and Binkley *et al*. 2013 [87]	1867 adult	59.2 ± 12.5	Lumbar spine	>175	130 - 175	< 130
Choi, Kim, and Lim *et al*. 2016 [89]	110 adult	59.5	Lumbar spine	167.9 ± 47.2	109.7 ± 28.9	80.4 ± 38.7
Johnson *et al*. 2016.[84]	45 female		Lumbar spine	392.94 ± 73.0	346 ± 67.53	239.43 ± 88.71
Pervaiz *et al*. 2013 [88]	230 adult	68.2	Proximal humerus	121.3 ± 27.9	103.4 ± 26.1	92.1 ± 29.1

1.4.1.5 Magnetic Resonance Imaging (MRI)

More recently, there has been increased usage of MRI in a variety of musculoskeletal disorders. MRI is regarded as a pivotal modality for accurate assessment of arthropathy as it is sensitive, safe and painless scan which is mostly used for symptomatic patients with joint pain. A powerful magnetic field and radio waves are used in an MRI scanner to obtain detailed images of the body part. Although the MR scan is non-invasive as there is no ionising radiation, it is an expensive procedure with some contraindications, which should be carefully considered. Practically, it is difficult for patients with severe

pain or those with neurodegenerative disorders to fit in the scanner and remain stable for a long time without moving [76].

There are a number of a published AKU case reports describing the imaging features which have been noted in MR images [66–68]. These findings introduce the advantage of MRI for detecting structural alteration and functional contrasts in soft tissue at an early stage of ochronotic arthritis, which may be difficult with other imaging techniques

1.4.1.5.1 MRI disc scoring system

Quantifying disc degeneration which appears in MRI is can be used as an sensitive assessment method. An easy, reliable and comprehensive MRI scoring system with sufficient reproducibility is needed to quantify disc degeneration in order to reflect the disc damage and disease progression. In the literature, a number of MRI assessment methods based on morphological change have been proposed to evaluate lumbar IVD degeneration. The most common MRI scoring system used to quantify degenerative disc disease is the Pfirrmann grading system which was introduced in 2001 by Pfirrmann *et al.* [90].

Pfirrmann disc degeneration system is one of the morphological disc degeneration scoring systems using T2-weighted MRI sequences [90]. The system mainly depends on the signal intensity from sagittal MRI sections of disc degeneration unit, IVD structure, the distinction between nucleus and anulus, and IVD height [90]. Initially, the Pfirrmann grading system was introduced with five scales. Although the Pfirrmann scoring system using five levels shows good discrimination and responsiveness, it may be non-discriminatory in elderly patients [91]. The main difference between Pfirrmann scales is the brightness and distinction of nucleus pulposus (NP) to disc membrane [92]. Indeed, using a five graded Pfirrmann disc degeneration scale can easily vary between different investigators or observers. Griffith *et al*. noted difficulties when scoring lumbar spine disc degeneration, specifically in the aged population [89]. Most of the discs were scored having third or fourth grade, and ambiguity was encountered. Griffith splits some scores, adding a privilege on using the Pfirrmann score system to increase its discriminatory power. The Pfirrmann grading system has been modified from five scores to eight scores by Griffith following the same principle criteria of the previous.

method. The third Pfirrmann grade was expanded to two scores, and the fourth Pfirrmann grade was expanded to three scores, adding three additional scores in total. The first, second and the fifth Pfirrmann grades were not changed. The modified Pfirrmann method expanded the visual representation of the disc and minimised ambiguity. In general, both five and eight Pfirrmann classifications of lumbar disc degeneration have reported a substantial to excellent intra- and inter-observer agreement rate in the literature [93–95]. The overall findings of the previous studies suggest that MRI can be used to detect and monitor degenerative alterations in the discovertebral joint, which are associated with ochronotic pigment in AKU patients.

1.4.1.6 Radionuclide bone imaging

Nuclear medicine is an alternative medical imaging field which can provide a regional assessment of bone formation, avoiding some drawbacks of other imaging techniques. Radionuclide bone scan is considered the preferred clinical method to identify bone metastasis, which often offers representations of the whole body with a single session. The widespread availability of nuclear medicine and molecular imaging scanners enhances the role of this imaging technique for diagnosing various musculoskeletal disorders [96]. Radionuclide bone scan also called scintigraphy. Nowadays, scintigraphy is one of the common imaging technique evaluating the pathophysiology of metabolic bone conditions, including infection, inflammation, trauma, benign and malignant tumor [97–99]. Scintigraphy is the most efficient imaging modalities assessing early changes in bone when correlated with other related imaging techniques such as X-rays, CT and MRI. Radionuclide bone imaging is a sensitive bone technique however it is non-specific. The abnormal uptake can be shown in the skeleton for several reasons such as fracture, infection, inflammation or even tumor depending on the osteoblastic activity and local blood flow.

The whole-body skeletal assessment in scintigraphy offers unique information reflecting active bone turnover, which can be assessed by qualitative and quantitative imaging methods. Besides whole skeleton evaluation, these imagery methods are flexible. It can analyse and quantify any selected region of interest within the whole body [100]. Although practically, there is no specific radiopharmaceutical to image the

articular cartilage, in the literature, several bone radiotracers have been used in advanced joint disorders [101].

1.4.1.6.1 Bone radiopharmaceuticals

Bone-seeking radiopharmaceuticals are primarily analogs similar to the basic mineral components of bone like hydroxyapatite, hydroxyl groups, or phosphate. In the 1960s, sodium fluoride labelled with fluorine-18, also known as ^{18}F-NaF was first proposed by Blau *et al*. as a radioisotope agent for bone imaging and was later approved for clinical use by the US FDA in 1972 [97]. Despite early awareness of the superior diagnostic efficiency of ^{18}F-NaF, the tracer was not used extensively because of its limited availability, comparatively high cost, and the technical issues relating to high-energy photons using the equipment which was available at that time. The introduction of the radioisotope technetium-99m (^{99m}Tc) contributed to the search for an alternative imaging marker which can be labelled with ^{99m}Tc presenting better physical characteristics than ^{18}F-NaF using conventional gamma cameras [55]. In the mid-1970s, ^{99m}Tc-labelled diphosphonate compounds was introduced by McAfee and Subramanian. Since then it has been widely employed for imaging both benign and malignant bone disorders [55]. Besides the suitability for imaging by a gamma camera, the radiotracer was more available with low cost and was simpler to prepare in the nuclear medicine department. For those reasons, the FDA withdrew its approval of using ^{18}F-NaF as a bone imaging radiotracer in 1975.

In the mid-1990s, gamma-cameras with thick crystals and high-energy collimators were implemented. In the late 90s, bone scan with ^{18}F-NaF came into its own with improved performance in PET scanners renewing the application of ^{18}F-NaF specifically for oncological imaging. The increasing number of PET scanners foster high-resolution skeletal imaging to be applied widely in various skeletal conditions [102]. In 2000, the FDA re-approved the use of ^{18}F-NaF as a bone imaging radiotracer. Since then, ^{18}F-NaF became the most commonly preferred bone imaging agent in nuclear medicine once again. A few more tracers are candidates for skeletal imaging however short half-life radiotracers are always the most recommended bone radiotracer in the clinical field to reduce radiation to the patients and clinical staff. In general, all bone-specific imaging tracers share a similar uptake mechanism.

Over the last decade, numerous radionuclide bone scan applications have been apparent in skeletal disorders using gamma photon tracers or positron emission tracers. Bone scintigraphy using both ^{18}F-NaF and ^{99m}Tc-Methylene diphosphonate (^{99m}Tc-MDP) has been found to be a useful technique for assessing disease activity in patients with OA [103]. Although both imaging techniques are sensitive, many technological advantages motivate the usage of ^{18}F-NaF PET scan as a superior imaging tool over ^{99m}Tc-MDP SPECT scan. The comparison between ^{18}F-NaF and ^{99m}Tc-MDP has been widely investigated. It has conclusively been shown that positron emission bone radiotracer has a superior ability to diagnose bone disorders compared to gamma bone radiotracer. In 2015, Beheshti *et al*. [104] compared the results of the conventional ^{99m}Tc-MDP bone scan and ^{18}F-NaF PET scan in detecting bone metastases in patients with prostate cancer. Beheshti reported that ^{18}F-NaF PET is more superior in terms of specificity and sensitivity compared to ^{99m}Tc-MDP in detecting the presence of malignant bone diseases. Lee *et al*. [103] compared the clinical utility of ^{18}F-NaF PET/CT with that of conventional ^{99m}Tc-MDP scintigraphy for 24 patients with temporomandibular disorder. In that study, ^{18}F-NaF PET/CT was reported having higher sensitivity and accuracy than ^{99m}Tc MDP scintigraphy to diagnose OA. Table 1.5 summarises and compares the characteristics of ^{99m}Tc-labelled diphosphonate compounds and ^{18}F-NaF PET bone scintigraphy. The following section reviews the pharmacokinetics of bone radiotracer and describes the main characteristics of ^{99m}Tc-MDP and ^{18}F-NaF.

Table 1.5. Comparison of ^{99m}Tc-labelled diphosphonate compounds and ^{18}F-NaF PET bone scan.

(Modified from [55,105])

Characteristic	**^{99m}Tc– MDP and ^{99m}Tc–HMDP**	**^{18}F-NaF PET**
Radiotracer physical half-life	6 hr	110 min
Protein binding in the blood	Yes	No
Types of emissions	Gamma	Positron, annihilation gamma
Energies of emissions	140 keV	511 keV
Imaging modality	Gamma cameras (planner/ SPECT)	PET scanner
The spatial resolution of the scanner (mm)	4–15	3–6
Organ receiving the highest dose	Bone	Bladder
Mechanism of localisation	Binds to bone matrix Glomerular	Binds to bone matrix Glomerular
Usual administered activity	600 MBq (planar) 800 MBq (SPECT) (25 mci)	185-370 MBq (5-10 mci)
Effective dose (mSv/MBq)	0.0057	0.024
Patient dose (mSv)	4.2 – 6.3	4.4 – 8.9
Imaging time after injection	3 – 6 hr	30 – 60 min
Advantages	• Inexpensive • Easily prepared on-site from generator • Well studied	• High spatial resolution of PET • Simple to prepare from cyclotron • No binding to plasma proteins.
Limitations	• Poorer spatial resolution of SPECT • Not a single chemical entity • Protein binding delays clearance • Instability of complex	• Expensive • Requires cyclotron production

1.4.1.6.1.1 Mechanism of radiopharmaceutical uptake

The pharmacokinetics of bone searching radiotracers rely fundamentally on the rate of bone absorption and the elimination from the body circulation by kidney excretion. ^{99m}Tc- labelled diphosphonates and ^{18}F-NaF are imaging radiomarkers for bone turnover and bone perfusion. The principal mechanism for the uptake of these radiotracers is absorption into or on the crystalline hydroxyapatite bone structure. After intravenous administration, the radiotracer distributes from the vascular to extravascular space, taking around 2 to 4 minutes [106]. The delivery of the tracer to the bone lesion mainly depends on the blood flow, regional osteoblastic activity, exposed bone surface area, and extraction rate of the tracer [97,107]. Therefore, the changes in radiotracer kinetics relate mainly to bone vascularity, osteoblastic activity, and kidney function [107]. In musculoskeletal disorders, it has been reported that there is an abnormal increase in vascularity and bone turnover in the affected site. [106].

Radionuclide bone imaging can be acquired at three imaging phases; first imaging phase is radiotracer angiography, immediately with the bolus injection; second phase is soft tissue phase or blood pool phase, and the third imaging phase is a delay phase or bone imaging phase [55]. Table 1.6 illustrates the movement of bone radiotracer during the three imaging phases.

Table 1.6. The movement of bone tracer during the three imaging phases.

Phase 1	Radionuclide angiography	Tracer intravascular administration
Phase 2	Soft tissue or blood pool phase imaging	Tracer distribute in the extravascular extracellular spaces
Phase 3	Delayed or metabolic imaging	Tracer accumulates in bone tissue

In scintigraphy, bone activity must be high, while soft tissue activity must be low at the delay imaging phase, reflecting the amount of circulating radiotracers in the blood pool. In adults, the distribution of bone tracers throughout the skeleton is generally uniform [55]. Bone lesions with increased or decreased tracer uptake reflects abnormal bone metabolism disorders. Although bone radiopharmaceuticals are mainly taken up

by the skeleton, extraskeleton tissue absorption can also be observed in scintigraphy [55]. These observations may be coincidental, because in some cases, it may indicate clues to other underlying diagnoses. Therefore, the accurate interpretation of scintigraphy relies on understanding the pathophysiology of the underlying condition and tracer absorption mechanisms in both bone and extraskeleton tissue. Some chronic diseases might alter regional bone formation or affect renal extraction causing the abnormal distribution of the bone radiotracer throughout the body. Furthermore, technical factors, such as formulation and quality of the radiopharmaceutical might also alter the tracer biodistribution causing abnormal accumulation of the tracer in extraskeleton tissues.

1.4.1.6.1.2 ^{99m}Tc- labelled diphosphonate

Both ^{99m}Tc-MDP (^{99m}Tc-Methylene diphosphonate) and ^{99m}Tc-HMDP (^{99m}Tc-hydroxymethylene diphosphonate) decay with a half-life of 6 hours, emitting 140 keV gamma-photons, generated from a ^{99}Mo/^{99m}Tc generator at the nuclear medicine department. ^{99m}Tc-MDP and ^{99m}Tc-HMDP have a similar molecular structure to etidronate, one of the first bisphosphonates used to treat osteoporosis [100]. In applications of nuclear medicine, substances with a P-C-P bond are typically referred to as diphosphonates. The simplest diphosphonates structures are preferred for scintigraphy due to their fast plasma clearance and a high urinary excretion, making a significant contribution to the better contrast between the bone and the soft tissue. Both ^{99m}Tc-MDP and ^{99m}Tc-HMDP undergo protein binding, rising over time from approximately 25% immediately after injection to around 50% at 4 hours after injection [97]. Protein binding complicates the bone scans, and only the non-protein-bound component or free ^{99m}Tc-MDP in plasma will be taken up by bone [97,100]. The kidneys excrete an average of 35% of the dose injected by glomerular filtration after three hours in a normally hydrated patient. Around 30 to 40% of the injected dose is accumulated within the bones, 10 to 15% in the soft tissues, and around 5% in the blood [106]. Usually, bone imaging with ^{99m}Tc-labeled diphosphonates is requested at three phases during the bone scans; immediately with the bolus injection, within 5 minutes after injection and 2-4 hours after the injection.

1.4.1.6.1.3 Sodium fluoride labelled with ^{18}F (^{18}F-NaF)

^{18}F-NaF is a positron emission radionuclide which decays with a physical half-life of 110-minutes, emitting a gamma photon at high energy of 511 keV. ^{18}F-NaF is produced on-site from medical cyclotron by bombarding Oxygen-18 enriched water (^{18}O-H_2O) with high energy protons [55]. Following IV administration, ^{18}F-NaF is rapidly cleared from the plasma. It has a high bone affinity, resulting in better tissue-to-background ratios leading to a high imaging quality. A minimal protein-bound fraction of ^{18}F-NaF causes fast clearance from blood. When ^{18}F-NaF gets into the bones, the inhilitation of fluoride and hydroxide ions occurs. $^{18}F–$ ion exchanges for hydroxy1 groups (OH-) on the surface of the hydroxyapatite matrix of bone-forming fluoroapatite (see Figure 1.9):

$$Ca_5\,(PO_4)_3OH + F^- \rightarrow Ca_5\,(PO_4)_3F + OH^-$$

^{18}F-NaF is accumulated at high osteoblastic sites, where fluoride ions bind to the new bone formation. About 50% of the ^{18}F-NaF injected dose is absorbed into the bone [108], and around 30% of the tracer goes into the red blood cells. The ^{18}F-NaF in the red blood cells has no effect on bone absorption of radiotracer since it easily spreads transversely through the cell membrane [108]. One hour after ^{18}F-NaF is injected, just about 10% of the administered dose remains in the bloodstream. Any remaining traces are excreted from the body through the renal system about 6 hours after being injected. This characteristics ensure proper absorption of ^{18}F-NaF, allowing the images to be performed 45-60 minutes after injection.

Radiotracer excretion is primarily through the kidneys and the urinary tract. In instances of renal insufficiency, the kidneys, and the ureters are usually visible in PET/CT image [108]. The localization of urinary tract level depends on the urine functionality, the level of hydration, and the time interval between injection and imaging. Localisation close to the site of construction will increase in the presence of urinary outflow obstruction. Soft tissue uptake indicates the amount of ^{18}F-NaF present in the blood during imaging and under normal circumstances, which should be minimal. ^{18}F-NaF uptake by the skeleton is homogeneous for adults with generally equal distribution on the right and left sides for all individual [109].

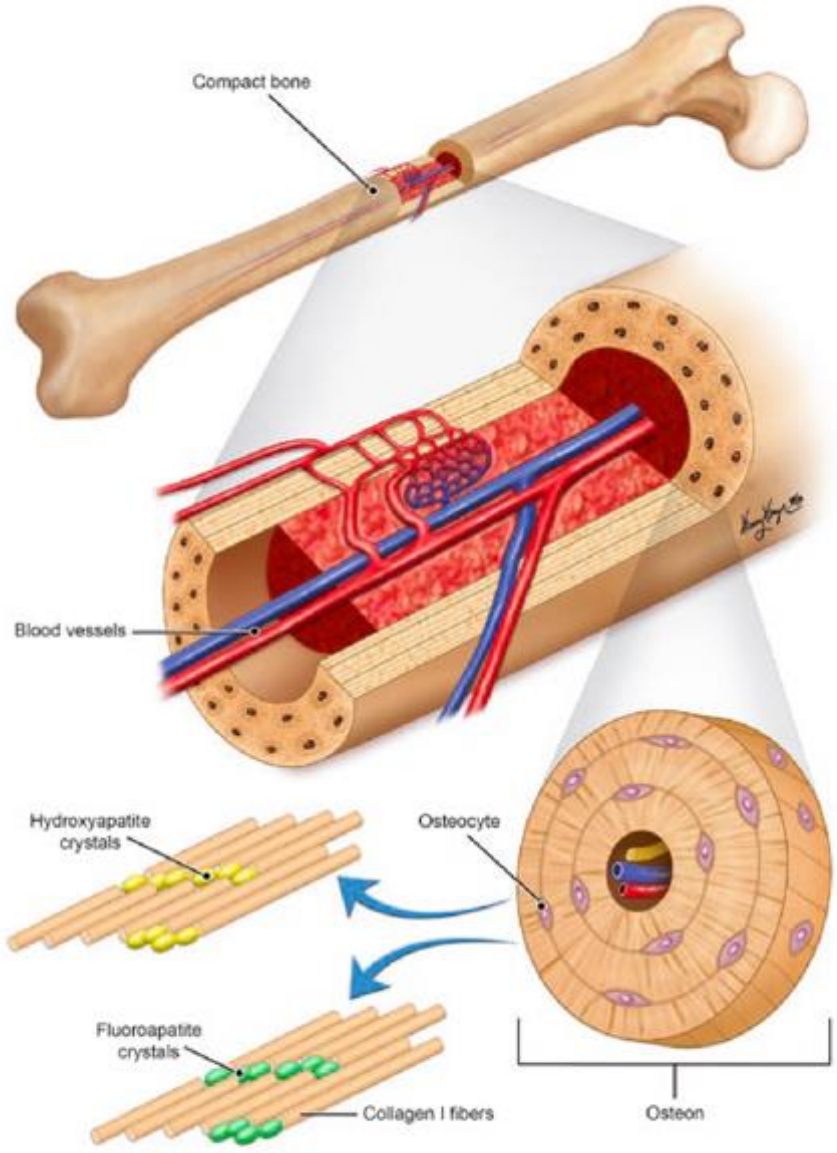

Figure 1.9. Incorporation of ^{18}F from NaF into the hydroxyapatite crystals of the mineral bone matrix to form the radioactive fluorapatite crystals.

(Figure illustration by Kelley Kage). (Figure from [110])

In 2010, the Society of Nuclear Medicine (SNM) proposed an international guideline for skeletal positron emission imaging with ^{18}F-NaF [109]. The paper summarised the most common clinical indications for ^{18}F-NaF PET scan, providing recommendations for patient preparation and precautions, the injection dose, imaging protocols and imaging acquisition, interpretation criteria, image processing, quality control, patient education concerns, infection control and radiation safety.

1.4.1.6.2 Imaging technology: instrumentation

Since the domain of nuclear medicine instrumentation is too broad to cover in this thesis, certain essential topics of instrumentation will be discussed in the following sections.

1.4.1.6.2.1 Gamma camera

The gamma camera imaging technique is designed to detect the decay of ^{99m}Tc atoms, which emit 140-keV gamma-rays and conversion electrons in low abundances during the radioactive decay process [111]. The gamma camera is built out of a large thin crystal, recording each gamma-ray arrival. In front of the crystal is a collimator made up of a dense lead block perforated by thousands of fine holes, which enables gamma-rays to pass precisely through the centre of the holes, forming an image of the distribution of the ^{99m}Tc atoms throughout the body [100]. Most modern gamma cameras have two heads, which allow the simultaneous acquisition of both anterior and posterior images. A two-dimension whole body image can be performed in a single scan taking 20-30 minutes. In some cases, confirming the presence of arthropathy may be a challenge with a 2D view as the planar image cannot precisely localise the site of an abnormality due to overlap and low resolution, specifically in joints [112]. By rotating the gamma camera around the ROI and taking a sequence of step-by-shoot images from multiple angles through a complete 360°, a three-dimensional (3D) image is created, a technique known as single-photon emission computed tomography (SPECT). Recently, SPECT has emerged as a useful imaging tool allowing higher accuracy localisation of suspicious lesions by separating the overlaying radiotracer activity into sequential tomographic planes. SPECT adds sensitivity and specificity to the findings

allowing a significantly higher reflection of early bone changes compared to 2D mages [112].

1.4.1.6.2.2 PET scanner

^{18}F atom decays into a neutron by emitting positrons which are particles similar to electrons but with a positive electric charge rather than a negative charge [100]. The positron constantly looses kinetic energy through interactions with the surrounding tissue atoms and deflects from its original path; usually it travels no more than 1mm through matter following emission from the nucleus. The positron finally combines with free electron and annihilates emitting two 511-keV photons which travel in opposite directions 180^o apart (see Figure 1.10).

A PET scanner consists of a large number of small crystal detectors which are organised as rings around the body. The fundamental measurement in the PET system is based on recording two photons simultaneously which emit from positron annihilation by two opposing detectors. When positron annihilate, the two 511-keV gamma rays are detected on the opposite sides of the ring detectors, which indicate that the ^{18}F atom decayed in the line between these two detectors [100]. This line is referred to as line of response (LOR). A detailed image of ROI can be built up after detecting millions of pairs of coincident gamma rays, which infer the distribution of ^{18}F atoms in the body of the patient. Most of the new PET systems are made of more than 12,000 detectors which have the ability to generate a 3D distribution image of ^{18}F atoms decaying within 15-20 cm-wide sections of the body [100,111]. By using a step-by-shoot technique, it is possible to produce an entire body image in about 40 minutes by recording the ^{18}F distribution in a sequence of bed positions [100].

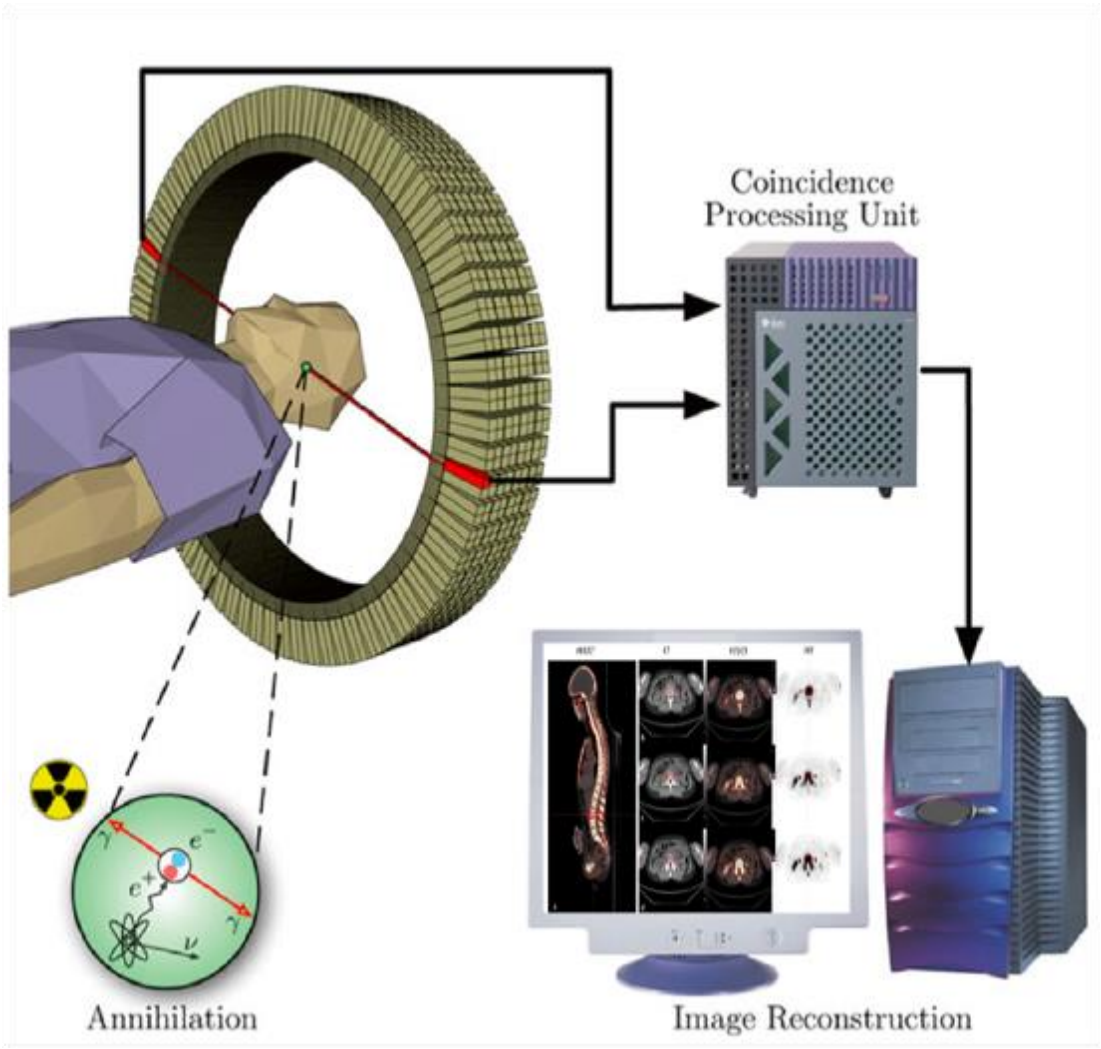

Figure 1.10. Basic principles of ^{18}F-NaF-PET/CT.

The figure shows the processing principles of a positron emission tomography (PET). The image illustrates how a positron (e +) is emitted from the nucleus of the radioisotope (^{18}F-) and attaches with an electron (e –), which results in the annihilation event that transforms their mass into two 511 keV gamma photons emitted in diametrically opposite directions. These photons are registered by the scanner's detector (the green-coloured ring). After the registration, the data is forwarded to a processing unit which determines if the two registered events are coincidence events (occurring at the same time) or not. All coincidences are forwarded to the image processing unit where the final image is produced via mathematical image reconstruction procedures. (This figure is adapted from the image released from [113].).

1.4.1.6.2.3 Hybrid scanner

Although a radionuclide bone scan is a sensitive imaging technique in detecting metabolic bone disorders, it delivers limited details on bone morphological information. Uptake of ^{18}F-NaF is a marker of specific diagnosis when the pattern of uptake is detected while the level of tracer uptake does not distinguish between benign and malignant bone lesions [114]. For this reason, the relationship between anatomical imaging and functional imaging may be critical to drawing a line in the middle of malignant and benign lesions.

Dual imaging modality, also known as hybrid imaging modality, provides several benefits for the clinical decision by combining functional and structural information in single scanning session [55]. Hybrid images can offer a precise localisation and size of lesion [115]. Previous investigations in this field have demonstrated the benefits of hybrid imaging for a wide range of clinical applications [114].

Over that last decade, PET scanners have been combined with anatomical imaging modalities such as CT or MRI in a single imaging system. In the same line, considerable attention has been devoted to increase the diagnostic accuracy of SPECT by combining a gamma camera with an anatomical scanner [116]. Hybrid imaging modalities which are available nowadays include SPECT/CT, SPECT/MR, PET/CT and PET/MR scans. These advance scanners offer satisfactory delineation of bone and soft tissues throughout the whole-body, providing well-detailed disease assessment. Although high ^{18}F-NaF uptake in subchondral bone does not always correspond to abnormal observations on MRI or CT images and vice versa, the abnormalities that can be observed separately in single imaging performance would notify the clinician to initiate further investigation [117].

It is hoped that hybrid imaging will provide useful information for AKU patients by evaluating structural and functional information in a single scanning session. Understanding the link between anatomical or molecular information will improve the diagnostic accuracy of AKU features and contribute to deeper understanding of this disease.

1.4.1.6.3 Qualitative and quantitative radionuclide assessment methods

Quantitative and semi-quantitative methods are significant, and an important aspect to consider during disease diagnoses, assessing disease progress, and evaluating treatment response. In the clinical field, there are two types of quantitative methods: imaging and non-imaging methods. Both techniques can provide useful information to detect early abnormal bone formation and assess accurate therapeutic response. Nowadays, there are a number of quantitative and semiquantitative imaging methods to diagnose, predict bone and joint abnormalities, and evaluate treatment response. Most of those quantitative methods are sensitive with good reliability; however, the best quantitative method has not been confirmed yet and will certainly change in the future. This will facilitate the determination of which technique is the most efficient for addressing regional bone turnover and joints degeneration for some rare disorders such as AKU.

Even though bone biopsy is regarded as the gold standard for quantifying bone turnover, it is restricted to one location at the iliac crest, making it reasonably complicated, invasive and expensive to execute, and may fail under considerable measurement mistakes [118]. Practically, one of the widely used methods for measuring bone turnover is biochemical bone markers or bone turnover markers (BTM). BTMs can estimate bone turnover from urine and serum, offering a practical and convenient alternative tool [119,120]. Different biochemical markers of bone resorption and bone formation have been studied, showing a significant association between the early change in BTM and predicting bone density response in clinical trials of osteoporosis treatment [119,120]. Although BTMs appear to be the most practical tool for evaluating bone turnover, they represent the global function of the skeleton. Therefore, BTMs cannot provide information on the regional bone sites or differentiate the effect of treatment in trabecular and cortical bone regions. A recent investigation showed an increase in bone resorption in AKU patients. Bone loss leads to high urinary excretion of type 1 collagen N-telopeptide [24]. Early results have demonstrated increased inflammation, bone resorption and cartilage remodelling among AKU patients compared to healthy control subjects using markers for remodelling [121].

Radioisotope quantitative methods are a powerful approach in the medical imaging field that provide an alternative technique to avoid some of the drawbacks of other bone quantitative methods. The broad usefulness of PET in research and in the clinical fields has led to efforts to simplify quantitative approaches which are comparatively reliable, and easy to use as a practical tool in the daily use of this modality. As mentioned earlier, the absorption of bone radiotracers throughout the entire skeleton should be almost equal and any discrepancies either lower or higher reflecting a change in bone metabolism. Those abnormal uptakes can be quantified using reliable radionuclide quantitation methods. Research studies involving radiotracers concentrate either on plasma clearance or bone uptake measurements. While a variety of radionuclide quantitative methods were defined in the literature, it is important to identify the best approaches based on study protocols, patient acquisition, processing time, and the availability of the software. Usually, each researcher or clinician chooses their preferred quantitation method considering it as the best method for the purpose of their study. Thus, the best radionuclide quantitation technique for clinical use will certainly improve as time goes. Hoekstra *et al*. [122] addressed nine classes of PET analytical approaches which have been used in literature for diagnosing, predicting, and evaluating the response to therapy.

At the moment, radionuclide quantitation can be approached by several methods from graded visual evaluation to complex kinetic assessments of dynamic imaging acquisition and blood collection. The following paragraphs briefly outline the main radionuclide quantitation methods which been described in literature.

1.4.1.6.3.1 Visual measurement

The simplest radionuclide assessment method is dichotomous visual inspiration; either a positive or negative scan. Clinically, bone scintigraphy interpretation is qualitative based primarily on visible assessment [123]. Visual inspection of a PET/CT image mainly depends on the opinion of the nuclear medicine physician who will look for signs of abnormal bone metabolism during the evaluation of the bone scan, however it is a subjective assessment method. Generally, positive bone lesions are detected visually by noting abnormal radiotracer uptake at any skeletal lesion. These regions seem to be either darker "hot spots" caused by absorbing more tracer or brighter "cold

spots" in the area of less tracer. Some theories are widely agreed as a reference when viewing ^{18}F-NaF PET images. Hot areas may point out tumor, infection, trauma, fibrous dysplasia, fracture, inflammation, Paget's disease, myositis ossificans or an arthritis, while cold areas may point out some certain types of cancer or lack of blood flow to the bone [107,124]. The viewer has two main challenges in deciding if a change in the absorption site is a normal tracer biodistribution and/or the degree of absorption is too high or low to support their final conclusion [125]. The expert observer will precisely determine whether an increasing or decreasing uptake at the specific site is likely to be related to bone disorder based on anatomical information, age, medical history and previous observations of the ^{18}F-NaF distribution throughout normal skeleton. However, it is difficult for even expert observers to accurately assess the degree of tracer uptake. The three theories are not descriptive on the meaning of normal, high or low tracer uptake throughout the skeleton. While more studies are carried out, it is clear that the concepts of normal, high and low tracer absorption vary from different bone disorders and clinical settings [125].

In 2011, an AKU study was performed seeking to describe practical methods to quantify the disease burden in a patient with AKU [70]. An alkaptonuria severity score index (AKUSSI) was used to score disease severity by performing systematic clinical evaluations, combining clinical assessment, imaging assessment, and questionnaires. Bone and joint lesions were subjectively scored by pain score and visual evaluation of abnormal radiotracer accumulation in the whole skeleton using ^{99m}Tc-MDP bone scanning [126]. A score system was used for whole body scintigraphy; 1 for a positive joint lesion and 0 for a normal region. The previous study led to the critical clinical imaging question of whether it is possible to quantify bone lesions by radionuclide bone imaging for AKU patients specifically and for arthropathy patients in general.

On the other hand, visual inspection might be graded to enhance the sensitivity and specificity. Many studies have graded the accumulation of radiotracer which was somewhat better [125]. In high resolution PET/CT images, the abnormality can be graded on a 4 or 5-point score level relative to normal bone structure. For instance, regional bone sites can be scored as: 0, normal; 1, mild; 2, moderate; 3, between moderate and high intense uptake; 4, high intense uptake; and 5, very high intense uptake. This gives the visual measurement some objective validity which can result in a fairly consistent

score between observers until explicitly established guidelines for abnormal regional level are performed. Using this approach, Vinjamuri *et al*. [76] addressed this hypothesis by visually scoring various lesions in whole-body ^{99m}Tc-MDP bone scans. Vinjamuri *et al*. quantified the radioisotope activity in AKU patients in order to create a reliable tool that might be used later to assess the response of treatment for those patients who will take nitisinone. The most affected OA bone and joint lesions were evaluated using a four-score level starting from 0 for normal, to 3 for the advanced degenerative site. In fact, the score scale was mainly based on his personal experience and might differ between clinical observers.

The scoring system based on visual assessment can be influenced by physical and physiological factors. Development of a non-subjective assessment method that demarcated the boundary between the normal distribution of radiotracer and increased tracer uptake in the skeleton is clinically required. Various research has focused on quantifying abnormal lesions to develop the best radionuclide quantitative method which can precisely measure radiotracer uptake and evaluate the treatment response.

1.4.1.6.3.2 Standardised uptake value (SUV)

Since 1941, tracer uptake normalisation was used as a technique to supplement visual interpretation which was described as a percentage of the injected dose divided by unit of body weight [127]. In 1980s, it was defined as the differential absorption ratio (DAR) and was being employed in PET scans evaluation. Occasionally, in the literature aliases like the differential uptake ratio (DUR) and a standardised uptake ratio (SUR) are also identified [123]. Currently, this is applied as standardised uptake value (SUV).

Nowadays, SUV is the most commonly employed semi-quantitative method owing to its popularity in clinical PET studies in comparison to other quantitative approaches. In many articles, this approach is addressed in detail [123,127,128]. SUV is represented as the tracer concentration in the tissue, divided by the injection dose normalised to body size, multiplied by a decay factor [123].

In practical application, SUV is measured automatically using commercial PET scanner software by dividing the ROI concentration of the radiotracer (kBq/mL), by the injecting dosage (kBq) divided by body size [123]. The basic SUV equation is:

$$\mathrm{SUV} = \frac{\text{activity concentration (kBq/ml)}}{\text{injected activity (kBq)} / \text{body size}}$$

Usually body size measurement is based on either lean body mass (LBM), body surface area (BSA) or total body weight (TBW) of the patient [123]. In fact, TBW is the most regularly used body size method which is used to calculate SUV values.

When radioactivity is retained and equally distributed throughout the body, the SUV in every part of the body will be found to be 1g/ml irrespective of the patient size and amount of tracer injected. SUV values have no dimensions and take the assumption that 1ml of tissues has a weight of 1g [129].

SUV was described as the best measurement method to adopt by many researchers and clinicians for PET investigations because of its attractive features [130,131]. The main advantage of SUV measurement is the fact that it is computationally simple to apply and can be used to quantify any site of the skeleton from only a single injection. Another advantage of SUV is that it needs substantially less scanner time than other complex acquisition protocols. Measuring the SUV value requires either a whole body scan or a static image for the chosen ROI rather than applying dynamic one-hour imaging for each region. Additionally, complex requirements such as blood sampling and blood analysis are not needed to calculate SUV values.

The reliability of SUV may be influenced by biological and physical/technical factors [123,127,129]. Some of these factors may lead to overestimation or underestimation of the SUV value if not considered carefully during image acquisition and image processing. Table 1.7 illustrates some of these factors [123,127,130]. Many consensus groups addressed these factors and established protocol guidelines in order to overcome the errors in such a broader sense. In 2010, Adams *et al*. [130] reviewed the main biological and technological factors which have a significant influence on the SUV measurements.

The article provided an overview recommendation to minimise the error during calculating SUV values in order to assess a precise response of the therapeutic plan and detect early degenerative changes. In another study done by Win *et al*. and his co-workers [107], the effect of several factors that can influence the uptake of ^{18}F-NaF uptake through the normal skeleton were tested including kidney function, patient age, height and weight. Although younger patients in that study had higher SUV values, they have not found a considerable correlation between age and the mean SUV value. On the other hand, they noticed a relationship between the mean bone SUV values and both height and weight of the patient in certain bone regions. Win also reported that there was no correlation between SUV value and serum creatinine because all the patients who were involved in his study had normal serum creatinine. The findings might have been far more relevant if the author had included patients with abnormal renal functions to find the relationship between the SUV values and serum creatinine levels.

In the literature, there are two popular existing ways of reporting SUV calculation within the ROI: maximum and mean SUV value (SUV_{mean} and SUV_{max}) [130]. SUV_{mean} incorporates multiple voxel information, which makes it less sensitive to the noise surrounding the ROI. Nevertheless, the calculated SUV_{mean} can differ depending on the voxels that are included within the ROI. It is therefore sensitive to the ROI definition, making it subject to intra-and interobserver variability [130]. In contrast, SUV_{max} is the maximum voxel value within the ROI and thus does not depend on the definition of ROI, assuming that there will be inclusion of the voxel having the highest activity concentration, however it is more susceptible to background activity and image noise. Therefore, it is important when measuring SUV_{max} to carefully avoid including areas of high radioactivity accumulation, like the urinary bladder. In PET research, SUV_{max} is the most convenient way of calculating SUV values making it the most popular employed method due to the fact that it more reproducible and less observer-dependent compared to SUV_{mean} [129,130]. Several clinical studies have revealed that SUV_{max} is a reliable method for evaluating treatment response specifically when serial images were analysed and compared in different occasions [129]. Usually, researchers prefer to use SUV_{max} to avoid underestimation of the radioactivity as the ROI may be misplaced. It is important to mention that radiotracers such as ^{18}F-NaF have high signal-to-noise ratio in bone, so that the soft tissues uptake is usually not visible, and the activity is mainly concentrated in the bone area and calcified tissues.

In this case, even slight region misplacement may result in significant drop in the mean measure of radioactivity uptake. It has been reported previously that there are no substantial variations between mean and maximum SUV values which have been measured from normal skeleton and extraskeleton tissue in negative or positive ^{18}F-NaF scans [132].

Data from several sources have identified the average SUV values for normal bone sites, trying to establish a threshold for normal bone SUV values. Win *et al.* [124] examined the data from 11 patients without a history of metabolic bone disease or cancer who underwent ^{18}F-NaF PET/CT bone scans. In that study, 31 bone sites throughout the axial and appendicular skeleton were analysed. Win *et al*. reported that mean SUV_{max} of cervical vertebrae was 6.84, thoracic vertebrae was 7.36, lumbar vertebrae was 7.27, femoral head was 2.22, humeral head was 1.82, mid sternum was 5.51, and parietal bone was 1.71. In another study, Puri *et al.* [131] quantified hip and lumbar spine lesions for 12 healthy postmenopausal women using six quantification methods including SUV measurement. In that study, normal SUV value for hip site was 2.324 ± 0.734, while for the lumbar spine was 6.005 ± 1.47. Similarly, Sabbah *et al.* [132] found that axial skeleton lesions had a significant higher SVU_{max} values (7.8 ± 2.0) compared with appendicular skeleton (2.9 ± 1.0). Together, these studies outline that each bone site has a different normal ^{18}F-NaF uptake measurement.

A considerable amount of literature has been published on using this approach to assess progression of disease and evaluate response to treatment. It is now well established from published studies that SUV can be used to quantify active lesions which can be noted in positive ^{18}F-NaF PET/CT scans. SUV has been extensively employed to detect bone metastases; it has recently been used in the degenerative joint disorder field [133,134]. Kobayashi *et al.* [133] measured the SUV at the hip joints and observed an accelerated rate of bone remodelling in various stages of OA. In his study, SUV values were compared with radiographic findings in MRI and the severity of pain scale. Kobayashi *et al*. pointed out that positive lesions in a PET scans had a SUV_{max} of 6.5 and higher. The authors reported also that the positive joint lesions were more detectable in PET scans in comparison to MRI (47 in PET vs 25 in MRI) suggesting that PET can identify abnormal bone turnover earlier than MRI in OA of the hip. Likewise, Dragana et. al [135] and Draper *et al.* [136] evaluated the bone and cartilage

damage from ^{18}F-NaF PET and MRI in patients with patellofemoral pain. The authors found that high SUV_{max} does not often relate to bone or cartilage structural damage which can be seen on MRI. Additionally, increased SUV showed a positive correlation with patient pain. These findings indicate that high radiotracer uptake in PET scans could indicate an early stage of a metabolic change, which may lead to joint degeneration.

To compare the distribution of ^{18}F-NaF uptake in normal, benign and malignant bone lesions, Sabbah *et al*. [132] compared SUV measurements from different skeleton lesions. Sabbah *et al*. reported that there was statistically significant difference in SUV_{max} between normal regions and benign bone lesions ($P < 0.0001$). Similarly, there was a statistically significant difference between SUV_{max} in bone metastases and SUV_{max} in the normal skeleton ($P < 0.0001$). Interestingly, when Sabbah compared the SUV_{max} in benign bone lesion with SUV_{max} in bone metastases, there was no statistically significant differences at any bone lesion ($P > 0.05$). Other authors argues that ^{18}F-NaF PET/CT scan may not be effective to differentiate between benign and metastatic bone lesions, however it still played a critical role in distinguishing between normal bone and benign or possibly malignant bone lesions [137]. Several other studies provided evidence that there is a definite difference in regional SUV values when comparing the values for normal lesions with abnormal findings in bone disorders or metastases lesions.

In the treatment field, ^{18}F-NaF PET is considered a promising tool to monitor the treatment response not only in cancer cases but also for various types of musculoskeletal diseases [138]. There is recent evidence indicating that serial measurements of SUV may discriminate between respondents or non-respondents to therapy as proposed by several researchers [139–142]. Frost *et al*. [138,140,141] carried out a number of investigations evaluating regional ^{18}F-NaF uptake before and after treatment for patients with osteoporosis. In his series of quantitative studies, Frost *et al*. noted a change in SUV values during treatment period which were different at various skeletal locations [141]. Installe *et al*. monitored the treatment in Paget's disease of bones by evaluating the changes in kinetic modelling, SUV_{max}, and biochemical markers of bone remodelling. In that study Installe *et al*. reported that SUV_{max} was an effective quantative approach which provided significantly useful infromation without

the need of dynamic acquisition or blood sampling. In another study, Uchida *et al* [143] found that both lumbar spine SUV and femoral neck SUV reduced significantly ($P < 0.01$) as a consequence of alendronate treatment, which correlated with an 8.2% rise in lumbar spine bone mineral density. All the studies reviewed here support the hypothesis that PET/CT semiquantitative radionuclide methods including SUV measurements can be used as an imaging biomarker to assess early changes in bone formation and detect evidence for nitisinone treatment response for AKU patients.

Table 1.7. Technical and biological factors influencing SUV determinations at ROI .

Factors	
Technical/ physical factors	Residual dose in the syringe Inter-scanner variability Injected radioactivity CT contrast material Imaging protocols Size of ROI Partial volume effect Attenuation correction and reconstruction methods Quality control point
Biological factors	Age Body size Uptake time Respiratory motion Kidney function

1.4.1.6.3.3 Other quantitative assessment

In addition to SUV, there are more accurate radionuclide quantitative approaches which are somewhat more complicated such as Hawkins method, and graphical Patlak analysis [125]. Despite their efficacy, previous methods have suffered from considerable methodological limitations. A major limitation of these methods is that each site or ROI needs a single bolus injection followed by a 60-minute dynamic scan [119,120]. It means that, if more than one region needs to be quantified, a patient needs to get another injection in order to quantify that ROI. Another drawback of these techniques is that the measurements are limited to only 15 cm, which is the PET scan field of

view. Also, these quantitative approaches require blood collection and analysis, making it a long, complex, and costly procedure. Because of the reasons above, these techniques are impractical to be used in day to day clinical studies but have been widely performed by researchers in experimental studies.

1.4.2 Radiographic evaluation of cardiac calcification using different imaging modalities

Atherosclerotic plaques may contain lipids, inflammatory cells or calcium, which usually remain asymptomatic until cardiovascular complications and events clinically appear without warning, such as myocardial infarction or stroke [98]. While cardiovascular imaging techniques are continuously improving, it is still challenging to efficiently detect atherosclerotic lesions at high-risk of rupture. These high-risk plaques, identified as vulnerable plaques, have key histopathological features including inflammation and early-stage microcalcification. It is proposed that intact high-risk plaques will demonstrate certain pathophysiological characteristics prior to the clinical rupturing incident so that detection of these features could have prospectively valuable information on plaque vulnerability. Moreover, early predicting of vulnerable patients could avoid serious consequences.

Although numerous studies have been trying to understand the mechanism of vascular calcification, it still remains elusive. Naturally, vascular calcification occurs during a two-phase process: the initial microcalcification stage and the subsequent macroscopic formulation of calcium, also known as macrocalcification [144]. Although there are no standardised sizing criteria of the plaque, there is a common agreement that microcalcification and macrocalcification are classified based on < 50 μm and ≥ 50 μm nodules, respectively. Microcalcification, a more clinically relevant representation of vascular mineralisation, describes the early phases of intimal calcium deposition and amplifying mechanical stress on the fibrous plaque surface, which can directly lead to its rupture. With incremental calcification of plaque, the inflammatory plaque becomes pacified with a necrotic core wall blocking off the blood flow. Therefore, later phases of macrocalcification include plaque stabilisation and a reduced possibility of plaque rupture. Table 1.8 illustrates the differences between

microcalcification and macrocalcification in vessels. The pathophysiological progression and vascular calcification imagery techniques are seen in Figure 1.11.

Table 1.8. Key differences between microcalcification and macrocalcification.
(Table from [145])

Characteristic	Microcalcification	Macrocalcification
Size	<5 μm	≥ 5 μm
Stage of calcification	Early	Late
Inflammation	Persistent	Healed
Surface area	High	Low
Exposed hydroxyapatite	High	Low
Risk of rupture	High risk of rupture	Low risk of rupture
Computed tomography/ X-ray angiography	Undetectable	Detectable
^{18}F-fluoride binding on positron emission tomography	Avid binding	Low binding

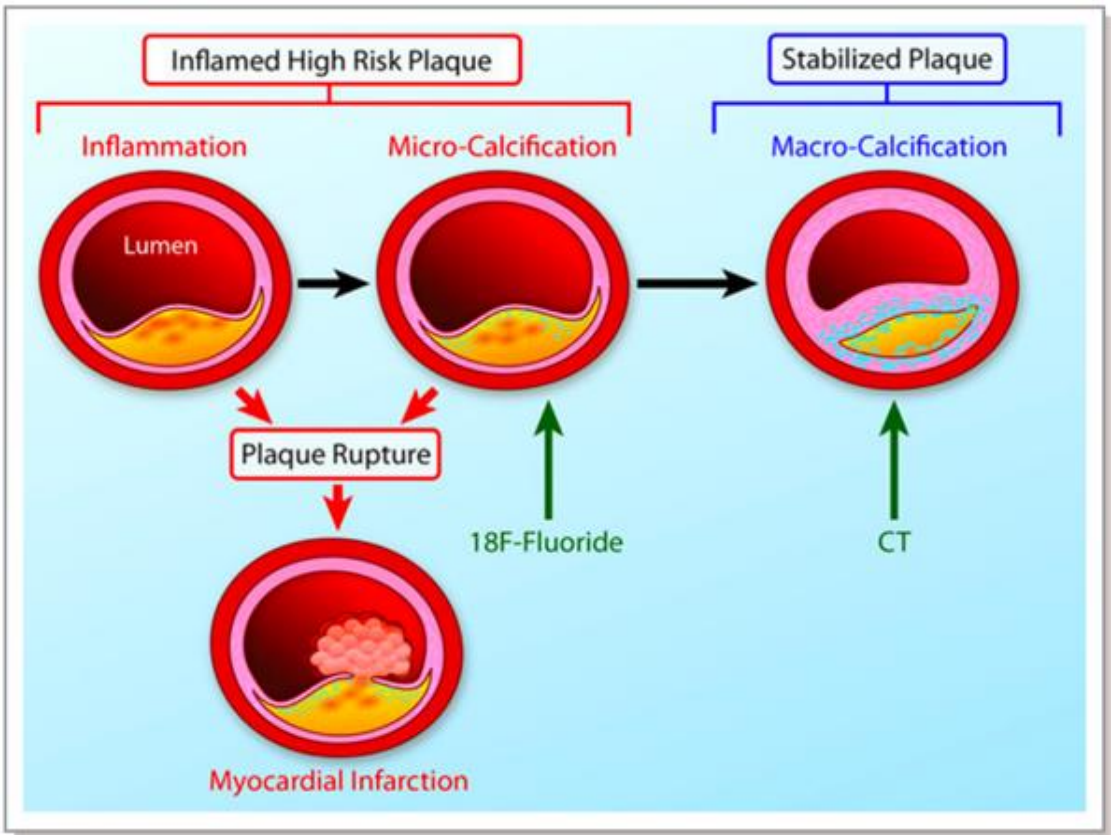

Figure 1.11. The link between inflammation, microcalcification, and macrocalcification. A large necrotic core, a thin fibrous cap, and an intense inflammation are key precipitants of acute plaque rupture and myocardial infarction. Intimal calcification is thought to occur as a healing response to this intense necrotic inflammation. However, the early stages of microcalcification detected by ^{18}F-fluoride positron emission tomography are conversely associated with an increased risk of rupture. In part, this is because of residual plaque inflammation and in part because microcalcification itself increases mechanical stress in the fibrous cap further increasing propensity to rupture. With progressive calcification, plaque inflammation becomes pacified, and the necrotic core walled off from the blood pool. The latter stages of macrocalcification detected by computed tomographic are therefore associated with plaque stability and a lower risk of that plaque rupturing (Illustration credit: Ben Smith). (figure from [146])

Imaging cardiac calcification may be crucial in terms of understanding the mechanism of vascular calcification, which may be associated with plaque rupture and adverse events. Conventional diagnostic modalities such as invasive coronary angiography and myocardial stress testing have consistently been unsuccessful in recognising such plaques, leading to an increase in the probability of having other factors than only the degree of luminal arterial stenosis which can relate to plaque rupture [145]. MRI angiography and US have also been used previously to detect atherosclerotic plaques [98,145]. Clinically, cardiac CT is a gold standard imaging technique for identifying macrocalcification in coronary arteries by providing a coronary artery calcium (CAC) score [147,148]. The advanced phase of calcification is conveniently imaged by CT angiography, which is assumed to show plaque stability. However, CT cannot detect microcalcification nor distinguish between active and inactive cardiovascular calcification. It has been argued by many researchers that CT can detect the irreversible stage of the atherosclerotic process but failed to prevent the evolution of vascular calcification as it cannot detect the earlier phase of microcalcification [148–150].

In nuclear imaging, different positron radiotracers have been used to detect and identify calcified vessels and improve cardiovascular risk prediction. To date, the majority of cardiovascular studies have employed 18Fluorine- labelled fluorodeoxyglucose (^{18}F-FDG) as an inflammation imaging radiomarker and ^{18}F-NaF as microcalcification imaging radiomarker [98]. Previous studies have used ^{18}F-FDG to quantify the extent of atherosclerosis and to determine therapeutic response [98,146,151]. In practice, imaging coronary arteries using ^{18}F-FDG is problematic as there is adjacent background myocardium uptake, which usually causes coronary signal obscuration [148]. Motion correction algorithms can help to address this problem by switching myocardial metabolism away from glucose [145]. Furthermore, the partial volume effect (PVE) restricts the use of ^{18}F-FDG-PET [98]. PVE contributes to a substantial underestimate of tracer absorption in structures smaller than the spatial resolution of PET system, which needs to be corrected when evaluating arterial inflammation.

Recently, positron bone agent ^{18}F-NaF has been proposed as a sensitive method to track microcalcification and active vascular calcification. There has been substantial interest for using ^{18}F-NaF in cardiac investigations [147,148,152,153]. ^{18}F-NaF PET/CT has

been employed before to evaluate vascular calcification within the coronary arteries [150], the aorta [154,155], femoral arteries [155], and carotid arteries [149]. Several clinical and preclinical works are investigating the use of ^{18}F-NaF as a vascular microcalcification biomarker [156].

As mentioned earlier, the mechanism of ^{18}F-NaF uptake includes the exchange between the fluoride ions and the hydroxyl group of hydroxyapatite after incorporating it into hydroxyapatite crystals forming the fluorapatite. The uptake of ^{18}F-NaF is associated with local blood flow, the surface area, and the permeability of the capillary system [97]. In atherosclerosis, vascular calcification commonly appears as hydroxyapatite deposits in the vascular wall sharing the same histological components of ectopic bone such as the existence of osteoclast-like and osteoblast-like cells. There is a high possibility that the same mechanism that underlies the ^{18}F-NaF uptake in osseous tissue is also occurring in the calcified vessels due to the strong biologic similarities between vascular calcification and bone formation [157]. Although the nature of vascular tissue is different to bone, in which there is constant blood supply via them, it is not likely to be considered as an active factor [145].

As it is in bone tissue, the essential structural component of the calcified vessels is hydroxyapatite. The arterial uptake is likely related to the fluoride ion deposition on hydroxyapatite crystals in the available surface area of the arterial wall [98]. In the subsequent stage of calcification or macrocalcification most hydroxyapatite is internally distributed and cannot be bound to ^{18}F-NaF. Furthermore, ^{18}F-NaF cannot penetrate to deeper vascular layers; ^{18}F-NaF can only bind to the outer surface [144]. Thus, macrocalcification cannot be precisely defined by ^{18}F-NaF PET scan.

In the literature, there are various assessment methods used to identify and quantify vascular calcification in ^{18}F-NaF PET/CT scans, such as visual assessment, SUV, target to background ratio (TBR), and entire myocardiac calcification measurement. In 2010, Derlin *et al*. described vascular ^{18}F-NaF uptake and arterial calcification in major arteries in a retrospective analysis of 75 patients with malignancy [155]. Both qualitative and semiquantitative analysis was performed. In that study, Derlin noted increased radiotracer uptake in femoral arteries, abdominal aorta, thoracic aorta and carotid arteries in about 75% of patients. Interestingly, only 12% of positive arterial

calcification sites, which have been detected from CT images, have shown an increased radiotracer uptake in PET images. The study indicated the feasibility of ^{18}F-NaF PET/CT for the imaging of mineral deposition in arterial wall alterations at the early stage of calcified plaques, providing different information to the CT images. A series of investigations were carried out by the same author in which he and his co-workers studied the vascular ^{18}F-NaF uptake [158–160].

In 2011, Beheshti *et al.* [152] created a unique method reflecting cardiac calcification in the entire heart structure. In that study, heart and aorta calcification were evaluated and quantified for 51 patients who underwent ^{18}F-NaF PET/CT scan for whole-body skeletal evaluation. For the quantitative analysis, the ROI was placed on a CT slice over the main cardiac arteries and then corresponded to PET images to measure SUV. After that, the molecular calcification score for each slice was estimated by multiplying the SUV_{mean} of each ROI by slice volume. The global cardiac calcification score (GCCS) was calculated by adding the previous molecular calcification scores for the entire ROIs. In that study, a strong correlation was noted between the age of patients and increased ^{18}F-NaF uptake. Beheshti provided a valuable insight into the detection of calcification from the large surface area of the cardiovascular structure, including the entire myocardium, to avoid miss diagnosis of patients at high-risk of cardiac events.

Irkle *et al.* [149] and his co-workers published a paper in 2015, which focused on the mechanism of ^{18}F-NaF uptake in the cardiovascular system. In that study, an electron microprobe was used on carotid atherosclerotic plaques to measure the presence of ^{18}F-NaF tracer directly within the calcified areas during carotid endarterectomy surgery. The authors noted that the binding of ^{18}F-NaF to the calcified areas was exceptionally specific. Also, the degree of ^{18}F-NaF absorption was seen to be strongly dependent upon the calcification surface area and was only able to absorb through the outer calcification layer without a deeper penetration. These results indicate that ^{18}F-NaF-PET/CT can detect microcalcifications since, with regard to its size, microcalcifications have large surface areas while macrocalcifications have limited surface areas. Several other researchers recorded similar conclusions which resulted in expanded interest for using ^{18}F-NaF to identify the microcalcification phase and visualise ongoing mineral deposition in the atherosclerotic plaque [147,152,153].

On the other hand, data from several studies have identified that the increased ^{18}F-NaF uptake in PET images was associated with coronary calcium score (CAC). Dweck *et al*. [148] noted that patients with CAC scores of 0 had low ^{18}F-NaF activity versus patients with CAC > 1000 (TBR_{max} ± SD; 1.23 ± 0.24 vs 1.64 ± 0.49, P = 0.003). In another study which set out to detect coronary atherosclerosis and evaluate the correlation between ^{18}F-NaF PET and CT quantitative assessments, Kitagawa *et al*. [150] classified his patients into four groups based on CT angiography results and HU values to; calcified plaque (CP), non-calcified plaque (NCP), partially calcified plaque (PCP), and high-risk features (HU < 30 and vascular remodelling index >1.1). In that study, TBR_{max} value for the PCP group was higher than the NCP and CP groups (1.17 ± 0.19 versus 1.00 ± 0.24 and 0.92 ± 0.18, respectively, P < 0.0001), and TBR_{max} value measured from high-risk lesions was higher than those in the other groups (1.20 ± 0.21 vs 1.02 ± 0.20, P = 0.0011).

It is important to point out that imaging of coronary artery disease using ^{18}F-NaF PET/CT scans has some limitations. The spatial resolution of the advanced PET system is around 4–5 mm, thus the target ROI has to be at least 8–10 mm in size in order to be observed [98]. This is especially relevant when imaging atherosclerotic plaques, since these plaques typically are a few millimetres in size. Moreover, cardiac motion and breathing rate are a significant cause of concern in attempts at imaging arteries. In order to overcome the limitations outlined, measuring uptake at the large vessels or global cardiac uptake enable better identification of cardiovascular inflammation or calcification [152].

Current evidence in the literature and ongoing studies strongly demonstrate the essential role of ^{18}F-NaF PET/CT imaging in assessing molecular calcification in the major vessels and coronary arteries. Overall, previous results clearly support the hypothesis that ^{18}F-NaF tracer can be used as an imaging marker to identify microcalcification and no doubt of becoming an intensive subject in future studies. Due to the substantial similarity between cardiac disorders and cardiovascular involvement in AKU, cardiac imaging modalities for identifying early vascular calcification could be utilised to diagnose and detect cardiac ochronosis. SONIA 2 patients underwent ^{18}F-NaF PET/CT scan to evaluate bone and joint abnormalities; the

images could be also used to detect early vascular calcification in AKU patients without adding extra radiation or cost.

1.5 Aims and objectives

This thesis provided an important opportunity to advance the understanding of the disease state and disease progression in AKU patients. The experimental works presented here in this thesis mainly investigates whether ^{18}F-NaF can be used as an imaging biomarker for evaluating early changes in bone tissue, identifying early calcification in the IVD area, and detecting early microvascular calcification in the main arteries for AKU patients. The impact of some biological factors such as age and gender that may influence the ^{18}F-NaF PET/CT semiquantitative values are also be tested. Part of this thesis seeks to investigate the relationship between semiquantitative radiographic values from different imaging modalities. Also, the progression of the ochronotic arthrophathy and the treatment response is investigated during the course of therapy. The specific objectives are as follows:

1. Assessment of bone involvement in the lumbar spine and hip regions for AKU patients by measuring Hounsfield units (HU) from CT and standardised uptake values (SUV_{max}) from ^{18}F-NaF PET.

2. Determine the link between structural disc changes and molecular changes in the lumbar disc area by comparing MRI disc degeneration grade and ^{18}F-NaF uptake in PET scan.

3. Evaluation of the changes in ^{18}F-NaF PET/CT semiquantitative values across five visits in order to track the progression of the disease and/or assess the response of treatment in the long term for AKU patients who treated with nitisinone for four years.

4. Using ^{18}F-NaF PET/CT images as a valuable imaging method to identify early cardiovascular calcification and assess future cardiovascular risk without adding extra cost or radiation to SONIA 2 patients.

The thesis is divided into seven chapters. The first chapter began by providing background information on AKU and medical imaging modalities, and reviewing the academic literature concerning the main findings in the radiographic evaluation of bone and cardiac involvements. The second chapter describes the methodology which was employed for this thesis. The overall structure of the experimental study takes the form of four chapters, form Chapter 3 to Chapter 6. Each experimental chapter examines one of the listed objectives, which was pointed out above. Each results chapter begins with a brief introduction and ends with a summary of the main findings, limitations of the study, suggestions for further research and followed by the conclusion. The final chapter gives a brief summary and discusses the overall findings, key methodological limitations, highlights the main contributions made by this thesis, reflects on the overall implications of the results for future research, and finally presents an overall conclusion .

2 Materials and Methods

2.1 Ethical approval

Ethical approval for the SONIA 2 clinical trial was given by the National Research Ethics Service, and the patients provided written informed consent (REC reference: 13/NW/0567), dated 17/9/2013.

2.2 Patient group

2.2.1 SONIA 2 patients

SONIA 2 has fully recruited 138 AKU patients over three sites: in Liverpool, United Kingdom; Paris, France, and Piešťany, Slovakia. The trial took place over four years, starting in 2014 and finishing in 2019. Each participant was required to make up to six visits to their nearest clinical site; at the baseline, after three months, after one, two and three years, and the final visit after four years. The participants were randomly divided into two equal groups of 69. The first group took nitisinone, 10 mg/day, and the second group was a control group. The comparison between the treatment and the non-treatment groups was aimed at identifying the effectiveness and the impact of nitisinone and provide evidence for nitisinone slowing the progression of AKU.

Only the patients who attended the Royal Liverpool University Hospital, Liverpool, England, for evaluation at the baseline in mid-2014/ early 2015 were included in the studies which were done here in this thesis. On the initial cohort of 41 adult AKU patients, 25 were males, and 16 were females with a mean age of 51 ± 10.9. The participants were aged between 30 and 68 at the beginning of the SONIA 2 trial. All patients underwent a number of clinical and biochemical tests, including the following; clinical eye photographs, ear cartilage biopsies, echocardiograms, blood samples, urine samples, X-Ray, ultrasound, spine MRI, DEXA, and ^{18}F-NaF PET/CT. Only ^{18}F-NaF PET/CT imaging data were analysed for the purpose of this thesis. The baseline ^{18}F-NaF PET/CT image was analysed for investigating ochronotic arthrophathy and cardiac ochronosis in Chapter 3, Chapter 4, and Chapter 6. The serial images from baseline through to the final visit were analysed and compared in Chapter 5. Data from other imaging modalities such as DEXA scan and MRI were compared with ^{18}F-NaF PET/CT findings in order to assess the correlation between different imaging

modalities in Chapter 3 and Chapter 4. **Error! Reference source not found.** showed the number of SONIA 2 patients, gender, age and standard deviation (SD) who were analysed in each result chapter.

Baseline ^{18}F-NaF PET/CT images at Visit 1 were available for all 41 patients. Only 32 AKU patients from the Liverpool site (78%) completed Visit 6. In SOINA2, 9 patients withdrew from the SONIA 2 trial after Visit 1 and before completing the rest of the scheduled visits. In practice, analysing some of the images was problematic for several reasons. Some of the patients had undergone ^{99m}Tc-MDP bone scans instead of ^{18}F-NaF PET/CT bone scans due to the failing production of ^{18}F-NaF on the scanning day. Another source of uncertainty in the analysis was that some of the patients had 2D ^{18}F-NaF PET/CT static images in specific body regions instead of 3D whole-body^{18}F-NaF PET/CT scans due to technical issues in the PET scanner on the day of imaging. In this thesis, neither ^{99m}Tc-MDP bone scans nor ^{18}F-NaF PET/CT static images were analysed or compared with the 3D ^{18}F-NaF PET/CT semiquantitative values.

SONIA 2 data was anonymised to protect the personal information of the patients. Limited data were shown while analysing the ^{18}F-NaF PET/CT images, such as gender, date of birth, weight, height, the amount of the administered dose, time of the scanning and imaging protocol.

Some SONIA 2 participants were excluded from some parts of this thesis. These include the patients who have lumbar disc implants, hip joint replacements, and those with very high bone density values. in Chapter 3, 2 SONIA 2 patients were excluded from the analysis; patient number 36 had multilevel spinal surgery, and patient number 38 had abnormally high bone density values, so that it was difficult to quantify the spine lesion for those patients. Patient number 16 had one lumbar disc implant placed between T12 and L1; this patient was included in this thesis by analysing the regions between L2-L5 levels instead of L1-L5.

Patients with a metal stem placed into the femur were excluded from femoral measurement only. In total, 5 patients had a right hip joint replacement and 9 patients had a left hip joint replacement; these patients were excluded from hip measurements in Chapter 3. The reason for excluding patients with metal implants is because, in CT

scans, X-rays would be completely absorbed by metal, causing streak artifacts which cause significant sources for error.

Table 2.1. SONIA 2 patients who were analysed in each result chapter. Y; included N; not included.

Patient number	Gender	Age	Chapter 3	Chapter 4	Chapter 5	Chapter 6
1	Male	42	Y	Y	Y	Y
2	Male	49	Y	Y	Y	Y
3	Male	62	Y	Y	Y	Y
4	Male	51	Y	Y	Y	Y
5	Male	65	Y	N	N	Y
6	Female	59	Y	Y	Y	Y
7	Female	53	Y	Y	Y	Y
8	Male	33	Y	Y	Y	Y
9	Female	45	Y	Y	Y	Y
10	Female	34	Y	Y	Y	Y
11	Female	43	Y	Y	Y	Y
12	Male	43	Y	Y	Y	Y
13	Male	39	Y	Y	Y	Y
14	Male	41	Y	Y	Y	Y
15	Male	47	Y	Y	Y	Y
16	Male	59	Y	Y	N	N
17	Male	46	Y	Y	Y	Y
18	Female	37	Y	Y	Y	Y
19	Female	55	Y	Y	Y	Y
20	Male	61	Y	Y	N	Y
21	Male	57	Y	Y	Y	Y
22	Male	65	Y	N	Y	Y
23	Female	37	Y	Y	Y	Y
24	Male	52	Y	Y	Y	Y
25	Female	56	Y	Y	Y	Y
26	Female	68	Y	N	N	Y
27	Female	54	Y	Y	N	Y
28	Male	44	Y	Y	Y	Y
29	Female	47	Y	Y	Y	Y
30	Male	67	Y	N	Y	Y
31	Female	64	Y	Y	Y	Y
32	Male	60	Y	N	Y	Y
33	Male	52	Y	Y	Y	Y
34	Female	68	Y	Y	Y	Y
35	Male	30	Y	Y	Y	Y
36	Male	55	N	N	N	Y
37	Female	30	Y	Y	Y	Y
38	Female	44	N	Y	Y	Y
39	Male	44	Y	N	Y	Y
40	Male	62	Y	Y	Y	Y
41	Female	49	Y	Y	N	Y
Total number of patients in each chapter			39	34	34	40

2.3 ^{18}F-NaF PET/CT procedure

Figure 2.1. illustrates the consecutive methodological steps for whole body ^{18}F-NaF PET/CT bone scan.

2.3.1 Patient preparation and precautions

1. Based on the Society of Nuclear Medicine (SNM) and European Association of Nuclear Medicine (EANM) Procedure Guideline for ^{18}F-NaF PET/CT Bone Scans [104,109], pregnant and breastfeeding patients were not involved in this study.

2. Before the schedule, the patient was informed about the procedure, and on the arrival day, one member of the PET/CT staffing team explained the process to the patient.

3. To decrease the radiation dose and improve image quality, patient was well hydrated one hour before the injection. Patients were asked to drink more than 200 ml (8-oz or two glasses) of water to promote the rapid renal extraction of the radiopharmaceutical.

4. Patients were asked to drink a second time, consuming more than 200 ml of water after receiving the ^{18}F-NaF injection to improve image quality and reduce background activity.

5. Patients emptied their bladder frequently and immediately before starting the scan to avoid high intense tracer activity in the urinary bladder, which could confound the interpretation of findings in the pelvis and degrade image quality.

6. Patients removed any metal objects to prevent attenuation artifacts.

7. Patients did not fast nor stop any of their medications.

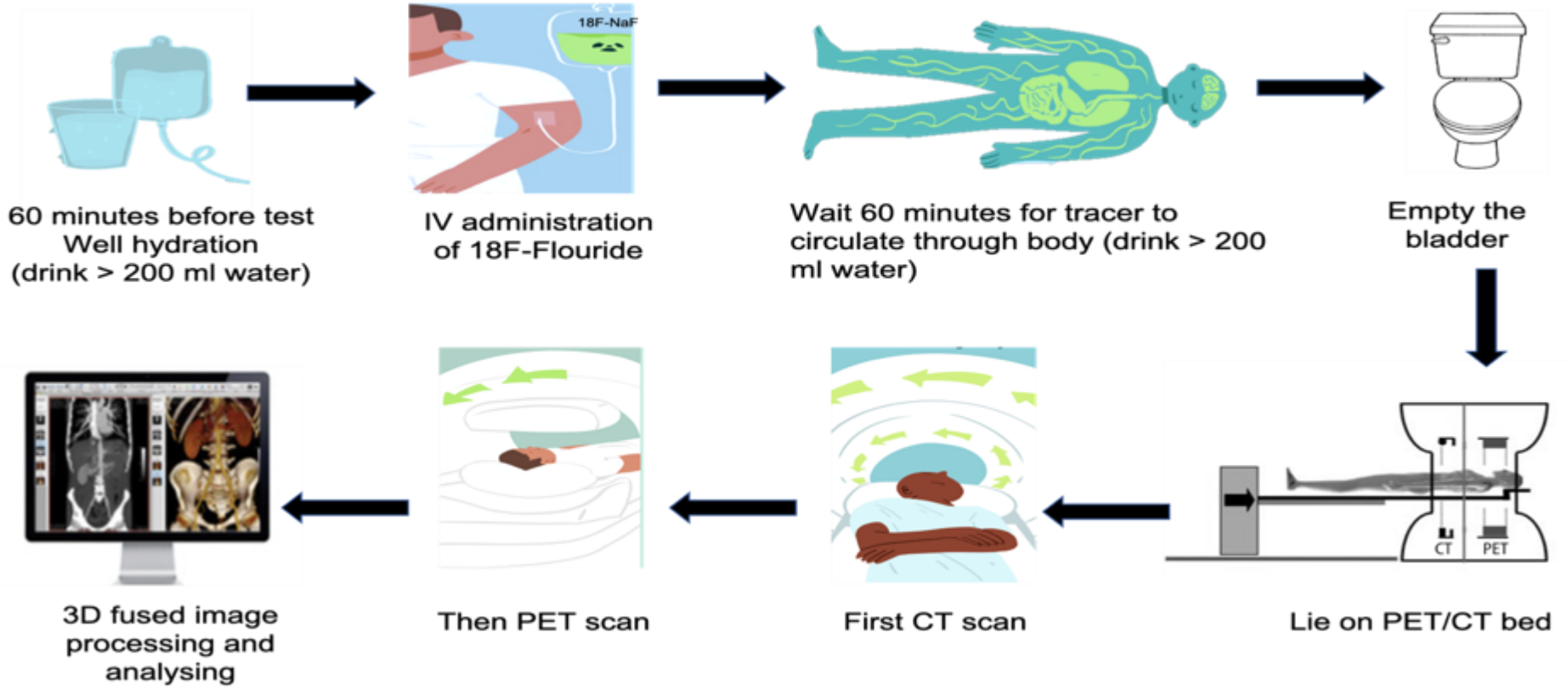

Figure 2.1. Illustrates ^{18}F-NaF PET/CT imaging produce.

One hour before the imaging, patient must be hydrated. After administration of the ^{18}F-NaF, patients must wait for around 60 minutes. During this waiting time, patients must drink water and empty his/her bladder. The patient lies supine in the scanner bed with a hand on the side. CT scan is acquired immediately before PET scan. Image workstation is used to display and analysis PET/CT images. Figure done in Biorender.com.

2.3.2 Radiopharmaceutical and dose administration

Patients were intravenously injected with 185-370 MBq (5-10 mCi) of ^{18}F-NaF by an intravenous catheter. Based on the SNM and EANM Procedure Guideline for ^{18}F-NaF PET/CT bone scans [104,109], the higher activity which could be used for obese patients was 370 MBq (10 mCi).

2.3.3 ^{18}F-NaF PET/CT protocol and imaging acquisition

^{18}F-NaF PET/CT images of the whole skeleton was performed 60 minutes after IV administration of ^{18}F-NaF in patients with normal renal function to ensure rapid localisation of radiotracer in the skeleton and rapid clearance from the soft tissues and circulation. Patients were placed in a supine position with their arms at the sides for whole-body imaging from the head to toes. Patients were asked to minimise their movements as much as possible during the scan.

The ^{18}F-NaF PET/CT images were performed using a GE Discovery 690 PET/CT scanner (General Electric Medical System, Waukesha, WI, USA). Two images were preformed; the first one from the vertex of the skull to one third of the way down the thigh, and the second one from the lower thigh to the toes. Low dose CT images without contrast media were acquired immediately before the PET scan for of the whole-body, for attenuation correction of emission images and lesion localisation purpose using X-ray tube current 30 mA, voltage of 120 kVp and rotation of 0.5 seconds. The duration of CT imaging was approximately 30 seconds.

The PET images were acquired by three-dimensional (3D) mode to ensure that higher count rates compensate for the shorter acquisition times, which were required for imaging a large imaging surface. The PET imaging parameter was matrix 128 x128, and the slice thickness was 2.5 mm. The acquisition time was 2 minutes per bed position. PET images were reconstructed using a 3D ordered-subset expectation-maximization algorithm (OSEM) which is ideal with iterative reconstruction. The duration of PET imaging was around 20 minutes.

2.4 Imaging display and processing

CT, PET, and co-registered fused PET/CT images were displayed and analysed using the PET/CT workstation. To ensure and facilitate lesion detection, maximum-intensity projections (MIP) was generated. Images were reconstructed in trans-axial, coronal and sagittal projections and interpreted from a workstation.

2.4.1 Image software

2.4.1.1 Hermes software

The 3D ^{18}F-NaF PET/CT images were displayed to identify any abnormalities in the whole skeleton and analysed the images using Hermes hybrid software (version 1.4) (Hermes medical solutions, Stockholm, Sweden). Hermes Hybrid Viewer is a molecular imaging software that displays the images which were generated for PET/CT and archives the data. Hermes software can display different images from different imaging modalities, which provides functional and morphological information. It is a fast and reliable software for PET/CT images, where the datasets are loaded simultaneously and processed. The trans-axial, coronal and sagittal PET, CT and fused PET/CT images can be viewed together. Hermes Hybrid Viewer also has a consistent and reproducible tool for a quantification purpose. Besides, it can save the quantitative values and export them as XML for further statistical analysis.

Hermes workstation was used to analyse data in Chapter 3 only. The ^{18}F-NaF PET/CT images were processed, analysed and quantified at the Department of Nuclear Medicine in the Royal Liverpool University Hospital Trust, England. Data were also analysed at Sheikh Jaber AlAhmad AlSabah Nuclear Medicine and Molecular Imaging Centre, Kuwait, using Hermes software.

2.4.1.2 Horos software

The second medical imaging software, which was used to display, and analyse the ^{18}F-NaF PET/CT data in this thesis, was Horos software. Horos software is a free medical imaging processing application for Mac dedicated to DICOM images produced by

different imaging modalities such as PET/CT. Horos viewer is based upon OsiriX^{TM} as well as other open-source medical imaging libraries. ^{18}F-NaF PET/CT data were downloaded from Hermes workstation in Royal Liverpool Hospital and uploaded in Horos software in MacBook Pro laptop. Horos software has the same imaging analysis tools that are available in Hermes software. It can display whole-body PET, CT and fused PET/CT images simultaneously. Like Hermes software, it can quantitative ROI, save the quantitative values and export them as XML for statistical analysis

Horos and OsiriX^{TM} Software have been selected by many researchers for their advantages as well as its reliability. One advantage of Horos software is that it can be used anytime, anywhere, without being in the hospital or clinical department. Using Horos software instead of Hermes software saved a lot of time and avoided using the imaging workstation during busy clinical weekdays. This software was used to view, analyse, and quantify ^{18}F-NaF PET/CT images in Chapter 4, Chapter 5, and Chapter 6.

2.5 Semiquantitative measurement for bone

2.5.1 Hounsfield unit (HU)

To date, various methods have been developed and introduced to assess osteoporosis by measuring bone density from different techniques. Each technique has its advantages and disadvantages. In this thesis, the linear attenuation coefficient measured from the CT scan was proposed to capture bone density from specific skeletal sites. Regional bone radiodensity was quantified from 3D CT images by measuring mean HU from specific ROI, without using phantom. In recent years, measuring HU have been employed to determine bone density in the lumbar spine using non-contrast CT image [81,83,85]. CT is mainly used in hybrid PET/CT scans for attenuation correction of emission images and lesion localisation. However, in this thesis, CT data was quantified to estimate regional bone density. Measuring bone density from the PET/CT image delivers an additional quantitative bone value without adding additional radiation or costs to the patients from data which are available but used for other purposes. PET/CT softwares calculated the average, minimum, and maximum HU values from the selected ROIs. In Chapter 3 and Chapter 5, mean HU

value was considered in order to assess regional bone density in the lumbar spine and femoral head, assess the progression of ochronotic arthropathy in the spine, and evaluate the regional efficacy of treatment over four years.

2.5.1.1 Lumbar vertebral body measurement

Lumbar spine density was quantified by measuring HU from lumbar vertebrae, from L1 to L5. Previously, CT scans have been used by many reserchers to assess osteoporosis using HU measurement from the lumbar spine. Across this research area, different authors have estimated lumbar bone density from diagnostic CT [81,83,85]. In this thesis, the CT lumbar quantitative assessment technique was based on the previous evidence in literature related to its reliability and validity. The HU measurement at each lumbar vertebral body was obtained using previously described protocols [81,83,85].

The following steps were done to evualate and quantify lumbar vertebrae bodies:

1. Displaying whole body CT, PET and PET/CT images side-by-side in sagittal, coronal and axial plans on one screen for easy viewing.
2. Scrolling through the images and adjusting the three orthogonal views to align with the appropriate spine till the best view of the spine at sagittal, coronal and axial plans is reached which is usually vary between the patients.
3. Placing the cursor over the intersection of the axes crosshairs in any image which will produce a cursor that translates the two axes in unison.
4. Draging the crosshair in to the centre of the spine which will automatically co-regisiter it in the three spine planes. Clicking on a location on one of the views will focuse the other two views on that specific location. Some patient may not laying straight ahead during the scan, causing the axial, coronal and sagittal reconstructions of the spine not being parallel to the the axial, coronal and sagittal planes of the body.
5. Use the magnifier tool to adjust the image size.
6. Placing the crosshairs on the sagittal plane for each lumbar vertebrae at three locations; superior to the inferior endplate, in the middle of the vertebral body and immediately inferior to the superior endplate (Figure 2.2).

7. In the axial CT images, the largest possible elliptical ROI was drawn covering the trabecular area only to prevent volume averaging from cortical margins. Note that the cortical bone region of the vertebrae is denser than the trabecular bone region which will show as a lighter area in CT images.

Following the steps above, the HU values were generated in the CT image for each ROI. Then the average value for each lumbar vertebral level was performed from the three axial slices. For for each patient, the average lumbar value of HU_{mean} was also performed, presenting the L1-L5 bone density value.

This method was used in Chapter 3 to assess the bone density for the baseline data and correlate the results with bone mineral density measured from the baseline DEXA reports. This method was also repeated throughout the serial data from Visit 1 to Visit 6, in Chapter 5, to assess the progression of disease and treatment response over four years.

2.5.1.2 Head of the femur measurement

The following steps were done to evaluate and quantify the head of the femur:

1. Magnifying the image using the magnifier tool to adjust the image size and maximise the view at the hip area.
2. In the coronal CT image, placing the crosshairs at the centre of each head of the femur.
3. Adjusting the three orthogonal views to align with the appropriate head of the femur till the best view of the ROI at sagittal, coronal and axial plans are reached.
4. In the axial images, round ROI was drawn around the head of the femur at ech side.

Following the previous steps, the HU values were generated in the CT image for both femoral sides (Figure 2.3). The average value of HU_{mean} for both the right and left head of the femur was calculated to give the mean HU value for each patient. In some patients, only one hip side was measured because the second hip joint was replaced

with artificial joint. The exclusion criteria for femoral measurement included bilateral hip replacements.

2.5.2 Standardised uptake value (SUV_{max})

It was decided that the best method to adopt in this thesis for quantifying bone and joint involvements was using SUV measurement. The exact ROI, which was drawn at the CT image to measure HU, was copied to the PET image to measure SUV at the lumbar spine and femoral head sites, as shown in Figure 2.2 and Figure 2.3. Both Hermes and Horos software were used to calculate: average standardised uptake value (SUV_{mean}), minimum standardised uptake value (SUV_{min}), and maximum standardised uptake value (SUV_{max}) value for the ROI. In the literature, it has been argued that the chosen value for any study would vary depending on the aim of the study. In this thesis, SUV_{max} was considered because the main objective of the investigation was to assess the progress of the disease and treatment response for AKU patients. The average value of SUV_{max} from the three axial slices was calcuated to provide the mean SUV_{max} for each lumbar vertebra. The average value of SUV_{max} for the lumbar vertebrae bodies for each patient was also performed. The average value of SUV_{max} of the right and left head of the femur was ued to calculate the mean SUV_{max} for the hip site. This method was used in Chapter 3 and Chapter 5.

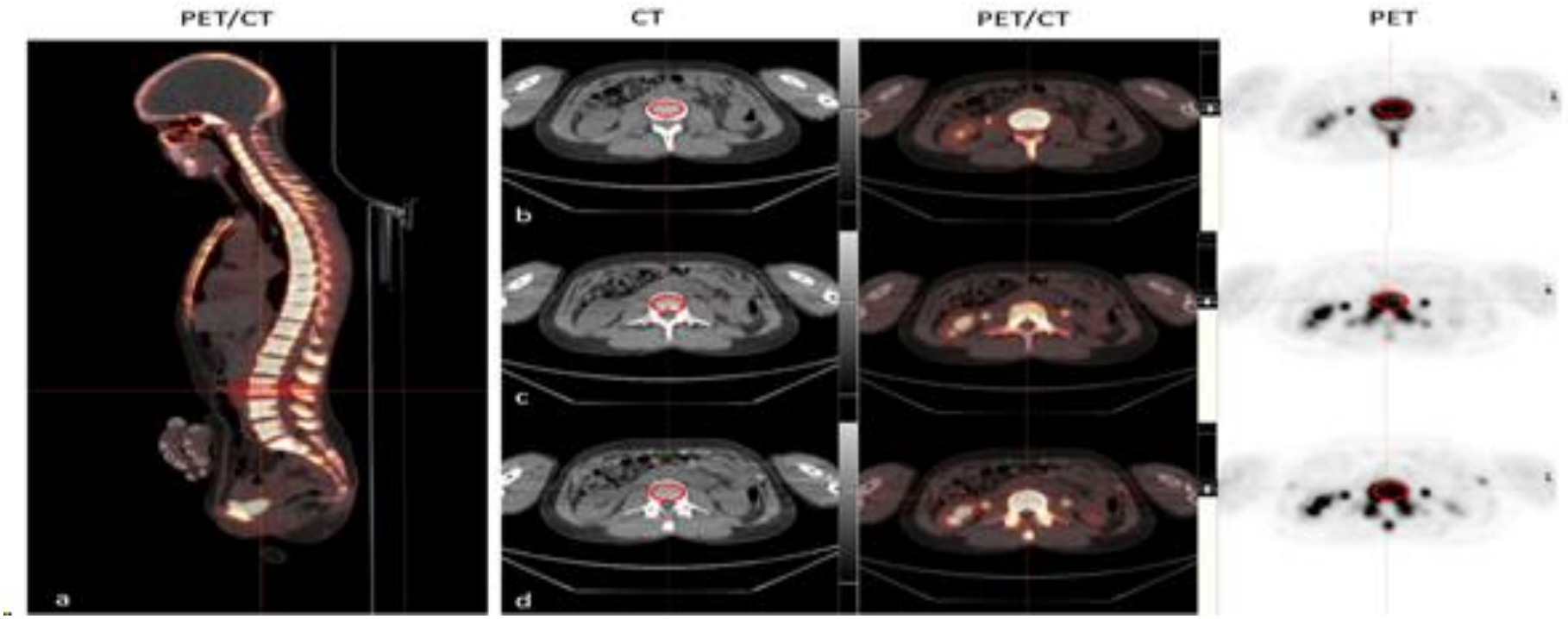

Figure 2.2. 3D ^{18}F-NaF PET/CT scan of the spine.

The images illustrate the methods for determining the Hounsfield unit (HU) values from CT scan and SUV from PET scan using an elliptical region of interest function. (a) Shows the vertebral bodies in a sagittal slice of ^{18}F-NaF PET/CT scan. In the panel, three axial locations are selected (b) immediately superior to inferior endplate slice (c), middle of the vertebral body, and slice (d), inferior to the superior endplate. The same region which was placed on the CT image at each level was copied to PET images to determine SUV_{max}.

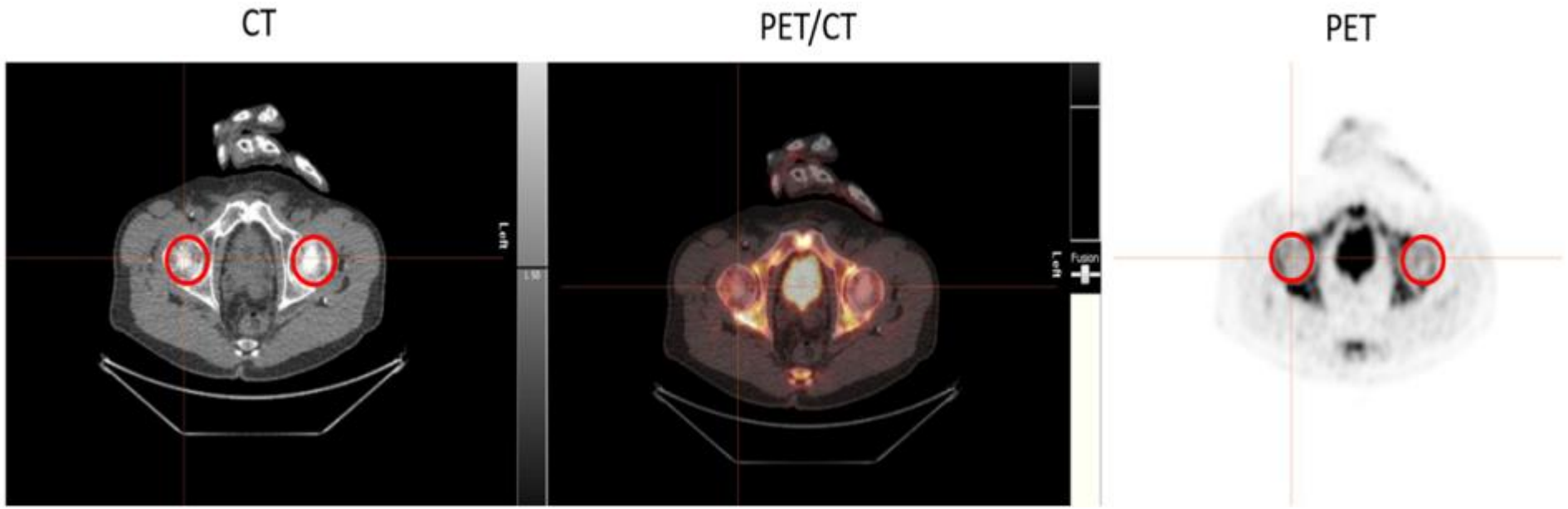

Figure 2.3. ^{18}F-NaF PET/CT axial slice of the head of the femur.

The image illustrates the analysing method for determining the HU and SUV values of the femoral head using round ROI function. The HU_{mean} and SUV_{max} values generated by the HERMES imaging software.

2.6 DEXA scan

Clinically, bone mineral density can be assessed by a dual-energy X-ray absorptiometry (DEXA) scan. All SONIA 2 patients underwent DEXA scanning annually to investigate the changes in bone density over the course of treatment. DEXA reports within the same year of performing ^{18}F-NaF PET/CT scan were evaluated. Bone density values were extracted from the baseline DEXA report to compare the data with semiquantatitive values which have been measured from baseline ^{18}F-NaF PET/CT scans. Based on the World Health Organisation (WHO) criteria, SONIA 2 patients have been classified into three groups according to T-score values. AKU patients who had a T-score -1 or greater were considered as normal, who had a T-score less than -1 and greater than -2.5 as osteopenia, and who had a T-score -2.5 or less as osteoporosis. Lumbar and femoral T-score values were compared with gender and age in Chapter 3. The relationship between ^{18}F-NaF PET/CT semiquantitative values and T-score was investigated in Chapter 3. Lumbar T-score value were correlated with mean lumbar HU_{mean} values and SUV_{max} values, whereas femoral T-score values were correlated with the head of the femur HU_{mean} and SUV_{max} values.

2.7 Semiquantitative measurement for discovertebral unit (DVU)

It was not possible to quantify IVDs because they were too thin and difficult to delineate. Thus, ROI including the IVD was used that included part of bone of the adjacent vertebrae to make it large enough to ensure that the cartilage region was placed within the drawn ROI. However, the measured value was not reflective of the disc alone, and so was referred to as the discovertebral unit (DVU). The concept of DVU delineation is based on covering the region between two horizontal lines at the middle point of two adjacent vertebrae, including the disc and endplates of the two adjacent vertebrae [161]. This term has been used previously in medical reports.

2.7.1 Standardised uptake value (SUV_{max})

Six lumbar discovertebral units (DVUs) from segment T12/L1 to segment L5/S1 were quantified at three consecutive sagittal slices from ^{18}F-NaF PET/CT images in order to assess and detect the extent of disc degradation in all three dimensions.

The following steps were done to evaluate and quantify the lumbar DVUs :

1. Displaying whole body CT, PET and PET/CT images side-by-side in sagittal, coronal and axial plans on one screen for easy viewing.
2. Scrolling through the images and adjusting the three orthogonal views to align with the appropriate spine till the best view of the spine at sagittal, coronal and axial plans is reached which is usually vary between the patients.
3. Placing the cursor over the intersection of the axes crosshairs in any image which will produce a cursor that translates the two axes in unison.
4. Draging the crosshair in to the centre of the spine which will automatically co-regisiter it in the three spine planes.
5. Magnifying the image using the magnifier tool to enhance the disc view.
6. Placing the crosshairs on the coronal plane for each lumbar IVD.
7. In the three sagittal CT images, ROI were drawn for each lumbar level covering the DVU area as shown in Figure 2.4.
8. Copying the same ROI which was drawn the the CT to PET images to measure the SUV_{max}.

Following the spteps above, the SUV_{max} values were generated in the PET image for each ROI. Then the average value for each lumbar vertebral level was performed from the three sagittal sections. This method was used to identify disc degeneration for AKU patients in Chapter 4, and to evaluate the disease progression and treatment response in Chapter 5.

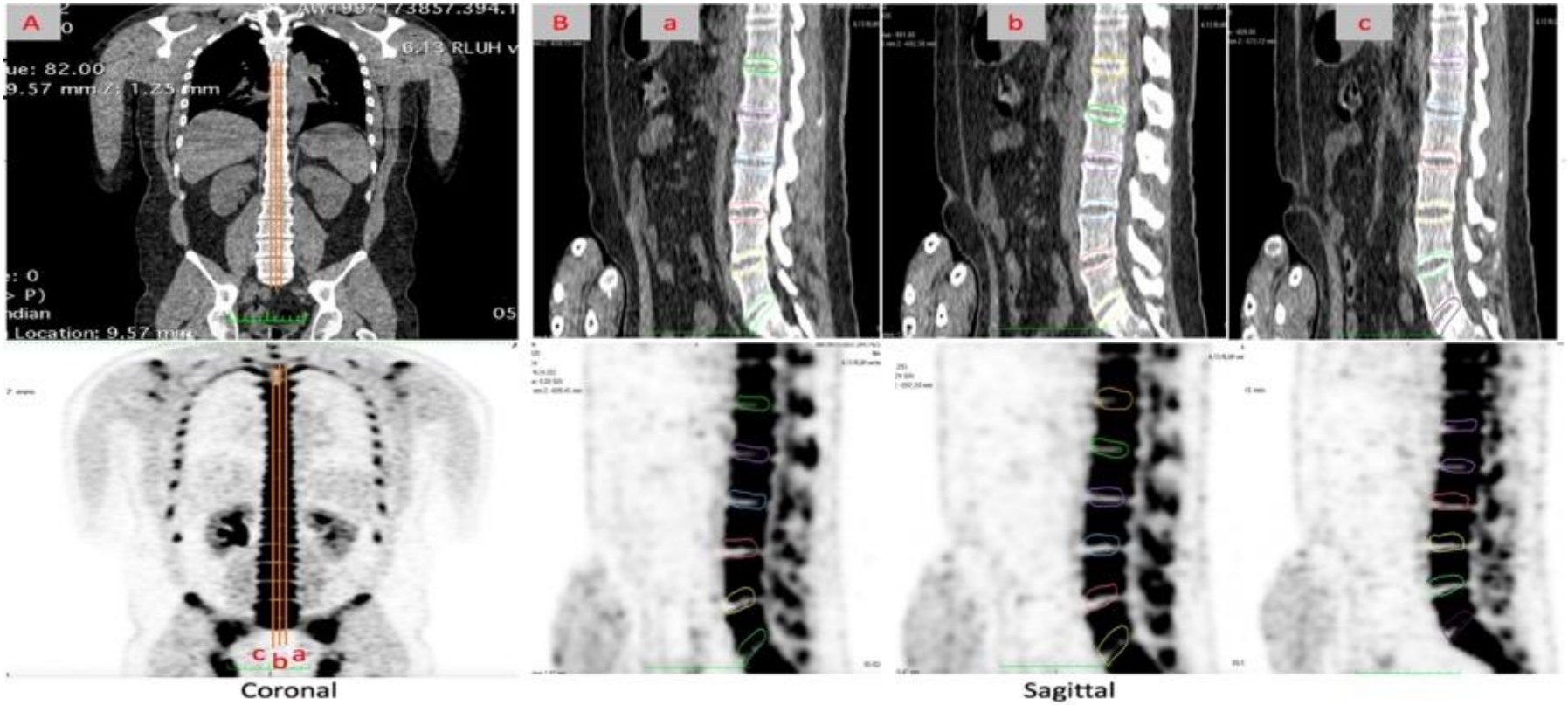

Figure 2.4. ^{18}F-NaF PET/CT for the lower spine.

The images illustrate the semiquantitative measurement method for the lumbar disc region. Upper images show the CT images, and lower images show ^{18}F-NaF PET images. A. coronal section with three different horizontal lines corresponds to the three sagittal sections in image B.

2.7.2 MRI scoring system

A spine MRI was performed for all SONIA 2 patients annually to investigate the changes in spine lesions over the course of treatment and assess the progression of the disease. Baseline MRIs were evaluated and analysed by an MRI consultant radiologist, experienced in musculoskeletal MRI, Dr Alpesh Mistry. Six regions of lumbar discovertebreal unit (DVUs) from segment T12/L1 to segment L5/S1 were scored using a validated MRI scoring system. The relationship between disc degeneration identified from MRI and ^{18}F-NaF PET/CT scan was investigated in Chapter 4.

2.7.2.1 MR imaging protocol

The MR images of the spine were performed on a 1-T scanner (Siemens Impact Expert; Siemens Medical Systems, Erlangen, Germany). The standard MR imaging protocol for degenerative disc disease included sagittal T1-weighted spin-echo (repetition time [TR] 700 msec/echo time [TE] 12 msec) and T2-weighted FSE (TR 5000 msec/TE 130 msec) images including the following parameters: matrix, 512x225; FOV, 225x300 mm; slice thickness, 4 mm; interslice gap, 0.8 mm; number of excitations, 4

T2-weighted images were used to allow a thorough view of disc anatomy. The T2-weighted sagittal images were utilised to evaluate the lumbar vertebral bodies, lumbar IVDs, the ligaments, facet joints, spinal canal and spinal cord and intervertebral foramen. Also, the STIR images were usually performed in the sagittal plane to detect bone marrow changes.

2.7.2.2 Pfirrmann scoring system

Various MRI scoring systems are available in the literature to classify disc degeneration. The Pfirrmann scoring system is one of the most common methods for lumbar disc degeneration. In this thesis, the Pfirrmann scoring system was selected by an MRI consultant to quantify disc degeneration for its reliability and validity. Lumbar DVUs were scored using a modified eight-level MRI based Pfirrmann scoring system. Table 2.2 describes the pertinent features of each Pfirrmann grade using T2-weighted sagittal plane. The reference images comprise 24 images, which reflect the changes in

the disc at each grade. The eight scores represent a progression of the disc degeneration from grade 1, which corresponds to healthy disc structure, to grade 8 for the end-stage of disc degeneration. The MR images were assessed and scored using a reference sheet of the Pfirrmann grading system. Figure 2.2 shows the images which were used as a reference panel.

Table 2.2. The eight-level grading scale of lumbar disc degeneration on sagittal MRI (T2-weighted) proposed by modified from five Pfirrmann grading system.

Table from [90,94].

Grade	Nucleus Structure	The distinction between inner and outer fibers	Nucleus Signal intensity	Height of IVD
1	Uniform, Homogeneous, bright white	Clear distinct	Hyperintense, isointense to cerebrospinal fluid	Normal
2	Homogeneous with or without horizontal bands	Clear distinct	Hyperintense, less than cerebrospinal fluid higher than presacral fat Or ± hypointense intranuclear cleft	Normal
3	Inhomogeneous, grey	Clear distinct	Hyperintense though less than fat	Normal
4	Inhomogeneous, grey to black	Unclear distinct	Intermediate, slightly higher than outer fibers of anulus	Normal
5	Inhomogeneous, grey to black	Lost distinct	Hypointense, equal to outer fibers of anulus	Normal to moderately decreased
6	Inhomogeneous, black	Lost distinct	Hypointense	Normal to moderately decreased (<30% reduction in disc height)
7	Inhomogeneous, black	Lost distinct	Hypointense	Moderately decreased (30% - 60% reduction in disc height)
8	Inhomogeneous, black	Lost distinct	Hypointense	Collapsed disc space (> 60% reduction in disc height)

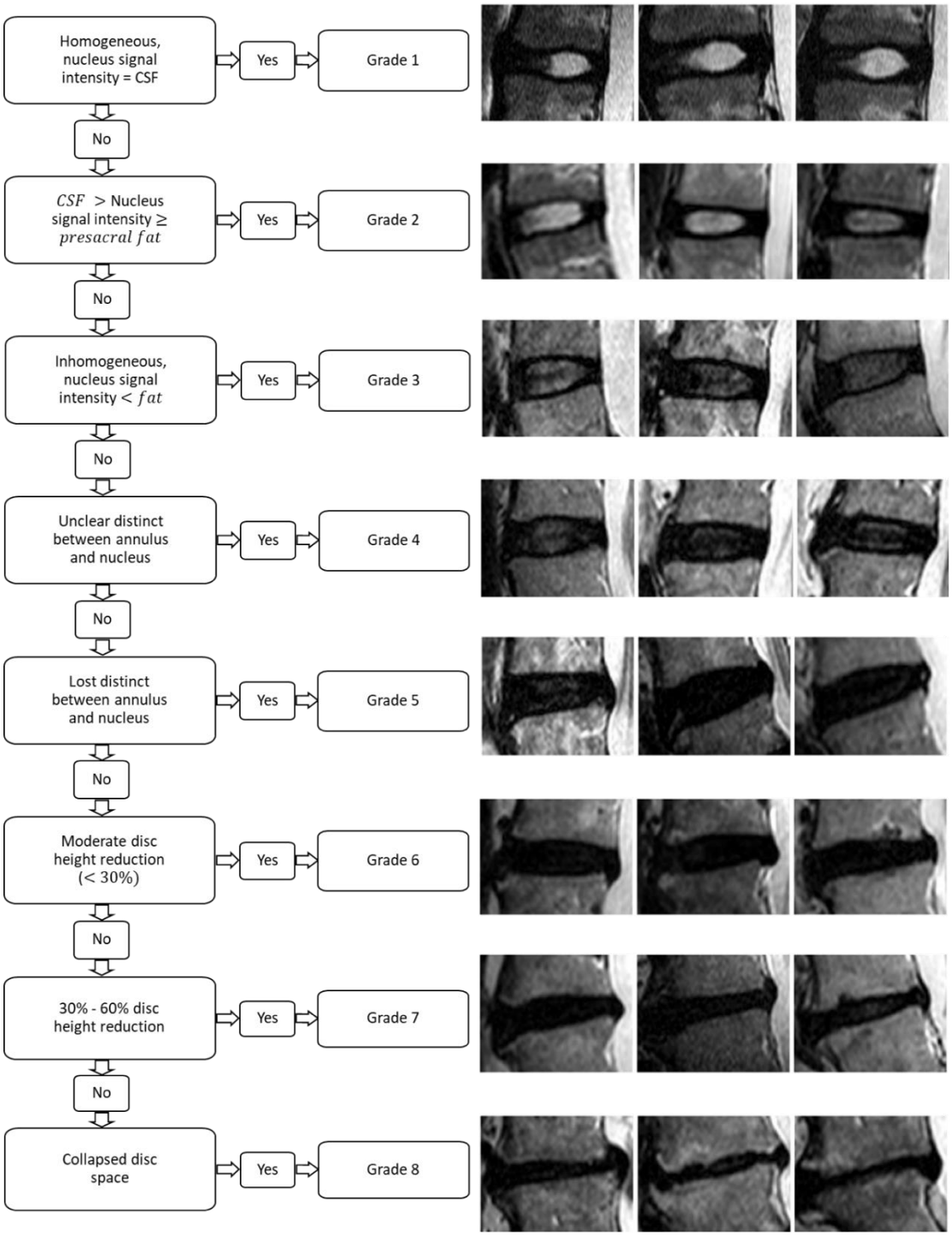

Figure 2.5 Algorithm for the modified Pfirrmann grading system for the assessment of lumbar disc degeneration, and the images of IVDs at each level.

Images cited from [89]. The image reference panel shows the eight-level modified grading system from three sagittal MRI T2-weighted images reflecting the inherent variability across each level. Table 2.2 describes the pertinent features at each disc degeneration level.

2.8 Semiquantitative measurement for cardiovascular arteries

Many SONIA 2 patients had dense areas in CT images and abnormal distributions of ^{18}F-NaF tracer in the PET images within the heart area was noted. A cross-sectional study was carried out for the baseline ^{18}F-NaF PET/CT data to capture the complexities of the phenomenon and allow a deeper understanding of cardiac involvements in AKU patients.

The main coronary arteries were visually recognised in CT images. The CT image was evaluated for abnormal focal density in the cardiac area. CT density for the calcified vessels was identified having high attenuation coefficient values. ^{18}F-NaF PET images were evaluated for increased bone radiotracer uptake in the main coronary arteries area.

In this thesis, the calcification of the main coronary and aortic artery was quantified in order to investigate the cardiac calcification in AKU patients. What follows is the description of the cardiovascular measurement method, which was used in Chapter 6.

2.8.1 Semiquantitative measurement for main coronary arteries

For the coronary arteries analysis, the four main branches of coronary arteries, including left coronary artery-left main stem (LCA), left anterior descending artery (LAD), left circumflex artery (LCA), and right coronary artery (RCA), were evaluated and quantified from the baseline ^{18}F-NaF PET/CT images for SONIA 2 participants.

The following steps were done to evaluate and quantify the main coronary arteries:

1. Displaying whole body CT, PET and PET/CT images side-by-side in sagittal, coronal and axial plans on one screen for easy viewing.
2. Scrolling through the images and adjusting the three orthogonal views to align with the appropriate view of the heart at sagittal, coronal and axial plans which is usually vary between the patients.

3. Placing the cursor over the intersection of the axes crosshairs at the centre of the heart in the coronal section which will produce a cursor that translates the two axes in unison.
4. Magnifying the image using the magnifier tool to enhance the the view of the main arteries.
5. Placing an individual circular ROI on axial CT slices in each arterial region over the four main coronary branches, as shown in Figure 2.6.
6. The HU_{mean} will be generated from the main coronary regions.
7. Copying the same ROI which was drawn in CT image to the PET image to measure mean, maximum and minimum SUV values (see Figure 2.6). It could be challenging to identify the exact border of cardiac arteries on non-contrast ^{18}F-NaF PET/CT images, so measuring the mean SUV value would not present the accurate uptake values. Because of that, measuring maximum SUV values for each ROI was the best option to choose in order to identify the active cardiovascular lesion in PET images and to predict future heart events. SUV_{max} from each coronary artery was generated individually.
8. To precisely evaluate the ^{18}F-NaF uptake at the arteries, it would be essential to extract the background ^{18}F-NaF activity from the blood pool, which could influence the arterial SUV measurements. To do that, blood pool SUV must be measured by placing three circular ROIs at the centre of inferior vena cava (IVC) and superior vena cava (SVC) on axial images.
9. Generating the maximum target to background ratio (TBR_{max}) for each ROI. TBR is also referred to us as tissue to background ratio or tumour to background ratio in the literature. TBR_{max} is calculated by dividing the SUV_{max} for each ROI with an averaged SUV_{mean} of the blood pool [148,150], see the equation below.

$$TBRmax = \frac{\text{SUVmax (artery)}}{SUVmean\ (blood\ pool)}$$

2.8.2 Semiquantitative measurement for aortic arteries

Aortic calcification was assessed by quantifying the ascending aorta (AA) and descending aorta (DA) from ^{18}F-NaF PET/CT images. The following steps were done to evaluate and quantify the aorta:

1. Displaying whole body CT, PET and PET/CT images side-by-side in sagittal, coronal and axial plans on one screen for easy viewing.
2. Scrolling through the images and adjusting the three orthogonal views to align with the appropriate view of the aorta at sagittal, coronal and axial plans which is usually vary between the patients.
3. Magnifying the image using the magnifier tool to enhance the aotra view.
4. Drawing an individual circular ROI on CT slices covering the maximal area just beyond the discernible border of the aortic artery at the axial CT slices.
5. The same principle, which was applied for coronary artery measurement (in section 2.8), was applied to generate HU_{mean}, SUV_{max} and TBR_{max} form ^{18}F-NaF PET/CT images for AA and DA (see Figure 2.7).

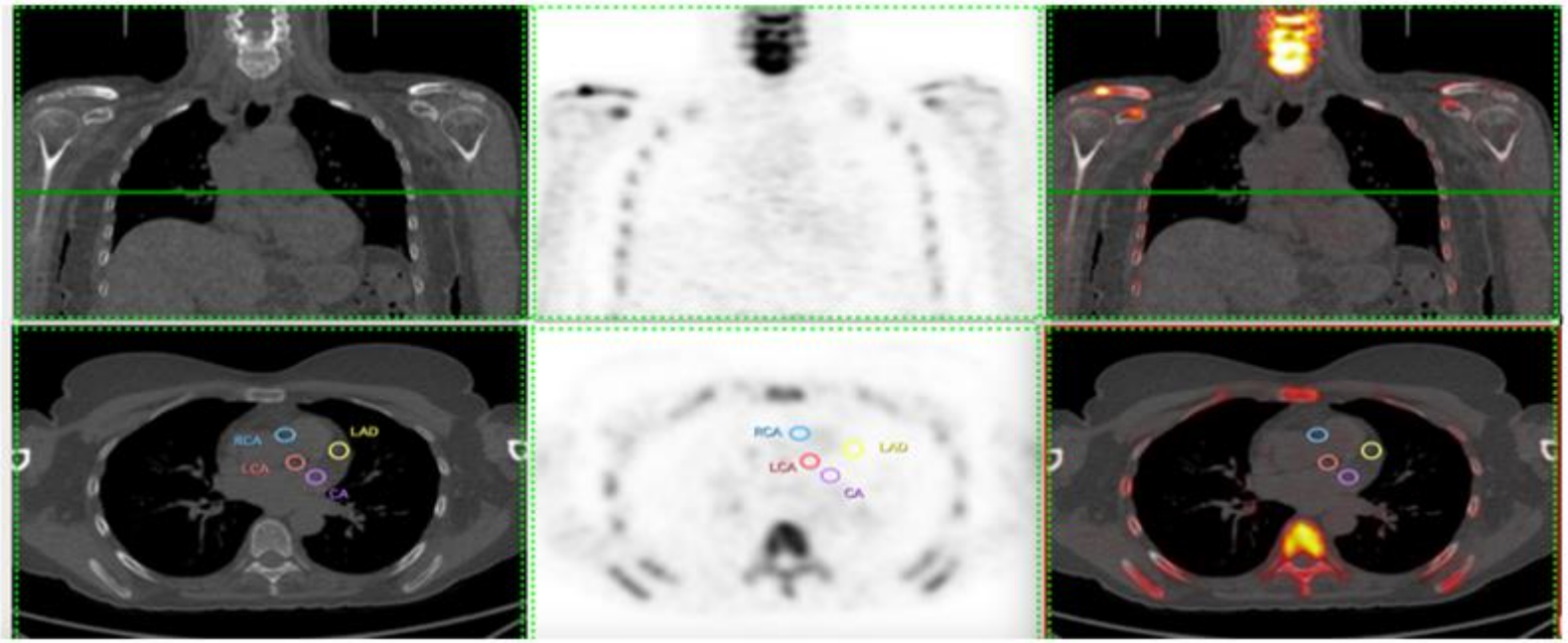

Figure 2.6. ^{18}F-NaF PET/CT scan of the chest illustrating the methods of determining the HU values from CT scan and SUV from PET scan for the main coronary arteries using a manual circle region of interest function.

The left panel shows CT images, middle ^{18}F-NaF PET image and right fused ^{18}F-NaF PET/CT image. The upper panel shows a coronal ^{18}F-NaF PET/CT slice of the chest. The lower panel shows an axial CT, PET, and fused ^{18}F-NaF PET/CT slice of the heart showing the main coronary arteries. Blue, RCA: right coronary artery; yellow, LAD: left anterior descending artery; red, LCA: left coronary artery-left main stem; purple, CA: left circumflex artery. The ROI was first drawn in the CT images to determine HU_{mean} was then copied to ^{18}F-NaF PET images to determine SUV_{max}. Horos imaging software automatically calculates the HU_{mean} values and SUV_{max} for each ROI.

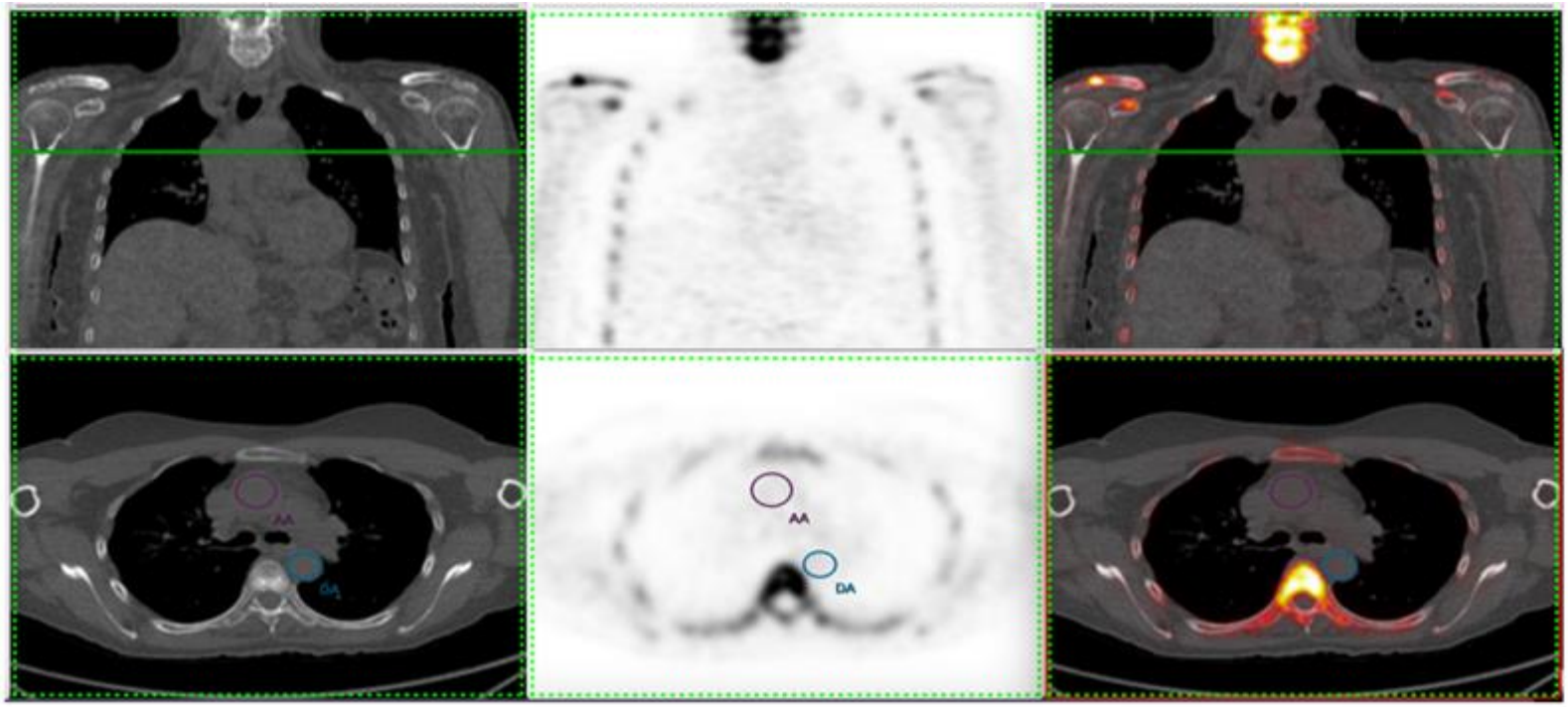

Figure 2.7. ^{18}F-NaF PET/CT scan of the chest illustrating the methods of determining the Hounsfield unit (HU) values from CT scan and SUV from PET scan for ascending aorta and descending aorta using a manual circle region of interest function.

The left panel shows CT images, middle PET image and right fused ^{18}F-NaF PET/CT image. The upper panel shows a coronal PET/CT slice of the chest. Lower panel shows CT, PET, and fused ^{18}F-NaF PET/CT axial slices of the heart, showing the ascending aorta and descending aorta. Blue, DA: descending aorta, and purple, AA: ascending aorta. The ROI was first drawn in the CT image to determine $HU_{mean,}$ then copied to PET images to determine SUV_{max}. Horos imaging software automatically calculates the HU_{mean} and SUV_{max} values for each ROI.

2.9 Statistical analysis

Descriptive data were generated for all variables. Statistical analysis and data management were performed using IBM SPSS Statistics software (version 24.0, Armonk, NY). Parametric tests were used to analyse data with a normal distribution. Non-parametric tests were used to compare data that was not normally distributed. Linear and non-linear regression were carried out to analyse numerical data and examine the linear relationship between two or more independent variables. Polynomial regression was applied, seeking for better correlation between age and the measured quantitative values. The data were presented as mean ± standard deviation (SD), minimum, maximum, median and percentage.

A Pearson correlation analysis was conducted to assess the relationship between all variables. A P value < 0.01 was considered strongly significant and $P < 0.05$ was considered significant. Pearson correlation was carried out to assess the correlation between the two variables. A correlation R-value of +1 is considered a perfect positive linear relationship between variables, -1 considered a perfect negative linear relationship and 0 considered no relationship.

Independent sample t-tests were used to compare the means values of two independent groups regarding the same variable to assess the statistically different variables, such as the difference between genders. The differences in variable values between the age groups were compared using one-way analysis of variance (ANOVA).

Statistical analysis comparing treated and control SONIA 2 groups was undertaken by Matt Gernall, medical statistician, Department of Liverpool Clinical Trials Centre LCTC. Because of missing values, data were analysed using the Kruskal-Wallis test for Chapter 5. In that chapter, a Kruskal-Wallis test was used to investigate the changes between the visits; pre-test, during-test, and post-test. A Kruskal-Wallis test is also known as one-way ANOVA on ranks. A Kruskal-Wallis test is a rank-based non-parametric test analog to the independent samples that is used to investigate whether there are statistically significant differences between two or more groups on the continuous dependent variable. Kruskal-Wallis test is an alternative test to the one-

way ANOVA and an extension of the Mann-Whitney U test, which compares more than two independent groups. The result of these tests provided P-values. A P-value < 0.01 was considered strongly significant, and P-value < 0.05 was deemed to be significant.

3 Cross-sectional study of bone involvement at baseline in alkaptonuria patients from the SONIA 2 study using ^{18}F-NaF PET/CT bone scans and DEXA in the lumbar spine and femoral head sites

3.1 Introduction

This part of the thesis proposes a molecular imaging methodology which allows better quantitative assessment of regional bone formation for patients with AKU using ^{18}F-NaF PET/CT scans. The primary aim of this study is to assess bone involvement in the lumbar spine and hip regions for AKU patients by measuring Hounsfield units (HU_{mean}) from CT and standardised uptake value (SUV_{max}) from ^{18}F-NaF PET scans. The secondary aim is to assess the impact of some biological factors such as gender and age in these semiquantitative values for AKU patients. This study also set out to determine if SUV_{max} and HU_{mean} obtained from PET/CT system correlate with each other and/or correlate with bone mineral density values measured from DEXA scans.

This chapter is subdivided into three sections. The first section identifies and quantifies bone involvements from CT images. The second section identifies and quantifies bone involvements from ^{18}F-NaF PET images. The third section investigates the relationship between semiquantitative radiographic values measured from different imaging modalities.

The diagnosis of ochronotic arthropathy may be technically and clinically challenging, especially in its early stages; however, it is an essential aspect to understand the pathophysiology of this rare metabolic disease. The spine and large joints have been found to be the most affected sites in patients with AKU. Several cases have required physical therapy and multiple joint replacements [10,12,64,65,162].

Radiographic imaging modalities utilised for evaluating ochronotic arthropathy must be sensitive in order to detect early bone and joint involvement. ^{18}F-NaF PET/CT scan is a promising imaging approach which has been widely employed for identifying early bone and joint abnormalities in various arthropathic conditions [76,101,103,131,163].

^{18}F-NaF is a positron bone radiotracer which is rapidly cleared from the plasma and has a high bone affinity resulting in better tissue-to-background ratio [108]. On the surface of the bone matrix where hydroxyapatite crystals are concentrated, ^{18}F-ion exchanges rapidly with the hydroxyl groups forming fluoroapatite. Sixty minutes after

injection, most of the ^{18}F-NaF administration dose deposits in areas of rich osteoblastic activity in the newly mineralising bone [55].

Increased ^{18}F-NaF uptake in PET images reflects abnormal manifestations, which can be detected *in vivo* by quantitative and qualitative measurement methods. Visual inspection of a positive lesion in a PET/CT image mainly depends on the opinion of the nuclear medicine specialist; therefore, it is a subjective method. Development of a non-subjective method that demarcated the boundary between the normal distribution of radiotracer and increased tracer uptake in the skeleton is clinically more needed. Standardised uptake value (SUV) is one of the simplest and reliable PET semiquantitative measurements that can be used to quantify active abnormal bone lesions throughout the whole skeleton from non-dynamic ^{18}F-NaF PET scans [101,103,131,163]. The accumulation of ^{18}F-NaF in the skeleton could be attributed to several factors such as regional osteoblastic activity, exposed surface area, blood flow, and renal function [107,108].

Over the few decades, most of the PET scanners have been combined with CT offering better functional and anatomical information. Although CT scanning is mainly acquired during PET imaging for lesion localisation purposes, valuable information can be extracted from CT images. Clinically, DEXA is a gold standard method for diagnosing osteoporosis by measuring bone mineral density value (T-score). As found previously in many studies, diagnostic CT scans shows the ability to estimate bone density, and predict fracture risk [81,83–85]. In this study, CT data were used to determine bone density in AKU patients by measuring HU without additional radiation or costs.

As part of the SONIA 2 clinical trial, whole-body ^{18}F-NaF PET/CT and DEXA scans were carried out annually at the Royal Liverpool University Hospital for each participant to evaluate bone and joint involvements (see section 2.2.1). It is hoped that this study will contribute to a deeper understanding of the disease state and progression in AKU patients.

3.2 Design of study

3.2.1 Patient group

In this study, a total of 39 AKU patients including 24 males and 15 females were analysed, with a mean age of 50.8 ± 10.8 years (range, 30 - 68-years old) at the beginning of the trial. No significant age differences were found between male and female groups (see Table 3.1). Patients with spinal surgery were excluded from the lumbar spine analysis, and those with hip replacement were excluded from the hip analysis. Although patient number 16 had one lumbar disc implant placed between T12 and L1, this patient was included by using the data from L2-L5 segments instead of L1-L5. In this chapter, 2 SONIA 2 patients were excluded from this study; patient number 36 had multilevel spinal surgery, so that it was difficult to quantify the lumbar bodies. Patient number 38, a 44-year-old female, had abnormally high bone density values in DEXA report, indicating a degenerative disorder, so she was excluded from this chapter analysis. On the other hand, patients who had at least one femoral replacement were excluded from hip measurements.

The patients were stratified by gender and decade of life, forming two and four groups, respectively, as shown in

Table 3.2. In this chapter, 7 patients (17.94%) were between 30 and 39 years old, 12 (30.77%) were between 40 and 49 years old, 10 (25.64%) were between 50 and 59 years old, and 10 (25.64%) were above 60 years old.

Table 3.1. Demographic baseline characteristics of AKU patients who were part of the SONIA 2 clinical trial.

Age of the patients displayed as mean ± SD, minimum and maximum.

Statistic	Patients no. (%)	Age ± SD years	Age range
Total	39	50.8 ± 10.8	30 – 68
Male	24 (61.5%)	51 ± 10	30 – 67
Female	15 (38.5%)	49 ± 12	30 – 68

Table 3.2. The number of AKU patients at the beginning of the SONIA 2 clinical trial classified by gender and age.

The participants were stratified by the decade of life into four age groups 30-39, 40-49, 50-59 and ≥ 60 years old.

Age group	Gender	Patient no.
30 – 39 years old	Total	7
	Male	3
	Female	4
40 49 years old	Total	12
	Male	8
	Female	4
50 – 59 years old	Total	10
	Male	6
	Female	4
≥ 60 years old	Total	10
	Male	7
	Female	3

3.2.2 Image analysis

Baseline data for SONIA 2 patients who had undergone ^{18}F-NaF PET/CT between 2014 and 2015 were retrospectively reviewed (see section 2.2.1). ^{18}F-NaF PET/CT images were viewed using Hermes hybrid software (see section 2.4.1.1). The ^{18}F-NaF PET/CT images were evaluated on a 3D fusion Hermes software imaging station. HU was measured from CT images from the lumbar spine and hip sites. For the lumbar spine measurement, the HU_{mean} was obtained from each lumbar vertebral body (L1-L5) at three different locations from axial CT slices by drawing the largest possible elliptical ROI covering the trabecular region (see a Figure 2.2). The average value of HU_{mean} for each lumbar level was generated. For the hip measurement, the HU_{mean} was obtained from the heads of the femurs, a circular ROI was drawn at the axial CT slice, and the HU generated from the right and the left head of the femur (see Figure 2.3). All the ROIs which obtained from the CT images were correlated to PET images to measure maximum SUV (see section 2.5.1.2). The average lower spine and hip measurement value for each patient was also generated.

3.2.3 Correlation

DEXA reports within the same year of performing the ^{18}F-NaF PET/CT scan were compared. Among the enrolled patients, 37 patients were included in the comparison section. T-score values from the lumbar spine (L1-L4) were correlated with HU_{mean} and SUV_{max} values of lumbar vertebrae measurements (L1-L4), and T-score value from the femoral region was correlated with HU_{mean} and SUV_{max} values of the head of the femur.

The differences in the measured quantitative values between gender and age were investigated using the Pearson correlation coefficient and multiple linear regression. Polynomial regression was also applied, seeking for better correlation between age and the measured values. The differences between age groups were investigated using one-way ANOVA. Correlations between the semiquantitative values were evaluated also using the Pearson correlation coefficient.

3.3 Results

3.3.1 HU mean measurements

The first section aimed to measure attenuation coefficients of bone regions from CT images at the lumbar spine and hip sites in order to estimate bone density from AKU patients, without adding extra radiation to the patients. All the measured data are found in the appendix section (Table 9.1), displaying the mean, minimum, and maximum HU values at each region of interest (ROIs).

3.3.1.1 Lumbar vertebrae body

The results of the mean HU value at each lumbar vertebrae level for 39 SONIA 2 patients are shown in Figure 3.1. The average HU_{mean} was obtained from the three levels of each lumbar vertebrae (L1, L2, L3, L4, and L5). The mean HU was 139.94 ± 60.06 at L1, 141.22 ± 63.85 at L2, 133.06 ± 53.67 at L3, 146.04 ± 61.92 at L4, and 182.41 ± 64.95 at L5 (see Table 9.1 in the appendix). Closer inspection of the data

show that the mean HU value measured at the lowest lumbar vertebrae body (L5) was statistically higher than the rest of lumbar vertebrae bodies (R = 0.726, R = 0.720, R = 0.723, R = 0.812, respectively and $P < 0.001$).

Figure 3.2 shows some examples of bone involvements in the lumbar spine in AKU cases, which were identified from spine CT images. The table below the images summarises the HU values measured from CT images for those patients. Closer inspection of the cases show that in normal cases, uniform high intensity area was noted throughout the skeleton in CT images, indicating normal bone density. In contrast, in abnormal cases, low bone intensity was noted in the skeleton indicating low bone density and weak and fragile bone lesions.

3.3.1.1.1 Lumbar vertebrae body HU_{mean} values and gender

Figure 3.1 and Table 9.1 (appendix) compare the mean HU values across the lumbar vertebrae (L1, L2, L3, L4, and L5) for each gender group. The mean HU value across L1 to L5 was 145.46 ± 54.33 (range 29.86 - 238.78) for males and 152.4 ± 59.77 (range 25.88- 221.05) for females. The mean HU was 138.25 ± 57.00 at L1, 133.02 ± 5 4.66 at L2, 130.05 ± 52.56 at L3, 145.31 ± 63.56 at L4, and 183.87 ± 69.80 at L5 for the male patients. While the mean HU was 142.52 ± 66.47 at L1, 154.33 ± 76.54 at L2, 137.87 ± 56.91 at L3, 147.22 ± 61.37 at L4, and 180.08 ± 58.62 at L5 for the female patients. The measured HU values across the lumbar vertebrae were very similar in both genders. The female patients had slightly higher HU_{mean} values across the lumbar vertebrae compared to the male patients. Independent t-tests were used to analyse the relationship between HU values and gender at each lumbar level. No statistically significant differences in the mean HU values between the two groups was found at any lumbar vertebrae level ($P > 0.05$)

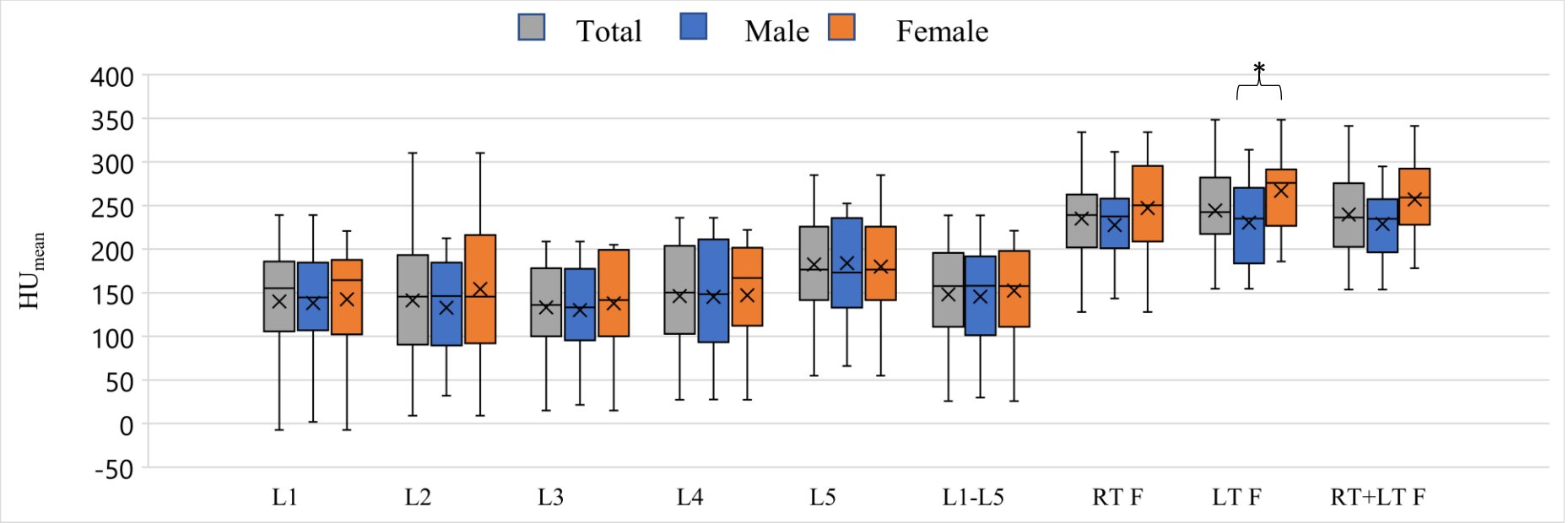

Figure 3.1. HU_{mean} obtained from CT scan at the lower spine and femoral sites for 39 AKU patients who were part of SONIA 2 clinical trial stratified by gender.

The results show the analysis of the baseline CT data for 24 males and 15 females, which have been measured from each lumbar vertebrae level (L1, L2, L3, L4, and L5), average lumbar levels (L1-L5), right femoral head (RTF), left femoral head (LTF), average femoral head (RT+LT F) for male and female patients. Table 9.1 (appendix) shows the statistical correlation between gender at all ROI. Independent t-tests revealed no statistically significant differences in HU values at L1, L2, L3, L4, L5, L1-L5, RTF nor RT+LF F between males and females (P-value was 0.83, 0.32, 0.66, 0.93, 0.86, 0.68, 0.23, and 0.09, respectively). A significant difference was found between male and female groups at the LTF site only ($P = 0.04$). *Groups which showed significant difference ($P < 0.05$). In box and whisker, x is the mean value, and the line is the median.

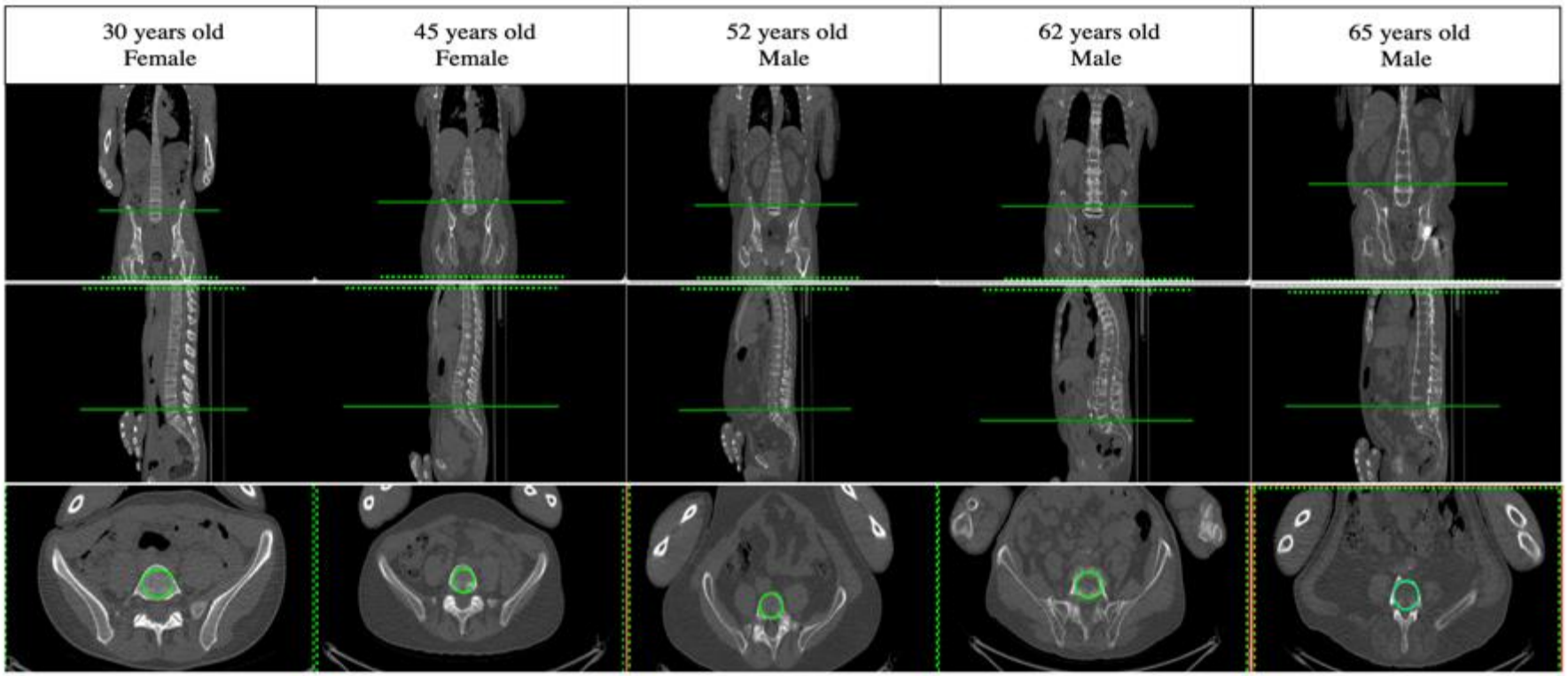

L1	186	157	117	141	2
L2	164	146	90	182	32
L3	199	152	85	130	22
L4	222	144	74	166	28
L5	220	190	122	184	66
L1-L5	198	158	98	161	30

Figure 3.2. Coronal, sagittal, and axial spine CT images for AKU patients.

Age and gender of the each patient display above each image. The table below illustrates HU_{mean} values for all lumbar levels.

3.3.1.1.2 Lumbar vertebrae body HU_{mean} values and age

The relationship between HU_{mean} and age was tested. The mean lumbar vertebrae (L1, L2, L3, L4, and L5) HU_{mean} was plotted against age for all patients, as shown in Figure 3.3. A clear reduction in HU_{mean} measurements with age was noted in AKU patients. Multiple linear regression was applied to demonstrate the trend in HU_{mean} at each lumbar level with age. On average, age was seen to have a statistically significant negative effect across the all lumbar vertebrae HU L1-L5 values ($R = -0.545$, $R = -0.588$, $R = -0.624$, $R = -0.646$, $R = -0.489$; all $P < 0.05$). Using polynomial regression, the correlation coefficient was not substantially improved (see Table 9.2 in the appendix).

The average HU_{mean} values measured from all lumbar ROI were stratified into four age groups, and subgroup analysis was performed, as shown in Figure 3.4, and Table 9.3 (appendix). The average HU_{mean} for L1-L5 was 181.95 ± 26.28 for 30-39 age group patients, 177.59 ± 45.9 for 40-49 age group patients, 142.44 ± 48 for 50-59 age group patients and 94.8 ± 50.27 for ≥ 60 years old patients. The youngest age group patients were shown to have the highest HU_{mean} values in most of the lumbar vertebrae levels (L1, L2, L3 and L4) and the oldest age group patients were shown to have the lowest HU_{mean} values. For all lumbar vertebral levels, the mean HU_{mean} values decreased consistently by increasing decade of life, ranging from 181.95 HU_{mean} in the 3rd decade of life to 94.8 HU_{mean} in the 6th decade of life and above. Looking at Figure 3.4, it is apparent that the mean HU_{mean} value in the average vertebral levels changed slightly from the 3rd to the 4th decade of life, and from the 4th to the 5th decade of life. Subgroup analysis using one-way ANOVA revealed that the differences were not statistically significant (all $P > 0.05$). Statistically, there was a significant difference in the average lumbar levels (L1-L5) between the 50s and 60s age groups only ($P = 0.045$). Interestingly, in the L5 level, HU_{mean} increased from the 30s to 40s age groups, then decreased; however, the differences were not statistically significant ($P > 0.05$). This observation was only noted at the lowest lumbar level.

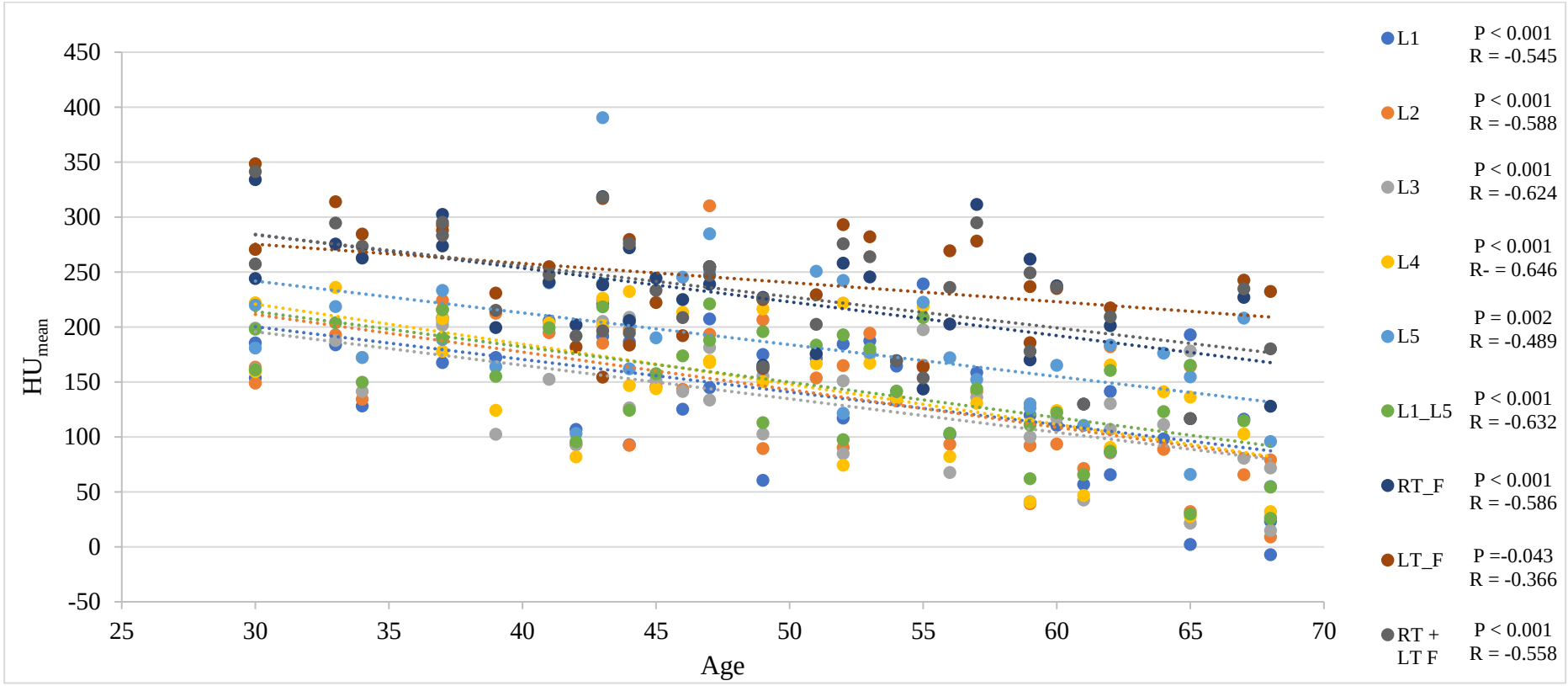

Figure 3.3. Scatter plots illustrating the correlation between age and HU_{mean} obtained from baseline CT scan at the lower spine and femoral sites for 39 AKU patients who were part of SONIA 2 clinical trial.

The results display HU_{mean} of each lumbar vertebrae level (L1, L2, L3, L4, and L5), average lumbar levels (L1-L5), right femoral head (RT_F), left femoral head (LT_F), average femoral head (RT+LT F) in individual AKU cases with age. Multiple linear regression analysis identified a negative statistically significant correlation between age and HU_{mean} values of lumbar vertebrae and head of the femur in AKU cases (all had $P < 0.05$).

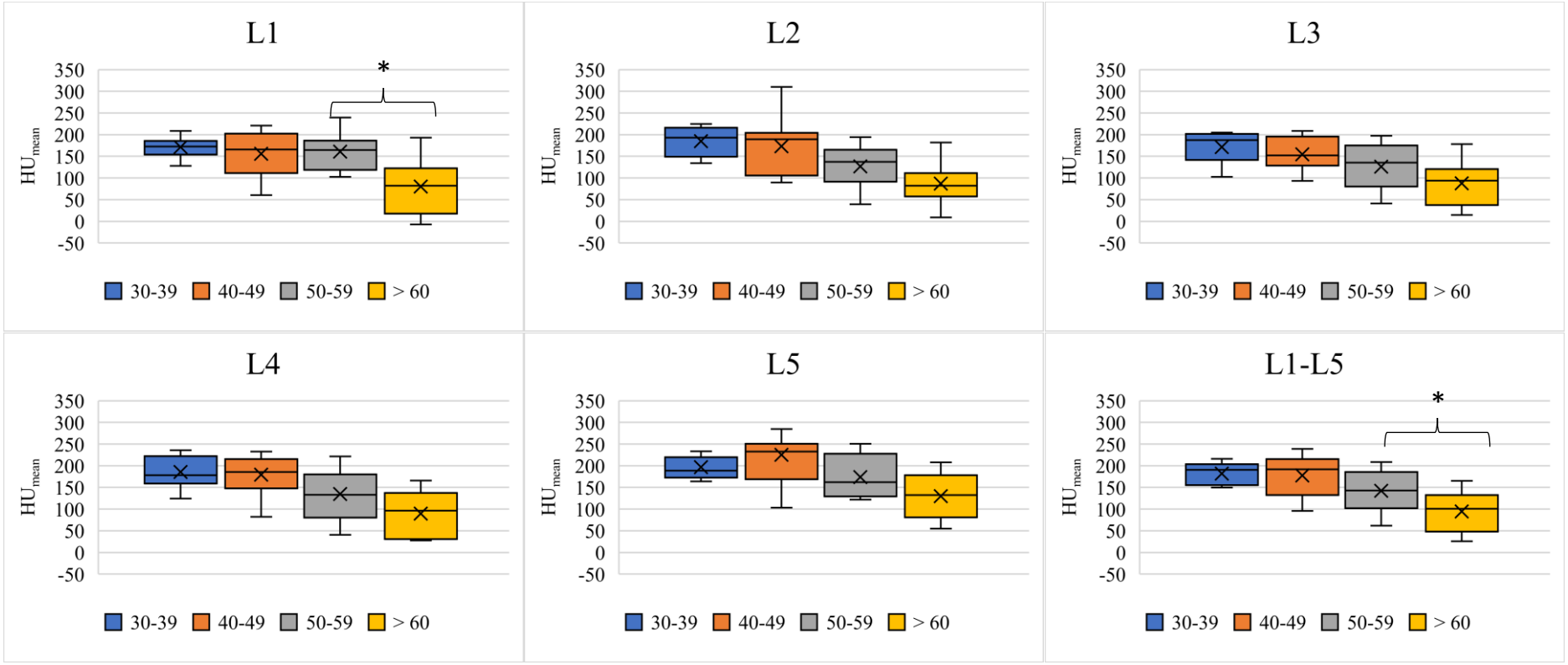

Figure 3.4. HU_{mean} for all lumbar vertebrae level among four decadal age groups measured from baseline CT scan for AKU patients who were part of SONIA 2 clinical trial.

Table 9.3 (appendix) shows the lumbar levels and four age groups which indicated a statistically significant difference between subgroup analyses. Lumbar HU_{mean} values show decreases as age increases. Statistically, there was a significant difference in the average L1 value between the 50s and 60s ($P = 0.005$) and in the average lumbar levels (L1-L5) between the 50s and 60s age groups ($P = 0.045$) only. *Groups which showed significant difference ($P < 0.05$). In box and whisker, x is the mean value, and the line is the median.

3.3.1.2 Head of the femur

Figure 3.1 displays the results of HU measurements at the head of the femurs for AKU patients. All the head of the femur data is found in Table 9.1 and Table 9.3 (appendix). The average head of the femur density measurement for all AKU patients was 240.00 ± 50.20 HU and ranged from 154.00 to 341.30 HU. The mean HU was 235.08 ± 59.78 at the head of the right femur, and ranged from 127.91 to 334.16; 244.42 ± 48.98 at the head of the left femur, and ranged from 154.5 to 348.44. Figure 3.1 shows the differences in HU value between right and left femoral sides. From this data, it is evident that the HU values of the right and left head of the femur was similar with no significant differences. On the other hand, as can be seen in the Figure 3.1, the femoral HU values were significantly higher than the lumbar HU values (R = 0.516, P = 0.002).

Figure 3.5 shows hip CT images for the same AKU patients which were decribed previously in the spine section (section 3.3.1.1). Likewise, in the spine area, uniform high intensity regions with high HU values were detected in femoral heads for young patients, indicating dense bone area, while the low intensity regions with low HU values were detected in the elderly patients indicating low bone density area.

3.3.1.2.1 Head of the femur HU_{mean} values and gender

Figure 3.1 demonstrates the mean HU_{mean} measured at the head of the femur in males and females. The mean head of femur HU_{mean} value was 229.00 ± 52.07 and ranged from 154.00 to 295.00 for the male patients and 257.00 ± 51.08, and ranged from 178.00 to 341.00 for female patients. The head of the femur HU_{mean} was 227.55 ± 52.54 at the right side and 311.52 ± 143.8 at the left side for males, while it was 247.02 ± 59.25 at righ side and 334.16 ± 127.91 at left side for females. There was no statistically significant difference between male and female group on the right side, but there was a statistical difference on the left sideHead of the femur HU_{mean} values and age

The mean head of femur HU_{mean} was plotted against age for all AKU patient in Figure 3.3. As noted in the lumbar vertebrae section, a noticeable trend demonstrating an apparent reduction in femur HU measurements with age in AKU patients was

observed. Multiple linear regression reflects the trend in HU_{mean} in the femoral region with age. Age had a statistically significant effect on the average head of femur HU_{mean} values ($R = -0.558$, $P < 0.05$).

As shown in Figure 3.6 and Table 9.3 (appendix), the average HU_{mean} for the head of the femur was 280.05 ± 38.68 for 30-39 age group patients, 229.83 ± 42.36 for 40-49 age group patients, 224.77 ± 50.71 for 50-59 age group patients and 184.46 ± 51.85 for ≥ 60 years old patients. On average, the youngest age group patients were noted to have the highest mean HU values in the head of the femur, and the oldest age group patients were observed to have the lowest HU values. The mean HU values decreased by age in the femoral area. Statistically, there was a significant difference in the average head of femur values between the 30s and 40s age groups only ($P = 0.02$). No statistically significant differences between the 40s and 50s age group or between the 50s and 60s age group were noted ($P = 0.806$ and $P = 0.159$, respectively). Separating out male and female findings indicates that there were very little changes in femoral HU_{mean} values for AKU male subjects between the age groups, while femoral HU_{mean} values for female subjects decreased by age from 30s to the 60s age groups, as shown in Figure 3.7.

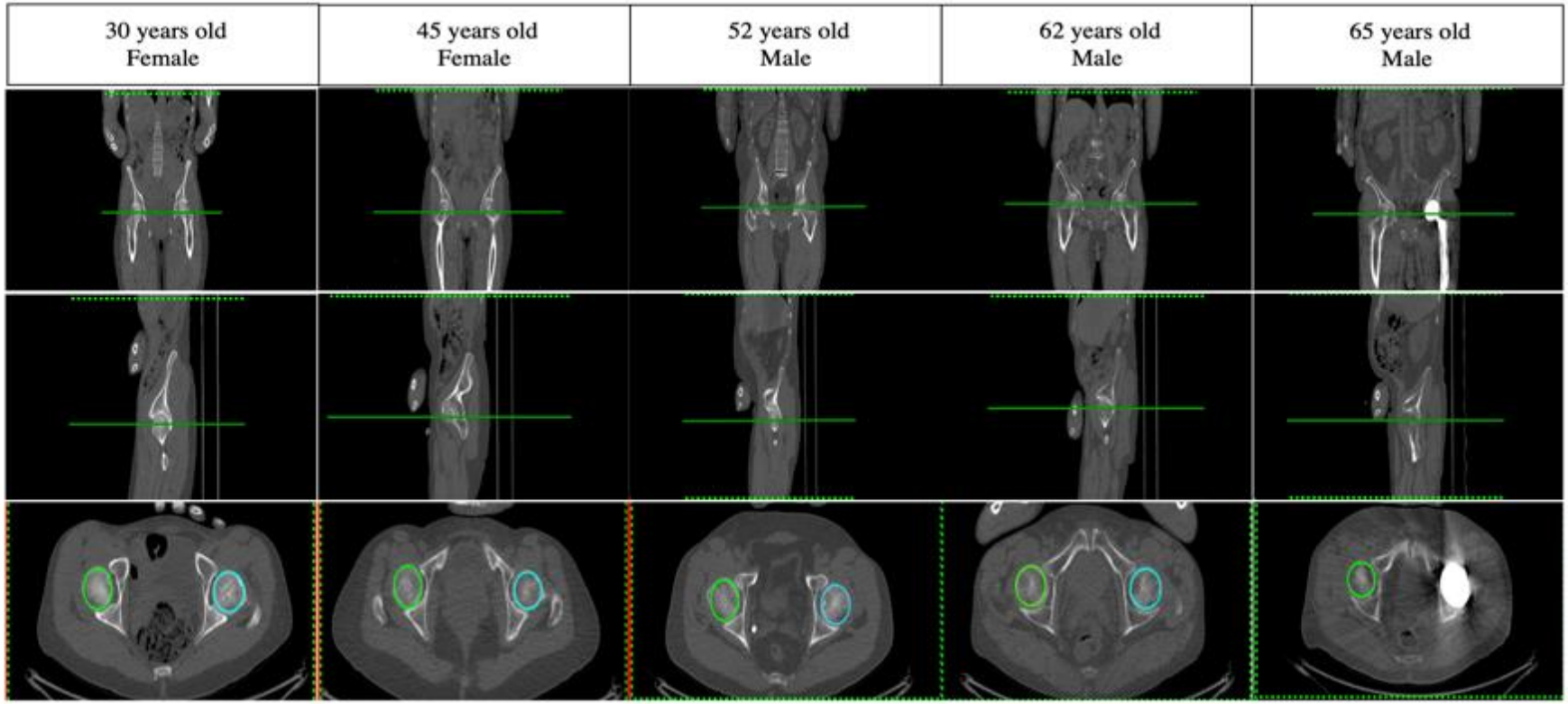

RT F	334.16	244.28	258.11	201.14	116.6
LT F	348.44	222.38	293.33	217.43	-
R+L F	341	233	276	209	-

Figure 3.5. Coronal, sagittal, and axial hip CT images for AKU patients.

Age and gender of each patient displayed above each image. The table below illustrates the HU_{mean} value for each femoral side. 65 years old male patient had left head of the femur replacement

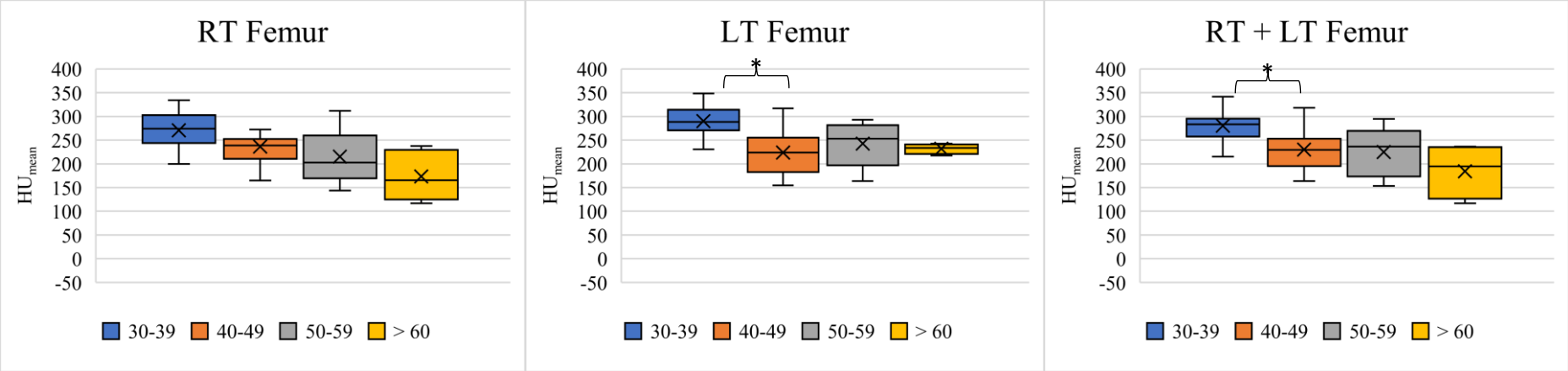

Figure 3.6. HU_{mean} for femoral heads among four decadal age groups measured from CT scan for AKU patients who were part of SONIA 2 clinical trial.

Table 9.3 (appendix) shows the right (RT), left (LT), and average femoral sites (RT +LT) and age groups, indicating a statistically significant difference between subgroup analyses. Femoral HU_{mean} values show slight decreases as age increases. Statistically, there was a significant difference in left femur value between the 30s and 40s ($P = 0.007$), and in the average femoral sites between the 30s and 40s age groups ($P = 0.02$) only. *Groups which showed significant difference ($P < 0.05$). In box and whisker, x is the mean value, and the line is the median.

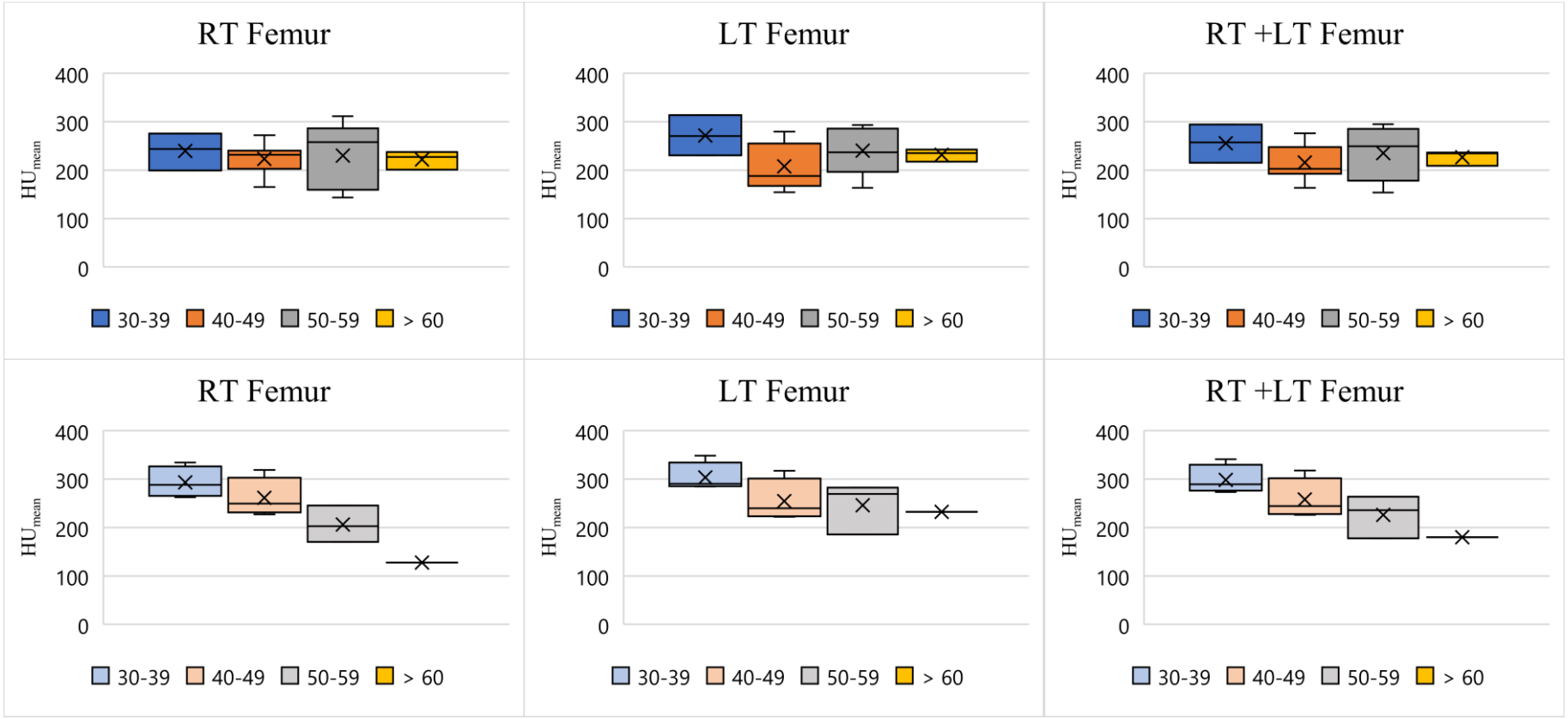

Figure 3.7. HU_{mean} for femoral heads among four decadal age groups for male (top row figures) and female (bottom row figures) measured from CT scan for AKU patients who were part of SONIA 2 clinical trial.

3.3.2 SUV_{max} measurement

The second section aimed to measure ^{18}F- NaF uptake from PET images at the lumbar spine and femoral sites from AKU patients. All the data are displayed in detail in the appendix section (Table 9.4 and Table 9.6), showing the mean, minimum, and maximum SUV_{max} values at each ROI for each gender and age group.

3.3.2.1 Lumbar vertebral body

The results of SUV_{max} measurements at each lumbar vertebrae level for SONIA 2 patients are shown in Figure 3.8. The mean lumbar SUV_{max} values for all AKU patients across L1 to L5 was 10.54 ± 2.17 (range, 5.20 – 15.91). The mean SUV_{max} was 10.19 ± 2.30 at L1, 10.67 ± 3.15 at L2; 10.08 ± 2.15 at L3, 10.59 ± 2.55 at L4, and 11.15 ± 2.62 at L5. It can be seen from the data in Figure 3.8 and Table 9.6 that mean SUV_{max} of L5 was slightly higher than the rest of the lumbar levels. Overall, the mean SUV_{max} value for all lumbar vertebrae levels were similar, with no statistically significant differences between the lumbar level values (all $P > 0.05$).

Figure 3.9 shows the spine ^{18}F-NaF PET images for some AKU cases. SUV_{max} values for L1-L5 are summarised in the table below the images. Figure 3.10 shows the fused ^{18}F-NaF PET/CT images for the patients shown in Figure 3.8. From these data, it can be seen that homogeneous distribution of ^{18}F-NaF tracer throughout the skeleton was noted in young patients at all spinal levels, indicating normal tracer uptake. In the abnormal AKU cases, unclear disc area and increased radiotracer uptake were noted, indicating metabolic bone disorder.

3.3.2.1.1 Lumbar vertebrae body SUV_{max} values and gender

Figure 3.8 illustrates the SUV_{max} across the lumbar vertebrae (L1, L2, L3, L4, and L5) in both gender groups. The mean lumbar SUV_{max} values across L1 to L5 was 10.92 ± 2.1 (range, 7.07 – 15.91) for males and 9.93 ± 2.22 (range, 5.2 – 14.64) for females. The mean SUV_{max} was 10.68 ± 2.27 at L1, 10.97 ± 3.20 at L2; 10.45 ± 2.25 at L3, 11.06 ± 2.45 at L4, and 11.43 ± 2.73 at L5 for the male patients. The mean SUV_{max} was 9.43 ± 2.21 at L1, 10.18 ± 3.11 at L2, 9.47 ±1.91 at L3, 9.84 ± 2.61 at L4, and

10.70 ± 2.47 at L5 for female patients. Looking at Figure 3.8, it is apparent that the SUV_{max} across all lumbar vertebrae levels of the male group was slightly higher than the female group; however, these differences were not statistically significant (all $P > 0.05$).

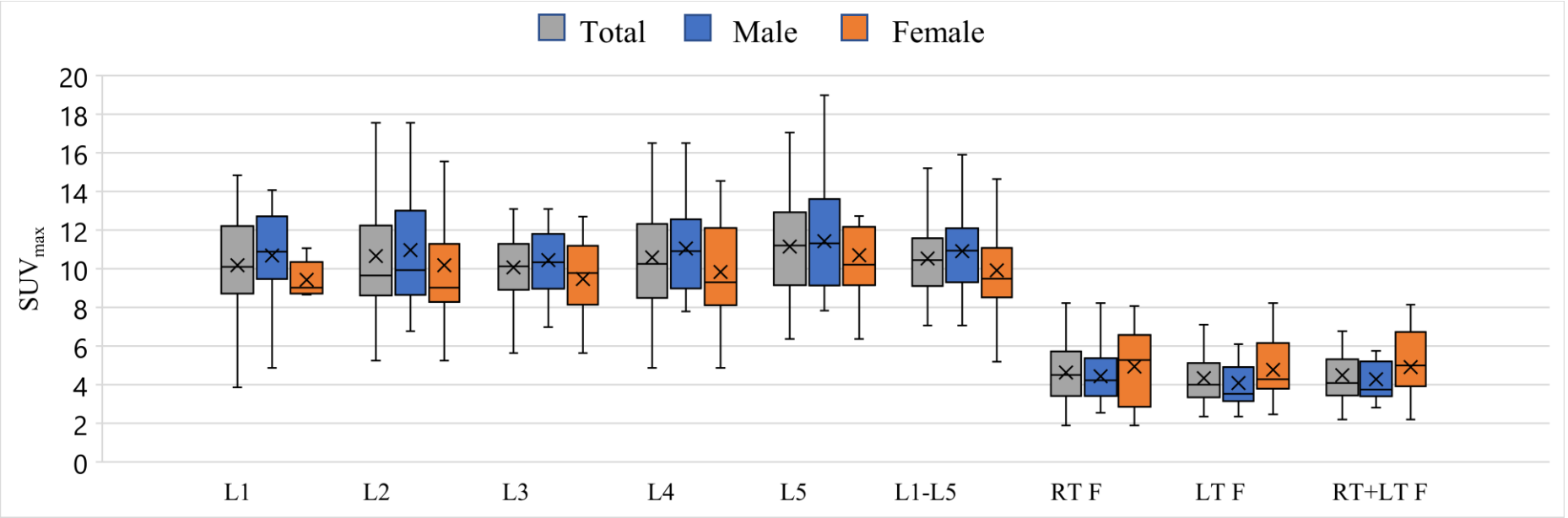

Figure 3.8. SUV_{max} obtained from the baseline ^{18}F-NaF PET scan at the lower spine and hip sites for 39 AKU patients who were part of SONIA 2 clinical trial stratified by gender.

This figure shows the analysis of ^{18}F-NaF uptake for 24 males and 15 females, which have been measured from each lumbar vertebrae level (L1, L2, L3, L4, and L5), average lumbar levels (L1-L5), right femoral head (RTF), left femoral head (LTF), average femoral head (RT+LT F) for male and female patients. Lumbar SUV_{max} values tend to be higher than femoral values in both male and female patients. The SUV value for all lumbar vertebrae levels were similar, with no statistically significant differences between the lumbar level values ($P > 0.05$). Likewise, The SUV value for the right and left femoral side was similar with no statistically significant differences ($P > 0.05$). Table 9.4 (appendix) shows that there are no significant differences between male and female patients at any ROI. P-value was 0.1, 0.045, 0.17, 0.15, 0.41, 0.17, 0.7, 0.25, 0.71 at L1, L2, L3, L4, L5, L1-L5, RTF, LTF, RT+LF F, respectively. In box and whisker, x is the mean value, and the line is the median.

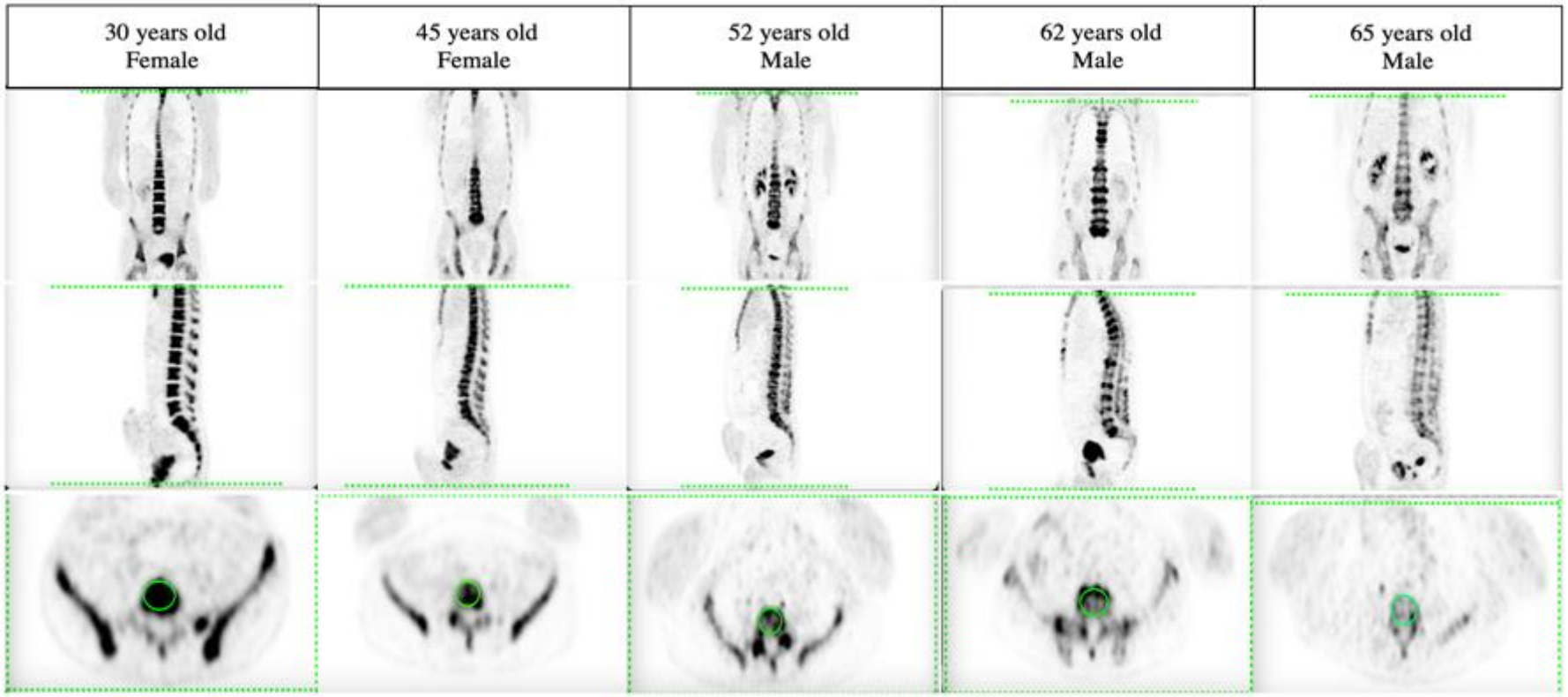

L1	8.98	8.66	12.9	12.57	4.87
L2	9.01	8.12	12.24	19.93	6.77
L3	9.27	7.24	11.22	13.10	6.99
L4	8.42	7.98	12.32	15.54	7.79
L5	8.92	12.17	12.93	14.56	8.93
L1-L5	8.92	8.83	12.16	15.2	7.07

Figure 3.9. Coronal, sagittal, and axial spine ^{18}F-NaF PET images for AKU patients.

Age and gender of each patient displayed above each image. The table below illustrates for SUV_{max} value for each lumbar level.

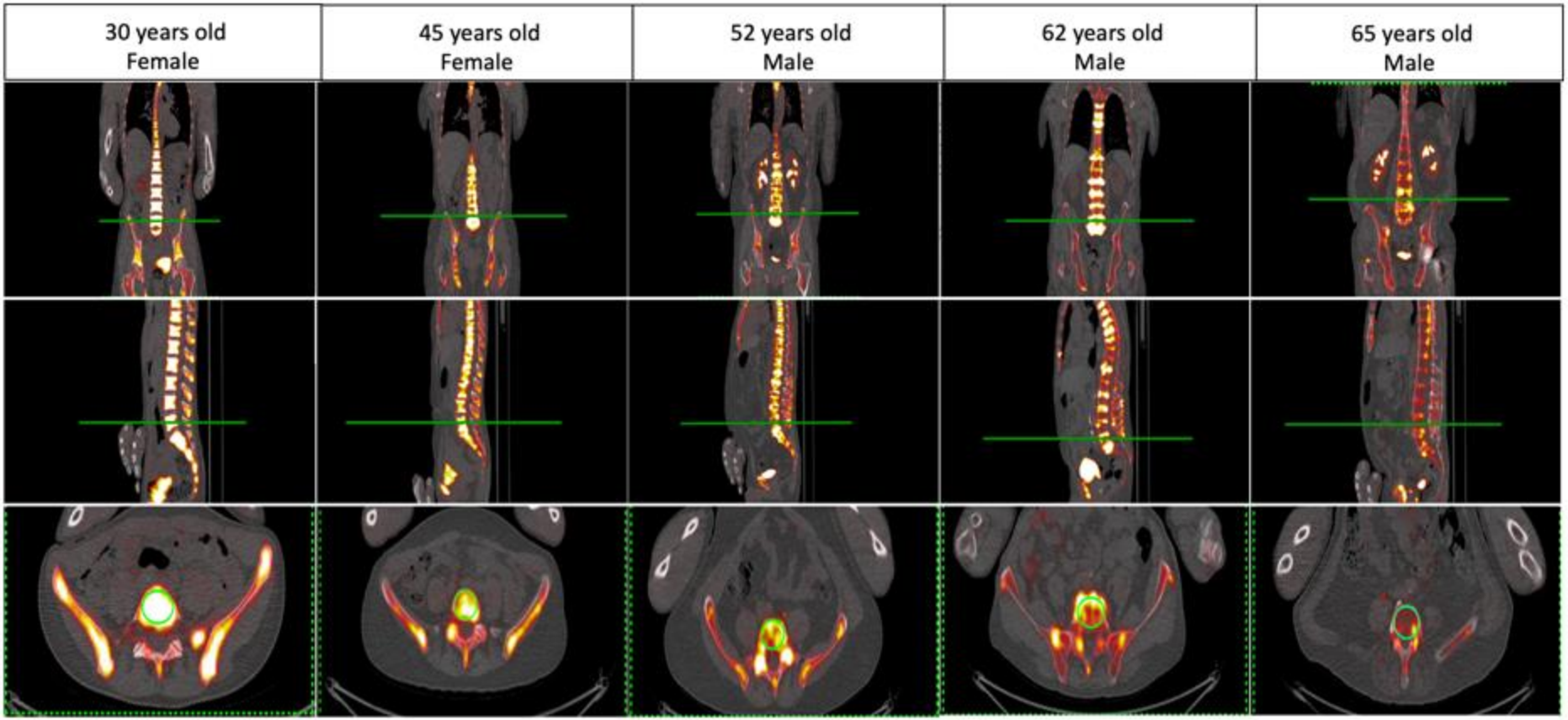

Figure 3.10 Coronal, sagittal, and axial spine fused ^{18}F-NaF PET/CT images for AKU patients.

Age and gender of each patient displayed above each image.

3.3.2.1.2 Lumbar vertebrae body SUV_{max} values and age

The results of the mean SUV_{max} across all lumbar vertebrae was plotted against age in Figure 3.11. Multiple linear regression was conducted to analyse the trend in the lumbar vertebrae SUV_{max} with age. The average SUV_{max} of L1-L5 was reduced with increasing age ($R = -0.438$, $P = 0.005$). Looking at each level individually, age was noted to have a statistically significant effect at L1, L3, L4 and L5 levels, with correlation coefficients of $R = -0.332$, $R = -0.391$, $R = -0.416$, and $R = -0.432$, respectively; all $P < 0.05$. Polynomial regression did not substantially improve the correlation coefficient (see Table 9.5 in the appendix).

The average SUV_{max} from the lumbar vertebrae across the L1 level to the L5 level for each age group was generated. The subgroup analysis results were compared and summarised in Figure 3.12 and Table 9.6 (appendix). Generally, young patients had higher SUV_{max} at all vertebrae bodies compared to older patients. As can be seen from the Figure 3.12, the average SUV_{max} values for all measured vertebrae body levels were decreased slightly by decade of life ranging from 11.86 ± 2.34 in the 3rd decade of life to 9.01 ± 2.60 in the 6th decade of life and above. Although the reduction in SUV_{max} was noted in the average lumbar levels, subgroup analysis using one-way ANOVA revealed that those differences between age groups were not statistically significant ($P > 0.05$). The only statistically significant differences between age groups has been noted between the 50s and 60s age groups in the L1 ($P = 0.025$) and between the 40s and 50s age group in the L5 ($P = 0.02$). As was found in the HU results, the measured values from the L5 level was increased from the 30s to 40s age group then decreased consistently in the 50s and 60s age group; however, these differences were not statistically significant ($P = 0.568$, $P = 0.451$ respectively).

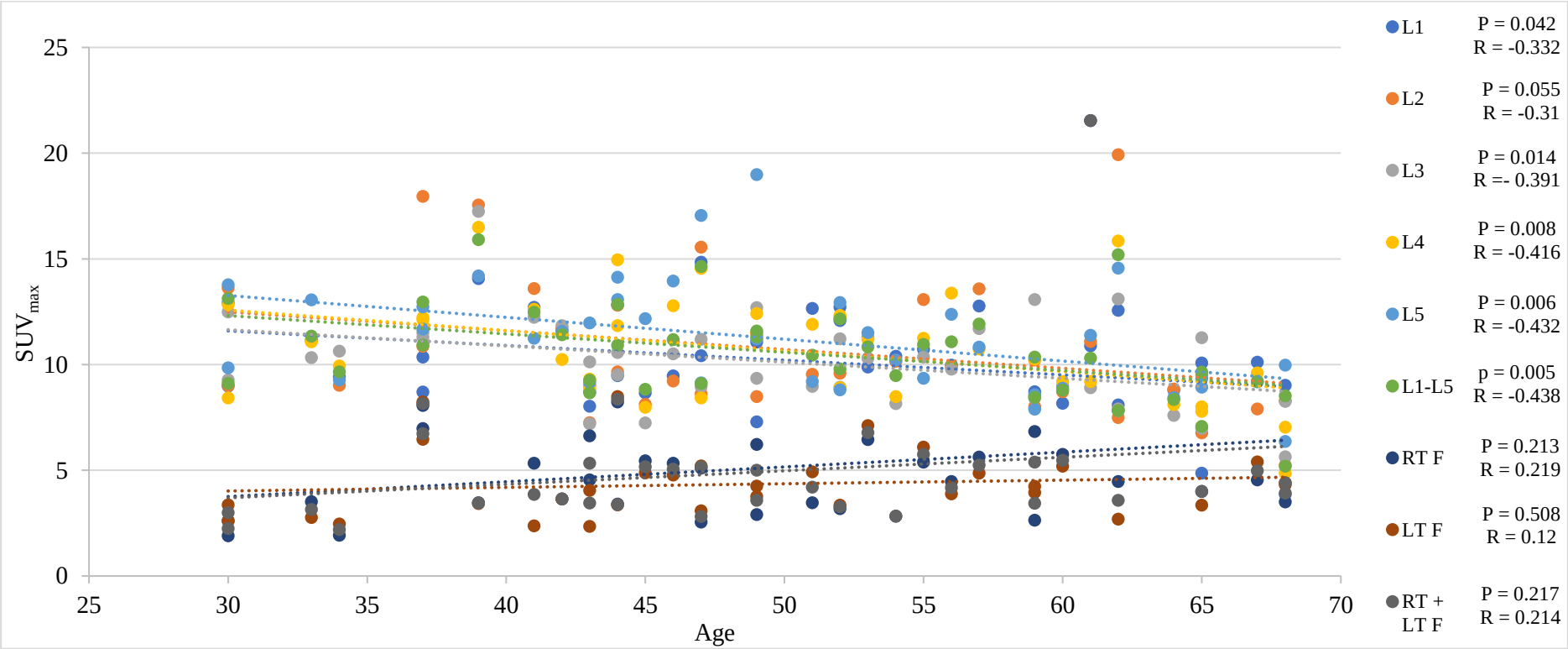

Figure 3.11. Scatter plots illustrating the correlation between age and SUV_{max} obtained from ^{18}F-NaF PET scan at the lower spine and femoral sites for 39 AKU patients who were part of SONIA 2 clinical trial.

The results display SUV_{max} of each lumbar vertebrae level (L1, L2, L3, L4, and L5), average lumbar levels (L1-L5), right femoral head (RTF), left femoral head (LTF), average femoral head (RT+LT F) in individual AKU cases with age. Multiple linear regression analysis identified a negative statistically significant correlation ($P < 0.05$) between age and SUV_{max} values measured from L1, L3, L4, and L5. Statistically, no significant correlation between SUV_{max} at L2 and age has been found ($P = 0.055$). There was no statistically significant correlation between age and SUV_{max} values measured from femoral sites ($P > 0.05$).

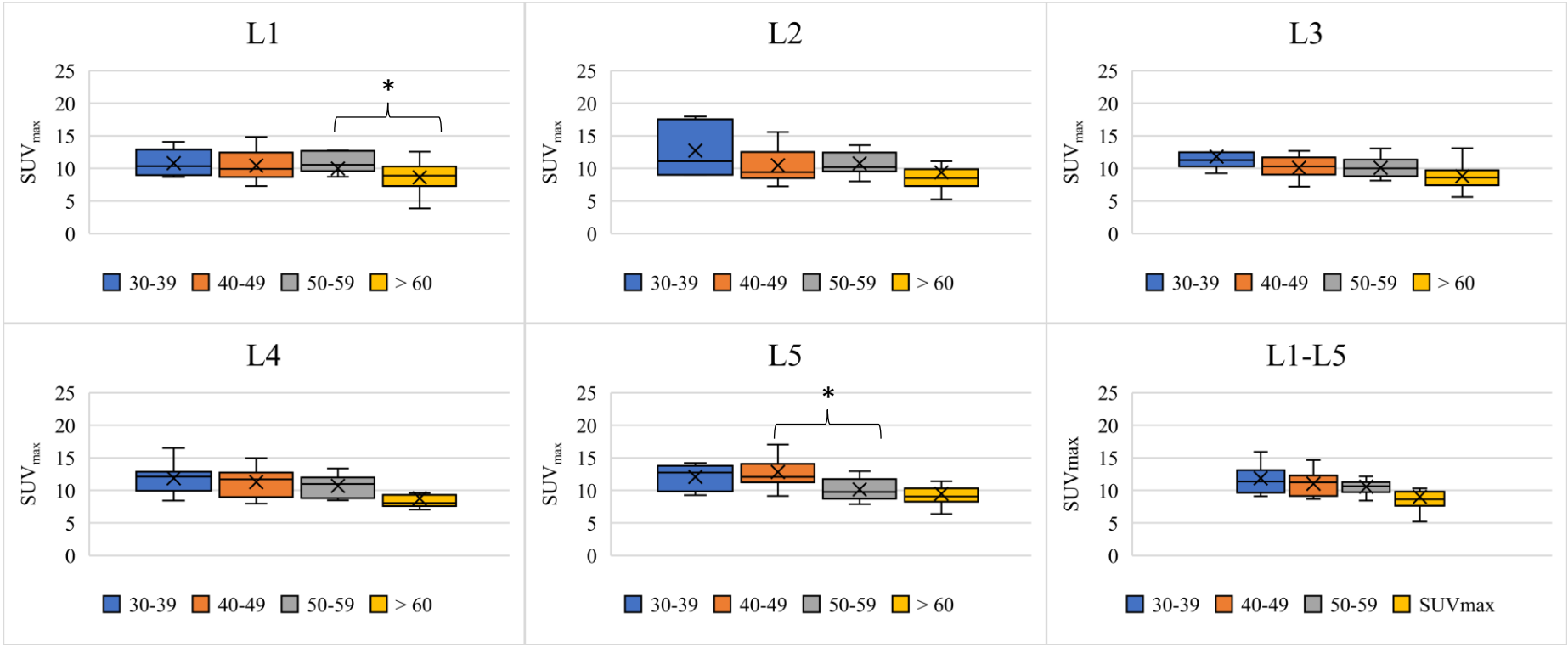

Figure 3.12. SUV_{max} for all lumbar vertebrae level among four decadal age groups measured from baseline ^{18}F-NaF PET scan for AKU patients who were part of SONIA 2 clinical trial.

Table 9.6 (appendix) shows the lumbar level, which indicated a statistically significant difference between subgroup analyses. Lumbar SUV_{max} values show slight decreases as age increases. Statistically, there was a significant difference in L1 value between the 50s and 60s ($P = 0.025$), and in the L5 between the 40s and 50s age groups ($P = 0.02$) only. * Groups which showed significant difference ($P < 0.05$). In box and whisker, x is the mean value, and the line is median

3.3.2.2 Head of the femur

Figure 3.8 and Table 9.4 (appendix) summarise the SUV_{max} results of the femoral regions. The mean SUV_{max} measured from the head of the femur was 4.50 ± 2.55 and ranged from 2.2 to 8.36. The mean SUV_{max} was 5.63 ± 2.36 at the head of the right femur and 4.34 ±1.57 at the head of the left femur for all patients. As shown in Figure 3.8, there was no statistically significant differences between right and left head of femur SUV measurements ($P > 0.05$). On the other hand, the mean head of femur SUV_{max} value was significantly lower than the average lumbar SUV_{max} value.

Figure 3.13 and Figure 3.15 show ^{18}F-NaF PET and fused ^{18}F-NaF PET/CT images, respectively for the hip regions for AKU cases. As noted from the figures and data, a normal femoral head structure had uniform distribution of ^{18}F-NaF throughout the bone, while increased ^{18}F-NaF uptake was noted in the abnormal hip lesions.

3.3.2.2.1 Head of the femur SUV_{max} values and gender

Figure 3.8 demonstrates the SUV_{max} of the head of the femur in males and females. The mean SUV_{max} measured from the head of the femur was 4.5 ± 2.08, ranged from 2.82 to 8.36 for males, and was 4.92 ± 1.92, ranged from 2.2 to 8.15 for females. From the Figure 3.8, it is clear that the male group had a higher SUV_{max} on the right side while the female group had higher values on the left side. For the average femoral value, males had higher values than females. However, the independent t-test identified that the differences were not statistically significant ($P > 0.05$). Previously in this chapter, HU measurements also showed that there was no evidence that gender has an influence on the average head of femur values.

3.3.2.2.2 Head of the femur SUV_{max} values and age

The results of the mean SUV_{max} of the head of the femur was plotted against age in Figure 3.16. Multiple linear regression was applied to analyse the trend in femoral SUV_{max} measurements with age. In contrast to the previous result in section 3.3.2.1.2, age was not found to be a statistically significant factor affecting the mean head of femur SUV_{max} ($R = 0.214$, and $P = 0.217$).

Subgroup analysis of the femoral measurement is shown in Figure 3.16 and Table 9.6 (appendix). The average SUV_{max} for femoral sides was 4.13 ± 2.34 for 30-39 age group patients, 4.57 ± 1.48 for 40-49 age group patients, 4.57 ± 1.31 for 50-59 age group patients, and 6.84 ± 6.51for ≥ 60 years old patients. In contrast to the lumbar level findings, the oldest age group patients had the highest SUV_{max} values, and the youngest age group patients had the lowest values. The mean SUV_{max} at the average head of the femur increased consistently by decade from 3rd decade of life to the 6th decade of life; however, there were no significant differences between any of the age groups at femoral sites ($P > 0.05$). Separating out male and female as shown in Figure 3.17 indicates that femoral SUV_{max} values for male subjects increased by age from 30s to the 60s age groups, while there were very little changes in femoral SUV_{max} values for AKU female subjects between the age groups.

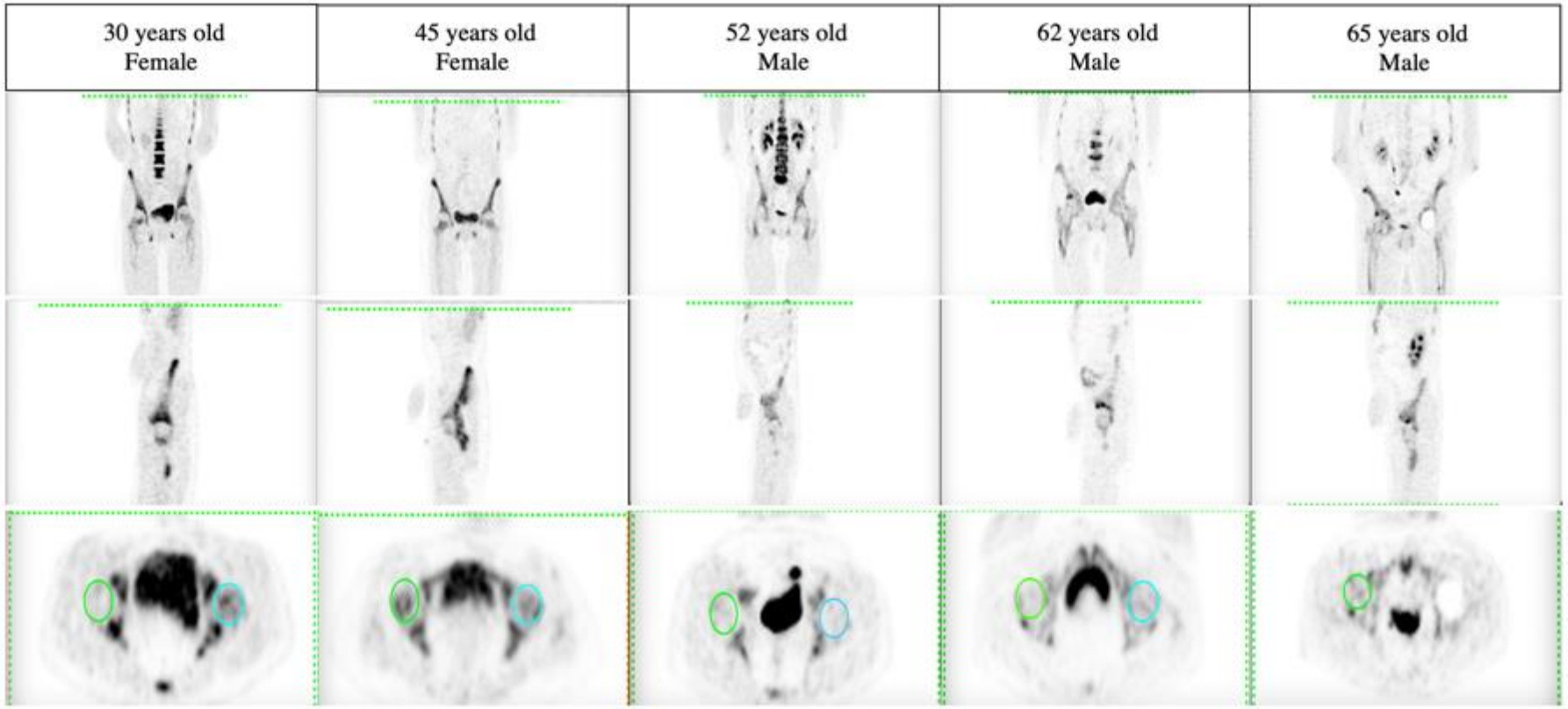

RT F	1.9	5.45	3.19	4.47	4.0
LT F	2.9	4.88	3.35	2.69	-
RT+LT F	2.25	5.12	3.27	3.58	-

Figure 3.13. Coronal, sagittal, and axial hip ^{18}F-NaF PET images for AKU patients.

Age and gender of each patient displayed above each image. The table below illustrates for SUV_{max} value for each femoral side.

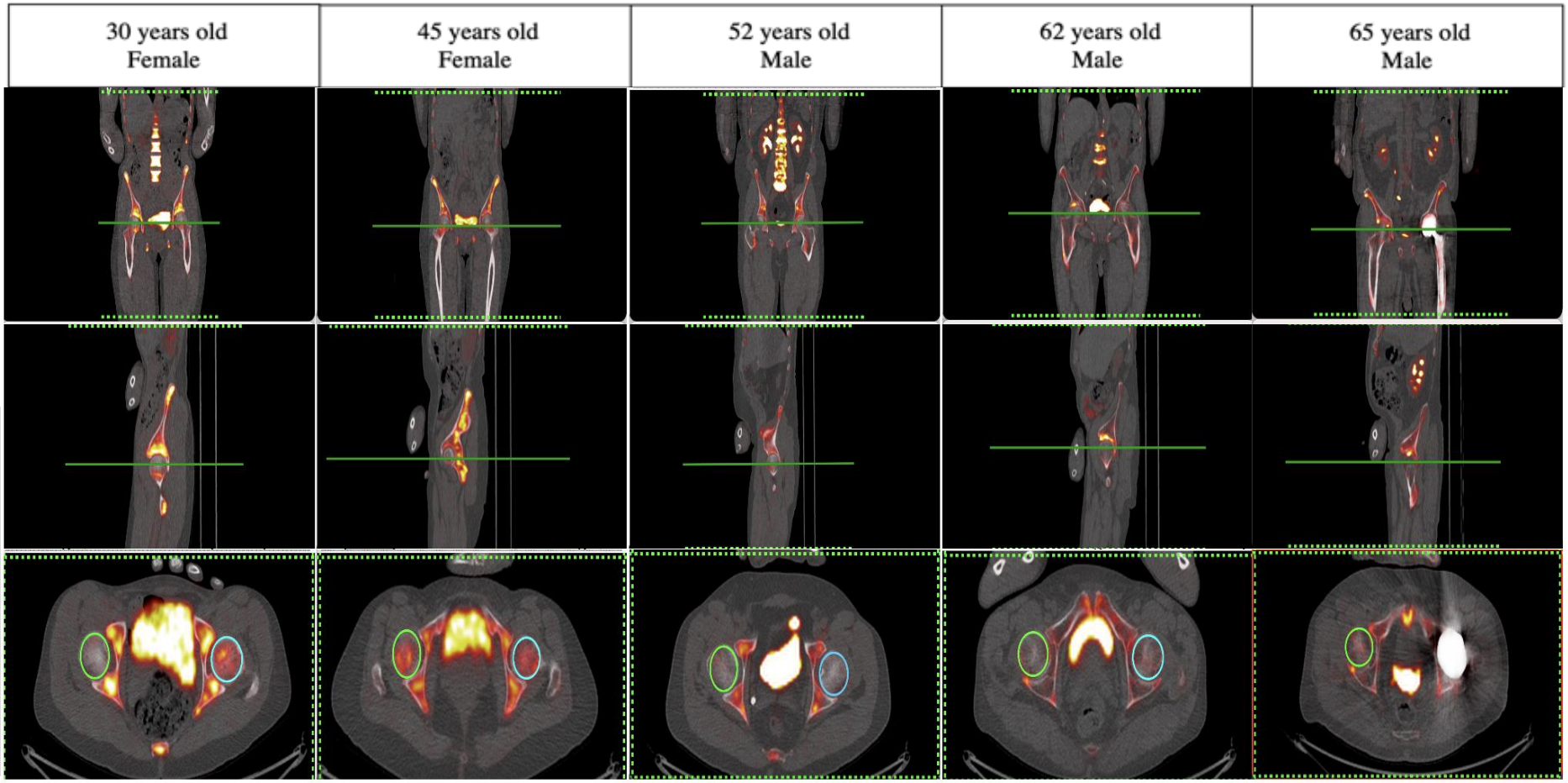

Figure 3.15. Coronal, sagittal, and axial fused ^{18}F-NaF PET/CT images for the hip region for AKU patients.

Age and gender of each patient displayed above each image.

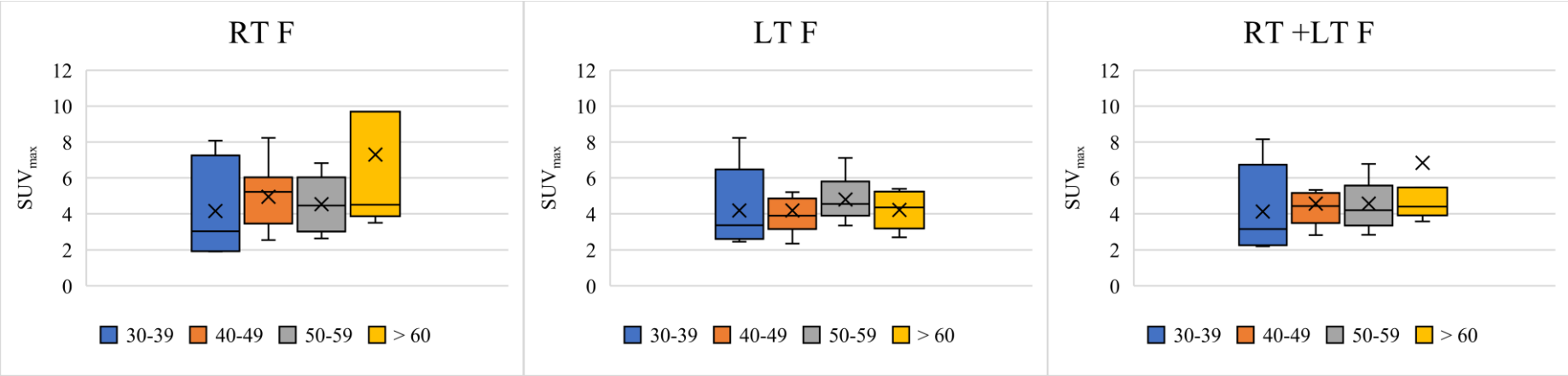

Figure 3.16. SUV_{max} for femoral heads among four decadal age groups measured from baseline ^{18}F-NaF PET scan for AKU patients who were part of SONIA 2 clinical trial.

Table 9.6 (appendix) shows the right (RT), left (LT), and average femoral sites (RT +LT) and age groups, indicating a statistically significant difference between subgroup analyses. The mean SUV_{max} at the average head of the femur increased consistently by decade from 3rd decade of life to the 6th decade of life; however, statistically, there were no significant differences between any of the age groups at femoral sites ($P > 0.05$). In box and whisker, x is the mean value, and the line is the median.

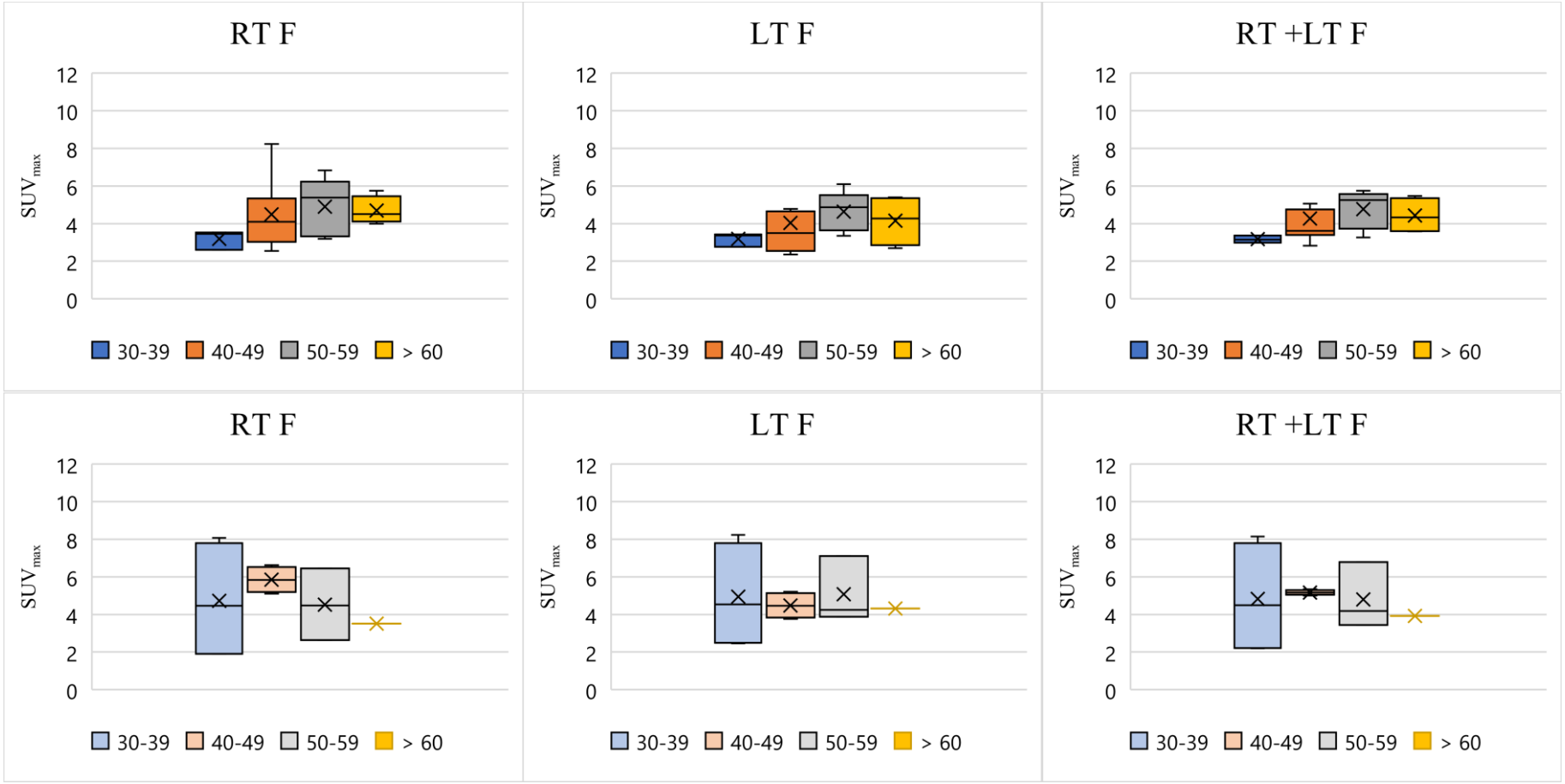

Figure 3.17. SUV_{max} for femoral heads among four decadal age groups for male (top row figures) and female (bottom row figures) measured from baseline ^{18}F-NaF PET scan for AKU patients who were part of SONIA 2 clinical trial.

3.3.3 DEXA bone density values

T-scores were extracted for each patient from the DEXA report to investigate the correlation between bone mineral density values and the semiquantitative values measured from the ^{18}F-NaF PET/CT image. The results of T-score values from the lumbar spine and hip sites reported from the DEXA scan were investigated, and the mean values displayed in Figure 3.18. All the data are summarised in Table 9.7 (appendix). The mean lumbar T-score values across L1 - L4 was 0.52 ± 1.79 (range, -3.2 – 5.4) and femoral T-score was -1.5 ± 1.06 (range, -3.1 – 1.3). The mean lumbar T- score was 0.9 ± 1.77 (range, -1.6 to 5.4) for male patients and -0.09 ± 1.7 (range, -3.2 to 3.5) for female patients while femoral T-score was -1.72 ± 0.9 (range, -3.1 to 0.3) for males and 1.27 ± 1.22 (range, -3.1 to 1.3) for females. Independent t-tests indicated a significant difference between the T-score values of males and females measured from L4 only (P = 0.04). No significant difference in the T-score values between males and females measured from the average lumbar spine and hip site was found (P = 0.1 and P = 0.25, respectively).

Based on World Health Organisation (WHO) criteria, AKU patients were stratified into three groups according to T-score values: normal when T-score is -1 or greater, osteopenic when T-score is less than -1 and greater than -2.5, and osteoporotic when T-score is -2.5 or less. According to WHO criteria, 81% of all patients were normal in the lumbar spine and 32.4% in the proximal femur, 16.2% of all patients had the diagnosis of osteopenia in the lumbar spine and 40.5% in the proximal femur, and 2.7% of all patients had a diagnosis of osteoporosis in lumbar spine and 21.6% in the proximal femur. It is apparent from the DEXA report that femoral T-scores seem to have a lower bone mineral density compared to the lumbar spine T-scores indicating the diagnosis of osteopenia and osteoporosis in AKU patients. Table 3.3 displays the T-score values for those patients described previously in the HU and SUV sections.

The mean T-score values measured from DEXA scans from the lumbar spine and left proximal femur were plotted against age in Figure 3.19. Multiple linear regression was applied to analyse the correlation of bone density values with age. No significant correlation was found between lumbar T-score and age at all levels L1-L4 (R = 0.032, R = -0.311, R = -0.158, and R = -0.009, respectively, all P > 0.05). In contrast, strong

correlation between femoral T-score and age was found (R= 0.571, P < 0.05). Polynomial regression did not improve the correlation coefficient (see Table 9.8 in the appendix). Looking at subgroup age analysis in Figure 3.20 and Table 9.9 (appendix), young patients had a normal T-score range, representing healthy bone density values, while most of the older patients, above 40 years old had osteopenia T-score range. For all lumbar vertebral levels, the mean T-score values increased consistently by increasing the decade of life from the 3rd decade of life to the 5th decade of life, then decreasing from the 5th decade of life to the 6th decade of life and above. Subgroup analysis using one-way ANOVA revealed that the differences were only significant at the L2 level between the 50s and 60s age groups (P = 0.006).

For the femoral site, the T-score values decreased consistently by increasing the decade of life, ranging from -0.486 in the 3rd decade of life to -2.186 in the 6th decade of life. There was a significant difference in the femoral T-score between the 30s and 40s age groups only (P = 0.028).

Table 3.3. lumbar and femoral T-score values for those patients in Figure 3.2, Figure 3.5, Figure 3.9 and Figure 3.11.

Age	30	45	52	62	65
Gender	Female	Female	Male	Male	Male
L1	0.6	-1.2	-0.4	-0.7	1.4
L2	1.0	-1.5	-0.6	-2.5	-0.3
L3	1.3	-1.0	-2.0	0.5	0.5
L4	0.4	-1.4	-1.6	0.6	1.3
L1-L4	0.8	-1.3	-1.4	-0.4	0.6
Femur	1.3	-2.1	-1.3	-2.8	-2.9

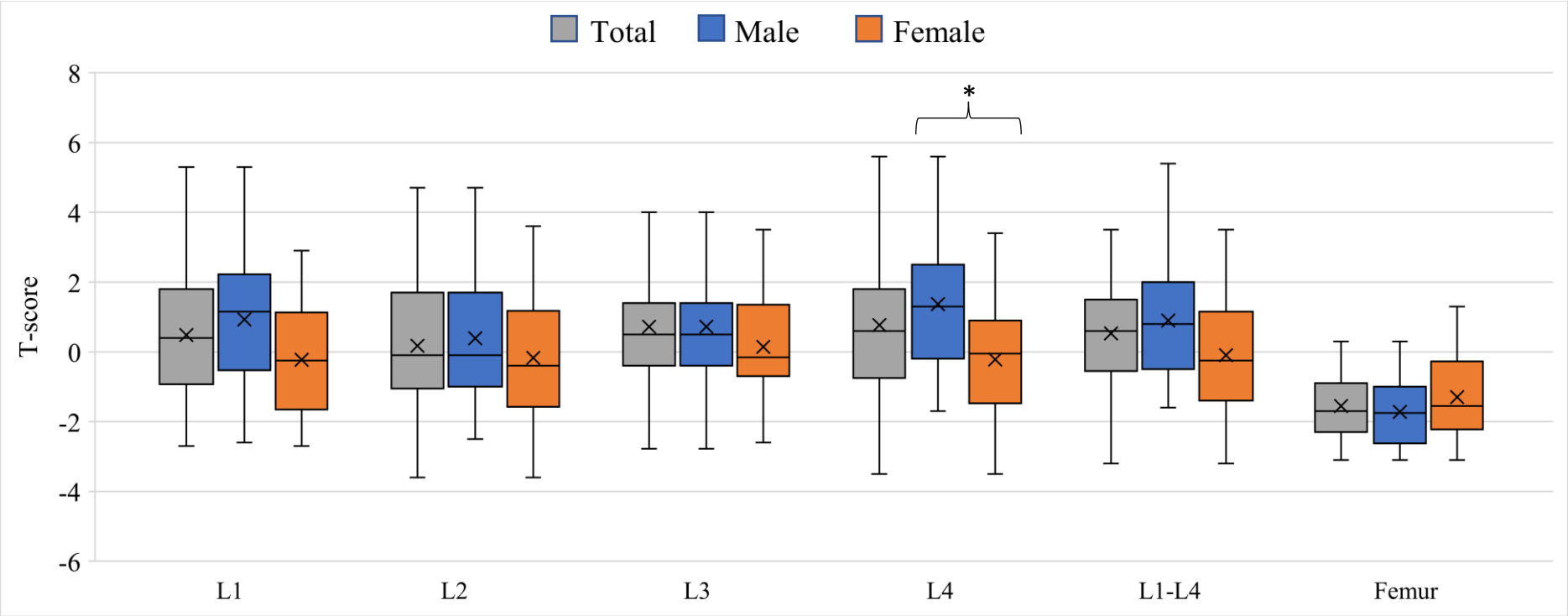

Figure 3.18. T-score obtained from baseline DEXA scan at the lower spine and femoral sites for 37 AKU patients who were part of SONIA 2 clinical trial stratified by gender.

The results show bone density analysis for 23 males and 14 females, measured from each lumbar vertebrae (L1, L2, L3, and L4), average lumbar levels (L1-L4), and the left proximal femur for male and female patients. Table 9.7 (appendix) shows significant differences in mean T-score value between male and female groups at L4 only (P = 0.04). No statistically significant differences in the T-score values were noted between males and females at the L1, L2, L4, or femoral site (P-value was 0.06, 0.39, 0.35, 0.10, 0.25, respectively). *Groups which showed significant difference (P < 0.05). In box and whisker, x is the mean value, and the line is the median.

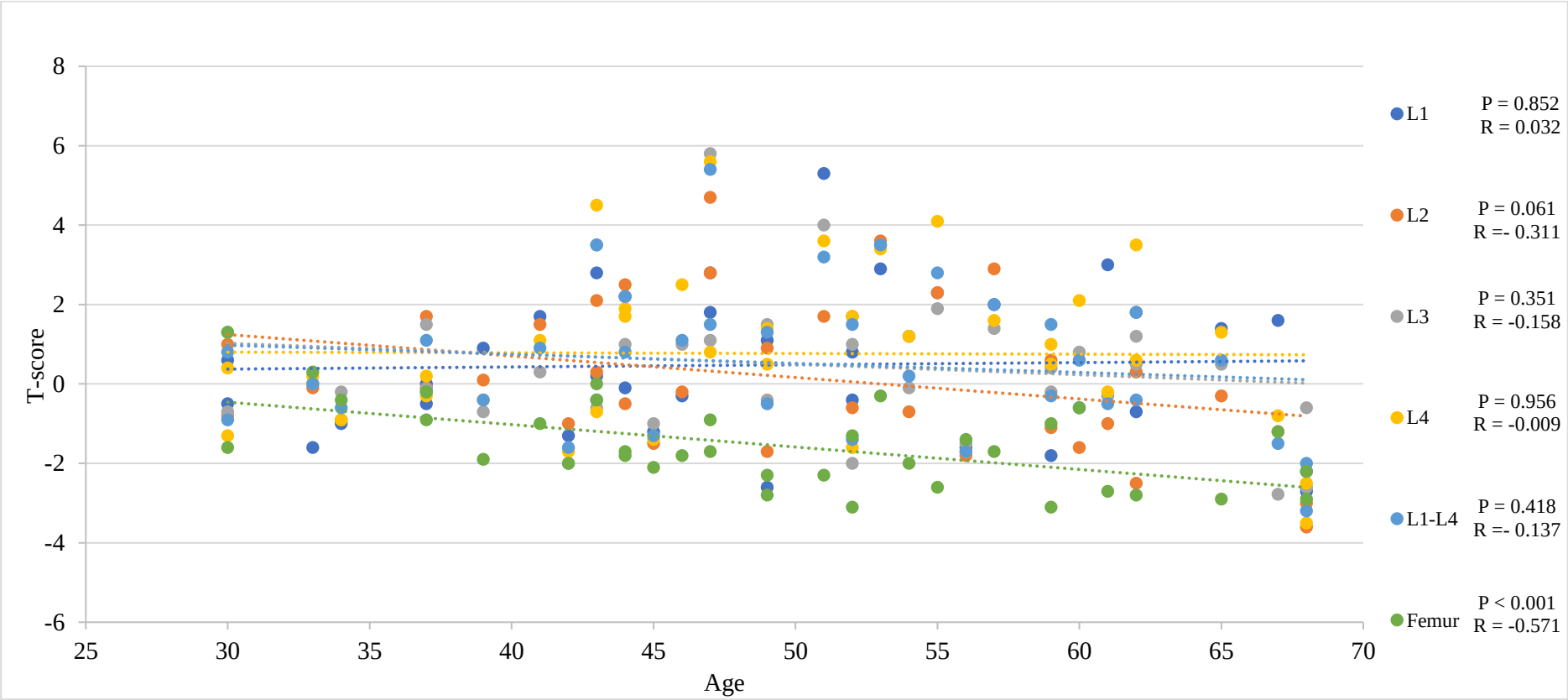

Figure 3.19. Scatter plots illustrating the correlation between age and T-score obtained from baseline DEXA scans at the lower spine and femoral regions for 37 AKU patients who were part of SONIA 2 clinical trial.

The results display the T-score of each lumbar vertebrae level (L1, L2, L3, and L4), average lumbar levels (L1-L4), and the left proximal femur in individual AKU cases with age. Femoral T-score values show consistent decreases as age increases ($P < 0.001$). Multiple linear regression analysis identified no statistical correlation between age and lumbar T-score values at all levels ($P > 0.05$).

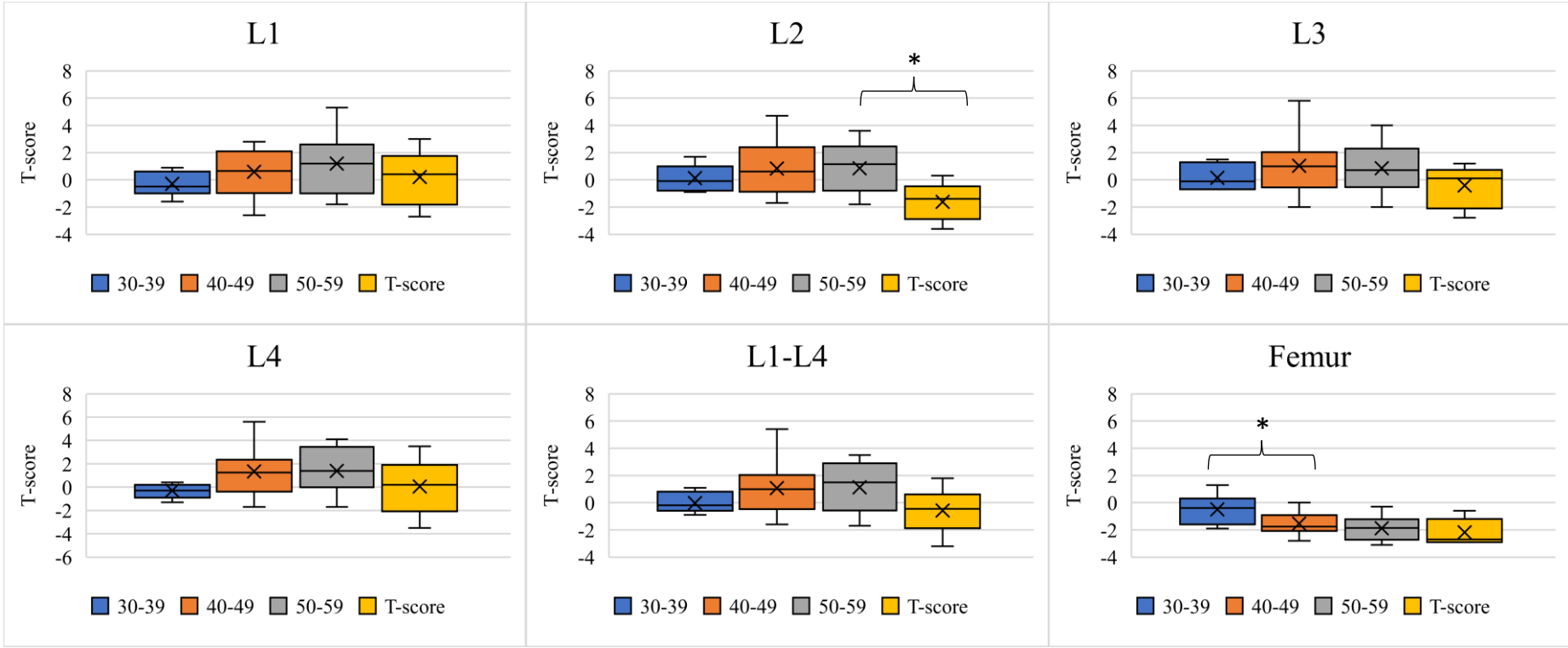

Figure 3.20. T-score for all lumbar vertebrae level and femoral regions measured from baseline DEXA scans among four decadal age groups for AKU patients who were part of SONIA 2 clinical trial.

Table 9.9 (appendix) shows the ROI, which indicated a statistically significant difference between subgroup analyses. *Groups which showed significant difference ($P < 0.05$). Statistically, there was a significant difference in L2 value between the 50s and 60s ($P = 0.006$), and in femur between the 30s and 40s age groups ($P = 0.028$) only. In box and whisker, x is the mean value, and the line is the median.

3.3.4 Correlation between the quantitative values

In this section, the relationship between the different quantitative values measured from different bone imaging techniques were addressed. The correlation between the semiquantitative values measured from CT, PET and those extracted from the DEXA report was tested. Simple statistical analysis was used to evaluate the relationship between HU_{mean} and T-score, between HU_{mean} and SUV_{max}, and between SUV_{max} and T-score.

3.3.4.1 Hounsfield Unit value (HU_{mean}) and (T-score) value

The relationship between the HU values measured from CT and T-score values measured from DEXA was evaluated for each lumbar level separately and compared, as shown in Figure 3.21. Moderate correlations were noted between the average lumbar level (L1-L4) HU value and the T-score value ($P < 0.05$ and $R = 0.503$). The R values were 0.398 for the L1 vertebra; 0.605 for L2; 0.563 for L3; 0.448 for L4. A strong correlation was found between HU values and T-score values in the femoral site with statistically significant values ($P < 0.01$, $R = 0.796$).

Based on DEXA scans, AKU patients were stratified into three groups according to T-score values; normal, osteopenic, and osteoporosis. Table 3.4 and Figure 3.22 summarised the mean HU value for each group. In the lumbar spine site, the mean HU value for normal patients was 152.93 ± 52.677 (95% CI, 133.26 to 172.6), and for osteopenic patients was 92.67 ± 33.44 (95% CI, 57.57 – 127.76). Only one patient had an osteoporotic T-score value in L1-L4 with HU 19. Using the t-test, the differences in mean HU values of L1-L4 between normal and osteopenic was significant ($P = 0.011$).

In the femoral site, the mean HU values for normal T-score patients was 270.53 ± 39.11 (95% CI, 245.68 to 295.38), for osteopenic patients was 231.37 ± 35.49 (95% CI 211.7 to 251.03), and for osteoporotic patients was 161.59 ± 31.596 (95% CI, 13.36 to 190.81) (Table 3.4). The differences in mean HU value of the head of the femur between normal and osteopenic, and between osteopenic and osteoporotic were statistically significant ($P = 0.012$, $P < 0.0001$, respectively).

Overall, patients who reported low HU values were also reporting low T-score. As noted from the examples in Table 3.3, Figure 3.2, and Figure 3.5, there is positive correlation between T-scores and HU values. This results indicate that normal T-score values can be detected in area with high HU values at both lumbar and femoral regions in the young 30 years old AKU patient. While low HU values in CT images were detected in the area of low T-score values in the elderly AKU patients.

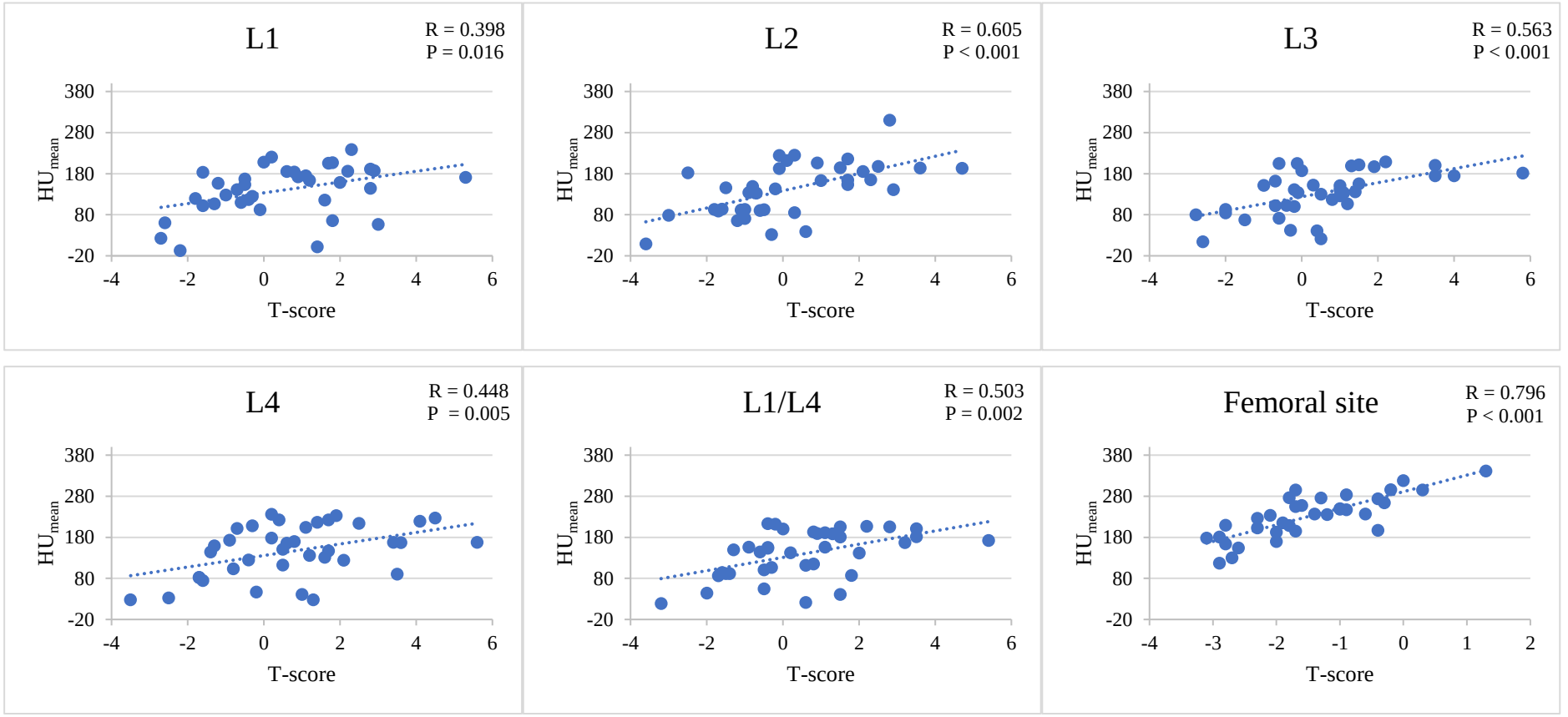

Figure 3.21. Scatter plots illustrating the correlation between HU_{mean} obtained from CT scan and T-score obtained from DEXA scan for each lumbar vertebrae level, and femoral site for AKU patients who were part of SONIA 2 clinical trial.

A strong positive, statistically significant correlation was found between HU_{mean}, and T-score, which were measured from all lumbar levels and femoral site ($P < 0.05$).

Table 3.4. Mean ± SD and 95% confidence intervals of HU_{mean} values for normal, osteopenic and osteoporotic AKU patients who were part of SONIA 2 clinical trial.
Based on WHO criteria, AKU patients were stratified into three groups according to lumbar and femoral T-score values. Pt no. = patient number, CI = confidence intervals.

T-score		Pt no.	Mean HU ± SD	95% CI
Lumbar spine				
Normal	-1 or greater	30	152.93 ± 52.677	133.26 – 172.6
Osteopenic	Less than -1 and greater than -2.5	6	92.67 ± 33.44	57.57 – 127.76
Osteoporotic	-2.5 or less	1	19	
Femur				
Normal	-1 or greater	12	270.53 ± 39.11	245.68 – 295.38
Osteopenic	Less than -1 and greater than -2.5	15	231.37 ± 35.49	211.7 – 251.03
Osteoporotic	-2.5 or less	7	161.59 ± 31.596	13.36 – 190.81

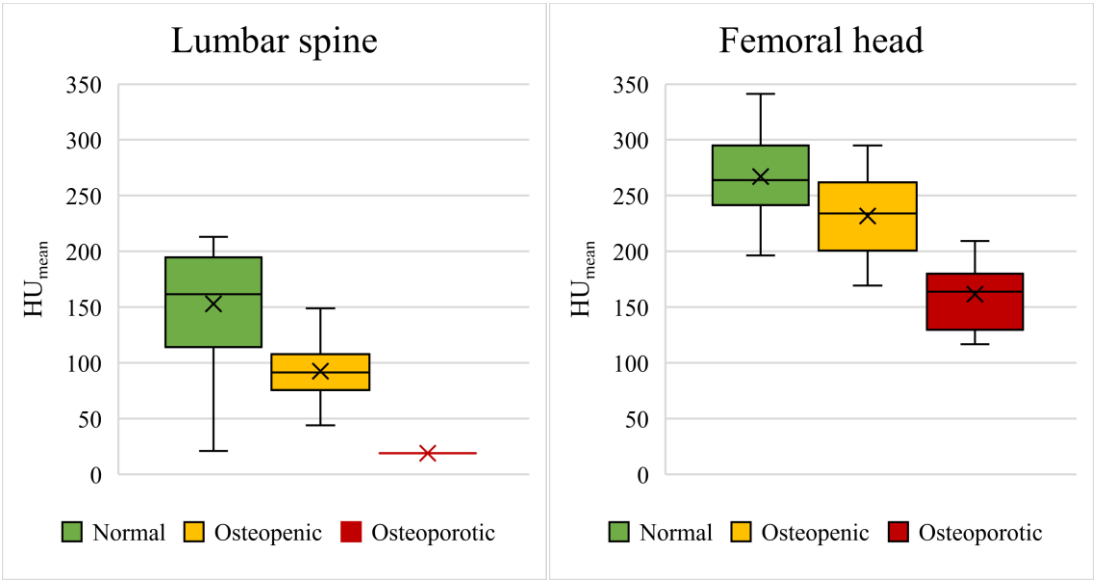

Figure 3.22. The HU_{mean} values for normal, osteopenic and osteoporotic AKU patients who were part of SONIA 2 clinical trial at the lumbar spine and femoral sites.
Based on lumbar T-score measurements, 30 patients were normal, 6 were osteopenic and 1 was osteoporotic. Based on femoral T-score, 12 patients were normal, 15 were osteopenic and 7 were osteoporotic. In box and whisker, x is the mean value, and the line is the median.

3.3.4.2 Hounsfield Unit value (HU_{mean}) and standardised uptake value (SUV_{max})

The relationship between HU values measured from CT and SUV_{max} values measured from ^{18}F-NaF PET were evaluated for lumbar spine and head of the femur, as shown in Figure 3.23 and Figure 3.24. It is apparent from Figure 3.23 and Figure 3.24 that there was a moderate correlation between the average lumbar HU_{mean} value and SUV_{max} with a correlation coefficient of 0.373, and P-value of 0.02. Regionally, there was statistical significant correlation between HU_{mean} value and SUV_{max} at L1, L2, and L4. The correlation coefficients and (P-value) was 0.517 (P = 0.001) for the L1 vertebra; 0.492 (P = 0.001) for L2; 0.13 (P = 0.429) for L3; 0.32 (P = 0.047) for L4 and 0.254 (P = 0.119) for L5. No significant correlation was found between HU_{mean} values and SUV_{max} values in the average femoral site R = -0.277 and P = 0.113.

As was shown in the examples in Figure 3.2 and Figure 3.9, younger AKU patients, had uniform high dense calcium areas in CT images with high HU values and homogeneous distribution of ^{18}F-NaF throughout the skeleton in PET images. Increased lumbar SUV_{max} values were noted in the area of low HU values in the 52 years old patient. On the other hand, the 65 years old AKU patient had very low HU values and low SUV_{max} at all lumbar level. Similar findings were noted in the hip region as shown in Figure 3.5 and Figure 3.10.

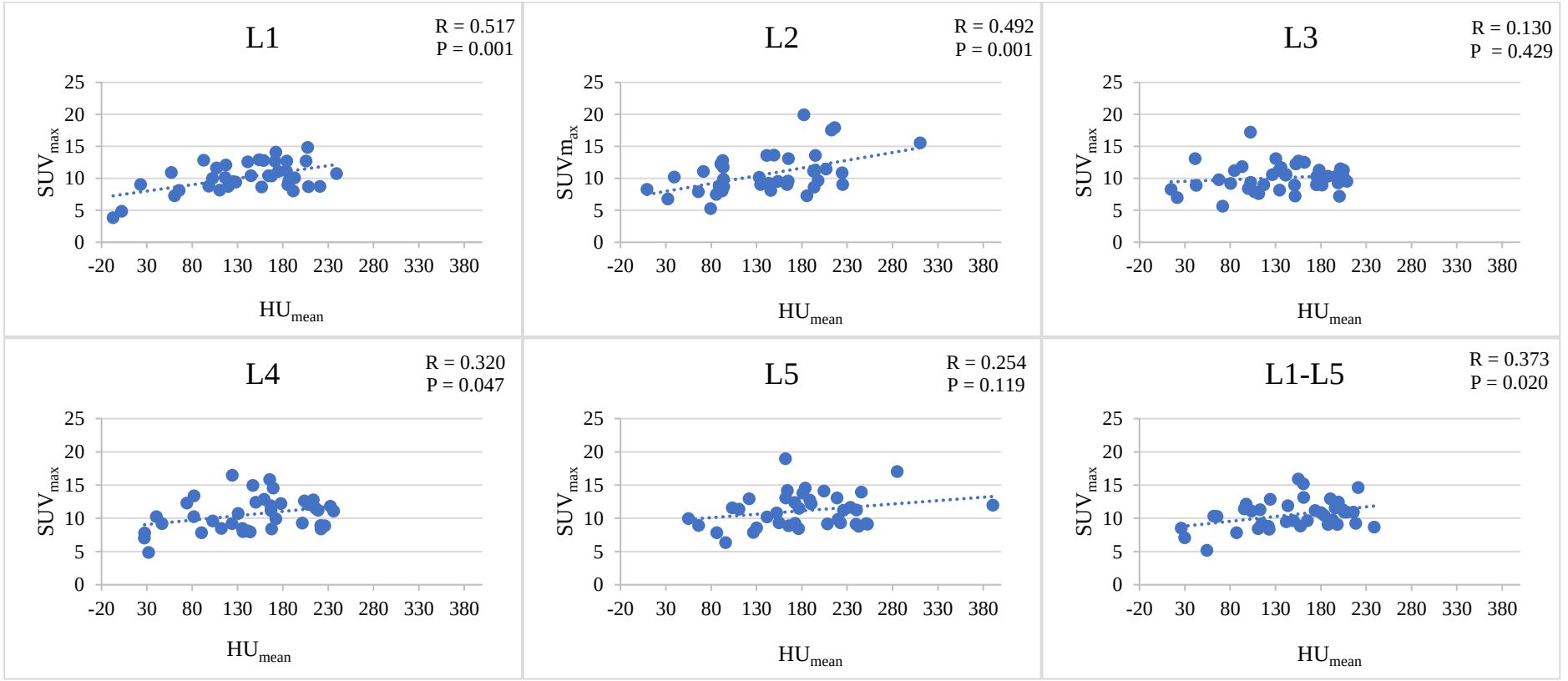

Figure 3.23. Scatter plots illustrating the correlation between mean HU_{mean} obtained from CT scan and SUV_{max} obtained from ^{18}F-NaF PET scan for each lumbar vertebrae level for AKU patients who were part of SONIA 2 clinical trial.

At L1, L2 and L4, there was a statistically significant correlation between HU_{mean} and SUV_{max} (P = 0.001, P = 0.001, and P = 0.047, respectively). No statistically significant correlation was noted at L3 and L5 levels (P = 0.429, and P = 0.119, respectively). In average lumbar levels, there was statistical correlation between HU_{mean} and SUV_{max} (P = 0.02, R = 0.373).

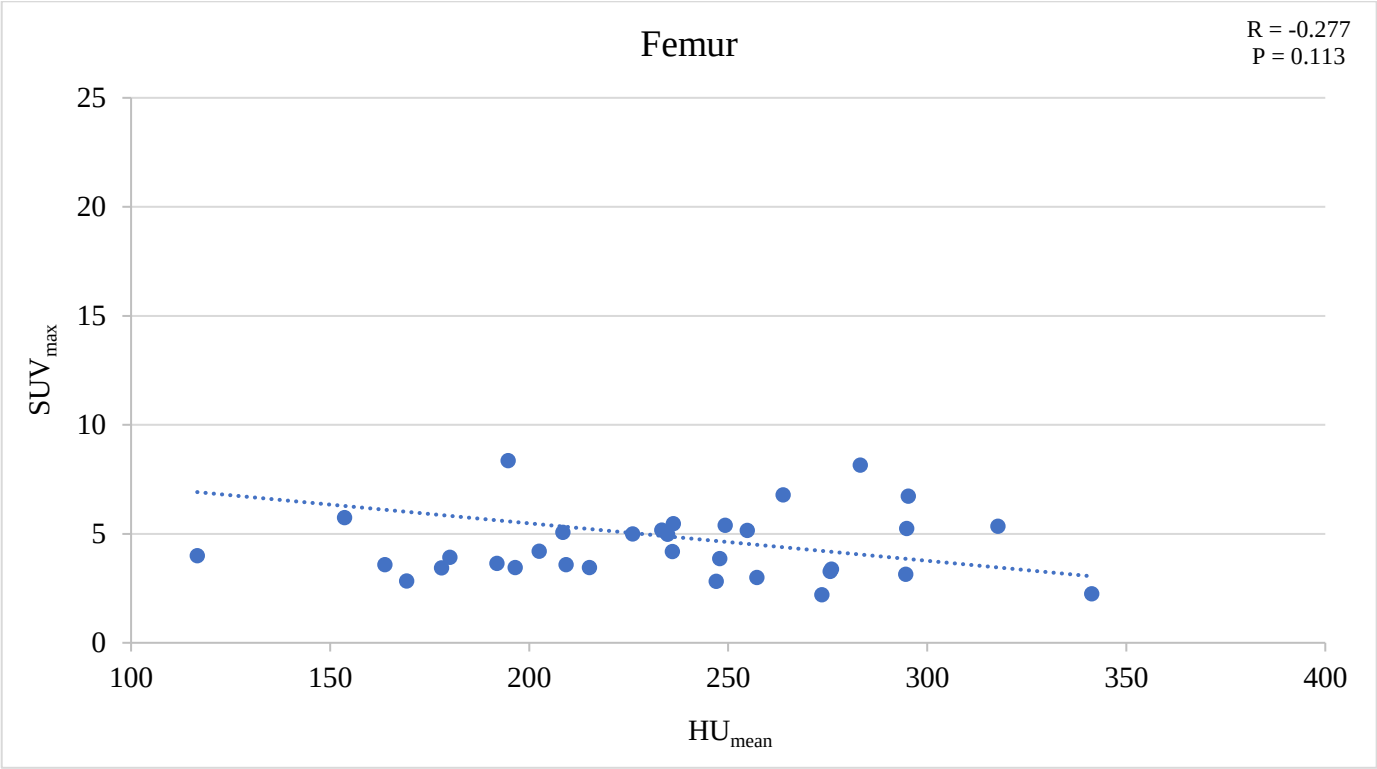

Figure 3.24. Scatter plots illustrating the correlation between HU_{mean} obtained from CT scan, and SUV_{max} obtained from ^{18}F-NaF PET scan for the femoral site AKU patients who were part of SONIA 2 clinical trial.

No statistically significant correlation was found between femoral SUV_{max} and HU_{mean} values (P = 0.113, R = 0.277).

3.3.4.3 Standardised uptake value (SUV_{max}) and T-score value

The relationship between SUV_{max} values measured from PET and T-score measured from DEXA was evaluated for each lumbar level, as shown in Figure 3.25. Data show that there was no correlations between SUV_{max} values and the T-score at the average lumbar vertebrae levels (P = 0.684) with a correlation coefficient (R) of 0.069. Regionally, the correlation coefficients and (P-value) was -0.292 (P = 0.085) for the L1 vertebra; 0.178 (P = 0.293) for L2; -0.096 (P = 0.572) for L3 and 0.047 (P = 0.781) for L4. Likewise, no significant correlation was found between femoral SUV_{max} value and femoral T-score value (P = 0.339, R = -0.166).

Based on WHO criteria for osteoporosis, mean SUV_{max} value for normal lumbar T-scores was 10.76 ± 2.22 (95% CI, 9.92 to 11.59), SUV_{max} value for osteopenic was 9.37 ± 2.62 (95% CI, 6.61 – 12.12), as summarised in Table 3.5 and presented in Figure 3.26. Only one patient had an osteoporotic T-score value in L1-L4 with SUV_{max} of 8.15. The differences in mean SUV_{max} value of L1-L4 between the normal and osteopenic group was not significant (P = 0.183).

In regard to the femoral site, mean SUV_{max} value for normal T-scores was 4.63 ± 1.96 (95% CI, 3.39 to 5.88), for osteopenic was 4.45 ± 1.34 (95% CI, 3.74 – 5.17), and for osteoporotic was 6.54 ± 6.66 (95% CI, 0.38 – 12.70). No statistically significant differences in the SUV_{max} value between normal and osteopenic nor between osteopenic and osteoporotic groups was found (P = 0.782, P = 0.231, respectively).

From Table 3.3, Figure 3.9, and Figure 3.11, it is clear that high SUV_{max} values in the PET image overlay with with low T-score values in DEXA image. From this data, it can be seen that the young AKU patient had normal T-score values at both spine and hip regions and low SUV values compared to 52 years old patient and 62 years old patients. The 45 years old AKU patient had a normal lumbar T-score value but an osteopenic femoral T-score value. In that patient, increased SUV_{max} values were noted in the lumbar vertebrae and femoral head. It was noted that the osteoporosic cases had low ^{18}F-NaF absorption in low-density areas. Although the 62 and 65 year old male patients had normal T-score values at the lumbar spine and osteoporotic T-score values at the femoral head, there was a significant difference in SUV_{max} values between the

two cases. The 62 year old patient had a very high SUV_{max} value, while the 65 years old patient had a very low SUV_{max} value.

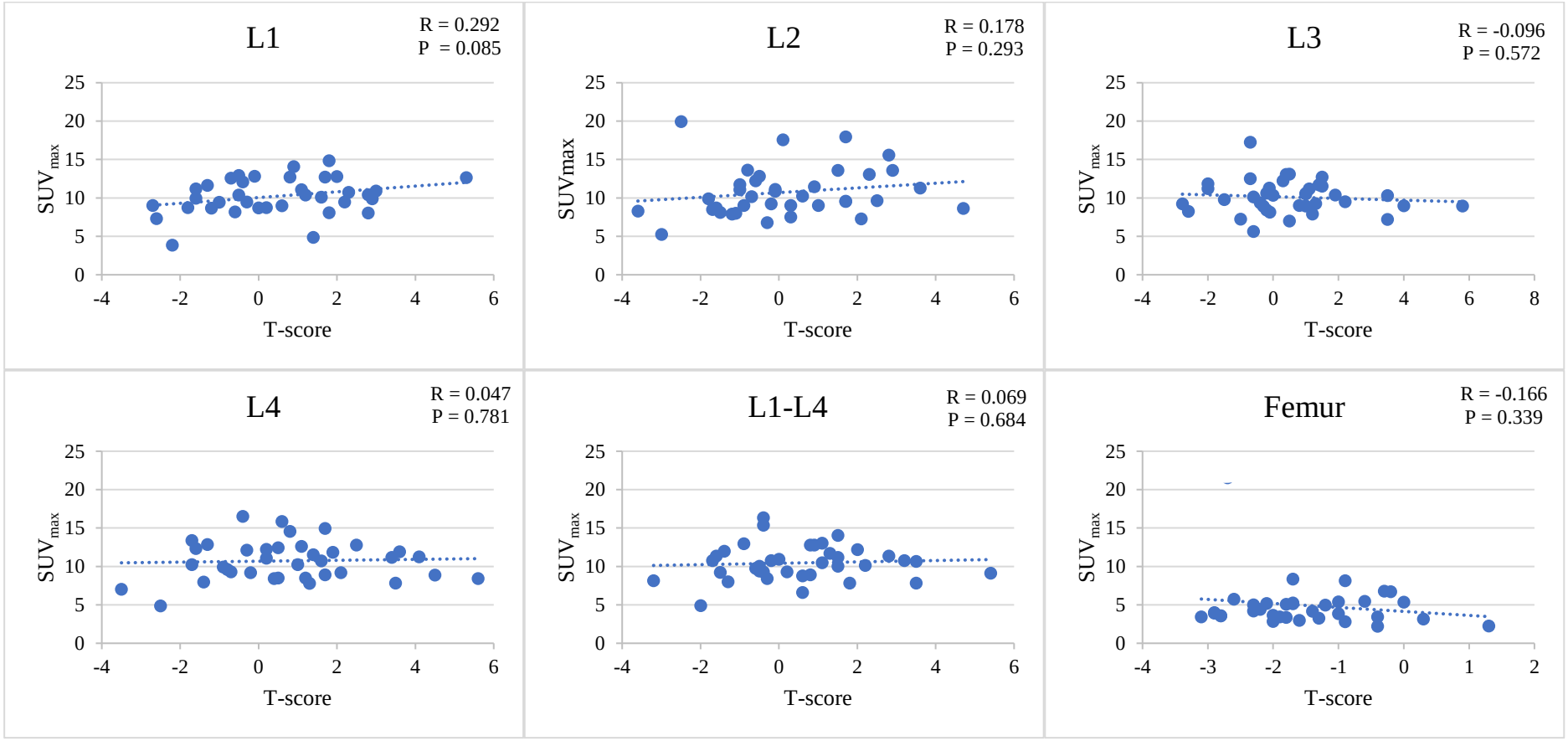

Figure 3.25. Scatter plots illustrating the correlation between SUV_{max} obtained from an ^{18}F-NaF PET scan, and T-score obtained from DEXA scan for each lumbar vertebrae level, and femoral site for 37 AKU patients who were part of SONIA 2 clinical trial.

No statistically significant correlation between SUV_{max} and T-scores was found at neither lumbar nor femoral sites (all had $P > 0.05$).

Table 3.5. Mean and 95% confidence intervals of SUV_{max} for normal, osteopenic and osteoporotic AKU patients who were part of SONIA 2 clinical trial.

Based on WHO criteria, AKU patients were stratified into three groups according to lumbar and femoral T-score values. Pt no. = patient number, CI = confidence intervals.

T-score		Pt no.	Mean SUV_{max} ± SD	95% CI
Lumbar spine				
Normal	-1 or greater	30	10.76 ± 2.22	9.92 – 11.59
Osteopenic	Less than -1 and greater than -2.5	6	9.37 ± 2.62	6.61 – 12.12
Osteoporotic	-2.5 or less	1		
Femur				
Normal	-1 or greater	12	4.63 ± 1.96	3.39 – 5.88
Osteopenic	Less than -1 and greater than -2.5	15	4.45 ± 1.34	3.74 – 5.17
Osteoporotic	-2.5 or less	7	6.54 ± 6.66	0.38 – 12.70

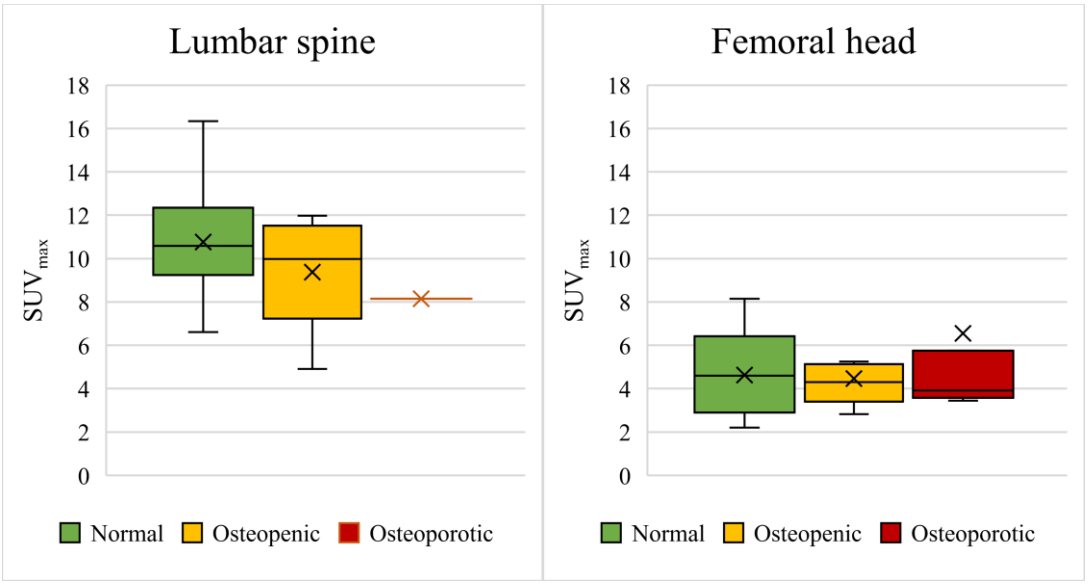

Figure 3.26. Figures show the mean SUV_{max} values for normal, osteopenic and osteoporotic AKU patients who were part of SONIA 2 clinical trial at the lumbar spine and femoral site.

Based on lumbar T-score measurements, 30 patients were normal, 6 were osteopenic, and 1 was osteoporotic, while based on femoral T-score, 12 patients were normal, 15 were osteopenic, and 7 were osteoporotic. In box and whisker, x is the mean value, and the line is the median.

3.4 Discussion

The current study is one of the few studies evaluating bone involvements for AKU patients quantitatively. The study set out to assess regional bone formation at the most affected skeletal sites for AKU patients using ^{18}F-NaF PET/CT scans. In this chapter, novel molecular imaging assessment methods have been introduced to quantify active bone turnover and estimate bone density at the lumbar spine and hip sites. The current study establishes a quantitative framework for detecting the early stage of ochronotic arthropathy in AKU patients using ^{18}F-NaF PET/CT semiquantitative methods.

3.4.1 HU measurements

Throughout this study, bone density for AKU patients was approximated by measuring HU from non-contrast CT scans. In the literature, several reports have identified patients at risk of fracture and those with bone density disorders by determining spine HU values from diagnostic CT systems when it is performed for other clinical purposes [81,83,85,164]. The results of this study showed that AKU patients had low HU values in the lumbar vertebrae and head of the femur, indicating low bone density. It is more likely that low bone density in AKU patients is associated with ochronosis. Several studies reported low bone desnity in patients with AKU [48,75]. It is more likely that ochronotic pigment in the joints cause unusual transmission of mechanical loading to the subchondral bone, which may alter bone remodelling in AKU patients.

As data showed in Figure 3.1, the mean HU measured at the lowest lumbar level (L5) was statistically higher than the rest of the lumbar levels. This suggests that the density of lumbar vertebrae may be different depending on the anatomical level. From lumbar HU values in both genders, females seem to have slightly higher HU values at all lumbar levels compared to male patients; however, there was no evidence that gender significantly influences the measured values. This suggests that the differences between HU values may not related to gender; instead, the effect may occur due to the individual difference between the measured patients. A previous study evaluating the relationship between lumbar HU values and sex for 18 females and 7 males supported the findings in this chapter [83]. Although the mean age of AKU patients in this chapter was 50.8 years old compared to 71.3 years old in Schreiber's study, similar findings

was found in both studies. Schreiber *et al*. found that male patients had slightly higher HU values compared to female patients; however, the differences were not statistically significant [83]. The measured HU values throughout L1-L4 by Schreiber were 175.7, 173.3, 169.5, 170.9 and 165.3, 165.1, 164.0, 164.4 for males and females, respectively, while in this chapter it was 138.25, 133.02, 130.05, 145.0 and 142.52, 154.33, 137.87, 147.00 for males and females, respectively. The differences between the results here and Schreiber study may be due to the small sample size and different mean age. Different CT systems may also influence the HU values, so caution must apply when comparing the quantitative values with the literature.

Regarding the head of the femur HU measurements, no data were found in the literature. Most of the published work has concentrated on lumbar spine measurements. In fact, the spine is considered as one of the best skeletal sites for quantitative assessment of bone metabolism by many researchers for several reasons. First of all, spinal bone turnover is usually greater than those detected at other bone sites. Anatomically, spine vertebrae is rich in trabecular bone, which is less dense but highly vascularised compared to cortical bone [107]. Cortical bone represents the minority of the bone mass, whilst trabecular bone accounts for the majority of bone turnover, which is associated with bone remodelling. Second of all, the spine is the primary weight-bearing region in the body, which is subjected to high mechanical stress, causing osteoblast differentiation and stimulation. As a result of these factors, bone turnover and osteoblastic activity will be increased in the spine area [124]. In the current study, the head of the femur result is consistent with lumbar spine findings where no significant differences between males and females were found. A possible explanation for this might be that the effect of losing bone tissues and developing osteoporosis in both genders is similar throughout the entire skeleton. These results may be due to menopause triggers in women, and physical inactivity in men. Therefore, hormonal changes in female and physical inactivity in men may cause an equal effect on bone density for AKU patients.

In relation to the age effect, it was noted that HU values obtained at L1-L5 decreased significantly with increasing age ($P < 0.01$, $R = -0.632$; Figure 3.11.). The differences in average lumbar levels HU values among different age groups were statistically significant between the 5^{th} and 6^{th} decade of life ($P = 0.045$), following the predictably

decreasing trend with increasing age. Femoral HU results seem to be consistent with lumbar HU results, where a significant decrease in the HU values with ageing was found ($P < 0.001$, $R = 0.558$). This finding broadly supports the work of other studies in this area linking low HU values with age. Batawil *et al*. measured HU in lumbar vertebrae (L1-L4) for 114 women who underwent an abdominal CT scan [85]. In that study, a strong correlation between decreased HU values at L1-L4 and increasing age was found; lumbar spine HU values were significantly decreased from 182 HU at the 4th decade to 82 HU at the 8th decade. Lee *et al*. [81] reported HU values in lumbar vertebrae L1-L4 in 128 female patients (mean age 66.4) with low back pain who underwent a CT scan. Lee *et al*. and his co-worker also found a decreasing trend at L1, L2, L3 and L4 with increasing age ($R = 0.673$, $R = 0.794$, $R = 0.766$, $R = 0.713$, respectively) [81]; subgroup analysis showed significant differences between the 50s and 60s groups, and between 70s and 80s groups at L1-L3. At the L4 level, a difference was noted between the 60s and 70s. Lee *et al*. also reported no significant differences between the 40s and 50s at any lumbar vertebrae levels. It is encouraging to compare the findings among age groups in this chapter with that found by Lee *et al*.[81], who found that the average lumbar HU values in the 40s were 175.0 ± 48.9, in 50s was 150.2 ± 40.4 and in 60s was 97.5 ± 39.7. Interestingly, a similar finding has been detected in this chapter where the average lumbar HU value was 177.59 ± 45.92, 142.44 ± 48.39, and 94.8 ± 50.27 among the 40s, 50s and 60s, respectively. These results reflect those of Batawil *et al*. [85] also who found very similar HU values among these age groups. Schreiber *et al*. also found linear decreasing HU values in the lumbar spine by decade, ranging from 225.1 HU in the 2nd decade of life to 78.7 in the 8th decade of life [83]. In this chapter, lumbar HU values followed a similar decreasing trend confirming the strong correlation between HU values and age.

There are several possible explanations of the age influence on HU measurements. These results may be explained by the fact that the structure of bone changes as ageing occurs, and causes a loss of bone tissue, calcium and other minerals, and therefore loss of bone mass [165]. Another possible explanation for this is the physical inactivity which will cause bone loss. Hormonal changes related to ageing may also be connected to losing bone tissue. From this point, decreased HU value in bone with age can be explained by bone mineral density reduction. In fact, it is more likely that the overlap

between ageing and ochronosis in AKU patients lead to more bone loss compared to the general population.

3.4.2 SUV measurements

This study is the first study that has investigated skeletal involvement for patients with AKU using semiquantitative ^{18}F-NaF PET assessment method. The results of this study showed abnormal ^{18}F-NaF uptake at lower spine and hip sites, refelecting bone turnover in AKU patients. Low SUV_{max} values in the lumbar vertebrae and head of the femur indicate low hydroxypeptite crystals which may be associated with ochronosis in AKU patients. High SUV_{max} values were detected in an area of early and active bone changes in AKU patients due to increased -^{18}F binding sites in the area of active bone formation. In fact, the accumulation of ^{18}F-NaF in the lumbar spine is associated with increased hydroxyapatite crystals of newly formed bone which reflects the active bone formation and bone remodelling lesions and can be identified as areas of increased SUV value. It is more likely that bone turnover and bone remodelling is associated with ochronotic pigment which deposited in the cartilage tissues. Although there was no previous PET quantitative data for patients with AKU in the literature to compare our reults with, it is more likely that AKU patients have abnormal ^{18}F-NaF measurements due to ochronotic arthropathy compared to the general population.

There are several published studies which reported bone SUV measurements from the normal cases and for those patients with bone disorders. Win *et al.* [124] reported the maximum SUV values from normal skeletons for 11 patients without a history of cancer or metabolic bone disease using ^{18}F-NaF -PET/CT bone scans. In that study, the mean SUV_{max} of the lumbar vertebrae (L1-L5) was 7.27 and ranged from 7.04 to 7.72, while lumbar SUV_{max} for AKU patients in this study was 10.54 and ranged from 5.2 to 15.91. Puri *et al.* [131] also reported lumbar spine SUV in 12 healthy postmenopausal women mean age 62.6 years, and found that SUV was 6.005 ± 1.47, significantly lower than the findings in this chapter. Although the findings of the current study do not match with literature, the differences in the values were expected due to the differences in the sample size and the nature of bone tissues between AKU patients and non-AKU patients. AKU patients more likely have degenerative bone and joint disease, therefore high SUV values in active and ongoing bone turnover area was

expected. This observation may support the hypothesis that HGA deposition in bone tissues may be correlated with increased bone resorption rate, leading to accelerated bone loss in patients with AKU. These damages would more likely increase the $^{-18}$F-NaF binding sites, therefore high SUV_{max} would be detected.

The results in this study showed that mean SUV_{max} values throughout L1-L5 were similar, with no statistically significant differences between the measured levels. The results reflect those of Win *et al*, who also found that lumbar levels have similar SUV_{max} values [124]. This suggests that the radiotracer uptake in the spine may be similar in all lumbar vertebrae levels.

In terms of quantifying the femoral site, similar mean SUV_{max} values were measured from both the right and left site which are far above those observed by Win *et al*. and Puri *et al*. The average SUV_{max} value at the femoral region in this chapter was 4.71, compared with 2.22 and 2.32 in literature. These differences are interesting, but also not surprising. These results may reflect differences in bone turnover between AKU patients and the general population. The comparison here appears to support the assumption that bone turnover increased ^{18}F-NaF uptake throughout whole skeleton in those patients with metabolic bone disorders compared to general population.

The findings of other osteoarthropathy studies confirm that the deposition of radiotracer in bone turnover lesions is higher than in healthy sites. Hip OA has been evaluated at various stages using SUV and compared with X-ray images and pain scale. The progressive OA stages showed significantly high SUV_{max} compared to the early-stage cases [166]. Even early OA stage cases without OA radiographic findings, but with pain showed a radiotracer accumulation in the affected sites [167]. Kobayashi *et al*. [133] assessed the SUV at the hip joints and he observed an accelerated bone remodelling rate in various stages of OA; SUV values were compared with radiographical findings in MRI and the severity of pain. Kobayashi *et al*. pointed out that positive lesions in PET scan had a SUV_{max} of 6.5 and higher. The authors reported that the positive joint lesions were more detectable in PET scans in comparison to MRI (47 in PET vs 25 in MRI), suggesting that PET can identify musculoskeletal involvements earlier than MRI.

As shown in Figure 3.8, the mean SUVs of all lumbar vertebrae levels were significantly higher than the mean SUVs of the femur regions (10.45 ± 2.17 and 4.94 ± 3.25, respectively). Comparing the findings with those of other studies confirms that ^{18}F-NaF uptake in the spine is higher than in the femoral bones. These results are consistent with that found by Win *et al.* [124], who reported that mean SUVs of the femoral bones are lower than the mean SUVs of the spine. This also accords with Puri *et al.* [118] findings who demonstrated higher bone turnover at the spine than the proximal femur. Therefore, a higher deposition of ^{18}F-NaF in the vertebrae compared to the head of the femur was expected and normal. This is a positive finding providing confidence in the quality of the outcomes reported in this study, and the measurement methods which have been used to quantify ROI in this study.

In reviewing the literature, no data were found on the question of sex effect on the bone SUV values measured from ^{18}F-NaF PET/CT scans. The results of this study found that there is no significant differences in lumbar and femoral SUV_{max} between males and females. Although male patients had slightly higher SUV_{max} values, it was not statistically significant ($P > 0.05$). This study produced results which corroborate the findings of Kaneta *et al.* [168]. Kaneta measured SUV in the normal vertebrae for 29 patients including 8 females and 21 males who underwent ^{99m}Tc MDP SPECT/CT scan. He reported that male patients had higher SUV values in the spine compared to the female patients, suggesting that these findings reflect differences in bone mineral density which is higher in males compared to females.

The results of this chapter found that age seems to affect ^{18}F-NaF uptake in the lumbar vertebrae in patients with AKU. As data showed, lumbar vertebrae SUV_{max} values decreased with age ($P = 0.006$, $R = 0.432$). This also accords with earlier observations in the HU (section 3.3.1.1.2), which showed a reduction in HU values with age in the lumbar vertebrae. The similar finding in both HU and SUV values could be linked. A reduction in HU_{mean} reflects low bone density which means less hydroxyapatite, resulting in a low ^{18}F-NaF uptake. Another possible explanation for this result may be related to spine perfusion. It was hypothesised that blood flow and osteoblastic activity reduced with age. Therefore, it is likely that the reduction in spine perfusion as a result of ageing would reduce the ^{18}F-NaF transfer to the spine vertebrae [118]. This finding may explain the decline in ^{18}F-NaF uptake with age. Therefore, it is not surprising that

a negative trend in lumbar levels SUV_{max} with age has been noted. In elderly patients, inactive or stable bone turnover lesions which were established years before might have fewer ^{18}F-ion binding sites, therefore decreased ^{18}F-NaF uptake, which can be identified as an area of low SUV values. Several studies have shown the same negative trend between lumbar SUV and age. Win *et al.* [107] examined the age effect in the normal spine, and he found a reduction in SUV_{max} in spine vertebrae at different levels with age; however, the reductions were not statistically significant. Ayubcha *et al.* [169] also reported a negative trend in lumbar spine SUV_{mean} with age but also without statistical significance.

In contrast to the earlier lumbar vertebrae findings, no significant reduction in the values were found between femoral SUVs and age. However, these findings are broadly consistent with those observed by Win *et al.* [107], who reported that age did not significantly affect the ^{18}F-NaF uptake in healthy bone regions. The findings of this chapter revealed that SUV_{max} of the femoral head had a similar trend with age as in the normal skeleton, suggesting that generalised rates of bone turnover in the hip region for AKU patients and normal patients are very similar. Although in this section no direct trend between SUVs and age was found, the results were limited to the number of patients who had not undergone femoral head replacement. Most of the eldery AKU patients had a metal stem placed into the femoral hollow centre; therefore, it is likely that these unmeasured cases could account for some aspect of findings here, causing a possible source of error.

Looking more deeply among age groups, patients in their 30s and 40s are more likely to have normal osteoblastic activity and normal blood supply to the spine and hip area; therefore, SUV measurement reflects the normal distribution of ^{18}F-NaF through the spine and femoral head in these AKU patients. In contrast, patients in their 50s and 60s tended to have a severe joint pain and disability. In older patients, they are more likely to have inactive osteoblast activity due to ageing and abnormal blood flow to the spine and hip area, which will cause fewer binding sites, leading to low ^{18}F-NaF deposition in bone. In general, most of pathological bone diseases are associated with an increase in local bone remodelling and vascularization [170]. On bone scans, this associated bone response is shown as a concentration of accelerated radioactive tracer absorption. The advance stage of bone or joint disorder provide minimal bone

remodelling and a disturbance in blood flow; therefore, in the late stage of bone and joints degeneration, the bone image findings are characterised by low radiotracer uptake area [171].

From the results of SUV values at each age group, young AKU patients were seen to have higher SUV_{max} values in the lumbar spine (L1-L5) compared to older patients. The average SUV_{max} in lumbar vertebrae levels decreased from the 30s to the 60s. Although the differences in the SUV_{max} for the average lumbar levels between age groups were only statistically significant between 50s and 60s, this result supports the idea of the association between ochronosis and age. It is probably that bone turnover is active in AKU pateints at the late 40s and can be detected in PET scans at the early 50s showing the peak bone turnover process.

3.4.3 T-score measurements

In this study, lumbar and femoral T-score values from DEXA reports were analysed and compared with gender and age. Statistically, no significant differences in T-score values between males and females were noted at neither lumbar spine nor the proximal femur (P = 0.1 and P = 0.25, respectively). These findings agree with HU and SUV results, suggesting that gender has no significant effect on bone radiographic quantitative values for AKU patients. As mentioned in the HU section, previous studies have reported that there are no significant differences in bone density values between males and females in non-AKU patients [83]. Therefore, it seems that this also applies to AKU patients. In contrast, Daly *et al.* [172] compared age and gender-specific changes in bone mineral density (BMD) over ten years of study, and found that the annual loss in BMD for female patients was significantly higher than male patients aged 60 years and older (0.5-0.7% greater).

In the current study, no correlation was noted between lumbar T-score and age for AKU patients (Figure 3.20), suggesting that there is no direct correlation between bone mineral density measured from DEXA scan and age. A reduction in lumbar T-score with age was expected due to bone loss with ageing; however, this trend was not evident in this part of the investigation. In contrast to the earlier lumbar spine T-score findings, there was a strong correlation between femoral T-score and age (R= 0.571,

P < 0.05). Young AKU patients had healthy femoral T-score ranges representing normal bone density, while most of the older patients had an osteopenic T-score range. There is no debate that bone density is reduced with age; but the results in this sections showing no statistically significant correlation between lumbar T-sore values and age which could also be related to the disease severity in AKU patients. It has been widely agreed that bone turnover is coupled very tightly in the first three decades of life to maintain a steady-state between bone formation and bone resorption. Around the age of 20 years in women and older in men, bone mass reaches a peak; after that, bone turnover continues causing a gradual bone mass reduction [173].

In AKU cases, bone density measurements may be problematic as extensive disc degeneration complicate bone densitometry in ochronotic patients. Spinal DEXA measurements may be influenced by severe disc calcification, and the results may not reflect a true representation of bone density. It has been reported previously that, hip BMD can be lower than spinal BMD due IVD calcification and the formation of osteophytes [48]. The spine calcification in conjunction with reactive arthritic changes mainly concentrates at the edges of vertebral bodies as osteophyte formation, which substantially alters spinal measurements and overestimate the measured bone density values in DEXA scan [48]. Abdominal aortic calcification, which is also common in AKU cases, can also cause a false high bone mineral density. For this reason, some articles suggested measuring bone density at the central or mid vertebral body rather than the posterior-anterior or lateral vertebral body to represent accurate vertebral density [48].

A number of large studies in this area suggest that spinal BMD from DEXA scan is not considered a significant surrogate marker for spinal osteoporosis in osteoarthritic patients. In some cases, DEXA reports may indicate normal spinal bone density while the patient is osteoporotic. This might be related to the DEXA imaging technique. In DEXA, bone density values represent the estimated amount of all mineral density in the path of X-ray beam between L2-L4 levels. Therefore, calcified regions within the X-ray path could interfere the lumbar bone density values.

In patients with ochronosis, IVD calcification is highly expected due to ochronotic deposition between the vertebrae. Therefore, this calcification and osteophyte

formation may likely influence the lumbar density measurements in a DEXA scan resulting in high T-score values. Therefore, lumbar bone density values measured from DEXA scans in AKU patients must be interpreted with caution. Furthermore, BMD assessment in ochronotic patients shows low bone mineral density at the hip region, while lumbar value was within or higher than the values of the control group [75]. In the current study, most of the AKU patients had lower femoral T-score values compared with the lumbar T-score values, giving a diagnosis of osteopenia and osteoporosis. According to the lumbar T-score, 81% of the AKU cases were diagnosed as normal, while only 32.4% of those cases were diagnosed as normal based on femoral T-score. These results are in agreement with Aliberti *et al*. [75] findings who investigated skeletal involvement in ochronotic patients. Aliberti *et al*. evaluated lumbar spine and femoral bone mineral density (BMD) from DEXA scans for 7 AKU patients (5 males and 2 females), age range from 26 to 82 years. In that study, Aliberti found that one patient had normal bone density at the femoral site, three patients were osteopenic, and three patients were osteoporotic. He reported that lumbar bone density provided overestimated T-score results caused by IVD calcification and osteophyte formation.

In general, DEXA measurements have several limitations. First, DEXA results reflects both cortical and trabecular bone, however, bone turnover appears earlier in the trabecular bone compared to cortical bone. Therefore, DEXA values may possibly fail in detecting early osteoarthropathy in the spine. Second, DEXA measurement is affected by the size of patient. Therefore, overweight and obese patients may have false T-score values. Notwithstanding these limitations, at present, T-score from DEXA scan is the only accepted method by WHO to diagnose osteopenia and osteoporosis. However, searching for more accurate diagnostic tools to estimate bone density is needed.

3.4.4 Correlation between HU and T-score

Throughout this study, a moderate correlation between HU values obtained from CT scans across lumbar vertebrae and bone mineral density values measured by DEXA scans was demonstrated with a $R = 0.503$ and $P = 0.002$ (Figure 3.22). This finding is consistent with that of Schreiber *et al*., who found a moderate correlation between HU values and T-score throughout L1-L4 ($R= 0.48$, $P < 0.0001$) [83]. This also accords with

Barawil *et al*. [85] observations, who reported correlation coefficients between HU and T-score throughout L1-L4 to be 0.509, 0.473, 0.492, and 0.525, respectively, similar to the results in this chapter. These findings significantly supported the results in this chapter.

On the other hand, several reports have shown that HU values measured from CT had a strong correlation with bone mineral density values (T-score and absolute BMD values) measured by DEXA scans throughout the lumbar levels. Lee *et al*. [81] reported a strong correlation across L1-L4 between HU and T-score with correlation coefficients of 0.673, 0.794, 0.766, and 0.713, respectively, and between HU and BMD with correlation coefficients of 0.657, 0.774, 0.737 and 0.673, respectively. Another clinically relevant finding was also found between HU measured from CT and BMD measured by quantitative computed tomography (QCT); a more complex CT technique. In a previous study of 30 healthy patients, Gerety et al. [164] reported a significant correlation between HU and QCT BMD measured from L1 level ($R = 0.83$, $P > 0.005$).

Since 2011, several studies have been published comparing HU values from CT scans with bone density measurement values from DEXA scans [83]. An initial objective of current and ongoing studies is to identify the sensitivity and specificity of HU values obtained from CT for the detection of osteopenia and osteoporosis. These findings might help us and others to establish the range of HU values that can be used to represent normal, osteopenia and osteoporosis. In the present study, AKU patients with normal T-score values in lumbar vertebrae had a mean HU value of 152.93 ± 52.677, and those with osteopenia had a mean HU value of 92.67 ± 33.44. It was difficult to represent and estimate the HU value for the osteoporotic group due to a limited number of patients who had osteoporosis T-score values at L1-L4. Only one patient had an osteoporotic T-score value of 19 HU, making this finding uncertain.

Although several studies suggested HU thresholds that represent high sensitivity and specificity for detecting normal, osteopenia and osteoporosis [81–85,87,89,164], these results should be interpreted with caution. Each study suggested a different range of HU values representing normal, osteopenia and osteoporosis cases (see Table 1.4). These results are likely to be related to bone radiodensity which can be influenced by several

factors. Vertebral bone density measurement from the CT scanner is dependent mainly on the CT system, the tube voltage (energy of the photons) and the imaging protocol. Therefore, the differences in the literature are expected as each CT department have their local CT system and use different imaging parameters. To develop a full picture in this area, additional work would be needed.

Regarding the femoral site, the head of femur HU values has a strong correlation with the femoral T-score ($R = 0.796$, $P < 0.001$), as shown in Figure 3.22. In the present study, AKU patients with normal T-score values in the proximal femoral head had a mean HU value of 270.53 ± 39.11, those with osteopenia had a mean HU value of 231.37 ± 35.49, and those with osteoporosis had a mean HU value of 161.59 ± 31.59.

Although no previous data were found on the correlation between femoral HU and T-score in the literature, the findings reported in this chapter are particularly interesting and encouraging. These findings suggest that the head of femur HU values can predict bone density at the femoral site. Therefore, it is a promising finding which introduces that HU values could be used to diagnose osteoporosis for those AKU patients who have not undergone a DEXA scan and had CT, SPECT/CT, or PET/CT scan for another reason.

3.4.5 Correlation between HU and SUV

To our knowledge, no study has investigated the correlation between bone HU values measured from CT and SUV values measured from ^{18}F-NaF PET. This study is the first study to examine the association between HU values and SUV values at lumbar and femoral bone regions. The results in this study showed an association between HU_{mean} values and SUV_{max} for average lumbar vertebrae levels ($R = 0.373$, $P = 0.002$). However, looking at each lumbar level individually in Figure 3.23, the significant correlations were noted only at the L1,L2 and L4 with a correlation coefficient of 0.517, 0.492 and 0.320, respectively and all had $P < 0.05$. At the same time, there was no significant correlation at L3, and L5 in which the correlation coefficients were 0.130, and 0.254, respectively, and all had $P > 0.05$. This inconsistency between the lumbar levels might be related to mechanical forces acting on the lumbar spine. It is possible that upper lumbar levels had increased axial forces acting upon them due to

its flexibility; therefore, the active bone turnover can be detected earlier in PET scan at those levels.

On the other hand, no significant correlation was noted between HU and SUV at the femoral site as shown in Figure 3.24. (R = 0.277, P = 0.113). This finding may be somewhat limited by the number of patients who were involved in this section. As mentioned earlier, patients who underwent joint replacement were excluded from the femoral measurements. So, these unmeasured cases may account for some aspects of the results.

Taken together, a correlation between the regional bone attenuation coefficient and regional ^{18}F-NaF uptake was expected due to strong correlation between bone density and hydroxyapatite sites. In fact, high-density area has higher HU values and therefore higher hydroxyapatite sites for ^{18}F-NaF to bind with, leading to high SUV. Further investigations are needed to confirm whether bone HU values obtained from CT correlate with ^{18}F-NaF uptake from PET scan or not.

3.4.6 Correlation between SUV and T-score

This study demonstrates no clear correlation between SUV_{max} values obtained from ^{18}F-NaF PET across lumbar vertebrae and bone mineral density values measured by DEXA scan with correlation coefficient 0.069 and P = 0.684. Similar findings have been noted in the femoral site, which also showed no correlation between the head of the femur SUV_{max} and femoral T-score (R = 0.166, and P = 0.339). Based on WHO criteria, in the present study, AKU patients with normal T-score values in lumbar vertebrae had a mean SUV_{max} value of 10.76 ± 2.22, and those with osteopenia had a mean SUV_{max} value of 9.37 ± 2.62. The SUV_{max} for an osteoporotic T-score is not certain as it is reflecting the value of one patient only who had lumbar vertebrae T-score below -2.5 and had 8.15 SUV_{max}. On the other hand, AKU patients with normal T-score values in the proximal femoral head had a mean SUV_{max} value of 4.63 ± 1.96, those with osteopenia had a mean SUV_{max} value of 4.45 ± 1.34, and those with osteoporosis had a mean SUV_{max} value of 6.54 ± 6.66.

The weak association between T-score and SUV_{max} was unexpected. The findings of the current study do not support the previous hypothesis, which suggests that low bone density is associated with low ^{18}F-NaF uptake in the bone. Following the expected correlation between HU and SUV, it was also expected to see a strong relationship between T-score values and SUV values due to limited hydroxyapatite sites in a low-density lesion. A possible explanation for this might be that the measurements of bone density value in DEXA scans is obtained from the trabecular and cortical bone regions, while in the current study, SUV values was measured from the trabecular areas only. It is possible that these unmeasured areas could account for some aspects of the relationship. The other possible reason could be explained by the fact that DEXA results are overestimated due to IVD calcification and vascular calcification, which may not represent true information about bone density.

As noted from the examples, patients who reported decreased SUV_{max} values had either very low or normal T-score values. The reason for this is not clear, but it may have something to do with bone formation and the stage of disease. For example, in case of active bone turnover or bone remodelling, it would be expected to detect high SUV values, and after that when the affected area becomes inactive or stable, the ^{18}F-NaF uptake in that area could become low. This could explain what was noted in this chapter.

3.5 Summary

In AKU patients, ochronotic pigment can cause unusual transmission of mechanical loading to the subchondral bone, which may alter bone remodelling. ^{18}F-NaF PET/CT is a sensitive and accurate imaging technique which can detect early bone metabolism and joint arthropathy throughout the entire skeleton, including high-risk regions such as the spine and hip. The present study proposes a novel radiographic semiquantitative method which can be used to assess the progression of skeletal involvement in the spine and hip regions for AKU patients. The results from this study contribute to a deeper understanding of the disease state and progression in AKU patients.

The accumulation of ^{18}F-NaF in PET images is associated with hydroxyapatite crystals of newly formed bone which can be identified as areas of increased SUV value. In

addition to performing CT for attenuation correction purpose, CT data can be used as a diagnostic tool alerting the physician to investigate abnormal bone density specifically for those patients with rare metabolic bone diseases which may not otherwise be suspected.

IVD calcification is highly expected in AKU patients due to ochronotic deposition between the vertebrae. This calcification and osteophyte formation may likely result in unusually high bone mineral density and T- score values in DEXA scans. Because of this, spinal DEXA measurements may not reflect a true representation of bone density for ochronotic patients.

Based on the significant correlation between vertebral and femoral HU values measured from PET/CT scan and T-score values measured from DEXA scan, HU measurements can be used to estimate bone mineral density and detect bone disorders without adding extra radiation or cost to the patient. These results may also help others to find new ways of quantifying and extracting valuable data which are available but has rarely been used for identifying patients at high risk of fracture. Although positive HU findings were noted in this study, these results are not strong enough to suggest the replacement of DEXA with CT for bone mineral density assessment purposes.

Spinal HU and SUV measurements from lumbar vertebrae consistently decrease with each decade of life studied here in AKU patients due to reduced bone density mass and active bone turnover which might be associated with ochronosis and ageing. However, a moderate correlation between the average HU of lumbar bodies and SUV_{max} may need more investigation.

3.6 Limitations

This study has some limitations which must be considered. First, interobserver and intraobserver reliability have not been tested due to limited time and collaboration. Second, only two skeletal sites were evaluated in the current study which may not represent the global disease progression. Third, a non-AKU control group was not studied to statistically compare the quantitative bone values for general population subjects with AKU patients. Fourth, in this study, HU values obtained from CT images

included only trabecular bone density, while T-score values from the DEXA reports represented both cortical and cancellous bone. Three axial sections may not precisely summarise the density of cancellous bone as it is a heterogeneous tissues. Although trabecular bone is more important than cortical bone in order to determine fracture risk, it is possible that HU results from CT images underestimate the true bone mineral density [81]. Therefore, in the current study, the correlation between T-scores and HU values may represent some error.

3.7 Future work

Future investigations are required to confirm and validate the findings which were found in this study. First, interobserver and intraobserver reliability of the SUV and HU values need to be tested. This would strongly support the PET/CT measurement methods which were proposed in this study. Second, other bone sites such as the shoulder, tibia and humerus bone need to be assessed and quantified, in order to evaluate the impact of ochronotic pigment in multiple skeleton sites. Third, a non-AKU control group is needed to statistically compare the results of AKU patients with the general population. Also, it would be interesting to establish HU thresholds for normal, osteopenia and osteoporosis in patients under local imaging protocols in the local CT department using a larger sample size.

3.8 Conclusions

This chapter has shown that:

- ^{18}F-NaF PET/CT scan is a promising imaging technique which can help to detect early ochronotic arthropathy.
- AKU patients had low HU values in the lumbar vertebrae and head of the femur indicating low bone density.
- The accumulation of ^{18}F-NaF in a PET image is associated with increased hydroxyapatite crystals of newly formed bone which reflects the active bone formation and bone remodelling lesions and can be identified as areas of increased SUV value.

- In elderly AKU patients, inactive or stable bone turnover lesions which were established years before might have low -^{18}F ion binding sites, and therefore decreased ^{18}F-NaF uptake, identifying as an area of low SUV value.
- Bone HU and SUV values in the lower spine consistently decrease with age, indicating decreased bone density and osteoblastic activity with age.
- The reduction in spine perfusion as a result of ageing would also reduce the ^{18}F-NaF transfer to the spine vertebrae.
- There were no significant differences between the ^{18}F-NaF PET/CT semiquantitative values nor DEXA measurement of males and females at neither spine nor femoral sites.
- Spinal DEXA measurements are influenced by severe disc calcification in AKU patients, and thus the results may not reflect a true representation of bone density.
- There was a strong correlation between vertebral and femoral HU values measured from PET/CT scans and T-score values measured from DEXA scans, suggesting that HU measurements can be used to estimate bone mineral density without adding extra radiation to the AKU patient.
- There was a moderate correlation between the average HU and SUV_{max} of the lumbar bodies, which needs further investigation.

4 Cross-sectional study of lumbar intervertebral disc degeneration at baseline in alkaptonuria patients from the SONIA 2 study using quantitative analysis by ^{18}F-NaF PET/CT and MRI

4.1 Introduction

In the previous chapter, regional bone formation in the lumbar spine and hip sites were quantitatively assessed in AKU patients from the SONIA 2 study by measuring HU_{mean} from CT and SUV_{max} from ^{18}F-NaF PET images. Also, the measured values were correlated with bone density values from DEXA reports. As pointed out in Chapter 3, ^{18}F-NaF PET/CT is a promising imaging technique which can successfully detect early bone involvements reflecting accelerated bone remodelling in ochronotic patients.

This chapter of the thesis is performed to detect and identify the lumbar joint changes for AKU patients. The present study is one of the first investigations to focus specifically on disc degeneration for ochronotic patients using two advanced molecular imaging modalities. The main aim of the current study is to evaluate the link between early molecular disc changes detected from ^{18}F-NaF PET/CT scans and the structural disc changes identified from MRI within lumbar spine. This study designed to identify lumbar intervertebral disc ^{18}F-NaF uptake by measuring SUV_{max} from PET images and identify disc structural changes by measuring the Pfirrmann score from MRI. Part of this study aimed to test the effect of gender and age on the SUV_{max} and disc degeneration score in AKU patients.

This study is divided into three sections. In the first section, lumbar disc degeneration is identified and quantified using ^{18}F-NaF PET/CT scans. In the second section, lumbar disc degeneration is scored from MRI. In the third section, the correlation between ^{18}F-NaF PET/CT and MRI results is investigated.

During the development of ochronosis, ochronotic pigment accumulates in the joints and articular cartilage, causing ochronotic arthropathy. In the spine, ochronotic pigment causes vertebral bone changes and joint degeneration, resulting in increased blood flow to spine, and accelerated bone remodelling in the affected area [3,35]. Ochronotic spinal changes manifest similar to spine arthritis through vertebral disc herniation, disk space narrowing, severe disc calcification, sclerosis, osteophytosis, and spondylitis [13,16]. In the early stages of disc degeneration, the interaction between the vertebral body and the IVD is critical not only to determine the disease profile but also to assess early changes in the spine.

Although there are no specific radiopharmaceuticals to image the articular cartilage, the ^{18}F-NaF radiotracer has been widely used to detect the changes relating to osteoarthritis and other joints disorders [101,103]. Early joint degradation assiocated with joint calcification is more likely be visible on ^{18}F-NaF PET imaging before other imaging techniques. The uptake of the bone radiotracer in the joint can be quantified using PET quantitative measurement methods such as SUV.

The principle of the MR scanner provides a clear separation between bone and soft tissues in vivo, offereing high-resolution images. The modified 8 level Pfirrmann grading system, is a simple, non-invasive, and convenient MRI method which can assess morphological changes and provide a visual evaluation of lumbar intervertebral disc degeneration; however, it is a subjective qualitative assessment method which can be inadequate for evaluating the end stage of disc degeneration [90,174].

4.2 Design of study

4.2.1 Patient group

In this chapter, a total of 34 AKU patients who were part of the SONIA 2 trial with a mean age of 48.38 ± 10.04 years old, ranging from 30 to 68 years old, were reviewed. These patients comprised of 19 males with a mean age of 48.68 ± 9.45 years, ranging from 30 to 62 years, and 15 females with a mean age of 48 ± 11.07 years, ranging from 30 to 68 years, with no statistical age difference between the groups ($P > 0.05$). The demographic characteristic of this population is summarised in Table 4.1. Patients with metal implants were not able to do an MRI and have been excluded from this analysis. Only patients who had both ^{18}F-NaF PET/CT and MRI within the same year were included in this study. Patients were grouped into four age groups, as shown in Table 4.2. In this study, 7 patients (21%) were between 30 and 39 years old, 12 (35%) were between 40 and 49 years old, 10 (29.3%) were between 50 and 59 years old, and 5 (14.7%) were above 60 years old.

Table 4.1. Demographic characteristics of 34 AKU patients who were part of SONIA 2 clinical trial and involved in this study classified by gender.

Data displayed as number of patients and percentage in each group. Age of the patients displayed as mean ± SD, minimum and maximum.

Gender	Patients no. (%)	Age ± SD (years)	Age range
Total	34	48.38 ±10.04	30 - 68
Male	19 (55.9%)	48.68 ±9.45	30 – 62
Female	15 (44.1%)	48.00 ±11.07	30 - 68

Table 4.2. The number of AKU patients at the beginning of the SONIA 2 clinical trial who underwent both ^{18}F-NaF PET/CT and MRI stratified by decade of life.

Age group	Gender	Patient no.
30 - 39 years old	Total	7
	Male	3
	Female	4
40 - 49 years old	Total	12
	Male	8
	Female	4
50 - 59 years old	Total	10
	Male	6
	Female	4
≥ 60 years old	Total	5
	Male	3
	Female	2

4.2.2 Image analysis

Baseline ^{18}F-NaF PET/CT images were displayed using Horos software. The images were analysed and interpreted, blinded to the MR images or results. As explained earlier in the Methods Chapter, (section 2.7) it was difficult to draw a ROI around the disc region only due to the advanced disc degeneration in most AKU cases; therefore, a ROI covering the disc area and the endplate of the two adjacent vertebrae was used and termed discovertebral unit (DVU).

Six regions of lumbar DVU from segment T12/L1 to segment L5/S1 from ^{18}F-NaF PET/CT and spine MR images were analysed. A total of 203 lumbar intervertebral discs were quantified as described in the Methods Chapter (see section 2.7). Patient

number 16 had metallic disc support at T12/L1, so only five DVUs were analysed for this patient.

^{18}F-NaF uptake within DVUs were quantitatively identified from PET images at three consecutive sagittal slices to assess and detect the extent of disc degradation. CT images were used in this chapter for attenuation correction and anatomical localisation of the disc area only. The ROI was drawn in CT image first to delineate the DVU clearly, than the same ROI was copied to PET image for SUV_{max} measurement. Lumbar discs from spine T2 weighted MR images were scored by a musculoskeletal radiologist, Dr. Alpesh Mistry, using the eight-level modified Pfirrmann grading system, blinded to the ^{18}F-NaF PET/CT images (see section 2.7.2).

4.2.3 Correlation

Differences in lumbar disc SUV_{max} values and Pfirrmann scores between gender and age were tested using the Pearson correlation coefficient. Multiple linear regression and polynomial regression were used, to assess the relationship between the quantitative values and age. Subgroup age analysis was investigated using one-way ANOVA. Within each lumbar DVU level, the SUV_{max} from the ^{18}F-NaF PET/CT scan and Pfirrmann score from MR images were compared to assess the relationships between ^{18}F-NaF PET/CT and MRI results using the Pearson correlation coefficient.

4.3 Results

4.3.1 SUV_{max} measurements

This section aimed to identify ^{18}F-NaF uptake by measuring SUV_{max} from PET images at the lumbar disc region to detect disc calcification for AKU patients. Figure 4.1 shows the lumbar SUV_{max} values, which were obtained from the lumbar DVUs across the T12/L1 segment to the L5/S1 segment for 34 SONIA 2 patients. Lumbar DVUs results from 18F-NaF PET/CT scan and MRI

Table 9.10 (appendix) displays the mean, minimum, and maximum SUV_{max} at each ROI. The mean SUV_{max} value of average lumbar DVU segments for all 34 AKU

patients was 15.12 ± 4.13, (range 6.93 – 23.84). Average SUV_{max} was 14.38 ± 5.10 (range 6.72 – 25.91) at T12/L1; 15.84 ± 6.41 (range 7.12 – 33.41) at L1/L2; 14.78 ± 5.2 (range 6.95 – 25.76) at L2/L3; 14.23 ± 5.01 (range 6.25 – 30.02) at L3/L4; 14.46 ± 5.06 (range 5.44 – 24.65) at L4/L5 and 17.11 ± 5.90 (range 7.14 – 27.20) at L5/S1. The highest mean SUV_{max} was detected at the lowest lumbar DVU (L5/S1) segment, as shown in Figure 4.1. Statistically, the SUV_{max} value of the L5/S1 segment was not significantly higher than to the rest lumbar segments ($P > 0.05$).

Figure 4.2 and Figure 4.3 show spine ^{18}F-NaF PET/CT images for four AKU patients. As noted from the images and the measured data in the table below the images, it appears that there is a clear separation between the vertebrae bodies with low ^{18}F-NaF uptake at DVUs in ^{18}F-NaF PET/CT images for young AKU patients. In contrast, in the elderly patients, focal hot areas were noted between the vertebrae with high SUV_{max} values.

4.3.1.1 Lumbar DUV SUV_{max} values and gender

Figure 4.1 and Table 9.10 (appendix) compare the SUV_{max} across the lumbar disc levels for each gender group. The mean SUV_{max} value for all lumbar DVUs across the T12/L1 segment to the L5/S1 segment was 16.15 ± 3.19 (range 8.59 - 21.58) for males and 14.11 ± 4.96 (range 6.93 – 23.84) for females. The SUV_{max} across the lumbar levels were very similar in both genders. Male patients had slightly higher SUV_{max} at all DVU levels than female patients except at L1/L2 level; the females had higher SUV_{max} value. However, statistical analysis using an independent t-test indicated that there was significant confounding differences between SUV_{max} for males and females at the L5/S1 level only ($P = 0.02$), while there were no statistically significant differences across the rest of the lumbar levels (all $P > 0.05$).

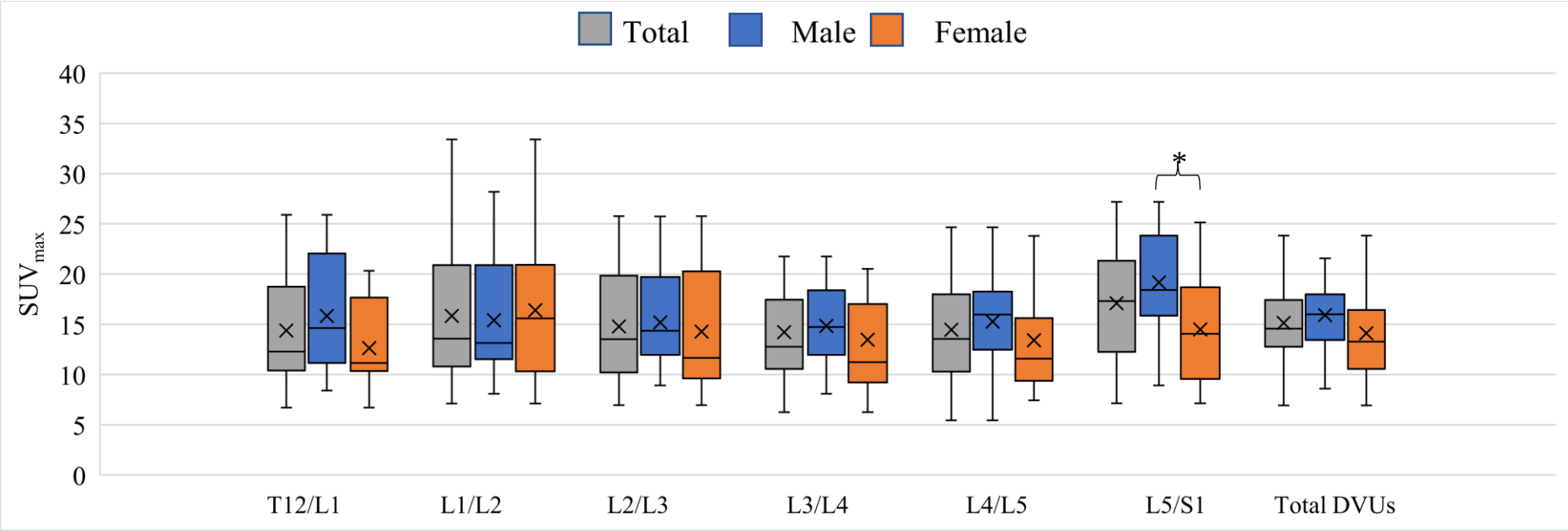

Figure 4.1. Mean SUV_{max} obtained from ^{18}F-NaF PET scan at each lumbar DVU for 34 AKU patients who were part of SONIA 2 clinical trial stratified by gender.

The results show the analysis of the baseline PET data for 19 males and 15 females AKU patients from six lumbar DVU regions from segment T12/L1 to segment L5/S1. SUV_{max} showed the highest value at the L5/S1 segment. Total DVUs; average DVU segments from T12/L1 to segment L5/S1. Table 9.10 (appendix) shows the statistical correlation between gender at all lumbar DVU segments. Males had slightly higher mean SUV_{max} at T12/L1, L2/L3, L3/L4, L4/L5 and L5/SI levels than females. By contrast, females tended to have slightly higher SUV_{max} at L1/L2 level only. The independent sample t-test revealed no statistically significant differences between males and females at T12/L1, L2/L3, L3/L4, L4/L5 ($P = 0.07$, $P = 0.67$, $P = 0.62$, $P = 0.44$, and $P = 0.3$, respectively). Statistically, AKU males had higher SUV_{max} value than the females at L5/S1 only ($P = 0.02$). In box and whisker, x is the mean value, and the line is the median.

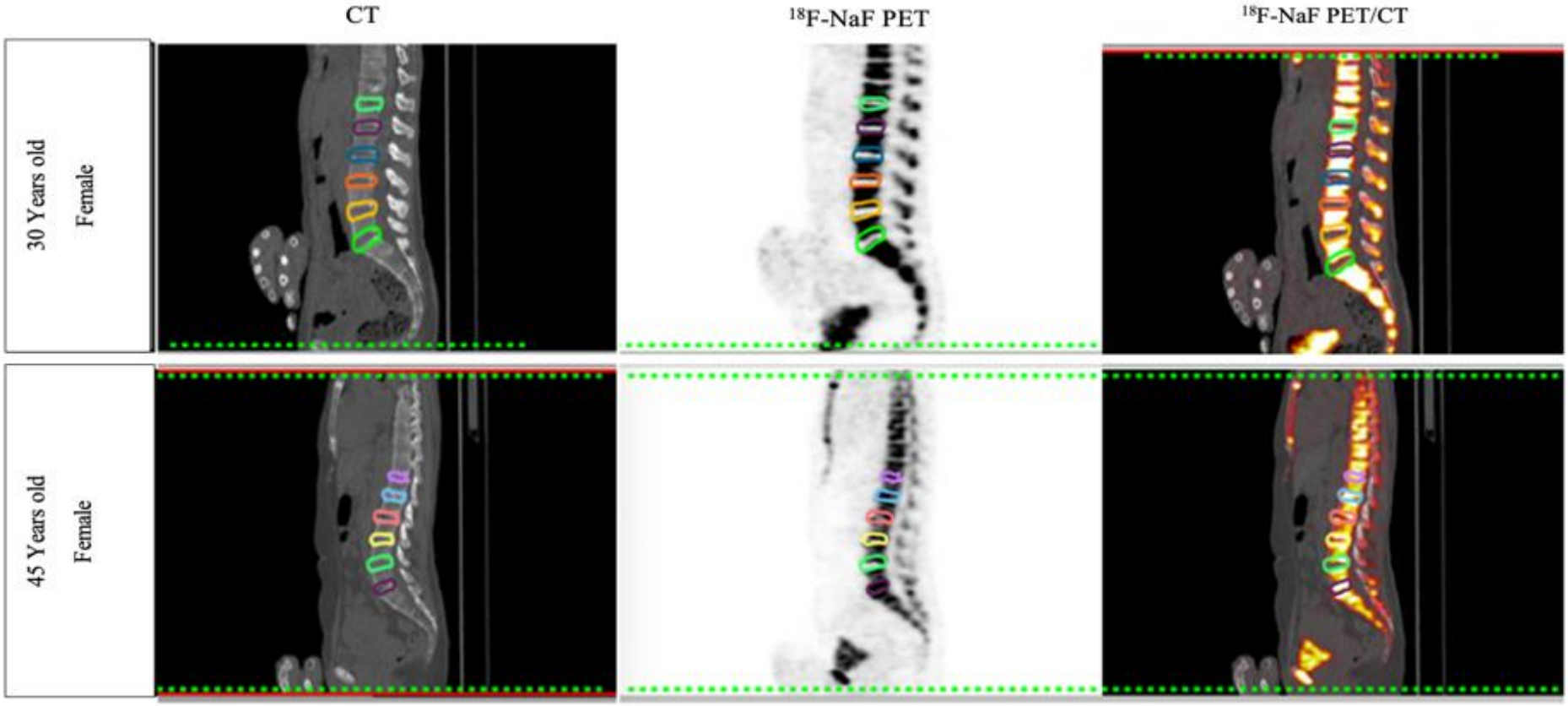

ROI	T12/L1		L1/L2		L2/L3		L3/L4		L4/L5		L5/S1		Total DVU	
	SUV_{max}	Grade	SUV_{max}	Grade	SUV_{max}	Grade	SUV_{max}	Grade	SUV_{max}	Grade	SUV_{max}	Grade	SUV_{max}	Grade
Pt #1	8.57	1	9.88	1	9.62	1	8.78	1	9.67	1	8.61	1	9.19	6
Pt #2	10.34	2	13.36	2	14.25	2	12.65	2	10.99	2	18.01	3	13.27	13

Figure 4.2. Coronal sections of CT, PET, and ^{18}F-NaF PET/CT for the lower spine for 30 years old and 45 years old AKU patients.

The SUV_{max} and Pfirrmann score (grade) for all lumbar DUV are displayed in the table below the images.

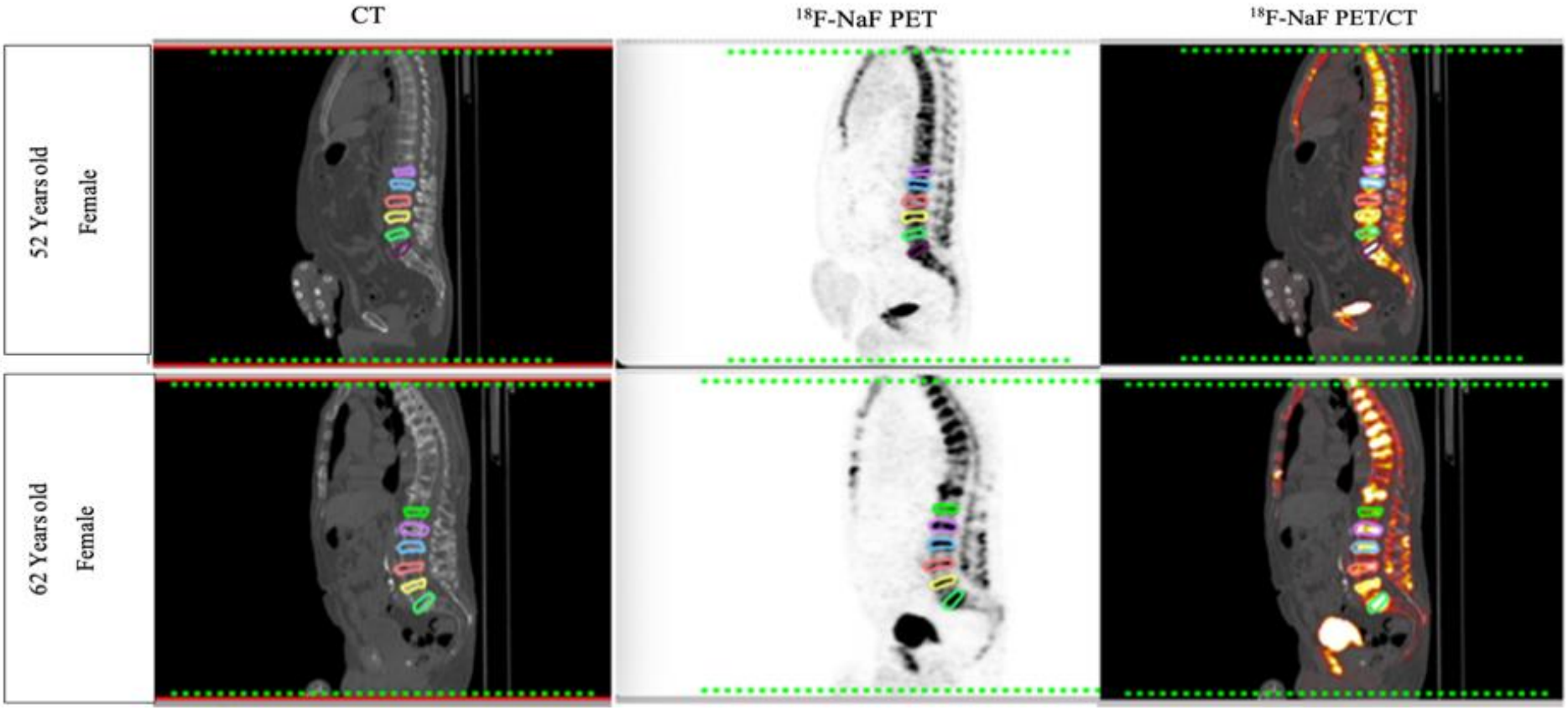

ROI	T12/L1		L1/L2		L2/L3		L3/L4		L4/L5		L5/S1		Total DVU	
	SUV_{max}	Grade	SUV_{max}	Grade	SUV_{max}	Grade	SUV_{max}	Grade	SUV_{max}	Grade	SUV_{max}	Grade	SUV_{max}	Grade
Pt #3	25.91	8	28.2	8	13.65	5	18.38	5	16.12	7	27.2	8	21.58	41
Pt #4	8.51	8	12.6	8	13.4	8	12.76	8	15.96	8	23.83	8	16.01	48

Figure 4.3.Coronal sections of CT, PET, and 18F-NaF PET/CT for the lower spine for 52 years old and 62 years old AKU patients.

The SUV_{max} and Pfirrmann score (grade) for all lumbar DUV are displayed in the table below the images.

4.3.1.2 Lumbar DUV SUV_{max} values and age

In this section, the effect of age on disc calcification was evaluated by examining the correlation between ^{18}F-NaF uptake and age at lumbar disc areas for AKU patients. Figure 4.4 shows the SUV_{max} against age for all AKU patients at each lumbar DVU. Multiple linear regression and polynomial regression were used, seeking for the best statistical correlation between SUV_{max} at each lumbar segment and age. The values of SUV_{max} increased gradually with age following by a declined in the later years. Young AKU patients had low SUV_{max} , below 15, then after the age of 40 years, the SUV_{max} values increased, reaching a maximum around the age of 44/50 years. From here, a general reduction in SUV_{max} measurements can be seen at most of DVU levels where the elderly AKU patients had a reduction in SUV_{max} measurements, decreasing to values comparable to that in young AKU patients.

Multiple linear regression indicated that SUV_{max} values were not significantly correlated with age at all DVU levels (R = -0.124, R = -0.034, R = -0.296 , R = -0.01 , R = -0.202, R= 0.143, respectively; all $P > 0.05$). As it is clear from Figure 4.4, a hill shaped trend in the data was noted at most of the lumbar disc levels; therefore, polynomial regression was fitted to the SUV_{max} data. The differences between multiple linear regression and polynomial regression analysis at each level is shown in Figure 4.4. When polynomial regression was applied, the R values were improved significantly in all DVU levels (R = 0.57, R = 0.44, R = 0.6 , R = 0.51 , R = 0.49, R= 0.52).

The mean SUV_{max} from the lumbar DVUs across the T12/L1 segment to the L5/S1 segment for each age group was measured, and subgroup analysis was performed as shown in Figure 4.5 and Table 9.11 (appendix). The average SUV_{max} for all lumbar levels was 12.99 ± 3.92 for 30-39 age group patients, 17.67 ± 3.97 for 40-49 age group patients, 15.45 ± 2.65 for 50-59 age group patients and 11.34 ± 3.6 for ≥ 60 years old patients. Generally, the youngest and oldest age group patients had low SUV_{max} in all DVU segments. Mean SUV_{max} values at all lumbar DVU segments increased from the 3rd decade of life to the 4th decade of life, where the highest mean SUV_{max} was detected at the average lumbar disc levels. Moreover, SUV_{max} values in the 5th decade patients were remarkably high. The SUV_{max} values started to decrease between the 50s and 60s

age groups in all lumbar disc levels. One-way ANOVA revealed that in the L2/L3, L4/L5 levels, there was a significant difference between the 30s and 40s age groups (P = 0.035 and P = 0.025, respectively). In L2/L3 and L4/L5 levels, there was significant differences between the 40s and 50s age groups (P = 0.002 and P = 0.003, respectively). In T12/L1 and L3/L4 levels, there was a significant difference in SUV_{max} values between the 50s and 60s age groups (P = 0.037 and P = 0.029, respectively). Interestingly, linear regression analysis showed that age did not affect the $SUV_{max,}$ but was found to be significant between the age subgroups at some of the measured lumbar disc levels. Therefore, in this section of the thesis, it was more precise to use polynomial regression rather than multiple linear regression to correlate SUV values at lumbar disc areas with age.

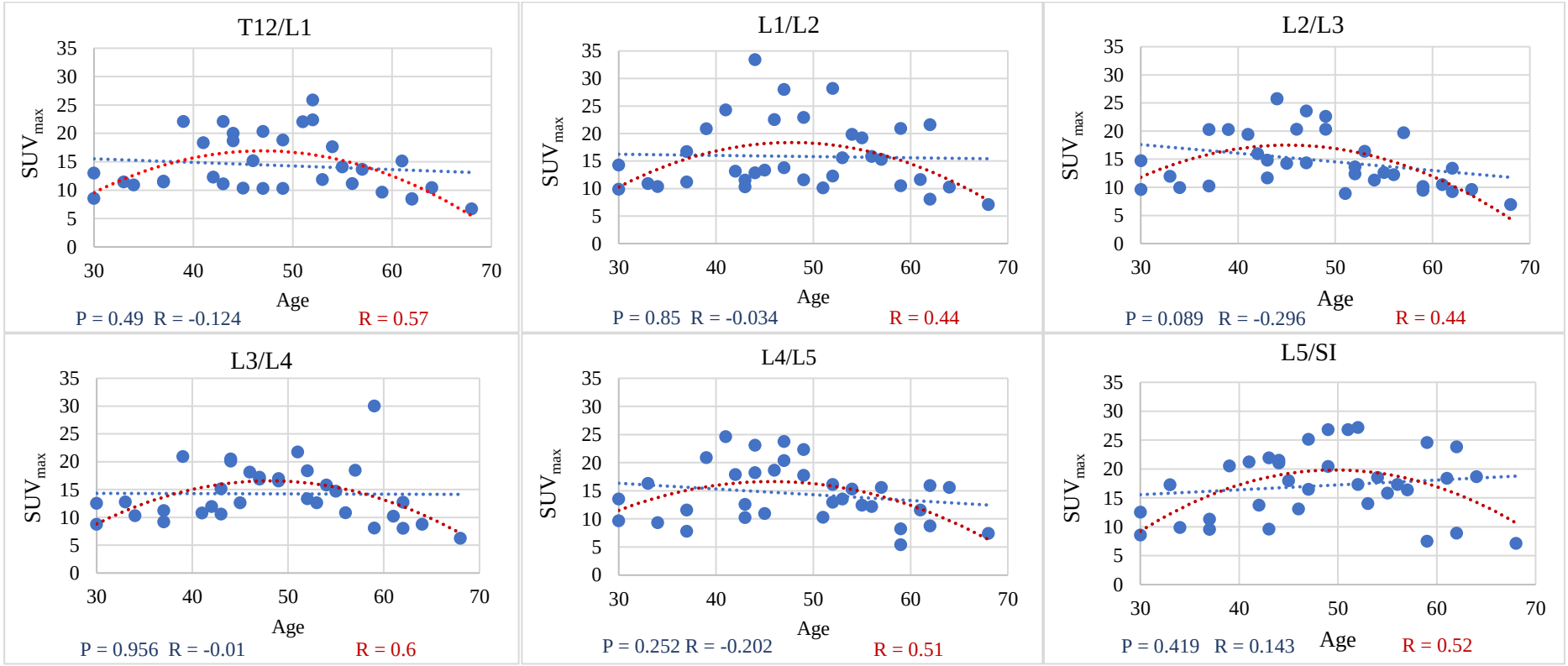

Figure 4.4. Scatter plots illustrating the correlation between SUV_{max} obtained from ^{18}F-NaF PET/CT and age at the lumbar DVU segments for 34 AKU patients who were part of SONIA 2 clinical trial.

The results display SUV_{max} of lumbar DVUs from T12/L1 segment to the L5/S1 segment in individual AKU patients with age. Linear regression analysis (blue dotted line) identified no statistically significant correlation between SUV_{max} and age in AKU patients at all DUV levels $P > 0.05$ (R = -0.124, R = -0.034, R = -0.296, R = -0.01, R = -0.202, R = 0.143, respectively). Polynomial function (order 2 polynomial line: red dotted line) was fitted to the AKU data (R = 0.57, R = 0.44, R = 0.6 , R = 0.51 , R = 0.49, R = 0.52, respectively).

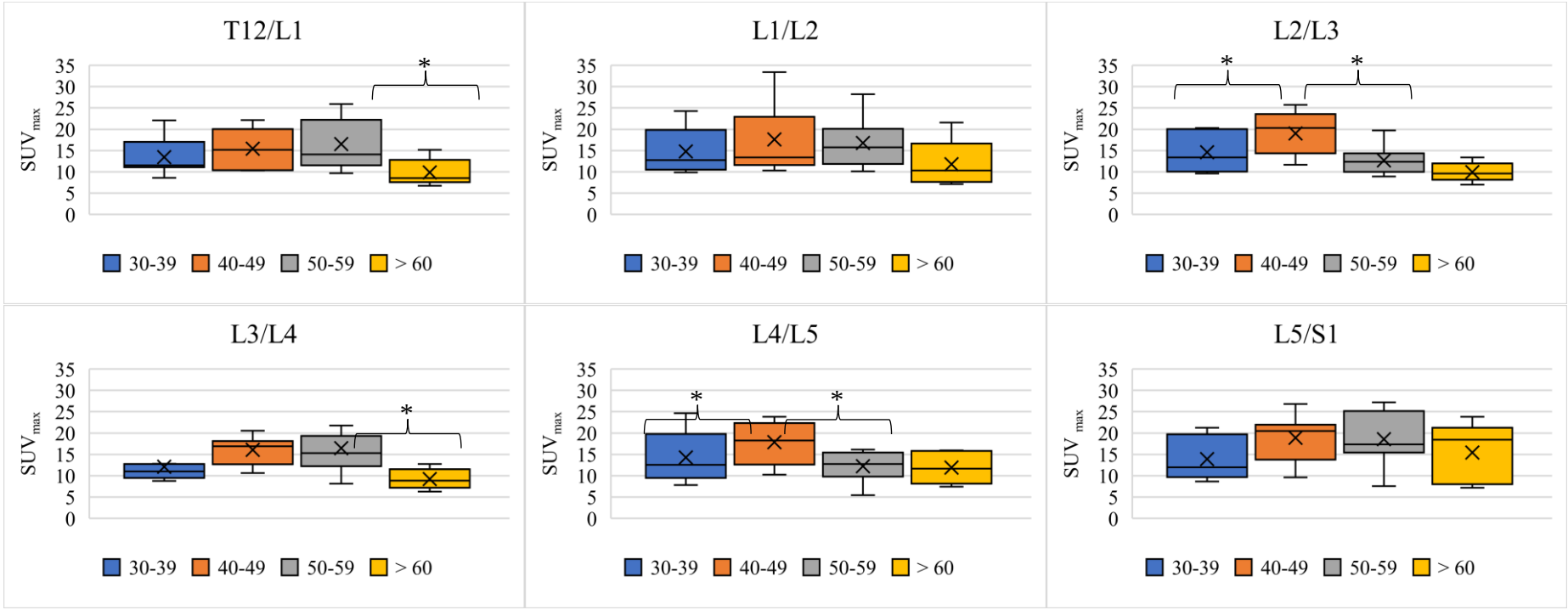

Figure 4.5. SUV_{max} for all lumbar DVU levels among four decadal age groups measured from baseline ^{18}F-NaF PET/CT scan for AKU patients who were part of the SONIA 2 clinical trial.

Table 9.11 (appendix) shows the lumbar DVU levels and age groups, indicating a statistically significant difference between subgroup analyses. *Groups which showed significant difference ($P < 0.05$). The difference between the 30s and 40s age groups SUV_{max} values were noted at L2/L3 and L4/L5 levels ($P = 0.035$, $P = 0.025$, respectively). The difference between the 50s and 60s age groups SUV_{max} values were noted at T12/L1 and L3/L4 levels ($P = 0.037$, $P = 0.029$, respectively). No significant differences were found in SUV_{max} values between any age group at level L1/L2 nor L5/S1. In box and whisker, x is the mean value, and the line is the median.

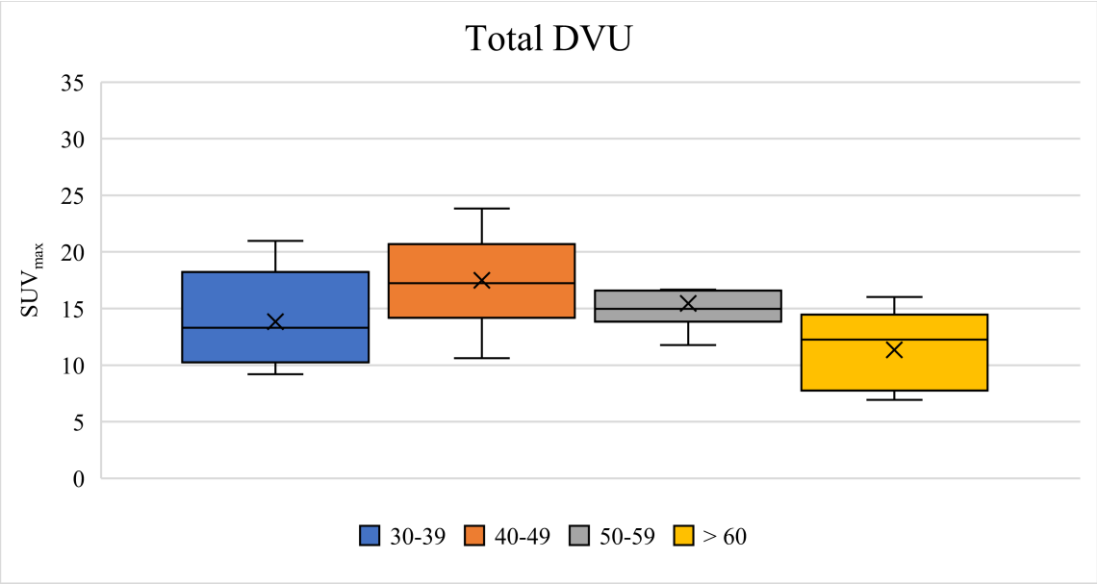

Figure 4.6. SUV_{max} for the average lumbar DVU level among four decadal age groups measured from baseline ^{18}F-NaF PET/CT scan for AKU patients who were part of the SONIA 2 clinical trial.

Table 9.11 (appendix) shows the lumbar DVU levels and age groups which indicated a statistically significant difference between subgroup analyses. No significant differences were found in SUV_{max} values between any age group at the average six lumbar DVU ($P > 0.05$). In box and whisker, x is the mean value, and the line is the median.

SONIA 2 patients were separated into four age groups by decade to look at the individual differences between the patients at each age group. ^{18}F-NaF uptake of individual cases was sensitive to the SUV_{max} measured at each lumbar DVU level. Substantial variation of SUV_{max} resulted in the classification of the individual patients into their absolute age at each DVU level, as highlighted in Figure 4.7. In the 30 to 39 age group (Figure 4.7), there was wide variation associated with the SUV_{max} measurement between the oldest patient in the group whose age was 39 years old and the rest of the patients whose ages were between 30 to 37 years old. The SUV_{max} values for that patient was closer to those patients in the 40s age group. It is evident that the patients in the 40s and 50s age groups had more differences between their values than in the other age group patients. In the age group 40-49 and 50-59, high SUV_{max} values were noted compared with the two other groups. The highest SUV_{max} (SUV_{max} = 33) was identified in a 44-year-old female, followed by a 59-year-old female with SUV_{max} = 30. The patients in the oldest age group (≥ 60 years old) mostly had low SUV_{max} values in all DVUs. The lowest SUV_{max} value was identified in a 68-year-old patient where the range of SUV_{max} values was 6.25 - 7.43 at lumbar DVU levels. The findings in this study show low SUV_{max} in the youngest patients in the 30s, followed by an exponential increase up to the end of the 50s, followed by a steady reduction in the oldest age group.

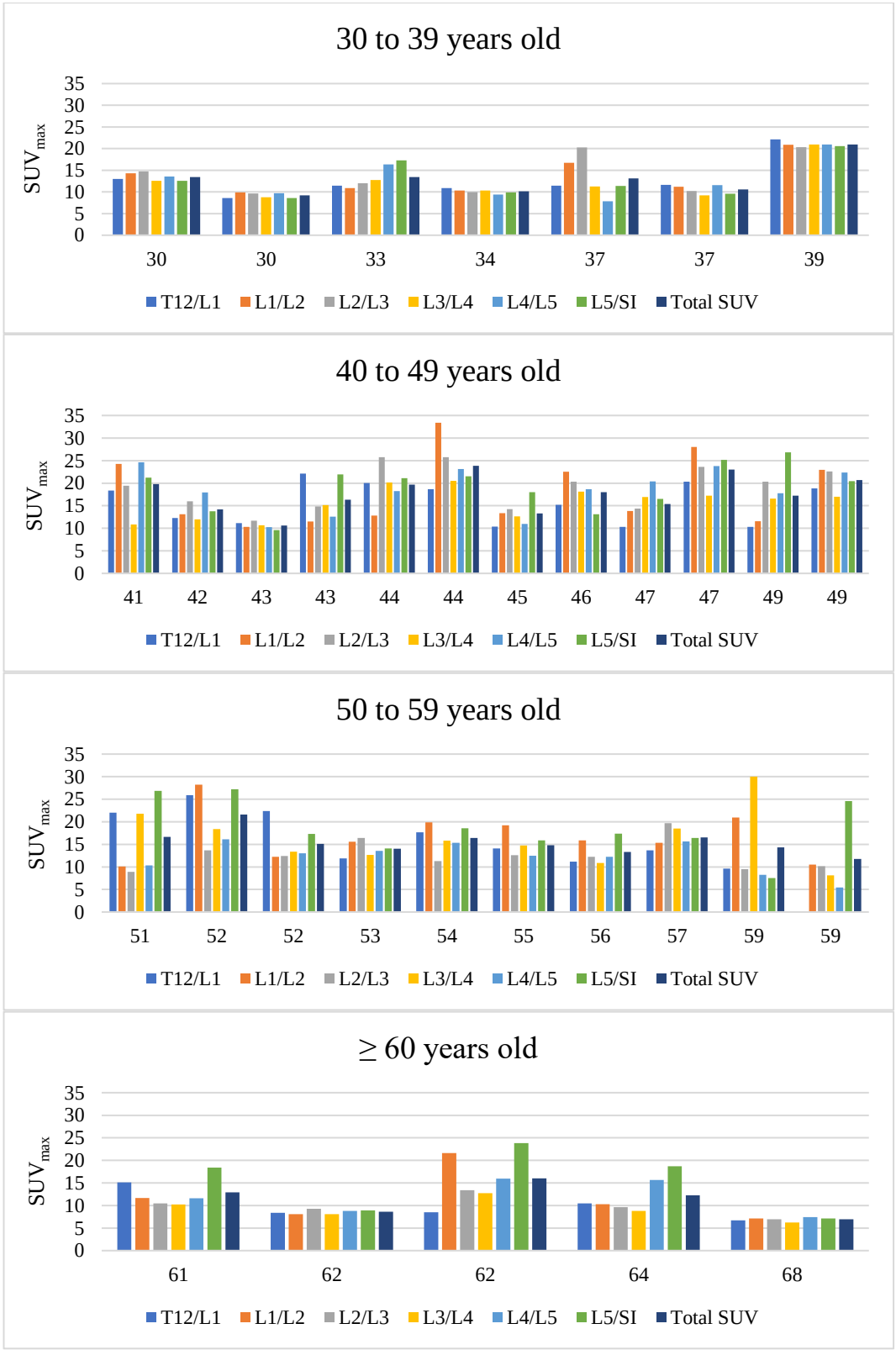

Figure 4.7. SUV_{max} measured from ^{18}F-NaF PET/CT scan at each lumbar DVU level for each individual 34 AKU case based on the age of patient.

In this chapter, 7 AKU patients in 30-39 years old group, 12 in 40-49 years old group, 10 in 50-59 years old group, and 5 in ≥ 60 years old group. Total SUV = average SUV_{max} across the 6 DVU's for each patient.

4.3.2 Pfirrmann grading score

The second section of this chapter aimed to assess disc degeneration from MR images at the lumbar spine region using Pfirrmann disc degeneration score for AKU patients. The results of Pfirrmann disc degeneration grade for 34 AKU patients are shown in Figure 4.8, and found in detail in Table 9.12 in the appendix section. The mean Pfirrmann score across the T12/L1 segment to the L5/S1 segment for all 34 AKU patients was 6.47 ± 2.65. There were no statistical differences between the average Pfirrmann score among lumbar disc levels ($P > 0.05$). Applying the modified 8 grade levels, 5 patients (14.7%) were classified as grade 1, 1 patient (2.9%) as grade 2, 1 patient (2.9%) as grade 3, 1 patient (2.9%) as grade 5, 1 patient (2.9%) as grade 6, 2 patients (5.9%) as grade 7 and 23 patients (67.6%) as grade 8 at the level of T12/L1; 4 patients (11.8%) were classified as grade 1, 1 patient (2.9%) as grade 2, 1 patient (2.9%) as grade 3, 1 patient (2.9%) as grade 5, 1 patient (2.9%) as grade 6, 3 patients (8.8%) as grade 7 and 23 patients (67.6%) as grade 8 at the level of L1/L2; 4 patients (11.8%) were classified as grade 1, 2 patients (5.9%) as grade 2, 1 patient (2.9%) as grade 3, 1 patient (2.9%) as grade 5, 1 patient (2.9%) as grade 6, 2 patients (5.9%) as grade 7 and 23 patients (67.6%) as grade 8 at the level of L2/L3; 5 patients (14.7%) were classified as grade 1, 2 patients (5.9%) as grade 2, 1 patient (2.9%) as grade 3, 1 patient (2.9%) as grade 5, 1 patient (2.9%) as grade 6, 1 patient (2.9%) as grade 7 and 23 patient (67.6%) as grade 8 at the level of L3/L4; 5 patients (14.7%) were classified as grade 1, 2 patients (5.9%) as grade 2, 1 patient (2.9%) as grade 3, 4 patients (11.8%) as grade 7 and 22 patients (64.7%) as grade 8 at the level of L4/L5; 3 patients (8.8%) were classified as grade 1, 2 patients (5.9%) as grade 2, 2 patients (5.9%) as grade 3, 4 patients (11.8%) as grade 7 and 25 patients (73%) as grade 8 at the level of L5/S1. No disc was scored as grade 4 for any of AKU patients, see Table 4.3.

According to the total Pfirrmann score at all IVD disc levels (Table 4.4), 2 AKU cases (5.9%) scored one at all lumbar IVD levels indicating normal discs in the lumbar spine. Also, 2 AKU patients (5.9%) had a total Pfirrmann score of 7, indicating that the overall lumbar disc structure was normal in height with a clear distinction between inner and outer fibers but without horizontal bands at only one lumbar disc level. On the other hand, 26 patients (76.4%) of SONIA 2 patients had a total Pfirrmann score of more than 40, indicating severe disc degeneration, while 20 (58.8%) had a total

Pfirrmann score of 48, having scored eight at all lumbar IVD levels, indicating collapsed disc space at all lumbar regions.

Table 4.3. Pfirrmann disc degeneration grade at each lumbar intervertebral disc scored from baseline MRI for 34 AKU patients who were part of SONIA 2 clinical trial.

Results displayed as the number of patients and % at each lumbar DVU level from segment T12/L1 to segment L5/S1.

Pfirrmann score	Number of patients	T12/L1	L1/L2	L2/L3	L3/L4	L4/L5	L5/S1
1	No of pts. (%)	5 (14.7%)	4 (11.8%)	4 (11.8%)	5 (14.%)	5 (14.%)	3 (8.8%)
2	No of pts. (%)	1 (2.9%)	1 (2.9%)	2 (5.9%)	2 (5.9%)	2 (5.9%)	2 (5.9%)
3	No of pts. (%)	1 (2.9%)	1 (2.9%)	1 (2.9%)	1 (2.9%)	1 (2.9%)	2 (5.9%)
4	No of pts. (%)						
5	No of pts. (%)	1 (2.9%)	1 (2.9%)	1 (2.9%)	1 (2.9%)		
6	No of pts. (%)	1 (2.9%)	1 (2.9%)	1 (2.9%)	1 (2.9%)		
7	No of pts. (%)	2 (5.9%)	3 (8.8%)	2 (5.9%)	1 (2.9%)	4 (11.%)	1 (2.9%)
8	No of pts. (%)	23 (67.6%)	23 (67.6%)	23 (67.6%)	23 (67.%)	22 (64.%)	25 (73%)

Table 4.4. Shows the total Pfirmman score for all lumbar DVU levels from T12/L1 to L5/S1 scored from baseline MRI for 34 AKU patients who were part of SONIA 2 clinical trial.

The minimum overall score for all DVUs is 6, indicating normal DVU at all lumbar levels, and a maximum score is 48 indicating abnormal DVU at all lumbar levels.

Total Pfrrmann score	Number of patients	%
6	2	5.9
7	2	5.9
13	1	2.9
17	1	2.9
18	1	2.9
21	1	2.9
41	1	2.9
43	1	2.9
44	1	2.9
45	2	5.9
46	1	2.9
48	20	58.8

4.3.2.1 Pfirrmann score and gender

Figure 4.8 demonstrates the Pfirrmann score across the lumbar disc levels in males and females. For both genders, there was no clear difference between the values across the lumbar disc levels. Males tended to have a greater Pfirrmann score than females at most of the lumbar disc levels. The average Pfirrmann score for average lumbar discs for male patients was 7.3 ± 1.7 and for female patients was 5.4 ± 3.3. Independent t-test identified that male patients had significantly higher Pfirrmann scores than female patients at the average lumbar DVU levels (P = 0.035). Regionally, there were significant differences between male and female patients at T12/L1, L1/L2, L3/L4 and L4/L5 levels with P-values of 0.021, 0.015, 0.046, 0.029, and 0.029, respectively. In contrast at L5/S1, there was no statistically significant difference between male and female scores (P = 0.071). The total Pfirrmann score across all lumbar disc levels for male patients was 43.0 ± 9.5, ranging from 17 to 48 compared to 32.3 ± 19.2, ranging from 6 to 48 for female patients. This means that the healthy lumbar disc structure was only noted in two female patient. Independent t-tests revealed statistically significant differences results in the total Pfirrmann score between males and females (P = 0.027).

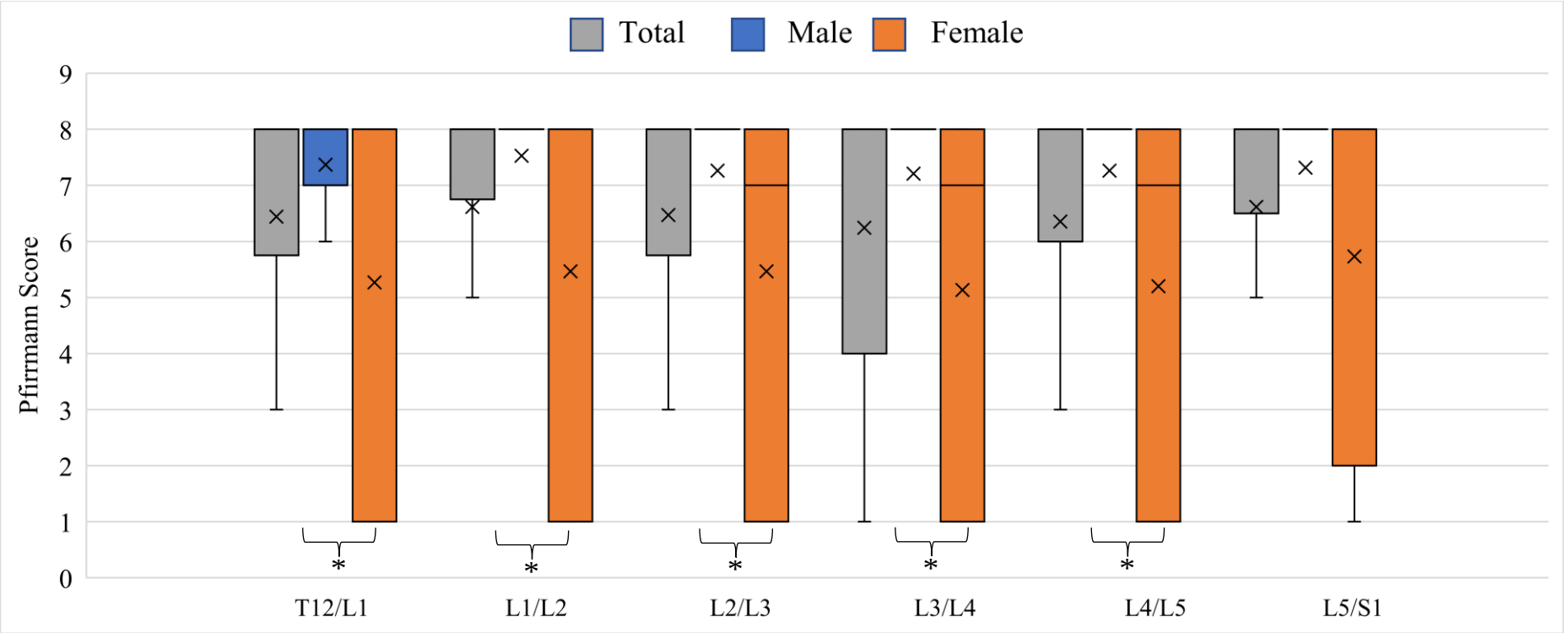

Figure 4.8. The Pfirrmann scoring values at each lumbar DVU values scored from baseline MRI for 34 AKU patients who were part of SONIA 2 clinical trial for each gender.

No difference in Pfirrmann score between the values across the lumbar disc levels were found. Table 9.12 (appendix) shows the statistical correlation between gender at most of the lumbar DVU segments. Male patients had statistically higher Pfirrmann scores compared to female patients at T12/L1, L1/L2, l2/l3, L3/L4 and L4/L5 (P = 0.021, P = 0.015, P = 0.046, P = 0.029, and P = 0.29, respectively). No statistically significant differences between male and female patients was noted at L5/S1 (P = 0.071). In box and whisker, x is the mean value, and the line is the median.

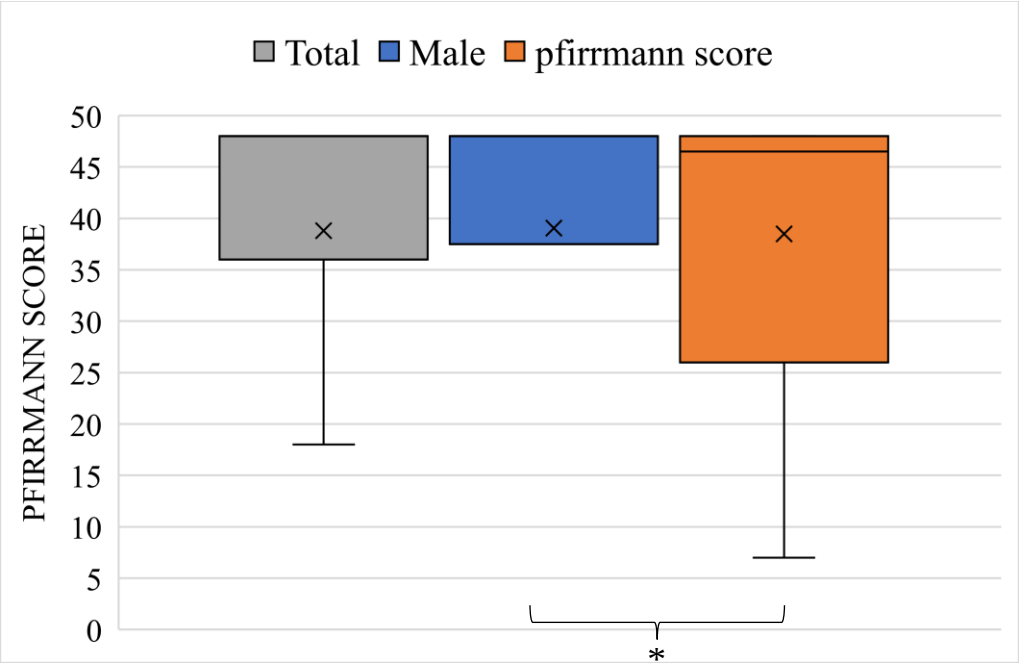

Figure 4.9. The Pfirrmann scoring values for the total lumbar DVUs values scored from baseline MRI for 34 AKU patients who were part of SONIA 2 clinical trial for each gender.

There was statistically significant differences in total Pfirrmann score across all lumbar DUV between male and female patients (P = 0.027). In box and whisker, x is the mean value, and the line is the median.

4.3.2.2 Pfirrmann and age

The results of the Pfirrmann score across all lumbar discs was plotted against age in Figure 4.10. Multiple linear regression and polynomial regression were conducted to examine the trend in the Pfirrmann score with age. From the graph below, it is clear that the Pfirrmann score of all lumbar discs was increased with age. Younge AKU patients had the low Pfirrmann score at most spinal levels that are in line with the Pfirrmann score of the normal disc structure in healthy non-AKU individuals. However, from the age of 39, the Pfirrmann score can be seen to increase sharply, reaching the maximum Pfirrmann score of 8. Linear regression revealed a strong correlation between the average Pfirrmann score and age at the average DVU levels ($R = 0.662$ and $P < 0.001$). Looking at each lumbar disc individually, age was noted to have a statistically significant effect at T12/L1, L1/L2, L2/L3, L3/L4, L4/L5, and L5/S1 levels, correlation coefficients $R = 0.602$, $R = 0.605$, $R = 0.642$, $R = 0.666$, $R = 0.684$ and $R = 0.681$, respectively, and all had $P < 0.001$. On the other hand, non-linear regression using polynomial function slightly improved the correlation coefficients at all disc levels ($R = 0.66$, $R = 0.67$, $R = 0.73$, $R = 0.75$, $R = 0.78$, and $R = 0.80$, respectively)

The Pfirrmann score across all lumbar discs from T12/L1 level to the L5/S1 level for each age group was performed. Figure 4.11 and Figure 4.12 illustrate the mean Pfirrmann score for the lumbar levels among the four age groups. There was a noticeable trend demonstrating a clear increment in Pfirrmann score with age between the age groups. Generally, the youngest patients had normal discs with low mean Pfirrmann scores of 2.9 ± 2.3 at the lumbar disc regions. Subgroup analysis indicated that age had a significant confounding effect on all lumbar DVUs between the 30s and 40s age groups ($P = 0.007$). The total Pfirrmann score for the patients in the 30-39 age group was 17.7 ± 13.6 compared to 41.2 ± 14.9 for the patients in the 40-49 age group. On the other hand, between the 40s and 50s, and 50s and 60s age groups, there was no significant difference in Pfirrmann score at any of the DVU levels. The mean Pfirmman score at all lumbar disc levels for 40-49 and 50-59 age group was 6.9 ± 2.5 and 7.7 ± 0.4, respectively. All the patients in the older age group had the highest Pfirrmann score (score of 8) at all lumbar disc levels and a total of 48 Pfirrmann scores at all levels, indicating the end stage of disc degeneration. Generally, the Pfirrmann

score increased with age, but it was statistically significant only between the youngest two age groups.

Figure 4.13 demonstrates the individual differences in the lumbar disc Pfirrmann score in four age groups. Substantial variation in the MRI graded score in the classification of the individual patient based on the absolute age was only noted in the 30s age group (Figure 4.13). It is evident from the graphs that young patients had healthy disc structure compared with the other patients. Most of the young patients (≤ 37 years old) had a Pfirrmann grade of 3 or lower at most of the lumbar levels except for a few exceptions. The oldest patient in the youngest age group who is 39 years old, had markedly different results from the rest of the 30-39 year old group patients, with a maximum Pfirrmann score at all lumbar disc levels. The majority of the cases in the 40s and 50s had grade 7 and 8 at most lumbar disc levels, which corresponded to having severe disc degeneration and collapsed disc spaces at most of the DVU levels. In the 40-49 age group, 2 patients had 1 and 2 Pfirrmann scores at most lumbar levels, indicating healthy lumbar disc structures in contrast to the rest of their age group. On the other hand, all elderly patients (≥ 60 years old) had collapsed lumbar disc space at all lumbar levels with the maximum Pfirrmann grade at all levels. It is clear that the youngest age group had the lowest Pfirrman score, and the oldest age group had the highest Pfirrmann score supporting the age-related trend shown in Figure 4.10.

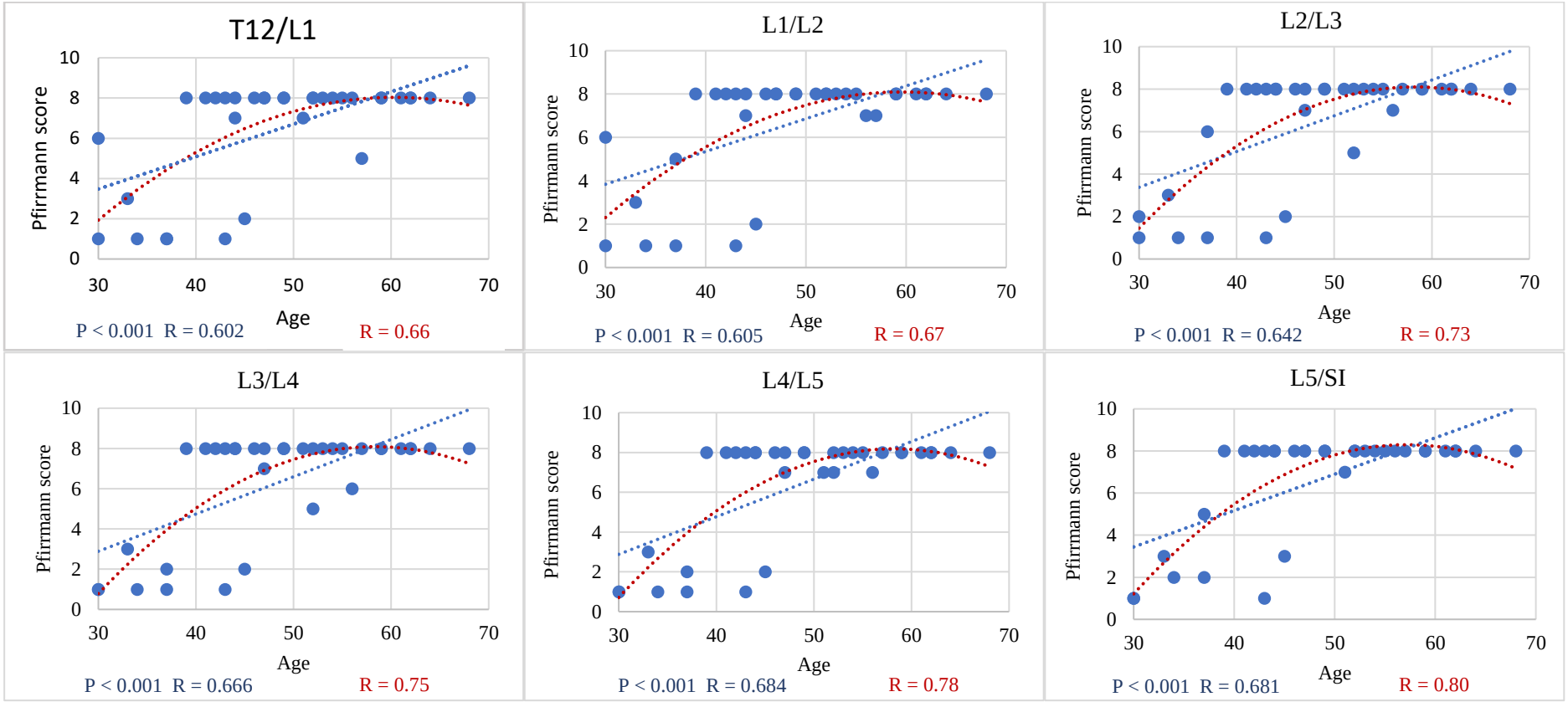

Figure 4.10. Scatter plots showing the correlation between Pfirrmann score values obtained from MRI and age for all lumbar disc levels.

Linear regression line (blue dotted line) shows that age have a strong positive statistically significant effect in Pfirrmann score at T12/L1, L1/L2, L2/L3, L3/L4, L4/L5, and L5/S1 levels, all had $P < 0.0001$ and correlation coefficients $R = 0.602$, $R = 0.605$, $R = 0.642$, $R = 0.666$, $R = 0.684$ and $R = 0.681$, respectively. Polynomial function (order 2; red doted line) found correlation coefficients $R = 0.66$, $R = 0.67$, $R = 0.73$, $R = 0.75$, $R = 0.78$ and $R = 0.80$, respectively.

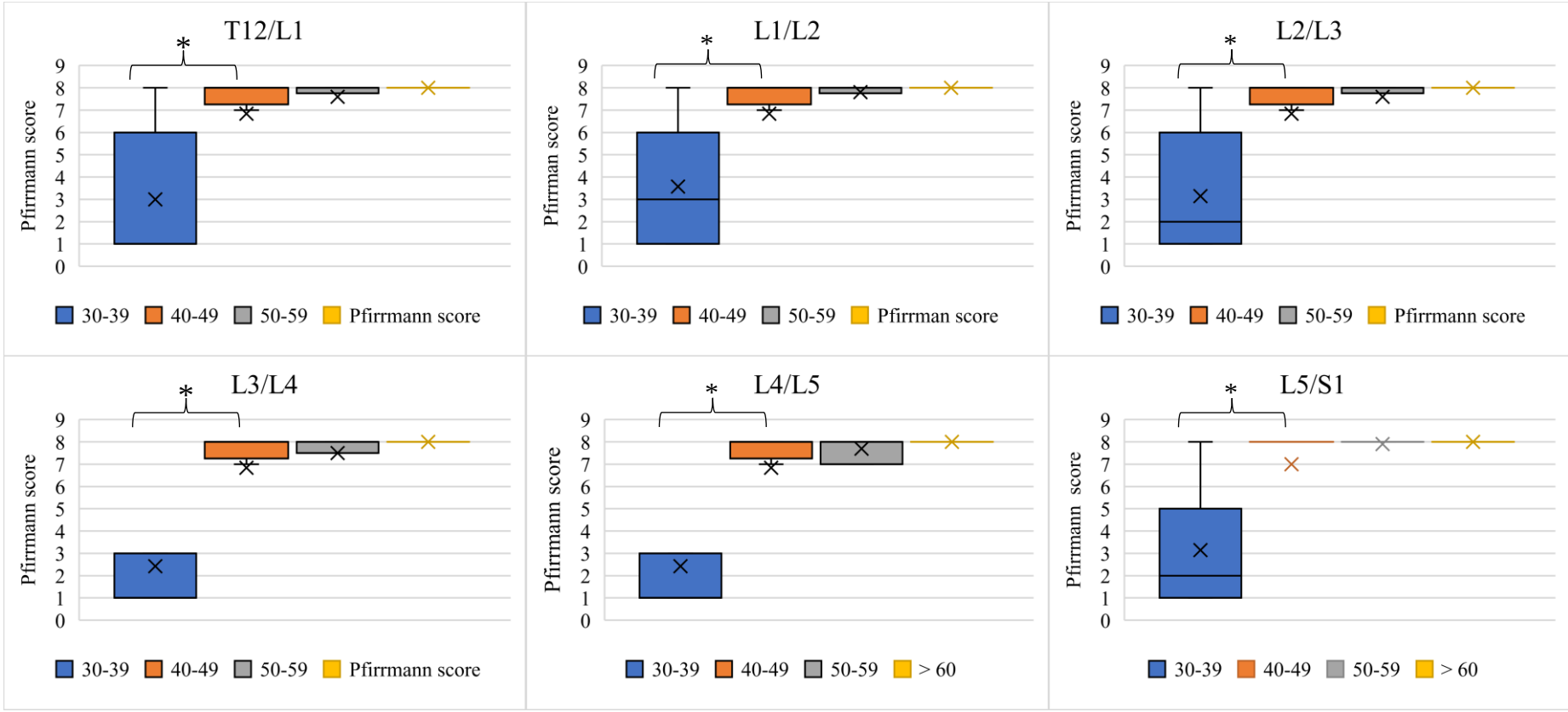

Figure 4.11. Pfirrmann score for all lumbar DVU level among four decadal age groups measured from baseline MRI for AKU patients who were part of the SONIA 2 clinical trial.

High Pfirrmann scores were noted at 40-49, 50-59, and ≥ 60 age groups at most of the disc levels. Table 9.13 (appendix) shows the lumbar DVU levels and age groups, indicating a statistically significant difference between subgroup analyses. The strong statistical differences in the Pfirrmann score were only found between the 30s and 40s age group patients ($P < 0.001$) at all lumbar disc levels. In box and whisker, x is the mean value, and the line is the median.

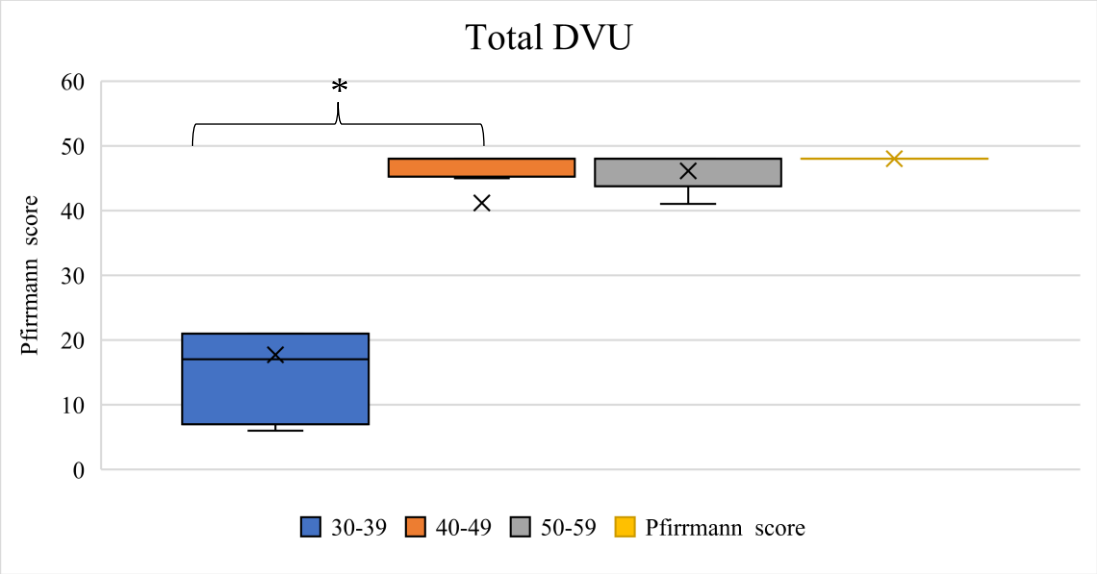

Figure 4.12. Pfirrmann score for the average lumbar DVU level among four decadal age groups measured from baseline MRI for AKU patients who were part of the SONIA 2 clinical trial.

High Pfirrmann scores were noted at 40-49, 50-59, and ≥ 60 age groups at the average lumbar disc levels. Table 9.13 (appendix) shows the lumbar DVU levels and age groups, indicating a statistically significant difference between subgroup analyses. The statistical differences in the Pfirrmann score were only found between the 30s and 40s age group patients (P = 0.004) at the average lumbar disc level. P-value between the 40s and 50 was 0.315, and between 50s and 60s was 0.139. In box and whisker, x is the mean value, and the line is the median.

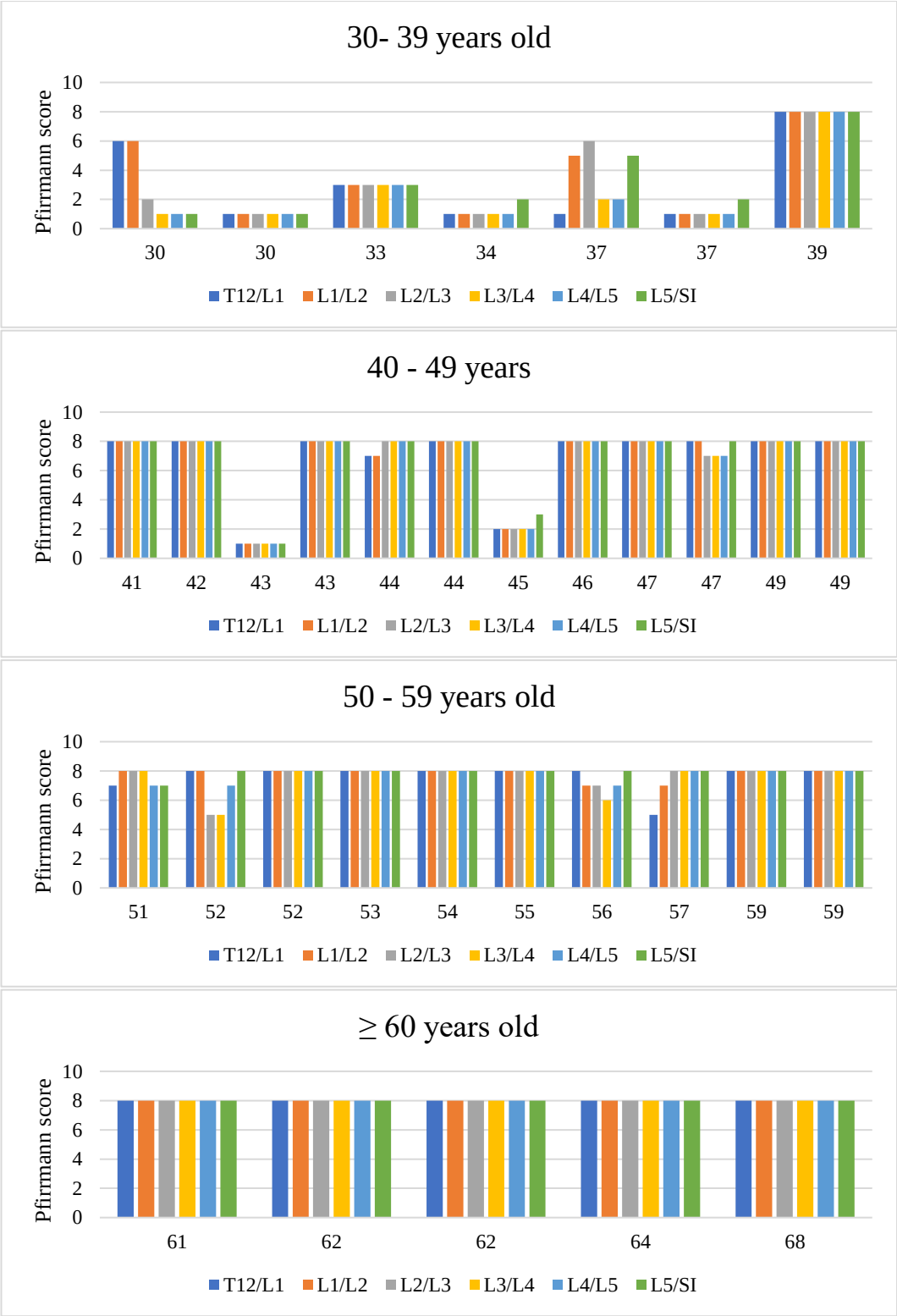

Figure 4.13. Pfirrmann score measured from MRI at each lumbar disc level for each individual 34 AKU case based on the age of each patient.

In this chapter, 7 AKU patients in 30-39 years old group, 12 in 40-49 years old group, 10 in 50-59 years old group, and 5 in ≥ 60 years old group. All patients in the 60s age group had the maximum Pfirrmann score at all lumbar disc levels.

4.3.3 Correlation between SUV_{max} and Pfirrmann score

The third section examines the relationship between semiquantitative values measured from ^{18}F-NaF PET and disc degeneration scores measured from MRI at the lumbar spine. Among the enrolled patients, the correlations of SUV_{max} values from PET images with MRI Pfirrmann score values were evaluated separately for each lumbar DVU level. Figure 4.14 shows the correlation between Pfirrmann score values and SUV_{max} at each lumbar DVU level. The Pearson correlation coefficients between the SUV_{max} value and Pfirrmann score for the T12/L1, L1/L2, L2/L3, L3/L4, L4/L5, and L5/S1 DVU were 0.358, 0.367, 0.282, 0.355, 0.371, and 0.472, respectively. All obtained correlations were statistical significant ($P < 0.05$) at all disc levels except at L2/L3, where there was no significant correlation ($P = 0.11$). Correlation between the total Pfirrmann score at the total lumbar disc levels and the average SUV_{max} at all lumbar DVU levels was also investigated. Figure 4.15 shows a positive, statistically significant correlation, which was identified between the total Pfirrmann score at all lumbar disc levels from T12/L1 segment to L5/S1 segment and the average DVUs SUV_{max} ($R = 0.459$ and $P = 0.006$).

From Figure 4.14, and the examples which were highlighted in section 4.3.1, it can be seen that the patients with low Pfirrmann scores had low SUV_{max} values. The young AKU patient with Pfirrmann score equal to 1 at all DVU levels, had SUV_{max} below 10 at all ROIs. The patient with Pfirrmann scores equal to 2/3 at lumbar levels, had an average SUV_{max} of 13.27; higher than the previous patient. On the other hand, the patient with Pfirrmann scores between 5 to 8 had a very high SUV_{max} value, even higher than those who had Pfirrmann scores equal to 8 at all lumbar levels. Interestingly, the 62 year old patient, who had end-stage disc degenerative had low SUV_{max} values. In this study, it was noted that elderly patients with grade 8 Pfirrman discs showed decreased SUV_{max} corresponding to low ^{18}F-NaF uptake on PET/CT at most affected levels.

.

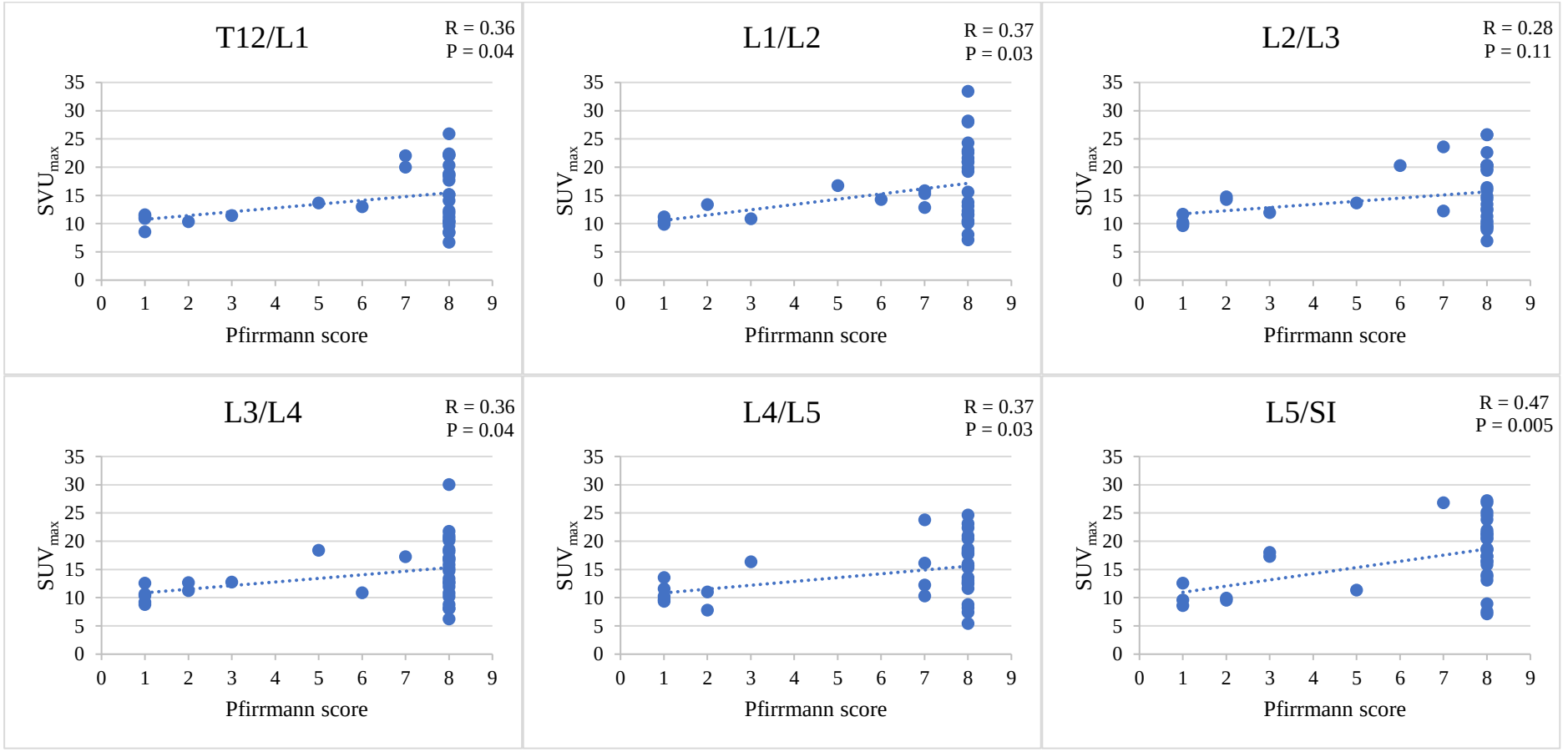

Figure 4.14. Scatter plots showing the correlation between SUV_{max} obtained from ^{18}F-NaF PET/CT scan and Pfirrmann score values obtained from MRI for all lumbar DVU levels for 34 AKU patients who were part of the SONIA 2 clinical trial.

SUV_{max} increased significantly as Pfirrmann score increased. Level T12/L1, L1/L2, L3/L4, L4/L5, and L5/S1 showed positive, statistically significant correlation coefficients between SUV_{max} and Pfirrmann score ($P < 0.05$). Level L2/L3 had shown no statistical correlation between SUV_{max} and Pfirrmann score ($P = 0.11$).

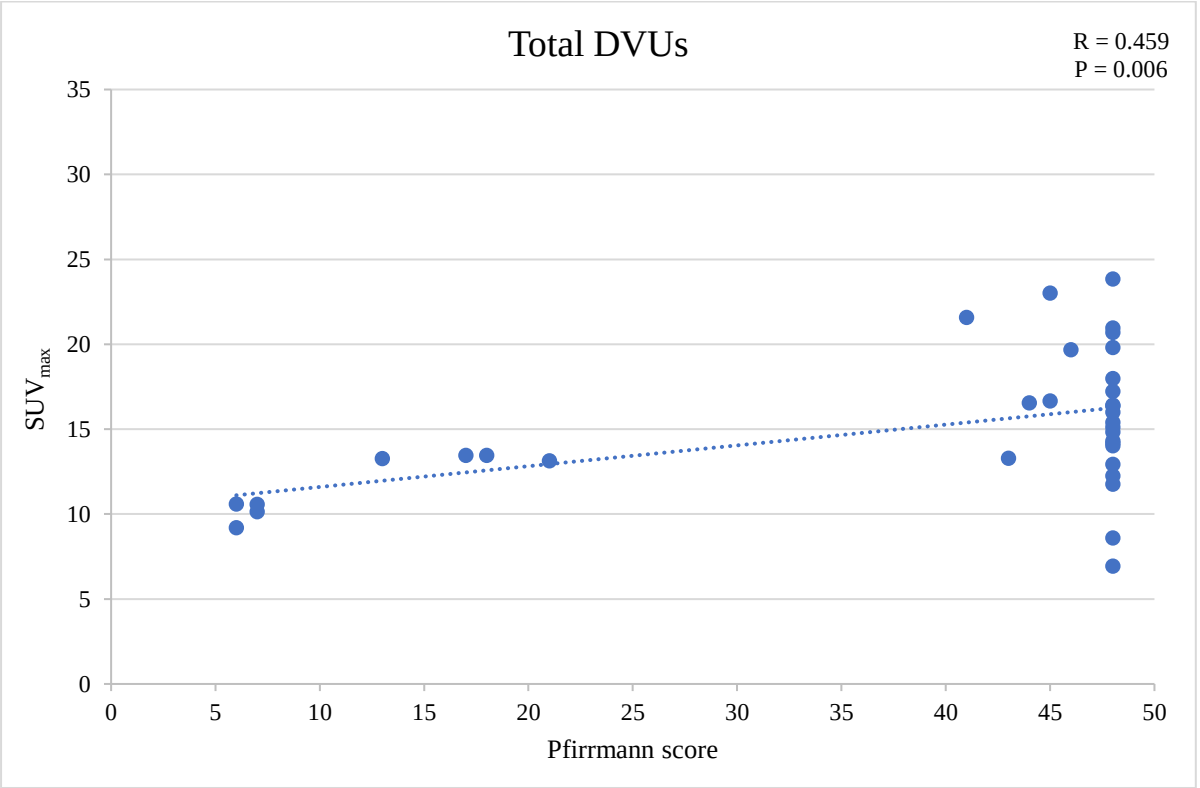

Figure 4.15. Scatter plots showing the correlation between the mean lumbar DVU SUV_{max} obtained from ^{18}F-NaF PET/CT scans and total Pfirrmann score values obtained from MRI for all lumbar DVU levels from T12/L1 to L5/S1 for 34 AKU patients who were part of the SONIA 2 clinical trial.

The minimum total Pfirrmann score is 6, indicating normal IVDs at all lumbar region, and the maximum Pfirrmann score is 48 indicating severe disc degeneration at all lumbar IVD regions. Mean lumbar DVU SUV_{max} increased significantly as Pfirrmann score increased (R = 0.459, P = 0.006). In some cases, the patient scored with 8 Pfirrmann scores but had low SUV_{max} at the measured disc region.

4.4 Discussion

This study is one of the first studies evaluating joint involvements for AKU patients by quantifying lumbar disc degeneration using advanced molecular imaging modalities. In this study, the relationship between molecular and morphological lumbar IVD changes was investigated by comparing the SUV_{max} from ^{18}F-NaF PET scans with the modified eight level Pfirrmann score from MRI. Although identification of early disc degeneration in AKU patients may be challenging using conventional imaging modalities, this study introduces a novel and sensitive semiquantitative ^{18}F-NaF PET/CT method which might detect disc calcification at its early stages, before its become symptomatic.

4.4.1 SUV_{max} measurement for lumbar DVUs

Abnormal scan manifestations at lower spine joints were noted in AKU patients as an area of increased ^{18}F-NaF uptake, reflecting disc abnormalities. Disc calcification was observed in the area between vertebrae having bone-like intensity in ^{18}F-NaF PET/CT scans. In reviewing the literature, no data were found on quantifying IVD changes in AKU patients using ^{18}F-NaF PET/CT scans. It was hypothesised that disc degeneration is associated with ongoing mineral deposition in the IVD area. Usually, disc degeneration in AKU patients occurs as lamellar calcification of the nucleus pulposus in the lumbar region and ascending to the rest of the spine region [175]. Jebaraj *et al.* [175] suggested that biochemical alteration of AKU can cause disc calcification. This pathological process will increase calcium hydroxyapatite crystals or calcium pyrophosphate dihydrate crystals in the disc area.

The mechanism of ^{18}F-NaF uptake in calcified discs and other calcified joints can be explained from the mechanism of ^{18}F-NaF uptake in bone tissues due to the strong biological similarities between joint calcification and bone formation. In fact, the main structural component in both events is hydroxyapatite crystals. After administration of ^{18}F-NaF, -^{18}F deposits in calcium-rich tissues including those in calcified joints. Therefore, it is not surprising that high radiotracer accumulation was identified between vertebrae in some AKU patients.

The changes in ^{18}F-NaF uptake at the disc area is strongly associated with disc degeneration stages, which may differ between the individual. In early and ongoing disc disease stages, ^{18}F-NaF mainly binds to the newly laid down hydroxyapatite in DVUs due to increased binding sites, therefore high ^{18}F-NaF uptake would be detected. In advanced disc degeneration, the calcified disc become stable and inactive causing low calcium hydroxyapatite crystal, therefore low ^{18}F-NaF uptake would be detected. In a separate study done in Kuwait, low ^{18}F-NaF uptake was noted in IVD regions for non-AKU patients (Alawadhi, unpublished). This can strongly suggest that disc degeneration in AKU patients is following different patterns compared to the general population.

As mentioned previously in the literature, there is a correlation between joint degeneration and increased ^{18}F-NaF uptake in the affected area. Kabayahi *et al*. evaluated ^{18}F-NaF uptake at the hip for various of OA stages and then compared the results with other clinical and radiographic findings [166]. Kabayahi found that the advanced stage of OA had a significantly higher SUV_{max} than early-stage OA. It was also noted that even patients with early-stage OA and without OA radiographic X-ray features had a significant ^{18}F-NaF accumulation at the hip joint. Interestingly, most of those patients had severe pain scores. This may strongly suggest that the early stages of disc degeneration in AKU patients could be identified as an area of increased ^{18}F-NaF uptake even before it becomes symptomatic.

Part of this chapter examines the gender effect on the value of SUV_{max} at the lumber DVUs for AKU patients. From Figure 4.1 and Table 9.10, it appears that females had slightly lower SUV_{max} values at most of the lumber DVU levels. However, the difference was not statistically significant at most of the levels except at the lowest lumber DVU level (L5/S1), where the most pressure may be experienced by the spine. Although there is no published study testing the gender effect in the disc regions, these results can be explained. A possible explanation could be that females generally weigh less than males, which will reduce the pressure on the lower spine region. Win *et al*. [107] tested some factors which may affect the ^{18}F-NaF uptake for normal patients at the spine. Win found that weight was one of the factors that affect the SUV measurements by putting mechanical stress on the spine, causing increased osteoblastic activity and therefore increased ^{18}F-NaF uptake. In another study, males showed higher bone SUV

values than female patients due to having a higher bone density than females [168]. These theories may possibly explain the slightly higher SUV_{max} in the male patients compared to female patients in this chapter.

Regarding the age effect, this study described that SUV_{max} across the lumbar disc increased gradually with age following by a decline in later years. This finding is contrary to the previous finding reported by Chanchairujira *et al*. who found that disc calcification noted by conventional radiography was linearly associated with age [176]. Close inspection between subgroup age showed that the youngest and oldest patients had lower SUV_{max} compared with other middle age group patients (Figure 4.5 and Table 9.11). Statistically, there was significant differences in the measured SUV_{max} values between some of the age groups. The average SUV_{max} of DVUs increased from the age of 30 to 59 years; after that, the SUV_{max} tended to reduce again. Several theories could explain this observation. With increasing age, disc changes in structure and calcium start to build up in the disc. In the 30s, it is more likely that AKU patients have healthy spine structures due to normal blood supply to the spine and therefore normal distribution of ^{18}F-NaF tracer would be noted in the spinal bone and disc. Interestingly, in this study, the oldest AKU patient in the youngest age group who was 39 years old, had significantly higher SUV_{max} values similar to the average SUV_{max} for those patients in their 40s. This means that the increased bone remodelling at the disc regions in AKU patients is more likely developed around the age of 38 and 40. It was reported previously during the late 30s, the onset of arthritic pain started in AKU patients specifically at the lower spine [3]. Patients in their 40s and 50s tended to have high SUV_{max}, in contrast to the other two age groups which indicates an active and ongoing calcification in the intervertebral space. This could be due to abnormal blood supply to the spine or it may be related to ochronosis.

Although the elderly patients tended to have disability and severe spinal pain, the SUV_{max} was low for the eldest patients, which is more likely due to inactive calcification in the disc space. By the 60s, the spine discs tend to be collapsed, and the calcification may become stable indicating end stage disc degeneration. Additionally, reduced perfusion to the bone as a result of ageing would result in reducing the radiotracer transfer to the spine regions, including those in vertebrae and the IVDs [118]. A similar finding was also observed in Chapter 3, an old AKU patient also had low

SUV_{max} at lumbar verebrae. These findings may explain the decline in ^{18}F-NaF uptake in the bone and calcified disc with age in general. Additionally, it has been widely described that bone mineral density reduces with age. Riggs *et al*. [165] investigated the differential changes in bone mineral density of the appendicular and axial skeleton with ageing. Riggs found that bone diminution from the vertebrae began in young adulthood and was linearly increased by ageing. This also accords with earlier observations in Chapter 3, which showed a significant reduction in lower spine HU_{mean} with age, indicating decreased bone density and osteoblastic activity with age. From this point, the reduction in SUV_{max} with age may be explained by the reduction of bone mineral density in the vertebrae, which would reduce the -^{18}F ion binding sites in the whole spinal structure including bone and disc.

Overall, the results in this section support the proposed theory that ^{18}F-NaF uptake corresponds to the deposition of hydroxyapatite crystals at disc areas which may be strongly associated with the deposition of ochrontic pigment in IVDs. These findings suggest that ^{18}F-NaF can be used as novel imaging marker to detect the early stage of ochronotic arthropathy by identifying early-stage disc calcification.

4.4.2 Pfirmann score

The second aim of this chapter was to evaluate lumbar intervertebral disc degeneration in MRI using the Pfirrmann scoring system. In this study, most of the lumbar discs for AKU patients were scored as grade 8, and ambiguity was encountered for the end disc degeneration stage. Although the MRI radiologist who scored the lumbar disc in this study suggested adding an extra grading score to separate the end stages of disc degeneration (very narrow intervertebral space and collapsed space); he preferred at that moment to score the lumbar disc degeneration for SONIA 2 patients using a validated MRI grading method.

Regarding the effects of gender on Pfirrmann score, this study demonstrated that male AKU patients have a strong tendency to develop more severe lumbar disc degeneration than their female age-matched counterparts (Figure 4.8 and Table 9.12). These results support the general clinical perception that females are less likely to have disc degeneration compared to males. From radiographic evaluation, males were more

likely to develop osteophytes, which appeared with greater frequency than females [177]. MRI data in this study confirms the previous radiographic findings, which showed a greater severity and frequency of osteophytes in men than women [177,178]. A possible explanation for the severity and greater frequency of disc abnormailites in the male patients, as mentioned earlier in section 4.4.1, may be due to the higher weight and higher bone mineral density in men.

In contrast to findings in this chapter, there are several studies that have suggested that females seem to be more susceptible to instability, structural deterioration, reduced lumbar disc height, and malalignment due to hormonal changes and menopause [179,180]. Although De Schepper *et al*. [177] found that osteophytes were the most frequent radiographic feature observed in males, he also noted that disc space narrowing was more frequent in females. On the other hand, Wang *et al*. [181] found that elderly female patients had slightly higher Pfirrmann scores than male patients indicating more severe disc degeneration at all lumbar levels. These results differ from the findings in this study, which show males tend to develop more severe disc degeneration than females. In general, degenerative disc changes can be observed in both genders, and concentrating on a specific gender may change the finding in some studies.

It was clear from Figure 4.10 that there are positive, statistical significant relationships between the Pfirrmann score and age in all lumbar disc levels ($P < 0.05$). However, this result has not previously been noted in this chapter when SUV_{max} was correlated with age. These results are likely related to the severity of the disc calcifications and whether the calcification is active or inactive in the IVD area. Looking at the subgroup age analysis in Figure 4.11 and Figure 4.12, the Pfirrmann score was statistically different between the 30s and 40s age groups only at all lumbar disc level ($P < 0.05$). As is shown in Figure 4.13, the individual changes in Pfirrmann score across the lumbar disc levels were noted for SONIA 2 patients. The youngest 6 SONIA 2 patients had low Pfirrmann scores with no score greater than 6. The majority of the patients after the age of 37 were graded with a grade 8, which indicated the end stage of the disc degeneration with totally collapsed disc spaces. Only, 1 patient in the late 30s had the maximum total Pfirrmann score at the lumbar disc levels, in which the values have nearly matched the results of the older age groups. The other three age groups had similar results with high Pfirrmann scores with insignificant differences between them.

Only a few individual differences were noted between cases within the 40s and 50s age groups. All the patients in the 60s age group had the highest possible total Pfirrmann score at all lumbar levels indicating the end stage of disc degeneration at all lumbar levels. It is somewhat surprising that some young AKU patients may had Pfirrmann grades of 7 and 8. The results show that even patients in their 30s and 40s have narrowed and collapsed disc spaces indicating advanced disc degeneration, likely due to the advanced ochronotic arthropathy stage.

4.4.3 Correlation between SUV_{max} and Pfirrmann score

The third objective in this study was to determine whether bone metabolic activity from ^{18}F-NaF PET images corresponded to the disc degeneration noted in MRI for AKU patients. When the SUV_{max} at each lumbar DVU was plotted against the Pfirrmann score (Figure 4.14 and Figure 4.15), a positive, statistically significant correlation was identified between SUV_{max} and Pfirrmann score at most of the lumbar DVUs ($R > 0.36$ and $P < 0.05$). This result demonstrates that high SUV_{max} is usually associated with a high Pfirrmann scores. However, the relationship between increased tracer uptake and disc damage was asymmetric at the end-stage of disc degeneration. This indicates that increased ^{18}F-NaF uptake on PET images may not always correspond to the structural damage in the discs which can be detected from MRI. For example, grade 1 and 2 Pfirrman scores were determined with SUV_{max} lower than 15 at all lumbar levels. As the lumbar disc graded higher in MRI, the SUV_{max} increased significantly. However, several advanced cases with structural disc abnormality had grade 8 Pfirrman scores, but showed decreased SUV_{max} values corresponding to low ^{18}F-NaF uptake on the PET/CT scan.

This asymmetry observed in the relationship between PET and MRI could be related to the disc degeneration stages. Although inactive or stable disc calcification would not present as high ^{18}F-NaF uptake in PET images, it can still be identified as an abnormal disc structure on an MRI. This does not mean that severe disc degeneration would appear as a normal disc in PET imaging; however it more likely that these calcified discs become stable, and therefore have low SUV_{max} values. A limited number of studies have compared ^{18}F-NaF PET/CT and MRI in the spine; however, the findings in this study can be compared to the findings of other joints areas, where

both PET scans and MRI have been used. Fischer *et al*. compared the distribution of increased bone tracer activity on PET with edema on MRI in the spine and sacroiliac joints (SIJ) for ankylosing spondylitis patients [182]. The study found that MRI detected more spinal lesions in comparison to what was detected in ^{18}F-NaF PET/CT (68 vs. 38), whereas there was a similarly positive results at SIJ in both modalities (19 vs 17). This is consistent with the findings in this chapter, indicating that active and inactive end-stage disc degeneration is more likely be noted in MRI compared to PET scans. Draper *et al*. [136] compared increased ^{18}F-NaF uptake on the PET images to cartilage damage visualised on MRI at the patellofemoral region; increased bone tracer detection did not always correspond to structural damage seen on MRI. Both Draper *et al*. [136] and Fischer *et al*. [183] found around 40% agreement between ^{18}F-NaF PET/CT and MRI. Another study was correlating increased bone uptake in ^{99m}Tc-MDP SPECT/CT image with MRI in the knee region [116]. In that study, a moderate correlation was found between bone tracer uptake and subchondral region, osteophytes and cartilage defects [116].

4.5 Summary

Advanced molecular imaging techniques such as ^{18}F-NaF PET/CT and MRI can detect and quantify early IVD changes in AKU patients. Lumbar disc degeneration of patients with ochronotic arthropathy was associated with increased ^{18}F-NaF uptake on PET images and high Pfirrmann scores on MR images. In AKU patients, disc degeneration is associated with increased ochronotic pigment in the joints and articular cartilage causing increased calcification in the IVD regions. Disc calcification will increase calcium hydroxyapatite crystals or calcium pyrophosphate dihydrate crystals at the affected area. In the early-stage of disc calcification, more binding sites would be available to bind with the ^{18}F-NaF radiotracer, therefore high SUV_{max} would be detected. Lumbar disc SUV_{max} values increased gradually with age following by a reduction in the later years. The age factor strongly influenced MRI scoring values at all DVU levels. Male AKU patients have a mild tendency to develop more severe lumbar disc degeneration than female patients. Several advanced grade 8 Pfirrmann score discs in MR images showed low ^{18}F-NaF uptake on PET/CT images. These cases were more likely to have fusion at that DVU level with inactive calcification or no clear bone formation at the intervertebral spaces. This study demonstrates the

correlation between functional PET images and anatomical MRI findings until IVD fusion occurs in ochronotic patients.

4.6 Limitations

This study has some limitations, which must be pointed out. First, the evaluation of interobserver and intraobserver reliability has not been tested. Lumbar disc Pfirrmann scoring was performed only once by one MRI radiologist experienced in musculoskeletal disease. Likewise, SUV_{max} for each lumbar DVU was also measured once. The agreement of detection and scoring the lumbar DVU between PET images and MRI by two or more viewers was not possible due to limited time and availablilty of experienced radiologists who collaborated in this study. Second, no control group was available to statistically compare the results of non-AKU patients with AKU patients.

4.7 Future work

Future work is needed to further exam the correlation between molecular PET and morphological MRI evaluations. Evaluation of the interobserver and intraobserver reliability of SUV_{max} assessments from PET image and Pfirrmann score from MR images for each lumbar DVU would be necessary to support the measurement methods which were used in this chapter. A modified MRI scoring system or a new grading system which can expand visual representation of the disc and minimise ambiguity for ochronotic patients would improve results. The modified scoring system for AKU patients could still follow the same principle criteria of the previously used method. It would be more valuable and precise if both PET and MR images are compared using the same qualitative principle measurement methods, such as grading both images with the same scoring system. Grading PET/CT images would need the collaboration from nuclear medicine specialists in ^{18}F-NaF PET/CT scans. Additionally, adding a control group of a similar age range would help to provide normal disc SUV_{max} threshold values.

4.8 Conclusion

This chapter has shown:

- Abnormal ^{18}F-NaF PET/CT scan manifestations were detected at lower spine joints in AKU patients as an area of increased ^{18}F-NaF uptake, reflecting disc degeneration.
- The values of SUV_{max} across the lumbar DVUs increased gradually with age following by a decline in the later years.
- Increased SUV_{max} at the lumbar disc site indicates high osteoblastic activity in the pathological area.
- Stable or inactive calcification in severe long-term disc degeneration was not identified as an area of high SUV_{max}, likely due to stable bone remodelling.
- Lumbar intervertebral disc degeneration was associated with high Pfirrmann scores on MR images.
- There were no statistically significant differences in SUV_{max} value between males and females across all lumbar DVUs except at L5/S1.
- Male patients have a statistically higher Pfirrmann score compared to the female patients at all lumbar DVUs except at L5/S1.
- Age was noted to have a positive, statistically significant effect on Pfirrmann scores at all lumbar disc levels.
- A positive, statistically significant correlation between SUV_{max} and Pfirrmann scores at most lumbar levels was observed.
- Several advanced disc degeneration cases had grade 8 Pfirrmann scores on MRI with low SUV_{max} on ^{18}F-NaF PET/CT scan, indicating fusion at that DVU lumbar level with inactive calcification at intervertebral spaces.

5 Determining treatment efficacy of nitisinone on spine ochronotic arthropathy in SONIA 2 patients using ^{18}F-NaF PET/CT scan

5.1 Introduction

In the previous chapters, ochronotic arthropathy in the spine and hip have been identified and quantified using different imaging techniques in patients with AKU. In Chapter 3, low bone density and active bone turnover have been identified in AKU patients by measuring HU_{mean} and SUV_{max} from lumbar vertebrae bodies and femoral heads using ^{18}F-NaF PET/CT. Then, in Chapter 4, lumbar intervertebral discs were quantified and scored from ^{18}F-NaF PET/CT and MR images.

This study examines the changes in ^{18}F-NaF PET/CT semiquantitative values across five visits for AKU patients who were part of the SONIA 2 clinical trial. The aim of this study was to investigate whether ^{18}F-NaF can be used as an imaging biomarker of regional treatment efficacy by evaluating the changes in the lumbar spine for AKU patients who were treated with nitisinone for four years. This chapter of the thesis is designed to assess the disease progression and effectiveness of nitisinone by evaluating the changes in HU_{mean} and SUV_{max} values measured from the lower spine using ^{18}F-NaF PET/CT scans.

The current chapter is divided into four main sections. The first section examines bone density by following the changes in lumbar spine HU_{mean} values measured from CT images for nitisinone treated and non-treated groups. The second section investigates the change in bone ^{18}F-NaF uptake by evaluating the changes in the mean lumbar vertebrae SUV_{max} values for both groups. The third section assesses the lumbar disc change by investigating the changes in SUV_{max} for the lumbar IVD regions. The fourth section evaluates the individual changes in the measured semiquantitative values between the visits for the nitisinone-treated patients and non-treated patients individually across the visits.

Recently, in July 2020, nitisinone received positive opinons from the European Medicines Agency for its use in alkaptonuria [39], and has since been approved as a therpay for AKU by the European Commission [49]. Nitisinone is a competitive inhibitor of hydroxyphenylpyruvic acid oxygenase, which is the second enzyme in the tyrosine catabolic pathway. Inhibiting this enzyme prevents production of the culprit molecule HGA, and should prevent or slow the progression of disease in patients with AKU

(Figure 1.1- Introduction). The main challenge faced to prove the efficacy of nitisinone is to stop or slow down the progression of ochronosis. It has been confirmed that nitisinone reduces plasma and urinary HGA levels [7,38,45–48,51]. Previous studies have noted this promising event in AKU patients [48] and also in the AKU mouse models [46] suggesting the beneficial effects of nitisinone in patients with ochronosis. It is suggested that early-stage treatment of AKU patients with nitisinone could prevent pigment deposition occurring, including within cartilage and joint tissues. The key research question here is whether or not the significant reduction in HGA levels after taking nitisinone has a significant impact in patients with AKU by stopping or slowing down the progression of ochronotic arthrophathy in the spine.

As pointed out in the introduction Chapter, SONIA 2 patients underwent a number of scans to monitor the disease progression, including scintigraphy, MRI and DEXA scans. In SONIA 2, scintigraphy was qualitatively evaluated to identify ochronotic arthropathy by counting the number of joints with increased or abnormal tracer uptake throughout the whole body. The results show that the number of joints involved were increased in both treatment and non-treatment groups. Looking at the spine result, the number of spinal regions with osteoarticular disease was also increased over time in both groups. DEXA scan reported a reduction in the hip T-score value over time in both groups, indicating reduced hip bone density. Regarding MRI results, the number of fractures was increased in both groups. SONIA 2 final analysis scan results are shown in the appendix (see section 9.4). In all the scans reviewed in the SONIA 2 trial, there were no significant differences in the mean change in imaging results between nitisinone-treated and non-treated patients. These analyses have failed to confirm the benefit of nitisinone on stopping ochronotic arthropathy for those patients who took a daily dose of nitisinone over four years. In fact, the previous SONIA 2 investigations have mostly foucsed on qualitative analyses which is a subjective assessment method. The current study aimed to detect any statistically significant differences in spinal bone or discs between nitisinone-treated patients and non-treated patients using reliable and sensitive quantitative methods.

With the development of new potential treatment for AKU patients, there is an increasing need to develop a new reliable method to examine drug efficacy, particularly in the early phases of clinical trials. In any clinical trial, it is important to

use accurate assessment methods to evaluate the success or failure of the treatment. Generally, bone mass is a major area of interest within the field of drug development for any bone or bone-related disorder due to the strong correlation between bone loss and disability. However, evaluating bone density changes using a traditional DEXA scans can be challenging because the changes in bone are usually mineral changes and may need years or decades to be visualise by conventional imaging techniques. Additionally, as was highlighted previously in Chapter 3, the calcified disc may strongly overestimate the DEXA scan BMD values. In the past decade, more recent attention has focused on bone biomarkers in clinical trials of therapies for various bone disorders. Although biochemical bone markers are widely used to measure bone turnover, they only reflect total skeletal function [138]. It would be more useful if the regional bone formation is monitored during the course of treatment wich will provide a better understanding of the treatment impact on bone for AKU patients.

^{18}F-NaF PET/CT can offer novel information about the drug efficacy at specific sites of the skeleton, by overcoming the major weakness of the conventional methods. A number of studies utilized bone isotopes to assess the direct effects of pharmacological therapies at different sites of the skeleton for many metabolic bone disorders, where the treatment response was tested using different semiquantitative assessment methods [98,138–142].

As mentioned earlier, ^{18}F-NaF PET/CT scan was part of the SONIA 2 clinical investigations, which were employed to evaluate the changes of clinical features in the skeleton over four years in order to track the progression of the disease and/or assess the response to treatment in the long term. This study may provide a better understanding of the impact of nitisinone on bone and joint disease in AKU patients, and evaluates the disease progression rate using a positron bone radiomarker.

5.2 Design of study

5.2.1 Patient group

In this study, 34 AKU patients including 22 males and 12 females who enrolled in the SONIA 2 clinical trial and attended the Liverpool AKU Trial Centre were used. All

participants were aged between 30 and 68 years old at the beginning of the trial. The participants were divided randomly into a treatment group and non-treatment group (control patient group). Participants in the treatment group were treated with nitisinone, 10 mg once a day, for four years. Table 5.1 shows the number of patients, age and gender at the baseline visit for both treatment and non-treatment groups who participated in this study. The trial period consisted of four years, during which each patient underwent a ^{18}F-NaF PET/CT scan annually for five consecutive visits; Visit 1 (at baseline, pre-treatment), Visit 3 (one year), Visit 4 (two-year), Visit 5 (three years), and Visit 6 (four years) (see section 2.2.1). In Visit 2, which was at 3 months follow up, no ^{18}F-NaF PET/CT scan was requested for all participants. Some patients dropped out of the SONIA 2 study therefore not all of the participants had a series of five ^{18}F-NaF PET/CT images. Patients with at least one recorded whole body ^{18}F-NaF PET/CT scan at baseline were included in this analysis. Table 5.2 shows the number of ^{18}F-NaF PET/CT images available and analysed at each visit for both groups.

Table 5.1. Age and gender of the 34 AKU patients who were part of the SONIA 2 clinical trial and involved in this study classified by treatment arm.

Not all of the SONIA 2 participants had a series of five ^{18}F-NaF PET/CT images.

Statistic	Untreated	Treated with nitisinone
Number of patients	17	17
Age		
Mean	47.88 ± 10.88	48.88 ± 10.42
Range of age	30 - 67	30 - 68
Gender (n, %)		
Male	10 (45.5%)	12 (54.5%)
Female	7 (58.3%)	5 (41.7%)

Table 5.2. Number of ^{18}F-NaF PET/CT images for AKU patients who were part of SONIA 2 per annual visit for nitisinone treatment and non-treatment groups.

Not all of the SONIA 2 participants had five serial ^{18}F-NaF PET/CT images.

Statistic		Untreated patients	Nitisinone-treated patients
No. patients at the visit (n)			
Visit 1	Baseline	17	17
Visit 3	Month 12	15	15
Visit 4	Month 24	14	16
Visit 5	Month 36	15	15
Visit 6	Month 48	14	12

5.2.2 Image analysis

^{18}F-NaF PET/CT images were analysed using Horos medical software (see section 2.4.1.2). A semiquantitative comparison was performed by measuring HU_{mean} and SUV_{max} for lumbar vertebral bodies (L1-L5) and SUV_{max} for lumbar disc units (T12/L1-L5/S1) for each patient (section 2.5 and 2.7). The measurement was obtained for each ROI at three sagittal sections, then the average value for each patient was generated for each visit. The longitudinal changes in the semiquantitative values for both groups over four years were tested. Kruskal-Wallis test was used to compare the data between treatment arms.

The patients were classified into four groups based on their age to investigate the treatment effect and evaluate the progression of the disease in each age group; 30-39 years, 40-49 years, 50-59 years and above 60 years. The individual changes in HU_{mean} and SUV_{max} over the serial visits in the average lumbar vertebrae and lumbar DVU was also evaluated for the nitisinone-treated patients and non-treated patients for accurate response assessment in individual cases. Any patient who has two or more imaging data was included in this part of the investigation.

5.3 Results

5.3.1 Change in semiquantitative values across 5 visits

HU_{mean} value was obtained from average lumbar vertebrae (L1-L5), and SUV_{max} was obtained from average lumbar vertebrae (L1-L5) and average lumbar DVU (T12/L1-L5/SI) for both nitisinone-treated and non-treated AKU patients across five annual visits.

5.3.1.1 Change in HU_{mean} measured from lumbar vertebrae body across 5 visits

Over time, the change in bone density was tested by investigating the mean change of vertebral HU measurements over four years (~48 months). Figure 5.1 and Table 9.23 (appendix) summarise the mean HU_{mean} values for the average lumbar vertebrae bodies (L1-L5), which were measured from CT images from Visit 1 at the baseline to Visit 6 at 48 months in the treatment group and non-treatment group. At the baseline, there was no significant difference in the mean lumbar spine HU_{mean} values between nitisinone-treated patients and non-treated patients (174.1 ± 104.3 and 152.7 ± 61.0, respectively). It is clear from the graph (Figure 5.1) that the mean lumbar HU_{mean} measurements were generally consistent across the visits in both groups. The mean plotted data for the treatment group showed little change in bone density in the lumbar vertebrae following treatment with nitisinone. In the same way, there was minimal change in the bone density for those patients in the control group over four years. Figure 5.2 shows the mean change from baseline to each visit for lumbar vertebrae body HU_{mean} values, for both groups. This data is also described in detail in Table 9.24 (appendix). At month 12, nitisinone-treated patients showed a significantly greater reduction in the mean lumbar HU_{mean} value (median change -5.3, range -48.7 to 35.9), compared with increase in the mean lumbar HU_{mean} value for non-treated patients (median change 6.1, range -38.5 to 50.8). Nitisinone-treated patients experienced a 8.64% mean reduction in vertebrae spine HU_{mean} values, compared with a 9.5% mean increase in HU_{mean} values in non-treated AKU patients (P = 0.036) at one year of follow up. After that, HU_{mean} values in the non-treated group started to decrease from 190.6 ± 111.4 in Visit 3 to 171.9 ± 112.2 in Visit 6. In nitisinone-treated AKU group, there was a slight rise in the HU_{mean} of lumbar vertebrae from 139.5 in Visit 3 to 144.4

in Visit 6. It can be clearly seen from the data in Figure 5.2 and Table 9.24 (appendix) that there were no statistically significant differences between treatment and non-treatment groups in the mean change in lumbar HU_{mean} measurements at neither month 24, month 36, nor month 48 (P = 0.739, 0.120, and 0.681, respectively). Overall, a clear impact of nitisinone in the HU could not be identified in this analysis.

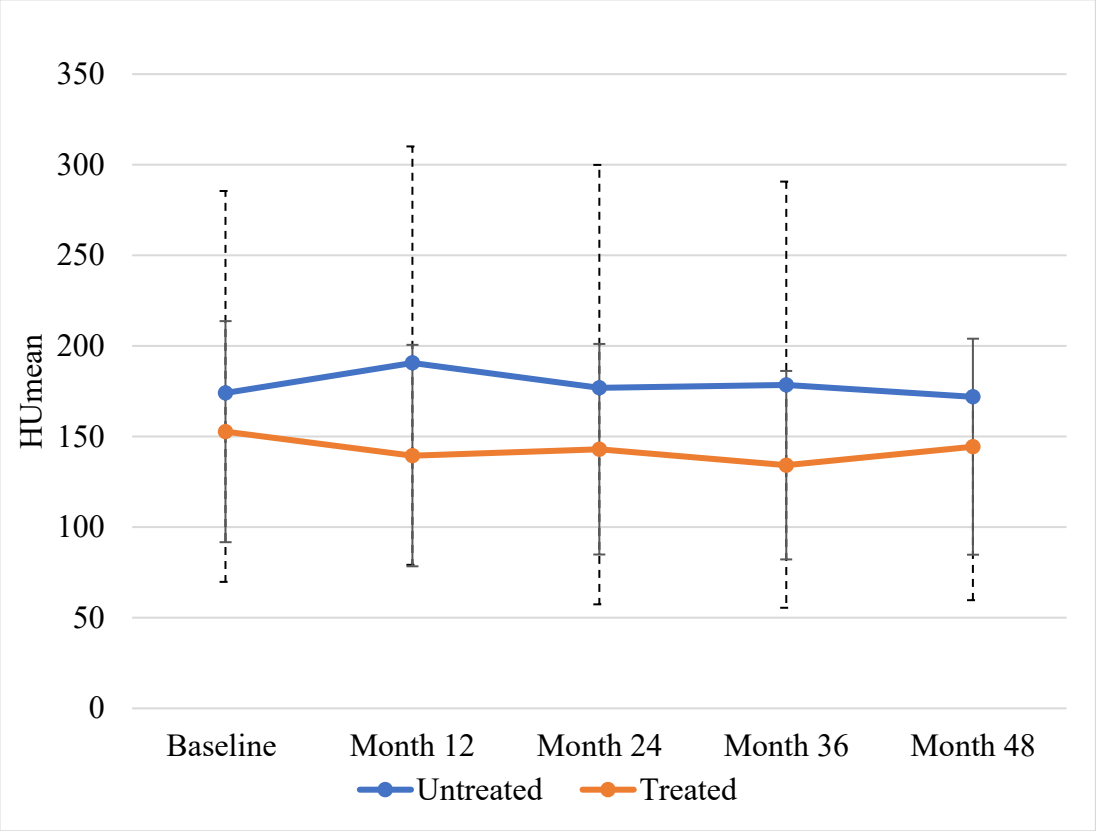

Figure 5.1. Mean lumbar vertebrae HU_{mean} values for nitisinone treated and untreated AKU patients who were part of the SONIA 2 clinical trial across 5 annual visits.

Blue line represents the non-treated SONIA 2 group; the orange line represents the nitisinone-treated SONIA 2 group. Each visit was one year apart, V1; baseline data (pre-nitisinone), V3; after 12 months, V4; 24 months, V5, 36 months and V6; 48 months. Error bars represent SD, dash line represents untreated group and solid line represents treated group. Table 9.23 (appendix) shows the summary statistics for HU values across the treatment and non-treatment AKU groups visits. At the baseline, there was no significant difference in mean lumbar spine HU_{mean} value between treatment and non-treatment group (174.1 ± 104.3 and 152.7 ± 61.0, respectively). Over four years, there were minimal changes in HU_{mean} values for nitisinone-treated and non-treated AKU patients

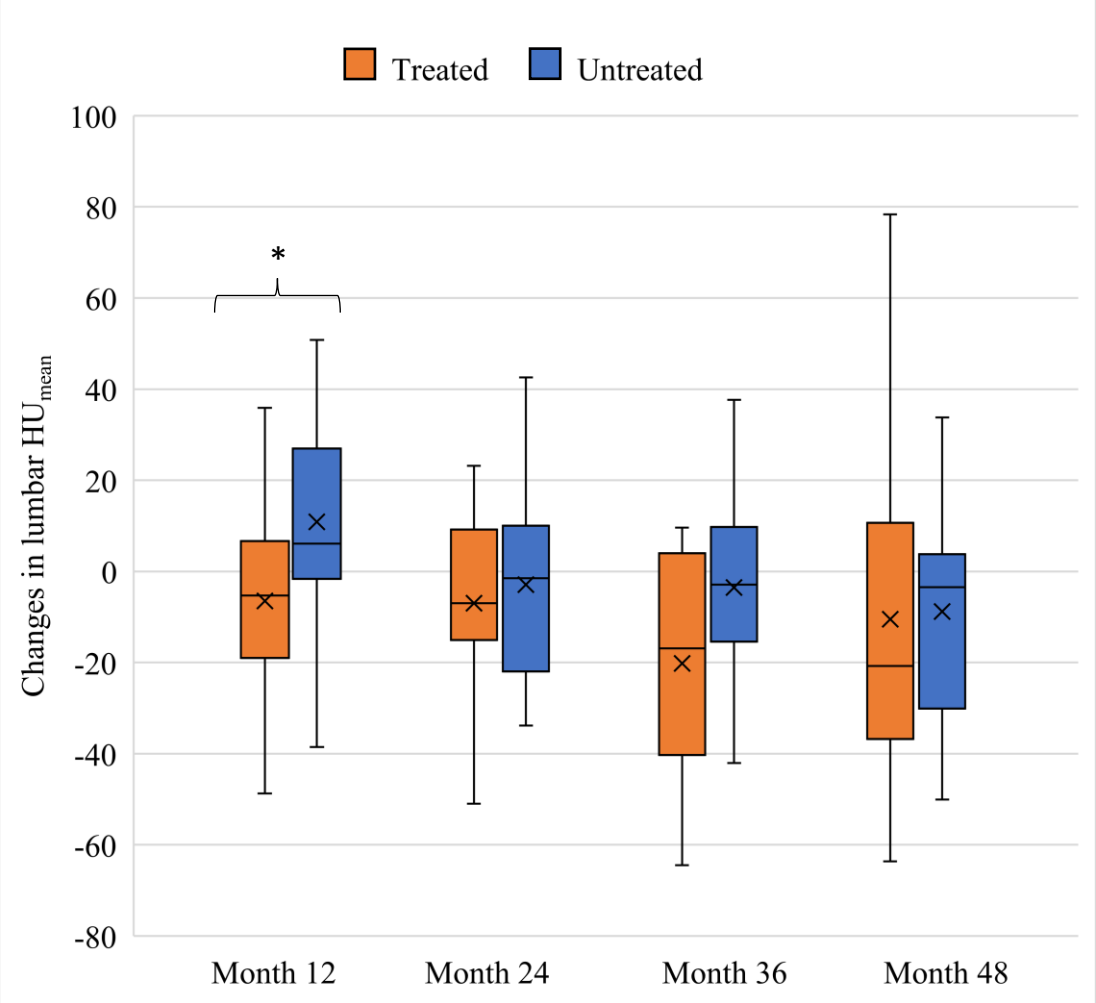

Figure 5.2. Changes in lumbar HU_{mean} from baseline to month 48 for nitisinone-treated and untreated AKU patients.

Blue represents the non-treatment SONIA 2 group; orange represents the nitisinone-treated SONIA 2 group. The graph shows the changes in HU values measured from CT images for lumbar vertebrae bodies (L1-L5) from baseline and the four follow up visits. Table 9.24 (appendix) shows the summary statistics for the changes in HU values for nitisinone-treated AKU patients and untreated patients who were part of the SONIA 2 clinical trial over four years. The changes in the mean HU values between the two groups were compared using the Kruskal-Wallis test. At month 12, nitisinone-treated AKU patients experienced a significant reduction in vertebrae spine HU_{mean} values, compared with non-treated AKU patients (P = 0.036). At month 24, month 36, and month 48, there were no statistically significant differences between treatment and non-treatment groups in the mean change in lumbar HU_{mean} measurements (P = 0.739, 0.120, and 0.681, respectively). *P-value < 0.05 indicate a statistically significant difference between treatment and non-treatment. In box and whisker, x is the mean value, and the line is the median

5.3.1.2 Change in SUV_{max} measured from lumbar vertebral body across 5 visits

The change in bone ^{18}F-NaF uptake during four years was investigated by following the changes in the mean lumbar spine SUV_{max} values. Figure 5.3 shows the mean lumbar SUV_{max} value comparison from Visit 1 at the baseline to Visit 6 at month 48 for each group. Table 9.25 (appendix) displays the summary statistics for SUV_{max} measured from the PET scans for lumbar vertebrae bodies (L1-L5) for both the treatment and non-treatment groups for each visit. Mean lumbar spine SUV_{max} results at the baseline for the treatment group was similar to the non-treatment group value (12.6 ± 4.2, 11.9 ± 2.0, respectively), with no statistically significant differences ($P > 0.05$). Looking at Figure 5.3, it is apparent that both groups reported no clear changes in SUV_{max} measurements from baseline to Visit 3 at month 12. After that, there was a gradual increasing trend in the mean vertebrae SUV_{max} measurement for the nitisinone-treated group. In the non-treated group, there was a rise in SUV_{max} from 12.7 at Visit 3 to 14.5 at Visit 5, and then the value slightly dropped to 13.9 at Visit 6. The change from baseline for the average lumbar vertebrae SUV_{max} for each group are displayed in Figure 5.4 and summarised in Table 9.26 (appendix). Using a Kruskal-Wallis test, there was no observed statistically significant difference in the mean change from baseline in vertebrae SUV_{max} values at neither month 12, 24, nor 36 (P-value = 0.206, 0.678, and 0.310, respectively). A clear influence of nitisinone in the bone ^{18}F-NaF uptake at the spine was noted by the end of the trial. At month 48, nitisinone-treated patients presented a significant higher increment in the mean lumbar vertebrae SUV_{max} values (median change 2.3, range -0.8 to 11.8) compared with non-treated patients (median change 0, range -2.2 to 5.0). Patients in the treatment group experienced a 26.89% mean increase in SUV_{max} measurements, compared with a 10.32% mean increase in SUV_{max} values in the control AKU group after four years ($P = 0.045$).

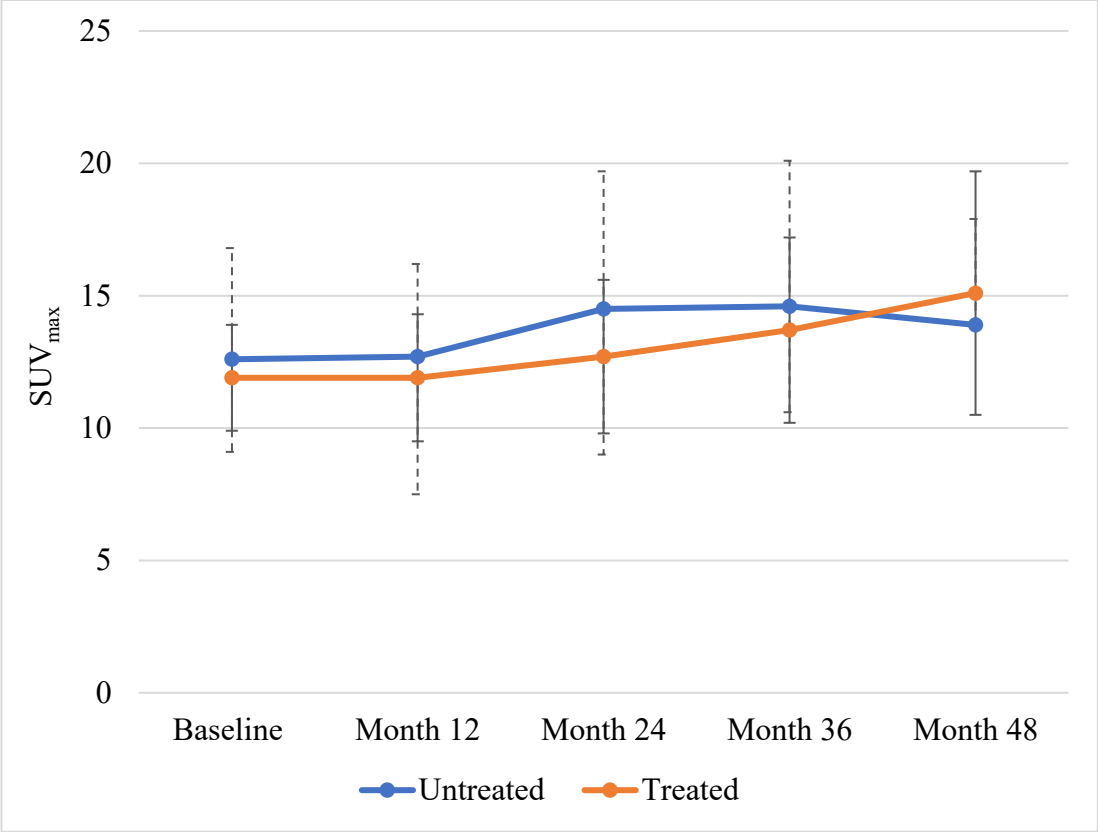

Figure 5.3. Mean lumbar SUV_{max} values for nitisinone-treated and untreated AKU patients who were part of the SONIA 2 clinical trial across 5 annual visits.

Blue line represents the non-treatment SONIA 2 group; the orange line represents the nitisinone-treat SONIA 2 group. Each visit was one year apart: V1; baseline (pre-nitisinone), V3; after 12 months, V4; 24 months, V5, 36 months and V6; 48 months. Error bars represent SD, dash type represents untreated group and solid represents treated group. Table 9.25 (appendix) shows the summary statistics for SUV_{max} values across the visits for both treatment and non-treatment AKU groups. At the baseline, there was no difference in mean lumbar spine SUV_{max} value between nitisinone-treated patients and non-treated patients (12.6 ± 4.2, 11.9 ± 2.0, respectively). There were no changes in SUV_{max} values for treated and non-treated AKU patients from baseline at Visit 3 (month 12), then the value increased for both groups from Visit 3 to Visit 4. After that, the value increased for the nitisinone-treated group and decreased for the non-treated group from Visit 4 to Visit 6.

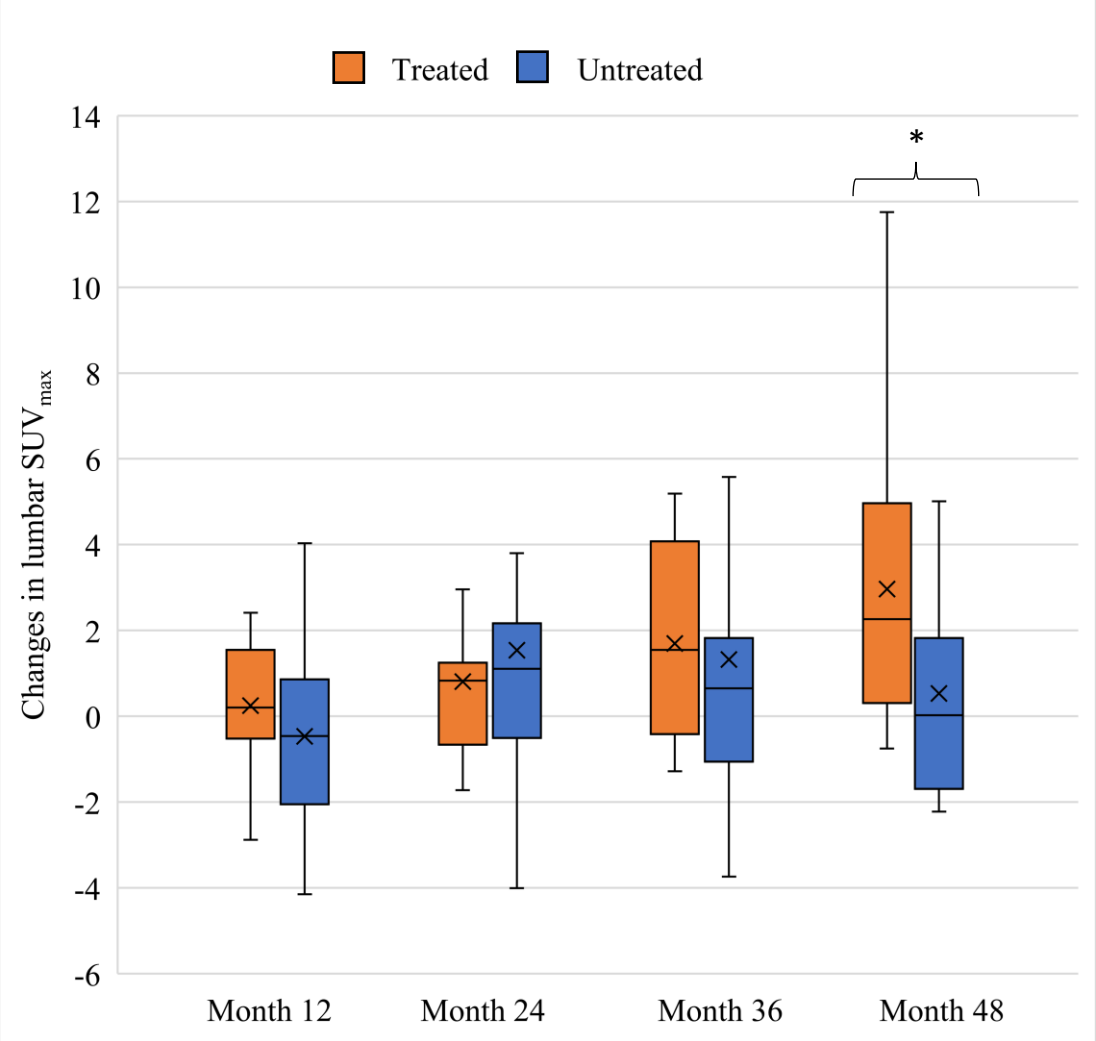

Figure 5.4. Changes in lumbar SUV_{max} from baseline to month 48 for nitisinone-treated patients and untreated patients.

Blue represents the non-treatment SONIA 2 group; orange represents the nitisinone-treat SONIA 2 group. The data summarises the change in SUV_{max} values measured from the PET images for lumbar vertebrae bodies (L1-L5) from baseline and the four follow up visits. Table 9.26 (appendix) summarises the statistics for the changes in SUV_{max} values for nitisinone-treated AKU patients and untreated patients who were part of the SONIA 2 clinical trial over four years. Kruskal-Wallis test shows that there was no statistically significant difference in the mean change from baseline in vertebrae SUV_{max} values at neither month 12, 24, nor 36 months (P-value = 0.206, 0.678, and 0.310, respectively). At month 48, patients in the treatment group presented a significant higher increment in the mean lumbar vertebrae SUV_{max} values compared with the control AKU group (P = 0.045). *P-value < 0.05 indicates a statistically significant difference between treatment and non-treatment. In box and whisker, x is the mean value, and the line is the median.

5.3.1.3 Change in SUV_{max} measured from lumbar disc vertebral unit DVU across 5 visits

The change in the regional joint was also evaluated by investigating the change of the lumbar intervertebral disc ^{18}F-NaF uptake over 48 months of treatment. Figure 5.5 displays the mean lumbar DVU SUV_{max} comparison from Visit 1 to Visit 6 for each patient group. Table 9.27 (appendix) compares the summary statistics for SUV_{max} measured from the PET scans for the average lumbar DVU (T12/L1-L5/S1) for each visit for both treatment and non-treatment groups. As can be seen from Figure 5.5, there was no significant difference in the mean SUV_{max} values in the lumbar DVUs between treatment and non-treatment AKU groups at baseline (17.7 ± 5.4, 14.6 ± 2.9, respectively) ($P > 0.05$). Generally, there were consistent SUV_{max} values for both groups with few changes across the five visits. The mean change from baseline for lumbar DVUs SUV_{max} are highlighted in Figure 5.6 and Table 9.28 (appendix). Close inspection of the figures shows that DVU SUV_{max} values for the nitisinone-treated patients reduced 5.48% from 14.6 at Visit 1 to 13.8 at Visit 4 (at month 36), then increased by 4.79% to 15.3 by month 48 at Visit 6. On the other hand, it appears that untreated patients experienced a 13.6% mean increase in lumbar DUV SUV_{max} value from baseline to month 24, then the value reduced back to the baseline pointt by month 48. In this section of the study, there were no statistically significant differences between treatment and non-treatment groups in the adjusted mean change from baseline in SUV_{max} values at any of the visits (P-value = 0.885, 0.124, 0.633 and 0.280, respectively). From this analysis, there was no clear evidence that nitisinone can influence the ^{18}F-NaF absorption in the disc area over four years.

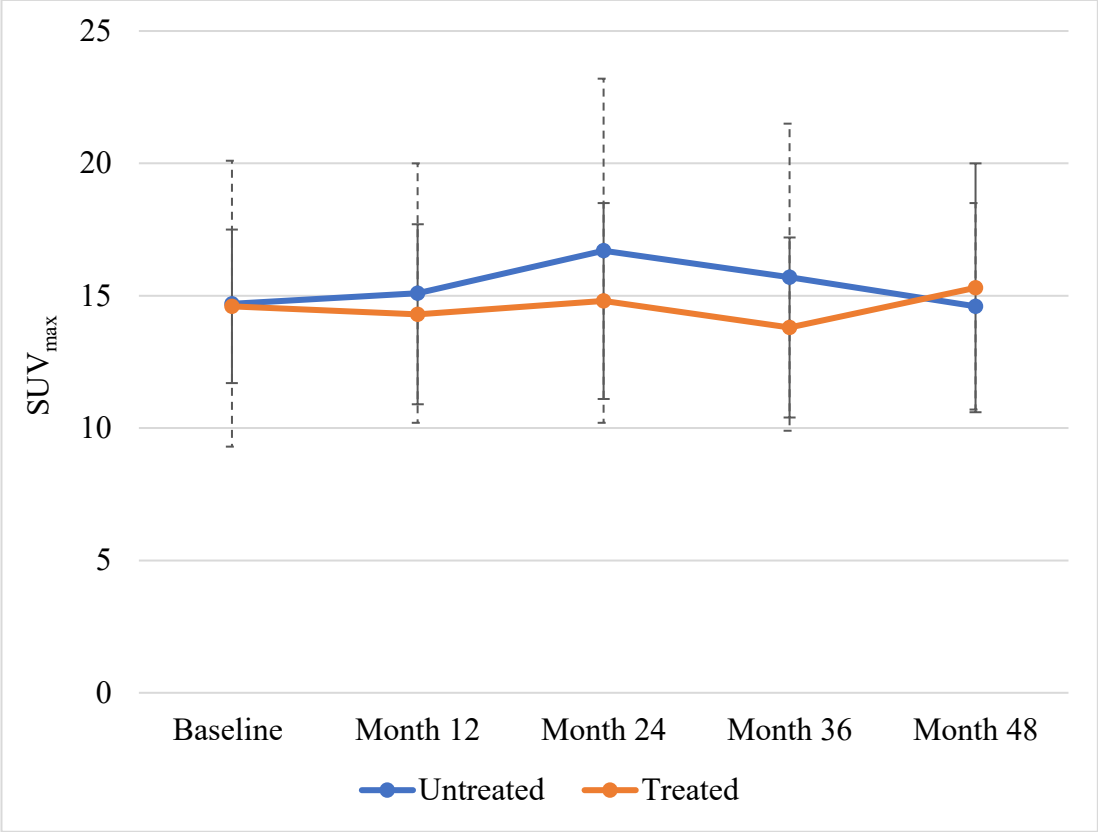

Figure 5.5. Mean SUV_{max} values for average lumbar DVUs (T12/L1-L5/S1) for nitisinone-treated and untreated AKU patients who were part of the SONIA 2 clinical trial across 5 annual visits.

Blue line represents the non-treated SONIA 2 group; the orange line represents nitisinone-treated SONIA 2 group. Each visit was one year apart, V1; baseline (pre-nitisinone), V3; after 12 months, V4; 24 months, V5, 36 months and V6; 48 months. Error bars represent SD, dash type represents untreated group and solid represents treated group. Table 9.27 shows the summary statistics for SUV_{max} values across the visits for both the treatment and non-treatment AKU groups. At baseline, there was no significant difference in the mean SUV_{max} values in the lumbar discovertebreal unit between the treatment and non-treatment AKU groups (17.7 ± 5.4, 14.6 ± 2.9, respectively). There was very little change in lumbar DVU SUV_{max} values for both groups, with few changes across the five visits.

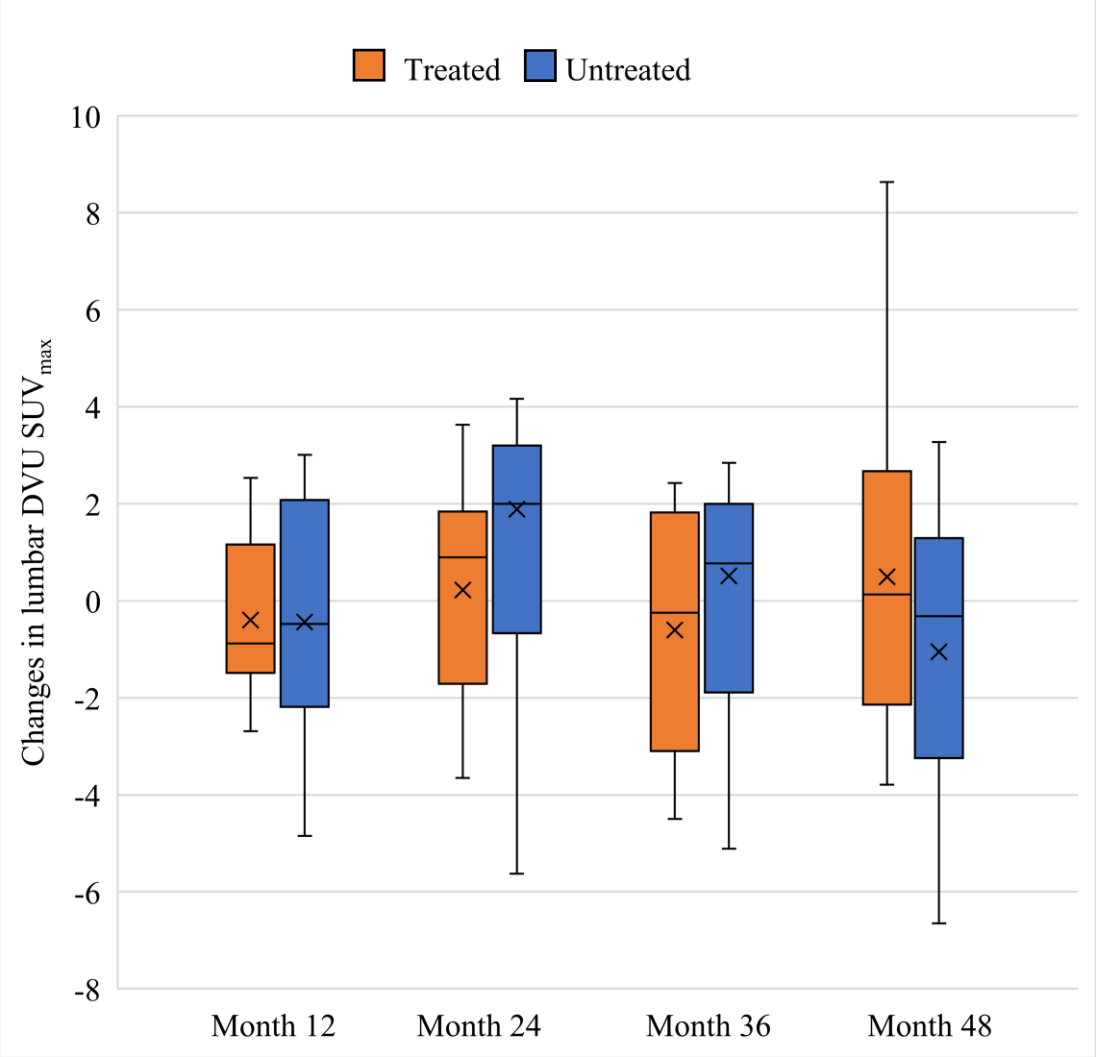

Figure 5.6. Changes in lumbar DVU SUV_{max} from baseline to month 48 for nitisinone treated and untreated AKU patients.

Blue represents the non-treated SONIA 2 group; orange represents the nitisinone-treat SONIA 2 group. The graph shows the changes in SUV_{max} values measured from the PET images for average lumbar DVUs (T12/L1-L5-S1) from baseline followed by up four visits. Table 9.28 (appendix) shows the summary statistics for the change in lumbar DVU SUV_{max} values for nitisinone treated AKU patients and untreated patients over four years. Kruskal-Wallis test indicates that there was no statistically significant difference between treatment and non-treatment group in the mean change from baseline in lumbar disc vertebrae SUV_{max} values to any of the visits (P-value = 0.885, 0.124, 0.633 and 0.280, respectively). In box and whisker, x is the mean value, and the line is median

5.3.2 Individual change in quantitative values across five visits

The individual changes in the measured values for the nitisinone-treated patients and non-treated patients were monitored individually.

5.3.2.1 HU_{mean} lumbar vertebral body

Figure 5.7 and Figure 5.8 display the individual changes in the mean lumbar vertebrae (L1-L5) HU_{mean} across the annual visits in the four age groups for both nitisinone-treated and non-treated patients, respectively. As can be seen from Figure 5.7, most of the nitisinone-treated patients had no significant change in HU values across the serial visits in all age groups. Of the nitisinone-treated patients, 9 patients had reduced lumbar HU_{mean} values, 7 had a small increase, and 1 had an almost consistent value over the four years. Likewise, most of the non-treated patients also showed a similar pattern in which no significant differences in lumbar HU_{mean} measurements were noted over the 4 years (Figure 5.8). One patient (43 year old female) in the control AKU group had a remarkably high lumbar HU value compared to other patients. Of the non-treated patients, 5 patients had experienced a reduction in baseline lumbar HU_{mean} value, 2 experienced an increase in the value, and 9 patients had almost the same value at Visit 6. It is apparent from this data that there was no direct trend in bone density for neither treatment or non-treatment patients across the visits. As seen in Chapter 3 (section 3.3.2.1.2), the oldest AKU patients ($\geq$ 60 years old) had the lowest HU_{mean} values compared to the patients in the other AKU age groups. Generally, there was little change in (L1-L5) HU_{mean} in the 30-39, 40-49, and $\geq$ 60 age groups in both treated and non-treated patients across the visits. These changes were not statistically significant. In the 50-59 age group, the HU_{mean} value fluctuated for nitisinone treated patients as well as for non-treated patients across the visits. Data shows that when the measured HU value was high initially at the beginning of the trial (Visit 1), it was likely to appear high across the visits in most cases, and the reverse is true.

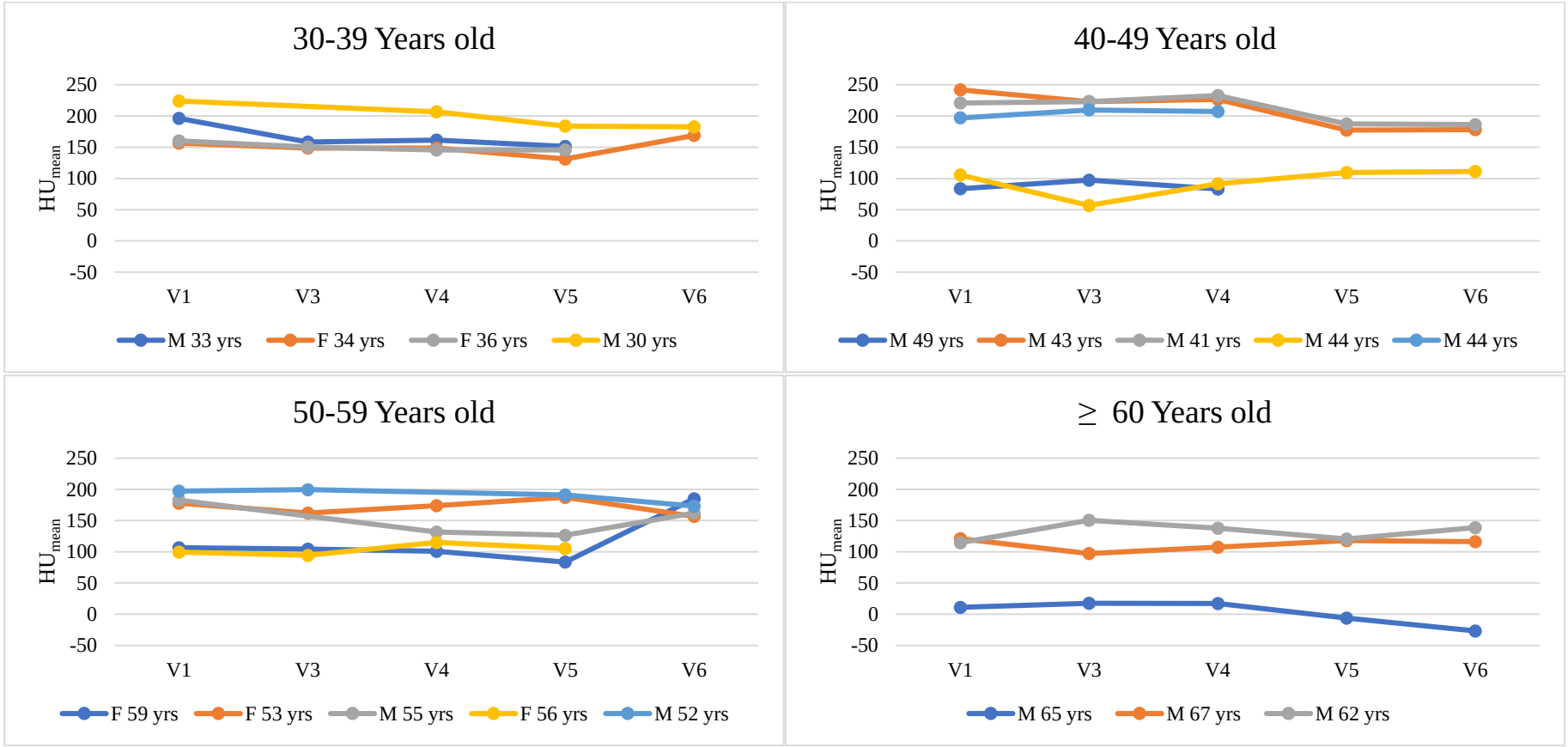

Figure 5.7. The average lumbar vertebrae bodies (L1-L5) HU_{mean} across the visits in the individual AKU patients who were part of the SONIA 2 clinical trial and treated with nitisinone classified by age.

The key defines the gender and age of each AKU patient. M-male, F-Female, yrs-years-old, V1- baseline, V3- at month 12, V4- at month 24, V5 at month 36, V6- at month 48.

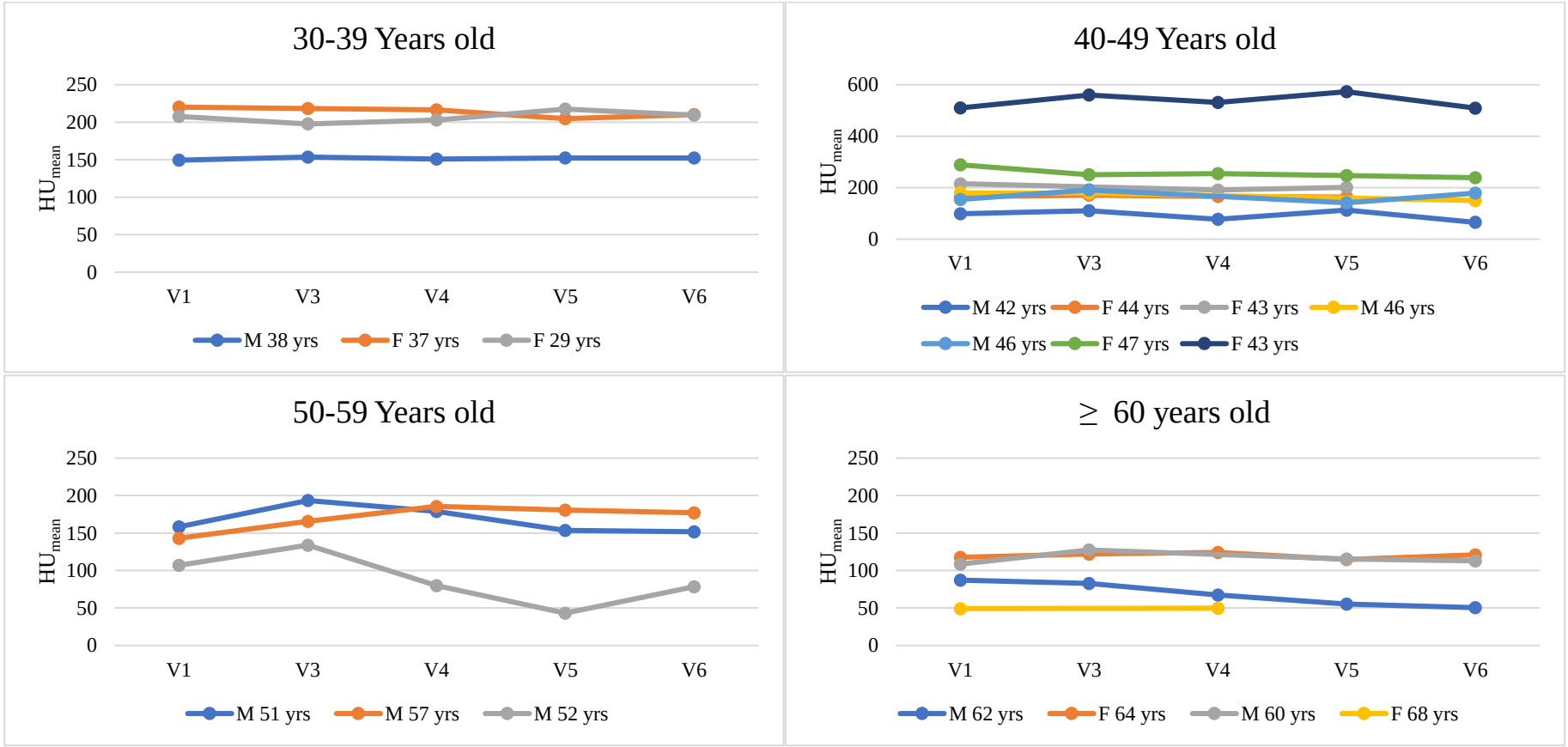

Figure 5.8. The average lumbar vertebrae bodies (L1-L5) HU_{mean} across the visits in the individual AKU patients who were part of the SONIA 2 clinical trial and been in control group classified by age.

The key defines the gender and age of each patient. M-male, F-Female, yrs-years-old, V1- baseline, V3- at month 12, V4- at month 24, V5 at month 36, V6- at month 48.

5.3.2.2 SUV_{max} in the lumbar vertebral body

Figure 5.9 and Figure 5.10 demonstrate the individual changes in the mean lumbar vertebrae (L1-L5) SUV_{max} across the four age groups from annual visits for treated and non-treated patients, respectively. Looking at the individual differences in the lumbar vertebrae SUV_{max} measurements for nitisinone-treated AKU patients among the four age groups (Figure 5.9), the mean lumbar SUV_{max} values were very consistent with little changes between the visits for most of the treated patients. It appears from the figures that the patients in the youngest and oldest age groups had consistent SUV_{max} across the visits with minimal changes between Visit 1 and Visit 6. Closer inspection of the figures shows that there was little difference in lumbar SUV_{max} values between Visit 1 and Visit 4 for most of the patients in the 40-49 and 50-59 age groups; the values started to increase between Visit 4 and Visit 6. Lumbar SUV_{max} value increased in 9 treated patients and remained the same in 8 patients. No clear reduction trend was noted in the lumbar SUV_{max} value for nitisinone-treated patients.

In the non-treatment group, the individual changes in the lumbar spine SUV_{max} measurements over time followed a similar pattern to that noted in the nitisinone-treated patients (Figure 5.10). As seen from the non-treated patient figures, some of the 40s and 50s patients showed fluctuations in the SUV_{max} during the visits. No significant difference in SUV_{max} for most of the 30s and 60s patients was noted. As shown un the Figure 5.10, 7 non-treated AKU patients showed increases in lumbar SUV_{max} values, 7 patients showed a decrease in the values, and 3 patients had almost the same values.

It is apparent that in most cases when the initial lumbar vertebrae SUV_{max} value was low at the beginning of the trial, it was more likely to be low across the visits. In general, elderly patients ($\geq$ 60 years old) in both groups had low SUV_{max} values compared to other age groups with little change from the Visit 1 to Visit 6. This finding was noted earlier in Chapter 3 (section 3.3.1.1.2), where it been found that elderly patients had low ^{18}F-NaF uptake at lumbar vertebral bodies compared to other age groups. Generally speaking, there was no direct trend in the individual changes for both treatment and non-treatment patients having very consistent lumbar SUV_{max} with little change across the five visits.

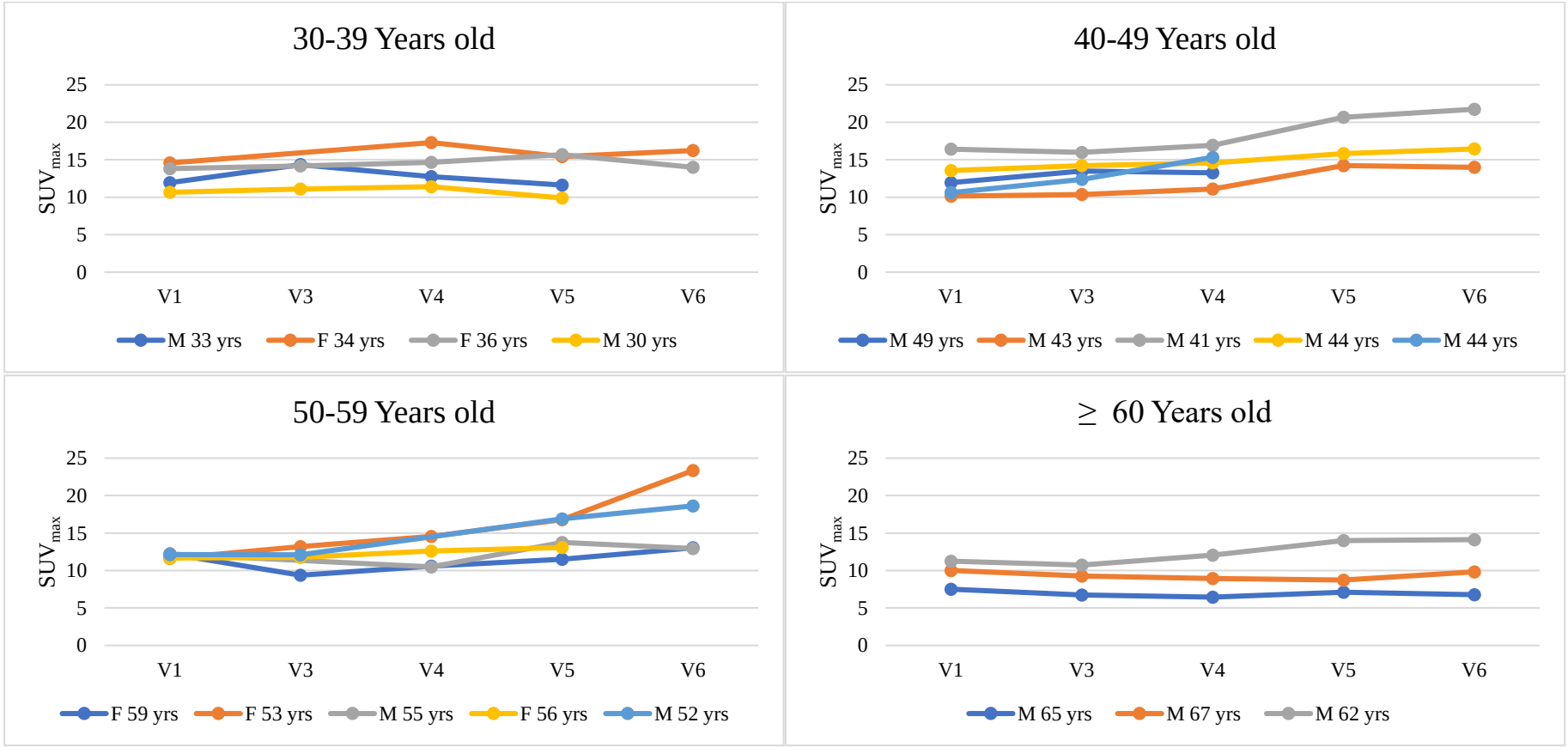

Figure 5.9. The average lumbar vertebrae bodies (L1-L5) SUV_{max} across the visits in the individual AKU patients who were part of the SONIA 2 clinical trial and treated with nitisinone classified by age.

The key defines the gender and age of each patient. M-male, F-Female, yrs-years-old, V1- baseline, V3- at month 12, V4- at month 24, V5 at month 36, V6- at month 48.

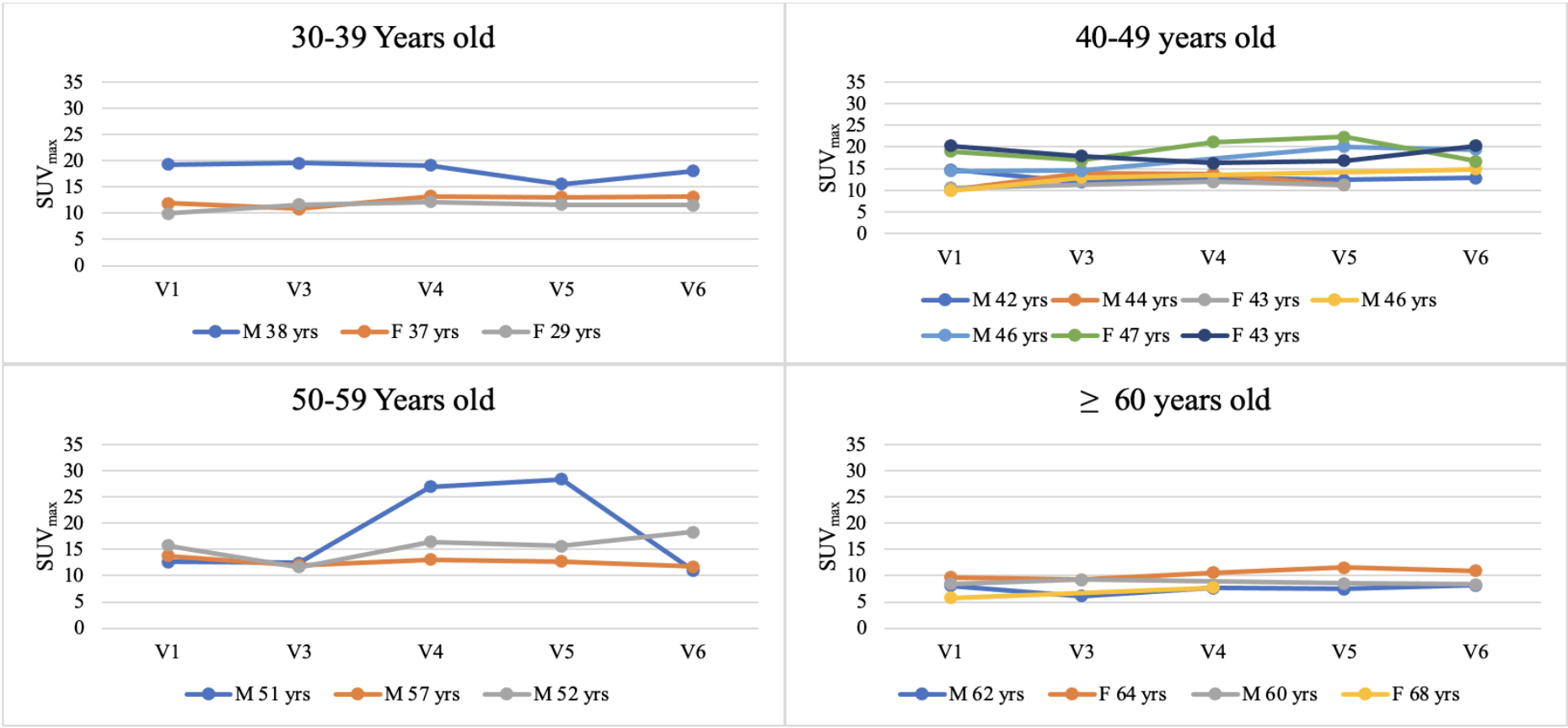

Figure 5.10. The average lumbar vertebrae bodies (L1-L5) SUV_{max} across the visits in the individual AKU patients who were part of the SONIA 2 clinical trial and been in control group classified by age.

The key defines the gender and age of each patient. M-male, F-Female, yrs-years-old, V1- baseline, V3- at month 12, V4- at month 24, V5 at month 36, V6- at month 48.

5.3.2.3 SUV_{max} in the lumbar discovertebral unit

Figure 5.11 and Figure 5.12 show the individual changes in the mean lumbar discovertebral unit (T12/L1-L5/S1) SUV_{max} values for treatment and non-treatment patients across the annual visits among the four age groups, respectively. It can be seen from Figure 5.11 that the lumbar DVU SUV_{max} measurements for the nitisinone-treated AKU patients in the 30-39, 40-49 and ≥ 60 age group were remarkably consistent across the five visits with little change between the visits. Treated patients in the 50-59 age group had constant SUV_{max} values between Visit 1 and Visit 5; after that the values started to increase from Visit 5 to Visit 6 for most of the cases. SUV_{max} at lumbar DVU increased in 8 nitisinone treated patients, decreased in 6 patients and remained the same in 3 patients.

In the non-treatment group, the lumbar disc SUV_{max} value fluctuated across the visits in all the age groups except in the oldest age group (≥ 60 years old), in which the SUV_{max} value was generally consistent across the five visits. As shown in Figure 5.12, 6 non-treated AKU patients showed increases in DVU SUV_{max} values,6 showed decreases in values, and 5 had no clear change in values.

From these findings, concerning the ^{18}F-NaF uptake in the IVD area, there seems to be no direct trend across the visits between the nitisinone-treated and non-treated AKU patients. Again, as with what was noted in lumbar vertebrae, when the SUV_{max} at the disc area was high initially at the baseline evaluation, it appears to be high across the following visits with minimal changes

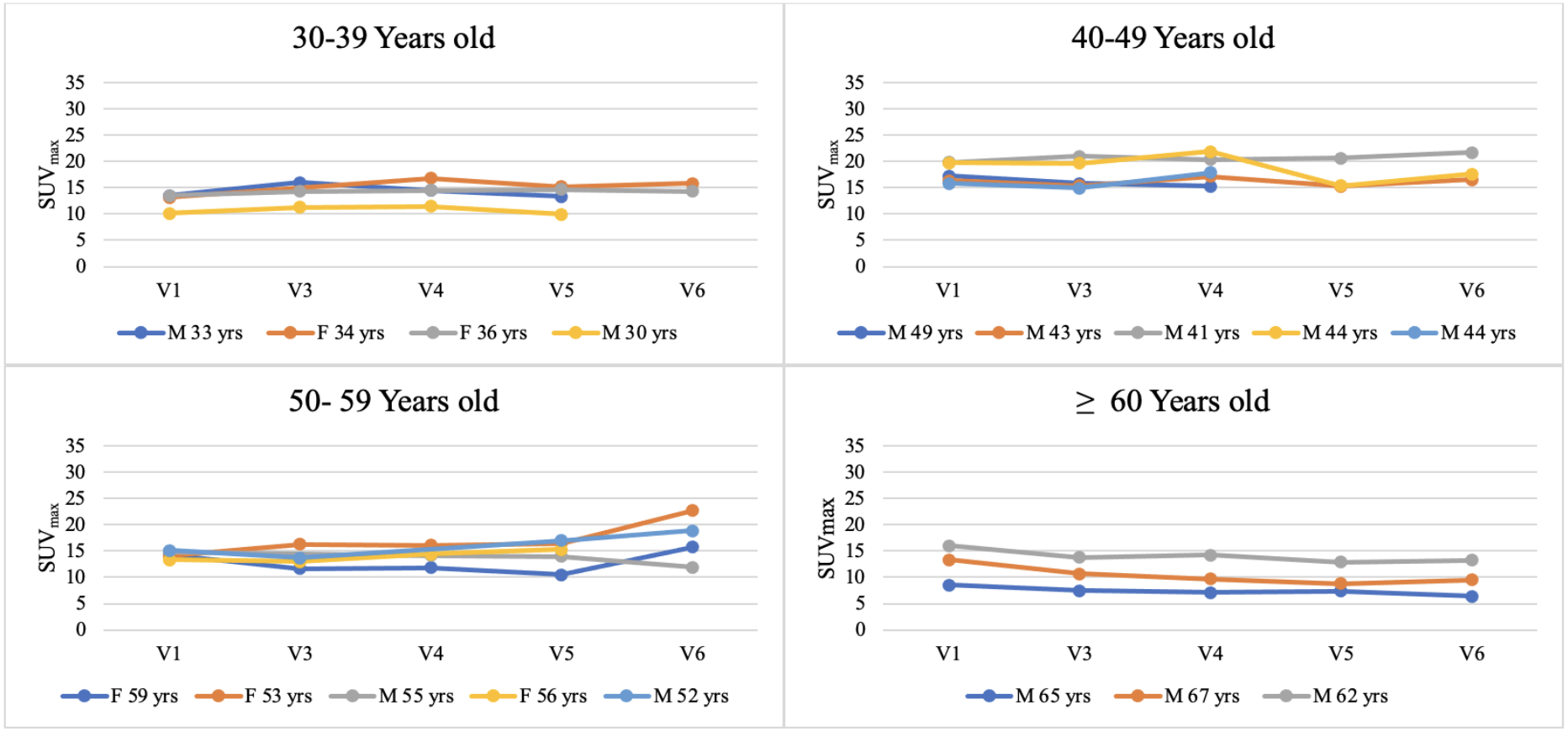

Figure 5.11. The average lumbar DVUs (T12/L1-L5/S1) SUV_{max} across the visits in the individual AKU patients who were part of the SONIA 2 clinical trial and treated with nitisinone classified by age.

The key defines the gender and age of each patient. M-male, F-Female, yrs-years-old, V1- baseline, V3- at month 12, V4- at month 24, V5 at month 36, V6- at month 48.

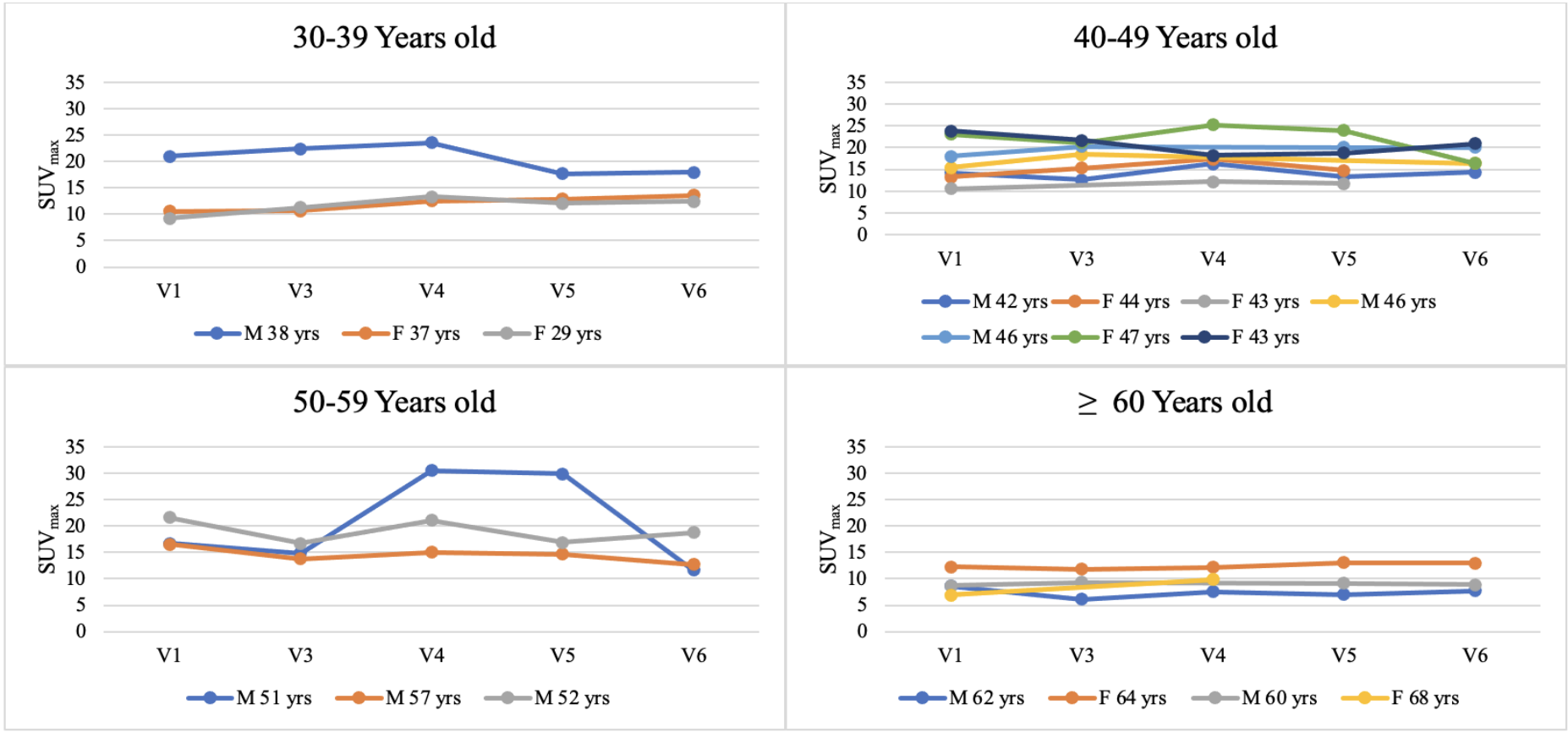

Figure 5.12. The average lumbar DVUs (T12/L1-L5/S1) SUV_{max} across the visits in the individual AKU patients who were part of the SONIA 2 clinical trial and been in control group classified by age.

The key defines the gender and age of each patient. M-male, F-Female, yrs-years-old, V1- baseline, V3- at month 12, V4- at month 24, V5 at month 36, V6- at month 48.

5.4 Discussion

In reviewing the literature, no previous data was found on the association between the changes that can be noted in scintigraphy and potential disease-modifying therapy in AKU patients. Previously, ^{18}F-NaF PET has been used as an isotopic imaging biomarker in a number of studies detecting the effect of pharmacological treatment on regional bone formation during drug development for various metabolic bone disorders, including osteoporosis[138–141]. Different PET semiquantitative methods were successfully utilised for identifying the changes in PET images over time.

This is the first longitudinal study investigating the effect of nitisinone in bone and cartilage for patients with AKU by quantifying ^{18}F-NaF PET/CT scans over four years. In the SONIA 2 clinical trial, serial ^{18}F-NaF PET/CT scans were performed to understand the disease progression better and/or assess possible responses to treatment. The progression of spinal arthrophathy in response to nitisinone was monitored annually by evaluating the changes in HU_{mean} values from CT scans and SUV_{max} values from PET scans in order to assess the longitudinal change throughout treatment. In this chapter, the methods described previously in Chapter 3 and Chapter 4, for quantifying the baseline ^{18}F-NaF PET/CT scans have been repeated over the other visits.

5.4.1 Annual change in the lumbar vertebrae HU_{mean} value

The first objective in this study was to determine the change in bone density over four years for those patients who received a daily dose of nitisinone and those who were treatment free. Although CT scans cannot detect early active bone biological processes, CT might still provide valuable information regarding the progression of the ochronotic arthrophathy during the course of treatment. There are few studies that evaluated the impact of nitisinone on osteopenia in AKU patients. To date, no previous study has investigated the impact of nitisinone on HU values. In this study, HU measurements from CT scans have been measured to assess the changes in bone density after receiving nitisinone for four years. The annual change in the mean HU_{mean} values in the lumbar spine was monitored, representing the change in the spine bone density (Table 9.23 and Table 9.24). As previously proposed, ochronosis alters the

bone matrix and interferes with bone metabolism causing loss in bone mass. Based on that assumption, it was expected to see a reduction in bone density with age in AKU patients who are in the control group compared to those in the nitisinone treatment group. Contrary to expectation, minimal annual changes in the mean bone density measurements over the visits have been noted in nitisinone-treated patients, as seen in Figure 5.1. In this four-year clinical trial, nitisinone did not change the mean lumbar spine HU measurements significantly for treated AKU patients. A clear benefit of nitisinone in preventing osteoporosis or preventing weakened bones was not detected in CT images by evaluating the changes in HU measurements. This indicates that it may not have a direct effect on bone density, or the impact of therapy on the bone may take more than four years to be noted. The results here further support the idea that rebuilding bone density/bone mass may not be possible once a significant amount of bone density has been lost. In the non-treatment group, no significant changes have also been noted over four years, suggesting that average bone density change in AKU patients may take years or decades to be detectable. The minimal HU changes in the non-treatment group represents the rate of bone density progression over time in AKU patients. Kruskal-Wallis tests revealed that the changes in HU values between the two groups was only statistically significant different after 12 months. Generally speaking, this study did not detect clear evidence regarding the differences between the treatment and non-treatment group in the mean changes of HU values between visits. This finding accords with the observations of Introne *et al.* [48], who evaluated the effect of nitisinone for 40 AKU patients over 36 months. In that study, although Introne observed HGA reduction in urine and plasma, total hip range of motion and musculoskeletal function did not improve following the medication. Ranganath *et al.* [51] suggested that the inconclusive results in that study may be due to insufficient nitisinone dosage (2 mg once daily). In the SONIA 2 trial, Ranganath and colleagues suggested giving SONIA 2 participants in the treatment group higher nitisinone dose of 10 mg once daily (based on the 4 week SONIA 1 study). Although the treatment group in SONIA 2 trial received five times more nitisinone than used in the Introne *et al.* [48] treatment group, the findings in the current chapter are in line with those of the Introne study; study duration is likely the common factor that has led to no effects on bone being detected. In another study, Suwannarat *et al.* [47] investigated the effect of nitisinone with a regular diet over the course of 3 to 4 months, and also found a consistent reduction of HGA in urine and plasma. That paper also provided little

evidence of positive therapeutic intervention on joints. Suwannarat noted that the pain in the affected joints was reduced, and that mobility improved in 6 out of the 7 patients. However, Suwannarat *et al*. only investigated a small number of cases and failed to use quantitative methods to assess the clinical effectiveness of nitisinone. The lack of quantitative outcome in that study makes it difficult to interpret these findings with confidence.

Comparing the findings in this Chapter with those of Ranganath *et al*. [53], confirms that nitisinone may be ineffective in bone tissue suggesting that co-therapy is required to prevent bone loss in AKU patients. In 2020, Ranganath investigated the relationship between potential therapy and bone density in the largest group of AKU patients. In this longitudinal study, Ranganath *et al*. examined the data from 87 AKU patients who attended the NAC between 2007 and 2020 and underwent serial clinical evaluations, including DEXA and CT densitometry. In that study, patients were classified into three groups: the nitisinone-treatment group, the nitisinone plus antiresorptive treatment group, and the non-treatment group. To determine the effect of treatment, the change in bone density values at the femoral neck, total hip and lumbar spine from DEXA and CT were examined in all groups. A group of AKU patients who undertook 2 mg daily dose of nitisinone showed a significant reduction in CT values measured at femoral and hip sites ($P < 0.05$) and slightly increased lumbar CT values ($P > 0.05$). Only patients on nitisinone plus antiresorptive had improved bone density values at all measured ROI ($P < 0.001$) and surprisingly had significantly more fractures than the nitisinone-treatment group and non-treatment group. These results also seem to be consistent with SONIA 2 final analysis scans results (appendix), which found increased fracture for both groups and no significant differences in hip bone density values from DEXA scans between treatment and non-treatment groups.

5.4.2 Annual change in SUV_{max} in the lumbar vertebrae and lumbar intervertebral disc

The second investigation in this chapter was to evaluate the change in ^{18}F-NaF uptake in the lower spine at the bone and joint regions over the four years for those nitisinone-treated and non-treated AKU patients. In this study, the annual changes in maximum SUV values measured from lumbar vertebrae bodies (L1-L5) and the lumbar intervertebral discs (T12/L1-L5/S1) for SONIA 2 patients were monitored for both

treatment and non-treatment groups, as shown in section 5.3.1.2 and 5.3.1.3. Looking at the annual changes in PET semiquantitative values, the results of this study show that there were very little changes in the mean SUV_{max} values for the average lumbar vertebral bodies across the visits. Kruskal-Wallis test revealed no statistically significant differences between nitisinone-treated and non-treated AKU patients in the mean changes from baseline in vertebrae SUV_{max} values at month 12, month 24, and month 36 (P-value = 0.206, 0.678, and 0.310, respectively); the only significant differences were noted at month 48 (P = 0.045). These results would seem to suggest that the effect of nitisinone in the lower spinal bone could not be noted in ^{18}F-NaF PET/CT scan before 48 months post-treatment. The finding in this section broadly supports the idea that it is hard to reproduce new bone after significant bone tissue damage. Further observations for a longer period may clarify these findings.

Regarding the effectiveness of the nitisinone on the spinal joints, the IVD changes were also not significant between the treatment arms. What can be clearly seen in this analysis is that nitisinone had no apparent benefit in treating disc degeneration in AKU patients. There were no statistically significant differences between nitisinone treatment and non-treatment groups at any visits in the adjusted mean change from baseline in lumbar DVU SUV_{max} values (P > 0.05). Generally, the SUV_{max} measurements for the average lumbar DVUs were remarkably stable for both groups. It is more likely that this observation can be explained by the molecular mechanisms of ^{18}F-NaF deposition in the calcified soft tissue, including calcified intervertebral disc lesions. Previously Chapter 4 shows that the relationship between increased SUV_{max} and disc damage was asymmetric in the severe disc degeneration cases and that increased ^{18}F-NaF uptake on PET scans did not always correspond to the structural disc damage in MRI. Patients with end-stage disc degeneration with structural disc abnormalities had a grade 8 Pfirrmann score but not a correspondingly high SUV_{max}. The change in ^{18}F-NaF uptake at the DVU was strongly associated with disc degeneration stages and whether the calcification was still active or had become stable. In the normal disc structure, no calcium deposition would be found in IVD area; therefore, no bone radiotracer accumulation at the non-calcified IVD would be expected. During the development of disc degeneration, the disc becomes thinner with unclear distinction between the vertebrae, causing a deformation of the vertebral bone. It is likely that calcium deposits in the IVD spaces in AKU patients increases with

disease progression, driving more ^{18}F ion binding sites, therefore high ^{18}F-NaF uptake. In severe disc degradation, it is more likely that most of the disc levels have complete calcification, causing the IVDs to begin to fuse together, which would lead to reduction of ^{18}F-NaF uptake due to an inactive and stable degeneration stage; therefore, low SUV could be noted at the end-stages of disc degeneration. Because of that, it was expected to see a significant reduction in SUV value over time for patients who received nitisinone as an indicator for a successful treatment before IVDs collapse at the end disc degenerative stage. It was also expected to identify increased ^{18}F-NaF uptake in the non-treated AKU group, which would indicate increased disc calcification before severe disc degeneration appears. Contrary to expectation, data did not show any significant differences in the SUV values between one visit and others in treatment and non-treatment AKU groups. It was surprising that the SUV_{max} values for the treatment group did not differ significantly from those of the non-treated AKU group. It may be challenging to explain this finding. However, a possible explanation for this result may be due to mineral calcium deposition over four years, which leads to few availability of -^{18}F-ion binding sites; therefore, no changes were noted in ^{18}F-NaF uptake during the trial. Also, nitisinone might not have the ability to treat stable disc calcification, which built up years ago. In fact, the severe damges in the spine tissues specifically in the disc area may not be treated by stopping or slowing down the ochronotic pigment deposition. Additionally, these results may demonstrate the stabilisation of the disease over four years.

Generally, the ^{18}F-NaF PET/CT results at lumbar vertebral and lumbar DVU of non-treated AKU patients are similar to those AKU patients who were treated with nitisinone, following a similar pattern over four years. In accordance with the present results, scintigraphy qualitative data from SONIA 2 trial have found no significant differences between treated and non-treated AKU patients, which showed that the number of affected joints in whole body and spine were increased over visits for both treatement and non-treatment groups. Although more accurate, reliable and sensitive semiquantitative PET methods have been used in the current study, similar finding have been observed in both groups. It is possible that bone turnover, vascularity and osteoblastic activity in the lumbar spine is increased over a few years, but the changes are minimal, therefore, ^{18}F-NaF uptake was almost stable in the measured sites.

According to these data, the effectiveness of nitisinone on ^{18}F-NaF uptake measured from the lower spine was inconclusive.

It was hypothesised that therapeutic interventions on bone disorders could be noted by evaluating the changes in ^{18}F-NaF uptake in bone and cartilage. However, the findings of the current study did not support this. Overall, the longitudinal changes in ^{18}F-NaF images in response to nitisinone were not significant, and minimal changes in bone and cartilage were observed over the period of four years. This observation may be explained by the fact that the number of patients was not enough to study the effectiveness of nitisinone on ^{18}F-NaF uptake for a long period. Although continued HGA deposition in cartilage leads to osteoarthropathy, monitoring the change using bone radiotracer uptake seems to need more years to be noted. As mentioned in the previous section (5.4.1), the PET findings were consistent with that of Introne *et al.* [48] who found that nitisinone did not appear to influence bone over a three-year clinical trial. The results observed in this study contradict with a previous preclinical study which suggested that taking nitisinone can completely prevent pigment deposition in cartilage tissues. Preston *et al.* [46] investigated the effectiveness of nitisinone in the knee joint using the AKU mouse model, and reported a beneficial impact of long-term treatment with nitisinone. Preston noted that ochronotic pigment was completely prevented in AKU mouse. It is important to point out that the observed impact of nitisinone in preventing ochronotic pigment in the cartilage or soft tissues is easier to assess and identify in preclinical studies, and it may be difficult to evaluate in human joints pre- and post-treatments with nitisinone. There is not currently a method that can assess deposition of HGA within human joints. Because of that, the alternative evaluation method in human research involves the use of imaging techniques as demonstrated here in this thesis.

5.4.3 Individual changes in the quantitative values across the visits

Due to the low number of patients in each age group, the trend of the change in the mean age group values may not be statistically convincing. The changes in lumbar vertebrae and IVD units from individual patients were plotted to examine any trends between the ^{18}F-NaF PET/CT semiquantitative values and age in both treatment and non-treatment AKU patients. This section aimed to investigate what is happening to

these semiquantitative values over four years on an individual basis. Are all nitisinone-treated AKU patients following the same pattern over the four years? These observational investigations helped to deliver an accurate assessment and show the disease progression in individual AKU patients. It is possible that the biological behaviour of the drug in the individual cases differs. In Chapter 3 and Chapter 4, the differences between the HU_{mean} and SUV_{max} for the lumbar vertebrae and SUV_{max} for the DVU in each age group were tested respectively to assess the age effect for the baseline data. Chapter 3 identifies that generally, there were no significant differences in lumbar vertebrae (L1-L5) HU_{mean} values between the age groups; also, no significant differences in lumbar vertebrae SUV_{max} between the age groups were observed. An interest finding has been noted in Chapter 4, in which lumbar disc SUV_{max} increased gradually with age following by a declined in the later years.

This study found little change in bone semiquantitative values (HU_{mean}) measured from the ^{18}F-NaF PET/CT image for the lumbar vertebrae across the five visits for most of the cases. Figure 5.7 and Figure 5.8 represent the individual changes in the mean lumbar vertebrae HU value for both nitisinone-treated and non-treated AKU patients across the five visits in four age groups (30-39, 40-49, 50-59, and $\geq$ 60). When the mean HU values were plotted for lumbar vertebrae across the visits, little change was noted from one year to the next for nitisinone-treated AKU patients and non-treated AKU patients. No definitive trends were observed in most of the cases. Although HU_{mean} values were fluctuating between visits for most of the AKU patients, the values in Visit 1 were very similar to the value in Visit 6.

The individual changes in ^{18}F-NaF uptake for lumbar bone have also been evaluated from Visit 1 to Visit 6. Figure 5.9 and Figure 5.10 show the individual changes in lumbar vertebrae SUV_{max} values in both nitisinone-treated and non-treated AKU patients. The results were similar to those shown in lumbar vertebrae HU_{mean} figures. Again, the lumbar vertebrae SUV_{max} remains stable across the five visits with minimal changes in most cases. Although small fluctuations were noted in lumbar bone SUV_{max} across the visits, no definitive trends were noted in AKU patients.

Regarding individual changes in the cartilage at the spine region, this study also observed small changes in the average SUV_{max} measured from the lumbar disc across

the five visits, as shown in Figure 5.11 and Figure 5.12. The lumbar DVUs SUV_{max} values were particularly stable with very little change in the values across the visits for most of the AKU cases. It was noted that if the SUV_{max} for the lumbar vertebral was high, it is likely that disc SUV_{max} value would also be high. It seems possible that these results were due to the inclusion of the endplate region in DVU measurements. As described in Chapter 2, it was impossible to define only the disc region in most of the spine levels, so the ROI was encompassed the DVU, covering the disc area and the endplate of the two adjacent vertebrae. Therefore, it is probable that the maximum SUV value was measured from the bone region rather than disc region.

Overall, it is somewhat surprising that the HU_{mean} and SUV_{max} measured from the lumbar spine for those AKU patients who undertook nitisinone and those who did not remained similar, with very little change in the measured values for most of the cases across the visits. Individually, no definitive trends were observed in any age groups. The similarites between the nitisinone-treated AKU patients and non-treated AKU patients was not expected but may be explained by several possible reasons. In the younger patients, the unchanged values may be explained by the fact that the deposition of the ochronotic pigment in spinal tissues is minimal in the third decade. These results are likely to be related to the stabilisation of the disease over four years for young patients. The reason for this is not clear but, it is possible that the effect of early-stage treatment for young AKU patients by nitisinone could prevent the development of ochronotic arthropathy and may be noted later in the 40s or 50s. In the 40s and 50s age groups, the HU and SUV values can be seen fluctuating; however, in most patients, the values of Visit 1 and Visit 6 were very similar. It is possible that the progression of the disease is active in the 40s and 50s, causing inconsistent results. On the other hand, the oldest patients have very stable quantitative values across the visits. These results may be explained by the fact that they have severe inactive bone turnover and inactive disc calcification in the spine region caused by a high level of ochronotic deposition. As explained in the previous chapters, the low SUV_{max} in the lumbar spine for elderly patients is expected due to inactive local osteoblastic reaction of bone which reduces -^{18}F ion binding sites, therefore low ^{18}F-NaF uptake. It is probably challenging to prevent or treat ochronotic arthropathy in elderly patients who already have severe degeneration, but it may have a beneficial impact in young patients. It has been widely argued that nitisinone might slow the progression of the ochronosis by arresting

ochronotic pigment; however, it is unlikely for nitisinone to reverse ochronosis, and importantly, reverse joint damage.

5.5 Summary

In summary, the ability of ^{18}F-NaF PET/CT to assess the early response in spinal arthropathy for AKU patients treated with nitisinone was limited. The semiquantitative evaluation of ^{18}F-NaF PET/CT reported a stable disease progression in the nitisinone-treat and non-treat groups over four years. Therefore, it seems that the effect of nitisinone in the lumbar spine was not confirmed due to unclear trends in nitisinone-treated and non-treated AKU patients. Patients who received nitisinone showed an absence of significant radiographic improvements; likewise, non-treated patients showed no evidence of substantial structural or molecular damage over four years. In fact, nitisinone might slow the progression of the ochronosis by arresting further ochronotic pigment deposition; however, it is unlikely to treat stable bone turnover or severe disc damage associated with a high level of pre-treatement ochronosis.

Whilst this study did not confirm the positive effect of nitisinone in the spine of AKU patients, it enhanced the understanding of disease progression over four years. The results raise the possibility that four years undertaking nitisinone may not be long enough to show bone and cartilage changes in the spinal tissues, particulary in patients who already had severe disease when treatment was initiated. It would not be unreasonable to expect a change in HU_{mean} and SUV_{max}, which represents the treatment effect or disease progression over a period of four years in AKU patients. However, there is a possibility that the outcome would be clearer in longer term evaluations. Additionally, the spinal regions may not represent the global progression of ochronotic arthrophathy among the skeletal sites. It is therefore likely that further investigation is needed to assess the longer-term impacts of nitisinone in reducing arthritis features for AKU patients to establish the effectiveness of the treatment. This study encourages further investigation into using isotopic imaging biomarkers as a response assessment method in the skeleton in a variety of treatment options for AKU patients. Close monitoring of individual treated and non-treated patients would be important to determine accurate treatment assessment in individual cases.

5.6 Limitations

The findings of this study are subject to certain limitations. First of all, interobserver and intraobserver reliability have not been tested due to limited time and clinical collaboration. Second of all, only one skeletal site was evaluated. It is more likely that one skeletal site does not represent the progression of the entire skeleton. Third of all, not all of the patients had all serial five scans due to withdrawal from the trial or technical issues in the PET/CT scanner or cyclotron on the scheduled day for imaging. These unmeasured scans may cause a source of error which should be considered carefully. Also, there were no control non-AKU patients to identify normal bone metabolism changes in the spine with age for the general population. Therefore it was not be possible to know whether the changes in the ^{18}F-NaF PET/CT semiquantitative values over four years in AKU patients is following the average changes in the general population and in-line with age. These limitations mean that the findings in this study need to be interpreted cautiously.

5.7 Future work

Further work is needed to support the ^{18}F-NaF PET/CT findings in regard to the effectiveness of nitisinone in bone and cartilage for AKU patients. More work is required to examine the interobserver and intraobserver agreements on the measured values. It would be more precise if other bones and joint sites such as the shoulder or knee are quantified to investigate the effect of nitisinone and assess the progression of the disease in more than one body site. This would represent a better understanding if nitisinone has a global and /or regional impact on bone and cartilage tissues. Additionally, more work is needed to develop a full picture of the correlation between nisitisone-treated and non-treated AKU patients over a long-term period.

5.8 Conclusion

This chapter has shown:

- There were no significant differences between the nitisinone treatment and non-treatment groups in the adjusted mean changes in HU_{mean} values for the lumbar spine.

- There were no significant differences between nitisinone-treated patients and non-treated patients in the adjusted mean changes in SUV_{max} values for lumbar vertebrae and lumbar disc SUV_{max} across the visits.
- There was no direct trend in the individual changes for both treatment and non-treatment patients having very consistent lumbar HU and SUV values, with little change across five visits.
- Four years undertaking nitisinone may not be long enough to detect the clear changes in the spinal tissues.
- Nitisinone might slow the progression of the ochronosis by arresting ochronotic pigment, but it is unlikely to reverse ochronosis and/or joint damage.

6 Cross-sectional study of cardiovascular calcification at baseline in alkaptonuria patients from the SONIA 2 study using quantitative analysis by ^{18}F-NaF PET/CT

6.1 Introduction

Thus far, this thesis has focused on evaluating ochronotic arthropathy from ^{18}F-NaF PET/CT scans in AKU patients. The previous chapters have shown increased ^{18}F-NaF uptake in abnormal bone lesions and active calcified disc lesions in AKU patients. After that, spine arthropathy progression in response to nitisinone was evaluated. The final study of this thesis will move on to consider cardiovascular ochronosis in patients with AKU. This cross-sectional study describes the prevailing characteristics of cardiovascular involvements in AKU patients from the SONIA 2 trial using ^{18}F-NaF PET/CT scans. The presence of abnormal cardiovascular calcifications were seen incidentally in the heart area while evaluating ^{18}F-NaF PET/CT scans in the previous studies. Initial observations suggested that calcified vessels can be analysed and quantifed using existing data without adding extra cost or radiation to those patients. ^{18}F-NaF PET/CT images was available for SONIA 2 patients but not been used previously to assess cardiac involvements in AKU patients. This study is the first study to evaluate and analysis the distribution of a bone radiotracer within the heart region of AKU patients. The main reason for this initial investigation was to evaluate whether measuring ^{18}F-NaF uptake in the heart could be used as a valuable imaging method to quantify molecular calcification in the cardiac vessels in order to identify calcified vessels and detect future cardiovascular risk in AKU patients. The current study set out to detect regional cardiac calcification by measuring the ^{18}F-NaF uptake from PET images and the attenuation coefficient from CT images.

In AKU, ochronotic pigment deposit in various body tissues, including cardiovascular tissues. It is understood in AKU that vessels become pigmented and calcified as part of the disease pathophysiology. The severe symptomatic cardiac disorder usually needs surgical intervention, so early diagnosis of cardiovascular disease could prevent surgical complications [28]. Several cases of cardiovascular disorder associated with ochronosis have been reported [28–32]. Additionally, numerous studies have been done to understand cardiovascular health in patients with AKU. In 1963, it was reported that there was no significant difference between the incidence of coronary artery disease in a patient suffering from AKU and those in the general population [184]. However, AKU patients may be more susceptible to cardiovascular disease. Theoretically, there is concern that ochronosis could lead to early heart diseases associated with ochronotic

pigment, including cardiovascular calcification and inflammation. In a study of 58 AKU patients, fifty percent of patients showed evidence of coronary-artery calcification detected from a non-contrast CT scan by the age of 59 years [7]. Interestingly, no correlation between the severity of aortic valve disease and urine HGA levels has been found. In that study Phornphutkul *et al.* [7] reported that, the mean age of detecting cardiovascular involvements, including cardiovascular calcification, was 54 years, with no cardiac abnormalities noted before the fifth decade. On the other hand, Pettit *et al.* [34] and Hwaida *et al.* [27] suggested a role for cardiac scans such as echocardiographic surveillance for AKU patients above 40 years old in order to assess the early cardiovascular involvements.

Although CT remains a gold standard to identify coronary artery calcification, it is a structural imaging modality which likely characterises vascular plaques and only detects macrocalcification. Detecting cardiovascular calcification before it becomes macroscopically visible will enable clinians to initiate further evaluation. Thus, for years, molecular imaging techniques have been employed to detect early abnormal cardiovascular lesions using isotopic biomarkers. Recently, ^{18}F-NaF has been reported as a promiseing non-invasive method to detect and identify active microvascular calcification by many researchers. Due to the strong biological similarities between vascular calcification and bone formation, ^{18}F-NaF can be used as a novel imaging biomarker for identifying early vascular calcification. Active vascular calcification commonly appears as hydroxyapatite deposits in the vascular walls, making it the best place for the exchange between the -^{18}F ions and the hydroxyl group of hydroxyapatite after incorporating it into hydroxyapatite crystals.

6.2 Design of study

In this chapter only baseline scans for SONIA 2 participants were analysed. SONIA 2 patients had subsequent scans; however, the analysis is beyond the scope of this thesis.

6.2.1 Patient group

Forty AKU patients including 24 males and 16 females who were part of the SONIA 2 trial and had undergone ^{18}F-NaF PET/CT scans to evaluate a variety of bone and joint abnormalities were analysed in this study. The exclusion criteria included previous myocardial surgery. The mean age of the patients involved in the current study was 50.25 ± 10.81 years old (range from 30 to 68), with no significant age difference between the gender groups; male mean age 50.92 ± 10.3 years old (range, 30-67) and female mean age 49.25 ± 11.8 years old (range 30-68). The demographic characteristic of this population is summarised in Table 6.1. As in previous chapters, the cohort was divided into four groups according to their age as shown in shows in Table 6.2, including 7 patients (17.5%) between 30 and 39 years old, 13 (32.2%) between 40 and 49 years old, 10 (25%) between 50 and 59 years old, and 10 (25%) above 60 years old.

Table 6.1 Demographic baseline characteristics of AKU patients who were part of the SONIA 2 clinical trial and analysised in this chapter.

Age of the patients displayed as mean ± SD, minimum and maximum.

Statistic	Patients no. (%)	Age ± SD years	Age range
Total	40	50.25 ± 10.81	30 – 68
Male	24 (60 %)	50.92 ± 10.3	30 – 67
Female	16 (40%)	49.25 ± 11.8	30 – 68

Table 6.2 The number of AKU patients at the beginning of the SONIA 2 clinical trial classified by gender and age who were included in this chapter.

The participants were stratified by the decade of life into four age groups 30-39, 40-49, 50-59 and ≥ 60 years old.

Age group	Gender	Patient no.
30 – 39 years old	Total	7
	Male	3
	Female	4
40 49 years old	Total	13
	Male	8
	Female	5
50 – 59 years old	Total	10
	Male	6
	Female	4
≥ 60 years old	Total	10
	Male	7
	Female	3

6.2.2 Image analysis

Baseline ^{18}F-NaF PET/CT data were analysed using Horos software, which allowed simultaneous display and analysis of PET, CT, and fusion PET/CT images in sagittal, coronal, and transverse planes. In this chapter, cardiac calcification was assessed in two main areas: coronary vessles and the aorta. The cardiac calcification assessment methods were described in detail in sections 2.8 and 2.8.2. Figure 6.1 briefly illustrates the assessment method which was applied in this chapter to quantify cardiovascular calcification. The main cardiac arterial regions, including coronary and aortic arterial regions, were evaluated and quantitatively analysed by measuring ^{18}F-NaF uptake from PET images and the mean HU from CT images. For coronary arteries analysis, the arteries were visually recognised in a CT image, and ROIs were placed over the area of the four main branches of coronary arteries, including left coronary artery-left main stem (LCA), left anterior descending artery (LAD), left circumflex artery (LCA) and right coronary artery (RCA). For aortic artery analysis, ROIs were placed over ascending aorta (AA) and descending aorta (DA) (see Figure 6.2). The same ROIs, which were drawn in CT images, then copied to the ^{18}F-NaF PET images to measure SUV values.

Maximum SUV and mean HU were generated from ^{18}F-NaF PET/CT images from the main coronary and aortic regions. Although the blood pool activity was minimal, it was more accurate excluding them from the measured uptake value. Background activity based on ^{18}F-NaF activity in the blood pool was measured from inferior vena cava (IVC) and superior vena cava (SVC). After that, the maximum target to background ratio (TBR_{max}) for each ROI was generated to avoid overestimating the SUV_{max} value. TBR_{max} was calculated by dividing the SUV_{max} value for each ROI with a mean SUV of the blood pool [148,150].

6.2.3 Correlation

SUV_{max}, $TBR_{max,}$ and HU_{mean} values from main coronary and aortic branches were correlated with gender and age to assess the degree of cardiac calcification in relation to sex and age. Differences between gender and age were tested using the Pearson

correlation coefficient. One-way ANOVA analysis was conducted to assess the differences between age groups.

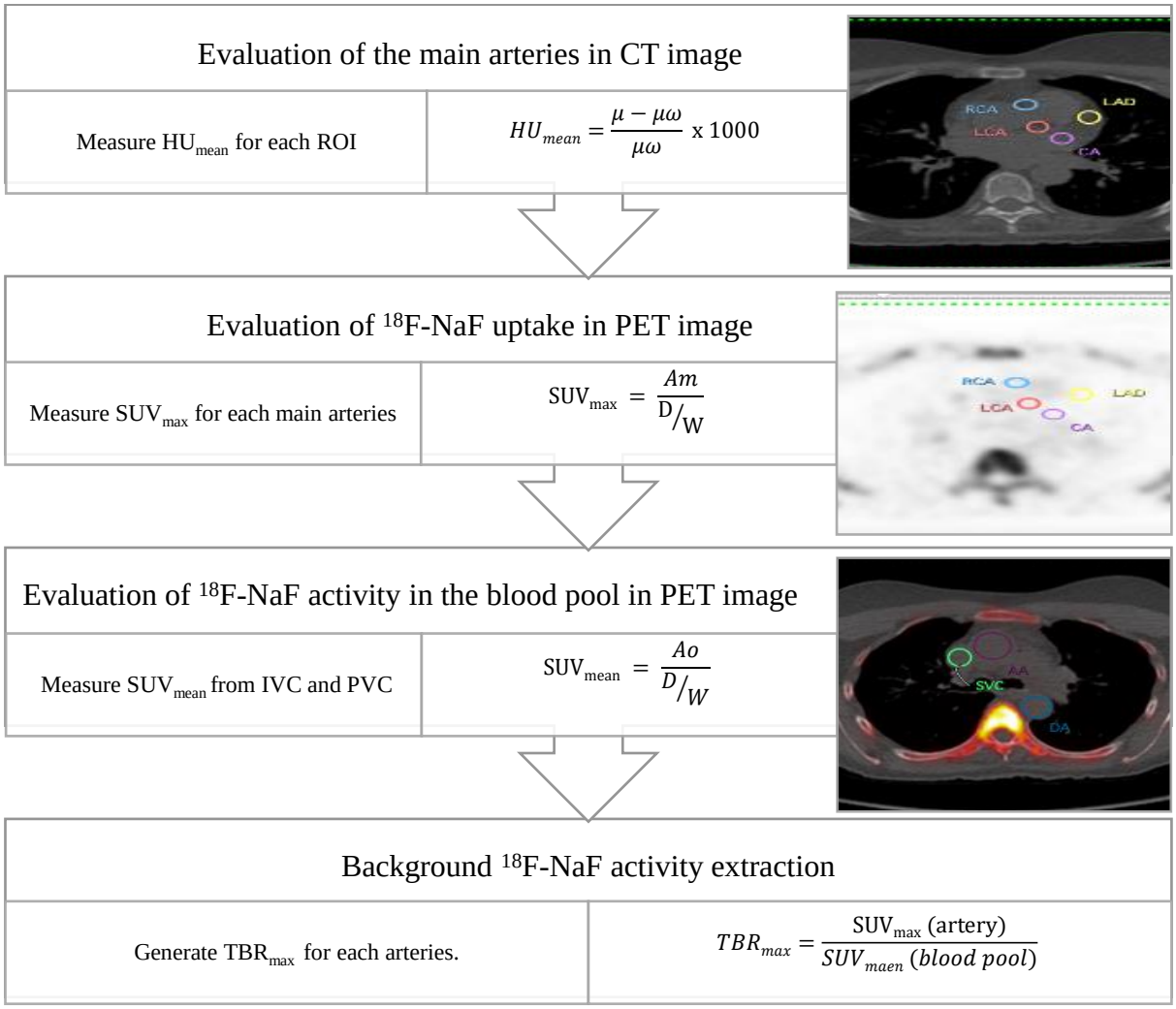

Figure 6.1. The assessment methods used in this chapter to quantify cardiovascular calcification from ^{18}F-NaF PET/CT images.

First step; HU_{mean} measurements from CT images by manually placing an individual circular ROI on axial CT slices over the four main coronary and aorta branches. Second step; SUV_{max} measurements from ^{18}F-NaF PET images. The same ROI, which was drawn in the CT image, was copied to the PET image to generate the SUV_{max} value. Third step; blood pool activity measurements. Blood pool SUV_{mean} was measured from SVC and IVC. Final step; background activity extraction. TRB_{max} was generated by dividing the value from the second step by the value of the third step for each ROI. HU_{mean}; mean Hounsfield unit, SUV_{max}; maximum standardised uptake value, TBR_{max}; maximum target to background ratio μ; is linear attenuation coefficient of ROI, μω; is linear attenuation of distilled water, Am; maximum activity concentration (kBq/ml), Ao; mean activity concentration (kBq/ml), D; injected dose (kBq), W; body weight.

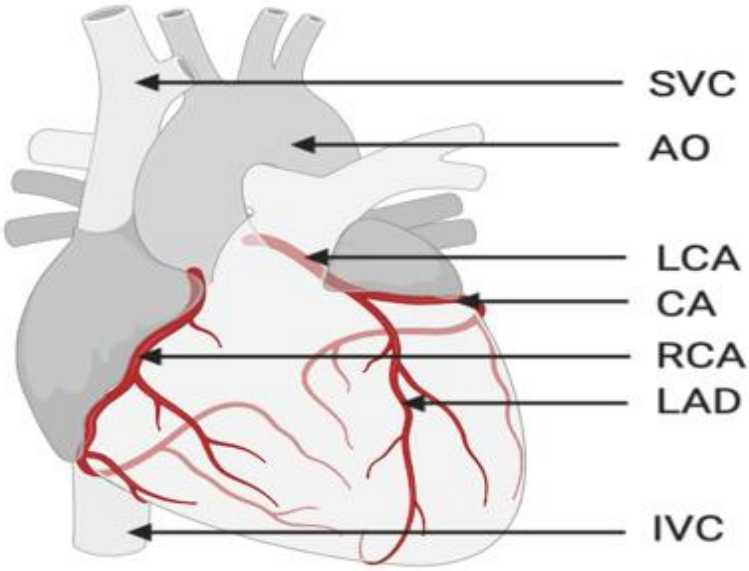

Figure 6.2. Three-dimensional reconstruction image of the heart depicting the main arteries and veins.

AO; aorta, SVC; superior vena cava, IVC; inferior vena cava, LCA; left coronary artery or left main stem, CA; left circumflex artery, RCA; right coronary artery, LAD; left anterior descending artery. Image done using BioRender.com

6.3 Results

6.3.1 SUV_{max} measurements

In the ^{18}F-NaF PET images, abnormal distribution of ^{18}F-NaF was visibly noted within the chest area in AKU patients. Intense focal tracer uptake was identified in the heart region having bone-like radiotracer intensity. In some cases, abnormal vascular involvement was more noticeable in the fused ^{18}F-NaF PET/CT images.

In the first part of this study, the ^{18}F-NaF uptake was analysed and quantified from coronary and aortic arteries by measuring maximum SUV from the main coronary arteries for 40 AKU patients. Figure 6.3 and Figure 6.4 show SUV_{max} measurements from the four main coronary arteries, aortic artery, and blood pool vessels. Table 9.29 (appendix) summarises the measured values for each ROI. The average SUV_{max} value of all measured coronary arteries was 1.39 ± 0.49 (range 0.73 – 2.55). Average SUV_{max}

was 1.57 ± 0.59 (range 0.78 – 3.73) at LCA; 1.12 ± 0.35 (range 0.55 – 1.97) at LAD; 1.18 ± 0.50 (range 0.45 – 2.64) at CA and 1.68 ± 1.04 (range 0.6 – 6.02) at RCA. The highest coronary arteries SUV_{max} value was detected at the RCA. The average SUV_{max} value at aortic artery was 2.06 ± 0.84 (range 0.94 – 4.76). Average SUV_{max} was 1.78 ± 0.57 (range 0.89 – 3.6) at AA and 2.38 ± 1.29 (range 0.99 – 7.1) at DA. Although DA value was slightly higher than AA, the t-test indicates no significant statistical difference between SUV_{max} measured from AA and DA. Blood pool ^{18}F-NaF uptake was also measured from IVC and SVC to generate TBR_{max} for the next section. The mean blood pool SUV_{max} was 0.82 ± 0.27 (range 0.43 – 1.83). Average SUV_{max} was 0.77 ± 0.30 (range 0.37– 1.79) at IVC and 0.86 ± 0.28 (range 0.43 – 1.86) at SVC. Among all measured ROIs, the highest SUV_{max} value was detected at the DA and the lowest at the blood pool vessels, showing statistical significance differences between the two values ($P < 0.05$).

6.3.1.1 Cardiovascular SUV_{max} and gender

To assess the gender effect, the differences in SUV_{max} values between male and female patients were tested. Figure 6.3 and Figure 6.4 demonstrate the SUV_{max} at all ROIs for male and female AKU patients. The average SUV_{max} value for all four measured coronary arteries was 1.52 ± 0.51 (range 0.76 - 2.55) for males and 1.23 ± 0.49 (range 0.6 – 2.25) for females. The SUV_{max} value at aorta was 2.14 ± 0.78 (range 1.18- 4.7) for males and 1.94 ± 0.93 (range 0.94– 4.76) for females. The blood pool SUV_{max} was 0.76 ± 0.21 (range 0.43- 1.2) for male and 0.90 ± 0.33 (range 0.53 - 1.83) for female. It can be seen from the charts and the data in Table 9.29 (appendix) that, SUV_{max} value at most of the ROIs were similar in both genders. Male patients had slightly higher SUV_{max} at coronary arteries and aorta than female patients, while the female patients had higher SUV_{max} values at blood pool vessels. The statistical analysis using an independent t-test indicated that males had significant higher SUV_{max} at the average four main coronary arteries than females ($P = 0.036$). As the data show, there was no significant difference between the two groups at the average aortic artery nor average blood pool vessels ($P = 0.471$ and $P = 0.123$, respectively).

Closer inspection of the figures show that regionally, there were significant confounding differences between coronary SUV_{max} value for males and females at

RCA only (P = 0.022), and at IVC (P = 0.003). No statistically significant differences in SUV_{max} values between males and females at LCA, LAD, CA, AA, DA, and SVC was found (P = 0.161, P = 0.066, P = 0.675, P = 0.222, P = 0.771, and P = 0.631, respectively).

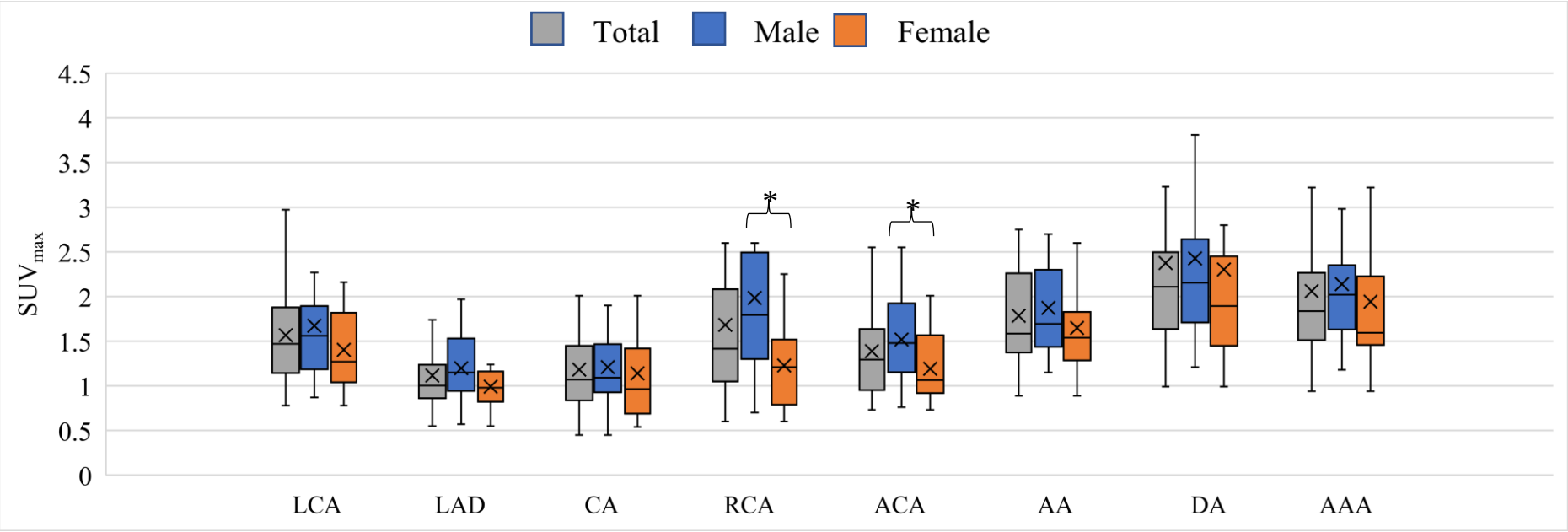

Figure 6.3. Mean SUV_{max} obtained from ^{18}F-NaF PET scan at each cardiac artery for 40 AKU patients who were part of the SONIA 2 clinical trial stratified by gender.

The results show the analysis of the baseline ^{18}F-NaF PET data for 24 males and 16 females from four main branches of coronary arteries, including left coronary artery-left main stem (LCA), left anterior descending artery (LAD), left circumflex artery (CA) and right coronary artery (RCA), average coronary arteries (ACA), and aortic artery analysis, ascending aorta (AA) and descending aorta (DA), average aortic artery (AAA). Table 9.29 (appendix) shows the statistical correlation between gender at all ROI. SUV_{max} was highest at the DA in both male and female. Independent sample t-test revealed that males tend to have significantly higher SUV_{max} value at RCA and ACA than females ($P = 0.022$, $P = 0.036$, respectively). No statistically significant differences between males and females across the aortic artery were noted ($P < 0.05$). *Groups which showed significant difference ($P < 0.05$). In box and whisker, x is the mean value, and the line is the median.

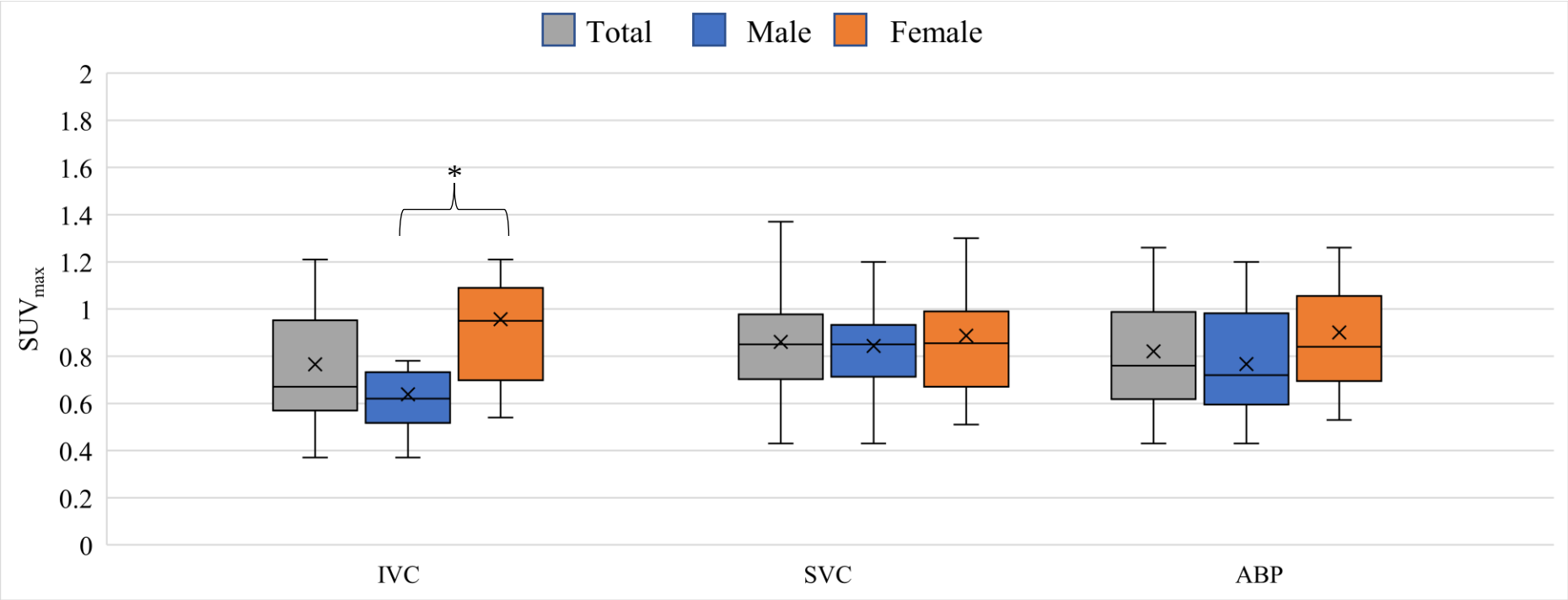

Figure 6.4. Mean SUV_{max} obtained from ^{18}F-NaF PET scan at blood pool vessels for 40 AKU patients who were part of the SONIA 2 clinical trial stratified by gender.

The results show the analysis of the baseline ^{18}F-NaF PET data for 24 males and 16 females from blood pool vessels; inferior vena cava (IVC), superior vena cava (SVC), and average blood pool (ABP). Table 9.29 (appendix) shows the statistical correlation between gender at all ROI. Females tend to have a significantly higher SUV_{max} value at IVC than males ($P = 0.003$). No statistically significant differences between males and females at SVC nor ABP were noted ($P = 0.123$, and $P = 0.631$, respectively) *Groups which showed significant difference ($P < 0.05$). In box and whisker, x is the mean value, and the line is the median.

6.3.1.2 Cardiovascular SUV_{max} and age

The correlation between cardiovascular SUV_{max} values and age was tested in this section. Figure 6.5, Figure 6.6 and Figure 6.7 show the changes in SUV_{max} against age for 40 AKU patients at each cardiovascular region. Figure 6.5 shows that SUV_{max} values at the coronary arteries increased slightly with age. In the average four coronary arteries, age had a significant statistical influence on SUV_{max} measurements ($R = 0.39$, $P = 0.013$). Regionally, there was a significant correlation between the SUV_{max} values and age at the RCA only ($R = 0.367$, $P = 0.02$). No significant difference between the SUV_{max} values and age was found at LCA, LAD, nor CA ($R= 0.276$, $R = 0.196$, $R = 0.281$, respectively, all $P > 0.05$). Likewise, as shown in Figure 6.6, aorta SUV_{max} values were not substantially correlated with age at neither AA nor DA ($R = 0.17$, $R = 0.144$, and $P = 0.293$, $P = 0.376$, respectively). On the other hand, as shown in Figure 6.7, the blood pool SUV_{max} value shows a moderate statistically significant correlation between age and SUV_{max} value at IVC ($R = 0.372$, $P = 0.04$), while no significant differences at SVC ($R = 0.115$, $P = 0.482$) were observed.

The SUV_{max} from all cardiovascular regions for each age group were analysed, as shown in Figure 6.8, Figure 6.9, and Figure 6.10. The SUV_{max} data for all ROIs is displayed in detail in Table 9.30 (appendix). The SUV_{max} at the average four main coronary arteries was 1.13 ± 0.25 for 30-39 age group patients, 1.31 ± 0.63 for 40-49 age group patients, 1.35 ± 0.34 for 50-59 age group patients and 1.71 ± 0.40 for 60 years old patients and above. Although the SUV_{max} at coronary arteries increased from the youngest age group patients to the oldest group of patients, it was not statistically significant between the 30s and 40s patients or between 40s and 50s. Statistically, there was significant differences for the average coronary arteries SUV_{max} between patients in their 50s and above 60 only ($P = 0.05$). The average SUV_{max} at the AA and DA was 1.73 ± 0.52 for 30-39 age group patients, 2.00 ± 0.93 for 40-49 age group patients, 2.28 ± 0.78 for 50-59 age group patients and 2.15 ± 0.98 for ≥ 60 years old patients. The youngest age group patients had slightly lower aortic SUV_{max} values than the other three age groups, but statistically, it was not significant ($P > 0.05$). Similarly, there were no significant differences in blood pool SUV_{max} among the age group patients ($P > 0.05$). The average blood pool SUV_{max} was 0.87 ± 0.47 for 30-39 age group patients,

0.77 ± 0.17 for 40 - 49 age group patients, 0.86 ± 0.23 for 50-59 age group patients and 0.81 ± 0.26 for ≥ 60 years old patients.

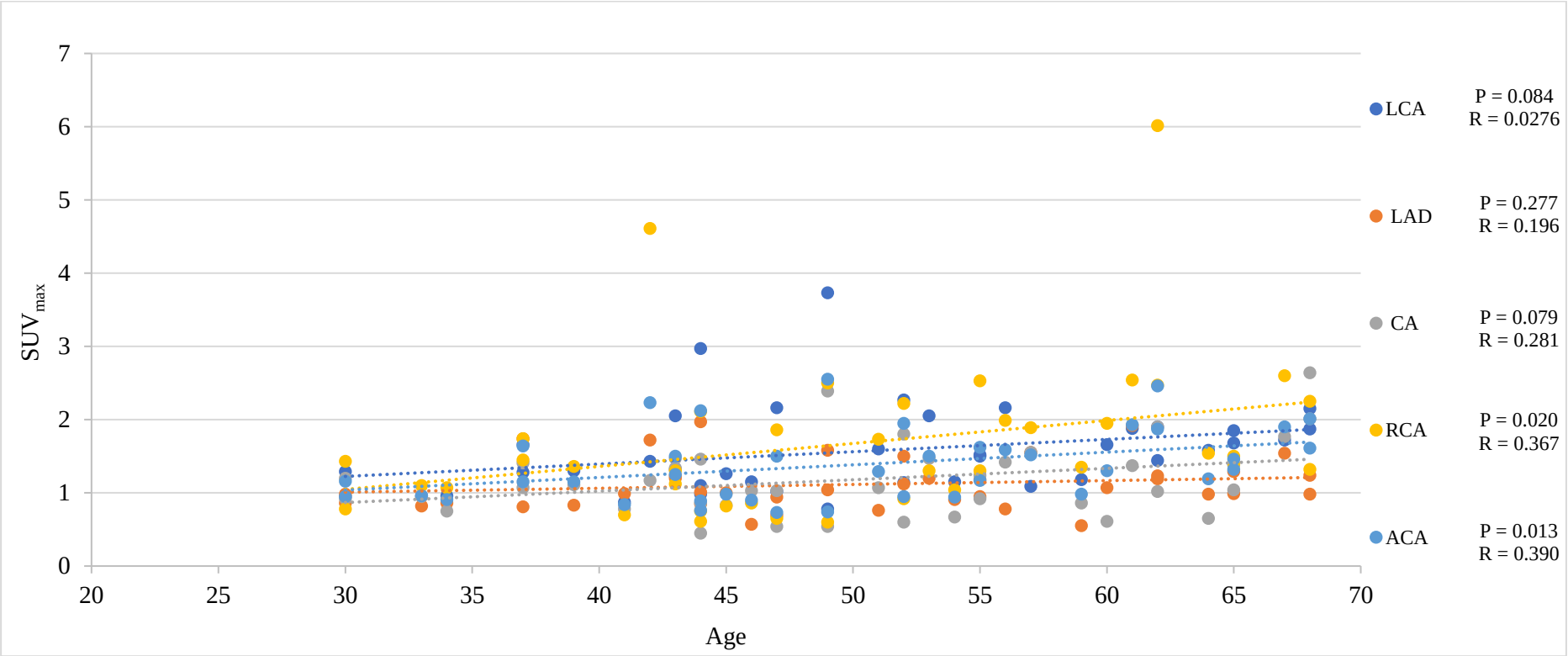

Figure 6.5. Scatter plots illustrating the correlation between SUV_{max} obtained from ^{18}F-NaF PET/CT and age at four main coronary arteries for 40 AKU patients who were part of the SONIA 2 clinical trial.

The results display left coronary artery-left main stem (LCA), left anterior descending artery (LAD), left circumflex artery (CA) and right coronary artery (RCA), average coronary arteries (ACA) in individual AKU cases with age. Multiple linear regression analysis identified no statistically significant correlation between regional SUV_{max} value and age in AKU cases measured at LCA, LAD, and CA (P = 0.084, P = 0.227, and P = 0.079, respectively). Age was noted to have a positive statistically significant effect in RCA (R = 0.367 and P = 0.02) and ACA (R = 0.39 and P = 0.013).

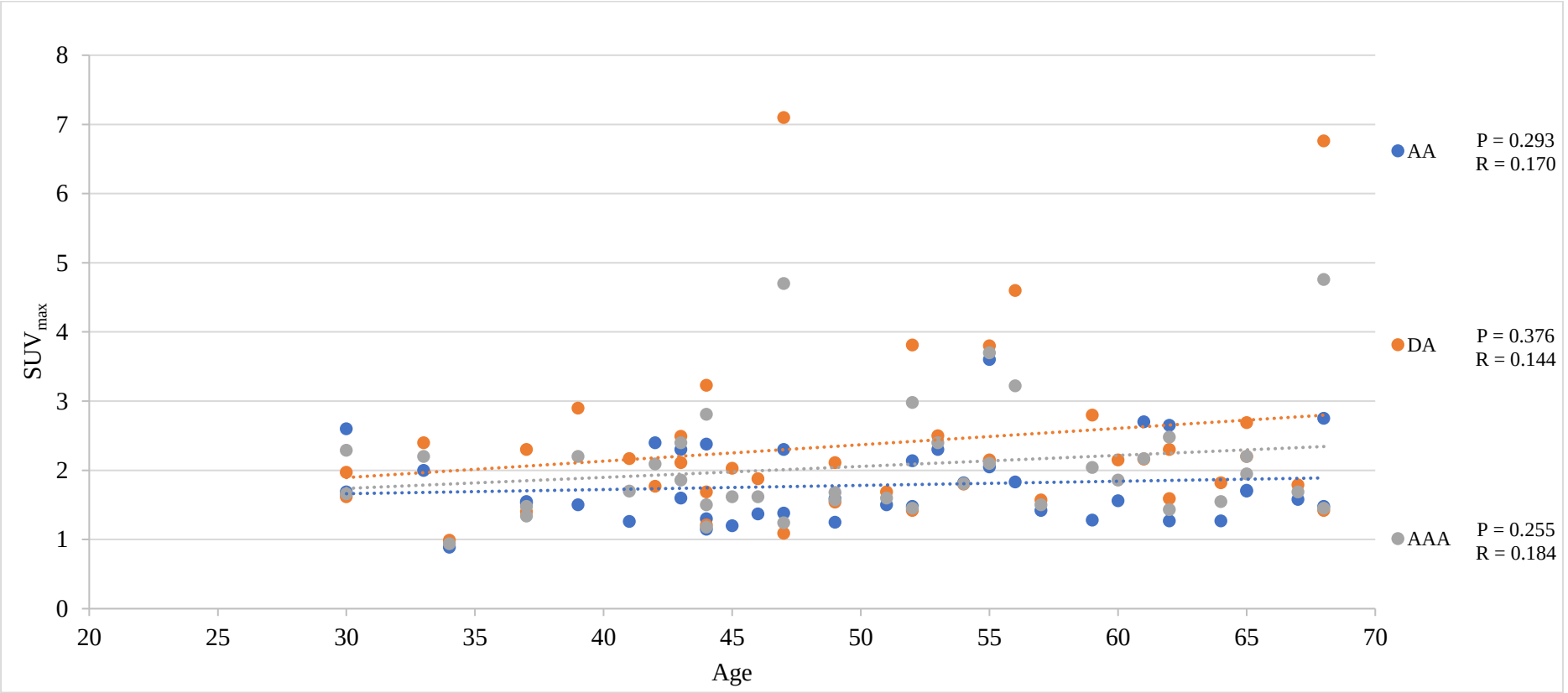

Figure 6.6. Scatter plots illustrating the correlation between SUV_{max} obtained from ^{18}F-NaF PET/CT and age at aortic artery for 40 AKU patients who were part of the SONIA 2 clinical trial.

The results display SUV_{max} of ascending aorta (AA) and descending aorta (DA), average aortic artery (AAA) in individual AKU cases with age. Multiple linear regression analysis identified that there was no significant correlation between SUV_{max} of AA nor DA and age in AKU cases (R = 0.17 and P = 0.293, R = 0.144 and P = 0.376, respectively).

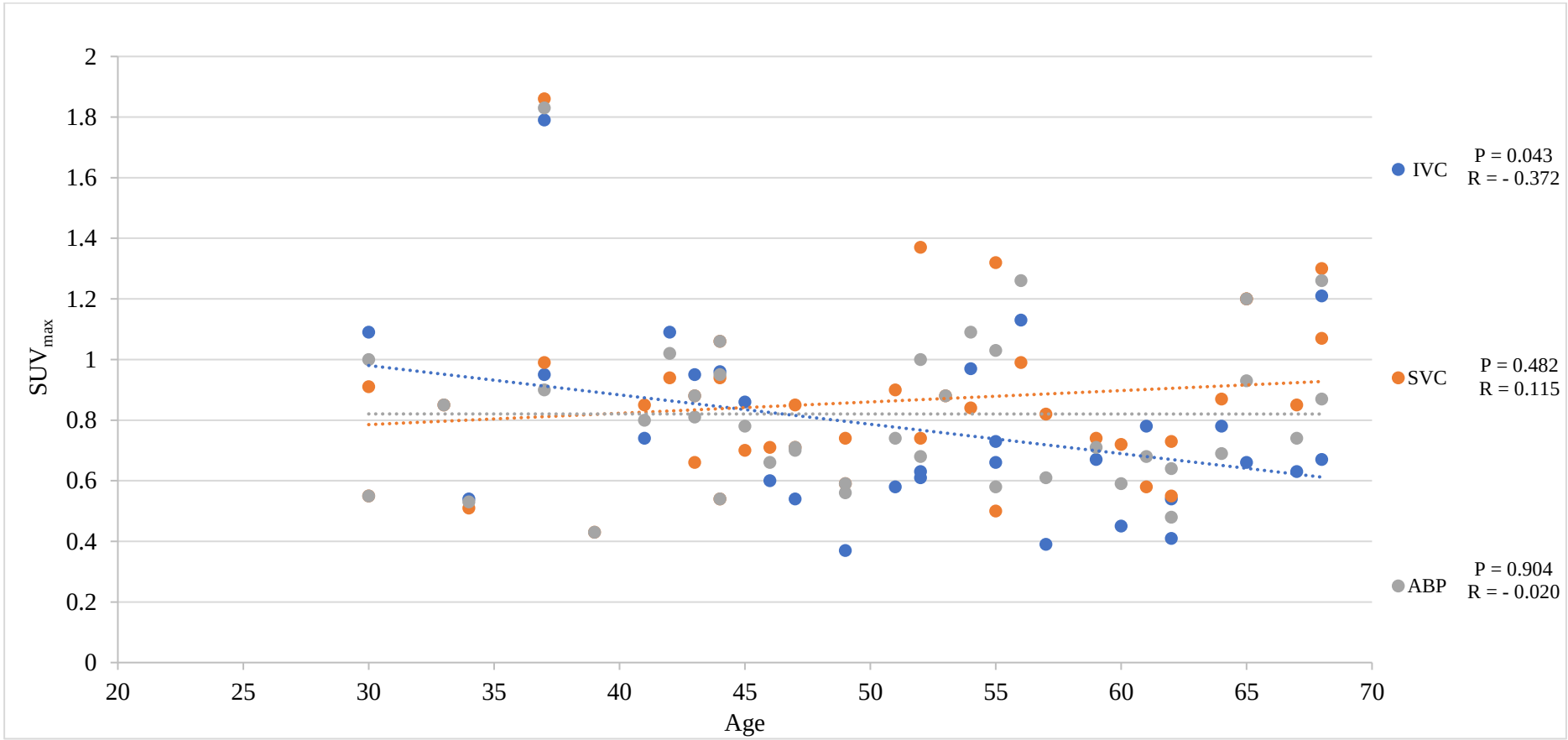

Figure 6.7. Scatter plots illustrating the correlation between SUV_{max} obtained from ^{18}F-NaF PET/CT and age at blood pool vessels for 40 AKU patients who were part of the SONIA 2 clinical trial.

The results display SUV_{max} of inferior vena cava (IVC), superior vena cava (SVC), and average blood pool (ABP) in individual AKU cases with age. Only SUV_{max} of IVC had shown a moderate correlation with age (R = -0.372, P = 0.043). At the same time, there was no correlation at SVC (R = 0.115, P = 0.48).

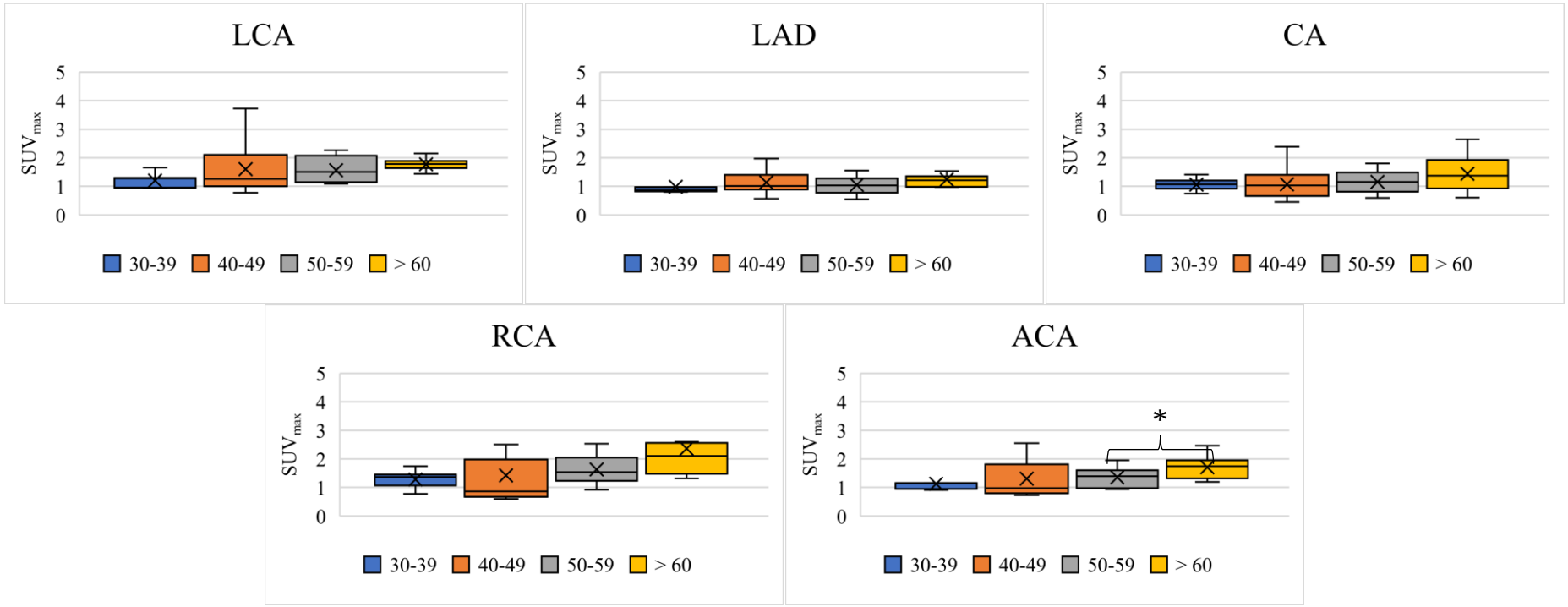

Figure 6.8. SUV_{max} measurements at the main coronary arteries measured from baseline ^{18}F-NaF PET/CT scan for 40 AKU patients who were part of the SONIA 2 clinical trial stratified by decade of life.

Table 9.30 (appendix) shows the coronary ROI and age groups which indicated a statistically significant difference between subgroup analyses. *Groups which showed significant difference ($P < 0.05$). One-way-ANOVA revealed no statistically significant difference between subgroup analyses at regional coronary arteries. There were substantial differences for SUV_{max} value between patients in their 50s and above 60 years only ($P = 0.05$) in the average four coronary arteries. Left coronary artery-left main stem (LCA), left anterior descending artery (LAD), left circumflex artery (CA) and right coronary artery (RCA), average coronary arteries (ACA). In box and whisker, x is the mean value, and the line is the median.

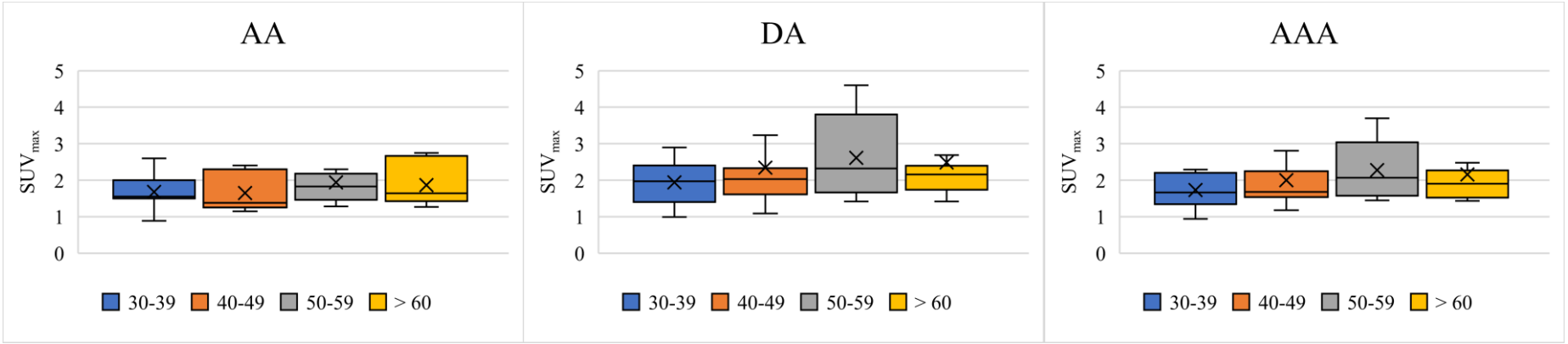

Figure 6.9. SUV_{max} measurements at the aortic artery measured from baseline ^{18}F-NaF PET/CT scan for 40 AKU patients who were part of the SONIA 2 clinical trial stratified by the decade of life.

Table 9.30 (appendix) shows the aortic ROIs and age groups which indicated a statistically significant difference between subgroup analyses. One-way-ANOVA revealed no statistically significant difference between subgroup analyses at regional aortic arteries. Ascending aorta (AA) and descending aorta (DA), average aortic artery (AAA). In box and whisker, x is the mean value, and the line is the median.

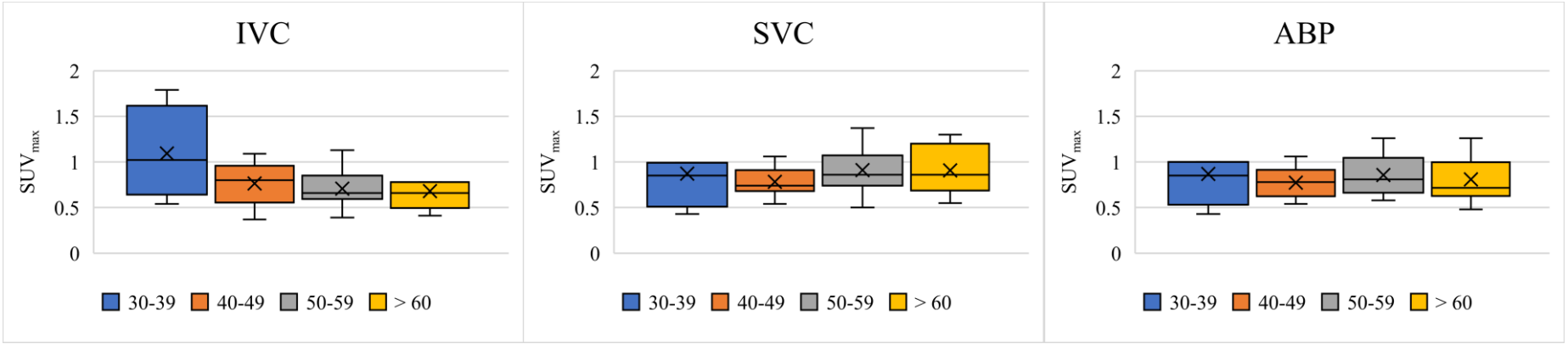

Figure 6.10. SUV_{max} measurements at the blood pool vessels measured from baseline ^{18}F-NaF PET/CT scan for 40 AKU patients who were part of the SONIA 2 clinical trial stratified by the decade of life.

Table 9.30 (appendix) shows the blood pool vascular ROIs and age groups which indicated a statistically significant difference between subgroup analyses. One-way-ANOVA revealed no statistically significant difference between subgroup analyses at regional blood pool vessels. Inferior vena cava (IVC), superior vena cava (SVC), and average blood pool (ABP). In box and whisker, x is the mean value, and the line is the median.

6.3.2 TBR_{max} measurements

The next section critically assesses the ^{18}F-NaF uptake from the cardiovascular region, excluding the background activity accumulated in blood pool vessels. The result of coronary arteries and aortic artery TBR_{max} for 40 SONIA 2 patients are shown in Figure 6.11, and in Table 9.31 (appendix). Among the coronary arteries, the RCA had the highest TBR_{max} with 2.21 ± 1.60, then LCA with 2.12 ± 1.44. Mean TBR_{max} at the LAD and CA was 1.45 ± 0.51 and 1.53 ± 0.77, respectively. No statistical differences between the four main coronary arteries TBR_{max} values were detected. Regarding the aortic artery, the DA showed a significantly higher TBR_{max} (3.03 ± 1.74) than the AA (2.31 ± 1.06) (P = 0.002). The average TBR_{max} was 1.80 ± 0.80 for coronary arteries ranging from 0.94 to 4.59, and 2.7 ± 1.24 for aortic artery ranging from 1.22 to 6.76. Statistically, aortic TBR_{max} values were considerably higher than coronary arteries TBR_{max} values (P < 0.005).

6.3.2.1 Cardiovascular TBR_{max} and gender

Figure 6.11 compares the SUV_{max} across the coronary arteries for male and female AKU patients. Table 9.31(appendix) summarises the coronary arteries TBR_{max} for each gender group. Independent t-test identified that male AKU patients had significantly higher TBR_{max} in the ACA than the female AKU patients (P = 0.012). The average TBR_{max} for coronary arteries for the male patient was 2.06 ± 0.93, while for the female patients was 1.42 ± 0.31. Regionally, there were differences in TBR_{max} between males and females at LAD and RCA (P = 0.018, P = 0.012, respectively). In contrast, there was no apparent difference in the TBR_{max} values at LCA nor CA between males and females (P = 0.1, P = 0.219, respectively).

Regarding the aortic artery, male patients had slightly higher aortic TBR_{max} values at both AA and DA regions, as shown in Figure 6.11 and Table 9.31. However, statistically, using an independent t-test, they were not significant (P = 0.175 and P = 0.275, respectively). The average TBR_{max} within the aorta was 2.94 ± 1.44 for male AKU patients ranging from 1.63 to 6.76 compared to 2.34 ± 0.80 for female AKU patients ranging from 1.22 to 4.15 (P = 0.141).

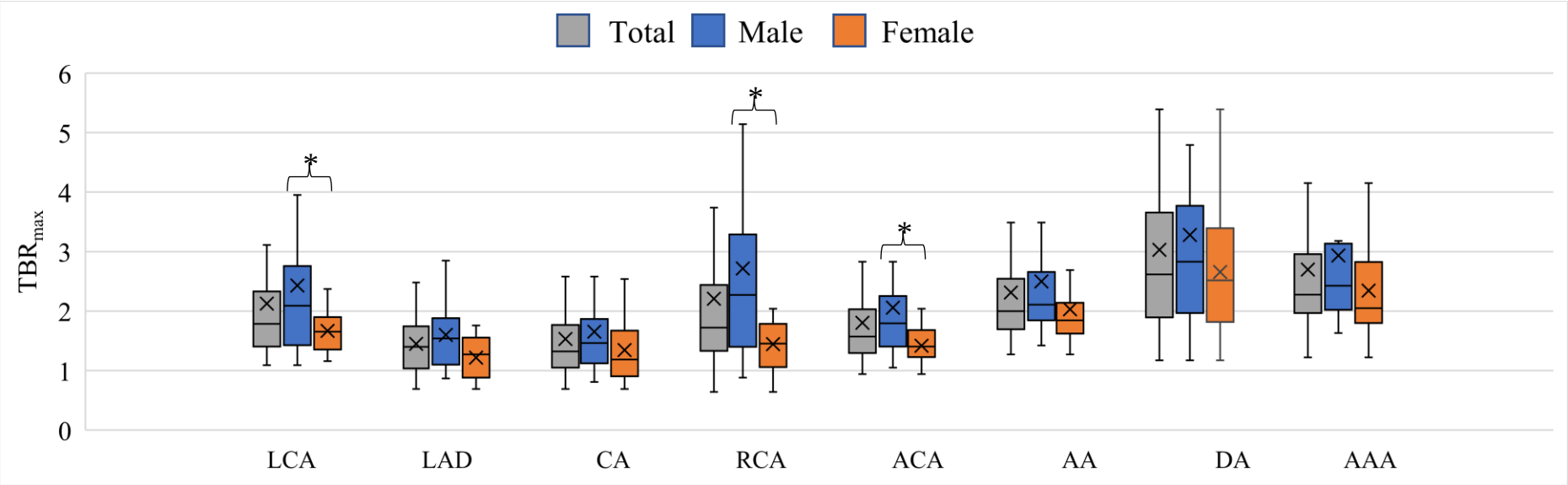

Figure 6.11. Mean TBR_{max} obtained from ^{18}F-NaF PET scan at each cardiac artery for 40 AKU patients who were part of the SONIA 2 clinical trial stratified by gender.

Baseline PET data for 24 males and 16 females from four main branches of coronary arteries, including left coronary artery-left main stem (LCA), left anterior descending artery (LAD), left circumflex artery (CA), and right coronary artery (RCA), average coronary arteries (ACA), and aortic artery analysis of the ascending aorta (AA) and descending aorta (DA) and average aortic artery (AAA). Table 9.31 (appendix) shows the statistical correlation between gender at all ROIs. TBR_{max} was highest at the DA and lowest at LAD at both male and female patients. *Groups which showed significant difference ($P < 0.05$). Statistically, aortic TBR_{max} values were considerably higher than coronary arteries TBR_{max} values ($P < 0.005$). Independent sample t-test revealed statistically significant differences between males and females at LAD, RCA, and ACA ($P = 0.01$, $P = 0.012$, $P = 0.012$ respectively). There was no apparent difference in the TBR_{max} values between both genders at LCA, CA, AA, DA, nor AAA ($P = 0.1$, $P = 0.219$, $P = 0.175$, $P = 0.275$, $P = 0.141$, respectively). In box and whisker, x is mean value, and the line is median.

6.3.2.2 Cardiovascular TBR_{max} and age

The TBR_{max} values were plotted against age, as shown in Figure 6.12 and Figure 6.13. Multiple linear regression analysis identified that there was no correlation between TBR_{max} obtained from the average four coronary arteries and age (R = 0.095, P = 0.268). Looking at each individual coronary artery, a moderate correlation was noted between TBR_{max} and age at RCA only (R = 0.336, P = 0.034). No correlation between TBR_{max} and age was observed at LCA, LAD, and CA (R = 0.76, R = 0.16, R = 0.148 respectively, all P > 0.05,). Similarly, there was no evidence that age had an influence on aortic TBR_{max} measurements, as shown in Figure 6.13. No statistically significant correlation coefficients were found between aorta TBR_{max} and age at neither AA nor DA (R = 0.006, P = 0.732 and R = 0.033, P = 0.971, respectively). From this result, it appears that age has no direct influence on the TBR_{max} measurements at both coronary and aortic arteries.

The mean TBR_{max} of the measured cardiovascular regions of each age group are compared in Figure 6.14 and Figure 6.15. The data are presented in detail in Table 9.31 (appendix). The TBR_{max} at the average four main coronary arteries was 1.62 ± 0.52 for 30-39 age group patients, 1.69 ± 0.96 for 40-49 age group patients, 1.59 ± 0.32 for 50-59 age group patients and 2.29 ± 0.97 for 60 years old patients and above. In terms of the aorta, TBR_{max} at the average value was 2.65 ± 1.44 for 30-39 age group patients, 2.64 ± 1.30 for 40-49 age group patients, 2.77 ± 1.35 for 50-59 age group patients and 2.73 ± 1.10 for 60 years old patients and above. Generally, patients with increased coronary and aortic arteries TBR_{max} values were more likely to be in the older groups. However, statistical analysis revealed that there was only a significant difference for the average coronary arteries TBR_{max} between patients in their 50s and above 60 years (P = 0.04). No statistically significant differences in the average aortic artery between the patients in any other age groups was found.

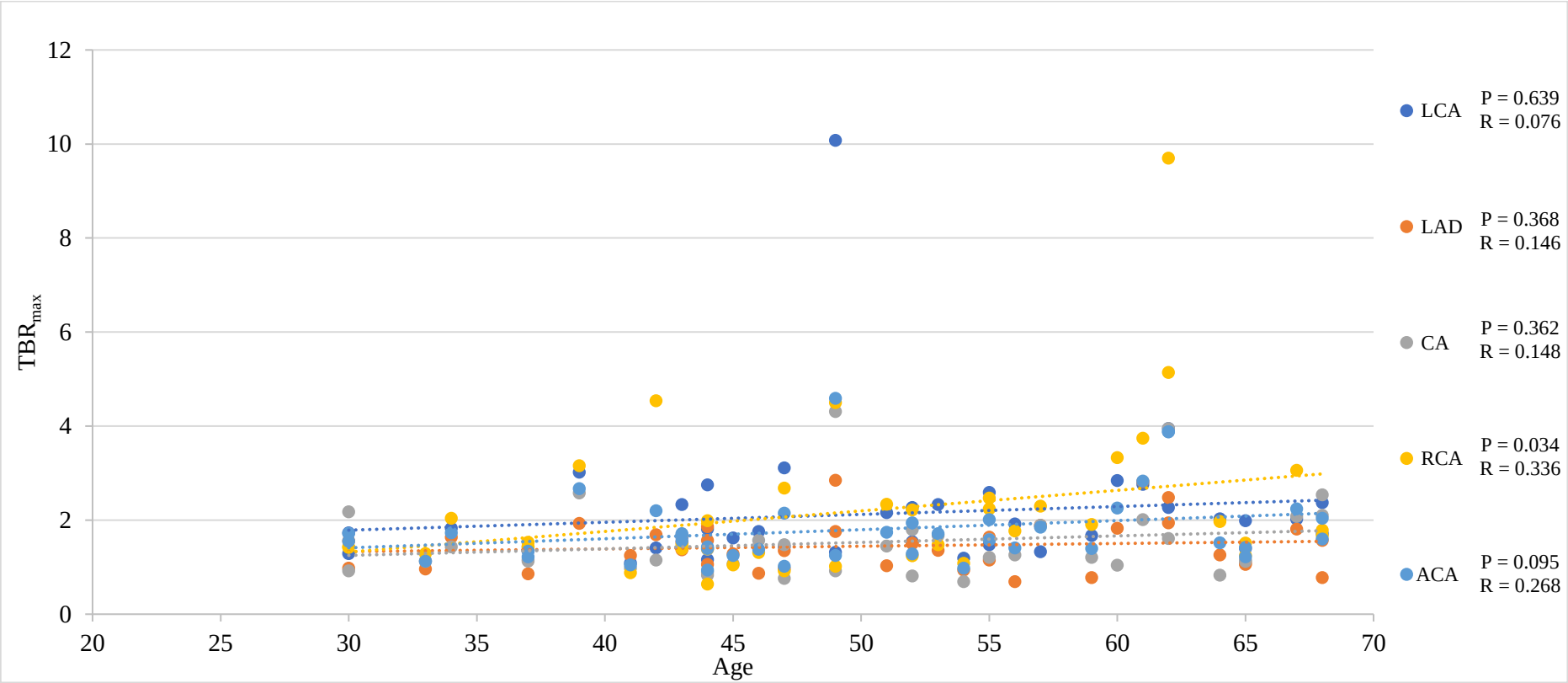

Figure 6.12. Scatter plots illustrating the correlation between TBR_{max} obtained from ^{18}F-NaF PET/CT and age at four main coronary arteries for 40 AKU patients who were part of the SONIA 2 clinical trial.

TBR_{max} of left coronary artery-left main stem (LCA), left anterior descending artery (LAD), left circumflex artery (CA) and right coronary artery (RCA), average coronary arteries (ACA) in individual AKU cases with age. Using multiple linear regression, coronary arteries showed no significant correlation between TBR_{max} values and age at most of the ROIs ($P > 0.05$), except at RCA; there was a significant correlation between TBR_{max} and age ($R = 0.034$, $P = 0.034$).

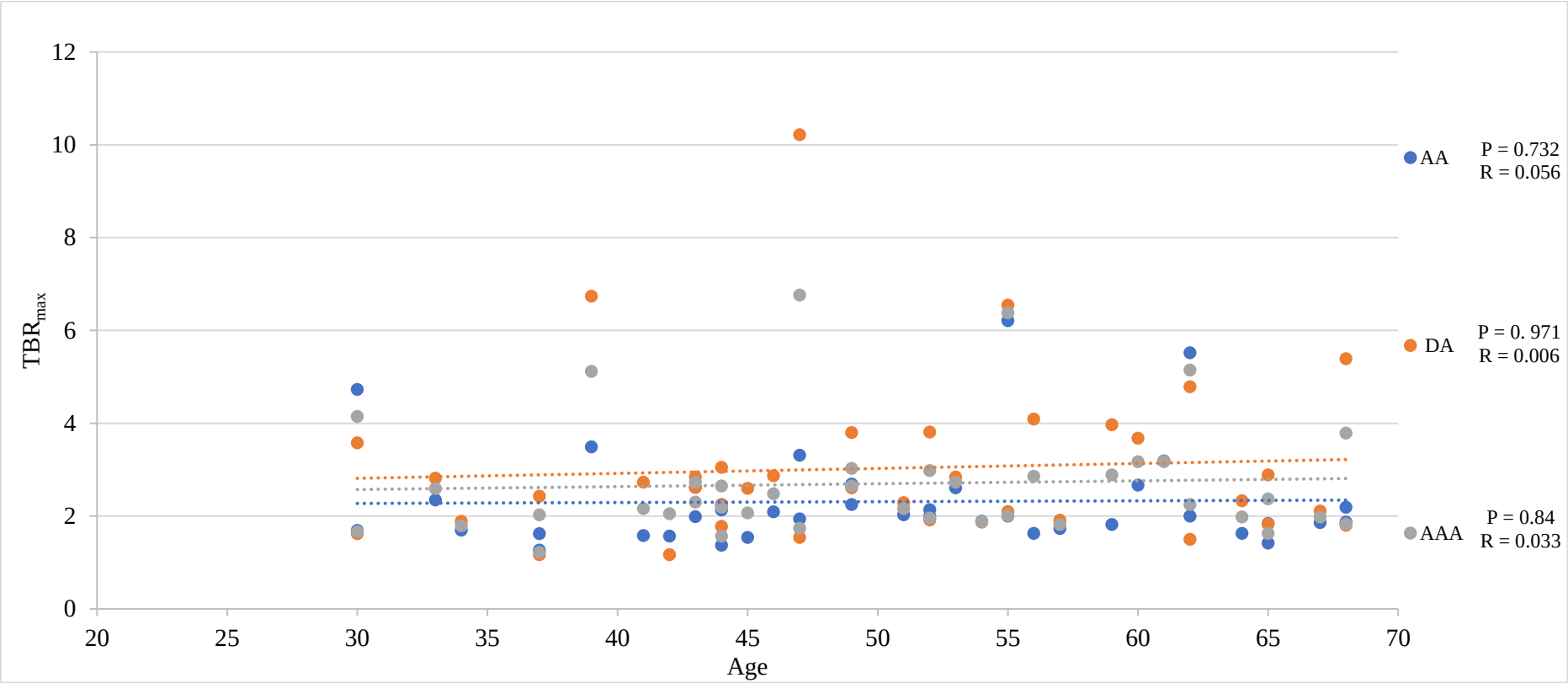

Figure 6.13. Scatter plots illustrating the correlation between aorta TBR_{max} obtained from ^{18}F-NaF PET/CT and age at aortic artery for 40 AKU patients who were part of the SONIA 2 clinical trial.

TBR_{max} of ascending aorta (AA) and descending aorta (DA), average aortic artery (AAA) in individual AKU cases with age. Multiple linear regression analysis identified that both AA and DA showed no significant correlation between TBR_{max} value and age in AKU cases (R = 0.056, P = 0.732, and R =0.006, P = 0.971 respectively).

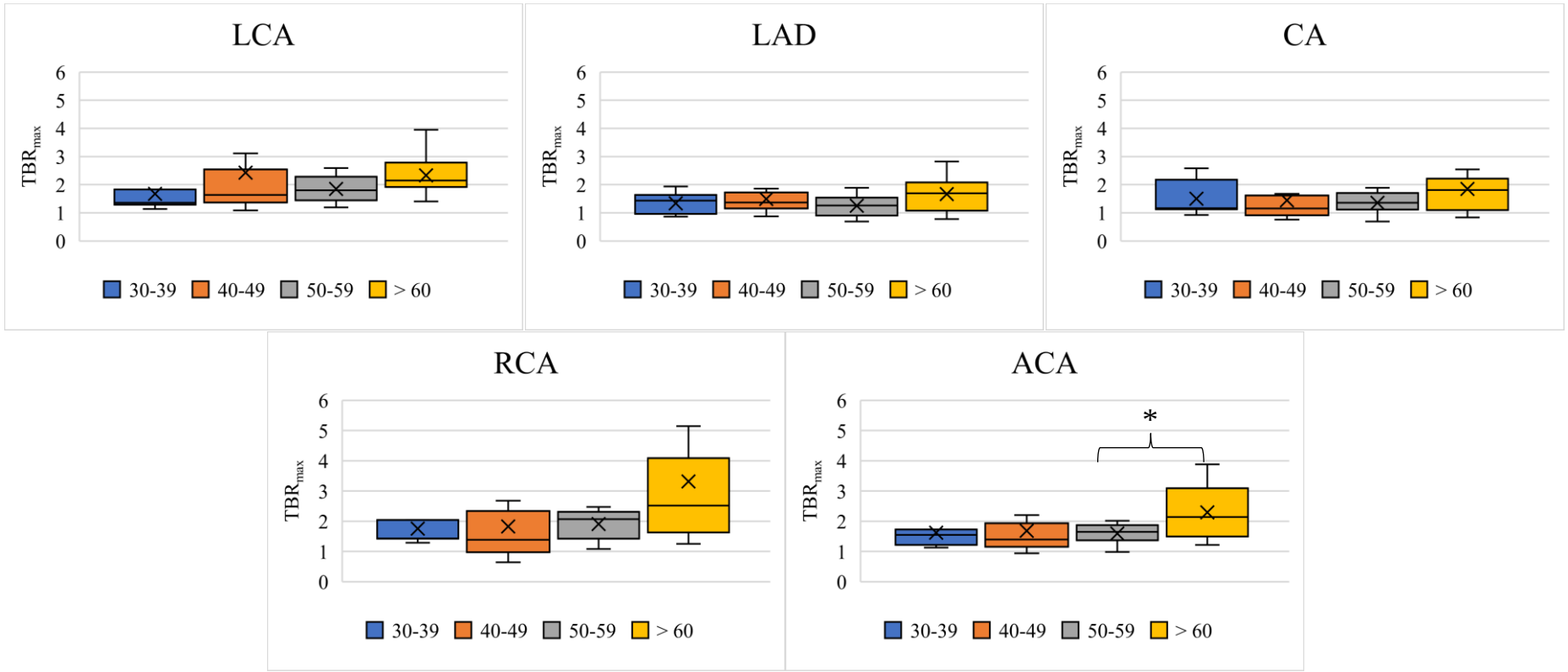

Figure 6.14. Mean main coronary arteries TBR_{max} among four decadal age groups measured from baseline ^{18}F-NaF PET/CT scan for 40 AKU patients who were part of the SONIA 2 clinical trial.

Table 9.31 (appendix) shows the four main coronary arteries and age groups which indicated a statistically significant difference between subgroup analyses. *Groups which showed significant difference ($P < 0.05$). There was a statistically significant difference between the 50s and 60s only at average coronary arteries ($P = 0.04$). Left coronary artery-left main stem (LCA), left anterior descending artery (LAD), left circumflex artery (CA) and right coronary artery (RCA), average coronary arteries (ACA). In box and whisker, x is the mean value, and the line is the median.

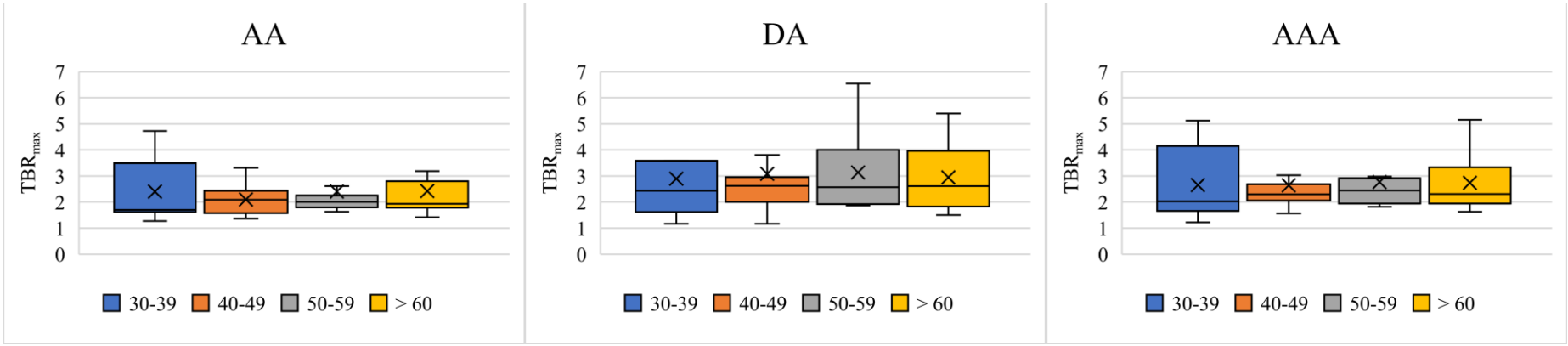

Figure 6.15. Mean aortic TBR_{max} among four decadal age groups measured from baseline ^{18}F-NaF PET/CT scan for 40 AKU patients who were part of the SONIA 2 clinical trial.

Table 9.31 (appendix) shows the aortic ROI and age groups which indicated a statistically significant difference between subgroup analyses. There was no statistically significant difference between subgroup analyses at aorta arteries. Ascending aorta (AA) and descending aorta (DA), average aortic artery (AAA) In box and whisker, x is the mean value, and the line is the median.

6.3.3 Mean HU measurements

So far, this study has focused on quantifying ^{18}F-NaF uptake at the cardiovascular regions in PET images. In CT investigations, abnormal vascular calcification signs were observed within the heart region having bone-like attenuation coefficient intensity. Some of the dense vascular areas in the CT image were adjacent to the existing intensive radiotracer in the PET image, which was cleared in the fused ^{18}F-NaF PET/CTT image. These high dense calcium lesions were quantitatively analysed by measuring HU_{mean} from CT images.

The results of the four main coronary arteries and aortic artery are shown in Figure 6.16 and Figure 6.17, and displayed in detail in Table 9.33. The mean HU value of all measured coronary arteries was 138.18 ± 139.41 (range 11 – 711). Average HU_{mean} was 127.42 ±153.91 (range -2– 700) at LCA; 115.75 ±124.66 (range 7 – 502) at LAD; 125.89 ±177.40 (range 3 – 937) at CA and 197.2 ±239.88 (range -29 – 1217) at RCA. The highest coronary arteries HU_{mean} value was detected at the RCA, as shown in Figure 6.16. This result correlates with the SUV_{max} data, where the highest SUV_{max} value at the RCA was found (see results section 6.3.1). The HU_{mean} value at the aorta was 133.71 ±143.48 (range 68.5 – 940). The average HU_{mean} was 134.33 ±141.74 (range 70 – 899) at AA and 133.1 ±147.11(range 67 – 981) at DA. Independent t-test indicates no significant differences in HU_{mean} values between the AA and DA regions. Mean blood pool HU_{mean} measured from IVC and SVC were 99.85 ± 15.99 and 92.9 ± 19.98, respectively, with no significant differences between the two values ($P > 0.05$).

6.3.3.1 Cardiovascular HU_{mean} and gender

The differences between male and female HU_{mean} values at all coronary and aortic ROIs are shown in Figure 6.16 and Figure 6.17 and summarised in Table 9.33 (appendix). The average HU_{mean} value for the four coronary arteries was 166.68 ±154.47 (range 43 - 711) for males and 95.44 ± 103.43 (range 11 - 370) for females. The HU_{mean} value at the aorta was 115.04 ± 64.68 (range 68.5 - 409) for males and 161.72 ± 213.81 (range 76.5 - 940) for females. The blood pool HU_{mean} was 92.75 ± 13.71 (range 66.5 - 126) for males and 100.54 ± 15.66 (range 83 - 133) for females.

Closer inspection of the figures show that male patients had slightly higher HU_{mean} at coronary arteries than female patients, while female patients had higher aortic and blood pool HU_{mean} values than male patients. However, an independent t-test indicated that there were no significant confounding differences in coronary arteries HU_{mean}, aortic artery $HU_{mean,}$ and blood pool HU_{mean} values between males and females AKU patients (P = 0.114, P = 0.32, and P = 0.129, respectively).

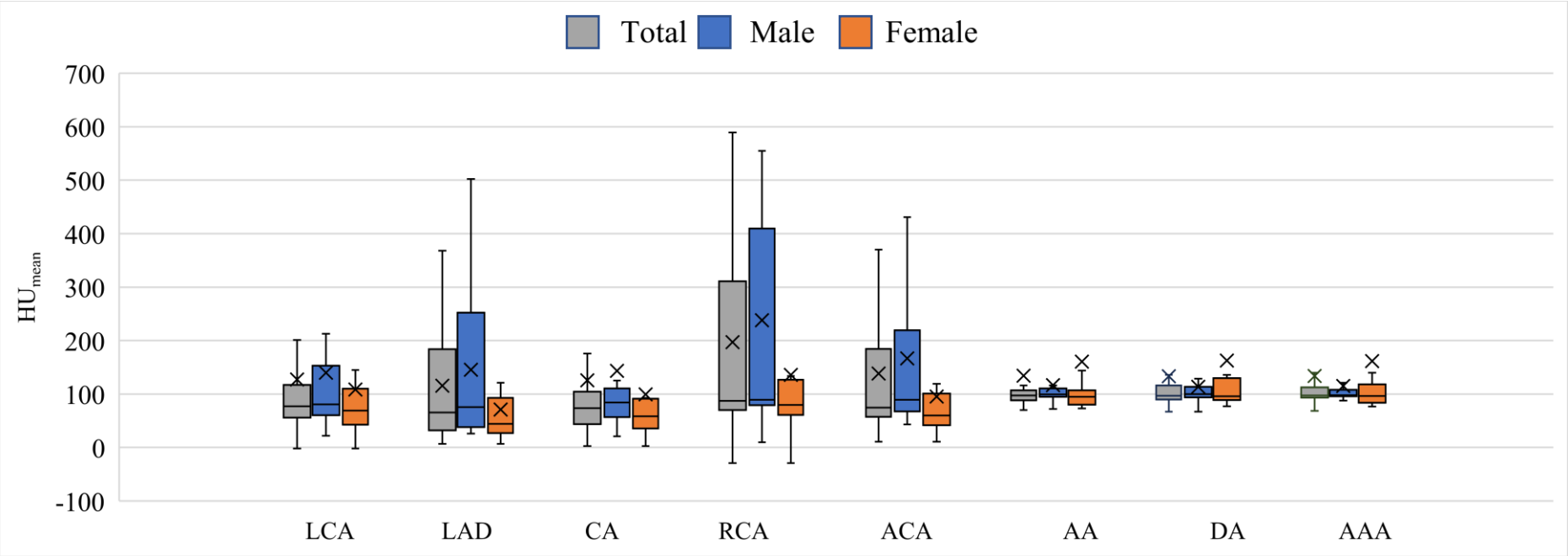

Figure 6.16. Mean HU_{mean} obtained from the CT scan at each cardiac artery for 40 AKU patients who were part of the SONIA 2 clinical trial stratified by gender.

The results show the analysis of the baseline PET data for 24 male and 16 female from four main branches of coronary arteries, including left coronary artery-left main stem (LCA), left anterior descending artery (LAD), left circumflex artery (CA) and right coronary artery (RCA), average coronary arteries (ACA), and aortic arteries analysis, ascending aorta (AA) and descending aorta (DA) and average aortic artery (AAA). Table 9.33 (appendix) shows the statistical correlation between gender at all cardiovascular ROIs. HU_{mean} is highest at the RCA in male patients and DA in female patients. Independent sample t-test revealed no statistically significant differences between males and females at all measured ROIs (all had $P > 0.05$). In box and whisker, x is the mean value, and the line is the median.

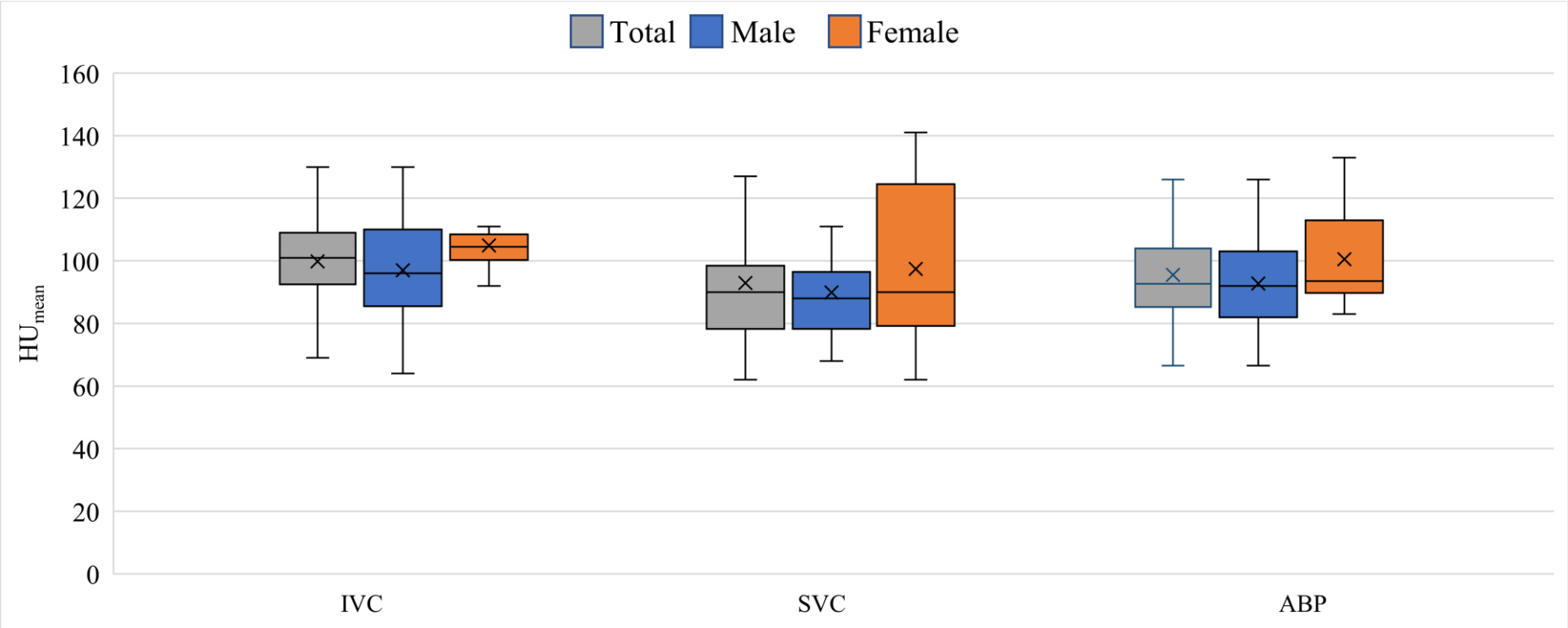

Figure 6.17. Mean HU_{mean} obtained from the CT scan at the blood pool vascular region for 40 AKU patients who were part of the SONIA 2 clinical trial stratified by gender.

The results show the analysis of the baseline PET data for 24 males and 16 females from blood pool vessels, including inferior vena cava (IVC) and superior vena cava (SVC), and average blood pool measurement (ABP). Table 9.33 (appendix) shows the statistical correlation between gender at all ROIs. Independent sample t-test revealed no statistically significant differences between males and females at AA, DA, nor ABP (P = 0.172, P = 0.246, and P = 0.129 respectively). In box and whisker, x is the mean value, and the line is the median.

6.3.3.2 Cardiovascular HU_{mean} and age

Figure 6.18, Figure 6.19, and Figure 6.20 shows the correlation between age and HU_{mean} across cardiovascular arteries. It is clear that HU_{mean} values were positively increased with age at all ROIs. The average coronary arteries HU_{mean} value was significantly correlated with age (P = 0.006, R = 0.427). Regionally, LCA, LAD, and RCA had a significant correlation with age with P-values of 0.003, 0.002, and 0.029, respectively. In contrast, there was no significant correlation between CA HU_{mean} values and age (P = 0.087, R = 0.274). The average aortic HU_{mean} value was also positively correlated with age (P = 0.022, R = 0.36), as shown in Figure 6.19. Regionally, both AA and DA HU_{mean} value had a positive trend with age (P = 0.017, R = 0.375 and P = 0.031, R= 0.341, respectively). Blood pool HU_{mean} measurement was not affected by age (P > 0.05), as shown in Figure 6.20.

Subgroup age analysis for the cardiac HU_{mean} was compared in Figure 6.21, Figure 6.22, and Figure 6.23 and presented in Table 9.34 (appendix). Generally, the youngest age group patients had low HU_{mean} values, while the oldest age group had the highest HU_{mean} values. The average HU_{mean} from the four measured coronary arteries was 78.32 ± 32.93 for 30-39 age group patients, 113.37 ± 182.69 for 40-49 age group patients, 100.63 ± 66.84 for 50-59 age group patients and 249.90 ± 124.18 for ≥ 60 year old patients. Statistically speaking, there were significant differences between the 50s and 60s age groups only for the HU_{mean} values, which were measured from LAD, LAD and RCA (P = 0.03, P = 0.05, and P = 0.02, respectively).

Subgroup age analysis from the aorta shows that the average HU_{mean} was 108.07 ± 23.62 for 30-39 age group patients, 92.92 ± 11.39 for 40-49 age group patients, 100.40 ± 10.45 for 50-59 age group patients and 238.00 ± 268.92 for ≥ 60 year old patients. Although aortic HU_{mean} values correlated with age, there was no clear trend between sub-age group values. The only statistically significant evidence was shown between the HU_{mean} values measured from AA for the youngest and the second youngest age groups (P = 0.04). On the other hand, most adolescent patients had significantly higher average blood pool HU_{mean} values (110.00 ± 15.22) compared with the patients in the 40-49 age group (86.83 ± 10.87), as shown in Figure 6.23. Regarding blood pool

vessels, no apparent differences were detected at the blood pool regions between the 40s and 50s nor 50s and 60s.

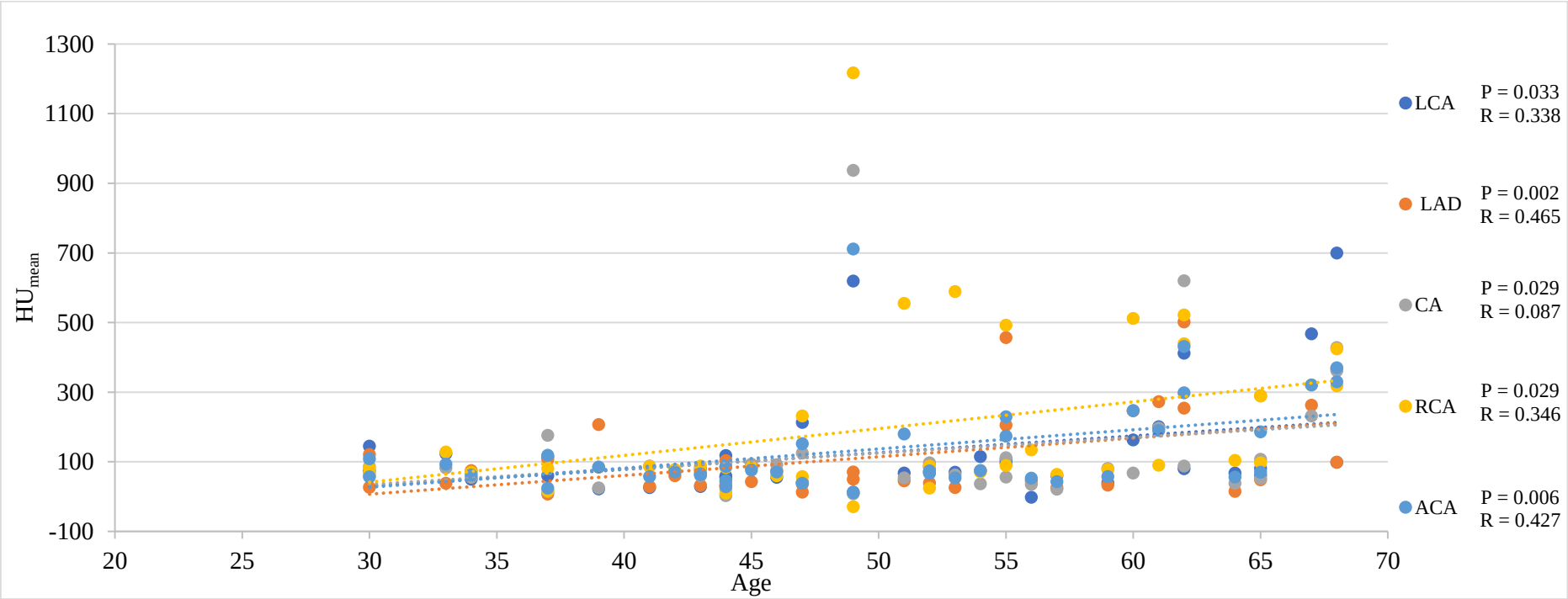

Figure 6.18. Scatter plots illustrating the correlation between HU_{mean} obtained from CT scan and age at four main coronary arteries for 40 AKU patients who were part of the SONIA 2 clinical trial.

The results display HU_{mean} of left coronary artery-left main stem (LCA), left anterior descending artery (LAD), left circumflex artery (CA) and right coronary artery (RCA), average coronary arteries (ACA) in individual AKU cases with age. Age had a positive, statistically significant effect in average main coronary arteries HU_{mean} value (R = 0.427, P = 0.006). Multiple linear regression analysis identified a statistically significant correlation between regional HU_{mean} and age in AKU cases measured at LCA, LAD, and RCA (R = 0.338, 0.465, and 0.346, respectively, all P > 0.05). No significant correlation between HU_{mean} values in CA and age (R = 0.274, P = 0.087).

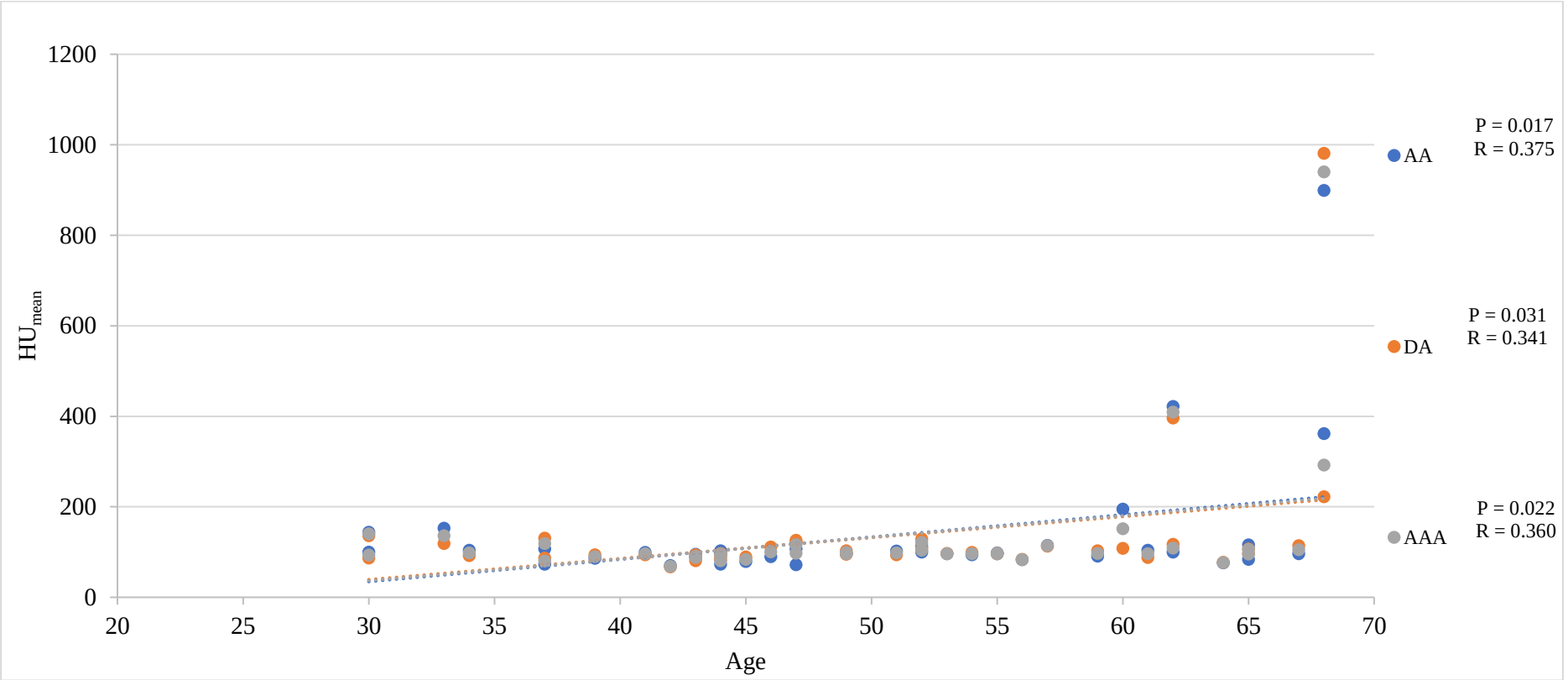

Figure 6.19. Scatter plots illustrating the correlation between aorta HU_{mean} obtained from CT scan and age for 40 AKU patients who were part of the SONIA 2 clinical trial.

The results display HU_{mean} of ascending aorta (AA) and descending aorta (DA), average aortic artery (AAA) in individual AKU cases with age. Multiple linear regression analysis identified that there was significant correlation between HU_{mean} and age in AKU cases at AA and DA (R = 0.375, P = 0.017, and R = 0.341, P = 0.031, respectively).

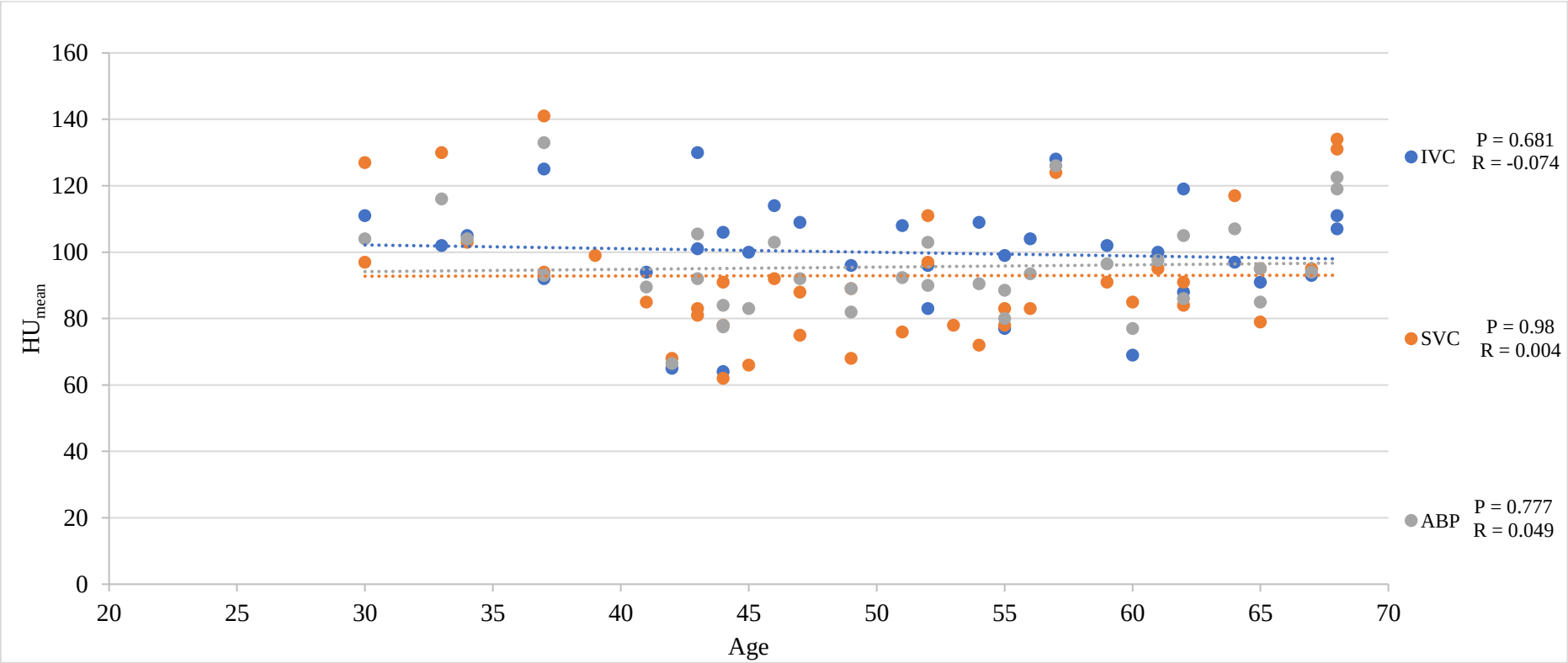

Figure 6.20. Scatter plots illustrating the correlation between blood pool HU_{mean} obtained from CT and age for 40 AKU patients who were part of the the SONIA 2 clinical trial.

The results display the HU_{mean} of inferior vena cava (IVC), superior vena cava (SVC), and average blood pool (ABP) in individual AKU cases with age. Multiple linear regression analysis identified that there was no significant correlation between HU_{mean} and age in AKU cases at IVC and SVC (R = -0.074, P = 0.681 and R = 0.004, P = 0.98, respectively)

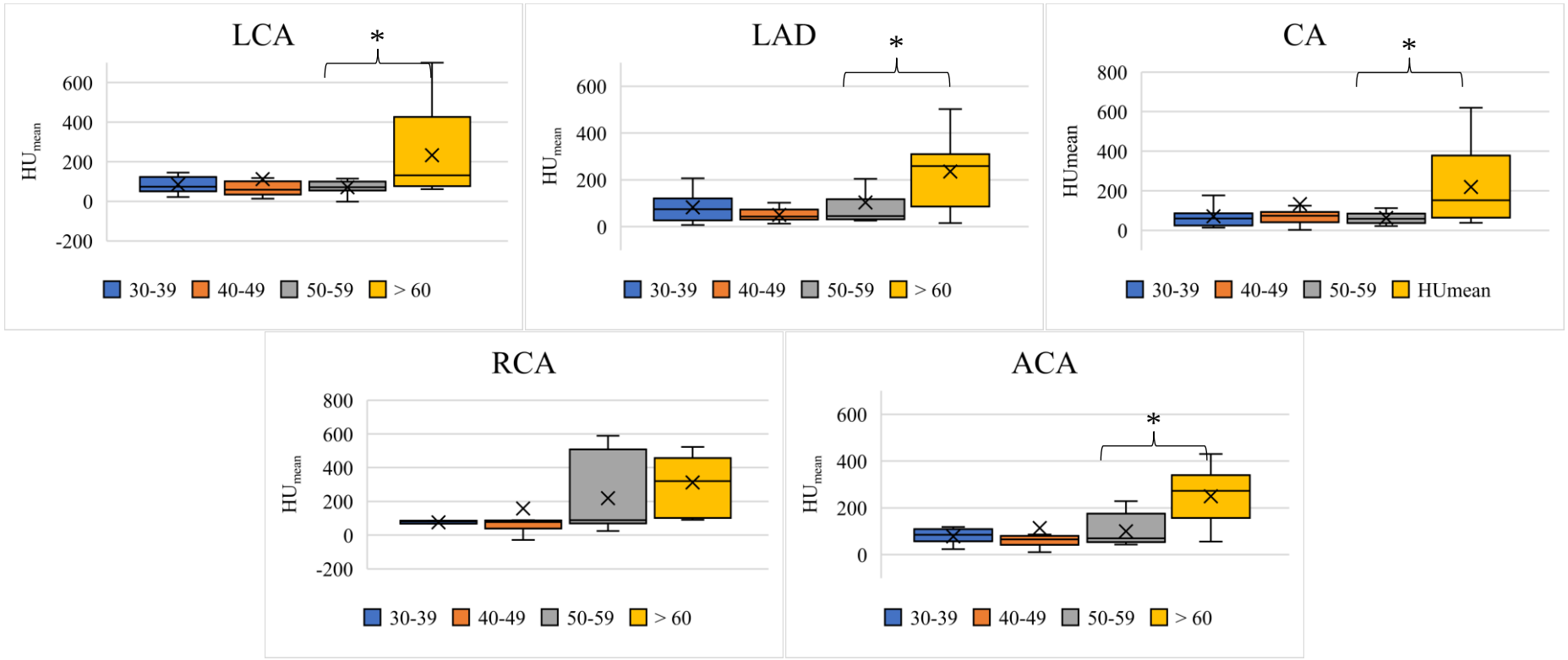

Figure 6.21. Mean coronary arteries HU_{mean} value among four decadal age groups measured from CT scan for AKU patients who were part of the SONIA 2 clinical trial.

Table 9.34 shows the ROI and age groups which indicated a statistically significant difference between subgroup analyses. *Groups which showed significant difference ($P < 0.05$). One-way-ANOVA revealed a statistically significant difference between the 50s and 60s age groups at LCA, LAD, CA, and ACA ($P = 0.03$, $P = 0.05$, $P = 0.02$, and $P = 0.001$, respectively). Left coronary artery-left main stem (LCA), left anterior descending artery (LAD), left circumflex artery (CA) and right coronary artery (RCA), average coronary arteries (ACA). In box and whisker, x is the mean value, and the line is the median.

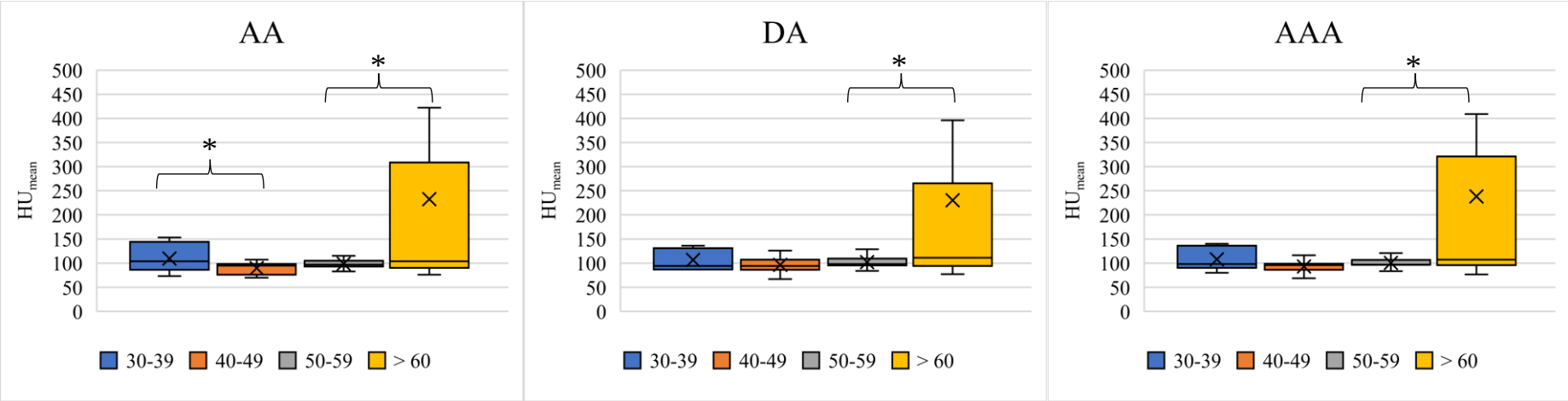

Figure 6.22. Mean aortic HU_{mean} values among four decadal age groups measured from CT scan for AKU patients who were part of the SONIA 2 clinical trial.

Table 9.34 shows the ROI and age groups which indicated a statistically significant difference between subgroup analyses. *Groups which showed significant difference ($P < 0.05$). One-way-ANOVA revealed a statistically significant difference between the 50s and 60s age groups at average coronary arteries, and between 30s and 40s at AA ($P = 0.04$), and between 50s and 60s at AA, DA, and AAA ($P = 0.009$, $P = 0.017$, and $P = 0.012$, respectively). Ascending aorta (AA) and descending aorta (DA), average aortic artery (AAA). In box and whisker, x is the mean value, and the line is the median.

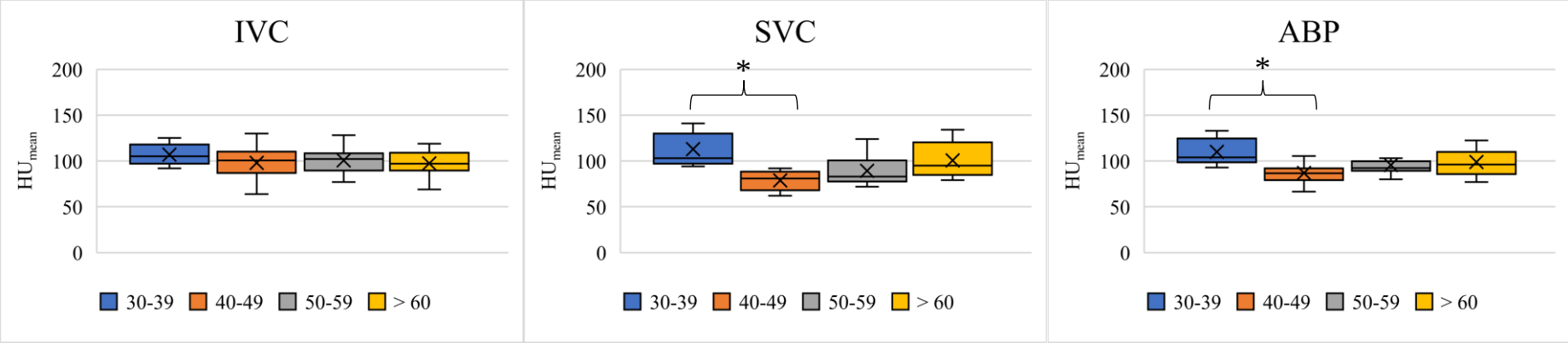

Figure 6.23. Mean blood pool HU_{mean} among four decadal age groups measured from CT scan for AKU patients who were part of the SONIA 2 clinical trial.

Table 9.34 shows the ROI and age groups which indicated a statistically significant difference between subgroup analyses.*Groups showed significant difference ($P < 0.05$). One-way-ANOVA revealed a statistically significant difference between the 30s and 40s age groups at SVC and ABP ($P = 0.0001$ and $P = 0.04$, respectively). Inferior vena cava (IVC), superior vena cava (SVC), and average blood pool (ABP). In box and whisker, x is the mean value, and the line is the median

6.3.4 Examples of some cases

Part of this chapter aimed to highlight the distribution of ^{18}F-NaF throughout the cardiac region in AKU patients. In a normal event, no coronary ^{18}F-NaF activity in the PET image nor coronary calcium in the CT image was noted, as shown in Figure 6.24. As the images show, the radiotracer was distributed homogeneously throughout the skeleton in the PET image with no abnormal accumulation of activity in the heart area. In the same way, normal soft tissue density had appeared in the CT image. A significant difference can be noted between bone intensity in vertebra, ribs and sternum and the cardiac soft tissue intensity. This indicates a typical young AKU case who had healthy cardiovascular arteries.

In abnormal cardiovascular events, three observations were noted in ^{18}F-NaF PET/CT scan. First, increased ^{18}F-NaF uptake in the PET image with the absence of local calcium in the CT image as shown in Figure 6.25 and Figure 6.26. The ^{18}F-NaF activity was pointed out in the aortic at both AA and DA walls, with no abnormal calcification signs in the CT image (Figure 6.25). Figure 6.26 shows intense ^{18}F-NaF uptake in the PET image in the femoral artery with no femoral artery calcium in the CT image. In those cases, uptake was identified as focal in nature, but the impact may be localised to individual plaques. Second, regional coronary calcification in CT images with no ^{18}F-NaF uptake. Area of coronary calcification and without any ^{18}F-NaF absorption was widely seen in AKU patients. Figure 6.27 shows an example of calcium in the AA wall with no unusual ^{18}F-NaF activity in PET image. Third, the focal distribution of radiotracer in PET images in the area adjacent or overlying to existing extensive calcification in the CT images. Figure 6.27 shows an advanced active cardiovascular calcification event. The patient had extensive calcification in LAD and DA in the CT image adjacent to a mineral ^{18}F-NaF uptake in the PET image. The affected area was clearly observed in the fused ^{18}F-NaF PET/CT. In that case, increased and intense focal ^{18}F-NaF uptake was observed in the RCA in the PET image overlaying with existing extensive calcification in that area in the CT image. Also, increased ^{18}F-NaF uptake was present in the abdominal aorta adjacent to the existing abdominal calcification area in the CT image. In that case, abnormal tracer distribution with bone-like tracer intensity in the PET image and bone-like intensity in the CT images was identified in the affected area.

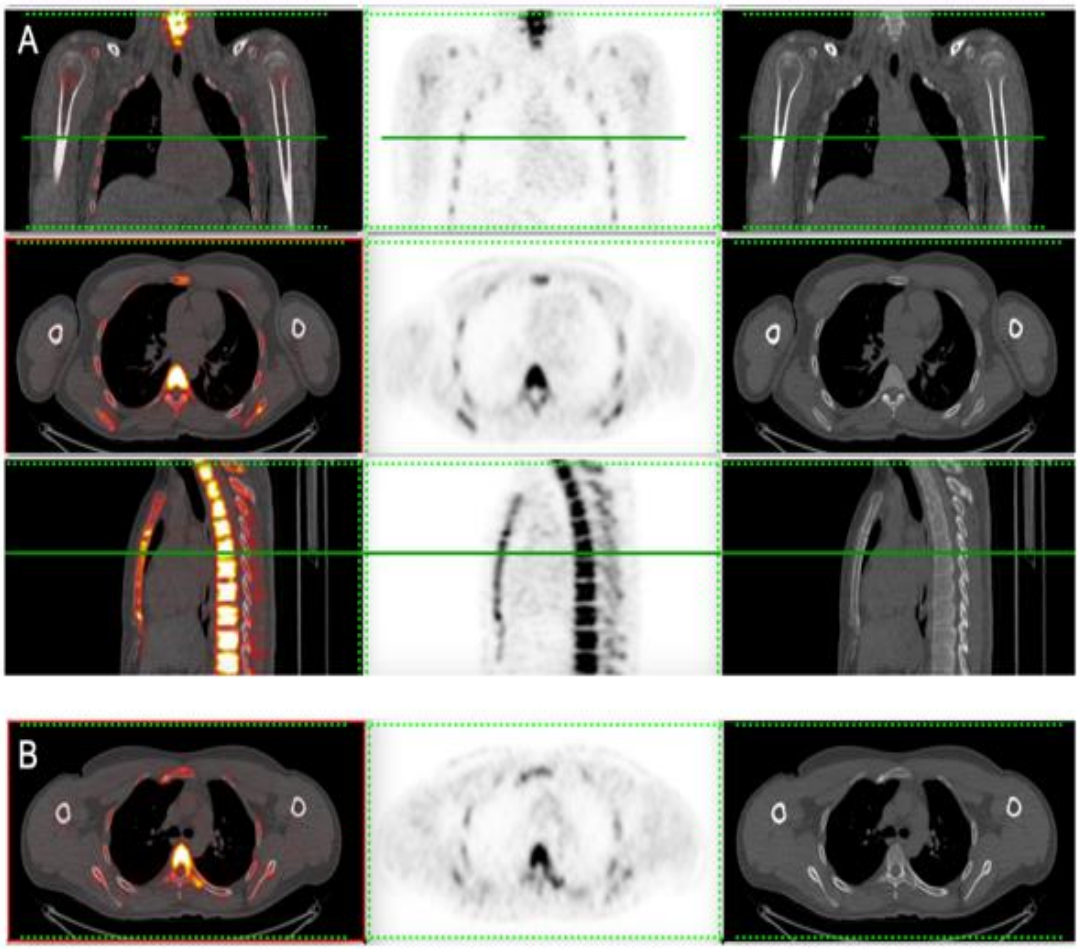

Figure 6.24. ^{18}F-NaF PET/CT images for a 33 year old, male AKU patient.

A. PET/CT image shows a normal distribution of ^{18}F-NaF throughout the skeleton, soft tissues and vessels. No abnormal ^{18}F-NaF uptake nor high-density region in the heart region was noted in PET/CT image. B) axial ^{18}F-NaF PET/CT image of aorta shows no abnormal ^{18}F-NaF uptake nor aortic calcification at neither AA nor DA. Note the intensity and activity in the vertebra, ribs and sternum.

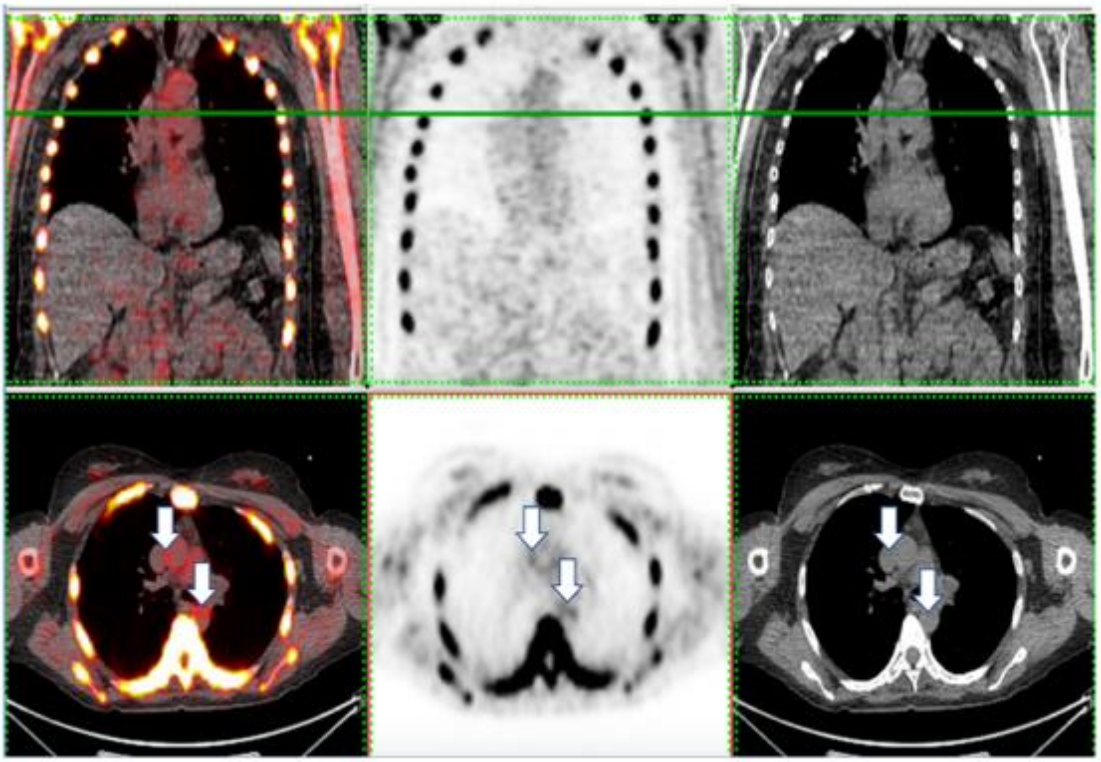

Figure 6.25. ^{18}F-NaF PET/CT image of the heart for a 44 year old, female AKU patient, showing high background activity in soft tissues, specifically in the heart region.

In the PET image, increased ^{18}F-NaF uptake was noted in AA and DA. In the CT image, the calcification in both AA and DA were not visible. In the fused ^{18}F-NaF PET/CT image, the abnormal uptake in both AA and DA were clearly noticeable. Arrows indicate increased ^{18}F-NaF uptake in PET image, which indicate micro-calcified vessels. In the previous chapter, it was noted that this patient had very high bone mineral density values in DEXA scan, high HU in CT images and high SUV values in PET images at lumbar spine lesions. Note the intensity and activity in the vertebra, ribs and sternum.

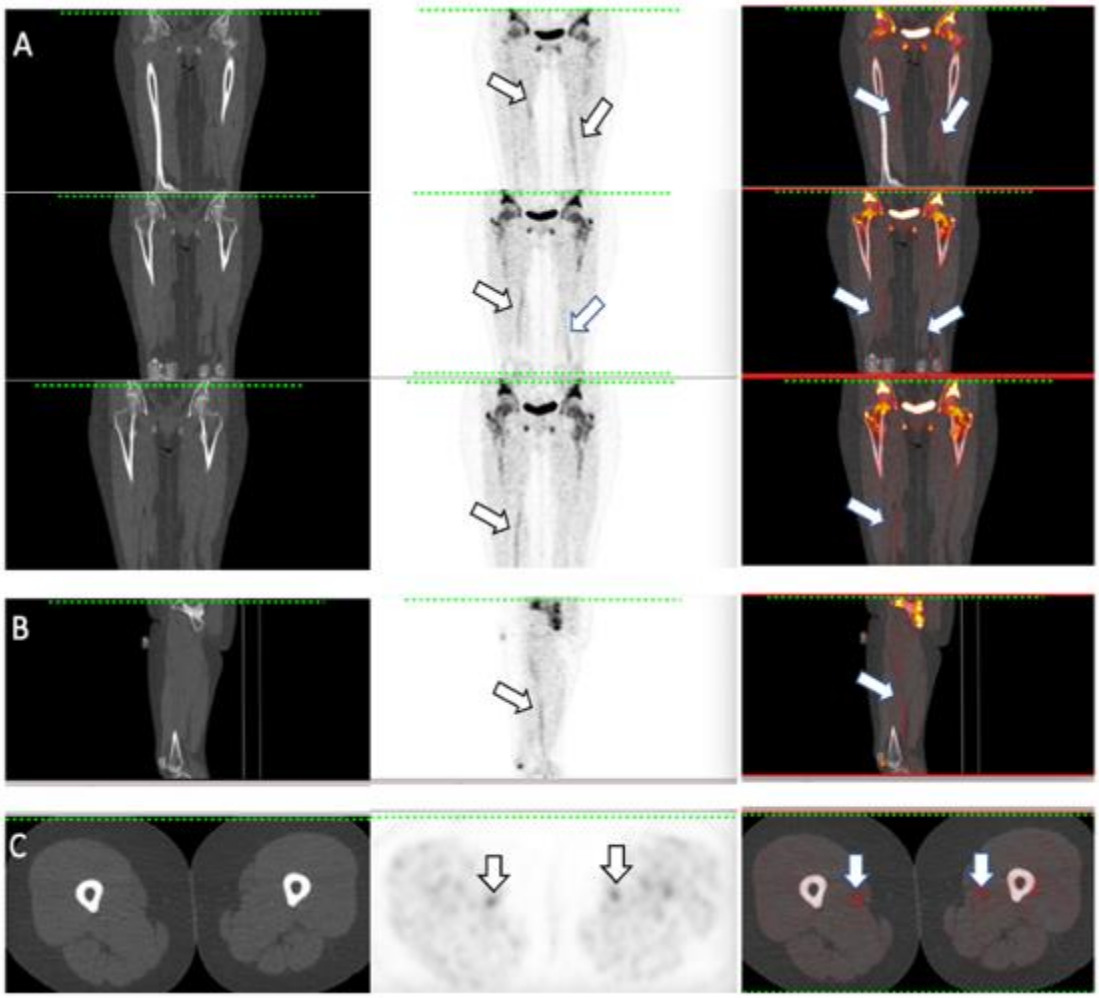

Figure 6.26. ^{18}F-NaF PET/CT image for a 56 year old, female AKU patient, showing high activity in the thigh.

A) Coronal B) Sagittal C) Axial ^{18}F-NaF PET/CT scan. In the PET image, increased ^{18}F-NaF uptake was noted in the femoral arteries. In the CT image, no calcification was identified. In the fused ^{18}F-NaF PET/CT image, the abnormal ^{18}F-NaF uptake in both femoral sides was clearly noted. Arrows indicated increased ^{18}F-NaF uptake in PET image and fused ^{18}F-NaFPET/CT image, indicating micro-calcified vessels in the right and left femoral sides. Note the intensity and activity in the femur.

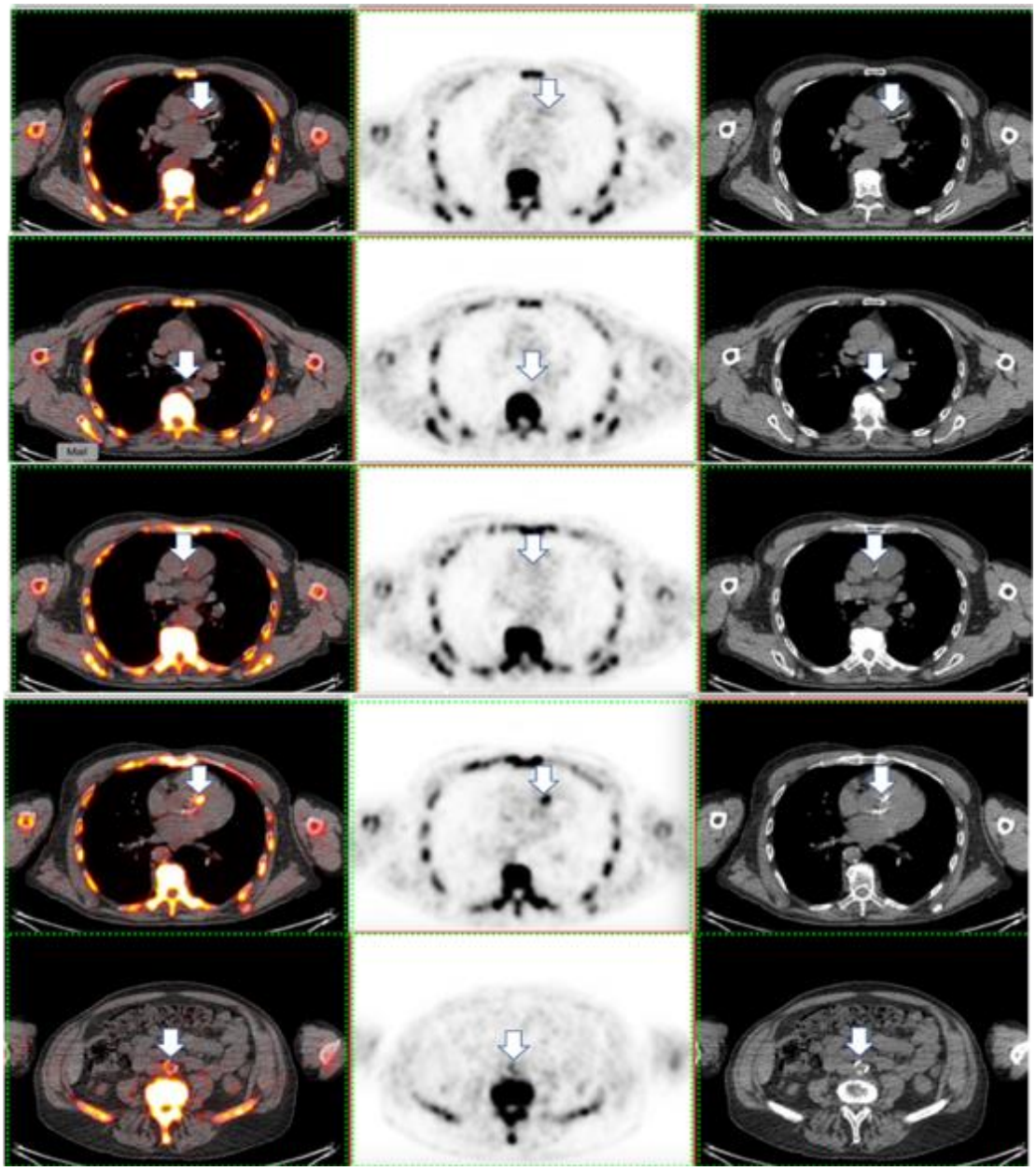

Figure 6.27. Axial ^{18}F-NaF PET/CT images for a 62 year old, male AKU patient.

The first upper row of images show extensive calcification in LAD in CT image adjacent to a minimally increased ^{18}F-NaF uptake in the PET image. The second-row of images show extensive calcification in DA, which was clearly noted in CT image and fused ^{18}F-NaF PET/CT image with no apparent abnormal ^{18}F-NaF uptake in PET image. The third-row of images show calcification in the AA wall in CT image and fused ^{18}F-NaF PET/CT image, with no intense ^{18}F-NaF activity in PET image. The fourth-row of images shows an intense focal ^{18}F-NaF uptake in PET image in RCA overlaying with existing extensive calcification in CT image. The bottom row of images shows intense focal ^{18}F-NaF uptake in PET image adjacent to an area of existing extensive calcification in the abdominal artery. Note the intensity and activity in the vertebra, ribs and sternum.

6.4 Discussion

This is the first study to describe vascular calcification in the main arteries in patients with AKU using ^{18}F-NaF PET/CT scan. While the ^{18}F-NaF PET/CT scan was performed to detect joint and bone abnormalities, cardiac involvements were accidentally noted in SONIA 2 participants, and the event has been investigated. Spotty hot areas and dense lesions were noted in ^{18}F-NaF PET/CT images, indicating vulnerable plaques which may be associated with cardiac ochronosis in AKU patients. Even minimal bone radiotracer uptake in coronary vessels was a piece of strong evidence for molecular cardiovascular calcification, which may lead to severe consequences if not treated. The purpose of this investigation came after noting unexpected bone radiotracer uptake in the heart area in AKU patients during ^{18}F-NaF PET/CT evaluation. This study aimed to determine ^{18}F-NaF uptake in the coronary arteries and aorta in order to assess early molecular calcification before detecting structural calcification by standard CT scan.

6.4.1 Cardiovascular calcification analysis method

In the present study, a novel method using a bone imaging radiomarker was employed, to quantify active cardiovascular calcification which may help to understand coronary artery disease in ochronotic patients. The assessment methods were chosen based on the previous studies in this area and the available resources, including data and software. The evaluation of coronary and aortic artery calcification using ^{18}F-NaF as a biomarker was previously tested in several non-AKU studies reporting successful findings [148,150,152,156,157].

In this study, it was not possible to identify the exact border of small vascular structures using non-contrast CT nor ^{18}F-NaF PET images. From this point, using maximum SUV would be the best value to choose, presenting abnormal ^{18}F-NaF uptake within small vessels. Clinically, there were no fixed or standard method to quantitatively analyse cardiovascular calcification in ^{18}F-NaF PET/CT images. Exciting efforts are ongoing to establish the optimal method for creating a standard protocol to use ^{18}F-NaF tracer as a microcalcification imaging biomarker. Several studies supported the analysis method, which has been selected in this chapter to quantify the vascular

uptake using maximum SUV [155,158]. In contrast, some studies preferred quantifying the cardiovascular ^{18}F-NaF uptake using mean SUV [185]. It is important to mention that a small fraction of the administered ^{18}F-NaF dose will remain in the plasma [152]. Therefore, this remaining background activity in the blood may affect the SUV measurements causing overestimation of the values. In order to avoid this issue, SUV_{max} was divided by the mean SUV of the blood pool to generate TBR_{max}..

The primary purpose of combining the CT scanner with the PET scanner is to improve the structural identification of the imaged regions. In this study, the CT image was used to identify the dense regions in the heart visually and analyse them quantitively by measuring HU values. Based on the HU scale, high HU values defined dense tissues, which are usually detected from bone or calcified soft tissue lesions. Therefore, detecting high HU values in cardiac vessels indicated an abnormal cardiac event, increasing the possibility of calcified vessels, which more likely caused by calcium deposition.

6.4.2 Increased ^{18}F-NaF uptake in the cardiovascular system.

Focal high intense ^{18}F-NaF activity was identified and localised at multiple sites within the coronary circulation in AKU patients. To understand the ^{18}F-NaF uptake within the cardiovascular system in AKU patients, the main arteries were identified and quantified in AKU patients. Although the evaluation of vascular calcification using ^{18}F-NaF PET/CT for AKU patients has not been described previously, the abnormal cardiac manifestations in ochronotic patients are well-known [7,25,28]. Over the last few years, cardiovascular ^{18}F-NaF uptake has been described in the general population and patients with heart disease using ^{18}F-NaF PET/CT scan. The precise mechanism of ^{18}F-NaF accumulation in the cardiovascular tissue is not clearly understood or established yet; however, it can be extrapolated from ^{18}F-NaF uptake in osseous tissue, which has been described previously by many studies over the decades. ^{18}F-NaF is a bone radiotracer which detects high-risk lesions of active bone formation and remodelling. After administration of ^{18}F-NaF, the -^{18}F ion binds to the calcium pyrophosphate dihydrate crystals, including those in the arterial walls. Calcification in the vascular tissues likely shows increased ^{18}F-NaF uptake, which can be indicated by the increase of SUV and TBR values. There is an assumption that ^{18}F-NaF uptake

represents an active and ongoing microcalcification, which usually occurs at the earliest stage of vascular calcium deposition. So, the focal spot areas of increased ^{18}F-NaF uptake in the AKU patients may reflect an active and ongoing cardiovascular calcification. This corroborates these earlier findings [148,150,152,155–157,186]. According to these observations, it is likely, therefore, to identify early cardiac involvements in AKU patients associated with active microvascular calcification before it becomes symptomatic. Increased ^{18}F-NaF uptake in the calcified vessels is a valuable finding which can predict future cardiovascular events in AKU patients, allowing earlier intervention and treatment of cardiac diseases.

Regarding the four main coronary arteries which have been measured in this chapter, the higher SUV_{max} was measured in the RCA followed by the LCA then CA and LAD (1.68 ± 1.04, 1.57 ± 0.59, 1.18 ± 0.05, and 1.12 ± 0.35, respectively). Dweck *et al.* [148] measured SUV_{max} and TBR_{max} in the RCA, LCA, CA, and LAD for 119 volunteers (age ± SD; 72 ± 8 years old) with and without aortic valve disease who underwent ^{18}F-NaF PET/CT. Dweck *et al*. reported the SUV_{max} of RCA, LCA, CA, and LAD to be 1.27 ± 0.41, 1.36 ± 0.4, 1.32 ± 0.46, and 1.38 ± 0.42, respectively. Interestingly, the mean SUV_{max} and TBR_{max} for the average four coronary arteries in that study reported being 1.56 ± 0.5 and 1.59 ± 0.48, respectively, which was very similar to the mean SUV_{max} and TBR_{max} for the average four coronary arteries of the AKU patients in this chapter, which had SUV_{max} of 1.39 ± 0.45 and TBR_{max} of 1.80 ± 0.8. In another study reporting coronary arteries SUV_{max}, Blomberg *et al*. and his co-workers [154] evaluated ^{18}F-NaF uptake in 89 healthy patients who been imaged by different PET/CT scanners, and they found that average coronary arteries SUV_{max} were 3.75 ± 0.91, which was higher than AKU patients here.

In the current study, descending aorta SUV_{max} values were higher than ascending aorta values (2.06 ± 0.84 and 1.78 ± 0.57, respectively), the same findings with almost similar values to those reported in both Dweck *et al.* [148] and Derlin *et al.* [155] studies. On the other hand, the descending aorta TBR_{max} was 3.03 ± 1.74 in AKU patients compared to ascending aorta value, which was 2.31± 1.06. This data is slightly higher than that reported in Derlin *et al.* [155] where he found that DA TBR_{max} was 2.06 ± 0.35 and AA was 2.01 ± 0.3, and also in Li *et al.* [147] who found that DA TBR_{max} was 1.57 ± 0.56 and AA was 2.0 ± 0.72. The results of this chapter revealed that SUV_{max} of the

aorta at both AA and DA regions for those patients with AKU were similar to the general population subjects, which have been published in the literature. This finding suggests that generalised rates of microvascular calcification in AKU and general population patients are very similar, reflected by arterial ^{18}F-NaF uptake.

From Figure 6.3 and Figure 6.11, ^{18}F-NaF introduced by SUV_{max} and TBR_{max} in the aortic artery were higher than those measured in coronary arteries. Li *et al*. [147] and Dweck *et al*. [148] reported the same finding in their studies. In contrast, Blomberg *et al*. [154] found different results in regard to the differences between coronary and aorta ^{18}F-NaF uptake. He found that coronary arteries had slightly higher SUV_{max} than the ascending aorta and descending aorta (3.74 ± 0.91, 3.32 ± 1.17 and 3.22 ± 0.88, respectively). In the current study, coronary arteries and aortic artery data were significantly lower than the previously published study. The possible explanation for this is that there were no active calcified regions, so there were few $^{-18}$F binding sites to bind with ^{18}F-NaF. Blomberg *et al*. found that both blood activity and the PET/CT system had a significant effect on the ^{18}F-NaF uptake measurements. In that study, a higher uptake was detected in patients who were imaged by Discovery 690/710 than those imaged by Discovery STE, VTC or RX. So, the differences in the values between the data in the literature and the current study could be due to the different PET/CT systems which have been used.

In general, less observation of calcification in coronary arteries compared to the aorta may be due to a few possible reasons. First of all, PET scanners have a limited spatial resolution, which could reduce the sensitivity to evaluate ^{18}F-NaF uptake in small arteries. Secondly, both cardiac and respiratory movements can further decrease the sensitivity of PET scans in the detection of small arteries. Another possible reason may be correlated with the partial volume effect, which interferes with evaluating the small size of the ROI. Anatomically, the proximal coronary arteries are surrounded by vascular structures, such as the heart valves, aorta, and pulmonary artery. These areas are highly susceptible to calcium deposition, which can easily affect the interpretation of radiotracer accumulation in coronary arteries. Generally, aortic calcification has been found to have high specificity in recognising severe coronary atherosclerosis in coronary artery disease patients [187]. Several studies suggested that cardiac calcification is more detectable in the aorta than coronary arteries because of its higher prevalence

and earlier onset [187]. Although no control patients have been analysed in this chapter, there is a high probability that AKU patients have higher cardiovascular ^{18}F-NaF uptake than healthy patients due to ochronosis. Dewck *et al*. found that patients with atherosclerosis had higher ^{18}F-NaF uptake than control patients, describing a progressive rise within coronary artery plaques [148].

6.4.2.1 Cardiovascular ^{18}F-NaF uptake and gender

The difference between cardiovascular ^{18}F-NaF uptake between males and females was tested. Male AKU patients had higher vascular ^{18}F-NaF uptake compared to female patients, demonstrated by higher SUV_{max} and TBR_{max} values at all measured coronary arteries and aortic artery. Higher ^{18}F-NaF uptake in cardiac vessels for males compared to females was expected due to several reasons. Based on the National Cholesterol Education Programme (NCEP), men have a higher risk of developing coronary heart disease ten years younger than women [188]. Although the difference was noted in this chapter, it was not significant in all coronary arteries. Statistically, no significant differences in SUV_{max} values have been identified between males and females at most of the coronary arteries except at RCA, where the P-value was 0.022. In regard to the TBR_{max}, there were substantial differences between males and females at LAD (P = 0.018), and at RCA only (P = 0.012). No statistically significant differences in SUV_{max} and TBR_{max} was noted at aortic artery at neither AA nor DA between males and females. The possible reason for that could be the odd ^{18}F-NaF distribution between the AKU patients throughout the body, which may be correlated to specific individual factors. For patients with AKU, cardiovascular calcification may be linked to the ochronosis process and pigment deposition in cardiac tissues. The gender difference regarding cardiovascular disease for AKU patients is incompletely understood. The results from this section suggest that when looking at the overall cardiovascular ^{18}F-NaF uptake to assess abnormal cardiac distribution in ^{18}F-NaF PET/CT image, gender should not be considered as a direct factor affecting cardiovascular uptake in AKU patients. Some published papers argue that aortic and coronary calcification is independently correlated with gender. In regard to the difference in ^{18}F-NaF uptake among males and females in the arteries, Derlin *et al*. [155] reported that the presence of arterial calcification and vascular uptake were more present in male patients compared with female patients. However, he pointed out that

this difference was not significant. This finding supports the results of this chapter. On the other hand, sex was found to have a significant impact in the cardiovascular calcification in elderly patients with severe aortic stenosis [188].

6.4.2.2 Cardiovascular ^{18}F-NaF uptake and age

Regarding age, a slight rise in the ^{18}F-NaF uptake of the average coronary arteries with age was observed. From Figure 6.5, and Figure 6.11, age was not statistically associated with increased regional SUV_{max} or TBR_{max} at LCA, LAD, and CA, in contrast to the theory indicating that age is one of the main risk factors for coronary artery calcification. Only one coronary artery out of the four measured arteries in this study, RCA, had a significant relationship between ^{18}F-NaF uptake and age, showing increased coronary arteries SUV_{max} and TBR_{max} with age. This result suggests that cardiovascular ^{18}F-NaF uptake is not always correlated with age in AKU patients.

In the current study the youngest age group of patients had minimal ^{18}F-NaF uptake, having low SUV_{max} and TBR_{max} values at all coronary arteries compared with the other age groups. The average SUV_{max} and TBR_{max} of the coronary arteries were increased slightly from 30s to the 60s; however, these increases were only significant between the 50s and 60s. The possible explanation for that might be due to the disease stages. It is more likely that the vascular calcifications are more common and progress faster between 50s and 60s in patients with AKU.

Generally, in the first four decades of life, cardiac vessels are likely to be healthy with no abnormal calcium deposition within the cardiovascular system. It seems possible that this result was due to a non-pigmented artery and/or non-calcified artery in young patients. Therefore, ^{18}F-NaF is rapidly cleared from the blood circulation and deposited in calcium-rich tissues, which are usually bone tissues and not a soft-tissues or vascular arteries. In young patients, the measured vascular regions expected to have low ^{18}F-NaF uptake due to a healthy vascular structure with no calcium deposits, therefore no or few ^{18}F-ion binding sites would be available in the vessels. This means that these AKU patients with healthy vessels would be more likely have low SUV and TBR values. With aging, ochronotic pigment is beginning to build up in all body tissues, including cardiac tissues. This deposition is usually linked with calcium

deposition in the cardiovascular wall. Due to this, increased ^{18}F-NaF uptake with age in the PET image was expected. As explained previously in this thesis, increased ^{18}F-NaF uptake can be detected in active and ongoing calcified area. It is important to bear in mind that the inactive or stable calcified artery may also have significantly low ^{18}F-NaF absorption. This does not mean that there is no vascular calcification, but that means, it may become undetectable by ^{18}F-NaF PET scan. The reason for this phenomenon is that ^{18}F- ion is usually bound to newly laid down hydroxyapatite in the affected artery, which generally has more binding sites due to the active disease processes. Stable and inactive macrocalcifications, which been established months or years before, usually have a large volume but small surface area compared to ongoing and active microcalcifications, which have a small volume but large surface area [149]. Since the degree of ^{18}F-NaF absorption depends on the calcification surface area and cannot absorb through the outer calcification layer without a deeper penetration, it is more likely that ^{18}F-NaF-PET/CT imaging detects microcalcifications only. Therefore, in macrocalcifications, ^{18}F-NaF signals are low. Several other researchers reported this, resulting in an expanded interest for using ^{18}F-NaF to image the microcalcification phase and visualise ongoing mineral deposition in the calcified vessels [147,152,153].

Aortic ^{18}F-NaF uptake values, which were measured by SUV_{max} and TBR_{max}, were also not correlated with age. In contrast, Beheshti *et al*. found a significant correlation between aortic SUV_{mean} and age [152]. The aortic SUV values in Beheshti *et al*. study were 0.72 ± 0.12 for a patient younger than 40 years old, 0.81 ± 0.06 in 40s years old patients, 0.86 ± 0.07 in 50s years old patients, and 0.99 ± 0.03 in patients more aged than 60, whereas in this chapter, the result was significantly higher. In the current study, the aortic SUV values were 1.73 ± 0.52, 2.00 ± 0.93, 2.28 ± 0.78 and 2.15 ± 0.98 for 30s, 40s, 50s, and 60s, respectively. Although Beheshti *et al*.'s research indicated a relationship between age and aortic calcification, which contrasts with the current findings, the differences may be due to several reasons. First of all, Beheshti and his co-workers measured mean SUV values, while here, the maximum SUV has been measured. The second significant difference between the two studies was the patients tested; Beheshti *et al*. evaluated the cardiovascular uptake for cancer patients, while in this study, AKU patients were evaluated. So, the pathological differences between cancer and AKU may cause those differences. Derlin *et al*. [155] also found that

both arterial calcification and ^{18}F-NaF accumulation was significantly associated with age. Although the early results are difficult to compare due to differences in inclusion criteria, the literature can provide us with approximate average ^{18}F-NaF uptake values, which can be useful for co-localisation of radiotracer uptake and calcification, specifically in patients at high risk of developing cardiac diseases such as AKU patients.

6.4.3 Increased HU_{mean} in the cardiovascular system

In the CT images, white spots were clearly noted in the heart region for many of the SONIA 2 patients, which indicates a structural macroscopic arterial calcification. CT images visually pointed out the presence of a calcified vessel, defined as high-density mural regions. Based on the measured attenuation coefficient values from coronary and aortic arteries areas, HU values were significantly higher than what would be expected from soft tissues and healthy vascular tissues. To our knowledge, this is the first study in which CT images have been used to quantify regional cardiovascular involvements in AKU patients by measuring HU from main arteries, making the results of this section in this thesis novel.

It was clear from the data that in the average measured coronary arteries and aortic artery, HU_{mean} were higher than 130 HU. Regionally, the HU_{mean} for AKU patients exceeded 115 in all coronary and aorta arteries. A study by Allison *et al*. [188] defined coronary calcification as a plaque with a density of more than 130 HU and an area larger than 2 pixels (0.67 mm^2) from the electron-beam computed tomography (EBCT) image. Derlin *et al*. [158] also defined calcified plaques in the wall of arteries from PET/CT studies, having high-density mural areas with HU higher than 130. The maximum HU in some AKU patients involved in this study exceeded 700 HU, indicating severely calcified vessels. The minimum HU for some of the measured arteries was below zero, which indicated fat present in the blood vessels. In regard to the coronary arteries, the highest HU_{mean} value was measured from RCA, which matched with the previous SUV_{max} and TBR_{max} findings. In contrast to the results in SUV_{max} and TBR_{max}, HU_{mean} of coronary arteries was almost the same as HU_{mean} of aortic artery.

6.4.3.1 Cardiovascular HU_{mean} and gender

This study demonstrated that male AKU patients have higher HU_{mean} than female AKU patients at all measured coronary arteries; however, this was not statistically significant ($P > 0.05$). A possible reason for that could be that men generally have a higher risk of coronary heart disease than women [188]. Therefore, male patients have denser arterial walls due to increased calcium deposition in the vessel walls, which begin as a plaque with high HU. Allison *et al*. [188] tested risk factors that strongly correlate with prevalent coronary artery calcification for 6086 consecutive patients. In that study, they found that coronary calcium score, which had been measured from EBCT for the male patients, was higher than female patients, with evidence of having a more substantial amount of plaque appearing at an earlier age. To avoid other risk factors contributing, Allison and co-workers adjusted other cardiovascular risk factors such as age, cholesterol levels, smoking, hypertension, and diabetes, and the same finding was reached. Although the previous study was designed differently from the current study, similar outcomes were noted where male AKU patients tend to have higher HU values than female patients. Another study done for very elderly patients found that male patients had significantly higher coronary artery calcification and aortic valve calcium than female patients [189]. Raggi *et al*. reported that female patients had lower calcification scores and a lower prevalence of coronary calcification than men ($P < 0.0001$) [190]. However, he found higher cumulative risk-adjusted mortality at five years for women than men despite controlling for other risk factors such as age, hypertension, and diabetes mellitus.

As presented in ^{18}F-NaF uptake section, males had higher SUV_{max} and TBR_{max} in coronary and aortic artery than females. Likewise, coronary arteries had higher HU_{mean} values for male patients compared to female patients. In contrast to ^{18}F-NaF uptake findings, aortic arteries had higher HU_{mean} values for female patients compared to male patients. The possible explanation for that could be due to the mechanism of calcification in larger arteries in which calcification would be more visible.

6.4.3.2 Cardiovascular HU_{mean} and age

In regard to age, the results describe a rise in HU_{mean} value measured from coronary arteries and aortic artery with age, as shown in Figure 6.18 and Figure 6.19. The current study found that age was positively correlated with vascular HU_{mean} values at most of the ROIs. Consistent with findings published by Allison *et al*. [188], which demonstrated age-associated coronary calcification measured by EBCT, which showed increased HU values at the calcified arteries with age. In that study, quantitative values measured from CT showed a significant correlation between age and Coronary Calcification Score (CCS) for both genders. The positive trend between age and CCS in that study was twice that of the next most significant correlation between CCS and body fat. Additionally, Allison *et al*. [188] noted that patients under 45 years old were not exhibiting any calcified plaques, and their EBCT test was negative.

On the other hand, Hwaida *et al*. [191] investigated the presence of vascular calcifications for 40 AKU patients who underwent non-contrast CT scans. In that study, it was found that the prevalence of vascular calcifications was significantly increased with age. These results supported the findings in this study showing a clear positive trend between non-contrast CT results and age in AKU patients. In general, age is one of the cardiovascular risk factors which cause calcium deposition in the arterial wall.

6.4.4 Relationship between ^{18}F-NaF uptake and calcification noted in CT images

The current study found that the results of PET and CT may vary such that the abnormality may be only visible in either PET or CT image depending on the calcification stage, as shown in Figure 6.25 and Figure 6.27. In the early calcification stage, ^{18}F-NaF uptake was noted in the PET image with no apparent calcification in the CT image. The ^{18}F-NaF activity was pointed out in some ROI, with no abnormal calcification signs observed in the CT image, as shown in Figure 6.25. In contrast, in stable macrocalcification, evident of vascular calcification was noted in the CT image without unusual ^{18}F-NaF activity in the PET image, as shown in the AA area in Figure 6.27. In advanced cases with very severe calcified plaques, intense ^{18}F-NaF activity was noted in the affected regions overlaying and adjacent with existing extensive

calcification in the CT image, which was observed in fused the ^{18}F-NaF PET/CT image as abnormal tracer distribution having bone-like intensity in calcified vessels.

These results suggested that the relationship between CT and PET images may not always be perfectly matched and correlated. This finding broadly supports the work of other studies in this area, demonstrating the mismatch between ^{18}F-NaF PET and CT images [148,149,155,157]. In fact, the mismatch between the two modalities might be expected due to the calcification stage, whether it is active or inactive. This finding was previously reported by Thang *et al.* [157] who evaluated ^{18}F-NaF PET/CT images to investigate vascular calcification in carotid plaques. The correlation between ^{18}F-NaF uptake and HU was tested in that study, and they found no clear relationship between the TBR_{max} and HU_{mean} ($P > 0.05$). Also, Derlin *et al.* [155] did not find a significant correlation between SUV_{max} measured in PET images and the calcification score measured from the CT scan. In another study done by Dwech *et al.* [148], he noted that 41% of his patients with high coronary calcium score (CAC >1000), had no significant increased ^{18}F-NaF activity; in addition, high activity has been observed in an area remote of calcification on CT image. In contrast, Li *et al.* [147] reported a strong correlation between ^{18}F-NaF and CT calcification in most of the coronary and aortic arteries, except in the abdominal aorta.

The previous results supported the findings in the current chapter which can be explained by the fact that ^{18}F-NaF binds to active microcalcification areas, which can be observed in PET images; in contrast, in CT image, inactive macrocalcification and stable calcification can be detected. Therefore, due to the difference in the calcification stages, mismatch results between PET and CT would be possible and expected. Irkle *et al.* [149] also reported that ^{18}F-NaF PET/CT imaging could distinguish between microcalcification and macrocalcification areas in carotid plaques. In that study, ^{18}F-NaF was strongly dependent on the surface area of calcification, as large microcalcification areas showed high ^{18}F-NaF uptake, in contrast to small macrocalcification areas.

6.5 Summary

Ochronotic pigment can affect all human tissues, including blood vessels causing calcium deposition within the cardiovascular system. This research sheds new light on detecting early stage of vascular calcification in AKU patients using advanced molecular imaging modalities. ^{18}F-NaF is a promising imaging biomarker for *in vivo* quantification and identification of calcified vessels which could be associated with ochronosis in AKU patients. ^{18}F-NaF PET/CT identified the presence and the extent of calcium deposition in the coronary arteries in SONIA 2 patients without adding extra cost or radiation. Additionally, ^{18}F-NaF PET/CT could distinguish between ongoing/active calcification process and those stable or structural calcification which may be established months or years before. In PET images, active and ongoing calcification was detected as an area of increased ^{18}F-NaF uptake, while in the CT image, stable and inactive calcified vessel was detected as a dense area having bone-like intensity.

Overall, this study considers a snapshot of the key characteristics of cardiac calcification in AKU patients, which would guide further longitudinal study. Identifying cardiac involvements at its early stage would educate the patients and clinical staff about symptoms and regular follow-up care. Future studies investigating cardiovascular involvements in AKU patients would be very interesting to develop a deeper understanding of the relationships between ochronosis and cardiovascular calcification in AKU patients.

6.6 Limitations

Several limitations to this study need to be acknowledged. First, the ^{18}F-NaF PET/CT image was scanned for detecting abnormal bone and joint regions and not for cardiac investigation; therefore, the images were not optimised with ECG gating. The degree of calcification may significantly be underestimated due to respiratory and cardiac motion, which can easily blur the coronary and aortic calcifications. Second, intraobserver and interobserver reliability and agreement were not tested due to time limitations. Third, this study was limited by the absence of non-AKU controls; therefore, the comparison between AKU patients and healthy patients without

coronary artery disease was not tested. Finally, since there are many cardiac risk factors such as obesity, smoking, dyslipidaemia, diabetes, cholesterol levels, and hypertension, the impact of these factors in AKU patients was not investigated. These traditional risk factors may increase calcium deposition in the vessels, which might influence the ^{18}F-NaF uptake in PET images and HU in CT images.

6.7 Future work

In terms of directions for future research, a number of studies are strongly recommended. It would be important to correlate the semiquantitative results from ^{18}F-NaF PET/CT scan with different clinical outcomes such as HGA level, ECG changes, and cardiac ultrasound, which could provide a better link between increased tracer uptake and/or present of calcium in the vascular wall and the disease progression in AKU patients. It is strongly suggested that intraobserver and interobserver reliability is tested in the future studies, to support the methods which have been used here. It would be intresting to compare the cardiovascular structures of non-AKU patients with AKU patients to better understand the natural history of AKU. Also, a larger sample size at each age group would help to determine the peak age where the microcalcification could be built up in AKU patients. Another possible area of future research would be to investigate the impact of nitisinone in calcified vessels for SONIA 2 patients. The longitudinal changes in cardiovascular quantitative values over a long time period would be an interesting area to consider in order to assess disease progression and early treatment response.

6.8 Conclusion

This chapter has shown:

- That the presence and extent of calcium deposition in the cardiac vessels can be detected by ^{18}F-NaF PET/CT scan without adding extra cost or radiation to AKU patients.

- Increased and intense focal tracer uptake at the cardiovascular regions in ^{18}F-NaF PET images reflected the early stage of microvascular calcification in AKU patients.
- The same mechanism that underlies the ^{18}F-NaF uptake in osseous tissue also occurs in the calcified vessels due to the strong biological similarities between vascular calcification and bone formation.
- Although the SUV_{max} and TBR_{max} at the average four coronary arteries increased from the youngest age group patients to the eldest age group of patients, it was statistically significant between the 50s and 60s age groups of patients only.
- An inactive calcified vessel identifies as an area of high HU value in CT image reflecting structural macrocalcification and plaque stability.
- HU_{mean} values were positively associated with age in most of the cardiovascular ROIs.
- There were no statistically significant differences in HU values and ^{18}F-NaF uptake between males and females across most of the cardiovascular ROIs in AKU patients was found.

7 General Discussion and Conclusion

This is the final chapter of the thesis, which will draw together the implications of the findings from the studies presented here. It will provide an overview of the main findings from the previous chapters in the light of the literature reviewed and the current knowledge, and examine and interpret key methodological strengths and limitations. This discussion chapter will show the unique contributions made by this thesis, reflect on the overall implications of these findings for future research and practice, and finally present an overall conclusion.

7.1 Discussion

This thesis has addressed four main questions, each investigated in one of the main result chapters. The specific questions are:

- Whether ^{18}F-NaF PET/CT scan can be used to assess and identify early regional bone formation for patients with AKU by measuring HU_{mean} from CT and SUV_{max} from PET.
- Whether there is a link between structural disc changes in MRI and increased ^{18}F-NaF uptake in PET images measured from lumbar disc units.
- Whether ^{18}F-NaF PET/CT can be used to assess the disease progression and evaluate the treatment response in the long term.
- Whether ^{18}F-NaF PET/CT can be used as a cardiovascular imaging biomarker to identify early cardiovascular calcification and assess future cardiovascular risk in AKU patients.

The work presented in this thesis demonstrates the most comprehensive imaging investigation for patients with AKU to date, which has played a key part in growing our awareness of the natural history of AKU. In this thesis, the quantitative data achieved from ^{18}F-NaF PET/CT images contributes in several ways to our understanding of AKU disease progression. The thesis was undertaken to investigate the utility of ^{18}F-NaF PET/CT as a molecular imaging biomarker for detecting and identifying the early stages of bone turnover, early disc degeneration, early stages of microvascular calcification, and to evaluate the therapy response in the long term for patients with AKU using novel assessment methods.

With respect to the first research question, it was found that ^{18}F-NaF PET/CT scans can be used as promising imaging technique to identify early musculoskeletal involvements in the lumbar spine and hip regions in AKU patients. In Chapter 3, low bone density was detected in the lower spine and hip regions from the CT images, indicating that there is a low bone density disorder in AKU patients. Also, high ^{18}F-NaF uptake was identified at spine and hip regions in AKU, indicating active bone turnover at the affected bone area. Although positive focal ^{18}F-NaF uptake and dense lesions were visibly observed in PET/CT images, visual assessment is a subjective assessment method which mainly depends on the opinion of the assesser. Therefore, Chapter 3 tested the use of non-subjective PET/CT assessment methods, which clearly defined the boundary between the normal distribution of radiotracer and increased uptake in the skeleton. The ROI has been quantified to accurately evaluate the change in ^{18}F-NaF uptake that may not clearly be detected by qualitative visual inspection. Although there are a number of PET quantitative methods, in this thesis, the data have been analysed and quantified using SUV; the most straightforward PET semiquantitative method. SUV reliably helped to accurately quantify active bone lesions in the lower spine and hip regions. Low SUV_{max} values and low HU_{mean} in the lumbar vertebrae and head of the femur indicated bone loss which may be associated with ochronosis in AKU patients. Comparing the results of AKU with the literature showed that AKU patients had higher SUV values than the general population. This could support the hypothesis that AKU patients have more active bone turnover than the general population.

On the question of gender effects, this study found that there was no significant difference between the quantitative values measured from males and females, suggesting that gender has no significant effect on bone ^{18}F-NaF uptake nor bone density values in AKU patients. On the other hand, lumbar HU and SUV values significantly decreased with age, indicating reduced active bone turnover and decreased bone density and bone perfusion in AKU patients which is likely to also be associated with ochronosis.

Regarding the correlation between HU and T-score values, in Chapter 3, a strong correlation was noted in the lumbar spine and hip regions. Thus, it can be suggested that HU values can be used to estimate BMD. Chapter 3 demonstrated that a CT scan

in a hybrid PET/CT system could be used as a valuable diagnostic tool to predict bone and bone-related disorders associated with low bone density. In fact, the quantitative data extracted from CT images was employed to predict osteoporosis using data which was available but rarely used for that purpose. The methods which have been proposed in Chapter 3 to measure regional bone density is a novel quantitative method that is generalisable. This method can be adopted for any other group of patients without exposing them to extra radiation when CT scans have been performed for other reasons. This would help to predict early fracture risk to high risk patients. The substantial evidence in the literature supports that HU measurements generated from diagnostic CT images may be utilised as a useful tool for determining regional bone density, therefore estimating early fracture risk. As pointed out, spinal DEXA measurements are influenced by severe disc calcification in AKU patients, and the results may not reflect a true representation of bone density. Some evidence suggests that quantitative CT can be used instead of DEXA to assess spinal density, although further work using this technique is required to confirm this finding. At this time, it may too soon to say that HU values can be a replacement for the gold standard bone mineral density measurements, which is clinically generated from the DEXA scan. Furthermore, the results in Chapter 3 provided a moderate correlation between lumbar HU and SUV values, suggesting further investigation to approve or reject the correlation between ^{18}F-NaF PET and CT findings.

The second question in this study sought to determine the link between structural disc changes and molecular changes in the intervertebral disc area. In Chapter 4, lumbar disc degeneration was identified from functional ^{18}F-NaF PET/CT images and anatomical MR images in order to investigate the relationships between the ^{18}F-NaF uptake and morphological intervertebral disc changes in the lumbar spine. The study was designed to detect disc degeneration by measuring SUV_{max} and Pfirrmann score for lumbar disc units from PET and MRI scans, respectively. Chapter 4 shows that high-quality molecular imaging modalities such as PET/CT and MRI may help to identify early and active bony changes and intervertebral disc degeneration before it progresses to severe symptomatic arthritis. Usually, advanced morphological bone changes caused by ochronosis and pigment deposition in the disc area may not be observed clearly by plain radiography, as most of these features appear in the late stages. The results of Chapter 4 reveal that lumbar intervertebral disc degeneration in

AKU patients was strongly associated with increased SUV_{max} in PET images and a high Pfirrmann score in MR images. Although male AKU patients had a statistically higher Pfirrmann score than the female patients at most lumbar DVUs, gender had no significant correlation to the ^{18}F-NaF uptake across the lumbar disc regions, similar to that noted in the lumbar vertebrae bodies in Chapter 3.

With regard to the age effect, the results in Chapter 4 indicated a strong correlation between age and Pfirrmann score in MRI. The most interesting finding to emerge from Chapter 4 is that the values of SUV_{max} across the lumbar DVUs increased gradually with age followed by a decrease in the later years. These results are likely to be related to degenerative disc disease progression. There is a high probability that disc calcification increased due to ochronotic pigment deposition within the cartilage, resulting in increased calcium hydroxyapatite deposition in the IVD area and therefore increased SUV values. In the early disc calcification stages, more binding sites would be available to bind with ^{18}F-NaF radiotracer; therefore, high SUV_{max} would be detected. As the disc become more calcified over time, it becomes more stable, and less binding sites will be available; therefore, low SUV_{max} would be detected in elderly patients.

In addition, Chapter 4 highlights that several advanced cases had high Pfirrmann scores but low SUV_{max} values. These observations suggest that these advanced cases probably had fusion of discs at the interbody lumbar level with inactive calcification at DVU. The overlap between disease progression and age leads to fewer free binding sites, due to complete disc calcification, inactive calcification, and/or vertebral fusion at that stage. These factors may explain the relative correlation between low SUV_{max} values in PET scan and high Pfirrmann scores in MRI.

Looking at the results from Chapter 3 and Chapter 4, it is apparent that the SUV_{max} across all lumbar vertebrae levels and lumbar DVUs of the male group was slightly higher than the female group; however, it is somewhat surprising that these differences were not statistically significant at most of the individual ROIs. It was expected to identify higher values in male patients compared to female patients. In the general population, males are more likely to have intervertebral disc degeneration, which appears with greater frequency than in females [177]. A possible explanation for this

might be that females generally weigh less than males, which will cause less pressure on the lower spine region. This non-significant result in AKU patients might be related to menopause triggers in women, and physical inactivity in men which might have an equal effect on losing bone density and developing osteoporosis in both genders. In general, degenerative disc changes can be observed in both genders in the literature.

A note of caution is also due here in this thesis since there was no comparison to a non-AKU control group. The ^{18}F-NaF uptake in the bony vertebrae and IVD from Chapter 3 and Chapter 4 described ochronotic arthropathy in AKU patients; these results demonstrating the biochemical alterations of the disease, which cause the active bone formation and therefore increase new hydroxyapatite for $^{-18}$F ion to bind to, thus increase SUV measurements in the bone and disc area. It can be assumed that the ochronotic pigment deposition within IVD areas could be the major factor causing disc calcification in AKU patients, increasing SUV values in the disc area. Also ochronotic pigment could alter the bone matrix and interfere with bone metabolism causing bone turnover and loss in bone density. Although AKU data in this thesis was not statistically compared with non-AKU patients, the initial observations from literature and unpublished data (Alawadhi- non-AKU patients from Kuwait) showed that non-AKU patients tend to have lower SUV values in bony vertebrae and IVD areas than AKU patients. These findings suggest that AKU patients are more likely to have advanced spinal arthropathy than the general population. What is now needed is a further study to establish whether these differences between AKU and the general population are statistically significant or not.

The third question in this research was whether ^{18}F-NaF PET/CT can be used to assess the progression of the disease and assess the response of treatment in the long term for AKU patients. Chapter 5 was designed to determine the effect of nitisinone in AKU patients over four years by evaluating the changes in HU_{mean} and SUV_{max} values measured from lumbar vertebrae and intervertebral disc units. At the beginning of the SONIA 2 trial, nitisinone had not yet been licensed to treat AKU, so this study aimed to detect the efficacy and effectiveness of nitisinone in AKU patients. Investigating the changes in bone and cartilage tissues over the years was one of the critical points which would strongly confirm or reject the efficacy of nitisinone in ochronotic arthropathy. Prior to the studies in this thesis, it was difficult to make an accurate

prediction about how nitisinone can treat or prevent the ochronotic arthropathy for those AKU patients treated with nitisinone for four years and whether there is a different response between AKU patients.

The results in Chapter 5 shows no clear trend in HU_{mean} nor SUV_{max} over the visits in neither the treatment nor non-treatment AKU groups. This also accords with SONIA 2 final analysis scans results, which showed that there were no significant differences in scintigraphy, MRI nor DEXA results between treatment and non-treatment groups. Comparison of the findings in this thesis with those of the final trial analysis confirms that nitisinone may not have direct impact on bone or cartilage. It was surprising that the treatment group trends did not differ significantly from those in the non-treatment groups. The reason for this is not clear, but it may be related to several possibilities. First, nitisinone might slow the progression of the ochronosis by stopping further pigmentation, but it is unlikely to reverse ochronosis or treat the severe damage which has been caused by ochronosis, specifically in the lumbar spine. Second, it is probable that the chosen spinal regions may not represent the overall bone change among the whole skeletal sites.

Although Chapter 5 did not confirm the positive impact of nitisinone in the spine for AKU patients, it enhanced the understanding of disease progression over four years. The results raise the possibility proposed that four years of taking nitisinone may not be long enough to reveal bone and cartilage changes in the spinal tissues. Since the biochemical efficacy had been confirmed previously by noting significant plasma and urine HGA reductions after receiving oral administration of nitisinone, it is probable that the clinical efficacy needs more time to be noticeable in bone. Therefore, it is likely that further investigation is required in order to assess the longer-term impacts of nitisinone in reducing arthritis features for AKU patients to establish the effectiveness of treatment.

Cardiac and vascular calcifications were incidentally noted on ^{18}F-NaF PET/CT scans in AKU patients who enrolled in SONIA 2 trial while evaluating bone and joint involvements in the previous studies. From this point, the aim of last study was to identify and quantify early cardiovascular calcification, allowing more in-depth insight into cardiac involvement in AKU patients without adding another dose of ionising

radiation to those patients. Chapter 6 found that ^{18}F-NaF PET/CT is a potential application which can provide novel function and structure information about vessels at no additional cost. ^{18}F-NaF was found to be a promising imaging biomarker for identifying and quantifying calcified vessels which could be associated with ochronosis in AKU patients. The vascular calcification appeared as a dense area in CT scans and focal hot spot area in ^{18}F-NaF PET images. In recent years, ^{18}F-NaF has been proposed as a sensitive imaging marker to identify early vascular calcification and has been developed for non-invasive coronary artery assessment in a promising way. This is possibly due to the strong biological similarities between bone formation and vascular calcification. The main structural component in both events is hydroxyapatite. Thus, this could likely mean that the mechanism of ^{18}F-NaF absorption by osseous tissues is also found in the calcified vessels.

In Chapter 6, the degree of coronary and aortic calcification was quantified by measuring SUV_{max}, TBR_{max}, and HU_{mean} values from ^{18}F-NaF PET/CT images in order to define early features of cardiovascular ochronosis in main coronary and aortic arteries. High SUV_{max}, TBR_{max}, and HU_{mean} values were detected from cardiovascular regions indicating vascular calcification in AKU patients. Although the coronary and aortic stenosis mechanism in AKU patients remains unclear, previous studies have identified pigment accumulation in various body tissues, including cardiovascular system tissues. The pigmentation pattern in the regions of higher pressures or turbulence indicates significant microvascular damage which introduces an optimal focus for HGA deposition. Damage linked to pigment tends to predispose the tissue to dystrophic calcification, even if these processes are not well understood. The most often diagnosed cardiac abnormality in AKU patients includes calcified aortic stenosis, for which patients often need a valve replacement. Early identification of cardiovascular calcification in AKU patients would prevent severe symptomatic cardiac disease and surgical complications. Therefore, early detection of these calcified vessels using a sensitive microcalcification marker would significantly benefit this area of research.

The findings in Chapter 6 indicate that neither gender nor age correlated directly to the degree of cardiovascular calcification in AKU patients. This outcome is contrary to the theoretical notion indicating that age is one of the significant cardiovascular risk

factors, which is most likely linked with the severity of cardiovascular calcification. Several possible reasons can explain this finding. In the early stage of microvascular calcification, calcium starts to build up in the vessels wall, resulting in increased calcium hydroxyapatite crystals. Therefore, more $^{-18}$F binding sites would be available in the vessels to bind with ^{18}F-NaF radiotracer. In the case of active and ongoing vascular calcification, high SUV_{max} and TBR_{max} values would be expected. By time, active vascular calcification becomes inactive and stable, less binding sites are available resulting in low SUV_{max} values. Another possible explanation for this is that ^{18}F-NaF cannot effectively identify macrocalcification because in the advanced calcification phase, hydroxyapatite is distributed deeply within vascular layers, and ^{18}F-NaF cannot penetrate deeper into vascular tissues. This can explain the statistically significant differences in the average coronary arteries ^{18}F-NaF uptake between the 50s and 60s age group patients only. These interesting results suggest that the level of cardiac vessel calcification is strongly related to individual cases in AKU patients. Therefore, it is indicated that the level of calcified deposition on the vascular walls in AKU patients depends on disease progress and disease stage.

The study done in Chapter 6 adds to the growing body of research by revealing a sensitive technique which could prevent the evolution of cardiac events by detecting early microvascular calcification using ^{18}F-NaF radiotracer. The novel assessment methods used here to analyse the main cardiac vessels in AKU patients may be applied to other patients elsewhere who underwent ^{18}F-NaF PET/CT for other reasons that include the heart area. In fact, ^{18}F-NaF PET/CT scans can be used for the retrospective and prospective interpretative investigation of calcified vessels and predict the early stage of cardiovascular calcification without additional radiation exposure or cost. Additionally, other bone radiotracers such as ^{99m}Tc-MDP can also be adapted to identify vascular calcification for those patients who had ^{99m}Tc-MDP or ^{99m}Tc-HMDP bone scintigraphy instead of ^{18}F-NaF PET/CT.

7.2 Limitations

The generalisability of this thesis is subject to a number of certain limitations. First, being limited to only one or two skeletal sites, this study lacks general progression for the entire skeleton. It is possible that the changes in ^{18}F-NaF uptake and bone density

in the lower spine does not accurately reflect the changes in the whole skeleton. Second, the most significant limitation lies in the fact that interobserver and intraobserver reliability of the measurement values have not been tested due to limited time and clinical collaboration. There are obvious difficulties in accepting the reliability of self-reported information or single observer findings. Third, ^{18}F-NaF PET/CT images were not designed to be used for cardiac investigation; therefore, the images have not been optimised by ECG gating or motion correction. Another major source of uncertainty in the data used to assess the progression of the disease and evaluate the response to treatment in Chapter 5 is that not all of the patients had all five serial scans making those unmeasured data sources of error. Finally, the thesis is also limited by the lack of a control non-AKU group; therefore, statistically comparing the values and evaluating the differences between the general population and AKU patients was not possible. Notwithstanding these limitations, this work offers valuable insights into the use of novel ^{18}F-NaF PET/CT semiquantitative methods.

7.3 Future work

Despite these promising results, which were presented within this thesis, several questions remain unanswered at present. Therefore, it is recommended that further research be undertaken in the following areas: First, clinical investigation using a larger sample size would be required to support the findings which were reported in this thesis. Second, the proposed methods which have been introduced here in this thesis needs to be applied to different skeletal sites such as the cervical spine, thoracic spine, shoulder or knee. It would be interesting to know the results from other body sites and compare them with lumbar and hip results. Third, it would be very important to test the interobserver and intraobserver reliability of the measurement values. In fact, good and excellent interobserver and intraobserver agreement would strongly be relevant in deciding the correct prognosis, treatment, and follow up strategy. Fourth, investigating the longitudinal changes in cardiovascular measurements for SONIA 2 patients is an important area for future research to evaluate disease progression over time. Finally, it would also be interesting to know the bone and joint progression over time in the general population and compare it with AKU patients in the SONIA 2 trial. Therefore, an additional investigation would be designed to examine the changes in ^{18}F-NaF PET/CT quantitative values for non-AKU patients over time. This

longitudinal comparison between non-AKU and AKU patients would be useful as it is highly expected that the non-AKU group will show the typical changes in bone density and ^{18}F-NaF uptake over the years, while the AKU patients will show the disease progression.

7.4 Conclusion

In conclusion, this thesis contributes significantly toward the validation of ^{18}F-NaF PET/CT as a sensitive and accurate molecular imaging biomarker for identifying and quantifying bone, disc and cardiovascular involvements in patients with AKU. The present studies support further investigations, which convey the metabolism of ochronotic arthropathy and cardiovascular ochronosis in patients with AKU. These studies establish a quantitative framework for detecting early bone turnover, early disc calcification and early microvascular calcification in AKU patients. Although the data presented here have not confirmed the positive effect of nitisinone in the spine for AKU patients, it enhanced our understanding of the natural history of AKU. This new understanding should help to improve predictions in the disease progression and the impact of therapy in AKU patients.

Furthermore, this thesis proposes novel ^{18}F-NaF PET/CT semiquantitative imaging methods using widely available data that is rarely used to identify co-existing pathology without additional radiation exposure or cost. These applications could serve as diagnostic tools for detecting regional bone density and early cardiovascular calcification when ^{18}F-NaF PET/CT is undertaken for other purposes, notifying and guiding the clinicians to initiate additional investigation on those who otherwise are not suspected of metabolic bone or cardiac disorders. Future investigations are required to confirm and validate the findings and build up the full picture of the correlation between the radioradiographic quantitative results and other clinical findings.

8 References

1. Reddy, O. J., Gafoor, J. A., Suresh, B. & Prasad, P. O. Alkaptonuria with review of literature. *Journal of Dr. NTR University of Health Sciences* **3**, 125–129 (2014).
2. Taylor, A. M., Preston, A. J., Paulk, N. K., Sutherland, H., Keenan, C. M., Wilson, P. J. M., Wlodarski, B., Grompe, M., Ranganath, L. R., Gallagher, J. A. & Jarvis, J. C. Ochronosis in a murine model of alkaptonuria is synonymous to that in the human condition. *Osteoarthritis and Cartilage* **20**, 880–886 (2012).
3. Ranganath, L. R., Jarvis, J. C. & Gallagher, J. A. Recent advances in management of alkaptonuria (invited review; Best practice article). *Journal of Clinical Pathology* **66**, 367–373 (2013).
4. Fisher, A. A., Medicine, G. & Hospital, T. C. Alkaptonuric Ochronosis with Aortic Valve and Joint Replacements and Femoral Fracture A Case Report and Literature Review. *Clinical medicine & research* **2**, 209–215 (2004).
5. Mannoni, A., Selvi, E., Lorenzini, S., Giorgi, M., Airò, P., Cammelli, D., Andreotti, L., Marcolongo, R. & Porfirio, B. Alkaptonuria, Ochronosis, and Ochronotic Arthropathy. *Seminars in Arthritis and Rheumatism* **33**, 239–248 (2004).
6. Raja Reddy, D. & Prasad, V. Alkaptonuria presenting as lumbar disc prolapse: Case report and review of literature. *Spinal Cord* **36**, 523–524 (1998).
7. Phornphutkul, C., Introne, W. J., Perry, M. B., Bernardini, I., Murphey, M. D., Fitzpatrick, D. L., Anderson, P. D., Huizing, M., Anikster, Y., Gerber, L. H. & Gahl, W. A. Natural History of Alkaptonuria. *New England Journal of Medicine* **347**, 2111–2121 (2002).
8. Milch, R. A. Studies of Alcaptonuria: Inheritance of 47 Cases in Eight Highly Inter-related Dominican Kindreds. *American journal of human genetics* **12**, 76–85 (1960).
9. Zatková, A., De Bernabé, D. B., Poláková, H., Zvarík, M., Feráková, E., Bosák, V., Ferák, V., Kádasi, L. & de Córdoba, S. R. High frequency of alkaptonuria in Slovakia: evidence for the appearance of multiple mutations in HGO involving different mutational hot spots. *American journal of human*

genetics **67**, 1333–9 (2000).

10. Rathore, F. A., Ayaz, S. B. & Mansoor, S. N. Ochronotic arthropathy: Two case reports from a developing country. *Clinical Medicine Insights: Arthritis and Musculoskeletal Disorders* **9**, 15–20 (2016).
11. Albers, S. E., Brozena, S. J., Glass, L. F., Fenske, N. A. & Tampa, M. D. Alkaptonuria and ochronosis : Case report and review. *journal of the american academy of dermatology* **27**, 609–614 (1992).
12. Hamdi, N., Cooke, T. D. & Hassan, B. Ochronotic arthropathy: case report and review of the literature. *International orthopaedics* **23**, 122–125 (1999).
13. Emel, E., Karago, F. & Seyithanog, M. H. Alkaptonuria With Lumbar Disc Herniation A Report of Two Cases. *Spine Journal* **25**, 2141–2144 (2000).
14. Aquaron, R. Alkaptonuria: A very rare metabolic disorder. *Indian Journal of Biochemistry and Biophysics* **50**, 339–344 (2013).
15. Ventura-Ríos, L., Hernández-Díaz, C., Gutiérrez-Pérez, L., Bernal-González, A., Pichardo-Bahena, R., Cedeño-Garcidueñas, A. L. & Pineda, C. Ochronotic arthropathy as a paradigm of metabolically induced degenerative joint disease. A case-based review. *Clinical rheumatology* **35**, 1389–1395 (2016).
16. Al-Sbou, M. & Mwafi, N. Nine cases of Alkaptonuria in one family in southern Jordan. *Rheumatology International* **32**, 621–625 (2012).
17. Al-Sbou, M., Mwafi, N. & Lubad, M. A. Identification of forty cases with alkaptonuria in one village in Jordan. *Rheumatology International* **32**, 3737–3740 (2012).
18. Gallagher, J. A., Ranganath, L. R. & Zatkova, A. Alkaptonuria. *Brenner's Encyclopedia of Genetics: Second Edition* 71–75 (2013) doi:10.1016/B978-0-12-374984-0.00030-9.
19. Ranganath, L. R. & Cox, T. F. Natural history of alkaptonuria revisited: Analyses based on scoring systems. *Journal of Inherited Metabolic Disease* vol. 34 1141–1151 (2011).
20. Gallagher, J. A., Dillon, J. P., Sireau, N., Timmis, O. & Ranganath, L. R. Alkaptonuria: An example of a 'fundamental disease'-A rare disease with important lessons for more common disorders. *Seminars in Cell and Developmental Biology* **52**, 53–57 (2016).
21. Ranganath, L. R., Norman, B. P. & Gallagher, J. A. Ochronotic pigmentation is caused by homogentisic acid and is the key event in alkaptonuria leading to

the destructive consequences of the disease—A review. *Journal of Inherited Metabolic Disease* **42**, 776–792 (2019).

22. Bayindir, P., Yilmaz Ovali, G., Pabuşçu, Y., Temiz, C. & Duruoz, T. Radiologic features of lumbar spine in ochronosis in late stages. *Clinical Rheumatology* **25**, 588–590 (2006).
23. Phatak, S. V, Kolwadkar, P. K., Hemnani, T. J., Phatak, M. S. & Hemnani, J. T. Pictorial essay : Alkaptonuria. *Ind. J. Radiol. Imagnd. J. Radiol. Imag* 2004–2007 (2006).
24. Keller, J. M., Macaulay, W., Nercessian, O. A. & Jaffe, I. A. New developments in ochronosis: Review of the literature. *Rheumatology International* **25**, 81–85 (2005).
25. Ffolkes, L. V., Brull, D., Krywawych, S., Hayward, M. & Hughes, S. E. Aortic stenosis in cardiovascular ochronosis. *Journal of Clinical Pathology* **60**, 92–93 (2007).
26. Stewart, B. F., Siscovick, D., Lind, B. K., Gardin, J. M., Gottdiener, J. S., Smith, V. E., Kitzman, D. W. & Otto, C. M. Clinical factors associated with calcific aortic valve disease. *Journal of the American College of Cardiology* **29**, 630–634 (1997).
27. Hannoush, H., Introne, W. J., Chen, M. Y., Lee, S. J., O'Brien, K., Suwannarat, P., Kayser, M. A., Gahl, W. A. & Sachdev, V. Aortic stenosis and vascular calcifications in alkaptonuria. *Molecular Genetics and Metabolism* **105**, 198–202 (2012).
28. Wauthy, P., Seghers, V., Mathonet, P. & Deuvaert, F. E. Cardiac ochronosis: not so benign. *European Journal of Cardio-thoracic Surgery* **35**, 732–733 (2009).
29. Kocyigit, H., Gurgan, A., Terzioglu, R. & Gurgan, U. Clinical, radiographic and echocardiographic findings in a patient with ochronosis. *Clinical rheumatology* **17**, 403–406 (1998).
30. Kragel, A. H., Lapa, J. A. & Roberts, W. C. Cardiovascular findings in alkaptonuric ochronosis. *American Heart Journal* **120**, 1460–1463 (1990).
31. Gaines, J. J. & Pai, G. M. Cardiovascular ochronosis. *Archives of Pathology and Laboratory Medicine* **111**, 991–994 (1987).
32. Atalay, A., Gocen, U., Basturk, Y., Kozanoglu, E. & Yaliniz, H. Ochronotic involvement of the aortic and mitral valves in a 72-year-old man. *Texas Heart*

Institute Journal **42**, 84–86 (2015).

33. Roser, M., Möller, J., Komoda, T., Knosalla, C. & Stawowy, P. Alkaptonuric aortic stenosis. *European Heart Journal* **29**, 444 (2008).
34. Pettit, S. J., Fisher, M., Gallagher, J. A. & Ranganath, L. R. Cardiovascular manifestations of Alkaptonuria. *Journal of Inherited Metabolic Disease* **34**, 1177–1181 (2011).
35. Zhao, B. H., Chen, B. C. & Zhang, Q. Osteoarthritis? Ochronotic arthritis! *Knee Surgery, Sports Traumatology, Arthroscopy* **17**, 778 (2009).
36. Taylor, A. M., Wlodarski, B., Prior, I. A., Wilson, P. J. M., Jarvis, J. C., Ranganath, L. R. & Gallagher, J. A. Ultrastructural examination of tissue in a patient with alkaptonuric arthropathy reveals a distinct pattern of binding of ochronotic pigment. *Rheumatology* **49**, 1412–1414 (2010).
37. Taylor, A. M., Boyde, A., Wilson, P. J. M., Jarvis, J. C., Davidson, J. S., Hunt, J. A., Ranganath, L. R. & Gallagher, J. A. The role of calcified cartilage and subchondral bone in the initiation and progression of ochronotic arthropathy in alkaptonuria. *Arthritis and Rheumatism* **63**, 3887–3896 (2011).
38. Ranganath, L. R., Khedr, M., Milan, A. M., Davison, A. S., Hughes, A. T., Usher, J. L., Taylor, S., Loftus, N., Daroszewska, A., West, E., Jones, A., Briggs, M., Fisher, M., McCormick, M., Judd, S., *et al.* Nitisinone arrests ochronosis and decreases rate of progression of Alkaptonuria: Evaluation of the effect of nitisinone in the United Kingdom National Alkaptonuria Centre. *Molecular Genetics and Metabolism* **125**, 127–134 (2018).
39. Sobi. Orfadin® (nitisinone) receives positive opinion from CHMP for treatment of AKU. *Swedish Orphan Biovitrum AB* https://www.sobi.com/en/press-releases/orfadinr-nitisinone-receives-positive-opinion-chmp-treatment-aku-1844542.
40. Sealock, R. R., Galdston, M. & Steele, J. M. Administration of Ascorbic Acid to an Alkaptonuric Patient. *Proceedings of the Society for Experimental Biology and Medicine* **44**, 580–583 (1940).
41. Wolff, J. A., Barshop, B., Nyhan, W. L., Leslie, J., Seegmiller, J. E., Gruber, H., Garst, M., Winter, S., Michals, K. & Matalon, R. Effects of ascorbic acid in alkaptonuria: alterations in benzoquinone acetic acid and an ontogenic effect in infancy. *Pediatric Research* **26**, 140–144 (1989).
42. De Haas, V., Carbasius Weber, E. C., De Klerk, J. B. C., Bakker, H. D., Smit,

G. P. A., Huijbers, W. A. R., Duran, M. & Poll-The, B. T. The success of dietary protein restriction in alkaptonuria patients is age-dependent. *Journal of Inherited Metabolic Disease* **21**, 791–798 (1998).

43. Morava, E., Kosztolányi, G., Engelke, U. F. H. & Wevers, R. A. Reversal of clinical symptoms and radiographic abnormalities with protein restriction and ascorbic acid in alkaptonuria. *Annals of Clinical Biochemistry* **40**, 108–111 (2003).
44. Anikster, Y., Nyhan, W. L. & Gahl, W. A. NTBC and alkaptonuria [8]. *American Journal of Human Genetics* **63**, 920–921 (1998).
45. Suzuki, Y., Oda, K., Yoshikawa, Y., Maeda, T. & Suzuki, T. A novel therapeutic trial of homogentisic aciduria in a murine model of alkaptonuria. *Journal of Human Genetics* **44**, 79–84 (1999).
46. Preston, A. J., Keenan, C. M., Sutherland, H., Wilson, P. J., Wlodarski, B., Taylor, A. M., Williams, D. P., Ranganath, L. R., Gallagher, J. A. & Jarvis, J. C. Ochronotic osteoarthropathy in a mouse model of alkaptonuria, and its inhibition by nitisinone. *Annals of the Rheumatic Diseases* **73**, 284–289 (2014).
47. Suwannarat, P., O'Brien, K., Perry, M. B., Sebring, N., Bernardini, I., Kaiser-Kupfer, M. I., Rubin, B. I., Tsilou, E., Gerber, L. H. & Gahl, W. A. Use of nitisinone in patients with alkaptonuria. *Metabolism: Clinical and Experimental* **54**, 719–728 (2005).
48. Introne, W. J., Perry, M. B., Troendle, J., Tsilou, E., Kayser, M. A., Suwannarat, P., O'Brien, K. E., Bryant, J., Sachdev, V., Reynolds, J. C., Moylan, E., Bernardini, I. & Gahl, W. A. A 3-year randomized therapeutic trial of nitisinone in alkaptonuria. *Molecular Genetics and Metabolism* **103**, 307–314 (2011).
49. European Commission. Success in DevelopAKUre: approval for Orfadin to treat patients with AKU. *ec.europa.eu* https://ec.europa.eu/info/news/success-developakure-approval-orfadin-treat-patients-aku-2020-oct-26_en.
50. AKU Clinical Trials. *akusociety.org* https://akusociety.org/aku-clinical-trials/ (2020).
51. Ranganath, L. R., Milan, a. M., Hughes, a. T., Dutton, J. J., Fitzgerald, R., Briggs, M. C., Bygott, H., Psarelli, E. E., Cox, T. F., Gallagher, J. a., Jarvis, J. C., van Kan, C., Hall, a. K., Laan, D., Olsson, B., *et al.* Suitability Of

Nitisinone In Alkaptonuria 1 (SONIA 1): an international, multicentre, randomised, open-label, no-treatment controlled, parallel-group, dose-response study to investigate the effect of once daily nitisinone on 24-h urinary homogentisic acid. *Annals of the Rheumatic Diseases* **1**, 1–6 (2014).

52. Cox, T., Psarelli, E. E., Taylor, S., Shepherd, H. R., Robinson, M., Barton, G., Mistry, A., Genovese, F., Braconi, D., Giustarini, D., Rossi, R., Santucci, A., Khedr, M., Hughes, A., Milan, A., *et al.* Subclinical ochronosis features in alkaptonuria: A cross-sectional study. *BMJ Innovations* **5**, 82–91 (2019).
53. Ranganath, L. R., Khedr, M., Vinjamuri, S. & Gallagher, J. A. Frequency, diagnosis, pathogenesis and management of osteoporosis in alkaptonuria: data analysis from the UK National Alkaptonuria Centre. *Osteoporosis International* (2020) doi:10.1007/s00198-020-05671-y.
54. Kobak, A. C., Oder, G., Kobak, Ş. ¸ Argin, M. & Inal, V. Ochronotic arthropathy: disappearance of alkaptonuria after liver transplantation for hepatitis B-related cirrhosis. *Journal of Clinical Rheumatology* **11**, 323–325 (2005).
55. Fogelman, I., Gnanasegaran, G. & van der wall, H. *radionuclide and hybrid bone imaging*. *Development* vol. 134 (2007).
56. Garg, S. Skeletal System. *Pediatric Pathology* 137–144 (2020) doi:10.1201/9781315382531-28.
57. Sophia Fox, A. J., Bedi, A. & Rodeo, S. A. The basic science of articular cartilage: Structure, composition, and function. *Sports Health* **1**, 461–468 (2009).
58. Manchikanti, L., Kaye, A. D., Falco, F. J. E. & Hirsch, J. A. *Essentials of interventional techniques in managing chronic pain*. *Essentials of Interventional Techniques in Managing Chronic Pain* (2018). doi:10.1007/978-3-319-60361-2.
59. Wang, F., Cai, F., Shi, R., Wang, X. H. & Wu, X. T. Aging and age related stresses: A senescence mechanism of intervertebral disc degeneration. *Osteoarthritis and Cartilage* **24**, 398–408 (2016).
60. Netter, F. H. Atlas of human anatomy. Philadelphia, PA: Saunders. *Elsevier* **548**, 547 (2006).
61. Standring, S. Gray's anatomy: the anatomical basis of clinical practice. (2005).

62. Athanasiou, L. S., Fotiadis, D. I. & Michalis, L. K. *Atherosclerotic Plaque Characterization Methods Based on Coronary Imaging*. (Academic Press, 2017).
63. Iaizzo, P. A. *Handbook of Cardiac Anatomy, Physiology, and Devices*. *Journal of Cardiac Surgery* vol. 21 (2006).
64. Acar, M. A., Erkocak, Ö. F., Aydin, B. K., Altan, E., Şenaran, H. & Elmadağ, N. M. Patients with black hip and black knee due to ochronotic arthropathy: Case report and review of literature. *Oman Medical Journal* **28**, 448–449 (2013).
65. Nas, K., Gür, A., Akdeniz, S., Çevik, R., Harman, M. & Saraç, A. J. Ochronosis: A case of severe ochronotic arthropathy. *Clinical Rheumatology* **21**, 170–172 (2002).
66. Hamdulay, S. S., Finegold, J., Boyer, L., Khanna, M., Akmal, M., Walker, A. & Kinderlerer, A. Clinical images: Magnetic resonance imaging appearance of alkaptonuria. *Arthritis and rheumatism* **64**, 129 (2012).
67. Sag, A. A., Silbergleit, R., Olson, R. E., Wilson, J. & Krishnan, A. T1 hyperintense disc in alkaptonuria. *Spine* **37**, 1361–1363 (2012).
68. Hamada, T., Yamamoto, T., Shida, J. I., Inokuchi, A. & Arizono, T. Subchondral insufficiency fracture of the femoral head in a patient with alkaptonuria. *Skeletal Radiology* **43**, 827–830 (2014).
69. Paul, R. & Ylinen, S. L. The 'whisker sign' as an indicator of ochronosis in skeletal scintigraphy. *Eur J Nucl Med* **18**, 222–224 (1991).
70. Cox, T. F. & Ranganath, L. A quantitative assessment of alkaptonuria: Testing the reliability of two disease severity scoring systems. *Journal of Inherited Metabolic Disease* **34**, 1153–1162 (2011).
71. Devauchelle-Pensec, V., D'Agostino, M. A., Marion, J., Lapierre, M., Jousse-Joulin, S., Colin, D., Chary-Valckenaere, I., Marcelli, C., Loeuille, D., Aegerter, P., Guis, S., Gaudin, P., Breban, M. & Saraux, A. Computed tomography scanning facilitates the diagnosis of sacroiliitis in patients with suspected spondylarthritis: Results of a prospective multicenter French cohort study. *Arthritis and Rheumatism* **64**, 1412–1419 (2012).
72. Mandl, P., Navarro-Compan, V., Terslev, L., Aegerter, P., van der Heijde, D., D'Agostino, M. a., Baraliakos, X., Pedersen, S. J., Jurik, a. G., Naredo, E., Schueller-Weidekamm, C., Weber, U., Wick, M. C., Bakker, P. a. C.,

Filippucci, E., *et al.* EULAR recommendations for the use of imaging in the diagnosis and management of spondyloarthritis in clinical practice. *Annals of the Rheumatic Diseases* 1–13 (2015) doi:10.1136/annrheumdis-2014-206971.

73. Jebaraj, I. Achilles tendon enthesopathy in ochronosis. *Journal of postgraduate medicine* **52**, 47–48 (2006).
74. Ferreira, M. E. G. & Scheinberg, M. A. Tendon involvement in patients with ochronosis: an ultrasonographic study. *Annals of the Rheumatic Diseases* **67**, 1784–1785 (2008).
75. Aliberti, G., Pulignano, I., Schiappoli, A., Minisola, S., Romagnoli, E. & Proietta, M. Bone metabolism in ochronotic patients. *Journal of Internal Medicine* **254**, 296–300 (2003).
76. Vinjamuri, S., Ramesh, C., Jarvis, J., Gallagher, J. & Ranganath, L. Nuclear medicine techniques in the assessment of alkaptonuria. *Nucl Med Commun* **32**, 880–886 (2011).
77. Lodder, M. C., De Jong, Z., Kostense, P. J., Molenaar, E. T. H., Staal, K., Voskuyl, A. E., Hazes, J. M. W., Dijkmans, B. A. C. & Lems, W. F. Bone mineral density in patients with rheumatoid arthritis: Relation between disease severity and low bone mineral density. *Annals of the Rheumatic Diseases* **63**, 1576–1580 (2004).
78. Yu, W., Glüer, C. C., Fuerst, T., Grampp, S., Li, J., Lu, Y. & Genant, H. K. Influence of degenerative joint disease on spinal bone mineral measurements in postmenopausal women. *Calcified Tissue International* **57**, 169–174 (1995).
79. Leone, A., Aulisa, L., Tamburrelli, F., Lupparelli, S. & Tartaglione, T. Ruolo della tomografia computerizzata e della risonanza magnetica nella valutazione della artropatia degenerativa delle facette articolari lombari. *Radiol Med* **88**, 547–552 (1994).
80. Weishaupt, D., Zanetti, M., Boos, N. & Hodler, J. MR imaging and CT in osteoarthritis of the lumbar facet joints. *Skeletal radiology* **28**, 215–219 (1999).
81. Lee, S., Chung, C. K., Oh, S. H. & Park, S. B. Correlation between bone mineral density measured by dual-energy X-ray absorptiometry and hounsfield units measured by diagnostic CT in lumbar spine. *Journal of Korean Neurosurgical Society* **54**, 384–389 (2013).
82. Schreiber, J. J., Anderson, P. A. & Hsu, W. K. Use of computed tomography

for assessing bone mineral density. *Neurosurgical Focus* **37**, E4 (2014).

83. Schreiber, J. J., Anderson, P. A., Rosas, H. G., Buchholz, A. L. & Au, A. G. Hounsfield units for assessing bone mineral density and strength: A tool for osteoporosis management. *Journal of Bone and Joint Surgery - Series A* **93**, 1057–1063 (2011).
84. Johnson, C. C., Gausden, E. B., Weiland, A. J., Lane, J. M. & Schreiber, J. J. Using Hounsfield Units to Assess Osteoporotic Status on Wrist Computed Tomography Scans: Comparison With Dual Energy X-Ray Absorptiometry. *Journal of Hand Surgery* **41**, 767–774 (2016).
85. Batawil, N. & Sabiq, S. Hounsfield unit for the diagnosis of bone mineral density disease: A proof of concept study. *Radiography* **22**, e93–e98 (2016).
86. Lee, D., Ohn, T., Chiang, Y., Quigley, G., Yao, G., Liu, Y. & Denis, C. L. Feasibility of Simultaneous Computed Tomographic Colonography and Fully Automated Bone Mineral Densitometry in a Single Examination. *Journal of Computer Assisted Tomography* **399**, 562–575 (2011).
87. Bruce, R. J. & Binkley, N. Opportunistic Screening for Osteoporosis Using Abdominal Computed Tomography Scans Obtained for Other Indications. *Bone* **158**, 588–595 (2013).
88. Pervaiz, K., Cabezas, A., Downes, K., Santoni, B. G. & Frankle, M. A. Osteoporosis and shoulder osteoarthritis: Incidence, risk factors, and surgical implications. *Journal of Shoulder and Elbow Surgery* **22**, e1 (2013).
89. Choi, M. K., Kim, S. M. & Lim, J. K. Diagnostic efficacy of Hounsfield units in spine CT for the assessment of real bone mineral density of degenerative spine: correlation study between T-scores determined by DEXA scan and Hounsfield units from CT. *Acta Neurochirurgica* **158**, 1421–1427 (2016).
90. Pfirrmann, C. W. A., Metzdorf, A., Zanetti, M., Hodler, J. & Boos, N. Magnetic resonance classification of lumbar intervertebral disc degeneration. *Spine* **26**, 1873–1878 (2001).
91. Griffith, J. F., Wang, Y. X. J., Antonio, G. E., Choi, K. C., Yu, A., Ahuja, A. T. & Leung, P. C. Modified Pfirrmann grading system for lumbar intervertebral disc degeneration. *Spine* **32**, 708–712 (2007).
92. Rim, D. C. Quantitative Pfirrmann Disc Degeneration Grading System to Overcome the Limitation of Pfirrmann Disc Degeneration Grade. *Korean Journal of Spine* **13**, 1 (2016).

93. Farshad-Amacker, N. A., Farshad, M., Winklehner, A. & Andreisek, G. MR imaging of degenerative disc disease. *European Journal of Radiology* **84**, 1768–1776 (2015).
94. Kettler, A. & Wilke, H. J. Review of existing grading systems for cervical or lumbar disc and facet joint degeneration. *European Spine Journal* **15**, 705–718 (2006).
95. Miyazaki, M., Hong, S. W., Yoon, S. H., Morishita, Y. & Wang, J. C. Reliability of a magnetic resonance imaging-based grading system for cervical intervertebral disc degeneration. *Journal of Spinal Disorders and Techniques* **21**, 288–292 (2008).
96. Jadvar, H., Desai, B. & Conti, P. S. Sodium 18F-fluoride PET/CT of bone, joint, and other disorders. *Seminars in Nuclear Medicine* **45**, 58–65 (2015).
97. Wong, K. K. & Piert, M. Dynamic Bone Imaging with 99mTc-Labeled Diphosphonates and 18F-NaF: Mechanisms and Applications. *Journal of Nuclear Medicine* **54**, 590–599 (2013).
98. Raynor, W., Houshmand, S., Gholami, S., Emamzadehfard, S., Rajapakse, C. S., Blomberg, B. A., Werner, T. J., Høilund-Carlsen, P. F., Baker, J. F. & Alavi, A. Evolving Role of Molecular Imaging with 18F-Sodium Fluoride PET as a Biomarker for Calcium Metabolism. *Current Osteoporosis Reports* **14**, 115–125 (2016).
99. Grant, F. D., Fahey, F. H., Packard, A. B., Davis, R. T., Alavi, A. & Treves, S. T. Skeletal PET with 18 F-Fluoride: Applying New Technology to an Old Tracer. *J Nucl Med* **49**, 68–78 (2008).
100. Blake, G. M., Frost, M. L., Moore, A. E. B., Siddique, M. & Fogelman, I. The Assessment of Regional Skeletal Metabolism: Studies of Osteoporosis Treatments Using Quantitative Radionuclide Imaging. *Journal of Clinical Densitometry* **14**, 263–271 (2011).
101. Omoumi, P., Mercier, G. A., Lecouvet, F., Simoni, P. & Vande Berg, B. C. CT Arthrography, MR Arthrography, PET, and Scintigraphy in Osteoarthritis. *Radiologic Clinics of North America* **47**, 595–615 (2009).
102. Even-Sapir, E., Metser, U., Mishani, E., Lievshitz, G., Lerman, H. & Leibovitch, I. The Detection of Bone Metastases in Patients with High-Risk Prostate Cancer : 99m Tc-MDP Planar. *Journal of Nuclear Medicine* **47**, 287–297 (2006).

103. Lee, J. W., Lee, S. M., Kim, S. J., Choi, J. W. & Baek, K. W. Clinical utility of fluoride-18 positron emission tomography/CT in temporomandibular disorder with osteoarthritis: Comparisons with 99mTc-MDP bone scan. *Dentomaxillofacial Radiology* **42**, 1–8 (2013).
104. Beheshti, M., Mottaghy, F. M., Payche, F., Behrendt, F. F. F., Van den Wyngaert, T., Fogelman, I., Strobel, K., Celli, M., Fanti, S., Giammarile, F., Krause, B. & Langsteger, W. 18F-NaF PET/CT: EANM procedure guidelines for bone imaging. *European Journal of Nuclear Medicine and Molecular Imaging* **42**, 1767–1777 (2015).
105. Mick, C. G., James, T., Hill, J. D., Williams, P. & Perry, M. Molecular imaging in oncology:18F-sodium fluoride PET imaging of osseous metastatic disease. *American Journal of Roentgenology* **203**, 263–271 (2014).
106. Holder, L. E. Clinical radionuclide bone imaging. *Radiology* vol. 176 607–614 (1990).
107. Win, A. Z. & Aparici, C. M. Factors Affecting Uptake of NaF-18 by the Normal Skeleton. *Journal of clinical medicine research* **6**, 435–42 (2014).
108. Czernin, J., Satyamurthy, N. & Schiepers, C. Molecular mechanisms of bone 18F-NaF deposition. *Journal of Nuclear Medicine* **51**, 1826–1829 (2010).
109. Segall, G., Delbeke, D., Stabin, M. G., Even-Sapir, E., Fair, J., Sajdak, R. & Smith, G. T. SNM Practice Guideline for Sodium 18F-Fluoride PET/CT Bone Scans 1.0. *Journal of Nuclear Medicine* **51**, 1813–1820 (2010).
110. Kairemo, K. & Macapinlac, H. A. *Sodium Fluoride PET/CT in Clinical Use*. *Sodium Fluoride PET/CT in Clinical Use* (2020). doi:10.1007/978-3-030-23577-2.
111. Grant, F. D., Fahey, F. H., Packard, A. B., Davis, R. T., Alavi, A. & Treves, S. T. Skeletal PET with 18F-Fluoride: Applying New Technology to an Old Tracer. *Journal of Nuclear Medicine* **49**, 68–78 (2007).
112. Kim, H. R., So, Y., Moon, S. G., Lee, I. S. & Lee, S. H. Clinical value of 99mTc-methylene diphosphonate (MDP) bone single photon emission computed tomography (SPECT) in patients with knee osteoarthritis. *Osteoarthritis and Cartilage* **16**, 212–218 (2008).
113. Singh, H., Neutze, J. A. & Jonathan R. Enterline, E. *Radiology fundamentals: Introduction to imaging & technology*. *Springer* (2014). doi:10.1017/CBO9781107415324.004.

114. Cal-Gonzalez, J., Rausch, I., Sundar, L. K. S., Lassen, M. L., Muzik, O., Moser, E., Papp, L. & Beyer, T. Hybrid imaging: Instrumentation and data processing. *Frontiers in Physics* **6**, (2018).
115. Idolazzi, L., Salgarello, M., Gatti, D., Viapiana, O., Vantaggiato, E., Fassio, A., Adami, S. & Rossini, M. 18F-fluoride PET/CT for detection of axial involvement in ankylosing spondylitis: correlation with disease activity. *Annals of Nuclear Medicine* **30**, 430–434 (2016).
116. Boegård, T., Rudling, O., Dahlström, J., Dirksen, H., Petersson, I. F. & Jonsson, K. Bone scintigraphy in chronic knee pain: Comparison with magnetic resonance imaging. *Annals of the Rheumatic Diseases* **58**, 20–26 (1999).
117. Kogan, F., Fan, A. P., McWalter, E. J., Oei, E. H. G., Quon, A. & Gold, G. E. PET/MRI of metabolic activity in osteoarthritis: A feasibility study. *Journal of Magnetic Resonance Imaging* **45**, 1736–1745 (2017).
118. Puri, T., Frost, M. L., Curran, K. M., Siddique, M., Moore, A. E. B., Cook, G. J. R., Marsden, P. K., Fogelman, I. & Blake, G. M. Differences in regional bone metabolism at the spine and hip: A quantitative study using 18F-fluoride positron emission tomography. *Osteoporosis International* **24**, 633–639 (2013).
119. Blake, G. M., Frost, M. L. & Fogelman, I. Quantitative radionuclide studies of bone. *Journal of Nuclear Medicine* **50**, 1747–1750 (2009).
120. Blake, G. M., Park-Holohan, S.-J., Cook, G. J. R. & Fogelman, I. Quantitative studies of bone with the use of 18 F-fluoride and 99m Tc-methylene diphosphonate. *Seminars in nuclear medicine* **31**, 28–49 (2001).
121. Genovese, F., Siebuhr, A. S., Musa, K., Gallagher, J. A., Milan, A. M., Karsdal, M. A., Rovensky, J., Bay-Jensen, A. C. & Ranganath, L. R. Investigating the robustness and diagnostic potential of extracellular matrix remodelling biomarkers in alkaptonuria. in *JIMD Reports* vol. 24 29–37 (Springer Berlin Heidelberg, 2015).
122. Hoekstra, C. J., Paglianiti, I., Hoekstra, O. S., Smit, E. F., Postmus, P. E., Teule, G. J. J. & Lammertsma, A. A. Monitoring response to therapy in cancer using tomography : an overview of different analytical methods. *European Journal of Nuclear Medicine* **27**, 731–743 (2000).
123. Basu, S., Zaidi, H., Houseni, M., Bural, G., Udupa, J., Acton, P., Torigian, D.

A. & Alavi, A. Novel Quantitative Techniques for Assessing Regional and Global Function and Structure Based on Modern Imaging Modalities: Implications for Normal Variation, Aging and Diseased States. *Seminars in Nuclear Medicine* **37**, 223–239 (2007).

124. Win, A. Z. & Aparici, C. M. Normal SUV values measured from NaF18-PET/CT bone scan studies. *PLoS ONE* **9**, 1–6 (2014).
125. Coleman, R. E. & Graham, M. M. Is quantitation necessary for oncological PET studies? *European Journal of Nuclear Medicine* **29**, 133–138 (2002).
126. Griffin, R., Psarelli, E. E., Cox, T. F., Khedr, M., Milan, A. M., Davison, A. S., Hughes, A. T., Usher, J. L., Taylor, S., Loftus, N., Daroszewska, A., West, E., Jones, A., Briggs, M., Fisher, M., *et al.* Data on items of AKUSSI in Alkaptonuria collected over three years from the United Kingdom National Alkaptonuria Centre and the impact of nitisinone. *Data in Brief* **20**, 1620–1628 (2018).
127. Thie, J. A. Understanding the standardized uptake value, its methods, and implications for usage. *Journal of Nuclear Medicine* **45**, 1431–1434 (2004).
128. Ota, N., Kato, K., Iwano, S., Ito, S., Abe, S., Fujita, N., Yamashiro, K., Yamamoto, S. & Naganawa, S. Comparison of 18F-fluoride PET/CT, 18F-FDG PET/CT and bone scintigraphy (planar and SPECT) in detection of bone metastases of differentiated thyroid cancer: A pilot study. *British Journal of Radiology* **87**, (2014).
129. Kinahan, P. E. & Fletcher, J. W. Positron emission tomography-computed tomography standardized uptake values in clinical practice and assessing response to therapy. *Seminars in Ultrasound, CT and MRI* **31**, 496–505 (2010).
130. Adams, M. C., Turkington, T. G., Wilson, J. M. & Wong, T. Z. A systematic review of the factors affecting accuracy of SUV measurements. *American Journal of Roentgenology* **195**, 310–320 (2010).
131. Puri, T., Blake, G. M., Frost, M. L., Siddique, M., Moore, A. E. B., Marsden, P. K., Cook, G. J. R., Fogelman, I. & Curran, K. M. Comparison of six quantitative methods for the measurement of bone turnover at the hip and lumbar spine using 18F-fluoride PET-CT. *Nuclear medicine communications* **33**, 597–606 (2012).
132. Sabbah, N., Jackson, T., Mosci, C., Jamali, M., Minamimoto, R., Quon, A.,

Mittra, E. S. & Iagaru, A. 18F-sodium fluoride PET/CT in oncology: an atlas of SUVs. *Clinical nuclear medicine* 228–231 (2015).

133. Kobayashi, N., Inaba, Y., Tateishi, U., Ike, H., Kubota, S., Inoue, T. & Saito, T. Comparison of 18F-fluoride positron emission tomography and magnetic resonance imaging in evaluating early-stage osteoarthritis of the hip. *Nuclear Medicine Communications* **36**, 84–89 (2015).
134. Draper, C. E., Quon, A., Fredericson, M., Besier, T. F., Delp, S. L., Beaupre, G. S. & Gold, G. E. Comparison of MRI and 18F-NaF PET/CT in patients with patellofemoral pain. *Journal of Magnetic Resonance Imaging* **36**, 928–932 (2012).
135. Savic, D., Pedoia, V., Seo, Y., Yang, J., Bucknor, M., Franc, B. L. & Majumdar, S. Imaging bone-cartilage interactions in osteoarthritis using [18F]-NaF PET-MRI. *Molecular Imaging* **15**, 1–12 (2016).
136. Draper, C. E., Quon, A., Fredericson, M., Besier, T. F., Delp, S. L., Beaupre, G. S. & Gold, G. E. Comparison of MRI and ^{18}F-NaF PET/CT in patients with patellofemoral pain. *Journal of magnetic resonance imaging : JMRI* **36**, 928–32 (2012).
137. Cook, G. J. & Fogelman, I. The role of positron emission tomography in skeletal disease. *Seminars in nuclear medicine* **31**, 50–61 (2001).
138. Frost, M. L., Moore, A. E., Siddique, M., Blake, G. M., Laurent, D., Borah, B., Schramm, U., Valentin, M. A., Pellas, T. C., Marsden, P. K., Schleyer, P. J. & Fogelman, I. 18F-fluoride PET as a noninvasive imaging biomarker for determining treatment efficacy of bone active agents at the hip: A prospective, randomized, controlled clinical study. *Journal of Bone and Mineral Research* **28**, 1337–1347 (2013).
139. Installe, J., Nzeusseu, A., Bol, A., Devogelaer, J. & Lonneux, M. PET for Monitoring Therapeutic Response in Paget's Disease of Bone. *The Journal of Nuclear Medicine* **46**, 1650–1658 (2005).
140. Frost, M. L., Cook, G. J. R., Blake, G. M., Marsden, P. K., Benatar, N. A. & Fogelman, I. A Prospective Study of Risedronate on Regional Bone Metabolism and Blood Flow at the Lumbar Spine Measured by 18F-Fluoride Positron Emission Tomography. *Journal of Bone and Mineral Research* **18**, 2215–2222 (2003).
141. Frost, M. L., Siddique, M., Blake, G. M., Moore, A. E., Schleyer, P. J., Dunn,

J. T., Somer, E. J., Marsden, P. K., Eastell, R. & Fogelman, I. Differential effects of teriparatide on regional bone formation using 18F-fluoride positron emission tomography. *Journal of Bone and Mineral Research* **26**, 1002–1011 (2011).

142. Vanderhoek, M., Perlman, S. B. & Jeraj, R. Impact of the Definition of Peak Standardized Uptake Value on Quantification of Treatment Response. *Journal of Nuclear Medicine* **53**, 4–11 (2012).
143. Uchida, K., Nakajima, H., Miyazaki, T., Yayama, T., Kawahara, H., Kobayashi, S., Tsuchida, T., Okazawa, H., Fujibayashi, Y. & Baba, H. Effects of Alendronate on Bone Metabolism in Glucocorticoid-Induced Osteoporosis Measured by 18F-Fluoride PET: A Prospective Study. *Journal of Nuclear Medicine* **50**, 1808–1814 (2009).
144. Wang, Y., Osborne, M. T., Tung, B., Li, M. & Li, Y. Imaging Cardiovascular Calcification. *Journal of the American Heart Association* **7**, 1–15 (2018).
145. Joshi, N. V., Vesey, A., Newby, D. E. & Dweck, M. R. Will 18F-Sodium Fluoride PET-CT Imaging Be the Magic Bullet for Identifying Vulnerable Coronary Atherosclerotic Plaques? *Current Cardiology Reports* **16**, 14–20 (2014).
146. Dweck, M. R., Aikawa, E., Newby, D. E., Tarkin, J. M., Rudd, J. H. F., Narula, J. & Fayad, Z. A. Noninvasive Molecular Imaging of Disease Activity in Atherosclerosis. *Circulation Research* **119**, 330–340 (2016).
147. Yuxin, L., Gholam, B. R., Shaba, W. F., Dadparvar, S., Berenji, G. R., Li, Y., Yevdayev, E. & Tafti, B. Association of vascular fluoride uptake with vascular calcification and coronary artery disease. *Nuclear Medicine Communications* **33**, 14–20 (2011).
148. Dweck, M. R., Chow, M. W. L., Joshi, N. V., Williams, M. C., Jones, C., Fletcher, A. M., Richardson, H., White, A., McKillop, G., Van Beek, E. J. R., Boon, N. A., Rudd, J. H. F. & Newby, D. E. Coronary arterial 18F-sodium fluoride uptake: A novel marker of plaque biology. *Journal of the American College of Cardiology* **59**, 1539–1548 (2012).
149. Irkle, A., Vesey, A. T., Lewis, D. Y., Skepper, J. N., Bird, J. L. E., Dweck, M. R., Joshi, F. R., Gallagher, F. A., Warburton, E. A., Bennett, M. R., Brindle, K. M., Newby, D. E., Rudd, J. H. & Davenport, A. P. Identifying active vascular microcalcification by 18F-sodium fluoride positron emission

tomography. *Nature Communications* **6**, (2015).

150. Kitagawa, T., Yamamoto, H., Toshimitsu, S., Sasaki, K., Senoo, A., Kubo, Y., Tatsugami, F., Awai, K., Hirokawa, Y. & Kihara, Y. 18F-sodium fluoride positron emission tomography for molecular imaging of coronary atherosclerosis based on computed tomography analysis. *Atherosclerosis* **263**, 385–392 (2017).
151. Libby, P., DiCarli, M. & Weissleder, R. The vascular biology of atherosclerosis and imaging targets. *Journal of Nuclear Medicine* **51**, (2010).
152. Beheshti, M., Saboury, B., Mehta, N. N., Torigian, D. A., Werner, T., Mohler, E., Wilensky, R., Newberg, A. B., Basu, S., Langsteger, W. & Alavi, A. Detection and global quantification of cardiovascular molecular calcification by fluoro-18-fluoride positron emission tomography/computed tomography-A novel concept. *Hellenic Journal of Nuclear Medicine* **14**, 114–120 (2011).
153. Kitagawa, T., Yamamoto, H., Toshimitsu, S., Sasaki, K., Senoo, A., Kubo, Y., Tatsugami, F., Awai, K., Hirokawa, Y. & Kihara, Y. Data on analysis of coronary atherosclerosis on computed tomography and 18F-sodium fluoride positron emission tomography. *Data in Brief* **13**, 341–345 (2017).
154. Blomberg, B. A., Thomassen, A., De Jong, P. A., Simonsen, J. A., Lam, M. G. E. H., Nielsen, A. L., Mickley, H., Mali, W. P. T. M., Alavi, A. & Høilund-Carlsen, P. F. Impact of personal characteristics and technical factors on quantification of sodium 18F-fluoride uptake in human arteries: Prospective evaluation of healthy subjects. *Journal of Nuclear Medicine* **56**, 1534–1540 (2015).
155. Derlin, T., Richter, U., Bannas, P., Begemann, P., Buchert, R., Mester, J. & Klutmann, S. Feasibility of 18F-sodium fluoride PET/CT for imaging of atherosclerotic plaque. *Journal of Nuclear Medicine* **51**, 862–865 (2010).
156. Basu, S., Høilund-Carlsen, P. F. & Alavi, A. Assessing global cardiovascular molecular calcification with 18F-fluoride PET/CT: Will this become a clinical reality and a challenge to CT calcification scoring? *European Journal of Nuclear Medicine and Molecular Imaging* **39**, 660–664 (2012).
157. Zhang, Y., Li, H., Jia, Y., Yang, P., Zhao, F., Wang, W., Liu, W., Chen, G., Zhuang, X. & Li, J. Noninvasive Assessment of Carotid Plaques Calcification by 18F-Sodium Fluoride Accumulation: Correlation with Pathology. *Journal of Stroke and Cerebrovascular Diseases* **27**, 1796–1801 (2018).

158. Derlin, T., Toth, Z., Papp, L., Wisotzki, C., Apostolova, I., Habermann, C. R., Mester, J. & Klutmann, S. Correlation of Inflammation Assessed by 18F-FDG PET, Active Mineral Deposition Assessed by 18F-Fluoride PET, and Vascular Calcification in Atherosclerotic Plaque: A Dual-Tracer PET/CT Study. *Journal of Nuclear Medicine* **52**, 1020–1027 (2011).

159. Bannas, P., Richter, U., Derlin, T., Wisotzki, C., Apostolova, I., Klutmann, S., Mester, J. & Weber, C. In Vivo Imaging of Mineral Deposition in Carotid Plaque Using 18F-Sodium Fluoride PET/CT: Correlation with Atherogenic Risk Factors. *Journal of Nuclear Medicine* **52**, 362–368 (2011).

160. Derlin, T., Janssen, T., Salamon, J., Veldhoen, S., Busch, J. D., Schön, G., Herrmann, J., Henes, F. O., Bannas, P. & Adam, G. Age-related differences in the activity of arterial mineral deposition and regional bone metabolism: a 18F-sodium fluoride positron emission tomography study. *Osteoporosis International* **26**, 199–207 (2014).

161. Braun, J., Baraliakos, X., Golder, W., Brandt, J., Rudwaleit, M., Listing, J., Bollow, M., Sieper, J. & Van der Heijde, D. Magnetic resonance imaging examinations of the spine in patients with ankylosing spondylitis, before and after successful therapy with infliximab: Evaluation of a new scoring system. *Arthritis and Rheumatism* **48**, 1126–1136 (2003).

162. Ventura-Rios, L., Hernandez-Diaz, C., Gutierrez-Perez, L., Bernal-Gonzalez, A., Pichardo-Bahena, R., Cedeno-Garciduenas, A. L. & Pineda, C. Ochronotic arthropathy as a paradigm of metabolically induced degenerative joint disease. A case-based review. *Clinical Rheumatology* **35**, 1389–1395 (2016).

163. Cook, G., Parker, C., Chua, S., Johnson, B., Aksnes, A.-K. & Lewington, V. J. 18F-fluoride PET: changes in uptake as a method to assess response in bone metastases from castrate-resistant prostate cancer patients treated with 223Ra-chloride (Alpharadin). *EJNMMI research* **1**, 4 (2011).

164. Gerety, E. L., Hopper, M. A. & Bearcroft, P. W. P. The reliability of measuring the density of the L1 vertebral body on CT imaging as a predictor of bone mineral density. *Clinical Radiology* **72**, 177.e9-177.e15 (2017).

165. Riggs, B. L., Wahner, H. W., Dunn, W. L., Mazess, R. B., Offord, K. P. & Melton, L. J. Differential changes in bone mineral density of the appendicular and axial skeleton with aging. Relationship to spinal osteoporosis. *Journal of Clinical Investigation* **67**, 328–335 (1981).

166. Kobayashi, N., Inaba, Y., Tateishi, U., Yukizawa, Y., Ike, H., Inoue, T. & Saito, T. New application of 18F-fluoride PET for the detection of bone remodeling in early-stage osteoarthritis of the hip. *Clinical nuclear medicine* **38**, e379-83 (2013).

167. Kobayashi, N., Inaba, Y., Yukizawa, Y., Ike, H., Kubota, S., Inoue, T. & Saito, T. Use of 18F-fluoride positron emission tomography as a predictor of the hip osteoarthritis progression. *Modern Rheumatology* **25**, 925–930 (2015).

168. Kaneta, T., Ogawa, M., Daisaki, H., Nawata, S., Yoshida, K. & Inoue, T. SUV measurement of normal vertebrae using SPECT/CT with Tc-99m methylene diphosphonate. *American journal of nuclear medicine and molecular imaging* **6**, 262–268 (2016).

169. Hartvigsen, J., Werner, T., Ayubcha, C., Høilund-Carlsen, P. F., Raynor, W., Zirakchian Zadeh, M., Rajapakse, C. S., Alavi, A., Stochkendahl, M. J., Al-Zaghal, A., Zhuang, H. & Thomassen, A. Quantitative evaluation of normal spinal osseous metabolism with 18F-NaF PET/CT. *Nuclear Medicine Communications* **39**, 945–950 (2018).

170. Brenner, A. I., Koshy, J., Morey, J., Lin, C. & Dipoce, J. The bone scan. *Seminars in Nuclear Medicine* **42**, 11–26 (2012).

171. Van den Wyngaert, T., Strobel, K., Kampen, W. U., Kuwert, T., van der Bruggen, W., Mohan, H. K., Gnanasegaran, G., Delgado-Bolton, R., Weber, W. A., Beheshti, M., Langsteger, W., Giammarile, F., Mottaghy, F. M. & Paycha, F. The EANM practice guidelines for bone scintigraphy. *European Journal of Nuclear Medicine and Molecular Imaging* **43**, 1723–1738 (2016).

172. Daly, R. M., Rosengren, B. E., Alwis, G., Ahlborg, H. G., Sernbo, I. & Karlsson, M. K. Gender specific age-related changes in bone density, muscle strength and functional performance in the elderly: A-10 year prospective population-based study. *BMC Geriatrics* **13**, (2013).

173. Demontiero, O., Vidal, C. & Duque, G. Aging and bone loss: New insights for the clinician. *Therapeutic Advances in Musculoskeletal Disease* **4**, 61–76 (2012).

174. Yu, L. P., Qian, W. W., Yin, G. Y., Ren, Y. X. & Hu, Z. Y. MRI Assessment of Lumbar Intervertebral Disc Degeneration with Lumbar Degenerative Disease Using the Pfirrmann Grading Systems. *PLoS ONE* **7**, 1–7 (2012).

175. Jebaraj, I., Chacko, B., Chiramel, G., Matthai, T. & Parameswaran, A. A

simplified staging system based on the radiological findings in different stages of ochronotic spondyloarthropathy. *Indian Journal of Radiology and Imaging* **23**, 101–105 (2013).

176. Chanchairujira, K., Chung, C. B., Kim, J. Y., Papakonstantinou, O., Lee, M. H., Clopton, P. & Resnick, D. Intervertebral Disk Calcification of the Spine in an Elderly Population: Radiographic Prevalence, Location, and Distribution and Correlation with Spinal Degeneration. *Radiology* **230**, 499–503 (2004).
177. De Schepper, E. I. T., Damen, J., Van Meurs, J. B. J., Ginai, A. Z., Popham, M., Hofman, A., Koes, B. W. & Bierma-Zeinstra, S. M. The association between lumbar disc degeneration and low back pain: The influence of age, gender, and individual radiographic features. *Spine* **35**, 531–536 (2010).
178. Biering-Sørensen, F., Hansen, F. R., Schroll, M. & Runeborg, O. The relation of spinal x-ray to low-back pain and physical activity among 60-year-old men and women. *Spine* **10**, 445–451 (1985).
179. Manson, N. A., Goldberg, E. J. & Andersson, G. B. J. Sexual dimorphism in degenerative disorders of the spine. *Orthopedic Clinics* **37**, 549–553 (2006).
180. Baron, Y. M., Brincat, M. P., Galea, R. & Calleja, N. Intervertebral disc height in treated and untreated overweight post-menopausal women. *Human Reproduction* **20**, 3566–3570 (2005).
181. Wang, Y. X. J., Kwok, A. W. L., Griffith, J. F., Leung, J. C. S., Ma, H. T., Ahuja, A. T. & Leung, P. C. Relationship between gender, bone mineral density, and disc degeneration in the lumbar spine: a study in elderly subjects using an eight-level MRI-based disc degeneration grading system. *Journal of Magnetic Resonance Imaging* **22**, 91–96 (2011).
182. Fischer, D. R., C. W. Pfirrmann, V. Zubler, K. D. Stumpe, B. Seifert, K. Strobel, G. Tamborrini, G. K. von Schulthess, B. A. Michel, and A. C. High bone turnover assessed by 18F-fluoride PET/CT in the spine of patients with ankylosing spondylitis: No redundancy to inflammatory lesions detected by whole body MRI. *Annals of the Rheumatic Disease* **71**, 1–9 (2013).
183. Fischer, D. R., Maquieira, G. J., Espinosa, N., Zanetti, M., Hesselmann, R., Johayem, A., Hany, T. F., Von Schulthess, G. K. & Strobel, K. Therapeutic impact of [18F]fluoride positron-emission tomography/computed tomography on patients with unclear foot pain. *Skeletal Radiology* **39**, 987–997 (2010).
184. O'brien, W. M., La Du, B. N. & Bunim, J. J. Biochemical, pathologic and

clinical aspects of alcaptonuria, ochronosis and ochronotic arthropathy. Review of world literature (1584-1962). *The American Journal of Medicine* **34**, 813–838 (1963).

185. Beheshti, M., Vali, R., Waldenberger, P., Fitz, F., Nader, M., Loidl, W., Broinger, G., Stoiber, F., Foglman, I. & Langsteger, W. Detection of bone metastases in patients with prostate cancer by 18F fluorocholine and 18F fluoride PET-CT: A comparative study. *European Journal of Nuclear Medicine and Molecular Imaging* **35**, 1766–1774 (2008).
186. Li, Y., Berenji, G. R., Shaba, W. F., Tafti, B., Yevdayev, E. & Dadparvar, S. Association of vascular fluoride uptake with vascular calcification and coronary artery disease. *Nuclear Medicine Communications* **33**, 14–20 (2012).
187. Kimani, C., Kadota, A., Miura, K., Fujiyoshi, A., Zaid, M., Kadowaki, S., Hisamatsu, T., Arima, H., Horie, M. & Ueshima, H. Differences between coronary artery calcification and aortic artery calcification in relation to cardiovascular disease risk factors in Japanese men. *Journal of Atherosclerosis and Thrombosis* **26**, 452–464 (2019).
188. Allison, M. A. & Wright, C. M. Age and gender are the strongest clinical correlates of prevalent coronary calcification (R1). *International Journal of Cardiology* **98**, 325–330 (2005).
189. Liyanage, L., Lee, N. J., Cook, T., Herrmann, H. C., Jagasia, D., Litt, H. & Han, Y. The impact of gender on cardiovascular system calcification in very elderly patients with severe aortic stenosis. *International Journal of Cardiovascular Imaging* **32**, 173–179 (2016).
190. Raggi, P., Shaw, L. J., Berman, D. S. & Callister, T. Q. Gender-based differences in the prognostic value of coronary calcification. *Journal of Women's Health* **13**, 273–283 (2004).
191. Hannoush, H., Introne, W. J., Chen, M. Y., Lee, S. J., O'Brien, K., Suwannarat, P., Kayser, M. A., Gahl, W. A. & Sachdev, V. Aortic stenosis and vascular calcifications in alkaptonuria. *Molecular Genetics and Metabolism* **105**, 198–202 (2012).

9 Appendix

9.1 Bone involvement results from the lumbar spine and femoral head site

Table 9.1. Gender difference in the severity of lower spine and hip degeneration measured from baseline CT scans for 39 AKU patients who were part of the SONIA 2 clinical trial.

The results display HU_{mean} ± SD, minimum, and maximum values at each lumbar vertebra body from L1 to L5, and head of the femur, for male and female patients. * Correlation is statistically significant between gender at the ROI ($P < 0.05$). L1- first lumbar vertebrae, L2- second lumbar vertebrae, L3- third lumbar vertebrae, L4- fourth lumbar vertebrae L5- fifth lumbar vertebrae, L1-L5 average lumbar vertebrae, RT F- right head of the femur, LT F- left head of the femur, F- average right and left head of the femur.

ROI	Gender	Patient no.	HU_{mean} (mean ±SD)	Minimum	Maximum	P-value
L1	Total	38	139.94 ± 60.06	-7.00	239.00	0.83
	M	23	138.25 ±57.00	2.00	239.00	
	F	15	142.52 ±66.47	-7.00	221.00	
L2	Total	39	141.22 ±63.85	9.00	310.00	0.32
	M	24	133.02 ±54.66	32.00	213.00	
	F	15	154.33 ±76.54	9.00	310.00	
L3	Total	39	133.06 ±53.67	15.00	209.00	0.66
	M	24	130.05 ±52.56	22.00	209.00	
	F	15	137.87 ±56.91	15.00	205.00	
L4	Total	39	146.04 ±61.92	27.00	236.00	0.93
	M	24	145.31 ±63.56	28.00	236.00	
	F	15	147.22 ±61.37	27.00	222.00	
L5	Total	39	182.41 ±64.95	55.00	390.00	0.86
	M	24	183.87 ±69.80	66.00	390.00	
	F	15	180.08 ±58.62	55.00	285.00	
L1-L5	Total	39	148.13 ±55.81	26.00	239.00	0.71
	M	24	145.46 ±54.33	30.00	239.00	
	F	15	152.40 ±59.77	26.00	221.00	
RT F	Total	31	235.08 ±59.78	127.91	334.16	0.68
	M	19	227.55 ±52.54	143.8	311.52	
	F	12	247.02 ±59.25	127.91	334.16	
LT F	Total	31	244.42 ±48.98	154.50	348.44	0.04*
	M	19	230.27 ±46.93	154.50	313.84	
	F	12	266.84 ±45.20	185.79	348.44	
Average F	Total	31	240.00 ±50.02	154.00	341.00	0.09
	M	19	229.00 ±52.07	154.00	295.00	
	F	12	257.00 ±51.08	178.00	341.00	

Table 9.2. Differences in R between multiple linear regression analysis and polynomial regression in relation to the correlation between age and HU_{mean} obtained from the lower spine and femoral sites for 39 AKU patients.

ROI	Linear regression	Polynomial
L1	0.545	0.624
L2	0.588	0.647
L3	0.624	0.644
L4	0.646	0.682
L5	0.489	0.576
L1-L5	0.632	0.69
RT F	0.586	0.586
LT F	0.366	0.501
RT + LT	0.558	0.569

Table 9.3.HU_{mean} measurements at the lower spine and femoral sites for 39 AKU patients who were part of the SONIA 2 clinical trial stratified by the decade of life.

Data display the HU_{mean} ± SD, minimum and maximum values and P-value obtained from the baseline CT scan at each lumbar vertebrae level, the mean of the lumbar levels measurement, right and left femurs and mean of femurs' measurements in four age groups. * Correlation is statistically significant between age group at the ROI ($P < 0.05$).

ROI	Age group	Mean HU ± SD	Minimum	Maximum	P-value
L1	30-39 40-49 50-59 > 60	171.37 ± 25.54 156.13 ± 50.87 160.53 ± 42.67 79.97 ± 63.86	128.00 60.00 102.00 -7.00	208.00 221.00 239.00 193.00	0.473 0.836 0.005*
L2	30-39 40-49 50-59 > 60	184.67 ± 35.70 173.07 ± 64.54 126.69 ± 46.87 87.10 ± 52.60	134.00 89.00 39.00 9.00	224.00 310.00 194.00 182.00	0.669 0.073 0.092
L3	30-39 40-49 50-59 > 60	171.31 ± 38.32 154.36 ± 38.36 126.30 ± 51.35 87.49 ± 51.44	102.00 93.00 41.00 15.00	205.00 209.00 198.00 178.00	0.366 0.158 0.109
L4	30-39 40-49 50-59 > 60	185.61 ± 38.85 179.45 ± 44.27 134.96 ± 60.13 89.35 ± 52.50	124.00 82.00 41.00 27.00	236.00 232.00 222.00 166.00	0.764 0.059 0.088
L5	30-39 40-49 50-59 > 60	196.78 ± 26.90 224.96 ± 71.99 173.62 ± 48.80 130.08 ± 53.92	164.00 103.00 122.00 55.00	233.00 390.00 251.00 208.00	0.338 0.070 0.075
L1-L5	30-39 40-49 50-59 > 60	181.95 ± 26.28 177.59 ± 45.92 142.44 ± 48.39 94.80 ± 50.27	150.00 96.00 62.00 26.00	216.00 239.00 209.00 165.00	0.822 0.096 0.045*
RT F	30-39 40-49 50-59 > 60	270.30 ± 42.63 236.08 ± 38.01 215.35 ± 56.14 173.33 ± 54.69	199.58 165.09 143.48 116.61	334.16 318.59 311.52 237.50	0.088 0.325 0.175
LT F	30-39 40-49 50-59 > 60	289.79 ± 36.32 223.58 ± 50.15 242.31 ± 47.44 231.80 ± 10.51	230.74 154.50 163.76 217.43	348.44 316.99 293.13 242.51	0.007* 0.414 0.678
RT+ LT F	30-39 40-49 50-59 > 60	280.05 ± 38.68 229.83 ± 42.36 224.77 ± 50.71 184.46 ± 51.85	215.00 164.00 154.00 117.00	341.00 318.00 295.00 236.00	0.020* 0.806 0.159

Table 9.4. Gender difference in the severity of the lower spine and hip degeneration measured from baseline ^{18}F-NaF PET scan for 39 AKU patients who were part of the SONIA 2 clinical trial.

The results display mean SUV_{max} ± SD, minimum, and maximum values at each lumbar vertebra body from L1 to L5, average lumbar vertebra levels (L1-L5), and head of the femur (right, left, and average sides) for males and females patients. No statistically significant differences in SUV_{max} values been found between male and female at any ROI was found ($P > 0.05$).

ROI	Gender	Patient no.	SUV_{max} (mean ±SD)	Minimum	maximum	P-value
L1	Total	38	10.19 ± 2.30	3.86	14.84	0.10
	M	23	10.68 ± 2.27	4.87	14.07	
	F	15	9.43 ± 2.21	3.86	14.84	
L2	Total	39	10.67 ± 3.15	5.25	19.93	0.45
	M	24	10.97 ± 3.20	6.77	19.93	
	F	15	10.18 ± 3.11	5.25	17.95	
L3	Total	39	10.08 ± 2.15	5.64	17.24	0.17
	M	24	10.45 ± 2.25	6.99	17.24	
	F	15	9.47 ± 1.91	5.64	12.70	
L4	Total	39	10.59 ± 2.55	4.87	16.50	0.15
	M	24	11.06 ± 2.45	7.79	16.50	
	F	15	9.84 ± 2.61	4.87	14.55	
L5	Total	39	11.15 ± 2.62	6.37	18.98	0.41
	M	24	11.43 ± 2.73	7.83	18.98	
	F	15	10.70 ± 2.47	6.37	17.05	
L1-L5	Total	39	10.54 ± 2.17	5.20	15.91	0.17
	M	24	10.92 ± 2.10	7.07	15.91	
	F	15	9.93 ± 2.22	5.20	14.64	
RT F	Total	31	4.63 ± 2.36	1.90	8.23	0.68
	M	19	4.44 ± 1.97	2.55	8.23	
	F	12	4.95 ± 2.06	1.90	8.07	
LT F	Total	31	4.34 ±1.57	2.35	8.49	0.25
	M	19	4.09 ±1.48	2.35	8.49	
	F	12	4.74 ±1.67	2.46	8.23	
Average F	Total	31	4.50 ± 2.55	2.20	8.36	0.77
	M	19	4.28 ± 2.08	2.82	8.36	
	F	12	4.92 ± 1.90	2.20	8.15	

Table 9.5. Differences in R between multiple linear regression analysis and polynomial regression in relate to the correlation between age and SUV_{max} obtained from the lower spine and femoral sites for 39 AKU patients.

ROI	Linear regression	Polynomial
L1	0.332	0.44
L2	0.31	0.338
L3	0.391	0.405
L4	0.416	0.528
L5	0.432	0.508
L1-L5	0.438	0.51
RT F	0.219	0.24
LT F	0.12	0.235
RT + LT	0.214	0.232

Table 9.6. SUV_{max} measurements at the lower spine and hip sites for 39 AKU patients who were part of the SONIA 2 clinical trial stratified by the decade of life.

Data display the SUV_{max} ± SD, minimum and maximum values and P-value obtained from the baseline ^{18}F-NaF PET/CT scan at each lumbar vertebrae level, the mean of the lumbar levels measurement, right and left femoral heads and average head of the femur measurement in four age groups. * Correlation is statistically significant at the level ($P < 0.05$).

ROI	Age group	Mean SUV_{max} ± SD	Minimum	Maximum	P-value
L1	30-39	10.80 ±2.05	8.7	14.07	0.722
	40-49	10.43 ±2.25	7.29	14.84	0.445
	50-59	11.10 ±1.49	8.72	12.77	0.025*
	> 60	8.65 ±2.64	3.86	12.57	
L2	30-39	12.73 ±3.76	9.01	17.95	0.134
	40-49	10.46 ±2.55	7.26	15.56	0.76
	50-59	10.76 ±1.75	8.02	13.58	0.334
	> 60	9.38 ±4.02	5.25	19.93	
L3	30-39	11.82 ±2.59	9.27	17.24	0.107
	40-49	10.12 ±1.78	7.2	12.7	0.966
	50-59	10.09 ±1.57	8.15	13.07	0.136
	> 60	8.79 ±2.12	5.64	13.1	
L4	30-39	11.87 ±2.55	8.42	16.5	0.619
	40-49	11.29 ±2.33	7.98	14.96	0.503
	50-59	10.69 ±1.66	8.49	13.38	0.078
	> 60	8.75 ±2.83	4.87	15.84	
L5	30-39	12.08 ±1.91	9.27	14.2	0.568
	40-49	12.80 ±2.92	9.13	18.98	0.02*
	50-59	10.17 ±1.70	7.89	12.93	0.451
	> 60	9.49 ±2.21	6.37	14.56	
L1-L5	30-39	11.86 ±2.34	9.11	15.91	0.391
	40-49	11.02 ±1.82	8.67	14.64	0.481
	50-59	10.55 ±1.11	8.45	12.16	0.103
	> 60	9.01 ±2.60	5.2	15.2	
RT F	30-39	4.07 ±2.47	1.9	8.07	0.363
	40-49	4.95 ±1.65	2.55	8.23	0.58
	50-59	4.54 ±1.59	2.64	6.83	0.268
	> 60	7.30 ±7.01	3.51	21.54	
LT F	30-39	4.19 ±2.25	2.46	8.23	0.996
	40-49	4.19 ±1.64	2.35	8.49	0.378
	50-59	4.80 ±1.26	3.35	7.11	0.38
	> 60	4.23 ±1.05	2.69	5.4	
RT+ LT F	30-39	4.13 ± 2.34	2.2	8.15	0.667
	40-49	4.57 ± 1.48	2.82	8.36	0.996
	50-59	4.57 ± 1.31	2.83	6.78	0.319
	> 60	6.84 ± 6.51	3.58	21.54	

Table 9.7. Gender difference in the severity of the lower spine and hip degeneration extracted from baseline DEXA reports for 39 AKU patients who were part of the SONIA 2 clinical trial.

The results show mean T-score ± SD, minimum, and maximum values at each lumbar vertebra body, average lumbar levels (L1-L4), and left femoral head for males and females patients. * Correlation is statistically significant at the ROI ($P < 0.05$). At L4, only male patients had statistically significant higher T-score values compared to female patients ($P = 0.02$).

ROI	Gender	Patient no.	T_{Score} (mean ±SD)	Minimum	Maximum	P-value
L1	Total	36	0.48 ±1.84	-2.70	5.30	0.06
	M	22	0.93 ±1.86	-2.60	5.30	
	F	14	-0.23 ±1.63	-2.70	2.90	
L2	Total	37	0.18 ±1.87	-3.60	4.70	0.39
	M	23	0.39 ±1.76	-2.50	4.70	
	F	14	-0.17 ±2.06	-3.60	3.60	
L3	Total	37	0.50 ±1.80	-2.78	5.80	0.35
	M	23	0.72 ±1.94	-2.78	5.80	
	F	14	0.14 ±1.52	-2.60	3.50	
L4	Total	37	0.77 ± 2.03	-3.50	5.60	0.02*
	M	23	1.37 ±1.97	-1.70	5.60	
	F	14	-0.22 ±1.76	-3.50	3.40	
L1-L4	Total	37	0.52 ±1.79	-3.20	5.40	0.10
	M	23	0.90 ±1.77	-1.60	5.40	
	F	14	-0.09 ±1.70	-3.20	3.50	
Femur	Total	36	-1.56 ±1.06	-3.10	1.30	0.25
	M	22	-1.72 ±0.90	-3.10	0.30	
	F	14	-1.30 ±1.26	-3.10	1.30	

Table 9.8. Differences in R between multiple linear regression analysis and polynomial regression in relate to the correlation between age and T- score obtained from the lower spine and femoral sites for 37 AKU patients.

ROI	Linear regression	Polynomial
L1	0.031	0.103
L2	-0.311	0.159
L3	-0.158	0.116
L4	-0.009	0.172
L1-L4	0.137	0.136
Femur	-0.571	0.176

Table 9.9. T-score measurements at the lower spine and femoral region extracted from DEXA reports for 37 AKU patients who were part of the SONIA 2 clinical trial stratified by the decade of life.

Data display the T-score ± SD, minimum and maximum values and P-value obtained from the baseline DEXA scan at each lumbar vertebrae level, the average lumbar levels, and femoral region in four age groups. * Correlation is statistically significant at the ROI ($P < 0.05$). Statistically, there were substantial differences in T-score value measured from L2 between the 50s and 60s age groups only ($P = 0.006$).

ROI	Age group	Mean T-score ± SD	Minimum	Maximum	P-value
L1	30-39	-0.300 ± 0.876	-1.6	0.9	0.228
	40-49	0.592 ± 1.750	-2.6	2.8	0.503
	50-59	1.189 ± 2.267	-1.8	5.3	0.363
	> 60	0.200 ± 2.050	-2.7	3	
L2	30-39	0.129 ± 0.936	-0.9	1.7	0.392
	40-49	0.825 ± 1.954	-1.7	4.7	0.966
	50-59	0.860 ± 1.847	-1.8	3.6	0.006*
	> 60	-1.613 ± 1.341	-3.6	0.3	
L3	30-39	0.154 ± 0.895	-0.7	1.5	0.313
	40-49	1.033 ± 2.110	-2	5.8	0.828
	50-59	0.840 ± 1.950	-2	4	0.157
	> 60	-0.410 ± 1.520	-2.78	1.2	
L4	30-39	-0.300 ± 0.627	-1.3	0.4	0.069
	40-49	1.350 ± 2.172	-1.7	5.6	0.974
	50-59	1.380 ± 1.997	-1.7	4.1	0.214
	> 60	0.063 ± 2.326	-3.5	3.5	
L1-L4	30-39	-0.029 ± 0.732	-0.9	1.1	0.18
	40-49	1.075 ± 1.992	-1.6	5.4	0.948
	50-59	1.130 ± 1.857	-1.7	3.5	0.057
	> 60	-0.575 ± 1.613	-3.2	1.8	
F	30-39	-0.486 ± 1.104	-1.9	1.3	0.028*
	40-49	-1.542 ± 0.812	-2.8	0	0.369
	50-59	-1.880 ± 0.916	-3.1	-0.3	0.511
	> 60	-2.186 ± 0.926	-2.9	-0.6	

9.2 Lumbar DVUs results from 18F-NaF PET/CT scan and MRI

Table 9.10. Gender difference in the SUV_{max} values for lumbar DVUs measured from baseline ^{18}F-NaF PET/CT scan for 34 AKU patients (19 males, 15 females) who were part of the SONIA 2 clinical trial.

The results show mean SUV_{max} ± SD, minimum, and maximum values at each lumbar DVU from T12/L1 to L5/S1 level for males and females. * Correlation is statistically significant between gender at the ROI ($P < 0.05$). A significant difference was found between male and female at L5/SI only ($P = 0.02$).

DVU level	Gender	SUV_{max} (mean – SD)	Minimum	Maximum	P-value
T12/L1	Total	14.38 ± 5.10	6.72	25.91	0.07
	M	15.85 ± 5.44	8.41	25.91	
	F	12.6 ± 4.14	6.72	20.33	
L1/L2	Total	15.84 ± 6.41	7.12	33.41	0.67
	M	15.67 ± 5.67	8.08	28.2	
	F	16.4 ± 7.45	7.12	33.41	
L2/L3	Total	14.78 ± 5.2	6.95	25.76	0.62
	M	15.46 ± 4.57	8.92	25.73	
	F	14.30 ± 5.99	6.95	25.76	
L3/L4	Total	14.23 ± 5.01	6.25	30.02	0.44
	M	15.21 ± 3.93	8.08	21.76	
	F	13.47 ± 5.98	6.25	30.02	
L4/L5	Total	14.46 ± 5.06	5.44	24.65	0.30
	M	15.83 ± 4.06	8.8	24.65	
	F	13.42 ± 5.58	7.43	23.79	
L5/SI	Total	17.11 ± 5.90	7.14	27.2	0.02*
	M	18.87 ± 5.24	8.92	27.2	
	F	14.50 ± 5.79	7.14	25.15	
Average lumbar DVU	Total	15.12 ± 4.13	6.93	23.84	0.29
	M	16.15 ± 3.19	8.59	21.58	
	F	14.11 ± 4.96	6.93	23.84	

Table 9.11. SUV_{max} measurements at the lumbar DVU for 34 AKU patients who were part of the SONIA 2 clinical trial stratified by the decade of life.

Data display the SUV_{max} ± SD, minimum and maximum values and P-value obtained from the baseline ^{18}F-NaF PET/CT scan at each lumbar DVU level, from T12/L1 segment to the L5/S1 segment in four age groups. * Correlation is statistically significant between age group at the DVU level ($P < 0.05$).

DVU level	Age group	SUV_{max} DVU (mean – SD)	Minimum	Maximum	P- value
T12/L1	30-39 years old	12.72 ± 4.34	8.57	22.10	0.185
	40-49 years old	15.66 ± 4.54	10.31	22.12	0.715
	50-59 years old	16.49 ± 5.76	9.64	25.91	0.037*
	≥ 60 years old	9.85 ± 3.24	6.72	15.14	
L1/L2	30-39 years old	13.46 ± 4.1	9.88	20.89	0.157
	40-49 years old	18.15 ± 7.71	10.32	33.41	0.645
	50-59 years old	16.79 ± 5.49	10.11	28.20	0.124
	≥ 60 years old	11.75 ± 5.79	7.12	21.6	
L2/L3	30-39 years old	13.87 ± 4.71	9.62	20.30	0.035*
	40-49 years old	19.07 ± 4.79	11.67	25.76	0.002*
	50-59 years old	12.70 ± 3.28	8.92	19.71	0.120
	≥ 60 years old	9.94 ± 2.33	6.95	13.40	
L3/L4	30-39 years old	12.26 ± 4.12	8.78	20.96	0.07
	40-49 years old	15.65 ± 3.42	10.64	20.53	0.717
	50-59 years old	16.42 ± 6.22	10.86	30.02	0.029*
	≥ 60 years old	9.22 ± 2.44	6.25	12.76	
L4/L5	30-39 years old	12.75 ± 4.61	7.81	20.94	0.025*
	40-49 years old	18.4 ± 4.91	10.26	24.65	0.003*
	50-59 years old	12.23 ± 3.41	8.23	16.12	0.864
	≥ 60 years old	11.89 ± 3.88	7.43	15.96	
L5/SI	30-39 years old	12.83 ± 4.45	8.61	20.54	0.015
	40-49 years old	19.10 ± 5.08	9.60	26.82	0.825
	50-59 years old	18.57 ± 6.11	7.54	27.20	0.288
	≥ 60 years old	15.4 ± 7.09	7.14	23.83	
Average lumbar DVU	30-39 years old	12.99 ± 3.92	9.19	20.96	0.546
	40-49 years old	17.67 ± 3.97	10.60	23.84	0.877
	50-59 years old	15.45 ± 2.65	13.29	21.58	0.528
	≥ 60 years old	11.34 ± 3.60	6.93	16.01	

Table 9.12. Gender difference in the severity of DVU degeneration measured from baseline MRI scan at each lumbar DVU level for 34 AKU patients who were part of the SONIA 2 clinical trial stratified by gender.

The results display the mean Pfirrmann grade ± SD, minimum, and maximum score from six lumbar DVU regions from segment T12/L1 to segment L5/S1 for both genders. The results show male patients have significantly higher Pfirrmann scoring grade in DVUs than female AKU patients. The independent sample t-test revealed statistically significant differences between males and females across the lumbar DVUs ($P < 0.05$) except at L5/S1 ($P = 0.07$) * Statistical significance ($P < 0.05$).

DVU level	Gender	Pfirmann grade (mean ± SD)	Minimum	Maximum	P-value
T12/L1	Total	6.4 ± 2.7	1	8	0.021*
	M	7.4 ± 1.3	3	8	
	F	5.3 ± 3.5	1	8	
L1/L2	Total	6.6 ± 2.5	1	8	0.015*
	M	7.5 ± 1.2	3	8	
	F	5.5 ± 3.2	1	8	
L2/L3	Total	6.5 ± 2.6	1	8	0.046*
	M	7.3 ± 1.8	2	8	
	F	5.5 ± 3.2	1	8	
L3/L4	Total	6.3 ± 2.8	1	8	0.029*
	M	7.2 ± 2.0	1	8	
	F	5.1 ± 3.3	1	8	
L4/L5	Total	6.4 ± 2.8	1	8	0.029*
	M	7.3 ± 1.9	1	8	
	F	5.2 ± 3.3	1	8	
L5/SI	Total	6.6 ± 2.5	1	8	.071
	M	7.3 ± 1.9	1	8	
	F	5.7 ± 3.0	1	8	
Average lumbar DVUs	Total	6.5 ± 2.7	1	8	0.035*
	M	7.3 ± 1.7	1	8	
	F	5.4 ± 3.3	1	8	
Total lumbar DVUs	Total	38.8 ± 15.5	6	48	0.027*
	M	43.0 ± 9.5	17	48	
	F	32.3 ± 19.2	6	48	

Table 9.13. The severity of DVU degeneration measured from baseline MRI scans at each lumbar DVU level for 34 AKU patients who were part of the SONIA 2 clinical trial stratified by the decade of life.

The results display the mean Pfirrmann grade ± SD, minimum, and maximum score from six lumbar DVU regions from segment T12/L1 to segment L5/S1. * Correlation is statistically significant between 30-39 age group and 40-49 age group at all DVU level ($P < 0.05$).

DVU level	Age group	Pfirmann DVU (mean±SD)	Minimum	Maximum	P- value
T12/L1	30-39 years old	3.0 ± 2.7	1	8	0.007*
	40-49 years old	6.8 ± 2.5	1	8	0.376
	50-59 years old	7.6 ± 1.0	5	8	0.38
	≥ 60 years old	8.0 ± 0	8		
L1/L2	30-39 years old	3.6 ± 2.6	1	8	0.018*
	40-49 years old	6.8 ± 2.5	1	8	0.246
	50-59 years old	7.8 ± 0.4	7	8	0.317
	≥ 60 years old	8.0 ± 0	8		
L2/L3	30-39 years old	3.1 ± 2.6	1	8	0.009*
	40-49 years old	6.8 ± 2.5	1	8	0.376
	50-59 years old	7.6 ± 1.0	5	8	0.38
	≥ 60 years old	8.0 ± 0	8		
L3/L4	30-39 years old	2.4 ± 2.4	1	8	0.002*
	40-49 years old	6.8 ± 2.5	1	8	0.446
	50-59 years old	7.5 ± 1.1	5	8	0.328
	≥ 60 years old	8.0 ± 0	8		
L4/L5	30-39 years old	2.4 ± 2.4	1	8	0.002*
	40-49 years old	6.8 ± 2.5	1	8	0.298
	50-59 years old	7.7 ± 0.5	7	8	0.196
	≥ 60 years old	8.0 ± 0	8		
L5/SI	30-39 years old	3.1 ± 2.4	1	8	0.004*
	40-49 years old	7 ± 2.4	1	8	0.250
	50-59 years old	7.9 ± 0.3	7	8	0.5
	≥ 60 years old	8.0 ± 0	8		
Average lumbar DVU	30-39 years old	2.9 ± 2.3	1	8	0.0007*
	40-49 years old	6.9 ± 2.5	1	8	0.332
	50-59 years old	7.7 ± 0.4	5	8	0.35
	≥ 60 years old	8.0 ± 0	8		
Total lumbar DVU	30-39 years old	17.7 ± 13.6	6	48	0.004*
	40-49 years old	41.2 ± 14.9	6	48	0.315
	50-59 years old	46.1 ± 2.6	41	48	0.139
	≥ 60 years old	48.0 ± 0	48		

9.4 SONIA 2 finial analysis scan results: osteoarticular disease of joints

Table 9.14. Shows the summary statistics for the number of joints with osteoarticular disease detected from scantigraphy throughout the whole body from Visit 1 to Visit 6 for 169 AKU patients who were part of SONIA 2 clinical.

Data are summarised by the number of patients (n), mean HU (SD), median (IQR), the minimum and maximum. This table is split by treatment arm and clinical trial visits.

Visit	Statistic	Untreated (N=69)		Nitisinone (N=69)	
		Value	Change from baseline	Value	Change from baseline
Baseline	n	69		67	
	Mean	6.7		6.1	
	SD	3.2		3.1	
	Median	8.0		6.0	
	min	0		0	
	max	14		14	
Month 12	n	62	62	66	65
	Mean	6.7	0.0	6.4	0.1
	SD	3.2	0.4	3.2	0.5
	Median	7.0	0.0	6.5	0.0
	min	1	-1	0	-1
	max	14	2	14	2
Month 24	n	54	54	62	60
	Mean	8.4	1.6	8.2	1.9
	SD	3.3	3.0	3.3	2.8
	Median	8.0	0.5	8.0	1.5
	min	1	-4	0	-4
	max	14	10	14	10
Month 36	n	52	52	55	53
	Mean	9.1	2.3	8.4	2.3
	SD	3.2	3.1	3.5	3.4
	Median	9.0	2.0	8.0	2.0
	min	0	-3	0	-6
	max	14	10	14	11
Month 48	n	48	48	52	51
	Mean	9.1	2.1	8.5	2.4
	SD	3.3	3.1	3.6	3.4
	Median	9.5	1.5	8.0	2.0
	min	2	-4	0	-4
	max	14	10	14	11

Table 9.15. Shows the change in the number of joints with osteoarticular disease for nitisinone treated AKU patients and untreated patients who were part of the SONIA 2 clinical trial over four years.

Data are summarised the change from baseline at each visit for number of joints detected from the scantigraphy using a mixed model with repeated measurements (MMRM).

Visit	Statistic	Untreated (N=69)	Nitisinone (N=69)
Month 12	Adjusted mean	0.1	0.1
	95% CI	0.0; 0.2	0.0; 0.3
	Adjusted mean (difference nitisinone-untreated)		0.0
	95% CI		-0.1; 0.2
	p-value*		0.576
Month 24	Adjusted mean	2.0	1.9
	95% CI	1.2; 2.7	1.2; 2.7
	Adjusted mean (difference nitisinone-untreated)		-0.1
	95% CI		-1.1; 1.0
	p-value*		0.893
Month 36	Adjusted mean	2.1	2.2
	95% CI	1.3; 3.0	1.3; 3.1
	Adjusted mean (difference nitisinone-untreated)		0.1
	95% CI		-1.1; 1.3
	p-value*		0.911
Month 48	Adjusted mean	2.2	2.1
	95% CI	1.4; 3.1	1.3; 3.0
	Adjusted mean (difference nitisinone-untreated)		-0.1
	95% CI		-1.3; 1.1
	p-value*		0.899

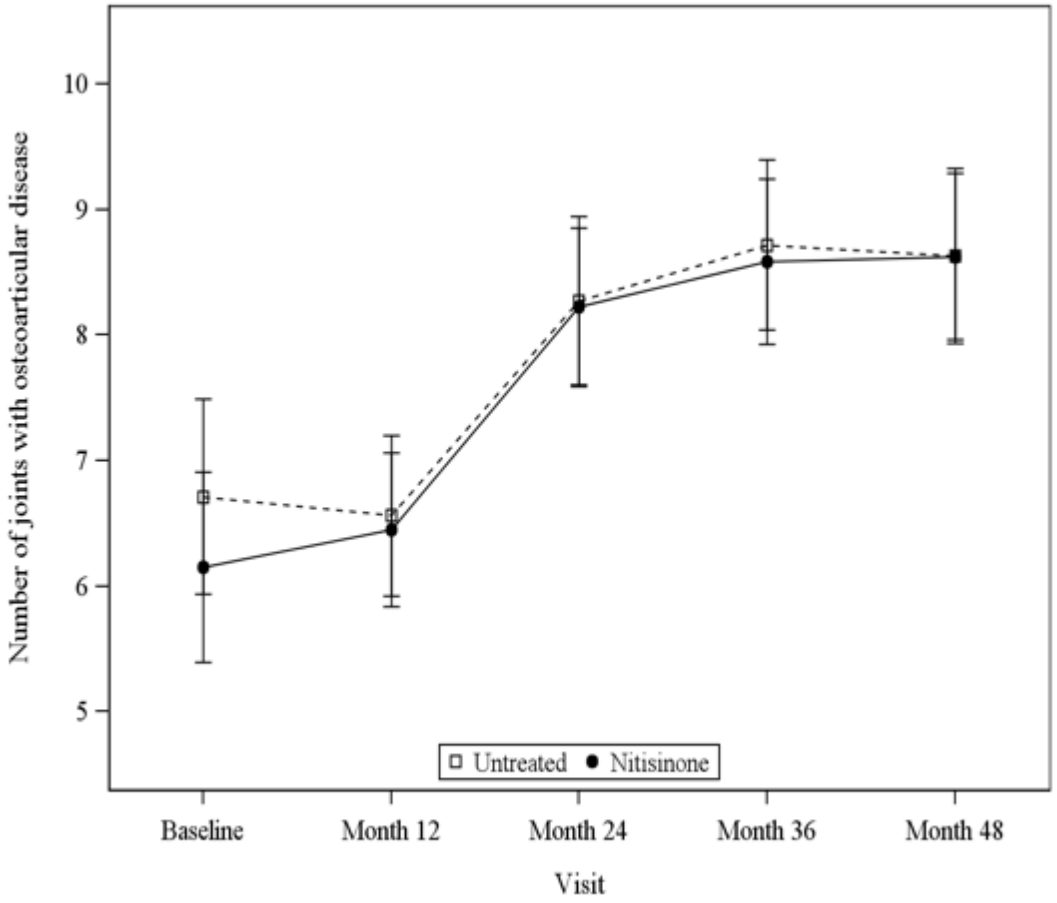

Figure 9.1. Changes in the number of joints with osteoarticular disease detected from scintigraphy from baseline to month 48 for nitisinone treated and untreated AKU patients.

Graph shows mean (95% CI) for baseline and adjusted mean (95% CI) for later time points.

Osteoarticular Disease of Spine

Table 9.16. Shows the summary statistics for the number of spinal regions with osteoarticular disease detected from scantigraphy throughout the whole body from Visit 1 to Visit 6 for 169 AKU patients who were part of SONIA 2 clinical.

Data are summarised by the number of patients (n), mean HU (SD), median (IQR), the minimum and maximum. This table is split by treatment arm and clinical trial visits.

Visit	Statistic	Untreated (N=69)		Nitisinone (N=69)	
		Value	Change from baseline	Value	Change from baseline
Baseline	N	69		67	
	Mean	3.0		3.4	
	SD	2.1		2.1	
	Median	3.0		4.0	
	Min	0		0	
	Max	6		6	
Month 12	N	62	62	66	65
	Mean	3.0	0.0	3.4	0.0
	SD	2.1	0.0	2.2	0.0
	Median	3.0	0.0	4.0	0.0
	Min	0	0	0	0
	Max	6	0	6	0
Month 24	N	54	54	62	60
	Mean	3.2	0.2	3.5	0.1
	SD	2.0	1.2	2.0	1.2
	Median	4.0	0.0	4.0	0.0
	Min	0	-3	0	-2
	Max	6	4	6	4
Month 36	N	52	52	55	53
	Mean	3.7	0.3	3.7	0.3
	SD	2.0	1.2	2.0	1.3
	Median	4.0	0.0	4.0	0.0
	Min	0	-3	0	-2
	Max	6	4	6	4
Month 48	N	48	48	52	51
	Mean	3.5	0.4	3.7	0.3
	SD	2.1	1.3	2.0	1.3
	Median	4.0	0.0	4.0	0.0
	Min	0	-3	0	-2
	Max	6	4	6	4

Table 9.17. Shows the change in the number of spinal regions with osteoarticular disease for nitisinone treated AKU patients and untreated patients who were part of the SONIA 2 clinical trial over four years.

Data are summarised the change from baseline at each visit for number of joints detected from the scantigraphy using a mixed model with repeated measurements (MMRM).

Visit	Statistic	Untreated (N=69)	Nitisinone (N=69)
Month 12	Adjusted mean	0.0	0.1
	95% CI	-0.2; 0.3	-0.2; 0.3
	Adjusted mean (difference nitisinone-untreated)		0.0
	95% CI		-0.3; 0.4
	p-value*		0.831
Month 24	Adjusted mean	0.3	0.2
	95% CI	0.0; 0.5	-0.1; 0.5
	Adjusted mean (difference nitisinone-untreated)		-0.1
	95% CI		-0.4; 0.3
	p-value*		0.641
Month 36	Adjusted mean	0.4	0.4
	95% CI	0.1; 0.6	0.1; 0.6
	Adjusted mean (difference nitisinone-untreated)		0.0
	95% CI		-0.4; 0.3
	p-value*		0.965
Month 48	Adjusted mean	0.4	0.3
	95% CI	0.2; 0.7	0.1; 0.6
	Adjusted mean (difference nitisinone-untreated)		-0.1
	95% CI		-0.4; 0.3
	p-value*		0.657

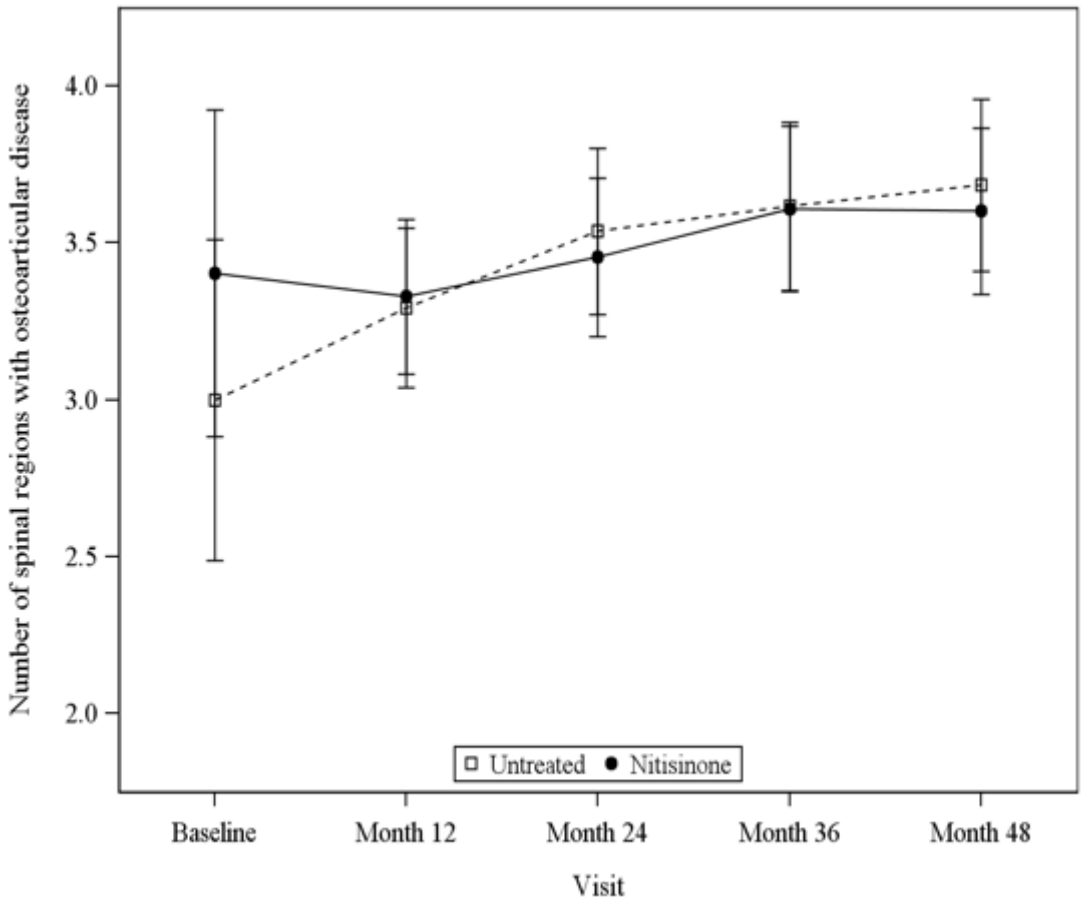

Figure 9.2. Changes in the number of spinal regions with osteoarticular diseas detected from scintigraphy from baseline to month 48 for nitisinone treated and untreated AKU patients.

Graph shows mean (95% CI) for baseline and adjusted mean (95% CI) for later time points.

Osteopenia of the Hip

Table 9.18. Shows the summary statistics for femur T-score values measured from DEXA scans from Visit 1 to Visit 6 for 169 AKU patients who were part of the SONIA 2 clinical.

Data are summarised by the number of patients (n), mean HU (SD), median (IQR), the minimum and maximum T-score. This table is split by treatment arm and clinical trial visits.

Visit	Statistic	Untreated (N=69)		Nitisinone (N=69)	
		Value	Change from baseline	Value	Change from baseline
Baseline	n	64		68	
	Mean	-1.26		-1.30	
	SD	0.98		1.20	
	Median	-1.25		-1.30	
	min	-3.9		-3.5	
	max	1.3		2.8	
Month 12	n	59	59	66	66
	Mean	-1.28	0.03	-1.39	-0.13
	SD	0.98	0.27	1.14	0.25
	Median	-1.20	0.00	-1.45	-0.10
	min	-3.3	-0.6	-3.4	-1.2
	max	1.6	1.1	2.5	0.4
Month 24	n	57	57	63	63
	Mean	-1.29	0.09	-1.37	-0.14
	SD	0.99	0.32	1.12	0.28
	Median	-1.30	-0.10	-1.40	-0.10
	min	-3.2	-0.6	-3.3	-1.1
	max	1.6	1.2	2.3	0.4
Month 36	n	57	57	58	58
	Mean	-1.37	0.07	-1.18	0.01
	SD	0.89	0.31	1.15	0.39
	Median	-1.40	-0.10	-1.25	-0.10
	min	-3.1	-0.7	-3.4	-0.8
	max	0.7	0.8	2.5	1.6
Month 48	n	50	50	53	53
	Mean	-1.41	-0.17	-1.22	0.04
	SD	0.81	0.35	1.17	0.41
	Median	-1.50	-0.20	-1.30	-0.10
	min	-3.1	-0.8	-3.3	-1.0
	max	0.2	0.8	2.9	1.6

Table 9.19. Shows the change in T-score values for nitisinone treated AKU patients and untreated patients who were part of the SONIA 2 clinical trial over four years.

Data are summarised the change from baseline at each visit for number of joints detected from the scantigraphy using a mixed model with repeated measurements (MMRM).

Visit	Statistic	Untreated (N=69)	Nitisinone (N=69)
Month 12	Adjusted mean	0.06	-0.15
	95% CI	-0.13; 0.01	-0.21; 0.09
	Adjusted mean (difference nitisinone-untreated)		0.09
	95% CI		-0.18; 0.01
	P-value*		0.030
Month 24	Adjusted mean	-0.12	-0.15
	95% CI	-0.20; 0.04	-0.23; 0.08
	Adjusted mean (difference nitisinone-untreated)		0.03
	95% CI		-0.13; 0.06
	P-value*		0.490
Month 36	Adjusted mean	-0.10	0.02
	95% CI	-0.20; 0.01	-0.12; 0.07
	Adjusted mean (difference nitisinone-untreated)		0.08
	95% CI		0.05; 0.21
	P-value*		0.211
Month 48	Adjusted mean	-0.19	0.05
	95% CI	-0.29; 0.09	-0.15; 0.05
	Adjusted mean (difference nitisinone-untreated)		0.14
	95% CI		0.00; 0.28
	P-value*		0.045

Table 9.20. Shows the summary statistics for the number of patients with osteopenia of the hip detected from DEXA scan from Visit 1 to Visit 6 for 169 AKU patients who were part of the SONIA 2 clinical.

Data are summarised by the number of patients (n), mean HU (SD), median (IQR), the minimum and maximum. This table is split by treatment arm and clinical trial visits. [a]Osteopenia/osteoporosis is categorised as Normal (T-score ≥-1.0), Osteopenia (T-score of -2.4 to -1.1) and Osteoporosis (T-score ≤-2.5).

Visit	Osteopenia/osteoporosis	Untreated	Nitisinone
Baseline	N **(%)**	64 (92.8)	68 (98.6)
	Normal	22 (31.9)	22 (31.9)
	Pts. with osteopenia or osteoporosis	42 (60.9)	46 (66.7)
	Osteopenia	35 (50.7)	33 (47.8)
	Osteoporosis	7 (10.1)	13 (18.8)
	Missing	5 (7.2)	1 (1.4)
Month 12	N **(%)**	59 (85.5)	66 (95.7)
	Normal	18 (26.1)	21 (30.4)
	Pts. with osteopenia or osteoporosis	41 (59.4)	45 (65.2)
	Osteopenia	36 (52.2)	32 (46.4)
	Osteoporosis	5 (7.2)	13 (18.8)
	Missing	10 (14.5)	3 (4.3)
Month 24	N **(%)**	57 (82.6)	63 (91.3)
	Normal	18 (26.1)	19 (27.5)
	Pts. with osteopenia or osteoporosis	39 (56.5)	44 (63.8)
	Osteopenia	33 (47.8)	30 (43.5)
	Osteoporosis	6 (8.7)	14 (20.3)
	Missing	12 (17.4)	6 (8.7)
Month 36	N **(%)**	57 (82.6)	58 (84.1)
	Normal	18 (26.1)	23 (33.3)
	Pts. with osteopenia or osteoporosis	39 (56.5)	35 (50.7)
	Osteopenia	35 (50.7)	24 (34.8)
	Osteoporosis	4 (5.8)	11 (15.9)
	Missing	12 (17.4)	11 (15.9)
Month 48	N **(%)**	50 (72.5)	53 (76.8)
	Normal	15 (21.7)	19 (27.5)
	Pts. with osteopenia or osteoporosis	35 (50.7)	34 (49.3)
	Osteopenia	33 (47.8)	26 (37.7)
	Osteoporosis	2 (2.9)	8 (11.6)
	Missing	19 (27.5)	16 (23.2)

Table 9.21. Shows the change in the number of patients with osteopenia of the hip for nitisinone treated AKU patients and untreated patients who were part of the SONIA 2 clinical trial over four years.

Data are summarised the change from baseline at each visit for number of joints detected from the scantigraphy using a general estimating equations (GEE) model.

Visit	Osteopenia/osteoporosis[a]	Untreated (N=69)	Nitisinone (N=69)
		n (%)	n (%)
Month 12	Improved by 1 category	3 (4.3)	0 (0.0)
	Unchanged	49 (71.0)	56 (81.2)
	Worsened by 1 category	7 (10.1)	10 (14.5)
	Missing	10 (14.5)	3 (4.3)
	P-value[*]		0.226
Month 24	Improved by 1 category	4 (5.8)	1 (1.4)
	Unchanged	42 (60.9)	48 (69.6)
	Worsened by 1 category	11 (15.9)	14 (20.3)
	Missing	12 (17.4)	6 (8.7)
	P-value[*]		0.379
Month 36	Improved by 1 category	8 (11.6)	4 (5.8)
	Unchanged	40 (58.0)	48 (69.6)
	Worsened by 1 category	9 (13.0)	6 (8.7)
	Missing	12 (17.4)	11 (15.9)
	P-value[*]		0.874
Month 48	Improved by 1 category	4 (5.8)	4 (5.8)
	Unchanged	34 (49.3)	41 (59.4)
	Worsened by 1 category	12 (17.4)	8 (11.6)
	Missing	19 (27.5)	16 (23.2)
	P-value[*]		0.376

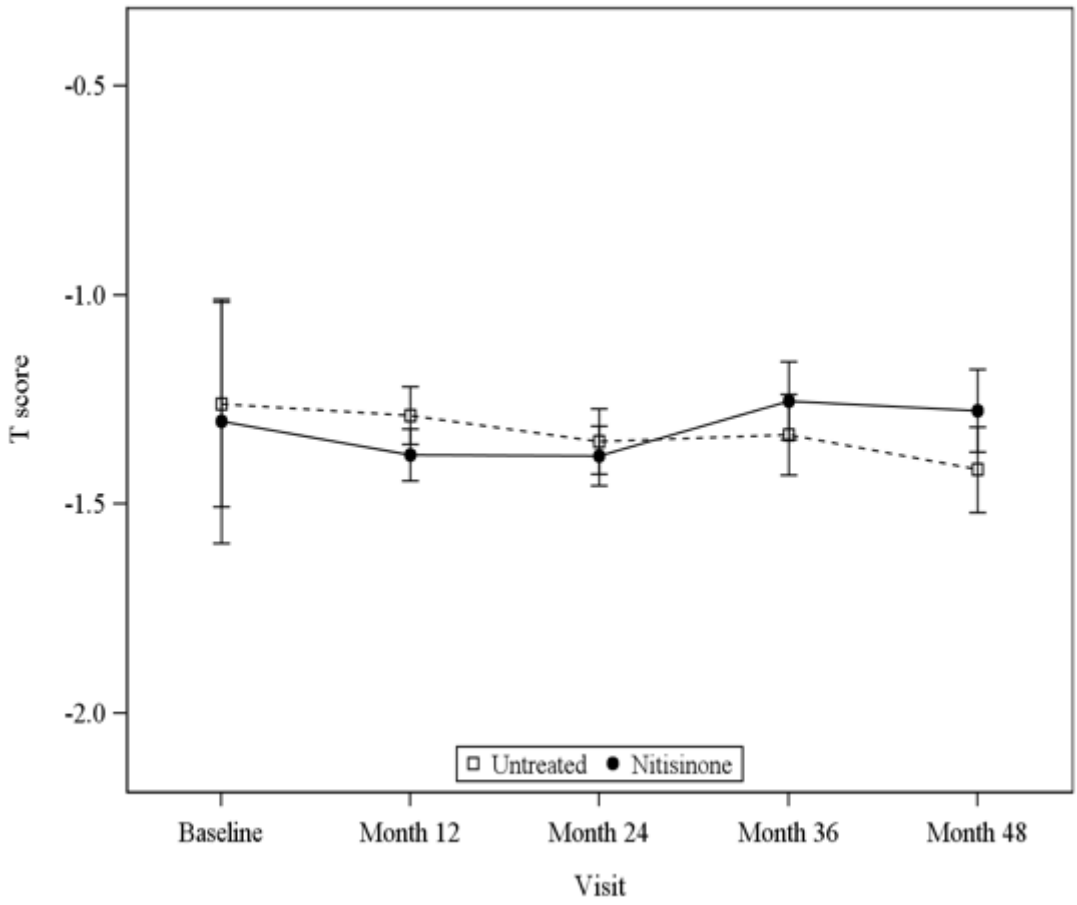

Figure 9.3. Changes in the femoral T-score measured from DEXA scan from baseline to month 48 for nitisinone treated and untreated AKU patients.

Graph shows mean (95% CI) for baseline and adjusted mean (95% CI) for later time points.

Fractures

Table 9.22. Shows the summary statistics for the number of fractures detected from MRI from Visit 1 to Visit 6 for 169 AKU patients who were part of the SONIA 2 clinical.

Data are summarised by the number of patients (n), mean HU (SD), median (IQR), the minimum and maximum. This table is split by treatment arm and clinical trial visits. Change from baseline is analysed using a generalised linear mixed model with an underlying Poisson distribution and a log-link function.

Visit	Number of episodes	Untreated (N=69) Since last visit n (%)	Number of patients with episodes		
			Since baseline n (%)	Nitisinone (N=69) Since last visit n (%)	Since baseline n (%)
Baseline	n	69	69	69	69
	0	58 (84.1)		54 (78.3)	
	1	8 (11.6)		11 (15.9)	
	2	0 (0.0)		2 (2.9)	
	3	1 (1.4)		2 (2.9)	
	4	0 (0.0)		0 (0.0)	
	5	2 (2.9)		0 (0.0)	
	Missing	0 (0.0)		0 (0.0)	
Month 12	n	63	63	67	67
	0	61 (88.4)	61 (88.4)	66 (95.7)	66 (95.7)
	1	2 (2.9)	2 (2.9)	1 (1.4)	1 (1.4)
	2	0 (0.0)	0 (0.0)	0 (0.0)	0 (0.0)
	3	0 (0.0)	0 (0.0)	0 (0.0)	0 (0.0)
	4	0 (0.0)	0 (0.0)	0 (0.0)	0 (0.0)
	5	0 (0.0)	0 (0.0)	0 (0.0)	0 (0.0)
	Missing	6 (8.7)	6 (8.7)	2 (2.9)	2 (2.9)
	P-value*				0.443
Month 24	n	61	61	65	65
	0	61 (88.4)	60 (87.0)	65 (94.2)	64 (92.8)
	1	0 (0.0)	1 (1.4)	0 (0.0)	1 (1.4)
	2	0 (0.0)	0 (0.0)	0 (0.0)	0 (0.0)
	3	0 (0.0)	0 (0.0)	0 (0.0)	0 (0.0)
	4	0 (0.0)	0 (0.0)	0 (0.0)	0 (0.0)
	5	0 (0.0)	0 (0.0)	0 (0.0)	0 (0.0)
	Missing	8 (11.6)	8 (11.6)	4 (5.8)	4 (5.8)
	P-value*				1.000
Month 36	n	61	61	60	60
	0	60 (87.0)	59 (85.5)	60 (87.0)	59 (85.5)
	1	1 (1.4)	2 (2.9)	0 (0.0)	1 (1.4)
	2	0 (0.0)	0 (0.0)	0 (0.0)	0 (0.0)

Visit	Number of episodes	Untreated (N=69) Since last visit n (%)	Number of patients with episodes		
			Since baseline n (%)	Nitisinone (N=69) Since last visit n (%)	Since baseline n (%)
	3	0 (0.0)	0 (0.0)	0 (0.0)	0 (0.0)
	4	0 (0.0)	0 (0.0)	0 (0.0)	0 (0.0)
	5	0 (0.0)	0 (0.0)	0 (0.0)	0 (0.0)
	Missing	8 (11.6)	8 (11.6)	9 (13.0)	9 (13.0)
	P-value*				0.998
Month 48	n	53	53	55	55
	0	48 (69.6)	46 (66.7)	53 (76.8)	52 (75.4)
	1	5 (7.2)	6 (8.7)	2 (2.9)	3 (4.3)
	2	0 (0.0)	1 (1.4)	0 (0.0)	0 (0.0)
	3	0 (0.0)	0 (0.0)	0 (0.0)	0 (0.0)
	4	0 (0.0)	0 (0.0)	0 (0.0)	0 (0.0)
	5	0 (0.0)	0 (0.0)	0 (0.0)	0 (0.0)
	Missing	16 (23.2)	16 (23.2)	14 (20.3)	14 (20.3)
	P-value*				0.160

*

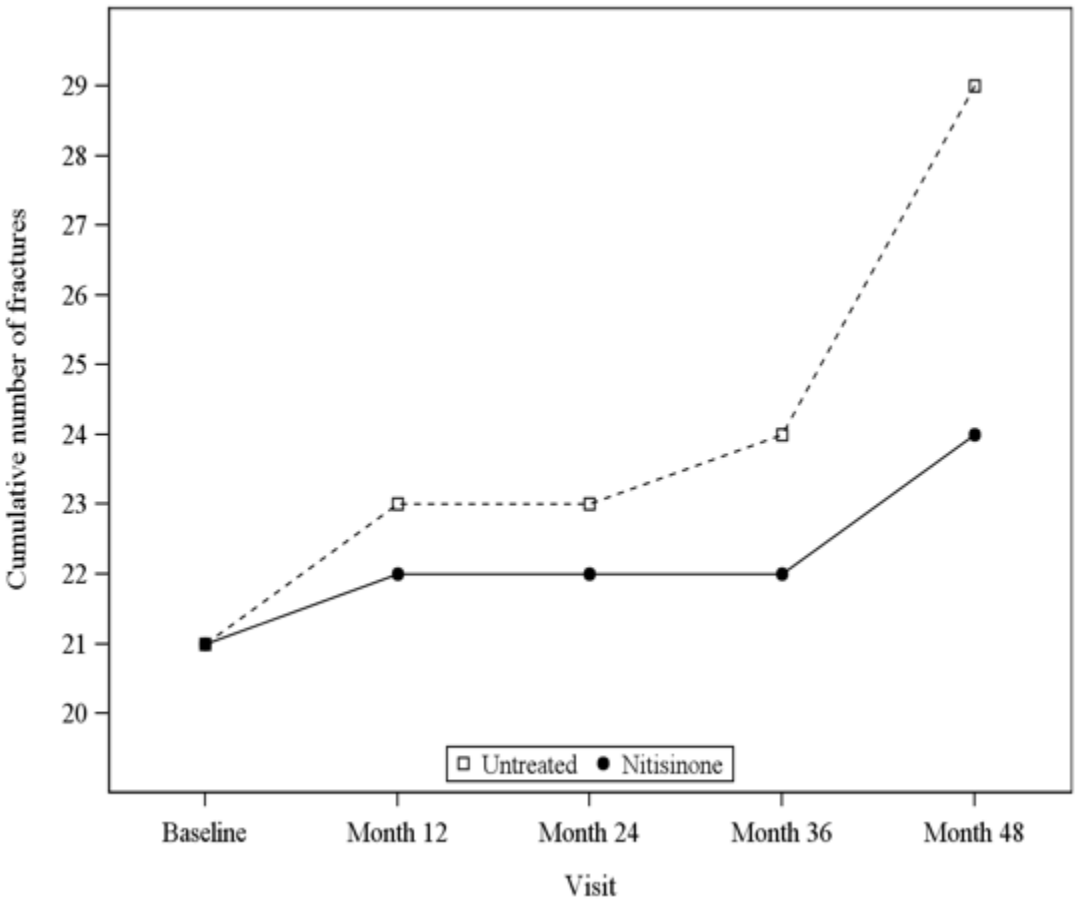

Figure 9.4. Changes in the number of fractures detected from MRI scans from baseline to month 48 for nitisinone treated and untreated AKU patients.

9.5 Treatment efficacy of nitisinone on spine ochronotic arthropathy in SONIA 2 patients using ^{18}F-NaF PET/CT scan

Table 9.23. Shows the summary statistics for HU measured from CT images for average lumbar vertebrae bodies (L1-L5) from Visit 1 to Visit 6 for 34 AKU patients who were part of the SONIA 2 clinical trial and involved in this study.

Data are summarised by the number of patients (n), mean HU (SD), median (IQR), the minimum and maximum HU values. This table is split by treatment arm and clinical trial visits.

Visit		Statistic	Untreated (N=17)	Nitisinone (N=17)
Visit 1	Baseline	N	17	17
		Mean (SD)	174.1 (104.3)	152.7 (61.0)
		Median (IQR)	154.2 (108.5,207.8)	160.2 (106.7,196.9)
		Min, max	49.1, 509.8	10.9, 242.0
Visit 3	Month 12	N	15	15
		Mean (SD)	190.6 (111.4)	139.5 (61.1)
		Median (IQR)	171.2 (127.4,197.8)	150.3 (97.2,199.6)
		Min, max	82.9, 560.6	17.5, 223.0
Visit 4	Month 24	N	14	16
		Mean (SD)	176.9 (119.5)	143.0 (58.1)
		Median (IQR)	172.3 (80.0,202.9)	141.8 (104.1,190.3)
		Min, max	49.7, 531.5	17.1, 232.9
Visit 5	Month 36	N	15	15
		Mean (SD)	178.5 (123.0)	134.2 (52.0)
		Median (IQR)	153.6 (114.7,204.8)	131.2 (109.5,183.8)
		Min, max	43.1, 573.3	-6.1, 191.0
Visit 6	Month 48	N	14	12
		Mean (SD)	171.9 (112.2)	144.4 (59.6)
		Median (IQR)	152.1 (113.0,209.5)	165.6 (127.6,180.5)
		Min, max	50.4, 509.5	-26.7, 186.3

Table 9.24. Shows the change in HU values for nitisinone treated AKU patients and untreated patients who were part of the SONIA 2 clinical trial over four years.

Data are summarised the change from baseline at each visit for HU values measured from the CT image for lumbar vertebrae bodies (L1-L5) using a Kruskal-Wallis test. *P-value < 0.05 indicate a statistically significant difference between treatment groups in the mean change from baseline in HU values. At month 12, nitisinone-treated patients showed significantly more reduction in the mean lumbar HU_{mean} value than non-treated patients (P = 0.036). There were no statistically significant differences between treatment and non-treatment groups in the mean change in lumbar HU_{mean} measurements at neither month 24, month 36, or month 48 (P = 0.739, 0.120, and 0.681, respectively).

Visit		Statistic	Untreated (N=17)	Nitisinone (N=17)	P-value
Visit 3	Month 12	N	15	15	
		Mean (SD)	10.9 (22.1)	-6.5 (21.1)	
		Median (IQR)	6.1 (-1.6,27.0)	-5.3 (-19.0,6.7)	***0.036**
		Min, max	-38.5, 50.8	-48.7, 35.9	
Visit 4	Month 24	N	14	16	
		Mean (SD)	-2.9 (21.4)	-7.0 (18.9)	
		Median (IQR)	-1.5 (-21.1,6.6)	-7.0 (-14.8,8.2)	0.739
		Min, max	-33.8, 42.5	-51.0, 23.2	
Visit 5	Month 36	N	15	15	
		Mean (SD)	-3.6 (30.6)	-20.2 (23.7)	
		Median (IQR)	-2.9 (-15.4,9.7)	-16.9 (-40.3,4.0)	0.120
		Min, max	-63.9, 63.5	-64.5, 9.6	
Visit 6	Month 48	N	14	12	
		Mean (SD)	-8.8 (24.0)	-10.5 (37.4)	
		Median (IQR)	-3.5 (-29.1,3.5)	-20.7 (-36.0,9.0)	0.681
		Min, max	-50.1, 33.8	-63.6, 78.3	

Table 9.25. Shows the summary statistics for SUV_{max} measured from PET scan for average lumbar vertebrae bodies (L1-L5) from Visit 1 to Visit 6 for 34 AKU patients who were part of the SONIA 2 clinical trial and involved in this study.

Data are summarised by the number of patients (n), mean SUV_{max} (SD), median (IQR), the minimum and maximum SUV_{max} values. This table is split by treatment arm and visits.

Visit		Statistic	Untreated (N=17)	Nitisinone (N=17)
Visit 1	Baseline	N	17	17
		Mean (SD)	12.6 (4.2)	11.9 (2.0)
		Median (IQR)	11.9 (9.9,14.8)	11.9 (10.6,12.3)
		Min, max	5.8, 20.3	7.5, 16.4
Visit 3	Month 12	N	15	15
		Mean (SD)	12.7 (3.5)	11.9 (2.4)
		Median (IQR)	12.0 (10.8,14.5)	12.1 (10.3,14.2)
		Min, max	6.1, 19.5	6.7, 16.0
Visit 4	Month 24	N	14	16
		Mean (SD)	14.5 (5.2)	12.7 (2.9)
		Median (IQR)	13.2 (12.0,16.4)	12.7 (10.9,14.6)
		Min, max	7.6, 27.0	6.5, 17.3
Visit 5	Month 36	N	15	15
		Mean (SD)	14.6 (5.5)	13.7 (3.5)
		Median (IQR)	12.7 (11.3,16.8)	14.0 (11.5,15.8)
		Min, max	7.4, 28.4	7.1, 20.7
Visit 6	Month 48	N	14	12
		Mean (SD)	13.9 (4.0)	15.1 (4.6)
		Median (IQR)	13.0 (11.0,18.0)	14.0 (13.0,17.5)
		Min, max	8.1, 20.2	6.8, 23.4

Table 9.26. Shows the change in SUV_{max} values for nitisinone treated and untreated AKU patients who were part of the SONIA 2 clinical trial over four years.

Data are summarised the change from baseline at each visit for SUV_{max} values measured from PET scan for lumbar vertebrae bodies (L1-L5) using a Kruskal-Wallis test. *P-value < 0.0,5 indicate a statistically significant difference between treatment groups in the mean change from baseline in SUV_{max} values. At month 12, month 24, and month 36, there was no statistically significant change from baseline in vertebrae SUV_{max} values. At month 48, nitisinone-treated patients presented a significantly higher increment in the mean lumbar vertebrae SUV_{max} values than non-treated patients.

Visit		Statistic	Untreated (N=17)	Nitisinone (N=17)	P-value
Visit 3	Month 12	n	15	15	
		Mean (SD)	-0.5 (2.2)	0.2 (1.3)	
		Median (IQR)	-0.5 (-2.0,0.9)	0.2 (-0.5,1.6)	0.206
		Min, max	-4.2, 4.0	-2.9, 2.4	
Visit 4	Month 24	n	14	16	
		Mean (SD)	1.5 (4.2)	0.8 (1.7)	
		Median (IQR)	1.1 (-0.5,2.1)	0.8 (-0.3,1.2)	0.678
		Min, max	-4.0, 14.3	-1.7, 4.7	
Visit 5	Month 36	n	15	15	
		Mean (SD)	1.3 (4.7)	1.7 (2.2)	
		Median (IQR)	0.7 (-1.1,1.8)	1.6 (-0.4,4.1)	0.310
		Min, max	-3.7, 15.7	-1.3, 5.2	
Visit 6	Month 48	n	14	12	
		Mean (SD)	0.5 (2.4)	3.0 (3.6)	
		Median (IQR)	0.0 (-1.6,1.6)	2.3 (0.5,4.6)	***0.045**
		Min, max	-2.2, 5.0	-0.8, 11.8	

Table 9.27. Shows the summary statistics for SUV_{max} measured from PET scan for average lumbar vertebrae disc units (T12/L1-L5/S1) from Visit 1 to Visit 6 for 34 AKU patients who were part of SINIA 2 clinical trial and involved in this study.

Data are summarised by the number of patients (n), mean SUV_{max} (SD), median (IQR), the minimum and maximum SUV_{max} values. This table is split by treatment arm and visits.

Visit		Statistic	Untreated (N=17)	Nitisinone (N=17)
Visit 1	Baseline	N	17	17
		Mean (SD)	14.7 (5.4)	14.6 (2.9)
		Median (IQR)	14.2 (10.6,18.0)	14.3 (13.3,16.0)
		Min, max	6.9, 23.8	8.6, 19.8
Visit 3	Month 12	N	15	15
		Mean (SD)	15.1 (4.9)	14.3 (3.4)
		Median (IQR)	14.8 (11.3,20.2)	14.3 (11.6,16.0)
		Min, max	6.1, 22.4	7.5, 21.0
Visit 4	Month 24	N	14	16
		Mean (SD)	16.7 (6.5)	14.8 (3.7)
		Median (IQR)	15.6 (12.2,21.1)	14.5 (13.0,17.0)
		Min, max	7.5, 30.5	7.1, 21.8
Visit 5	Month 36	N	15	15
		Mean (SD)	15.7 (5.8)	13.8 (3.4)
		Median (IQR)	14.7 (12.0,18.7)	14.7 (10.5,15.3)
		Min, max	7.0, 29.8	7.3, 20.6
Visit 6	Month 48	N	14	12
		Mean (SD)	14.6 (3.9)	15.3 (4.7)
		Median (IQR)	14.0 (12.5,17.9)	15.8 (12.6,18.2)
		Min, max	7.8, 20.1	6.4, 22.7

Table 9.28. Shows the change in lumbar DVU SUV_{max} values for nitisinone treated and untreated AKU patients who were part of the SONIA 2 clinical trial over four years.

Data are summarised the change from baseline for SUV_{max} measured from PET scan for lumbar DVU (T12/L1-L5-S1) using a Kruskal-Wallis test. There was no statistically significant difference between treatment and non-treatment groups in the adjusted mean change from baseline in SUV_{max} values at none of the visits ($P > 0.05$).

Visit		Statistic	Untreated (N=17)	Nitisinone (N=17)	P-value
Visit 3	Month 12	N	15	15	
		Mean (SD)	-0.4 (2.3)	-0.4 (1.7)	
		Median (IQR)	-0.5 (-2.2,2.1)	-0.9 (-1.5,1.2)	0.885
		Min, max	-4.8, 3.0	-2.7, 2.5	
Visit 4	Month 24	N	14	16	
		Mean (SD)	1.8 (4.3)	0.2 (2.0)	
		Median (IQR)	2.0 (-0.5,2.9)	0.9 (-1.6,1.6)	0.124
		Min, max	-5.6, 13.8	-3.7, 3.6	
Visit 5	Month 36	N	15	15	
		Mean (SD)	0.5 (4.3)	-0.6 (2.4)	
		Median (IQR)	0.8 (-1.9,2.0)	-0.3 (-3.1,1.8)	0.633
		Min, max	-5.1, 13.2	-4.5, 2.4	
Visit 6	Month 48	N	14	12	
		Mean (SD)	-1.1 (3.1)	0.5 (3.6)	
		Median (IQR)	-0.3 (-3.8,1.0)	0.5 (-2.5,2.3)	0.280
		Min, max	-6.7, 3.3	-3.8, 8.6	

9.6 Cardiovascular calcification in alkaptonuria patients using quantitative analysis by ^{18}F-NaF PET/CT

Table 9.29. Gender difference in the severity of cardiovascular calcification measured from ^{18}F-NaF PET/CT scan for 40 AKU patients who were part of the SONIA 2 trial.

The results show mean SUV_{max} ± SD, minimum, and maximum values for main branches of arteries for males and females. * Correlation is statistically significant between gender at the ROI ($P < 0.05$). Left coronary artery-left main stem (LCA), left anterior descending artery (LAD), left circumflex artery (CA) and right coronary artery (RCA), ascending aorta (AA) and descending aorta (DA), inferior vena cava (IVC) and superior vena cava (SVC).

ROI	Gender	SUV_{max} ± SD	Minimum	Maximum	P-value
LCA	Total	1.57 ± 0.59	0.78	3.73	0.161
	Male	1.67 ± 0.65	0.87	3.73	
	Female	1.40 ± 0.45	0.78	2.16	
LAD	Total	1.12 ± 0.35	0.55	1.97	0.066
	Male	1.2 ± 0.37	0.57	1.97	
	Female	0.99 ± 0.27	0.55	1.74	
CA	Total	1.18 ± 0.50	0.45	2.64	0.675
	Male	1.21 ± 0.45	0.45	2.39	
	Female	1.14 ± 0.57	0.54	2.64	
RCA	Total	1.68 ± 1.04	0.6	6.02	0.022*
	Male	1.99 ± 1.20	0.7	6.02	
	Female	1.23 ± 0.49	0.6	2.25	
All main coronary arteries	Total	1.39 ± 0.49	0.73	2.55	0.036*
	Male	1.52 ± 0.51	0.76	2.55	
	Female	1.23 ± 0.49	0.6	2.25	
AA	Total	1.78 ± 0.57	0.89	3.6	0.222
	Male	1.87 ± 0.59	1.15	3.6	
	Female	1.65 ± 0.51	0.89	2.75	
DA	Total	2.38 ± 1.29	0.99	7.1	0.771
	Male	2.43 ± 1.20	1.21	7.1	
	Female	2.30 ± 1.46	0.99	6.76	
All aorta	Total	2.06 ± 0.84	0.94	4.76	0.471
	Male	2.14 ± 0.78	1.18	4.7	
	Female	1.94 ± 0.93	0.94	4.76	
IVC	Total	0.77 ± 0.30	0.37	1.79	0.003*
	Male	0.64 ± 0.20	0.37	1.09	
	Female	0.96 ± 0.33	0.54	1.79	
SVC	Total	0.86 ± 0.28	0.43	1.86	0.631
	Male	0.84 ± 0.25	0.43	1.37	
	Female	0.89 ± 0.33	0.51	1.86	
Average BP	Total	0.82 ± 0.27	0.43	1.83	0.123
	Male	0.76 ± 0.21	0.43	1.2	
	Female	0.90 ± 0.33	0.53	1.83	

Table 9.30. SUV_{max} measurements at the cardiac arteries for 40 AKU patients who were part of the SONIA 2 clinical trial stratified by the decade of life.

Data display the SUV_{max} ± SD, minimum and maximum values, and P-value obtained from the baseline ^{18}F-NaF PET/CT scan at the main coronary arteries (LCA, LAD, CA, and RCA), aorta (AA, and DA), and blood pool vessels (IVc, and SVC) in four age groups. * Correlation is statistically significant between age group at the ROI ($P < 0.05$).

ROI	Age group	SUV_{max} ± SD	Minimum	Maximum	P-value
LCA	30-39 years old	1.20 ± 0.26	0.95	1.66	0.26
	40-49 years old	1.60 ± 0.89	0.78	3.73	0.91
	50-59 years old	1.57 ± 0.45	1.09	2.27	0.20
	> 60 years old	1.77 ± 0.20	1.44	2.15	
LAD	30-39 years old	0.99 ± 0.34	0.81	1.74	0.41
	40-49 years old	1.14 ± 0.40	0.57	1.97	0.58
	50-59 years old	1.05 ± 0.32	0.55	1.55	0.18
	> 60 years old	1.24 ± 0.30	0.98	1.92	
CA	30-39 years old	1.06 ± 0.21	0.75	1.41	0.96
	40-49 years old	1.07 ± 0.52	0.45	2.39	0.61
	50-59 years old	1.16 ± 0.40	0.60	1.80	0.26
	> 60 years old	1.44 ± 0.64	0.61	2.64	
RCA	30-39 years old	1.28 ± 0.32	0.78	1.74	0.75
	40-49 years old	1.42 ± 1.14	0.60	4.61	0.61
	50-59 years old	1.63 ± 0.53	0.92	2.53	0.13
	> 60 years old	2.36 ± 1.38	1.32	6.02	
All coronary arteries	30-39 years old	1.13 ± 0.25	0.91	1.64	0.49
	40-49 years old	1.31 ± 0.63	0.73	2.55	0.84
	50-59 years old	1.35 ± 0.34	0.94	1.95	0.05*
	> 60 years old	1.71 ± 0.40	1.19	2.46	
AA	30-39 years old	1.68 ± 0.52	0.89	2.60	0.91
	40-49 years old	1.65 ± 0.50	1.15	2.40	0.25
	50-59 years old	1.94 ± 0.67	1.28	3.60	0.80
	> 60 years old	1.87 ± 0.59	1.27	2.75	
DA	30-39 years old	1.94 ± 0.65	0.99	2.90	0.52
	40-49 years old	2.34 ± 1.53	1.09	7.10	0.64
	50-59 years old	2.61 ± 1.11	1.42	4.60	0.84
	> 60 years old	2.49 ± 1.55	1.42	6.76	
All aorta	30-39 years old	1.73 ± 0.52	0.94	2.29	0.49
	40-49 years old	2.00 ± 0.93	1.18	4.70	0.45
	50-59 years old	2.28 ± 0.78	1.45	3.70	0.75
	> 60 years old	2.15 ± 0.98	1.43	4.76	
IVC	30-39 years old	1.09 ± 0.52	0.54	1.79	0.16
	40-49 years old	0.76 ± 0.25	0.37	1.09	0.62
	50-59 years old	0.71 ± 0.22	0.39	1.13	0.82
	> 60 years old	0.68 ± 0.24	0.41	1.21	
SVC	30-39 years old	0.87 ± 0.49	0.43	1.86	0.54
	40-49 years old	0.78 ± 0.15	0.54	1.06	0.16
	50-59 years old	0.91 ± 0.26	0.50	1.37	0.98
	> 60 years old	0.91 ± 0.27	0.55	1.30	
Average BP	30-39 years old	0.87 ± 0.47	0.43	1.83	0.51
	40-49 years old	0.77 ± 0.17	0.54	1.06	0.33
	50-59 years old	0.86 ± 0.23	0.58	1.26	0.66
	> 60 years old	0.81 ± 0.26	0.48	1.26	

Table 9.31. Gender difference in the severity of cardiovascular calcification measured from baseline ^{18}F-NaF PET/CT scans for 40 AKU patients who were part of the SONIA 2 clinical trial.

The results show mean TBR_{max} ± SD, minimum, and maximum values for main branches of coronary arteries and aortic arteries for males and females. * Correlation is statistically significant between gender at the ROI ($P < 0.05$). A significant difference was found between male and female at LAD and RCA only ($P = 0.018$, $P = 0.0\ 12$, respectively). Left coronary artery-left main stem (LCA), left anterior descending artery (LAD), left circumflex artery (-CA) and right coronary artery (RCA).

ROI	Gender	TBR_{max} ± SD	Minimum	Maximum	P-value
LCA	Total male female	2.12 ±1.44 2.43 ±1.78 1.67 ±0.37	1.09 1.09 1.16	10.08 10.08 2.37	0.1
LAD	Total male female	1.45 ± 0.51 1.60 ±0.55 1.22 ±0.35	0.69 0.87 0.69	2.85 2.85 1.76	0.018*
CA	Total male female	1.53 ±0.77 1.65 ±0.87 1.35 ± 0.55	0.69 0.81 0.69	4.31 4.31 2.54	0.219
RCA	Total male female	2.21 ±1.60 2.72 ±1.89 1.44 ±0.41	0.64 0.88 0.64	9.7 9.7 2.04	0.012*
All main coronary arteries	Total male female	1.80 ±0.80 2.06 ±0.93 1.42 ±0.31	0.94 1.05 0.94	4.59 4.59 2.04	0.012*
AA	Total male female	2.31 ±1.06 2.50 ±1.17 2.03 ±0.82	1.27 1.42 1.27	6.21 6.21 4.73	0.175
DA	Total male female	3.03 ±1.74 3.28 ±2.042 2.66 ±1.11	1.17 1.17 1.17	10.22 10.22 5.39	0.275
All Aorta	Total male female	2.7 ±1.24 2.94 ±1.44 2.34 ± 0.80	1.22 1.63 1.22	6.76 6.76 4.15	0.141

Table 9.32. TBR_{max} measurements at the cardiac arteries for 40 AKU patients who were part of the SONIA 2 clinical trial stratified by the decade of life.

Data display the TBR_{max} ± SD, minimum and maximum values and P-value obtained from the baseline ^{18}F-NaF PET/CT scan at the main coronary arteries and aorta in four age groups. Statistically, no significant difference between the values of TBR_{max} of age groups at neither coronary nor aortic arterial regions (P > 0.05).

ROI	Age Group	TBR_{max} ± SD	Minimum	Maximum	P-value
LCA	30-39 years old	1.67 ± 0.64	1.13	3.02	0.43
	40-49 years old	2.42 ± 2.38	1.09	10.08	0.46
	50-59 years old	1.85 ± 0.47	1.19	2.59	0.09
	> 60 years old	2.33 ± 0.72	1.40	3.95	
LAD	30-39 years old	1.34 ± 0.41	0.86	1.93	0.50
	40-49 years old	1.49 ± 0.51	0.87	2.85	0.22
	50-59 years old	1.25 ± 0.39	0.69	1.89	0.10
	> 60 years old	1.66 ± 0.65	0.78	2.82	
CA	30-39 years old	1.50 ± 0.63	0.92	2.58	0.87
	40-49 years old	1.44 ± 0.92	0.76	4.31	0.80
	50-59 years old	1.36 ± 0.40	0.69	1.89	0.15
	> 60 years old	1.84 ± 0.93	0.83	3.95	
RCA	30-39 years old	1.76 ± 0.66	1.29	3.16	0.89
	40-49 years old	1.83 ± 1.30	0.64	4.54	0.87
	50-59 years old	1.91 ± 0.49	1.08	2.47	0.10
	> 60 years old	3.32 ± 2.55	1.25	9.70	
All main coronary arteries	30-39 years old	1.62 ± 0.52	1.13	2.67	0.87
	40-49 years old	1.69 ± 0.96	0.94	4.59	0.76
	50-59 years old	1.59 ± 0.32	0.98	2.01	0.04*
	> 60 years old	2.29 ± 0.97	1.22	3.88	
AA	30-39 years old	2.41 ± 1.26	1.27	4.73	0.46
	40-49 years old	2.10 ± 0.54	1.37	3.31	0.47
	50-59 years old	2.41 ± 1.36	1.63	6.21	0.98
	> 60 years old	2.42 ± 1.21	1.42	5.52	
DA	30-39 years old	2.89 ± 1.87	1.17	6.74	0.85
	40-49 years old	3.08 ± 2.25	1.17	10.22	0.95
	50-59 years old	3.14 ± 1.50	1.87	6.55	0.77
	> 60 years old	2.95 ± 1.32	1.50	5.39	
All aorta	30-39 years old	2.65 ± 1.44	1.22	5.12	0.99
	40-49 years old	2.64 ± 1.30	1.57	6.76	0.83
	50-59 years old	2.77 ± 1.35	1.82	6.38	0.95
	> 60 years old	2.73 ± 1.10	1.63	5.15	

Table 9.33. Gender difference in the severity of cardiovascular calcification measured from CT scans for 40 AKU patients who were part of the SONIA 2 clinical trial.

The results show mean HU_{mean} ± SD, minimum, and maximum values for main branches of arteries for males and females. * Correlation is statistically significant between gender at the ROI ($P < 0.05$). Left coronary artery-left main stem (LCA), left anterior descending artery (LAD), left circumflex artery (CA) and right coronary artery (RCA), aortic arteries, including ascending aorta (AA) and descending aorta (DA), and blood pool vessels, including inferior vena cava (IVC) and superior vena cava (SVC).

ROI	Gender	HU_{mean} ± SD	Minimum	Maximum	P-value
LCA	Total male female	127.42 ± 153.91 140.00 ± 150.30 108.56 ± 162.22	-2 22 -2	700 619 700	0.534
LAD	Total male female	115.75 ± 124.66 145.42 ± 138.54 71.25 ± 86.33	7 26 7	502 502 368	0.064
CA	Total male female	125.89 ± 177.40 143.44 ±2 06.56 99.56 ± 123.16	3 21 3	937 937 428	0.451
RCA	Total male female	197.2 ± 239.88 238.21 ± 274.65 135.69 ± 164.99	-29 10 -29	1217 1217 589	0.189
All coronary arteries	Total male female	138.18 ± 139.41 166.68 ± 154.47 95.44 ± 103.43	11 43 11	711 711 370	0.114
AA	Total male female	134.33 ± 141.74 116.67 ± 69.74 160.81 ± 208.64	70 70 73	899 422 899	0.341
DA	Total male female	133.1 ±1 47.11 113.42 ± 61.92 162.63 ± 220.99	67 67 77	981 396 981	0.306
All Aorta	Total male female	133.71 ± 143.48 115.04 ± 64.68 161.72 ± 213.81	68.5 68.5 76.5	940 409 940	0.32
IVC	Total male female	99.85 ± 15.99 96.95 ± 18.65 104.92 ±8.21	64 64 92	130 130 125	0.172
SVC	Total male female	92.9 ±19.98 89.88 ±15.42 97.43 ± 25.23	62 68 62	141 130 141	0.246
Average BP	Total male female	95.57 ± 14.71 92.75 ± 13.71 100.54 ± 15.66	66.5 66.5 83	133 126 133	0.129

Table 9.34. HU_{mean} measurements at the cardiac arteries for 40 AKU patients who were part of the SONIA 2 clinical trial stratified by the decade of life.

Data display the HU_{mean} ± SD, minimum and maximum values, and P-value obtained from the CT scan at the main coronary arteries, aorta, and blood pool in four age groups. * Correlation is statistically significant between age group at the ROI ($P < 0.05$).

ROI	Age Group	HU_{mean} ± SD	Minimum	Maximum	P-value
LCA	30-39 years old	84.00 ± 44.38	22.00	145.00	0.65
	40-49 years old	112.77 ± 160.48	13.00	619.00	0.43
	50-59 years old	71.00 ± 34.08	-2.00	115.00	0.03*
	> 60 years old	233.30 ± 219.23	61.00	700.00	
LAD	30-39 years old	83.00 ± 68.74	7.00	207.00	0.13
	40-49 years old	50.00 ± 25.42	13.00	103.00	0.17
	50-59 years old	104.10 ± 135.05	26.00	457.00	0.05*
	> 60 years old	235.80 ± 147.79	15.00	502.00	
CA	30-39 years old	71.14 ± 53.41	14.00	176.00	0.53
	40-49 years old	132.31 ± 244.27	3.00	937.00	0.38
	50-59 years old	62.60 ± 28.48	21.00	112.00	0.02*
	> 60 years old	219.15 ± 193.89	38.00	620.00	
RCA	30-39 years old	75.57 ± 33.07	16.00	128.00	0.51
	40-49 years old	158.38 ± 323.72	-29.00	1217.00	0.62
	50-59 years old	218.40 ± 228.39	24.00	589.00	0.31
	> 60 years old	311.60 ± 167.40	90.00	522.00	
All coronary arteries	30-39 years old	78.32 ± 32.93	24.00	119.00	0.63
	40-49 years old	113.37 ± 182.69	11.00	711.00	0.84
	50-59 years old	100.63 ± 66.84	43.00	229.00	0.0001*
	> 60 years old	249.90 ± 124.18	56.00	431.00	
AA	30-39 years old	109.57 ± 29.14	73.00	153.00	0.04*
	40-49 years old	89.54 ± 12.28	70.00	107.00	0.06
	50-59 years old	98.80 ± 9.58	83.00	115.00	0.009*
	> 60 years old	245.40 ± 260.23	76.00	899.00	
DA	30-39 years old	106.57 ± 21.42	87.00	136.00	0.25
	40-49 years old	96.31 ± 16.44	67.00	126.00	0.37
	50-59 years old	102.00 ± 12.34	84.00	129.00	0.017
	> 60 years old	230.60 ± 280.75	77.00	981.00	
All aorta	30-39 years old	108.07 ± 23.62	80.00	140.00	0.07
	40-49 years old	92.92 ± 11.39	68.50	116.50	0.12
	50-59 years old	100.40 ± 10.45	83.50	121.00	0.012*
	> 60 years old	238.00 ± 268.92	76.50	940.00	
IVC	30-39 years old	107.00 ± 12.19	92.00	125.00	0.38
	40-49 years old	97.90 ± 20.39	64.00	130.00	0.74
	50-59 years old	100.67 ± 14.92	77.00	128.00	0.63
	> 60 years old	97.22 ± 14.60	69.00	119.00	
SVC	30-39 years old	113.00 ± 19.07	94.00	141.00	0.00*
	40-49 years old	78.92 ± 10.28	62.00	92.00	0.08
	50-59 years old	89.30 ±1 6.83	72.00	124.00	0.18
	> 60 years old	100.60 ± 19.66	79.00	134.00	
Average BP	30-39 years old	110.00 ± 15.22	93.00	133.00	0.00*
	40-49 years old	86.83 ± 10.87	66.50	105.50	0.11
	50-59 years old	95.59 ± 12.97	80.00	126.00	0.62
	> 60 years old	98.80 ± 14.70	77.00	122.50	